The Extraction and Characterization of Bio-oils from Woody Biomass and Investigation of Their Use as Antioxidants in Model Biodiesel

Abdulrahman Saleh A Alwehaibi

Doctor of Philosophy

University of York

Chemistry

December 2016

Abstract

Currently, antioxidants used in biodiesel to prevent degradation by autoxidation are synthesized from petroleum, which is non-renewable and has had a volatile price in recent years. Therefore, this thesis examines the possibility of using phenolic species from bio-oils derived from woodchips as antioxidants to protect biodiesel.

Crude bio-oil (18.5% w/w of woodchips) was obtained by microwave-enhanced pyrolysis of spruce woodchips (*picea abies*). Characterization by multiple analytical techniques shows that a noticeable portion of the bio-oil consisted of aromatics (mostly phenols) and sugars. The phenolic content of the bio-oil was quantified and identified by GC-FID & GC-MS and was found to be *ca.* 6% (w/w), while the total phenolic content was determined by Folin-Ciocalteu (FC) assay was *ca.* 23% (w/w). To isolate these phenols, the crude bio-oil was further fractionated by supercritical CO_2, and by two multi-solvent fractionation methods, namely: water-insoluble phase and water-soluble phase. The extract obtained with the highest phenolic content was a diethyl ether extract isolated from the water-soluble phase of crude bio-oil, at *ca.* 56% (w/w) by FC assay, with *ca.* 9% (w/w) identified and quantified by GC-MS & FID.

The effectiveness of these renewable phenols in a model biodiesel was examined using methyl linoleate autoxidation in 1 bar of oxygen at 120 $^{\circ}$C. Addition of low amounts of crude bio-oil to methyl linoleate was sufficient to increase its induction time, and was comparable with a commercial antioxidant (butylated hydroxy-toluene). Further examination of methyl linoleate with bio-oil isolated extracts indicated that these were less effective than the parent crude bio-oil. This was striking because some of the isolated extracts contained higher phenolic concentrations than the bio-oil. The antioxidancy of a chemical model of the crude bio-oil phenol consisting of six representative components at appropriate concentrations was approximately three times less active than the crude bio-oil, suggesting that components with noticeable antioxidancy remain to be identified.

List of Contents

Abstract 3

List of Contents 5

List of Figures 13

List of Tables 47

Acknowledgments 53

Author's Declaration 55

Chapter 1: Introduction 57

1.1 Thesis Aims 58

1.2 The Twelve Principles of Green Chemistry & Green Engineering 59

1.3 Biomass 62

1.3.1 Definition and resources 62

1.3.2 Composition of lignocellulosic biomass 64

1.3.3 Treatments 67

1.3.4 The use of biomass in the concept of a biorefinery 72

1.4 Microwave-Enhanced Chemistry 74

1.4.1 Principles of microwave heating 75

1.4.2 Microwave-enhanced pyrolysis of biomass 79

1.5 Composition of Bio-oils 82

1.5.1 Quantification and identification of bio-oil components 84

1.6 Biodiesel 85

1.6.1 Overview 85

1.6.2 Production 88

1.6.3 Composition 92

1.6.4 Degradation 93

1.7 Autoxidation Mechanisms of Lipids 93

1.8 Inhibition of Autoxidation by Different Classes of Antioxidants 96

1.8.1 Breaking the oxidation chains by the reaction with peroxyl ($ROO^{\bullet}$) radicals 97

1.8.2 Breaking the oxidation chains by the reaction with alkyl ($R^{\bullet}$) radicals .. 106

1.8.3 Reducing the rate of chain branching by the reaction of hydroperoxides with peroxide decomposing antioxidants 106

1.9 Commercial Radical Scavenging Antioxidants 108

1.9.1 Phenolic antioxidants 108

1.9.2 Aminic antioxidants 110

1.10 Biomass-Derived Antioxidants 112

1.11 Contextualization of Thesis 117

Chapter 2: Experimental 119

2.1 Microwave-Assisted Pyrolysis 120

2.2 Crude Bio-oil Fractionation 121

2.2.1 Solvent fractionation 121

2.2.2 Supercritical CO_2 fractionation 124

2.3 Analysis 124

2.3.1 Thermogravimetric analysis 124

2.3.2 Carbon-Hydrogen-Nitrogen analysis 125

2.3.3 Karl Fischer titration 125

2.3.4 Inductively coupled plasma-mass spectrometry analysis 126

2.3.5 Gas chromatography 127

2.3.6 Folin-Ciocalteu assay 129

2.3.7 Ultraviolet-visible spectrophotometry 130

2.3.8 Attenuated total reflectance-Fourier transform infrared spectroscopy ... 131

2.3.9 Nuclear magnetic resonance spectroscopy 131

2.3.10 High performance liquid chromatography 132

2.3.11 Gel permeation chromatography 132

2.4 Oxidation Tests 133

2.4.1 Static oxidation 133

2.4.2 Rancimat test 135

2.5 Chemical Materials and Reagents 136

Chapter 3: Extraction of Crude Bio-oils *via* Microwave-Enhanced Pyrolysis and Identification of Components 139

3.1 Introduction 140

3.2 Microwave Pyrolysis of Spruce Woodchips 141

3.3 Proximate and Ultimate Analysis of Spruce Woodchips and its Microwave-Enhanced Pyrolysis Products 143

3.4 ICP-MS Analysis of Spruce Woodchips and its Microwave-Enhanced Pyrolysis Products 146

3.5 ATR-IR Analysis of Spruce Woodchips and its Microwave-Enhanced Pyrolysis Products 148

3.6 NMR Analysis of Crude Bio-oil 152

3.7 GC-MS Characterization of Spruce Pyrolysis Liquids 157

3.7.1 Results 157

3.7.2 Discussion 167

3.8 Conclusion 170

Chapter 4: Extraction and Characterisation of Phenols from Spruce-Derived Bio-oils 173

4.1 Introduction 174

4.2 Identification and Quantification of Phenolic Compounds in Crude Bio-oil Extracts 174

4.3 Multi-Solvent Fractionation of Crude Bio-oil 180

4.3.1 Water-insoluble phase fractionation 180

4.3.2 Water-soluble phase fractionation 195

4.4 Supercritical CO_2 Extraction 210

4.4.1 Overview 210

4.4.2 Results and discussion 214

4.5 Discussion of the Phenolic Separation and Quantification 222

4.6 Conclusion 226

Chapter 5: Effect of Spruce-Derived Phenols on Oxidative Stability of Methyl Linoleate 229

5.1 Introduction 230

5.1.1 Methyl linoleate autoxidation mechanism 231

5.1.2 Antioxidant mechanism by phenols 234

5.2 Results 236

5.2.1 Effect of crude bio-oil derived phenols on methyl linoleate 236

5.2.2 Effect of Isolated Extracts on Methyl linoleate 240

5.2.3 Effect of phenolic standards on methyl linoleate 246

5.3 Discussion 251

5.3.1 Effect of isolated extracts total weight addition on induction time 251

5.3.2 Effect of isolated extracts total phenols on induction time 254

5.3.3 Effect of mixed phenolic standard on induction time 263

5.3.4 Discussion of the mechanism of antioxidant activity of bio-oil 266

5.3.5 The reduction of catechol antioxidancy at higher concentrations 274

5.4 Conclusion 280

Chapter 6: Conclusions and Future Work 283

6.1 Concluding Remarks 284

6.2 Future Work on Biomass Pyrolysis 287

6.3 Future Work on Antioxidant Testing and Antioxidants 287

Appendix A: Mass Spectra 289

A.1 Mass Spectra of Major Identified Compounds in Pyrolysis Liquids 290

A.1.1 Mass spectra of major identified compounds in crude bio-oil 290

A.1.2 Mass spectra of major identified compounds in aqueous fraction 305

A.2 Mass Spectra of Identified Phenolic Peaks in Crude Bio-oil 317

A.2.1 Mass spectra of identified phenolic peaks in 1st extract of crude bio-oil and their best NIST library match 317

A.2.2 Mass spectra of identified phenolic peaks in 2nd extract of crude bio-oil and their best NIST library match 323

A.3 Mass Spectra of Identified Phenolic Peaks in Water-Insoluble Phase Fractionation Experiment 332

A.3.1 Mass spectra of identified phenolic peaks in 2nd extract of crude bio-oil and their best NIST library match 332

A.3.2 Mass spectra of identified phenolic peaks in water-soluble extract and their best NIST library match 333

A.3.3 Mass spectra of identified phenolic peaks in neutral extract and their best NIST library match 337

A.3.4 Mass spectra of identified phenolic peaks in phenolic extract and their best NIST library match 343

A.3.5 Mass spectra of identified phenolic peaks in organic acids extract and their best NIST library match 352

A.4 Mass Spectra of Identified Phenolic Peaks in Water-Soluble Phase Fractionation Experiment 359

A.4.1 Mass spectra of identified phenolic peaks in 2nd extract of crude bio-oil and their best NIST library match 359

A.4.2 Mass spectra of identified phenolic peaks in water-soluble extract and their best NIST library match 367

A.4.3 Mass spectra of identified phenolic peaks in diethyl ether extract and their best NIST library match 372

A.5 Mass Spectra of Identified Phenolic Peaks in Supercritical CO_2 Extraction Experiment 380

A.5.1 Mass spectra of identified phenolic peaks in 1st extract of crude bio-oil and their best library match 380

A.5.2 Mass spectra of identified phenolic peaks in CO_2-1 and their best library match 380

A.5.3 Mass spectra of identified phenolic peaks in CO_2-2 and their best library match 386

A.5.4 Mass spectra of identified phenolic peaks in CO_2-3 and their best library match 393

A.5.5 Mass spectra of identified phenolic peaks in CO_2-4 and their best library match 399

Appendix B: ECN Calculations 407

Appendix C: Phenolic Concentrations in Methyl Linoleate 413

Appendix D: Microwave Pyrolysis 423

Abbreviations 427

References 433

List of Figures

Figure 1.1: Chemical structure of cellulose.[21] 65

Figure 1.2: Main monomers of hemicellulose.[21] 65

Figure 1.3: The chemical structures of the three main building blocks of lignin (monolignols).[21] 66

Figure 1.4: Thermal treatment technologies for biomass.[29] 68

Figure 1.5: Electromagnetic spectrum. 76

Figure 1.6: Schematic diagram of temperature distribution and heat development in wood by microwave irradiation, and the temperature distribution and heat transfer in wood by conventional heating.[120] 80

Figure 1.7: General equation for transesterification of triglyceride to biodiesel.[139] . 87

Figure 1.8: Top biodiesel producing countries in 2014. 90

Figure 1.9: Basic chain reactions of autoxidation in lipids.[186, 187] 96

Figure 1.10: Autoxidation degradation cycle and chain breaking mechanism by radical scavenging antioxidant.[187] 97

Figure 1.11: The well-known mechanism of a hindered phenolic antioxidant action.[190] 98

Figure 1.12: The well-known radical scavenging mechanism of diphenylamine antioxidant.[191-193] 99

Figure 1.13: *Ortho*- and *para*-quinolide peroxides formation in the case of 2,4,6-tri-*tert*-butylphenol (TTBP).[197] 100

Figure 1.14: The decomposition of peroxyl-antioxidant adducts to form a quinone.[197, 200] 101

Figure 1.15: The reaction of a hindered phenoxyl radical with dioxygen and the formation of quinolide peroxide.[186, 204] 101

Figure 1.16: Recombination of 2,6-di-*tert*-butylphenoxyl radicals with the formation of C-C dimer.[206] 102

Figure 1.17: The two proposed ways for the formation of a quinonemethide and BHT from 2,6-di-*tert*-butyl-4-methylphenoxyl radicals.[208-210] 103

Figure 1.18: The chemical structures of stilbene quinone and galvinoxyl. 103

Figure 1.19: The suggested mechanism for the formation of stilbene quinone from BHT through the dimerization of benzyl radicals.[213-215] 104

Figure 1.20: Proposed mechanisms of the formation of stilbene quinone and galvinoxyl from the simultaneous dimerisation and rearrangement of 2,6-di-*tert*-butyl-4-methylphenoxyl radicals.[217] 105

Figure 1.21: The dimerization of methylenequinone to stilbene quinone and ethylene bisphenol.[218] 105

Figure 1.22: The reactions of alkyl radical with: ia) benzoquinone; ib) dioxygen.[221-223] 106

Figure 1.23: The chemical structure of zinc dialkyl dithiophosphate (ZDDP). 107

Figure 2.1: The microwave pyrolysis set-up: A) Milestone ROTO SYNTH microwave reactor; B) Rotative 2 dm^3 microwave glass flask; C) Crude bio-oil collection point; D) Aqueous collection point; E) Vacuum pump; F) Pyrolysis gas release point..... 120

Figure 2.2: Schematic diagram of water-insoluble phase fractionation steps..... 122

Figure 2.3: Schematic diagram of water-soluble phase fractionation steps. 123

Figure 2.4: Illustration of proximate analysis (moisture, volatile matter, fixed carbon and ash contents) determination from spruce woodchips TG analysis data. 125

Figure 2.5: A schematic diagram of the oxidation test reactor in a sealed mode used in this study. 133

Figure 2.6: Diagrammatic illustration of induction time (IT) determination in a typical pressure trace of an oxidation experiment carried out in sealed reactor. 135

Figure 3.1: Schematic diagram of the microwave set-up, including an illustration of the obtained products (char, crude bio-oil and aqueous extracts) after the pyrolysis experiment. 141

Figure 3.2: The TG analysis curves and an illustration of proximate analysis (moisture, volatile matter, fixed carbon, and ash contents) determination of: A) spruce char; B) spruce woodchips 144

Figure 3.3: ATR-IR spectra of crude bio-oil and the aqueous fraction generated from the microwave enhanced pyrolysis of spruce woodchips. (Spectra offset vertically for clarity) 148

Figure 3.4: ^{13}C NMR spectra of crude bio-oil and aqueous fraction produced from the microwave enhanced pyrolysis of spruce woodchips. (spectra offset vertically for clarity) 154

Figure 3.5: GC-MS spectrum of crude bio-oil derived from the microwave enhanced pyrolysis of spruce woodchips; A) Spectrum retention time from 3 to 20 min, B) The follow-up of spectrum retention time from 20 to 37 min. 159

Figure 3.6: GC-MS spectrum of aqueous fraction obtained from the microwave enhanced pyrolysis of spruce woodchips. 164

Figure 3.7: The suggested mechanism of 1,2-benzenediol formation from guaiacol during pyrolysis.[290] 168

Figure 4.1: The GC-MS chromatograms of: (A) identified phenolic compounds in 1st extract of crude bio-oil; (B) identified phenolic compounds in 2nd extract of crude bio-oil (some phenolic peaks were identified later in Table 4.3, therefore, for consistency the phenolic peaks numbering were labeled here according to the phenolic peak retention times of Table 4.3). 175

Figure 4.2: The GC-MS chromatograms of the identified phenolic compounds in: A) 2nd extract of crude bio-oil; B) Water-soluble extract; C) Neutral extract; D) Phenolic extract; and E) Organic acids extracts. 182

Figure 4.3: ATR-IR spectra of: A) Crude bio-oil; B) Water-soluble extract; C) Neutral extract; D) Phenolic extract; and E) Organic acids extract. 191

Figure 4.4: ^{13}C NMR spectra of: A) 2nd extract of crude bio-oil; B) Water-soluble extract; C) Neutral extract; D) Phenolic extract; and E) Organic acids extract. 193

Figure 4.5: HPLC spectra of sugars standards and water-soluble extract (red trace: ELSD detector, and black trace: DAD detector). 195

Figure 4.6: The GC-FID chromatograms of the identified phenolic compounds in: A) 2nd extract of crude bio-oil; B) Water-soluble extract; C) Diethyl ether extract; D) DCM extract; and E) Water-soluble residue. (For consistency, the 2nd crude bio-oil and the water soluble extracts were reanalyzed again together with the rest of extracts *via* another GC-FID apparatus with different programmed method at the point of this experiment. Therefore, the retention time of phenolic peaks differ from previous GC-MS chromatograms in Figure 4.2). 197

Figure 4.7: ATR-IR spectra of: A) Crude bio-oil; B) Water-soluble extract; C) Diethyl ether extract; D) DCM extract; and E) Water-soluble residue. 205

Figure 4.8: ^{13}C NMR spectra of: A) Crude bio-oil; B) Water-soluble extract; C) Diethyl ether extract; D) DCM extract; and E) Water-soluble residue. 207

Figure 4.9: ^{13}C NMR spectra of diethyl ether extract and catechol standard. 208

Figure 4.10: GPC-ELSD spectra of: A) water-soluble extract; B) di-ethyl ether extract; C) DCM extract; and D) water-soluble residue. 209

Figure 4.11: Typical pressure-temperature phase diagram of supercritical fluid.[299] 211

Figure 4.12: The GC-MS chromatograms of the identified phenolic compounds in 1st crude bio-oil extract and in CO_2 isolated fractions. 216

Figure 4.13: ATR-IR spectra of crude bio-oil and its supercritical CO_2 isolated extracts (spectra offset vertically for clarity). 222

Figure 5.1: Initial stages of the mechanism of methyl linoleate autoxidation.[329] ... 232

Figure 5.2: Proposed reactions of the phenoxyl radical with peroxyl radical to produce alcohol and *ortho*- and *para*-quinones.[186] 235

Figure 5.3: Examples of phenolic species and their experimental BDE values (kJ mol^{-1}).[339] 235

Figure 5.4: Oxidation pressure traces of 2 ml methyl linoleate with concentrations of crude bio-oil from 0 to 69.5 x 10^{-3} (mol dm^{-3}) at 120 °C and 1 bar of oxygen (phenolic concentrations determined by FC assay that assume only mono-phenolic present). 237

Figure 5.5: Oxidation pressure traces of 2 ml methyl linoleate with concentrations of BHT from 0 to 80 x 10^{-3} (mol dm^{-3}) at 120 °C and 1 bar of oxygen. 238

Figure 5.6: The average Rancimat test (EN 14112) induction times of 3 g methyl linoleate without antioxidant, and with concentrations of 20.21 and 34.80 (x10^{-3} mol dm^{-3}) respectively of BHT and crude bio-oil at 110 °C (the induction times here are the average of four independent runs and the error bars are ±standard deviation. the phenolic concentration quoted for the crude bio-oil was determined by FC assay that assume only mono-phenolic present). 239

Figure 5.7: Schematic diagram of water-insoluble phase fractionation steps..... 240

Figure 5.8: Oxidation pressure traces of 2 ml methyl linoleate with concentrations of: (A) water-soluble extract from 0 to 41.5 x 10^{-3} mol dm^{-3}; (B) neutral extract from 0 to 34.5 x 10^{-3} mol dm^{-3}; (C) phenolic extract from 0 to 151 x 10^{-3} mol dm^{-3}; (D) organic acids extract from 0 to 116.5 x 10^{-3} mol dm^{-3}, at 120 °C and 1 bar of oxygen. (Phenolic concentrations determined by FC assay assuming only mono-phenolic present). 242

Figure 5.9: Schematic diagram of water-soluble phase fractionation steps..... 244

Figure 5.10: Oxidation pressure traces of 2 ml methyl linoleate with concentrations of: (A) water-soluble extract from 0 to 41.5 x 10^{-3} (mol dm^{-3}); (B) diethyl ether extract from 0 to 169.5 x 10^{-3} (mol dm^{-3}); (C) DCM extract from 0 to 39 x 10^{-3} (mol dm^{-3}); (D) water-soluble residue extract from 0 to 4.5 x 10^{-3} (mol dm^{-3}), at 120 °C and 1 bar of oxygen. (Phenolic concentrations determined by FC assay assume only mono-phenolic present). 245

Figure 5.11: Chemical structures of eugenol, catechol and trans-isoeugenol. 246

Figure 5.12: Oxidation pressure traces of 2 ml methyl linoleate with concentrations of 4-allyl-2-methoxyphenol (eugenol) from 0 to 162 x 10^{-3} (mol dm^{-3}) at 120 °C and 1 bar of oxygen. 247

Figure 5.13: Oxidation pressure traces of 2 ml methyl linoleate with concentrations of 1,2-benzenediol (catechol) from 0 to 162 x 10^{-3} (mol dm^{-3}) at 120 °C and 1 bar of oxygen (catechol here was a 1st experimental run) 247

Figure 5.14: Oxidation pressure traces of 2 ml methyl linoleate with concentrations of 1,2-benzenediol (catechol) from 0 to 60 x 10^{-3} (mol dm^{-3}) at 120 °C and 1 bar of oxygen (catechol here was a 2nd experimental run). 248

Figure 5.15: Oxidation pressure traces of 2 ml methyl linoleate with concentrations of isoeugenol from 0 to 60 x 10^{-3} (mol dm^{-3}) at 120 °C and 1 bar of oxygen. 249

Figure 5.16: Oxidation pressure traces of 2 ml methyl linoleate with concentrations of mixed phenolic standard from 0 to 119 x 10^{-3} (mol dm^{-3}) at 120 °C and 1 bar of oxygen. 251

Figure 5.17: The induction time of 2 ml methyl linoleate at three total weight addition % (w/w) of crude bio-oil, water-soluble extract, neutral extract, phenolic extract and organic acids extract at 120 °C and 1 bar of oxygen. 252

Figure 5.18: The induction times of 2 ml methyl linoleate at three total weight addition % (w/w) of crude bio-oil, water-soluble extract, diethyl ether extract, DCM extract and water-soluble residue at 120 °C and 1 bar of oxygen (crude bio-oil and water-soluble extract results are presented here again for ease of comparison). 253

Figure 5.19: The induction times of 2 ml methyl linoleate with increasing concentrations of: (A) crude bio-oil, water-soluble, neutral, phenolic and organic acids extracts; (B) BHT, eugenol and catechol at 120 °C and 1 bar of oxygen..... 255

Figure 5.20: The induction times of 2 ml methyl linoleate with increasing concentrations of: (A) crude bio-oil, water-soluble, diethyl ether, DCM and water-soluble residue extracts; (B) BHT, isoeugenol and catechol, at 120 °C and 1 bar of oxygen (crude bio-oil, water-soluble extract, BHT and catechol are presented again for ease of comparison). 260

Figure 5.21: The ^{13}C NMR spectrum of catechol standard and the ^{13}C NMR spectra of methyl linoleate with the addition of 170 x 10^{-3} mol dm^{-3} of diethyl ether extract before and after oxidation at 120 °C and 1 bar oxygen. 261

Figure 5.22: The ^{13}C NMR spectrum of catechol standard and the ^{13}C NMR spectra of methyl linoleate with the addition of 20 x 10^{-3} mol dm^{-3} of catechol standard before and after oxidation at 120 °C and 1 bar oxygen. 262

Figure 5.23: The induction times of 2 ml methyl linoleate with increasing concentrations of: (A) crude bio-oil and mixed phenolic standard; (B) BHT, eugenol, isoeugenol, catechol and mixed phenolic standard at 120 °C and 1 bar of oxygen (the induction time of catechol at 40 x 10^{-3} mol/dm^3 presented here is the average of two independent experiments). 264

Figure 5.24: Potential reaction mechanism and oxidation products of eugenol.[349] 267

Figure 5.25: The formation of isoeugenol-derived phenoxyl radical and its radical stabilization. 268

Figure 5.26: The chemical structures of caffeic, *p*-coumaric, gallic, protocatechuic, gentisic and γ-resorcylic acids. 269

Figure 5.27: The formation of intramolecular hydrogen bond in the catechol-derived phenoxyl radical, and the formation *ortho*-quinone by either the reaction of the formed phenoxyl radical with a second peroxyl radical or by the regeneration mechanism of a catechol.[341, 349, 354] 270

Figure 5.28: The formation of diphenol dimer by either the reaction between two phenoxyl radicals or the reaction between an *ortho*-quinone and a diphenol.[355, 356] 271

Figure 5.29: Two possible types of dimer formation from the reaction of *ortho*-quinones with *ortho*-diphenols.[357] 271

Figure 5.30: The trapping of two peroxyl radicals by the formed C-O dimer of *ortho*-diphenol.[357] 272

Figure 5.31: The trapping of four peroxyl radicals by the formed C-C dimer of *ortho*-diphenol.[357] 272

Figure 5.32: The chemical structures of quercetin, rosmarinic acid, α-tocopherol, and caffeic acid. 273

Figure 5.33: The suggested regeneration mechanism of an antioxidant by another one in a mixture.[359] 274

Figure 5.34: Proposed change in antiradical mechanism of catechol at higher concentration during autoxidation reaction. 275

Figure 5.35: The proposed oxidation products of catechol during oxidation reactions.[361] 276

Figure 5.36: Proposed oxidative reaction pathway for the formation of triphenylene (product 1) from catechol.[361-363] 276

Figure 5.37: Proposed mechanism for the formation of triphenylene (product 1) from catechol during oxidation reactions. 277

Figure 5.38: Proposed mechanistic pathway for the formation of polycyclic quinone (product 2) from catechol-derived biphenyl during oxidation reactions.[361] 278

Figure 5.39: The chemical structure of 2,5,6,9,12,13-hexamethoxy-1,8-quinone. . 278

Figure A.1: Matching mass spectrum of peak number 1 in crude bio-oil GC-MS: A) MS of peak number 1 in crude bio-oil sample; B) MS of furfural according to NIST library database. 290

Figure A.2: Matching mass spectrum of peak number 2 in crude bio-oil GC-MS: A) MS of peak number 2 in crude bio-oil sample; B) MS of 2-furanmethanol according to NIST library database. 290

Figure A.3: Matching mass spectrum of peak number 3 in crude bio-oil GC-MS: A) MS of peak number 3 in crude bio-oil sample; B) MS of 2(5H)-furanone according to NIST library database. 291

Figure A.4: Matching mass spectrum of peak number 4 in crude bio-oil GC-MS: A) MS of peak number 4 in crude bio-oil sample; B) MS of 1,2-cyclopentanedione according to NIST library database..... 291

Figure A.5: Matching mass spectrum of peak number 5 in crude bio-oil GC-MS: A) MS of peak number 5 in crude bio-oil sample; B) MS of 2-hydroxy-gamma-butyrolactone according to NIST library database..... 292

Figure A.6: Matching mass spectrum of peak number 6 in crude bio-oil GC-MS: A) MS of peak number 6 in crude bio-oil sample; B) MS of 1,2-cyclopentanedione, 3-methyl- according to NIST library database. 292

Figure A.7: Matching mass spectrum of peak number 7 in crude bio-oil GC-MS: A) MS of peak number 7 in crude bio-oil sample; B) MS of phenol, 2-methoxy- according to NIST library database..... 293

Figure A.8: Matching mass spectrum of peak number 8 in crude bio-oil GC-MS: A) MS of peak number 8 in crude bio-oil sample; B) MS of cyclopropyl carbinol according to NIST library database..... 293

Figure A.9: Matching mass spectrum of peak number 9 in crude bio-oil GC-MS: A) MS of peak number 9 in crude bio-oil sample; B) MS of 2(3H)-furanone, dihydro-4-hydroxy- according to NIST library database. 294

Figure A.10: Matching mass spectrum of peak number 10 in crude bio-oil GC-MS: A) MS of peak number 10 in crude bio-oil sample; B) MS of phenol, 2-methoxy-4-methyl- according to NIST library database. 294

Figure A.11: Matching mass spectrum of peak number 11 in crude bio-oil GC-MS: A) MS of peak number 11 in crude bio-oil sample; B) MS of 1,2-benzenediol according to NIST library database. 295

Figure A.12: Matching mass spectrum of peak number 12 in crude bio-oil GC-MS: A) MS of peak number 12 in crude bio-oil sample; B) MS of 1,4:3,6-dianhydro-α-d-glucopyranose according to NIST library database. 295

Figure A.13: Matching mass spectrum of peak number 13 in crude bio-oil GC-MS: A) MS of peak number 13 in crude bio-oil sample; B) MS of 2-furancarboxaldehyde, 5-(hydroxymethyl)- according to NIST library database. 296

Figure A.14: Matching mass spectrum of peak number 14 in crude bio-oil GC-MS: A) MS of peak number 14 in crude bio-oil sample; B) MS of 1,2-benzenediol, 4-methyl- according to NIST library database. 296

Figure A.15: Matching mass spectrum of peak number 15 in crude bio-oil GC-MS: A) MS of peak number 15 in crude bio-oil sample; B) MS of phenol, 4-ethyl-2-methoxy- according to NIST library database. 297

Figure A.16: Matching mass spectrum of peak number 16 in crude bio-oil GC-MS: A) MS of peak number 16 in crude bio-oil sample; B) MS of 2-methoxy-4-vinylphenol according to NIST library database. 297

Figure A.17: Matching mass spectrum of peak number 17 in crude bio-oil GC-MS: A) MS of peak number 17 in crude bio-oil sample; B) MS of 3-allyl-6-methoxyphenol according to NIST library database. 298

Figure A.18: Matching mass spectrum of peak number 18 in crude bio-oil GC-MS: A) MS of peak number 18 in crude bio-oil sample; B) MS of benzaldehyde, 3-hydroxy-4-methoxy- according to NIST library database. 298

Figure A.19: Matching mass spectrum of peak number 19 in crude bio-oil GC-MS: A) MS of peak number 19 in crude bio-oil sample; B) MS of phenol, 2-methoxy-4-(1-propenyl)- according to NIST library database. 299

Figure A.20: Matching mass spectrum of peak number 20 in crude bio-oil GC-MS: A) MS of peak number 20 in crude bio-oil sample; B) MS of phenol, 2-methoxy-4-(1-propenyl)-, (Z)- according to NIST library database..... 299

Figure A.21: Matching mass spectrum of peak number 21 in crude bio-oil GC-MS: A) MS of peak number 21 in crude bio-oil sample; B) MS of phenol, 2-methoxy-4-propyl- according to NIST library database. 300

Figure A.22: Matching mass spectrum of peak number 22 in crude bio-oil GC-MS: A) MS of peak number 22 in crude bio-oil sample; B) MS of β-D-glucopyranose, 1,6-anhydro- according to NIST library database. 300

Figure A.23: Matching mass spectrum of peak number 23 in crude bio-oil GC-MS: A) MS of peak number 23 in crude bio-oil sample; B) MS of ethanone, 1-(4-hydroxy-3-methoxyphenyl)- according to NIST library database. 301

Figure A.24: Matching mass spectrum of peak number 24 in crude bio-oil GC-MS: A) MS of peak number 24 in crude bio-oil sample; B) MS of 2-propanone, 1-(4-hydroxy-3-methoxyphenyl)- according to NIST library database. 301

Figure A.25: Matching mass spectrum of peak number 25 in crude bio-oil GC-MS: A) MS of peak number 25 in crude bio-oil sample; B) MS of β-D-glucopyranose, 1,6-anhydro- according to NIST library database. 302

Figure A.26: Matching mass spectrum of peak number 26 in crude bio-oil GC-MS: A) MS of peak number 26 in crude bio-oil sample; B) MS of phenol, 4-(3-hydroxy-1-propenyl)-2-methoxy- according to NIST library database. 302

Figure A.27: Matching mass spectrum of peak number 27 in crude bio-oil GC-MS: A) MS of peak number 27 in crude bio-oil sample; B) MS of benzeneacetic acid, 4-hydroxy-3-methoxy- according to NIST library database. 303

Figure A.28: Matching mass spectrum of peak number 28 in crude bio-oil GC-MS: A) MS of peak number 28 in crude bio-oil sample; B) MS of 4-hydroxy-2-methoxycinnamaldehyde according to NIST library database. 303

Figure A.29: Matching mass spectrum of peak number 29 in crude bio-oil GC-MS: A) MS of peak number 29 in crude bio-oil sample; B) MS of 10,11-dihydro-10-hydroxy-2,3-dimethoxydibenz(b,f)oxepin according to NIST library database. 304

Figure A.30: Unidentified MS of peak 30 in crude bio-oil sample. 304

Figure A.31: Matching mass spectrum of peak number 1 in aqueous fraction GC-MS: A) MS of peak number 1 in aqueous fraction sample; B) MS of 2-furanmethanol according to NIST library database. 305

Figure A.32: Matching mass spectrum of peak number 2 in aqueous fraction GC-MS: A) MS of peak number 2 in aqueous fraction sample; B) MS of butanoic acid, 4-hydroxy- according to NIST library database. 305

Figure A.33: Matching mass spectrum of peak number 3 in aqueous fraction GC-MS: A) MS of peak number 3 in aqueous fraction sample; B) MS of 2(5H)-furanone according to NIST library database. 306

Figure A.34: Matching mass spectrum of peak number 4 in aqueous fraction GC-MS: A) MS of peak number 4 in aqueous fraction sample; B) MS of 2-cyclohexen-1-ol according to NIST library database. 306

Figure A.35: Matching mass spectrum of peak number 5 in aqueous fraction GC-MS: A) MS of peak number 5 in aqueous fraction sample; B) MS of ethanol, 2,2-diethoxy- according to NIST library database. 307

Figure A.36: Matching mass spectrum of peak number 6 in aqueous fraction GC-MS: A) MS of peak number 6 in aqueous fraction sample; B) MS of 2-furancarboxaldehyde, 5-methyl- according to NIST library database. 307

Figure A.37: Matching mass spectrum of peak number 7 in aqueous fraction GC-MS: A) MS of peak number 7 in aqueous fraction sample; B) MS of phenol according to NIST library database. 308

Figure A.38: Matching mass spectrum of peak number 8 in aqueous fraction GC-MS: A) MS of peak number 8 in aqueous fraction sample; B) MS of furan, 2,5-diethoxytetrahydro- according to NIST library database. 308

Figure A.39: Matching mass spectrum of peak number 9 in aqueous fraction GC-MS: A) MS of peak number 9 in aqueous fraction sample; B) MS of 1,2-cyclopentanedione, 3-methyl- according to NIST library database. 309

Figure A.40: Matching mass spectrum of peak number 10 in aqueous fraction GC-MS: A) MS of peak number 10 in aqueous fraction sample; B) MS of phenol, 2-methoxy- according to NIST library database. 309

Figure A.41: Matching mass spectrum of peak number 11 in aqueous fraction GC-MS: A) MS of peak number 11 in aqueous fraction sample; B) MS of 2-cyclopenten-1-one, 3-ethyl-2-hydroxy- according to NIST library database. 310

Figure A.42: Matching mass spectrum of peak number 12 in aqueous fraction GC-MS: A) MS of peak number 12 in aqueous fraction sample; B) MS of cis-3-hexenal diethyl acetal according to NIST library database. 310

Figure A.43: Matching mass spectrum of peak number 13 in aqueous fraction GC-MS: A) MS of peak number 13 in aqueous fraction sample; B) MS of cyclohexanone, 2,3-dimethyl- according to NIST library database. 311

Figure A.44: Matching mass spectrum of peak number 14 in aqueous fraction GC-MS: A) MS of peak number 14 in aqueous fraction sample; B) MS of 1,3-benzenediol, 4-ethyl- according to NIST library database 311

Figure A.45: Matching mass spectrum of peak number 15 in aqueous fraction GC-MS: A) MS of peak number 15 in aqueous fraction sample; B) MS of phenol, 2-methoxy-4-methyl- according to NIST library database. 312

Figure A.46: Matching mass spectrum of peak number 16 in aqueous fraction GC-MS: A) MS of peak number 16 in aqueous fraction sample; B) MS of 3,4-dimethoxytoluene according to NIST library database. 312

Figure A.47: Matching mass spectrum of peak number 17 in aqueous fraction GC-MS: A) MS of peak number 17 in aqueous fraction sample; B) MS of 1,2-benzenediol according to NIST library database. 313

Figure A.48: Matching mass spectrum of peak number 18 in aqueous fraction GC-MS: A) MS of peak number 18 in aqueous fraction sample; B) MS of phenol, 4-ethyl-2-methoxy- according to NIST library database. 313

Figure A.49: Matching mass spectrum of peak number 19 in aqueous fraction GC-MS: A) MS of peak number 19 in aqueous fraction sample; B) MS of 2-methoxy-4-vinylphenol according to NIST library database. 314

Figure A.50: Matching mass spectrum of peak number 20 in aqueous fraction GC-MS: A) MS of peak number 20 in aqueous fraction sample; B) MS of 3-allyl-6-methoxyphenol according to NIST library database. 314

Figure A.51: Matching mass spectrum of peak number 21 in aqueous fraction GC-MS: A) MS of peak number 21 in aqueous fraction sample; B) MS of phenol, 2-methoxy-4-propyl- according to NIST library database. 315

Figure A.52: Matching mass spectrum of peak number 22 in aqueous fraction GC-MS: A) MS of peak number 22 in aqueous fraction sample; B) MS of benzaldehyde, 3-hydroxy-4-methoxy- according to NIST library database. 315

Figure A.53: Matching mass spectrum of peak number 23 in aqueous fraction GC-MS: A) MS of peak number 23 in aqueous fraction sample; B) MS of phenol, 2-methoxy-4-(1-propenyl)- according to NIST library database. 316

Figure A.54: Matching mass spectrum of peak number 24 in aqueous fraction GC-MS: A) MS of peak number 24 in aqueous fraction sample; B) MS of phenol, 2-methoxy-4-(1-propenyl)-, (Z)- according to NIST library database. 316

Figure A.55: Matching mass spectrum of peak number 25 in aqueous fraction GC-MS: A) MS of peak number 25 in aqueous fraction sample; B) MS of 2-propanone, 1-(4-hydroxy-3-methoxyphenyl)- according to NIST library database. 317

Figure A.56: Matching mass spectrum of peak number 4 in 1st extract of crude bio-oil GC-MS: A) MS of peak number 4 in 1st extract of crude bio-oil sample; B) MS of phenol, 2-methoxy- according to NIST library database. 317

Figure A.57: Matching mass spectrum of peak number 7 in 1st extract of crude bio-oil GC-MS: A) MS of peak number 7 in 1st extract of crude bio-oil sample; B) MS of phenol, 2-methoxy-4-methyl- according to NIST library database. 318

Figure A.58: Matching mass spectrum of peak number 8 in 1st extract of crude bio-oil GC-MS: A) MS of peak number 8 in 1st extract of crude bio-oil sample; B) MS of 1,2-benzenediol according to NIST library database. 318

Figure A.59: Matching mass spectrum of peak number 10 in 1st extract of crude bio-oil GC-MS: A) MS of peak number 10 in 1st extract of crude bio-oil sample; B) MS of phenol, 4-ethyl-2-methoxy- according to NIST library database. 319

Figure A.60: Matching mass spectrum of peak number 12 in 1st extract of crude bio-oil GC-MS: A) MS of peak number 12 in 1st extract of crude bio-oil sample; B) MS of 2-methoxy-4-vinylphenol according to NIST library database. 319

Figure A.61: Matching mass spectrum of peak number 14 in 1st extract of crude bio-oil GC-MS: A) MS of peak number 14 in 1st extract of crude bio-oil sample; B) MS of 3-allyl-6-methoxyphenol according to NIST library database. 320

Figure A.62: Matching mass spectrum of peak number 16 in 1st extract of crude bio-oil GC-MS: A) MS of peak number 16 in 1st extract of crude bio-oil sample; B) MS of benzaldehyde, 3-hydroxy-4-methoxy- according to NIST library database..... 320

Figure A.63: Matching mass spectrum of peak number 17 in 1st extract of crude bio-oil GC-MS: A) MS of peak number 17 in 1st extract of crude bio-oil sample; B) MS of phenol, 2-methoxy-4-(1-propenyl)- according to NIST library database. 321

Figure A.64: Matching mass spectrum of peak number 18 in 1st extract of crude bio-oil GC-MS: A) MS of peak number 18 in 1st extract of crude bio-oil sample; B) MS of phenol, 2-methoxy-4-(1-propenyl)-, (Z)- according to NIST library database. .. 321

Figure A.65: Matching mass spectrum of peak number 20 in 1st extract of crude bio-oil GC-MS: A) MS of peak number 20 in 1st extract of crude bio-oil sample; B) MS of ethanone, 1-(4-hydroxy-3-methoxyphenyl)- according to NIST library database. 322

Figure A.66: Matching mass spectrum of peak number 21 in 1st extract of crude bio-oil GC-MS: A) MS of peak number 21 in 1st extract of crude bio-oil sample; B) MS of 2-propanone, 1-(4-hydroxy-3-methoxyphenyl)- according to NIST library database. 322

Figure A.67: Matching mass spectrum of peak number 24 in 1st extract of crude bio-oil GC-MS: A) MS of peak number 24 in 1st extract of crude bio-oil sample; B) MS of benzeneacetic acid, 4-hydroxy-3-methoxy- according to NIST library database. 323

Figure A.68: Matching mass spectrum of peak number 26 in 1st extract of crude bio-oil GC-MS: A) MS of peak number 26 in 1st extract of crude bio-oil sample; B) MS of 4-hydroxy-2-methoxycinnamaldehyde according to NIST library database. 323

Figure A.69: Matching MS spectrum of peak number 1 MS in 2nd extract of crude bio-oil GC-MS: A) MS of Peak number 1 in 2nd extract of crude bio-oil sample; B) MS of phenol according to NIST library database. 324

Figure A.70: Matching MS spectrum of peak number 3 MS in 2nd extract of crude bio-oil GC-MS: A) MS of peak number 3 in 2nd extract of crude bio-oil sample; B) MS of Phenol, 4-methyl- according to NIST library database. 324

Figure A.71: Matching MS spectrum of peak number 4 MS in 2nd extract of crude bio-oil GC-MS: A) MS of peak number 4 in 2nd extract of crude bio-oil sample; B) MS of Phenol, 2-methoxy- according to NIST library database. 325

Figure A.72: Matching MS spectrum of peak number 7 MS in 2nd extract of crude bio-oil GC-MS: A) MS of peak number 7 in 2nd extract of crude bio-oil sample; B) MS of Phenol, 2-methoxy-4-methyl- according to NIST library database. 325

Figure A.73: Matching MS spectrum of peak number 8 MS in 2nd extract of crude bio-oil GC-MS: A) MS of peak number 8 in 2nd extract of crude bio-oil sample; B) MS of 1,2-Benzenediol according to NIST library database. 326

Figure A.74: Matching MS spectrum of peak number 10 MS in 2nd extract of crude bio-oil GC-MS: A) MS of peak number 10 in 2nd extract of crude bio-oil sample; B) MS of Phenol, 4-ethyl-2-methoxy- according to NIST library database. 326

Figure A.75: Matching MS spectrum of peak number 11 MS in 2nd extract of crude bio-oil GC-MS: A) MS of peak number 11 in 2nd extract of crude bio-oil sample; B) MS of 1,2-Benzenediol, 4-methyl- according to NIST library database. 327

Figure A.76: Matching MS spectrum of peak number 12 MS in 2nd extract of crude bio-oil GC-MS: A) MS of peak number 12 in 2nd extract of crude bio-oil sample; B) MS of 2-Methoxy-4-vinylphenol according to NIST library database. 327

Figure A.77: Matching MS spectrum of peak number 14 MS in 2nd extract of crude bio-oil GC-MS: A) MS of peak number 14 in 2nd extract of crude bio-oil sample; B) MS of 3-Allyl-6-methoxyphenol according to NIST library database. 328

Figure A.78: Matching MS spectrum of peak number 15 MS in 2nd extract of crude bio-oil GC-MS: A) MS of peak number 15 in 2nd extract of crude bio-oil sample; B) MS of Phenol, 2-methoxy-4-propyl- according to NIST library database..... 328

Figure A.79: Matching MS spectrum of peak number 16 MS in 2nd extract of crude bio-oil GC-MS: A) MS of peak number 16 in 2nd extract of crude bio-oil sample; B) MS of Benzaldehyde, 3-hydroxy-4-methoxy- according to NIST library database. 329

Figure A.80: Matching MS spectrum of peak number 17 MS in 2nd extract of crude bio-oil GC-MS: A) MS of peak number 17 in 2nd extract of crude bio-oil sample; B) MS of Phenol, 2-methoxy-4-(1-propenyl)- according to NIST library database. 329

Figure A.81: Matching MS spectrum of peak number 18 MS in 2nd extract of crude bio-oil GC-MS: A) MS of peak number 18 in 2nd extract of crude bio-oil sample; B) MS of Phenol, 2-methoxy-4-(1-propenyl)-, (Z)- according to NIST library database. 330

Figure A.82: Matching MS spectrum of peak number 20 MS in 2nd extract of crude bio-oil GC-MS: A) MS of peak number 20 in 2nd extract of crude bio-oil sample; B)

MS of Ethanone, 1-(4-hydroxy-3-methoxyphenyl)- according to NIST library database. 330

Figure A.83: Matching MS spectrum of peak number 21 MS in 2nd extract of crude bio-oil GC-MS: A) MS of peak number 21 in 2nd extract of crude bio-oil sample; B) MS of 2-Propanone, 1-(4-hydroxy-3-methoxyphenyl)- according to NIST library database. 331

Figure A.84: Matching MS spectrum of peak number 22 MS in 2nd extract of crude bio-oil GC-MS: A) MS of peak number 22 in 2nd extract of crude bio-oil sample; B) MS of Phenol, 4-(3-hydroxy-1-propenyl)-2-methoxy- according to NIST library.. 331

Figure A.85: Matching MS spectrum of peak number 24 MS in 2nd extract of crude bio-oil GC-MS: A) MS of peak number 24 in 2nd extract of crude bio-oil sample; B) MS of Benzeneacetic acid, 4-hydroxy-3-methoxy- according to NIST library. 332

Figure A.86: Matching MS spectrum of peak number 26 MS in 2nd extract of crude bio-oil GC-MS: A) MS of peak number 26 in 2nd extract of crude bio-oil sample; B) MS of 4-Hydroxy-2-methoxycinnamaldehyde according to NIST library. 332

Figure A.87: Matching MS spectrum of peak number 7 MS in water-soluble extract GC-MS: A) MS of peak number 7 in water-soluble extract sample; B) MS of Phenol, 2-methoxy-4-methyl- according to NIST library. 333

Figure A.88: Matching MS spectrum of peak number 8 MS in water-soluble extract GC-MS: A) MS of peak number 8 in water-soluble extract sample; B) MS of 1,2-Benzenediol according to NIST library. 333

Figure A.89: Matching MS spectrum of peak number 16 MS in water-soluble extract GC-MS: A) MS of peak number 16 in water-soluble extract sample; B) MS of Benzaldehyde, 3-hydroxy-4-methoxy- according to NIST library. 334

Figure A.90: Matching MS spectrum of peak number 20 MS in water-soluble extract GC-MS: A) MS of peak number 20 in water-soluble extract sample; B) MS of Ethanone, 1-(4-hydroxy-3-methoxyphenyl)- according to NIST library. 334

Figure A.91: Matching MS spectrum of peak number 21 MS in water-soluble extract GC-MS: A) MS of peak number 21 in water-soluble extract sample; B) MS of 2-Propanone, 1-(4-hydroxy-3-methoxyphenyl)- according to NIST library..... 335

Figure A.92: Matching MS spectrum of peak number 22 MS in water-soluble extract GC-MS: A) MS of peak number 22 in water-soluble extract sample; B) MS of Phenol, 4-(3-hydroxy-1-propenyl)-2-methoxy- according to NIST library..... 335

Figure A.93: Matching MS spectrum of peak number 24 MS in water-soluble extract GC-MS: A) MS of peak number 24 in water-soluble extract sample; B) MS of Benzeneacetic acid, 4-hydroxy-3-methoxy- according to NIST library..... 336

Figure A.94: Matching MS spectrum of peak number 26 MS in water-soluble extract GC-MS: A) MS of peak number 26 in water-soluble extract sample; B) MS of 4-Hydroxy-2-methoxycinnamaldehyde according to NIST library. 336

Figure A.95: Matching MS spectrum of peak number 4 MS in neutral extract GC-MS: A) MS of peak number 4 in neutral extract sample; B) MS of Phenol, 2-methoxy- according to NIST library. 337

Figure A.96: Matching MS spectrum of peak number 6 MS in neutral extract GC-MS: A) MS of peak number 6 in neutral extract sample; B) MS of 1,3-Benzenediol, 4-ethyl- according to NIST library..... 337

Figure A.97: Matching MS spectrum of peak number 7 MS in neutral extract GC-MS: A) MS of peak number 7 in neutral extract sample; B) MS of Phenol, 2-methoxy-4-methyl- according to NIST library. 338

Figure A.98: Matching MS spectrum of peak number 10 MS in neutral extract GC-MS: A) MS of peak number 10 in neutral extract sample; B) MS of Phenol, 4-ethyl-2-methoxy- according to NIST library..... 338

Figure A.99: Matching MS spectrum of peak number 12 MS in neutral extract GC-MS: A) MS of peak number 12 in neutral extract sample; B) MS of 2-Methoxy-4-vinylphenol according to NIST library. 339

Figure A.100: Matching MS spectrum of peak number 14 MS in neutral extract GC-MS: A) MS of peak number 14 in neutral extract sample; B) MS of 3-Allyl-6-methoxyphenol according to NIST library. 339

Figure A.101: Matching MS spectrum of peak number 15 MS in neutral extract GC-MS: A) MS of peak number 15 in neutral extract sample; B) MS of Phenol, 2-methoxy-4-propyl- according to NIST library. 340

Figure A.102: Matching MS spectrum of peak number 17 MS in neutral extract GC-MS: A) MS of peak number 17 in neutral extract sample; B) MS of Phenol, 2-methoxy-4-(1-propenyl)- according to NIST library. 340

Figure A.103: Matching MS spectrum of peak number 18 MS in neutral extract GC-MS: A) MS of peak number 18 in neutral extract sample; B) MS of Phenol, 2-methoxy-4-(1-propenyl)-, (Z)- according to NIST library. 341

Figure A.104: Matching MS spectrum of peak number 19 MS in neutral extract GC-MS: A) MS of peak number 19 in neutral extract sample; B) MS of 3,7-Benzofurandiol, 2,3-dihydro-2,2-dimethyl- according to NIST library. 341

Figure A.105: Matching MS spectrum of peak number 24 MS in neutral extract GC-MS: A) MS of peak number 24 in neutral extract sample; B) MS of Benzeneacetic acid, 4-hydroxy-3-methoxy- according to NIST library. 342

Figure A.106: Matching MS spectrum of peak number 31 MS in neutral extract GC-MS: A) MS of peak number 31 in neutral extract sample; B) MS of Podocarpa-8,11,13-triene-7β,13-diol, 14-isopropyl- according to NIST library. 342

Figure A.107: Matching MS spectrum of peak number 1 MS in phenolic extract GC-MS: A) MS of peak number 1 in phenolic extract sample; B) MS of Phenol according to NIST library. 343

Figure A.108: Matching MS spectrum of peak number 2 MS in phenolic extract GC-MS: A) MS of peak number 2 in phenolic extract sample; B) MS of Phenol, 2-methyl- according to NIST library. 343

Figure A.109: Matching MS spectrum of peak number 3 MS in phenolic extract GC-MS: A) MS of peak number 3 in phenolic extract sample; B) MS of Phenol, 4-methyl- according to NIST library. 344

Figure A.110: Matching MS spectrum of peak number 4 MS in phenolic extract GC-MS: A) MS of peak number 4 in phenolic extract sample; B) MS of Phenol, 2-methoxy- according to NIST library. 344

Figure A.111: Matching MS spectrum of peak number 5 MS in phenolic extract GC-MS: A) MS of peak number 5 in phenolic extract sample; B) MS of Phenol, 2,5-dimethyl- according to NIST library. 345

Figure A.112: Matching MS spectrum of peak number 7 MS in phenolic extract GC-MS: A) MS of peak number 7 in phenolic extract sample; B) MS of Phenol, 2-methoxy-4-methyl- according to NIST library. 345

Figure A.113: Matching MS spectrum of peak number 10 MS in phenolic extract GC-MS: A) MS of peak number 10 in phenolic extract sample; B) MS of Phenol, 4-ethyl-2-methoxy- according to NIST library. 346

Figure A.114: Matching MS spectrum of peak number 12 MS in phenolic extract GC-MS: A) MS of peak number 12 in phenolic extract sample; B) MS of 2-Methoxy-4-vinylphenol according to NIST library. 346

Figure A.115: Matching MS spectrum of peak number 13 MS in phenolic extract GC-MS: A) MS of peak number 13 in phenolic extract sample; B) MS of Phenol, 4-(2-propenyl)- according to NIST library. 347

Figure A.116: Matching MS spectrum of peak number 14 MS in phenolic extract GC-MS: A) MS of peak number 14 in phenolic extract sample; B) MS of 3-Allyl-6-methoxyphenol according to NIST library. 347

Figure A.117: Matching MS spectrum of peak number 15 MS in phenolic extract GC-MS: A) MS of peak number 15 in phenolic extract sample; B) MS of Phenol, 2-methoxy-4-propyl- according to NIST library. 348

Figure A.118: Matching MS spectrum of peak number 16 MS in phenolic extract GC-MS: A) MS of peak number 16 in phenolic extract sample; B) MS of Benzaldehyde, 3-hydroxy-4-methoxy- according to NIST library. 348

Figure A.119: Matching MS spectrum of peak number 17 MS in phenolic extract GC-MS: A) MS of peak number 17 in phenolic extract sample; B) MS of Phenol, 2-methoxy-4-(1-propenyl)- according to NIST library. 349

Figure A.120: Matching MS spectrum of peak number 18 MS in phenolic extract GC-MS: A) MS of peak number 18 in phenolic extract sample; B) MS of Phenol, 2-methoxy-4-(1-propenyl)-, (Z)- according to NIST library. 349

Figure A.121: Matching MS spectrum of peak number 20 MS in phenolic extract GC-MS: A) MS of peak number 20 in phenolic extract sample; B) MS of Ethanone, 1-(4-hydroxy-3-methoxyphenyl)- according to NIST library. 350

Figure A.122: Matching MS spectrum of peak number 24 MS in phenolic extract GC-MS: A) MS of peak number 24 in phenolic extract sample; B) MS of Benzeneacetic acid, 4-hydroxy-3-methoxy- according to NIST library. 350

Figure A.123: Matching MS spectrum of peak number 25 MS in phenolic extract GC-MS: A) MS of peak number 25 in phenolic extract sample; B) MS of 4-((1E)-3-Hydroxy-1-propenyl)-2-methoxyphenol according to NIST library. 351

Figure A.124: Matching MS spectrum of peak number 26 MS in phenolic extract GC-MS: A) MS of peak number 26 in phenolic extract sample; B) MS of 4-Hydroxy-2-methoxycinnamaldehyde according to NIST library. 351

Figure A.125: Matching MS spectrum of peak number 4 MS in organic acids extract GC-MS: A) MS of peak number 4 in organic acids extract sample; B) MS of Phenol, 2-methoxy- according to NIST library. 352

Figure A.126: Matching MS spectrum of peak number 8 MS in organic acids extract GC-MS: A) MS of peak number 8 in organic acids extract sample; B) MS of 1,2-Benzenediol according to NIST library. 352

Figure A.127: Matching MS spectrum of peak number 9 MS in organic acids extract GC-MS: A) MS of peak number 9 in organic acids extract sample; B) MS of 1,2-Benzenediol, 3-methyl- according to NIST library..... 353

Figure A.128: Matching MS spectrum of peak number 12 MS in organic acids extract GC-MS: A) MS of peak number 12 in organic acids extract sample; B) MS of 2-Methoxy-4-vinylphenol according to NIST library..... 353

Figure A.129: Matching MS spectrum of peak number 16 MS in organic acids extract GC-MS: A) MS of peak number 16 in organic acids extract sample; B) MS of Benzaldehyde, 3-hydroxy-4-methoxy- according to NIST library. 354

Figure A.130: Matching MS spectrum of peak number 18 MS in organic acids extract GC-MS: A) MS of peak number 18 in organic acids extract sample; B) MS of Phenol, 2-methoxy-4-(1-propenyl)-, (Z)- according to NIST library. 354

Figure A.131: Matching MS spectrum of peak number 23 MS in organic acids extract GC-MS: A) MS of peak number 23 in organic acids extract sample; B) MS of Benzoic acid, 4-hydroxy-3-methoxy- according to NIST library..... 355

Figure A.132: Matching MS spectrum of peak number 24 MS in organic acids extract GC-MS: A) MS of peak number 24 in organic acids extract sample; B) MS of Benzeneacetic acid, 4-hydroxy-3-methoxy- according to NIST library..... 355

Figure A.133: Matching MS spectrum of peak number 27 MS in organic acids extract GC-MS: A) MS of peak number 27 in organic acids extract sample; B) MS of Benzeneacetic acid, 4-hydroxy-3-methoxy-, methyl ester according to NIST library. 356

Figure A.134: Matching MS spectrum of peak number 28 MS in organic acids extract GC-MS: A) MS of peak number 28 in organic acids extract sample; B) MS of Phenylacetylformic acid, 4-hydroxy-3-methoxy- according to NIST library..... 356

Figure A.135: Matching MS spectrum of peak number 29 MS in organic acids extract GC-MS: A) MS of peak number 29 in organic acids extract sample; B) MS of

Naphtho[2,3-c]furan-1,4-dione, 3,3a,9,9a-tetrahydro-6-hydroxy-7-methoxy- according to NIST library. 357

Figure A.136: Matching MS spectrum of peak number 30 MS in organic acids extract GC-MS: A) MS of peak number 30 in organic acids extract sample; B) MS of 2H-1-Benzopyran-7-ol, 3,4-dihydro-3-(4-hydroxy-2-methoxyphenyl)- according to NIST library. 357

Figure A.137: Matching MS spectrum of peak number 32 MS in organic acids extract GC-MS: A) MS of peak number 32 in organic acids extract sample; B) MS of Phenol, 4-[2,3-dihydro-7-methoxy-3-methyl-5-(1-propenyl)-2-benzofuranyl]-2-methoxy- according to NIST library. 358

Figure A.138: Matching MS spectrum of peak number 33 MS in organic acids extract GC-MS: A) MS of peak number 33 in organic acids extract sample; B) MS of 2(3H)-Furanone, dihydro-3,4-bis[(4-hydroxy-3-methoxyphenyl)methyl]-, (3R-trans)- according to NIST library. 358

Figure A.139: Matching MS spectrum of peak number 34 MS in organic acids extract GC-MS: A) MS of peak number 34 in organic acids extract sample; B) MS of Naphtho[2,3-c]furan-1(3H)-one, 3a,4,9,9a-tetrahydro-6-hydroxy-4-(4-hydroxy-3-methoxyphenyl)-7-methoxy-, [3aR-(3aα,4α,9aβ)]- according to NIST library. 359

Figure A.140: Matching MS spectrum of peak number 4 MS in 2nd crude bio-oil extract GC-MS: A) MS of peak number 4 in 2nd crude bio-oil extract sample; B) MS of Phenol, 2-methoxy- according to NIST library. 360

Figure A.141: Matching MS spectrum of peak number 7 MS in 2nd crude bio-oil extract GC-MS: A) MS of peak number 7 in 2nd crude bio-oil extract sample; B) MS of Phenol, 2-methoxy-4-methyl- according to NIST library. 360

Figure A.142: Matching MS spectrum of peak number 8 MS in 2nd crude bio-oil extract GC-MS: A) MS of peak number 8 in 2nd crude bio-oil extract sample; B) MS of 1,2-Benzenediol according to NIST library. 361

Figure A.143: Matching MS spectrum of peak number 10 MS in 2nd crude bio-oil extract GC-MS: A) MS of peak number 10 in 2nd crude bio-oil extract sample; B) MS of Phenol, 4-ethyl-2-methoxy- according to NIST library. 361

Figure A.144: Matching MS spectrum of peak number 12 MS in 2nd crude bio-oil extract GC-MS: A) MS of peak number 12 in 2nd crude bio-oil extract sample; B) MS of 2-Methoxy-4-vinylphenol according to NIST library. 362

Figure A.145: Matching MS spectrum of peak number 14 MS in 2nd crude bio-oil extract GC-MS: A) MS of peak number 14 in 2nd crude bio-oil extract sample; B) MS of 3-Allyl-6-methoxyphenol according to NIST library. 362

Figure A.146: Matching MS spectrum of peak number 15 MS in 2nd crude bio-oil extract GC-MS: A) MS of peak number 15 in 2nd crude bio-oil extract sample; B) MS of Phenol, 2-methoxy-4-propyl- according to NIST library. 363

Figure A.147: Matching MS spectrum of peak number 16 MS in 2nd crude bio-oil extract GC-MS: A) MS of peak number 16 in 2nd crude bio-oil extract sample; B) MS of Benzaldehyde, 3-hydroxy-4-methoxy- according to NIST library. 363

Figure A.148: Matching MS spectrum of peak number 17 MS in 2nd crude bio-oil extract GC-MS: A) MS of peak number 17 in 2nd crude bio-oil extract sample; B) MS of Phenol, 2-methoxy-4-(1-propenyl)- according to NIST library 364

Figure A.149: Matching MS spectrum of peak number 18 MS in 2nd crude bio-oil extract GC-MS: A) MS of peak number 18 in 2nd crude bio-oil extract sample; B) MS of Phenol, 2-methoxy-4-(1-propenyl)-, (Z)- according to NIST library. 364

Figure A.150: Matching MS spectrum of peak number 20 MS in 2nd crude bio-oil extract GC-MS: A) MS of peak number 20 in 2nd crude bio-oil extract sample; B) MS of Ethanone, 1-(4-hydroxy-3-methoxyphenyl)- according to NIST library..... 365

Figure A.151: Matching MS spectrum of peak number 21 MS in 2nd crude bio-oil extract GC-MS: A) MS of peak number 21 in 2nd crude bio-oil extract sample; B) MS of 2-Propanone, 1-(4-hydroxy-3-methoxyphenyl)- according to NIST library. 365

Figure A.152: Matching MS spectrum of peak number 24 MS in 2nd crude bio-oil extract GC-MS: A) MS of peak number 24 in 2nd crude bio-oil extract sample; B) MS of Benzeneacetic acid, 4-hydroxy-3-methoxy- according to NIST library. 366

Figure A.153: Matching MS spectrum of peak number 28 MS in 2nd crude bio-oil extract GC-MS: A) MS of peak number 28 in 2nd crude bio-oil extract sample; B) MS of Phenylacetylformic acid, 4-hydroxy-3-methoxy- according to NIST library. 366

Figure A.154: Matching MS spectrum of peak number 26 MS in 2nd crude bio-oil extract GC-MS: A) MS of peak number 26 in 2nd crude bio-oil extract sample; B) MS of 4-Hydroxy-2-methoxycinnamaldehyde according to NIST library. 367

Figure A.155: Matching MS spectrum of peak number 7 MS in water-soluble extract GC-MS: A) MS of peak number 7 in water-soluble extract sample; B) MS of Phenol, 2-methoxy-4-methyl- according to NIST library. 368

Figure A.156: Matching MS spectrum of peak number 8 MS in water-soluble extract GC-MS: A) MS of peak number 8 in water-soluble extract sample; B) MS of 1,2-Benzenediol according to NIST library. 368

Figure A.157: Matching MS spectrum of peak number 10 MS in water-soluble extract GC-MS: A) MS of peak number 10 in water-soluble extract sample; B) MS of Phenol, 4-ethyl-2-methoxy- according to NIST library. 369

Figure A.158: Matching MS spectrum of peak number 14 MS in water-soluble extract GC-MS: A) MS of peak number 14 in water-soluble extract sample; B) MS of 3-Allyl-6-methoxyphenol according to NIST library. 369

Figure A.159: Matching MS spectrum of peak number 16 MS in water-soluble extract GC-MS: A) MS of peak number 16 in water-soluble extract sample; B) MS of Benzaldehyde, 3-hydroxy-4-methoxy- according to NIST library. 370

Figure A.160: Matching MS spectrum of peak number 18 MS in water-soluble extract GC-MS: A) MS of peak number 18 in water-soluble extract sample; B) MS of Phenol, 2-methoxy-4-(1-propenyl)-, (Z)- according to NIST library. 370

Figure A.161: Matching MS spectrum of peak number 20 MS in water-soluble extract GC-MS: A) MS of peak number 20 in water-soluble extract sample; B) MS of Ethanone, 1-(4-hydroxy-3-methoxyphenyl)- according to NIST library. 371

Figure A.162: Matching MS spectrum of peak number 21 MS in water-soluble extract GC-MS: A) MS of peak number 21 in water-soluble extract sample; B) MS of 2-Propanone, 1-(4-hydroxy-3-methoxyphenyl)- according to NIST library. 371

Figure A.163: Matching MS spectrum of peak number 24 MS in water-soluble extract GC-MS: A) MS of peak number 24 in water-soluble extract sample; B) MS of Benzeneacetic acid, 4-hydroxy-3-methoxy- according to NIST library..... 372

Figure A.164: Matching MS spectrum of peak number 4 MS in diethyl ether extract GC-MS: A) MS of peak number 4 in diethyl ether extract sample; B) MS of Phenol, 2-methoxy- according to NIST library..... 372

Figure A.165: Matching MS spectrum of peak number 7 MS in diethyl ether extract GC-MS: A) MS of peak number 7 in diethyl ether extract sample; B) MS of Phenol, 2-methoxy-4-methyl- according to NIST library. 373

Figure A.166: Matching MS spectrum of peak number 8 MS in diethyl ether extract GC-MS: A) MS of peak number 8 in diethyl ether extract sample; B) MS of 1,2-Benzenediol according to NIST library. 373

Figure A.167: Matching MS spectrum of peak number 10 MS in diethyl ether extract GC-MS: A) MS of peak number 10 in diethyl ether extract sample; B) MS of Phenol, 4-ethyl-2-methoxy- according to NIST library. 374

Figure A.168: Matching MS spectrum of peak number 9 MS in diethyl ether extract GC-MS: A) MS of peak number 9 in diethyl ether extract sample; B) MS of 1,2-Benzenediol, 3-methyl- according to NIST library..... 374

Figure A.169: Matching MS spectrum of peak number 11 MS in diethyl ether extract GC-MS: A) MS of peak number 11 in diethyl ether extract sample; B) MS of 1,2-Benzenediol, 4-methyl- according to NIST library. 375

Figure A.170: Matching MS spectrum of peak number 14 MS in diethyl ether extract GC-MS: A) MS of peak number 14 in diethyl ether extract sample; B) MS of 3-Allyl-6-methoxyphenol according to NIST library. 375

Figure A.171: Matching MS spectrum of peak number 16 MS in diethyl ether extract GC-MS: A) MS of peak number 16 in diethyl ether extract sample; B) MS of Benzaldehyde, 3-hydroxy-4-methoxy- according to NIST library. 376

Figure A.172: Matching MS spectrum of peak number 18 MS in diethyl ether extract GC-MS: A) MS of peak number 18 in diethyl ether extract sample; B) MS of Phenol, 2-methoxy-4-(1-propenyl)-, (Z)- according to NIST library. 376

Figure A.173: Matching MS spectrum of peak number 20 MS in diethyl ether extract GC-MS: A) MS of peak number 20 in diethyl ether extract sample; B) MS of Ethanone, 1-(4-hydroxy-3-methoxyphenyl)- according to NIST library. 377

Figure A.174: Matching MS spectrum of peak number 35 MS in diethyl ether extract GC-MS: A) MS of peak number 35 in diethyl ether extract sample; B) MS of Benzoic acid, 4-hydroxy-3-methoxy-, methyl ester according to NIST library. 377

Figure A.175: Matching MS spectrum of peak number 21 MS in diethyl ether extract GC-MS: A) MS of peak number 21 in diethyl ether extract sample; B) MS of 2-Propanone, 1-(4-hydroxy-3-methoxyphenyl)- according to NIST library. 378

Figure A.176: Matching MS spectrum of peak number 24 MS in diethyl ether extract GC-MS: A) MS of peak number 24 in diethyl ether extract sample; B) MS of Benzeneacetic acid, 4-hydroxy-3-methoxy- according to NIST library. 378

Figure A.177: Matching MS spectrum of peak number 26 MS in diethyl ether extract GC-MS: A) MS of peak number 26 in diethyl ether extract sample; B) MS of 4-Hydroxy-2-methoxycinnamaldehyde according to NIST library. 379

Figure A.178: Matching MS spectrum of peak number 36 MS in diethyl ether extract GC-MS: A) MS of peak number 36 in diethyl ether extract sample; B) MS of β-(4-Hydroxy-3-methoxyphenyl)propionic acid according to NIST library. 379

Figure A.179: Matching MS spectrum of peak number 4 MS in CO_2-1 extract GC-MS: A) MS of peak number 4 in CO_2-1 extract sample; B) MS of Phenol, 2-methoxy- according to NIST library. 380

Figure A.180: Matching MS spectrum of peak number 7 MS in CO_2-1 extract GC-MS: A) MS of peak number 7 in CO_2-1 extract sample; B) MS of Phenol, 2-methoxy-4-methyl- according to NIST library. 381

Figure A.181: Matching MS spectrum of peak number 10 MS in CO_2-1 extract GC-MS: A) MS of peak number 10 in CO_2-1 extract sample; B) MS of Phenol, 4-ethyl-2-methoxy- according to NIST library. 381

Figure A.182: Matching MS spectrum of peak number 12 MS in CO_2-1 extract GC-MS: A) MS of peak number 12 in CO_2-1 extract sample; B) MS of 2-Methoxy-4-vinylphenol according to NIST library. 382

Figure A.183: Matching MS spectrum of peak number 14 MS in CO_2-1 extract GC-MS: A) MS of peak number 14 in CO_2-1 extract sample; B) MS of 3-Allyl-6-methoxyphenol according to NIST library. 382

Figure A.184: Matching MS spectrum of peak number 16 MS in CO_2-1 extract GC-MS: A) MS of peak number 16 in CO_2-1 extract sample; B) MS of Benzaldehyde, 3-hydroxy-4-methoxy- according to NIST library. 383

Figure A.185: Matching MS spectrum of peak number 17 MS in CO_2-1 extract GC-MS: A) MS of peak number 17 in CO_2-1 extract sample; B) MS of Phenol, 2-methoxy-4-(1-propenyl)- according to NIST library. 383

Figure A.186: Matching MS spectrum of peak number 18 MS in CO_2-1 extract GC-MS: A) MS of peak number 18 in CO_2-1 extract sample; B) MS of Phenol, 2-methoxy-4-(1-propenyl)-, (Z)- according to NIST library. 384

Figure A.187: Matching MS spectrum of peak number 20 MS in CO_2-1 extract GC-MS: A) MS of peak number 20 in CO_2-1 extract sample; B) MS of Ethanone, 1-(4-hydroxy-3-methoxyphenyl)- according to NIST library. 384

Figure A.188: Matching MS spectrum of peak number 21 MS in CO_2-1 extract GC-MS: A) MS of peak number 21 in CO_2-1 extract sample; B) MS of 2-Propanone, 1-(4-hydroxy-3-methoxyphenyl)- according to NIST library. 385

Figure A.189: Matching MS spectrum of peak number 24 MS in CO_2-1 extract GC-MS: A) MS of peak number 24 in CO_2-1 extract sample; B) MS of Benzeneacetic acid, 4-hydroxy-3-methoxy- according to NIST library. 385

Figure A.190: Matching MS spectrum of peak number 26 MS in CO_2-1 extract GC-MS: A) MS of peak number 26 in CO_2-1 extract sample; B) MS of 4-Hydroxy-2-methoxycinnamaldehyde according to NIST library. 386

Figure A.191: Matching MS spectrum of peak number 4 MS in CO_2-2 extract GC-MS: A) MS of peak number 4 in CO_2-2 extract sample; B) MS of Phenol, 2-methoxy- according to NIST library. 386

Figure A.192: Matching MS spectrum of peak number 7 MS in CO_2-2 extract GC-MS: A) MS of peak number 7 in CO_2-2 extract sample; B) MS of Phenol, 2-methoxy-4-methyl- according to NIST library. 387

Figure A.193: Matching MS spectrum of peak number 8 MS in CO_2-2 extract GC-MS: A) MS of peak number 8 in CO_2-2 extract sample; B) MS of 1,2-Benzenediol according to NIST library. 387

Figure A.194: Matching MS spectrum of peak number 10 MS in CO_2-2 extract GC-MS: A) MS of peak number 10 in CO_2-2 extract sample; B) MS of Phenol, 4-ethyl-2-methoxy- according to NIST library. 388

Figure A.195: Matching MS spectrum of peak number 12 MS in CO_2-2 extract GC-MS: A) MS of peak number 12 in CO_2-2 extract sample; B) MS of 2-Methoxy-4-vinylphenol according to NIST library. 388

Figure A.196: Matching MS spectrum of peak number 14 MS in CO_2-2 extract GC-MS: A) MS of peak number 14 in CO_2-2 extract sample; B) MS of 3-Allyl-6-methoxyphenol according to NIST library. 389

Figure A.197: Matching MS spectrum of peak number 16 MS in CO_2-2 extract GC-MS: A) MS of peak number 16 in CO_2-2 extract sample; B) MS of Benzaldehyde, 3-hydroxy-4-methoxy- according to NIST library. 389

Figure A.198: Matching MS spectrum of peak number 17 MS in CO_2-2 extract GC-MS: A) MS of peak number 17 in CO_2-2 extract sample; B) MS of Phenol, 2-methoxy-4-(1-propenyl)- according to NIST library. 390

Figure A.199: Matching MS spectrum of peak number 18 MS in CO_2-2 extract GC-MS: A) MS of peak number 18 in CO_2-2 extract sample; B) MS of Phenol, 2-methoxy-4-(1-propenyl)-, (Z)- according to NIST library. 390

Figure A.200: Matching MS spectrum of peak number 20 MS in CO_2-2 extract GC-MS: A) MS of peak number 20 in CO_2-2 extract sample; B) MS of Ethanone, 1-(4-hydroxy-3-methoxyphenyl)- according to NIST library. 391

Figure A.201: Matching MS spectrum of peak number 21 MS in CO_2-2 extract GC-MS: A) MS of peak number 21 in CO_2-2 extract sample; B) MS of 2-Propanone, 1-(4-hydroxy-3-methoxyphenyl)- according to NIST library. 391

Figure A.202: Matching MS spectrum of peak number 24 MS in CO_2-2 extract GC-MS: A) MS of peak number 24 in CO_2-2 extract sample; B) MS of Benzeneacetic acid, 4-hydroxy-3-methoxy- according to NIST library. 392

Figure A.203: Matching MS spectrum of peak number 26 MS in CO_2-2 extract GC-MS: A) MS of peak number 26 in CO_2-2 extract sample; B) MS of 4-Hydroxy-2-methoxycinnamaldehyde according to NIST library. 392

Figure A.204: Matching MS spectrum of peak number 4 MS in CO_2-3 extract GC-MS: A) MS of peak number 4 in CO_2-3 extract sample; B) MS of Phenol, 2-methoxy- according to NIST library. 393

Figure A.205: Matching MS spectrum of peak number 7 MS in CO_2-3 extract GC-MS: A) MS of peak number 7 in CO_2-3 extract sample; B) MS of Phenol, 2-methoxy-4-methyl- according to NIST library. 393

Figure A.206: Matching MS spectrum of peak number 8 MS in CO_2-3 extract GC-MS: A) MS of peak number 8 in CO_2-3 extract sample; B) MS of 1,2-Benzenediol according to NIST library. 394

Figure A.207: Matching MS spectrum of peak number 10 MS in CO_2-3 extract GC-MS: A) MS of peak number 10 in CO_2-3 extract sample; B) MS of Phenol, 4-ethyl-2-methoxy- according to NIST library. 394

Figure A.208: Matching MS spectrum of peak number 12 MS in CO_2-3 extract GC-MS: A) MS of peak number 12 in CO_2-3 extract sample; B) MS of 2-Methoxy-4-vinylphenol according to NIST library. 395

Figure A.209: Matching MS spectrum of peak number 14 MS in CO_2-3 extract GC-MS: A) MS of peak number 14 in CO_2-3 extract sample; B) MS of 3-Allyl-6-methoxyphenol according to NIST library..... 395

Figure A.210: Matching MS spectrum of peak number 16 MS in CO_2-3 extract GC-MS: A) MS of peak number 16 in CO_2-3 extract sample; B) MS of Benzaldehyde, 3-hydroxy-4-methoxy- according to NIST library. 396

Figure A.211: Matching MS spectrum of peak number 17 MS in CO_2-3 extract GC-MS: A) MS of peak number 17 in CO_2-3 extract sample; B) MS of Phenol, 2-methoxy-4-(1-propenyl)- according to NIST library. 396

Figure A.212: Matching MS spectrum of peak number 18 MS in CO_2-3 extract GC-MS: A) MS of peak number 18 in CO_2-3 extract sample; B) MS of Phenol, 2-methoxy-4-(1-propenyl)-, (Z)- according to NIST library..... 397

Figure A.213: Matching MS spectrum of peak number 20 MS in CO_2-3 extract GC-MS: A) MS of peak number 20 in CO_2-3 extract sample; B) MS of Ethanone, 1-(4-hydroxy-3-methoxyphenyl)- according to NIST library. 397

Figure A.214: Matching MS spectrum of peak number 21 MS in CO_2-3 extract GC-MS: A) MS of peak number 21 in CO_2-3 extract sample; B) MS of 2-Propanone, 1-(4-hydroxy-3-methoxyphenyl)- according to NIST library. 398

Figure A.215: Matching MS spectrum of peak number 24 MS in CO_2-3 extract GC-MS: A) MS of peak number 24 in CO_2-3 extract sample; B) MS of Benzeneacetic acid, 4-hydroxy-3-methoxy- according to NIST library. 398

Figure A.216: Matching MS spectrum of peak number 26 MS in CO_2-3 extract GC-MS: A) MS of peak number 26 in CO_2-3 extract sample; B) MS of 4-Hydroxy-2-methoxycinnamaldehyde according to NIST library. 399

Figure A.217: Matching MS spectrum of peak number 4 MS in CO_2-4 extract GC-MS: A) MS of peak number 4 in CO_2-4 extract sample; B) MS of Phenol, 2-methoxy- according to NIST library. 399

Figure A.218: Matching MS spectrum of peak number 7 MS in CO_2-4 extract GC-MS: A) MS of peak number 7 in CO_2-4 extract sample; B) MS of Phenol, 2-methoxy-4-methyl- according to NIST library. 400

Figure A.219: Matching MS spectrum of peak number 8 MS in CO_2-4 extract GC-MS: A) MS of peak number 8 in CO_2-4 extract sample; B) MS of 1,2-Benzenediol according to NIST library. 400

Figure A.220: Matching MS spectrum of peak number 10 MS in CO_2-4 extract GC-MS: A) MS of peak number 10 in CO_2-4 extract sample; B) MS of Phenol, 4-ethyl-2-methoxy- according to NIST library. 401

Figure A.221: Matching MS spectrum of peak number 12 MS in CO_2-4 extract GC-MS: A) MS of peak number 12 in CO_2-4 extract sample; B) MS of 2-Methoxy-4-vinylphenol according to NIST library. 401

Figure A.222: Matching MS spectrum of peak number 14 MS in CO_2-4 extract GC-MS: A) MS of peak number 14 in CO_2-4 extract sample; B) MS of 3-Allyl-6-methoxyphenol according to NIST library. 402

Figure A.223: Matching MS spectrum of peak number 16 MS in CO_2-4 extract GC-MS: A) MS of peak number 16 in CO_2-4 extract sample; B) MS of Benzaldehyde, 3-hydroxy-4-methoxy- according to NIST library. 402

Figure A.224: Matching MS spectrum of peak number 17 MS in CO_2-4 extract GC-MS: A) MS of peak number 17 in CO_2-4 extract sample; B) MS of Phenol, 2-methoxy-4-(1-propenyl)- according to NIST library. 403

Figure A.225: Matching MS spectrum of peak number 18 MS in CO_2-4 extract GC-MS: A) MS of peak number 18 in CO_2-4 extract sample; B) MS of Phenol, 2-methoxy-4-(1-propenyl)-, (Z)- according to NIST library. 403

Figure A.226: Matching MS spectrum of peak number 20 MS in CO_2-4 extract GC-MS: A) MS of peak number 20 in CO_2-4 extract sample; B) MS of Ethanone, 1-(4-hydroxy-3-methoxyphenyl)- according to NIST library. 404

Figure A.227: Matching MS spectrum of peak number 21 MS in CO_2-4 extract GC-MS: A) MS of peak number 21 in CO_2-4 extract sample; B) MS of 2-Propanone, 1-(4-hydroxy-3-methoxyphenyl)- according to NIST library. 404

Figure A.228: Matching MS spectrum of peak number 24 MS in CO_2-4 extract GC-MS: A) MS of peak number 24 in CO_2-4 extract sample; B) MS of Benzeneacetic acid, 4-hydroxy-3-methoxy- according to NIST library. 405

Figure A.229: Matching MS spectrum of peak number 26 MS in CO_2-4 extract GC-MS: A) MS of peak number 26 in CO_2-4 extract sample; B) MS of 4-Hydroxy-2-methoxycinnamaldehyde according to NIST library. 405

List of Tables

Table 1.1: The twelve principles of green chemistry.[7] 60

Table 1.2: The twelve principles of green engineering.[8] 61

Table 1.3: The classification of biomass resources.[13] 63

Table 1.4: Typical cellulose, hemicellulose and lignin content of selected biomass species.[19] 64

Table 1.5: Ranges of pyrolysis operating parameters for the three main pyrolysis processes.[55, 63] 70

Table 1.6: Boiling point (°C), dielectric constant (ε′), dielectric loss (ε″), and loss tangent (tanδ) of 30 common organic solvents.[108] 78

Table 1.7: Typical properties of crude bio-oil derived from conventional fast pyrolysis of wood.[124] 83

Table 1.8: Selected fuel properties of petroleum-derived diesel and biodiesel.[133, 136] 86

Table 1.9: Major feedstocks used for biodiesel production in different countries.[135, 150] 89

Table 1.10: Biodiesel average productions and consumptions from 2012 to 2014, and there 2024 projections in the world's top biodiesel producing countries.[151] 90

Table 1.11: Chemical composition of biodiesel FAME produced from various feedstocks.[170] 92

Table 1.12: Measured stoichiometric inhibition coefficient (f) per one molecule of some key phenolic antioxidants. 99

Table 1.13: Some common synthetic phenolic antioxidants previously investigated for improving the oxidation stability of biodiesel. 108

Table 1.14: Some synthetic aminic antioxidants previously investigated for use in biodiesel. 111

Table 1.15: Some previous investigations on renewable antioxidants from biomass for use in fuels or lubricants. 113

Table 2.1: General parameters applied for the UV-Vis spectrophotometry..... 131

Table 2.2: Reaction specification for all oxidation experiments carried out in sealed mode. 134

Table 2.3: General parameters associated with Rancimat test. 136

Table 2.4: Description of biomass, chemical materials and reagents. 137

Table 3.1: The microwave enhanced pyrolysis fraction yields distribution per run (150 g) and the average yields distribution per 6 runs (900 g) of spruce woodchips. 142

Table 3.2: Proximate and ultimate analysis data of spruce woodchips and its microwave enhanced pyrolysis products. 143

Table 3.3: Mineral contents of spruce woodchips and its microwave enhanced pyrolysis products. 147

Table 3.4: ATR-IR data of functional groups and compound classes for crude bio-oil and aqueous fraction.[250, 269-271] 149

Table 3.5: Carbon assignments based on ^{13}C NMR analysis of bio-oil and aqueous fraction produced from the microwave enhanced pyrolysis of spruce woodchips, and the assignments arranged according to chemical shift range. (reproduced from[286]) 155

Table 3.6: Major identified compounds in crude bio-oil derived from the microwave enhanced pyrolysis of spruce woodchips. 160

Table 3.7: Major identified compounds in aqueous fraction obtained from the microwave enhanced pyrolysis of spruce woodchips. 164

Table 4.1: The quantification and identification of GC detectable phenolic compounds in 1st and 2nd extracts of crude bio-oil. 176

Table 4.2: Fractional weight distribution recovered from crude bio-oil *via* the water-insoluble phase fractionation experiment and its equivalent recovery percentage from the original woodchips. 181

Table 4.3: Identification and quantification of phenolic compounds in 2nd extract of crude bio-oil and in its extracted fractions. 183

Table 4.4: Summary of the phenols content estimated by GC-FID and by Folin-Ciocalteu (FC) assay, and the ratio of these. 190

Table 4.5: ATR-IR data of functional groups and compound class.[250] 192

Table 4.6: Peak assignments for ^{13}C NMR spectra.[286] 194

Table 4.7: Fractional weight distribution recovered from crude bio-oil *via* the water-soluble phase fractionation experiment and its equivalent recovery percentage from the original woodchips. 196

Table 4.8: Identification and quantification of phenolic compounds in 2nd crude bio-oil extract and in its water-soluble phase extracted fractions. 199

Table 4.9: Summary of the phenolic content estimated by GC-FID and by Folin-Ciocalteu (FC) assay, and the ratio of these. 204

Table 4.10: The weight average molecular weight (Mw) of water-soluble extract and its fractions estimated by GPC-ELSD. 210

Table 4.11: Range values of some physicochemical properties of gases, liquids and supercritical fluids.[299] 211

Table 4.12: Critical properties of some selected solvents used in supercritical fluid extraction.[303] 212

Table 4.13: Fractions weight distribution recovered from crude bio-oil *via* supercritical CO_2 fractionation experiment at 350 bar and 50 $^{\circ}C$. 215

Table 4.14: The identification and quantification of GC detectable phenolic compounds in crude bio-oil and in the CO_2 isolated fractions. 217

Table 4.15: Summary of the phenolic content estimated by GC-FID for 1st crude bio-oil extract and its supercritical CO_2 extracts. 220

Table 4.16: Summary of some previous work on phenolic separation from bio-oil by liquid-liquid extraction. 223

Table 5.1: The BDEs of major types of C-H bonds in biodiesel FAME chains and their rate constants (*k*) at 30 °C for hydrogen-atom abstraction. 233

Table 5.2: Major FAMEs in biodiesel and their typical concentrations in soybean and rapeseed derived biodiesel.[335] 233

Table 5.3: The phenolic composition of mixed phenolic standard and their molar concentrations in methyl linoleate samples before oxidation. 250

Table 5.4: Bond dissociation energies (BDE) of some selected phenols O-H bond (kJ mol^{-1}) and their rate constant (M^{-1} s^{-1}) at 30 °C for H abstraction by peroxy radicals ($ROO^{\bullet}$). 256

Table B.1: ECN reduction values by functional group used for analysis of phenols in all GC-FID experiments. 408

Table B.2: ECN reduction by functional group for each identified phenolic compound including the standard compound. 409

Table C.1: The exact amounts of phenolic standard antioxidants blended with 2 ml methyl linoleate and their measured induction times at 120 °C and 1 bar of oxygen. 414

Table C.2: The exact amounts of crude extracts blended with 2 ml methyl linoleate and their measured induction times at 120 °C and 1 bar of oxygen 415

Table C.3: The equivalent molar concentrations of each detected phenolic compound *via* GC-FID when blending 100 mg of crude bio-oil or its water-insoluble extracts with 2 ml methyl linoleate. [a] 417

Table C.4: The equivalent molar concentrations of each detected phenolic compound *via* GC-FID when blending 100 mg of crude bio-oil or its water-soluble extracts with 2 ml methyl linoleate. [a] 421

Table D.1: Recorded observations during the 1st microwave pyrolysis experiment. 424

Table D.2: Recorded observations during the 2nd microwave pyrolysis experiment. 424

Acknowledgments

In the Name of Allah, the Most Gracious, the Most Merciful. All praise and thanks to Allah for the strengths and His blessing in completing this thesis.

My sincere appreciation must go to my supervisors Dr. Moray Stark and Dr. Duncan Macquarrie for giving me the opportunity to carry out my PhD at the University of York. With enthusiasm and patience, they have continuously guided, motivated and supported me during my study. Without them, I doubt this thesis will ever have got to this final stage! Thanks also to Dr. Andrew Hunt for being my IPM and giving much needed feedback throughout the TAP meetings.

For financial support, I would like to acknowledge the Ministry of Education of the Kingdom of Saudi Arabia for the PhD scholarship. I also appreciate the Saudi Arabian Cultural Bureau in London for their administration and legal support during my PhD scholarship in the UK.

I would like to thank all the current and previous members of the Green Chemistry Center of Excellence for all their help and friendship. Special thanks to Dr. Vitaly Budarin for advice and assistance with microwave pyrolysis. Similarly, thanks to Dr. Thomas Dugmore for discussion on the Folin-Ciocalteu assay. Big thanks must go to Paul Elliott and Charlotte Brannigan for their assistance with lab equipment. Likewise thanks must go to Dr. Mark Gronnow and Dr. Raymond Sloan for their assistance with equipment at the Biorenewables Development Centre (BDC).

Warm thanks must go to Rachel Crooks, Alice Duckett, Sharon Stewart and Lauren Hunt in the Graduate Office of the Department of Chemistry for their kindness and continuous support during my study.

In particular and most sincerely, I would like to pay my warmest tribute to my beloved wife for her dedication, patience, understanding, and lots more. With her support, she made my life much pleasant even at the hardest times.

Last and definitely by no means least, the greatest gratitude goes to my lovely parents and the rest of my family for all their endless support over the years.

Author's Declaration

Some of the results presented herein were obtained by, or in collaboration with other co-workers. They are all fully acknowledged in the list below along with their corresponding institution.

Piece of work	Collaborator	Institution
Elemental (CHN) analysis	Dr. Graeme McAllister	Department of Chemistry service, University of York
ICP-MS analysis	Dr. Helen Parker, Andrea García	Green Chemistry Centre of Excellence, University of York
GPC analysis	Dr. Raymond Sloan, Yuan Yuan	Biorenewables Development Centre (BDC) & Green Chemistry Centre of Excellence, University of York
HPLC analysis	Dr. Raymond Sloan, Tianzong Li	Biorenewables Development Centre (BDC) & Green Chemistry Centre of Excellence, University of York
Rancimat test (EN 14112)	Dr. Raymond Sloan	Biorenewables Development Centre (BDC), University of York
Microwave pyrolysis	Dr. Vitaly Budarin	Green Chemistry Centre of Excellence, University of York
Supercritical CO_2 extraction	Dr. Andrew Hunt	Green Chemistry Centre of Excellence, University of York

The other results presented within this thesis are the work of the author and some parts of work described in this thesis have been previously presented in a publication:

- A. S. Alwehaibi, D. J. Macquarrie and M. S. Stark, *Green Chemistry*, 2016, **18**, 2762-2774.

Abdulrahman S. Alwehaibi

December 2016

Chapter 1: Introduction

1.1 Thesis Aims

Crude bio-oil, which is generally produced by the pyrolysis of lignocellulosic materials, is a complex mixture that consists of several hundred individual components including aldehydes, ketones, furans, alcohols, organic acids, sugars, phenols, oligomeric lignin, and oligomeric carbohydrates.[1, 2] Therefore, crude bio-oils have a great potential to be used as a source for many high-value chemicals. The phenols, in particular, have been of growing interest due to their potential antioxidant nature that can be further exploited for a wide range of useful applications. An example of such applications is to use them as antioxidants in biofuels, particularly in biodiesel.

Biodiesel is a renewable automotive fuel, and is currently considered as a promising alternative to petroleum diesel. However, using pure biodiesel directly into diesel engines is not viable due to some problems associated with its physical and chemical properties. A significant downside of pure biodiesel is its poor oxidation stability, which can be significantly improved by adding antioxidants.[3, 4] Generally, most current antioxidants used in the biodiesel industry are synthetic antioxidants derived from petroleum, such as butylated hydroxytoluene (BHT).[5, 6] The fact that these antioxidants are non-renewable, as well the instability of petroleum prices, prompted the investigation reported in this thesis into alternative sources of antioxidants that are renewable and can easily be extracted from low-cost resources, specifically examining the antioxidancy of crude bio-oil and its extracts.

In order to have a better understanding of the nature and antioxidancy of phenolic species in crude bio-oils, the work described in this thesis aimed to:

a) Extract crude bio-oil from a woody biomass (spruce woodchips) using a novel green technology: microwave-enhanced pyrolysis, with characterization of components.
b) Identify and quantify phenolic compounds in the crude bio-oil using multiple analytical techniques: GC-FID, GC-MS, ATR-FTIR, ^{13}C NMR, and Folin-Ciocalteu (FC) assay.

c) Experimentally investigate the antioxidant power of the crude bio-oil in a chemical model of biodiesel: methyl linoleate.
d) An initial investigation to identify which phenolic components of the bio-oil may be the cause of the antioxidancy.

1.2 The Twelve Principles of Green Chemistry & Green Engineering

In earlier decades, the traditional role of synthetic chemists within the world of chemistry would be viewed as to synthesize new chemicals in the laboratory, and later design large-scale processes for their manufacture, with any environmental impact not being a pre-eminent concern.[7] It could be argued by synthetic chemists that most problems with new chemicals, such as the waste stream, were only identified at the end of the process whereas their job are centered around the fact that they just get involved with the beginning of the process, which revolves around researching the ways to make these new chemicals.[7] However, the public holds synthetic chemists responsible for the toxicity of those chemicals and for the chemical waste generated by the chemical industry.[7] Synthetic chemists should be however considering these problems as well during their research, as their views can have a strong positive impact on avoiding a great deal of the 'end of the pipe' problems.[7]

In the past, synthetic chemists designed synthetic pathways to make target molecules in the maximum yield for the cheapest cost.[7] However, at present, the costs of producing new chemicals must include not only the costs for raw materials and equipment, but also the entire cost of regulatory compliance, for instance, the cost of waste disposal, liability costs, and treatment costs, as well as plant modifications for end-of-pipe treatment.[7] The consideration of these extra costs has pushed the whole cost of many syntheses to an excessive levels.[7] Therefore, the precise calculation of the full cost is very important to provide new standards for the economics of manufacturing new chemicals.[7]

All previous indirect costs can be minimized by chemists who have the ability to reduce these costs significantly by redesigning chemicals and their processes.[7] Chemists have the knowledge to decide whether hazardous materials will be used,

will have to be handled by workers, or their waste or by-products will need special disposal.[7] All of these decisions are inherent in the concept of 'Green Chemistry'. The aim of green chemistry is to eliminate or reduce the use or the production of toxic feedstocks, solvents, by-products, and all other related products.[7] A synthetic chemist who applies the concept of green chemistry in a synthetic process is likely to generate a more cost-effective product where all direct and indirect costs are considered.[7]

Green chemistry can be defined as "the utilization of a set of principles that reduces or eliminates the use or generation of hazardous substances in the design, manufacture and application of chemical products".[7] The set of principles associated with this definition were expanded into 12 principles listed in Table 1.1.

Table 1.1: The twelve principles of green chemistry.[7]

1.	It is better to prevent waste than to treat or clean up waste after it is formed.
2.	Synthetic methods should be designed to maximize the incorporation of all materials used in the process into the final product.
3.	Wherever practicable, synthetic methodologies should be designed to use and generate substances that possess little or no toxicity to human health and the environment.
4.	Chemical products should be designed to preserve efficacy of function while reducing toxicity.
5.	The use of auxiliary substances (*e.g.* solvents, separation agents, etc.) should be made unnecessary wherever possible and, innocuous when used.
6.	Energy requirements should be recognized for their environmental and economic impacts and should be minimized. Synthetic methods should be conducted at ambient temperature and pressure.
7.	A raw material of feedstock should be renewable rather than depleting wherever technically and economically practicable.
8.	Unnecessary derivatization (blocking group, protection /deprotection, temporary modification of physical/chemical processes) should be avoided whenever possible.
9.	Catalytic reagents (as selective as possible) are superior to stoichiometric reagents.
10.	Chemical products should be designed so that at the end of their function they do not persist in the environment and break down into innocuous degradation products.
11.	Analytical methodologies need to be further developed to allow for real-time, in-process monitoring and control prior to the formation of hazardous substances.
12.	Substances and the form of a substance used in a chemical process should be chosen so as to minimize the potential for chemical accidents, including releases, explosions, and fires.

Green chemistry principles are guides towards sustainability, and when they are applied successfully, they would reduce the negative human impacts on the planet. These principles encourage specific novel goals to be accomplished, for instance minimizing waste, reducing dependency on fossil fuels, and more importantly avoiding the generation of substances that could be harmful to humans and the environment. However, these novel goals can only be effective when they are turned into reality. New methodologies have to be developed in order to achieve these green novel goals through disciplines, industries, and sectors.

In order to achieve sustainability in the engineering sector through science and technology, Anastas and Zimmerman[8] have introduced the 12 Principles of Green Engineering, see Table 1.2.

Table 1.2: The twelve principles of green engineering.[8]

1. Designers need to strive to ensure that all material and energy inputs and outputs are as inherently nonhazardous as possible.
2. It is better to prevent waste than to treat or clean up waste after it is formed.
3. Separation and purification operations should be designed to minimize energy consumption and materials use.
4. Products, processes, and systems should be designed to maximize mass, energy, space, and time efficiency.
5. Products, processes, and systems should be "output pulled" rather than "input pushed" through the use of energy and materials.
6. Embedded entropy and complexity must be viewed as an investment when making design choices on recycle, reuse, or beneficial disposition.
7. Targeted durability, not immortality, should be a design goal.
8. Design for unnecessary capacity or capability (*e.g.*, "one size fits all") solutions should be considered a design flaw.
9. Material diversity in multicomponent products should be minimized to promote disassembly and value retention.
10. Design of products, processes, and systems must include integration and interconnectivity with available energy and materials flows.
11. Products, processes, and systems should be designed for performance in a commercial "afterlife".
12. Material and energy inputs should be renewable rather than depleting.

The 12 Principles of Green Engineering are other guides towards sustainability. They have been introduced to help scientists and engineers to design new materials, products, processes, and systems that are harmless to human health and the environment.[8] When applying the 12 principles of Green Engineering to a design, they would consequently improve the design engineering quality and its safety specification to fulfill with the environmental, economic, and social needs.[8] The Green Engineering principals should not simply be viewed as a list of goals, but rather viewed as a novel set of methodologies to achieve the goals of green design and sustainability.[8]

To sum up, the movement towards sustainability using green technologies is a novel approach due to practical, logistical, economic, inertial, and institutional reasons.[8] Green technologies are necessary to improve unsustainable products, processes, and systems that are currently in use.[8] Together, Green Chemistry and Green Engineering principals can provide valuable guides for accomplishing these improvements. Practicing these principles is fundamental toward achieving real sustainability in the design of molecules, products, processes, and systems, for the simultaneous benefit of society, economy, and the environment, as well as the eventual goal of sustainability.[8]

1.3 Biomass

1.3.1 Definition and resources

To be able to outline the global biomass resources, it is first appropriate to find a clear definition for the term biomass. The UK Biomass Task Force[9] definition of biomass as follows:

"literally, any biological mass derived from plant or animal matter. This includes material from forests, crop-derived biomass including timber crops, short rotation forestry, straw, chicken litter and waste material."[9]

Biomass is plentifully available and is thought to be the fourth largest energy resource in the world after petroleum, natural gas and coal.[10] In the long term use; biomass can be sustainable and ideally it would not interfere with the other land

demands such as food production if managed carefully. Currently, biomass provides about 10% of the world's energy demand and by 2050 it is predicted that sustainable sources of biomass could provide 20-50% of the world's primary energy needs.[10] In the UK, it is projected that by 2020 the UK could depend on sustainable biomass for supplying the equivalent of 20% of its total primary energy demand, and more than double or even treble by 2030.[11]

Biomass has the potential to be the leading global primary energy sources through the next century.[12] Biomass resources are plentiful in volume on earth, carbon-neutral, renewable, have low sulfur contents, and can be the best alternative to fossil fuel resources.[13] The use of biomass as an alternative energy source can reduce pollution and global warming, alleviate the energy crisis, and its contribution can lead to sustainable development.[14, 15] Therefore, in order to reach sustainable developments in the near future, the efficient utilization of biomass resources is essential.[13] The categorization of biomass resources is the first step towards the development of these resources.[13] Motasemi and Afzal[13] have illustrated the classification of biomass resources into three major categories: virgin resources, residues, and municipal solid waste (MSW), see Table 1.3. According Motasemi and Afzal,[13] all of these biomass resources can be promising sources for the future energy production using suitable conversion processes.

Table 1.3: The classification of biomass resources.[13]

Biomass resources		
Virgin resources	Forest resources	Any type of wood like pine beetle wood, or new types of woody and forest biomass such as willow, hybrid poplar, balsam poplar, aspen
	Oil/crops	Wheat, barley, tame hay, corn, canola, palm oil, soybean, flax, oat, straw, pasture grasses
Residues	Wood residues	Bark, branches, leftover treetop, and leaves from harvest and thinning operations or left over from felling, sawdust, shavings from pulp mills and saw mills
	Agricultural residues and wastes	Residual fraction of primary crop (wheat, barley, tame hay, oat, etc.) harvest, waste oil/fat
	Livestock residues	Readily available source of waste biomass like livestock excrement and livestock carcass

Municipal solid waste (MSW)	Residential	Newsprint, cardboard and boxboard, mixed paper, glass, ferrous metals, copper and aluminium.
	Non-residential	Mixed metals, white goods, electronics, plastics, tires, construction, renovation and demolition, organics, other materials

1.3.2 Composition of lignocellulosic biomass

Lignocellulosic (plant) biomass, particularly woody biomass, is a complex material constructed from oxygen-containing organic polymers, which consist of three major high molar masses components: cellulose, hemicellulose and lignin.[16] Low molar masses of extraneous materials, such as organic extractives (waxes, fats, resins, terpenes, *etc.*) and inorganic minerals, are also present at small percentage (usually <10% w/w) in wood species.[17, 18] The weight distribution percentage of cellulose, hemicellulose and lignin can vary depending on the woody biomass species.[16]

Table 1.4 shows the typical cellulose, hemicellulose and lignin content in some plant materials.

Table 1.4: Typical cellulose, hemicellulose and lignin content of selected biomass species.[19]

Biomass material	Content (% w/w)		
	Cellulose	Hemicellulose	Lignin
Softwood	45.8	24.4	28.0
Hardwood	45.2	31.3	21.7
Spruce wood	50.8	21.2	27.5
Beech wood	45.8	31.8	21.9
Ailanthus wood	46.7	26.6	26.2
Wood bark	24.8	29.8	43.8
Wheat straw	28.8	39.1	18.6
Corn stover	51.2	30.7	14.4

Cellulose

Cellulose is currently ranked as the most abundant terrestrial biopolymer.[20] The cellulose fibers provide a physical support to woody plants and its content in dry wood was generally estimated to be ~40-50 % (w/w).[18] Cellulose is a linear polysaccharide polymer consisting of ~5000-10000 of β-(1→4)-D-glucopyranose units.[16, 17] The cellulose polymer has a basic repeating unit that consists of two glucose anhydride units, named as a cellobiose unit, see Figure 1.1.[16, 17]

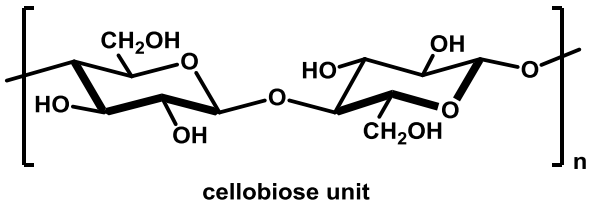

Figure 1.1: Chemical structure of cellulose.[21]

Hemicellulose

Hemicellulose is a heterogeneous polysaccharide polymer that consist of various polymerized monosaccharides, mostly glucose, galactose, mannose, xylose, arabinose, 4-*O*-methylglucuronic acid, and galacturonic acid residues, see Figure 1.2.[16, 17]

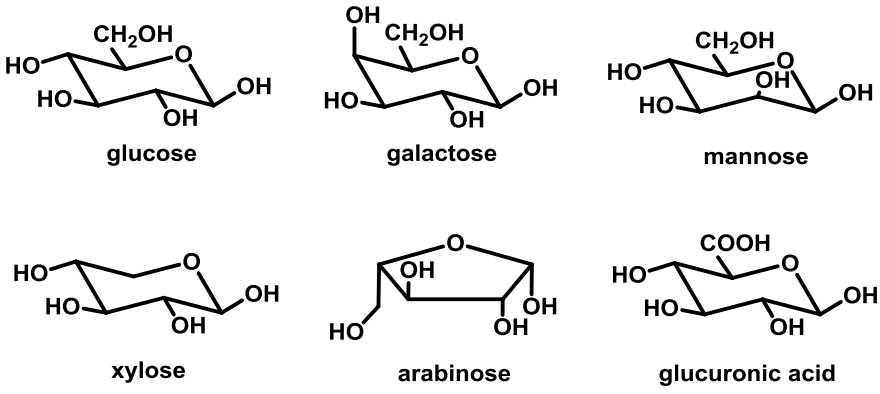

Figure 1.2: Main monomers of hemicellulose.[21]

The ratio of these saccharide monomers varies depending on the species of woody biomass and the growing environment. However, hemicelluloses generally account

for 25-35% (w/w) in dry wood.[18] Furthermore, in comparison with cellulose, hemicellulose has lower molecular weight than cellulose.[16] The average number of repeating saccharide monomers in hemicellulose is only ~100-200, whereas in cellulose, the number is greatly more than 5000 repeating glucose units.[16, 17]

Lignin

Lignin is considered the second most abundant biopolymer on earth after cellulose.[20] Lignin is an important structural component of woody plants that is found in plant cell walls.[20] The prime functions of lignin in plants are to provide physical strength to plants, to form networks of water conducting vascular by hydrophobic interactions, and to protect plants from insects and microorganisms.[20]

Lignin is an aromatic polymer constructed of complex, three-dimensional, highly branched polyphenolic substance with various types of functional groups: aliphatic and phenolic hydroxyls, carboxylic, carbonyl and methoxyl groups.[16, 22, 23] Generally, lignin chemical structure is also often described as consisting of phenylpropane units, originating from three aromatic alcohol precursors (monolignols), namely *p*-coumaryl alcohol, coniferyl alcohol, and sinapyl alcohol, see Figure 1.3.[24] The further phenolic substructures that generate by these monolignols are named: *p*-hydroxyphenyl (H, from *p*-coumaryl alcohol), guaiacyl (G, from coniferyl alcohol) and syringyl (S, from sinapylalcohol) moieties in lignin.[24]

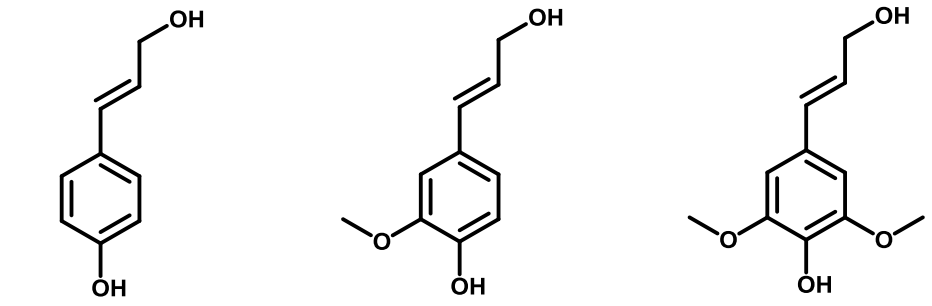

***p*-coumaryl alcohol** **coniferyl alcohol** **sinapyl alcohol**

Figure 1.3: The chemical structures of the three main building blocks of lignin (monolignols).[21]

Lignin composition and content are typically influenced by the species of woody biomass and also by the growing environment.[23] Therefore, lignins derived from hardwood consist principally of G and S units, as well as traces of H units.[25] However, lignins derived from softwood consist mostly of G units and low levels of H units.[25] In addition, lignins from grasses are built up from H, G and S units, where grasses (monocots) incorporate G and S units at comparable levels, and more H units than grasses (dicots).[25, 26]

1.3.3 Treatments

Different types and sources of biomass can be converted into energy and chemicals *via* a wide range of different technologies.[27] The conversion technology option is dependent on many factors, for instance biomass feedstock type and quantity, the required form of energy (*i.e.*, end-use applications), environmental obligations, economic situations, etc.[27] However, in most cases, the process route is designed depending on mainly the form in which the energy is required as well as the types and quantities of biomass feedstock.[27]

Three significant products can be obtained from the conversion of biomass: power/heat generation, transportation fuels and chemical feedstock.[28] The process technologies currently being used for the conversion of biomass are classified as thermo-chemical, bio-chemical/biological, and mechanical extraction (with esterification).[27]

1.7.3.1 Thermo-chemical conversion

There are three well-known major processes used to thermo-chemically convert the biomass to energy and chemicals: combustion, gasification and pyrolysis, see Figure 1.4.[27, 29]

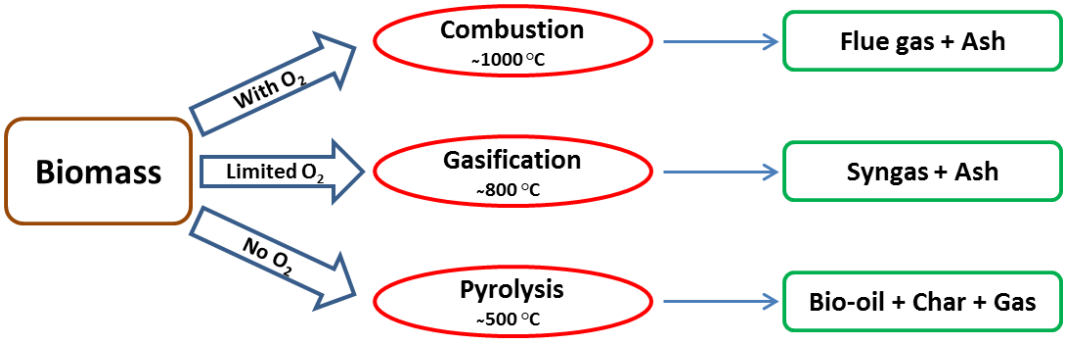

Figure 1.4: Thermal treatment technologies for biomass.[29]

The key difference between combustion, gasification and pyrolysis thermal treatments is the amount of oxygen supplied into the thermal reactor.[29] For combustion, the process occurs under full oxidation of the biomass with sufficient supply of oxygen, producing carbon dioxide, water and ash including other minor products, such as metals, trace hydrocarbons and acid gases.[29] For gasification, the process involves supplying limited oxygen to avoid complete combustion to produce combustible gases like carbon monoxide and hydrogen.[29] For pyrolysis, the reaction takes place under the absence of oxygen for the production of bio-oil, char and gas.[29]

Combustion

Combustion is simply the burning of biomass in air, which converts the stored chemical energy of biomass into electricity, heat, or mechanical power.[30] During biomass combustion, hot gases are produced (*e.g.*, carbon dioxide and acid gases) at temperatures about 800-1000 °C.[27] Any type of biomass can be used for combustion, however, in practice, it is preferable to pre-dry biomass to achieve a moisture content of less than 50% (w/w) prior to combustion.[27]

Gasification

Gasification is the conversion of biomass into a combustible gas mixture (*e.g.*, carbon monoxide and hydrogen), where the biomass is partially oxidised under limited air supply at high temperatures of approximately 800-900 °C.[27, 29] The gas mixture produced can be burnt directly to generate heat and electricity, or can be stored as a fuel for later use in gas engines or gas turbines.[27] The stored gas mixture can also be used as feedstock (syngas) for making chemicals, such as methanol.[27]

Gasification is a comparatively clean energy technology and has received much of interest for the utilisation of biomass, coal, sewage sludge, and municipal solid waste (MSW).[31-49] The use of gasification to generate heat and power offers some advantages when compared to the traditional direct combustion of the hydrocarbon materials.[50] For instance, using the gasification thermal treatment enables the elimination of nitrogen- and sulfur-containing compounds from syngas during its production, which is beneficial as the presence of these compounds cause emissions of NO_X and SO_X during combustion.[50] Also, the gasification-combustion process has a higher net efficiency than the traditional direct combustion of raw feedstocks for heat and power generation.[50, 51]

Pyrolysis

Pyrolysis is the conversion of biomass into liquid (bio-oil), char and combustible gases.[52] The pyrolysis process is generally carried out by heating biomass under an air-free environment to a temperature around 500 $^{\circ}$C. The pyrolysis liquid fraction is typically described as bio-oil, however, it has also been referred to with other names such as pyrolysis liquid, pyrolysis oil, wood oil, wood liquid, wood distillates, liquid wood, liquid smoke, pyroligneous acid, pyroligneous tar, bio-crude oil, and bio-fuel oil.[53] The bio-oil can be used as a fuel in engines, turbines, furnaces and boilers.[54] However, the bio-oil can also be used as a feedstock to extract a wide range of chemicals including food flavouring, resins and fertilisers.[54] extensive studies have been previously reported for the pyrolysis treatments of different types of feedstocks including biomass, sewage sludge, tyres, plastics and municipal solid waste (MSW).[55-62]

The ratios of the pyrolysis products (liquid, solid and gaseous fractions) are very much dependent on reaction temperature and residence time.[52] Altering these reaction parameters can increase the yield of one fraction and decrease another, depending on the required application. For example, a pyrolysis process with a lower reaction temperature and longer residence time is desired for the production of charcoal, whereas a pyrolysis process with a moderate reaction temperature and short residence time is optimum for the production of bio-oil.[53] Furthermore, pyrolysis processes with high reaction temperature and longer residence time increases the

conversion of biomass to gas.[53] Therefore, because of these influencing pyrolysis operating parameters, generally the modes of pyrolysis processes are often divided into three types: slow pyrolysis, fast pyrolysis and flash pyrolysis.[63] The range of the values of the operating parameters for these pyrolysis types are summarised in Table 1.5.

Table 1.5: Ranges of pyrolysis operating parameters for the three main pyrolysis processes.[55, 63]

	Slow pyrolysis	Fast pyrolysis	Flash pyrolysis
Operating temperature (°C)	300-700	600-1000	800-1000
Heating rate (°C/s)	0.1-1	10-200	≥1000
Solid residence time (s)	600-6000	0.5-5	<0.5
Major products	Char	Liquids	Liquids, gases

Slow pyrolysis

Slow pyrolysis, or sometimes referred to as conventional pyrolysis, is a pyrolysis process that take place under a low heating rate and long residence time.[29, 52] This mode of pyrolysis has been in use for thousands of years and has been mostly limited to charcoal production.[16]

Fast pyrolysis

This mode of pyrolysis is more favourable for the production of liquids (bio-oils).[64] Lately, the fast pyrolysis process of biomass has gained many attentions for maximizing the process liquid yields.[64] Generally, depending on the biomass used, fast pyrolysis processes can yield up to 60-75% (w/w) of bio-oil, 15-25% (w/w) of char, and 10-20% (w/w) of gases.[16] Maximizing liquid products using fast pyrolysis of biomass would require a process condition of low temperature, high heating rate, and short residence time.[65] However, gaseous products can also be maximized using the fast pyrolysis mode if the process condition modified to high temperature, low heating rate, and long residence time.[65]

Flash pyrolysis

Flash pyrolysis is similar to fast pyrolysis, with the only difference between these two modes of pyrolysis being the heating rates and hence the residence times. Generally, the heating rates for flash pyrolysis are higher than about ~1000 $^{\circ}$C/s, and the residence times are extremely short (<1 s).[66] The flash pyrolysis process of biomass is a promising technology for the production of bio-oils.[67] An efficiency of up to 70% (w/w) conversion of biomass to liquid bio-oil can be achieved using flash pyrolysis processes.[29]

1.7.3.2 Bio-chemical conversion

The bio-chemical conversion of biomass is mainly associated with two processes: fermentation and aerobic digestion (AD).

Fermentation

Fermentation is a well-known process for the conversion of sugars to mainly alcohols, which can be used as an alternative biofuels to replace gasoline or kerosene: the petroleum-based fuels.[27, 30] The fermentation process has been used commercially on a large scale in many countries, such as the US and Brazil, to produce ethanol from sugar crops (*e.g.*, sugar cane) or starch crops (*e.g.*, wheat).[27, 30] Starch is a natural polysaccharide and can be converted to sugars by enzymes, and then these sugars converted to ethanol by the fermentation process.[27]

Anaerobic digestion

Anaerobic digestion (AD) is a biological process that directly converts organic materials in the absence of oxygen to gas, often referred to as biogas, which is a mixture of mainly methane and carbon dioxide (CO_2).[27, 30] Generally, bacteria are used in an anaerobic environment to convert the biomass to a biogas. [27, 30]AD is commonly used for the treatment of organic wastes with relatively high moisture content (>80%).[27] Commercially, AD is a valuable technology as its main product (biogas) offers many useful applications. Biogas can be either used directly or upgraded to a higher quality, by removing CO_2, for use as a fuel to produce electricity using gas turbines.[27, 30]

1.7.3.3 Mechanical extraction

Mechanical extraction is a process that mechanically extracts oil from seeds.[27] Various types of biomass crops, for instance, rape seed and cotton seed, are used for the oil production.[27, 30] These oils can be chemically processed further by the reaction with an alcohol (methanol or ethanol) using a process often referred to as transesterification to produce biodiesel.[27] Biodiesel is used as a transportation fuel and largely produced in EU countries from rapeseed oil.[30]

1.3.4 The use of biomass in the concept of a biorefinery

The International Energy Agency (IEA) Bioenergy Task 42 introduced a general definition of a biorefinery as *"the sustainable processing of biomass into a spectrum of bio-based products (food, feed, materials, chemicals) and bioenergy (biofuels, power, heat)"*.[68] Therefore, a biorefinery can be achieved through a concept, a facility, a process, a plant, or even a group of facilities that require the combination of many different areas of knowledge including chemistry, biochemistry and biology, chemical engineering and biomolecular engineering.[69, 70] All types of biomass can be used in a biorefinery including forest residues, agricultural crops, organic residues (both animal and plant derived), industrial wastes, aquatic biomass (sea weeds and algae) and wood.[68] The main goal of a biorefinery is to deliver a sustainable route to high value products, which in turn improve the biomass processing economics as well as the environmental carbon footprint.[70]

The concept of a biorefinery is not a recent one.[68] A lot of the traditional biomass-converting technologies, such as the starch, sugar and, pulp and paper industry, use some features related to the biorefinery approach.[68] However, the most significant drawback associated with these traditional biomass-converting industries is perhaps the misuse of the generated waste. For example, the hemicellulose encountered in traditional kraft pulping industry is mostly dissolved in the form of saccharified mono sugars, together with lignin and inorganic pulping chemicals, in black liquor that is traditionally combusted for generating power.[71] However, as hemicellulose has a lower heating value than lignin, this represents an inefficient use of the resource.[71] Therefore, a separation of the hemicellulose from lignin prior to combustion would be optimal for more economic use of hemicellulose.[71] For

instance, it could be used as a feedstock for the production of biofuels (bioethanol) or higher value chemicals.[71] Thus, many traditional bio-industries can combine their material flows in order to achieve a complete utilization of all biomass components: the 'waste' from one bio-industry becomes a feedstock for other industries, leading to integrated bio-industrial systems.[72]

In a similar way within a biorefinery concept, integrated facilities can help to create flexibility for the conversion of biomass into multiple high-value products including energy, chemicals and materials with zero, or close to zero waste.[73] The technologies available to the biorefinery are mainly classed as mechanical/physical, chemical, biochemical and thermochemical processes.[72] Most studies nowadays are usually focusing on investigating one methodology rather than a combination of methodologies.[73] Indeed, there are some pros and cons associated with each of these available technologies, however, recognizing them all is essential to enable the integration and blending of different technologies and feedstocks to help maximizing the diversity of applications and products formed.[73]

Budarin *et al.*[73] have investigated this area and proposed a new concept for an integrated close to zero waste wheat straw biorefinery. As demonstrated by Budarin *et al.*,[73] two novel green technologies can be combined, supercritical CO_2 extraction and low temperature microwave pyrolysis, in order to enhance the economic feasibility of a wheat straw biorefinery. The first stage of their integrated biorefinery is the extraction of secondary metabolites, including wax esters, fatty acids and fatty alcohols, *via* supercritical CO_2,[73] while the second stage of their integrated biorefinery is the use of low temperature microwave pyrolysis (<200 $^{\circ}$C) to produce char (*ca.* 30% w/w), bio-oil (*ca.* 20% w/w), aqueous solution (*ca.* 35% w/w) and gas (*ca.* 14% w/w).[73]

According to Budarin *et al.*,[73] the char fraction is suitable for co-firing, while the bio-oil can be further fractionated to produce transportation fuels and high-value chemicals. The *in-situ* separated aqueous fraction from the organic matter (bio-oil) contains mainly formic acid, acetic acid, formaldehyde and acetaldehyde, which according to Budarin *et al.*,[73] can be used as platform molecules for downstream processing to high-value products. The incondensable gas fraction contains mainly

carbon dioxide, carbon monoxide and methane, and as demonstrated by Budarin *et al.*,[73] the carbon dioxide can be recycled internally for the supercritical CO_2 extraction, while carbon monoxide and methane could also be recycled internally for power generation.

Other utilizations of the pyrolysis char that might be applicable in the concept of a biorefinery have also been reported.[74, 75] According to Wu *et al.*,[74] the pyrolysis char can be used as bio-char for soil improvement, or upgraded to activated carbon. In addition, it can also be gasified to produce syngas and hydrogen.[74, 75] The gases produced, as described by Wu *et al.*,[74] have medium to high calorific values and may contain sufficient energy to provide the energy needs of a pyrolysis plant.

An alternative lignocellulosic biomass biorefinery model based on just one technology has been reported by Meier.[1] According to Meier,[1] fast pyrolysis as a thermo-chemical process within a biorefinery model provides a viable option that can convert lignocellulosic biomass into higher-value-added products with no waste streams other than ash and flue gas. As demonstrated by Meier,[1] the design of a biorefinery based on pyrolysis bio-oil is very much like a traditional refinery. In the first step, the biomass is converted into bio-oil by fast pyrolysis, with obtainable yields of up to 75% (w/w; on a dry feed basis), and the by-product char and gas are recycled internally to provide the process heat requirements.[1] In the second step, the bio-oil collected from different installations at the biorefinery is divided into different fractions. Each fraction can be further upgraded by different technology to produce finally the optimal combination of high- and low-value products from the bio-oil. The high-value chemicals, which are predicted by Meier,[1] are mainly organic acids, hydroxymethylfurfural (HMF), furfural, levoglucosan and phenols.

1.4 Microwave-Enhanced Chemistry

The earliest common application of microwave technology was to heat and cook food, and the first appearance of domestic and commercial microwave appliances were in 1950s.[76] However, these microwave appliances introduced in 1950s were too large and expensive for home use.[76] Therefore, the widespread use of general home microwave ovens did not occur until 1970s, which by then the first generation issues

were solved.[76] Processing food with microwaves was discovered by accident in 1940s,[76] when Percy Spencer, a self-taught engineer, was working on an active radar set that he built and noticed a chocolate bar in his pocket started to melt.[76]

Heating chemical reactions using microwave energy is a new technology which is growing rapidly. Microwave energy offers new and innovative applications in organic and peptide synthesis, polymer chemistry, nanotechnology, material science, and biochemical processes.[77-92] The use of microwave heating to drive organic chemical reactions can be significantly more energy efficient than using conventional heating.[93] A considerable number of reported studies have demonstrated that using microwave heating can dramatically decrease processing times, improve product yields and enhance product quality or material properties when compared to the use of conventional heating methods.[94-96] In addition, it has been demonstrated that heating using microwave irradiation is a clean, cheap, and convenient method for carbohydrate chemistry.[97] In comparison with conventional methods, short reaction times, large rate enhancement, and comparable, or sometimes much higher, yields (especially in reactions where the short reaction time prevents decomposition) are observed.[97] Furthermore, in the medicinal and organic chemistry communities, this new technology has been accepted as a standard practice just after a few years of laboratory investigations.[98, 99] Therefore, the use of microwave heating is predicted to continue to be an important technique in these areas.[97, 99, 100]

1.4.1 Principles of microwave heating

In the electromagnetic spectrum (see Figure 1.5), the microwave region is between infra-red radiation and radio frequencies, which corresponds to wavelengths of 1 cm to 1 m and frequencies of 30 GHz to 300 MHz, respectively.[101] The wavelength range between 1 cm and 25 cm are extensively used for RADAR transmissions and the remaining range of wavelengths is used for telecommunications.[101] Therefore, to avoid any interference with these uses, industrial and domestic microwave heaters are designed to operate at two fixed wavelengths, at either 12.2 cm (2.45 GHz) or 33.3 cm (900 MHz).[101] However, most domestic microwave ovens nowadays operate at 2.45 GHz, which corresponds to the wavelength of 12.2 cm.[101]

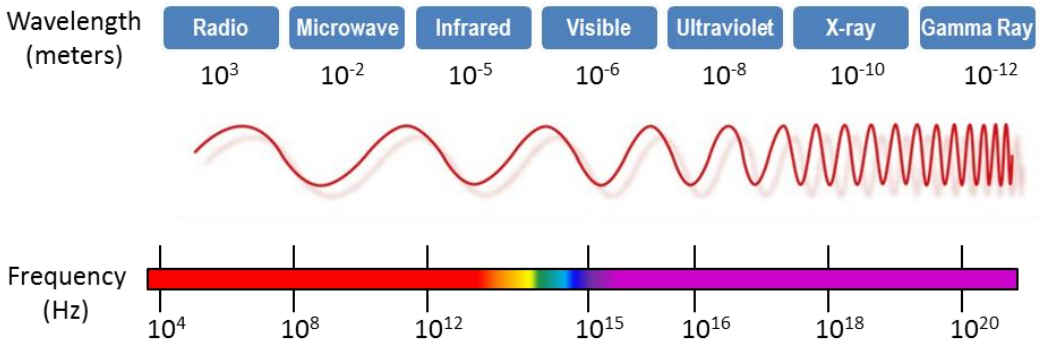

Figure 1.5: Electromagnetic spectrum.

Generally, microwaves are described as the electromagnetic waves that consist of two perpendicular components, namely electric and magnetic fields. These components interact with anything that can be electrically or magnetically polarised.[93] The interaction of electric-field component within the electromagnetic wave with a material causes the heating effect.[93] The overall mechanism of how a material is heated by the effect of microwave radiation is commonly explained under two main mechanisms: dipolar polarisation and ionic conduction.[101-105] A further third mechanism called "interfacial polarisation" could also contributes to the overall heating mechanism of a material.[101, 104, 105]

Dipolar polarisation is an important heating mechanism of microwave radiation, and this heating mechanism is more dominant with materials containing polar compounds.[104] These materials are regularly classified as "dielectric materials" in order to indicate that they have the ability to store energy when subjected to an external electric field.[93] When a dielectric material is exposed to an electric field, the dipoles rotate to align themselves according to the direction of the electric field.[106] The alignment of the dipoles changes with the magnitude and the direction of the electric field.[106] Molecules can realign in time with applied frequencies of 10^6 Hz in liquids and gases.[102] However, it is not possible for them to follow the electric field inversion at microwave frequencies of *ca.* 10^{12} Hz.[102] Therefore, dielectric losses and phase shifts are the result.[106] In addition to the dielectric coefficient (permittivity), the excited molecules size (mass) is also relevant.[102, 106] The field is released in to the medium as electrical energy which further transformed into kinetic or thermal energy.[106] This behaviour is also referred to as molecular friction (*i.e.*, friction

between the rotating molecules), and hence causes the heat to be generated within the whole medium.[104]

For the ionic conduction mechanism, this heating mechanism (due to the subjected microwave radiation) is more associated with highly conductive materials. When these materials interact with microwave radiation, electric currents are formed as a result of the charged particles (*e.g.*, ions) oscillating back and forth within these materials under the influence of the external electric force.[86, 105] Therefore, as the electric currents flow within these materials, heating is developed due to the currents facing an internal resistance in the form of collisions of charged particles with neighbouring molecules.[86, 105] Moreover, it is noteworthy that this ionic conduction mechanism contributes a much stronger effect than the dipolar polarisation mechanism in the terms of heat-generating capacity.[86, 105]

Interfacial polarisation, also known as Maxwell-Wagner effect, is a third heat-contributing mechanism that arises from the combination of dipolar polarisation and ionic conduction.[101, 104, 105] This mechanism becomes noticeably effective with inhomogeneous systems—a suspension of conducting particles in a non-conducting medium.[101, 105] When microwave irradiation is applied to these systems, charges are built-up between the interfaces of different components leading to field distortions and dielectric loss, which further contribute to the systems overall heating.[104]

In order to determine the dielectric properties of a material, two parameters are regularly considered: dielectric constant ε', and dielectric loss ε''.[86, 101, 107-109] The dielectric constant, ε', specifies the ability of the molecule to be polarized by the electric field,[101] whereas, ε'', the dielectric loss evaluates the amount of input microwave energy that is lost to the medium by being dissipated as heat.[108] The ratio of these two parameters defines what often referred to as the loss tangent ($\tan\delta = \varepsilon''/\varepsilon'$).[86, 101] This loss factor ($\tan\delta$) indicates the ability of a material to convert electromagnetic energy into heat at a given frequency and temperature.[86, 101] A reaction medium with a high $\tan\delta$ value is required for efficient absorption of microwaves and rapid heating.[86]

Table 1.6 shows the boiling point ($^{\circ}$C), dielectric constant (ε'), dielectric loss (ε''), and loss tangent ($\tan\delta$) of 30 common organic solvents.[108]

Table 1.6: Boiling point (°C), dielectric constant (ε′), dielectric loss (ε″), and loss tangent (tanδ) of 30 common organic solvents.[108]

Solvent	Bp °C	ε′[a]	ε″[a]	tanδ[a]
Ethylene glycol	197	37.0	49.950	1.350
Ethanol	78	24.3	42.237	0.941
DMSO	189	45.0	37.125	0.825
2-Propanol	82	18.3	14.622	0.799
1-Propanol	97	20.1	15.216	0.757
Formic acid	100	58.5	42.237	0.722
Methanol	65	32.6	21.483	0.659
Nitrobenzene	202	34.8	20.497	0.589
1-Butanol	118	17.1	9.764	0.571
Isobutanol	108	15.8	8.248	0.522
2-Butanol	100	15.8	7.063	0.447
2-Methoxyethanol	124	16.9	6.929	0.410
o-Dichlorobenzene	180	9.9	2.772	0.280
NMP	215	32.2	8.855	0.275
Acetic acid	113	6.2	1.079	0.174
DMF	153	37.7	6.070	0.161
1,2-Dichloroethane	83	10.4	1.321	0.127
Water	100	80.4	9.889	0.123
Chlorobenzene	132	2.6	0.263	0.101
Chloroform	61	4.8	0.437	0.091
MEK	80	18.5	1.462	0.079
Nitromethane	101	36.0	2.304	0.064
Acetonitrile	82	37.5	2.325	0.062
Ethyl Acetate	77	6.0	0.354	0.059
Acetone	56	20.7	1.118	0.054
THF	66	7.4	0.348	0.047
Dichloromethane	40	9.1	0.382	0.042

Solvent	Bp °C	ε'^{a}	ε''^{a}	$\tan\delta^{a}$
Toluene	111	2.4	0.096	0.040
Hexane	69	1.9	0.038	0.020
o-Xylene	144	2.6	0.047	0.018

[a] Measured at 20 °C, and at 2.45 GHz.

1.4.2 Microwave-enhanced pyrolysis of biomass

The conversion of biomass into fuels and chemicals using microwave pyrolysis is a quite new approach and is rapidly growing. This recent attention is mainly due to the advantages that microwaves can offer, such as rapid, direct and energy-efficient mode of heating, when compared to conventional heating methods.[110] In addition, conventional methods for converting biomass into fuels and chemicals are often carried out at very high temperatures (usually >500 °C), whereas conversion of biomass *via* microwave as a heating tool can be achieved at considerably lower temperatures (<200 °C).[110]

In the last fifteen years or so, several published papers have investigated the use of microwave pyrolysis with different types of biomass including coffee hulls,[111] wheatstraw,[112] rice straw,[113, 114] seaweed (macroalgae),[115, 116] and corn stover.[117-119]

Miura *et al.*[120] have investigated the microwave pyrolysis of cylindrical wood blocks, with varying diameters from 6 to 30 cm and masses up to 12 kg. As demonstrated by Miura *et al.*,[120] the heat development during a microwave pyrolysis of a wood block begins at the center of the wood whereas, by contrast in conventional pyrolysis, the heat transfers gradually from the surface to the wood center as illustrated in Figure 1.6.

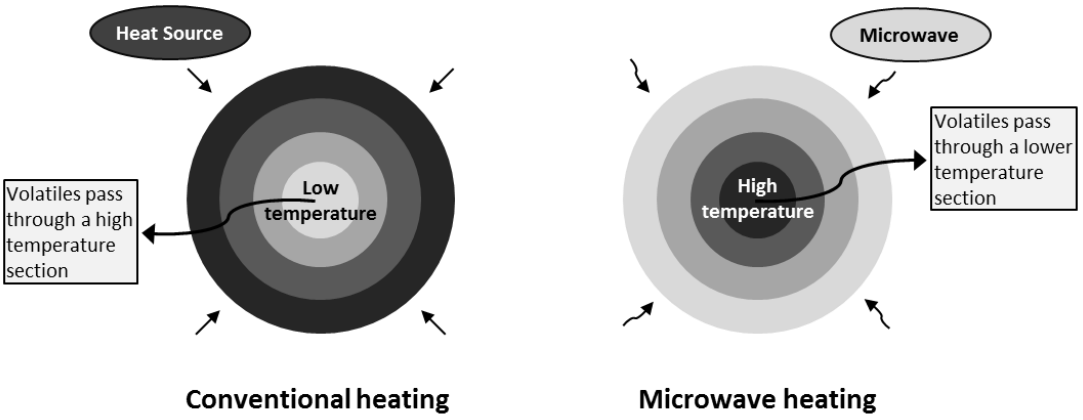

Figure 1.6: Schematic diagram of temperature distribution and heat development in wood by microwave irradiation, and the temperature distribution and heat transfer in wood by conventional heating.[120]

According to Miura *et al.*,[120] this different heating development mechanism of microwaves can reduce undesirable secondary reactions of the wood volatiles as these volatiles formed in the wood center pass through a lower temperature section towards the wood surface layer and subsequently into a cooler gas phase, as also illustrated in Figure 1.6. Furthermore, Miura *et al.*[120] also showed that the obtained char of the microwave pyrolysis of wood has greater surface area than the chars prepared by conventional pyrolysis. The pores of the char obtained by microwave pyrolysis were also found to be 'cleaner' and have less debris deposits in them than those prepared by conventional pyrolysis. The maximum tar yield (up to *ca.* 30% based on wood weight) was obtained after 12 minutes of microwave irradiation. The tar composition was found to include low molecular weight acids, furfural, phenols, and a series of saccharides including levoglucosan being the major saccharide component at concentrations up to *ca.* 9% based on the tar weight.

Robinson *et al.*[121] have studied the microwave pyrolysis of wood pellets. During their investigation, they found that water is the only effective microwave absorber in wood at temperatures up to 600 °C. Substantial amount of water is naturally present in wood biomass, and as the temperature increases by the microwave irradiation, this amount of water will drop, but it is still enough to absorb microwave energy and carry on the pyrolysis. Robinson *et al.*[121] have also demonstrated that increasing the amount of water in wood above its natural content will have a negative effect on the yields of liquid and gas formed during the microwave pyrolysis. According to

Robinson *et al.*,[121] the wood pellets received have natural water content of *ca.* 6% (w/w), and under the conditions used in their investigation, the microwave pyrolysis of this stock sample has produced 13% (w/w) liquid and over 19% (w/w) gas. However, when the amount of water was increased (to *ca.* 22% w/w of the wood pellets), the yield of the microwave pyrolysis liquid and gas, under the same conditions, were found to be reduced to *ca.* 4% (w/w) and *ca.* 5% (w/w), respectively.

Budarin *et al.*[122] have identified four physical parameters that affect the results of microwave pyrolysis of biomass: microwave power, sample mass, water content and biomass density. According to Budarin *et al.*,[122] any changes on these parameters will eventually affect the heating rate of the microwave pyrolysis, which is critical to the formation of pyrolysis liquids. From Budarin *et al.*,[122] a 60% (w/w) liquid yield was obtained from the microwave pyrolysis of Spruce, which, according to their discussion, is equivalent to those obtained by conventional fast pyrolysis. In addition, Budarin *et al.*[122] have also stated that using microwave pyrolysis can avoid the need for further pyrolysis liquid upgrading steps as required when using conventional pyrolysis. The *in-situ* separation of pyrolysis liquid during microwave pyrolysis separates the water and acidic compounds from the bio-oil, and thus, according to Budarin *et al.*,[122] this is the most significant benefit of microwave pyrolysis over conventional pyrolysis methods.

Moreover, in order to improve microwave absorption, microwave absorbers can be added with the biomass prior to pyrolysis. These are solid substances, such as SiC or graphite, which can absorb microwave energy at relatively high temperatures, especially, at temperatures higher than 200 $^{\circ}$C.[110] Therefore, for microwave pyrolysis at low temperatures, below *ca.* 250 $^{\circ}$C, the addition of these microwave absorbers will not considerably improve the pyrolysis process, but they could contribute much more significantly when much higher temperatures are required.[110]

Luo *et al.*[123] have investigated the microwave pyrolysis of wood sawdust (a residue from pine wood pelleting process) in the presence of SiC. According to their investigation, the addition of SiC as a microwave absorber has significantly improved the pyrolysis liquid yields, reaching a maximum yield of *ca.* 59% (w/w; of

the initial wood sawdust) at 500 °C, which, according to Luo *et al.*,[123] was closer to those obtained by conventional fast pyrolysis (60-75% w/w) under similar conditions.

Nonetheless, there are other factors that need attention when using microwave absorbers. For instance, a relatively uniform mixing of the biomass and the microwave absorber must be achieved.[110] Therefore, processing large biomass pieces to smaller ones is essential to enhance the uniform mixing, but this clearly will bring undesirable additional costs.[110] The other factor that can be most concerning is contamination. The addition of SiC as a microwave absorber can release silicon to the pyrolysis products which can be undesirable, especially if some enters a bio-oil used as a fuel, where it could have serious effects on the performance of an engine.[110]

In summary, despite the advantages discussed above for microwave pyrolysis over conventional pyrolysis, it still has not attracted the attention that has been paid to conventional pyrolysis methods.[110] Microwave pyrolysis of biomass can offer a much better energy efficient route to low water and acidic content bio-oils, good quality chars, and beneficial syngas than conventional pyrolysis.[110, 122] Many types of biomass can be pyrolysed using microwave irradiation, and the distribution of products are broadly close to the ones obtained by conventional pyrolysis.[110] The future challenge however of microwaves is perhaps to develop them to larger-scale units.[110] In fact, Biorenewables Development Centre (BDC) at York, UK, has developed a microwave pyrolysis unit capable of continuous flow up to 30 kg/h.[110] This step could attract more attention to the field, which will help in driving the microwave-enhanced pyrolysis of biomass forward.[110]

1.5 Composition of Bio-oils

Crude bio-oil or pyrolysis liquid is dark brown and approximates to its original biomass in elemental composition.[124] It arises from fragmentation and depolymerization of the three major plant components, cellulose, hemicellulose and lignin.[125] Generally, it is composed of a very complex mixture of oxygenated compounds with an appreciable amount of water from both the pyrolysis reaction

product and initial biomass moisture.[124] Table 1.7 summarizes some further typical properties of this pyrolysis liquid.

Table 1.7: Typical properties of crude bio-oil derived from conventional fast pyrolysis of wood.[124]

Physical property	Typical value
Moisture content	25% (w/w)
pH	2.5
Specific gravity	1.20
Elemental analysis	
C	56% (w/w)
H	6% (w/w)
O	38% (w/w)
N	0-0.1% (w/w)
HHV (as produced)	17 MJ/kg
Viscosity (at 40 °C and 25% water)	40-100 mPa s
Solids (char)	0.1% (w/w)
Vacuum distillation residue	up to 50% (w/w)

The crude bio-oil produced by conventional fast pyrolysis contains varying amounts of water, and typically ranging from about 15% to a maximum limit of about 30-50% (w/w) depending on the biomass feedstock.[124] Also, it contains a wide variety of functional groups including aldehydes, ketones, alcohols, ethers, carboxylic acids, furans, esters, phenols and sugars.[125] Thus, it reveals an extremely wide range of boiling points.[125]

In addition, the bio-oil is completely immiscible with petroleum-derived fuels due to the high oxygen content, which is around 35-40% (w/w).[124] However, it is miscible with polar solvents such as acetone and methanol.[124] Furthermore, the bio-oil is acidic, has a heating value of less than half of that of conventional fuel oil (~42 MJ/kg), and it tends to polymerize when heated.[126]

The bio-oil acidity is most likely attributed to carboxylic acid compounds, with acetic acid and formic acid being the most abundant, respectively representing 5% and 3% (w/w) of the bio-oil.[127] As with regards to its low heating value, it probably arises from two causes: (a) water content in bio-oil; and (b) the presence of oxygenated compounds.[125] Moreover, the bio-oil contains large quantities of non-volatile compounds such as lignin oligomers and sugars, and their presence may be responsible for the bio-oil polymerization upon heating.[125]

1.5.1 Quantification and identification of bio-oil components

Due to the diversity and complexity of the bio-oils, an accurate analysis of their complete chemical composition is a very complicated task.[128] The analysis techniques of bio-oil usually involve gas chromatography-mass spectroscopy (GC-MS), gas chromatography-flame ionization detector (GC-FID), high-performance liquid chromatography (HPLC), nuclear magnetic resonance (NMR) spectroscopy, and/or ion-exchange chromatography.[128]

GC-MS and GC-FID are by far the most appropriate methods for analyzing more complex organic mixtures and identifying individual components that are volatile enough to pass through the GC column.[129] However, in the case of bio-oil, partial chemical information can be obtained from GC-MS analysis of bio-oil because of the large number of compounds and chromatographic co-elutions.[129] Therefore, the quantification of crude bio-oil components remains an expensive and time-consuming analytical procedure.[128] Hence, the majority of conducted studies focus on semi-quantitative analysis of bio-oil, or on the more comprehensive analysis of either a single component or group of components.[128] Frequently, the analyses do not take into account variables such as likely retention times and rely solely on automated and, sometimes, unreliable library matching of mass spectra, leading to erroneous results.

Nonetheless, even when narrowing the analysis to just classes of components in bio-oil, considerable inaccuracies in the analysis may occur. For instance, a large number of studies rely on just GC-MS and GC-FID for identifying and quantifying phenolic species in bio-oil. However, a lot of phenolics are present in bio-oil as oligomers, where these generally have molecular weight distributions of several hundred to

5000 g/mol depending on the pyrolysis conditions.[130] Thus, the conventional GC cannot detect such high molecular weights in bio-oil, and this inevitably leads to the provision of unreliable analytical information.

1.6 Biodiesel

1.6.1 Overview

Diesel fuel has an important part in the industrial development of any country. This is due to the significant role that these fuels play in the transport sector, thus, the demand for these diesel fuels is steadily increasing.[131] Nowadays, fuel consumption intensity can directly reflect the development of a society.[132] Engines running on diesel have been used globally in automobiles, engineering equipment and shipping equipment due to their thermal efficiency and excellent drivability and durability. Diesel fuels are currently used in electricity generators, city transport buses, heavy-duty trucks, farm machinery and many other applications.[132]

For many years, fossil fuels were consumed to generate energy, which without a doubt has participated in numerous technological advancements as well as growing the community economic.[132] But, on the other hand, it has at the same time raised many environmental concerns, which can be a risk to the sustainability of our planet.[132] The increasing demand for diesel fuel by the world's industry and pollution problems caused by its excessive use make it crucial to look for renewable energy sources that have lower environmental impact than these traditional sources.[132]

Therefore, the renewable fuel that could replace the petroleum diesel fuel is biodiesel. Biodiesel is a renewable fuel that has gained attention due to the ease of synthesis from vegetable oils or animal fats by a chemical process called 'transesterification'.[133] Also, it is non-toxic, biodegradable, and it has lower emissions than the typical diesel derived from petroleum.[134, 135] Nonetheless, biodiesel provides other advantages when compared to the petroleum-derived diesel, for example a) higher cetane number and higher flash point, which indicates a safer and better performance, b) higher lubricity, which increases engine lifetime and reduces the regularity of replacing engine parts, and c) the existence of oxygen in

biodiesel (~11%) improves combustion, and reduces CO and hydrocarbon emissions.[133] For the other diesel-biodiesel properties, see Table 1.8.

Table 1.8: Selected fuel properties of petroleum-derived diesel and biodiesel.[133, 136]

Fuel Property	Diesel	Biodiesel
Fuel Standard	ASTM D975	ASTM D6751
Fuel composition	C10-C21 HC [a]	C12-C22 FAME [b]
Higher Heating Value, Btu/gal	~137,640	~127,042
Lower Heating Value, Btu/gal	~129,050	~118,170
Kinematic Viscosity, @ 40 °C	1.3-4.1	4.0-6.0
Specific Gravity kg/l @ 15.5 °C	0.85	0.88
Density, lb/gal	7.1	7.3
Carbon, wt %	87	77
Hydrogen, wt %	13	12
Oxygen, by dif. wt %	0	11
Sulfur, wt %	0.0015 max	0.0-0.0024
Boiling Point, °C	180-340	315-350
Flash Point, °C	60-80	100-170
Cloud Point, °C	-35 to 5	-3 to 15
Pour Point, °C	-35 to -15	-5 to 10
Cetane Number	40-55	48-65

[a] Hydrocarbons [b] Fatty acid methyl esters

Biodiesel consists chemically of fatty acid methyl (or ethyl) esters (FAME) and is synthesised by a chemical process called transesterification of vegetable oil or animal fat feedstocks.[137] The main product of this transesterification is a mixture of mono-alkyl esters of long chain fatty acids (biodiesel), and glycerol as a by-product,[138] see Figure 1.7.

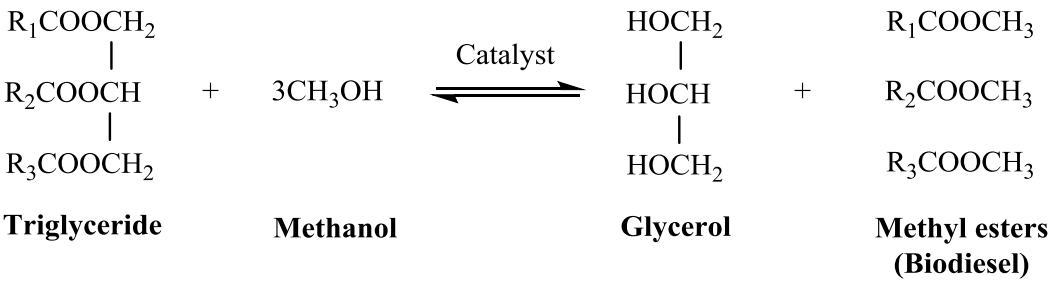

Figure 1.7: General equation for transesterification of triglyceride to biodiesel.[139]

In the past, before the invention of electric lights and even gas lights, vegetable oils and animal fats were commonly applied in oil lamps for lighting in late 18th century.[140] However, using vegetable oils and animal fats to produce biodiesel did not happen until 1930s.[141] The idea of using vegetable oil to power diesel engine was first introduced by the German engineer Rudolf Diesel who invented the eponymous compression-ignited diesel engine in 1893.[141] He implied that pure vegetable oil could be used as a fuel to run machines for agriculture in remote areas, and thus, farmers could eventually be able to power-up the farm's machinery using their on-site produced fuels.[141] This idea by Rudolf Diesel became first practical in early 20th century, at the 1900 World's Fair held in Paris, when the French Otto Company demonstrated publically their diesel engine running on peanut oil.[142] However, this engineering/scientific breakthrough was passed over due to the later widespread accessibility of petroleum-derived diesel at extremely low price.[141, 142] In spite of this, at that time there was still interests in powering internal combustion engines with vegetable oil.[141] Much research has been carried out to investigate the use of vegetable oils without modification in diesel engine and all concluded that vegetable oils have higher viscosity than petroleum-derived diesel, and this is the main disadvantage preventing the direct use of vegetable oils in diesel engines.[141-144] Therefore, to overcome this negative side of vegetable oils, a number of methods were investigated, for example blending the vegetable oil with petroleum diesel, pre-heating it, and thermochemically cracking the oil.[141, 144] However, none of these methods were fully successful, and finally in 1937, a patent registered by the Belgian scientist George Chavanne under the title of "Procedure for the transformation of vegetable oils for their uses as fuels",[145] which demonstrates the transesterification (alcoholysis) method for breaking down triglyceride molecules (oil and fat) *via*

replacing the glycerin moiety with methanol or ethanol. This patent by George Chavanne[145] was the first introduction of fatty acid methyl esters (biodiesel) production.[142, 143]

The world's first industrial-scale plant to produce biodiesel did not come into operation until 1989, when rapeseed oil was used as a feedstock to produce biodiesel in Asperhofen, Austria.[141] It took over 50 years, since George Chavanne[145] patented the synthesis of biodiesel, to start an industrial-scale plant to produce biodiesel from vegetable oil.[141] This was probably again due to the influence of the widespread use of petroleum diesel at low prices.[141] Therefore, the historical petroleum prices increase after 2001 as well as the global increased attention of energy security promoted biodiesel to a popular alternative fuel on the marketplace.[141]

1.6.2 Production

Using feedstocks to produce biodiesel could raise some problems associated with food security. There are some concerns that increasing demand for food feedstocks by the biodiesel industry will affect the prices of these food feedstocks and steadily became no longer affordable for a given region.[146] This issue can create a competition between food in developing countries and biodiesel in developed countries. Furthermore, lands used to grow food crops may gradually change to grow crops that can be used as a feedstock to produce biodiesel.[146, 147] Therefore, it is necessary to encourage using non-food feedstocks where possible to overcome these potential issues.[147, 148]

To date, the world's current and most common feedstock oils used to produce biodiesel are oils derived from rapeseed, sunflower, soybean, palm, cotton seed, canola and jatropha, with the top used feedstock oils in terms of quantity are those derived from rapeseed and soybean.[147] Rapeseed derived biodiesel is most intensively produced in Europe, whereas soybean derived biodiesel is most intensively produced in the United States.[149] Table 1.9 shows the current major feedstocks used to produce biodiesel in leading biodiesel producing countries.

Table 1.9: Major feedstocks used for biodiesel production in different countries.[135, 150]

Country	Feedstock used for biodiesel production
Europe	Rapeseed oil (>80%), sunflower oil
Spain	Linseed, olive oil
France	Sunflower oil
Italy	Sunflower oil
Germany	Rapeseed oil
Ireland	Animals fats, frying oils
UK	Waste oils
USA	Soybean oil
Canada	Canola oil, animal fat
Brazil	Soybean oil
Argentina	Soybean oil
India	Jatropha oil, neem oil, mahua oil
Indonesia	Palm oil
Malaysia	Palm oil
Australia	Animals fats, rapeseed oil

Figure 1.8 shows the worldwide top biodiesel producing countries, and Table 1.10 shows the average productions and consumptions from 2012 to 2014 in the world's top biodiesel producing countries. Also, it shows the average projections of productions and consumptions by 2024 in these top biodiesel producing countries.

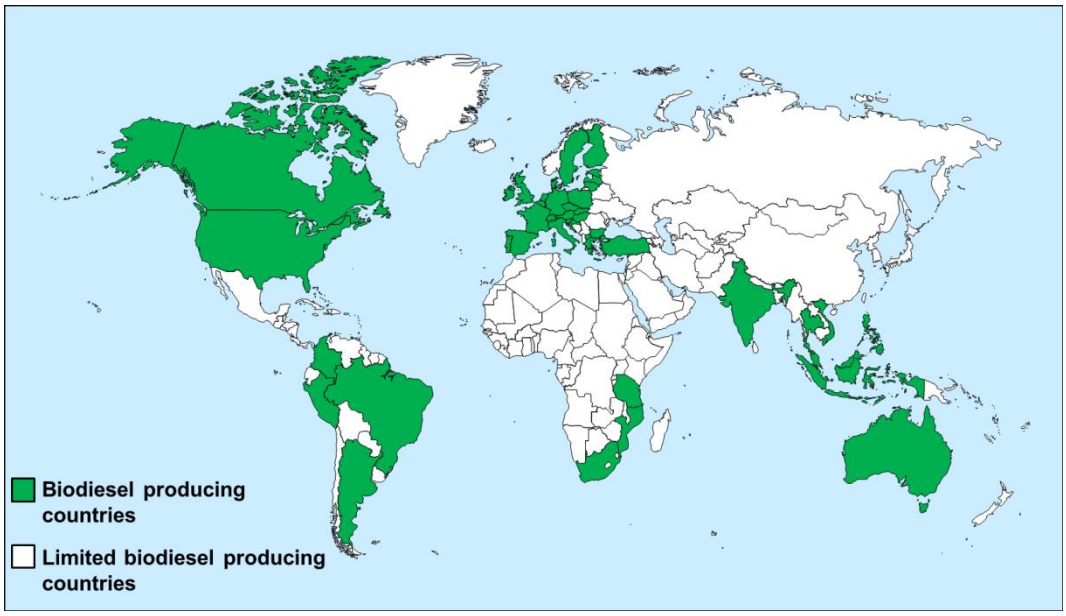

Figure 1.8: Top biodiesel producing countries in 2014.

Table 1.10: Biodiesel average productions and consumptions from 2012 to 2014, and there 2024 projections in the world's top biodiesel producing countries.[151]

	PRODUCTION (Mln L)		DOMESTIC USE (Mln L)	
	Average 2012-14est[a]	2024	Average 2012-14est[a]	2024
NORTH AMERICA				
Canada	392	486	538	794
United States	5149	4723	5719	6633
EUROPE				
European Union	11599	13120	13014	13452
of which second generation	52	185	..[b]	..
OCEANIA DEVELOPED				
Australia	63	280	72	276
OTHER DEVELOPED				
South Africa	77	268	77	268
SUB-SAHARAN AFRICA				
Mozambique	74	78	29	42
Tanzania	63	101	6	38

	PRODUCTION (Mln L)		DOMESTIC USE (Mln L)	
	Average 2012-14est[a]	2024	Average 2012-14est[a]	2024
LATIN AMERICA AND CARIBBEAN				
Argentina	2565	2923	1043	1429
Brazil	3118	5094	3119	5070
Colombia	666	968	665	968
Peru	98	108	275	272
ASIA AND PACIFIC				
India	300	792	433	900
Indonesia	2044	6789	1007	5638
Malaysia	240	619	105	294
Philippines	187	281	187	281
Thailand	944	1001	944	1001
Turkey	13	14	13	14
Vietnam	28	145	28	145
TOTAL	27913	38569	27568	38297

[a] Data for 2014 are estimated according to the source.[151]

[b] Not available.

The global average biodiesel production in 2014 was approximately 28 billion litres (Bln L), and this is expected to increase to reach nearly 39 Bln L by 2024. European Union (EU), the United States (US) and Brazil were the world's top leading countries in the average production of biodiesel in 2014 at approximately 11.6, 5.1 and 3.1 Bln L, respectively. However, by 2024, Indonesia is predicted to surpass the US and Brazil to become the second leading biodiesel producer after the EU. In the EU, the Renewable Energy Directive (RED) percentage target of using energy coming from biofuels is expected to reach 7% by 2019.[152] Therefore, within the EU, biodiesel consumption is predicted to rise to its maximum level in 2019 to fulfil the RED target. Argentina and Indonesia were the world's top exporting countries of

biodiesel in 2014 at approximately 1.5 and 1 Bln L, respectively, and they are predicted to continue to dominate biodiesel exports by 2024. Furthermore, EU and the US were the world's leading importing countries of biodiesel in 2014 at approximately 1.4 and 0.6 Bln L, respectively, and they are predicted to remain the only significant biodiesel importers by 2024.

1.6.3 Composition

The fatty acid methyl esters (FAME) composition of biodiesel derived from different feedstocks was previously investigated by many scientists,[153-169] and Table 1.11 shows the fatty acid compositions in both the oil feedstocks and the FAME obtained from these feedstocks, which is commonly assumed that the feedstock's fatty acid compositions remain unaffected after the transesterification reaction.[138]

Table 1.11: Chemical composition of biodiesel FAME produced from various feedstocks.[170]

Oil/Fat	Fatty acid composition % (w/w)							
	12:0 [a]	14:0	16:0	18:0	18:1	18:2	18:3	22:1
Canola	..	..	3-7	1-3	51-70	15-30	5-14	< 2
Coconut	45-53	17-21	8-10	2-4	5-10	1-3	..	..
Corn	..	..	8-17	< 3	20-42	34-66	< 2	..
Cottonseed	..	0.6-1	21-26	2-3	15-22	47-58	..	..
Jatropha	..	..	10-17	5-10	36-64	18-45	..	..
Linseed[163, 167, 170] [b]	..	..	5-7	2-4	19-22	16-24	47-55	..
Olive	..	< 1	8-20	1-4	55-83	4-21	..	..
Palm	..	0.5-2	39-48	4-6	36-44	9-12	..	..
Peanut	..	..	8-14	1-5	35-69	12-43	..	..
Rapeseed	..	..	2-6	1-3	8-60	11-23	5-13	2-60
Safflower[163, 167, 171] [b]	..	..	6-7	2-3	14-18	73-77	..	..
Sesame	..	..	8-12	5-6	36-42	42-48	..	..
Soybean	..	..	8-14	2-5	17-30	48-59	5-11	..

Oil/Fat	Fatty acid composition % (w/w)							
	12:0 [a]	14:0	16:0	18:0	18:1	18:2	18:3	22:1
Sunflower	..	..	5-8	3-7	14-39	48-74	..	..
Tallow (beef)	..	2-6	20-30	15-30	30-45	1-6	< 1.5	..

[a] Number of C: Number of C=C. [b] Data are the range of three sources.

It is clear from Table 1.11 that each feedstock has a distinct distribution of fatty acids, and therefore, the FAME compositional profile of a biodiesel is generally dependent on the feedstock used in the transesterification reactions. For example, the biodiesel produced from soybean feedstocks has relatively higher linoleic acid methyl ester (18:2) than the one produced from palm feedstocks.

1.6.4 Degradation

Biodiesel is typically highly sensitive to autoxidation, unlike normal diesel that is derived from crude oil. The commonly known reason for this poor oxidation stability is that the biodiesel contains high levels of unsaturated fatty acid methyl esters (FAME), particularly polyunsaturated fatty acid (PUFA).[172] The autoxidation process rate of biodiesel is very much dependent on the number and location of methylene-interrupted double bonds (as will be discussed later in Chapter 5), which can eventually increase the biodiesel viscosity, and further can cause the appearance of insoluble deposit that could seriously block fuel filters and injection system of automotive diesel engines.[173] Furthermore, the change to higher acidity and the forming of peroxides as a result of autoxidation reactions could also lead to the corrosion of fuel system parts, destroying rubber joints, and fusion of moving parts.[174]

1.7 Autoxidation Mechanisms of Lipids

Oxidation in lipids can occur by a self-accelerating process called autoxidation.[175] The starting stage normally occurs *via* a slow reaction with oxygen followed by a cycle of chain reactions until the process slows due to depletion of reactants (radicals, lipids, and/or oxygen).[175, 176] The deterioration is motivated by an auto-

catalytic reaction that is well-described in the literature through a free radical chain mechanism.[177-180] The chain mechanism is frequently described by the following four distinct stages: initiation, propagation, chain branching, and termination.[175, 181]

Initiation

The initiation stage involves the formation of lipid free radicals ($R^{\bullet}$) by the reaction of the initial lipid with the dissolved oxygen molecule as in reaction 1.1.[182] The exposure of lipids to oxygen and energy as heat, or UV light can also enhance initiation.[183] Generally, the chain initiation reaction rate is very slow under normal conditions. However, this reaction is temperature dependent and can go noticeably faster with increasing temperature, as well as the presence of transition metal ions catalysis like iron, copper, nickel, manganese, vanadium, cobalt, *etc*.[181, 184]

$$RH + O_2 \longrightarrow R\bullet + HOO\bullet \qquad (1.1)$$

Propagation:

The first propagation stage is the reaction of the lipid free radical ($R^{\bullet}$) with an oxygen molecule to produce a lipid peroxyl radical ($ROO^{\bullet}$), see reaction 1.2.[182] This reaction is very rapid, and the rate is dependent on the free radical's substituents.[175] As soon as the lipid peroxyl radical ($ROO^{\bullet}$) is produced, it can abstract hydrogen from another lipid molecule to produce a lipid hydroperoxide (ROOH) and another new lipid free radical ($R^{\bullet}$), as in reaction 1.3.[182]

$$R\bullet + O_2 \longrightarrow ROO\bullet \qquad (1.2)$$

$$ROO\bullet + RH \longrightarrow ROOH + R\bullet \qquad (1.3)$$

Chain branching:

The chain branching stage starts with the decomposition of lipid hydroperoxides (ROOH) to lipid alkoxyl radical ($RO^{\bullet}$) and hydroxyl radical ($HO^{\bullet}$),[182] since the O-O

bond is the weakest bond in a hydroperoxide ($D_{RO\text{-}OH}$ ~175.7 kJ/mol),[185] see reaction 1.4. However, this reaction is typically slow at ambient temperatures due to the noticeable activation energy, though, it increases strongly at higher temperatures or with traces of metal ions catalysis present.[181] Hydroxyl and lipid alkoxyl radicals are very reactive, so they rapidly abstract hydrogen atoms from a lipid molecule to form an addition lipid free radical which increases the rate of autoxidation,[175] see reactions 1.5 and 1.6.

$$ROOH \longrightarrow RO\bullet + HO\bullet \quad (1.4)$$

$$RO\bullet + RH \longrightarrow ROH + R\bullet \quad (1.5)$$

$$HO\bullet + RH \longrightarrow H_2O + R\bullet \quad (1.6)$$

Termination:

The chain termination reactions will start when the lipid medium has reached a point that consumption of oxygen is significantly limited.[181] As shown in reactions 1.7 and 1.8, the lipid free radical ($R^{\bullet}$) can join another lipid free radical ($R^{\bullet}$) to produce a lipid molecule.[175, 181] Furthermore, the lipid free radical ($R^{\bullet}$) can also join a lipid peroxyl radical ($ROO^{\bullet}$) to produce a lipid peroxide.[175, 181] However, this lipid peroxide is not stable and can simply breakdown to produce further lipid alkoxyl radicals.[181] Nonetheless, the lipid peroxyl radical ($ROO^{\bullet}$) can join another lipid peroxyl radical ($ROO^{\bullet}$) to produce non-radical products,[184] see reaction 1.9.

$$R\bullet + R'\bullet \longrightarrow R - R' \quad (1.7)$$

$$R\bullet + R'OO\bullet \longrightarrow ROOR' \quad (1.8)$$

$$ROO\bullet + R'OO\bullet \longrightarrow \text{Non-radical products} \quad (1.9)$$

Figure 1.9 shows the basic chain reactions for autoxidation in lipids.

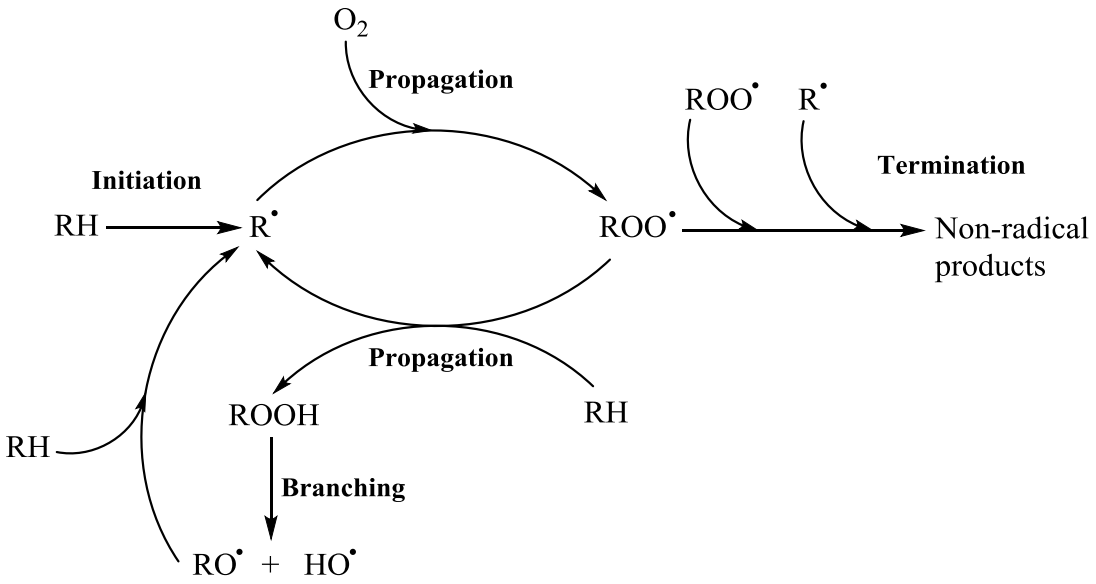

Figure 1.9: Basic chain reactions of autoxidation in lipids.[186, 187]

1.8 Inhibition of Autoxidation by Different Classes of Antioxidants

Oxidation of lipids takes place by the chain reaction mechanism involving the reactions of alkyl ($R^{\bullet}$) and peroxyl ($ROO^{\bullet}$) radicals (as discussed earlier in section 1.7).[186] Hydroperoxides (ROOH) formed during autoxidation reactions can also further decompose into additional radicals hence, increasing the rate of oxidation.[186] Therefore, the oxidation of lipids can be inhibited chemically by any of the following three ways:

- Breaking the oxidation chains by the destruction of peroxyl ($ROO^{\bullet}$) radicals by reaction with $ROO^{\bullet}$ radical scavenging antioxidants (chain breaking donor antioxidants).
- Breaking the oxidation chains by the destruction of alkyl ($R^{\bullet}$) radicals by reaction with $R^{\bullet}$ radical scavenging antioxidants (chain breaking acceptor antioxidants).
- Reducing the rate of chain branching by the destruction of hydroperoxides (ROOH) by reaction with peroxide decomposing antioxidants.

1.8.1 Breaking the oxidation chains by the reaction with peroxyl ($ROO^{\bullet}$) radicals

This class of radical scavenging antioxidants includes hindered phenols, aromatic amines and aminophenols, all of which are reductive agents[187] with relatively weak O-H and N-H bonds, which readily donate hydrogen atoms to peroxyl ($ROO^{\bullet}$) radicals to break the autoxidation chain reactions cycle and form relatively stable intermediate radicals giving rise to a number of molecular products that can also help inhibit autoxidation.[186, 187]

Generally, the most common examples of this type of antioxidant are phenolic and aminic antioxidants, where these are known to have low O-H and N-H bond dissociation energies (BDEs), lower than the C-H BDE of the corresponding lipid molecule and hence favorably react with peroxyl ($ROO^{\bullet}$) radicals formed during the autoxidation of lipids. By the reaction of radical scaveners with peroxyl radicals, the propagation reactions in autoxidation will be broken, therefore breaking the autoxidation chain cycle and hence preventing the lipid molecules from being substantially oxidised, as shown in Figure 1.10.

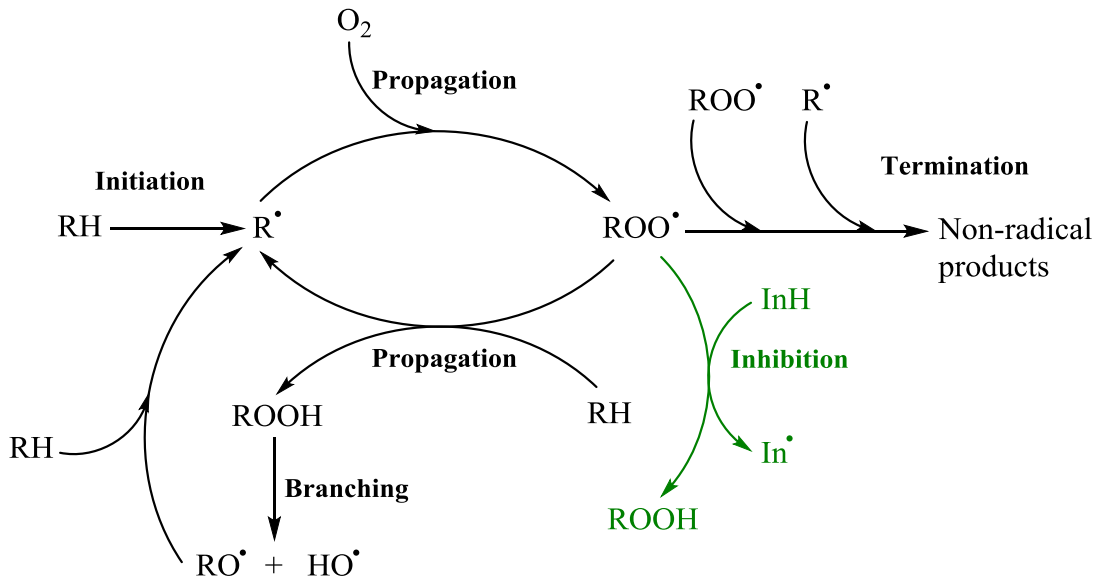

Figure 1.10: Autoxidation degradation cycle and chain breaking mechanism by radical scavenging antioxidant.[187]

With regards to the phenolic type antioxidant, the hydrogen atom abstraction by a peroxyl ($ROO^{\bullet}$) radical will lead to the formation of a phenoxyl radical (reaction i in Figure 1.11). The phenoxyl free radical will be resonance stabilised *via* the phenoxyl aromatic ring (reaction ii in Figure 1.11). A second peroxyl ($ROO^{\bullet}$) radical can then react with the resonance stabilised structure to form a peroxide molecule (reaction iii in Figure 1.11).[188, 189] Thereby, one phenol antioxidant can, ideally, remove two peroxyl ($ROO^{\bullet}$) radicals from the system, *i.e.* it has a stoichiometric inhibition coefficient (f) of two.

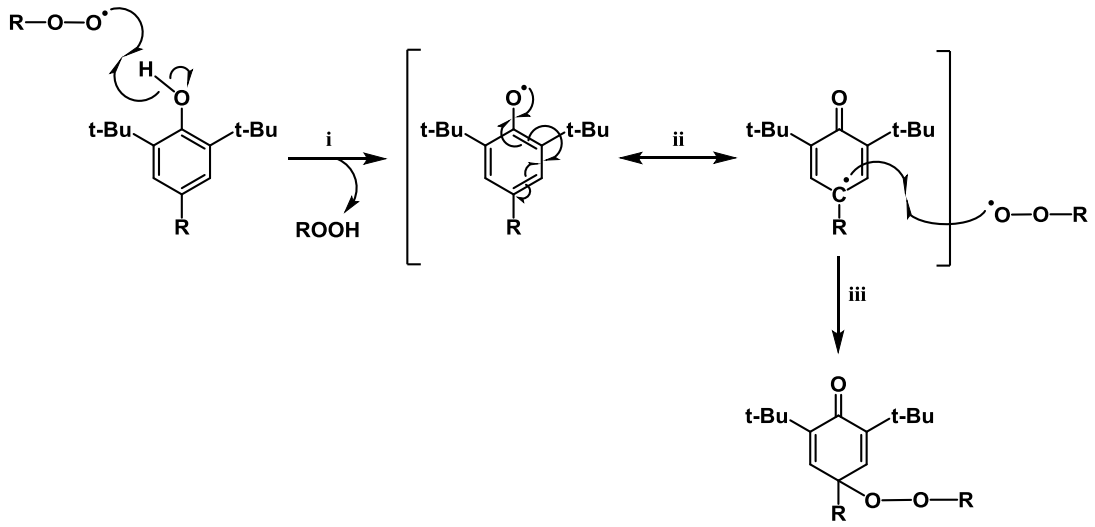

Figure 1.11: The well-known mechanism of a hindered phenolic antioxidant action.[190]

For aminic antioxidants, such as diphenylamine,[191] it uses a comparable mechanism to the phenolic radical scavenging antioxidant, where initially a peroxyl radical abstracts the weakest hydrogen (the N-H bond in a diphenylamine) to form a diphenylaminyl radical (reaction i in Figure 1.12), and the latter can further react with another peroxyl radical leading to the formation of a peroxide molecule (reaction ii in Figure 1.12).[192] Therefore, one diphenylamine antioxidant can inhibit the propagation of two autoxidative chain reactions and hence, it has a stoichiometry coefficient of two.[191]

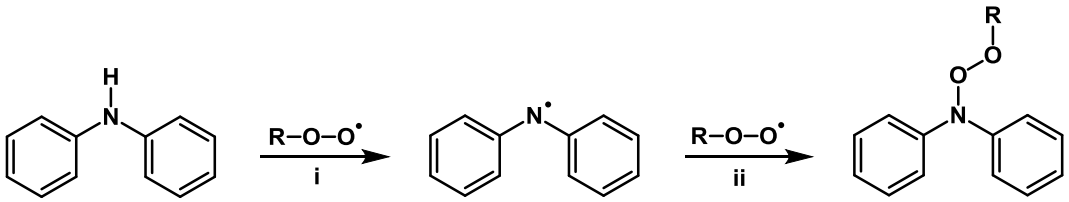

Figure 1.12: The well-known radical scavenging mechanism of diphenylamine antioxidant.[191-193]

The stoichiometric inhibition coefficient (f) of antioxidants measures the number of oxidation chains that are broken by one molecule of an antioxidant *via* reactions of chain carriers with antioxidant molecules.[194] Table 1.12 shows the experimentally measured stoichiometric inhibition coefficient (f) of some key phenolic antioxidants.

Table 1.12: Measured stoichiometric inhibition coefficient (f) per one molecule of some key phenolic antioxidants.

Antioxidant	Solvent	Temp. (°C)	f	Ref.
Phenol	Chlorobenzene	62.5	2.0	[195]
BHT	Cumene / chlorobenzene	50	2.0	[196]
Catechol	Styrene / chlorobenzene	37	2.1 ± 0.2	[194]
Caffeic acid	Styrene / chlorobenzene	37	1.5 ± 0.1	[194]
Gallic acid	Styrene / chlorobenzene	37	1.0 ± 0.1	[194]
Catechin	Cumene / chlorobenzene	50	1.7	[196]
α-tocopherol	Cumene / chlorobenzene	50	2.0	[196]

In principal, the addition of the second peroxyl ($ROO^{\bullet}$) radical with respect to the phenoxyl aromatic ring can be in *ortho*- and *para*-positions where the density of the unpaired electron is considerable.[197] The ratio of probabilities for the peroxyl radical

recombination in either position is dependent on the nature of the substituents in the phenoxyl radical. For example, in case with 2,4,6-tri-*tert*-butylphenol (TTBP; Figure 1.13), both *ortho*-positions and the *para*-position of the phenol aromatic ring are occupied by the same bulky substituent and, therefore, the ratio of probabilities of the peroxyl radical recombination in *ortho*-position over the *para*-position is approximately 0.25.[197]

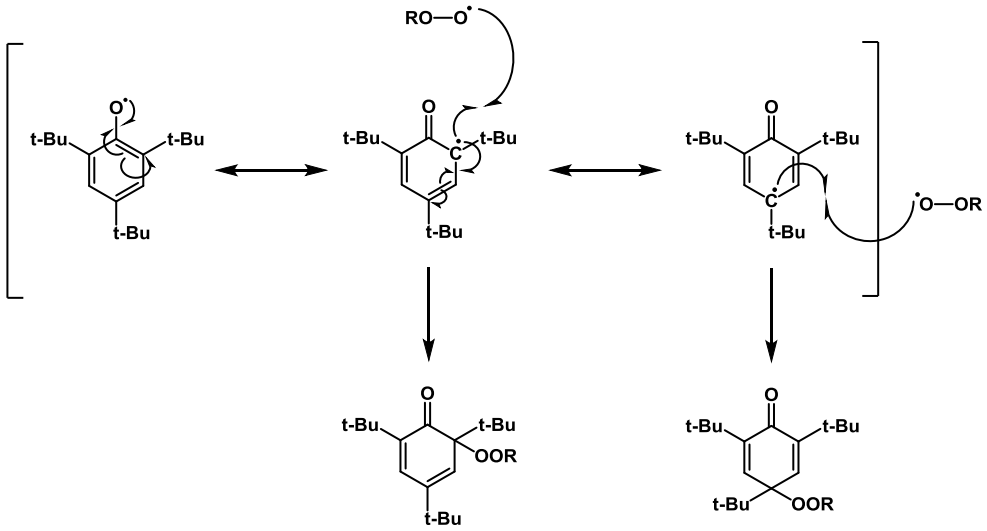

Figure 1.13: *Ortho*- and *para*-quinolide peroxides formation in the case of 2,4,6-tri-*tert*-butylphenol (TTBP).[197]

Moreover, in the case with 2,6-di-*tert*-butyl-4-methylphenol (BHT), its *para*-position is occupied by a non-bulky substituent (-CH_3) and, therefore, this ratio of probabilities of the peroxyl radical recombination in *ortho*-position over the *para*-position falls to 0.01, indicating recombination, in this case, at *para*-position is more dominant.[197] However, in the case with 4,6-di-*tert*-butyl-2-methylphenol, one of the *ortho*-positions is occupied by a non-bulky substituent (-CH_3) and, thus, peroxyl radical recombination, in this case, is found to be more dominant at this *ortho*-position.[197] Therefore, from the last two examples, it can be denoted that a peroxyl radical recombines predominantly at a position bearing no bulky substituent.

These peroxyl-antioxidant adducts can, eventually, decompose to form two alkoxyl-like radicals (reaction i in Figure 1.14), with the antioxidant-derived alkoxyl radical losing an alkyl radical to form a quinone (reaction ii in Figure 1.14).[198, 199]

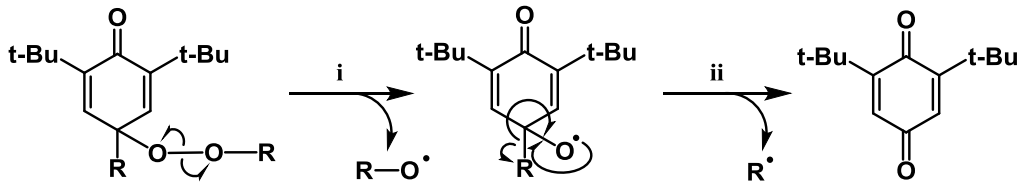

Figure 1.14: The decomposition of peroxyl-antioxidant adducts to form a quinone.[197, 200]

Additionally, the quinone formed is thought to have the ability to further react with both alkyl ($R^{\bullet}$) and peroxyl ($ROO^{\bullet}$) radicals.[186, 201] However, due to the presence of oxygen and the fact that these reactions are relatively slower when compared to the reaction of alkyl radical with oxygen and/or the reaction of peroxyl radical with either an antioxidant or a lipid molecule, these reactions are believed to have little contribution during the autoxidation of oxygen-saturated substrates.[202]

The primary oxidation products of hindered phenols were found to be stable in the absence of oxygen but, in the presence of oxygen, most further react rapidly by addition of dioxygen to form peroxyl ($ROO^{\bullet}$) radicals.[203] Therefore, this antioxidant-derived peroxyl radical was found to react irreversibly with another phenoxyl radical to form a quinolide peroxide.[186, 203] An example for this was studied for the 2,4,6-tri-*tert*-butylphenoxyl radical,[204] see Figure 1.15.

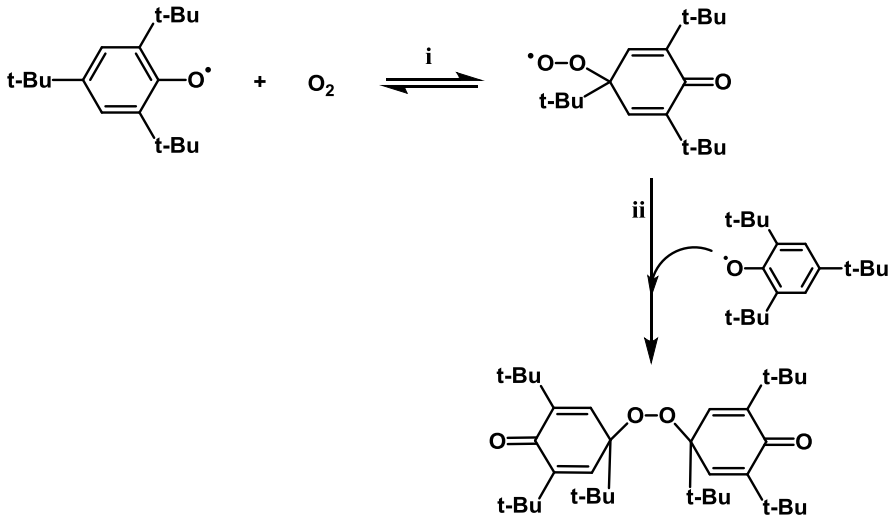

Figure 1.15: The reaction of a hindered phenoxyl radical with dioxygen and the formation of quinolide peroxide.[186, 204]

The substituents of a phenoxyl radical can dramatically influence the mechanism of self-reactions in the presence of oxygen.[186] If the *para*-position of a phenoxyl radical is free, no dioxygen is added and, instead, these phenoxyls recombine to form a C-C unstable dimer.[205] This denotes that an unhindered phenoxyl radical will self-react rapidly and not react with oxygen.[205] An example for this was studied for 2,6-di-*tert*-butylphenoxyl radical,[206] see Figure 1.16.

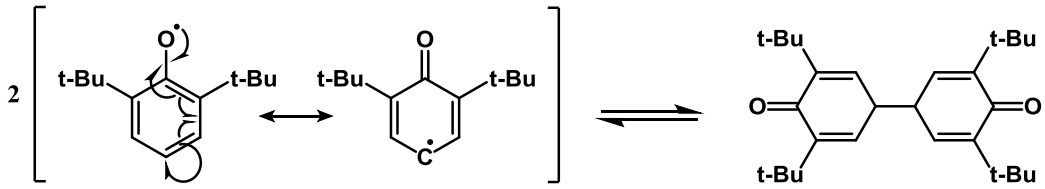

Figure 1.16: Recombination of 2,6-di-*tert*-butylphenoxyl radicals with the formation of C-C dimer.[206]

Other reported recombination mechanism of hindered phenoxyl radicals is the formation of C-O unstable dimer (reaction ia in Figure 1.17).[207] This C-O unstable dimer has been proposed to further decay to form a hindered phenol and a methylenequinone (reaction iia in Figure 1.17).[208, 209] The same products have also been proposed to form by direct disproportionation of hindered phenoxyl radicals (reaction ib in Figure 1.17).[210]

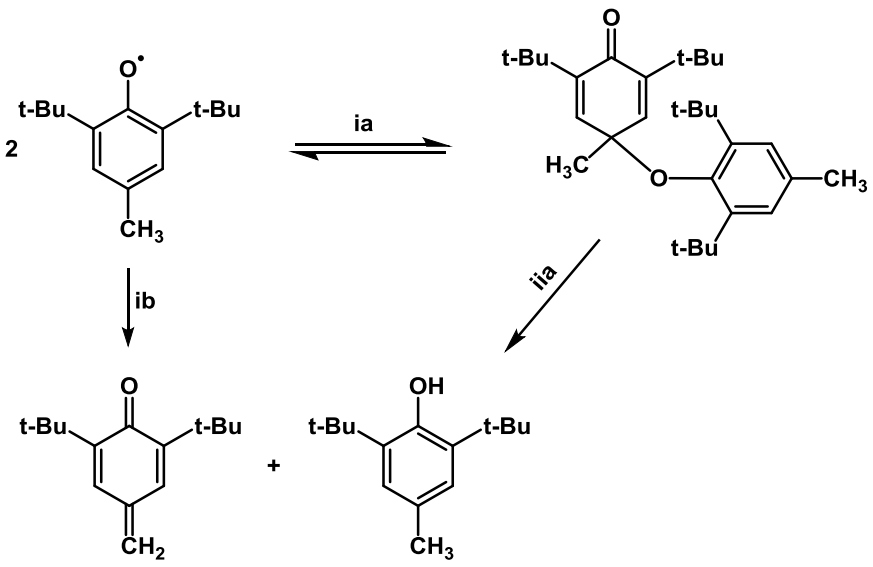

Figure 1.17: The two proposed ways for the formation of a quinonemethide and BHT from 2,6-di-*tert*-butyl-4-methylphenoxyl radicals.[208-210]

In addition, further studies on the oxidation of BHT have shown the formation of stilbene quinone and a very stable radical product, namely galvinoxyl.[211, 212] The chemical structures of these two oxidation products of BHT are provided in Figure 1.18.

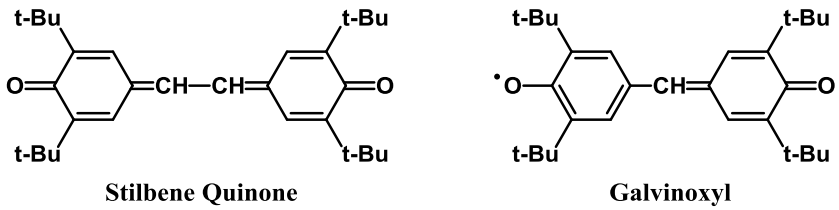

Figure 1.18: The chemical structures of stilbene quinone and galvinoxyl.

The detailed mechanisms of these reactions are still somewhat obscure.[203] Some studies[213-215] interpret the stilbene quinone formation from BHT to the dimerization of a benzyl radical to ethylene bisphenol (reaction ii in Figure 1.19), and the latter is oxidized easily to the stilbene quinone (reaction iii in Figure 1.19).

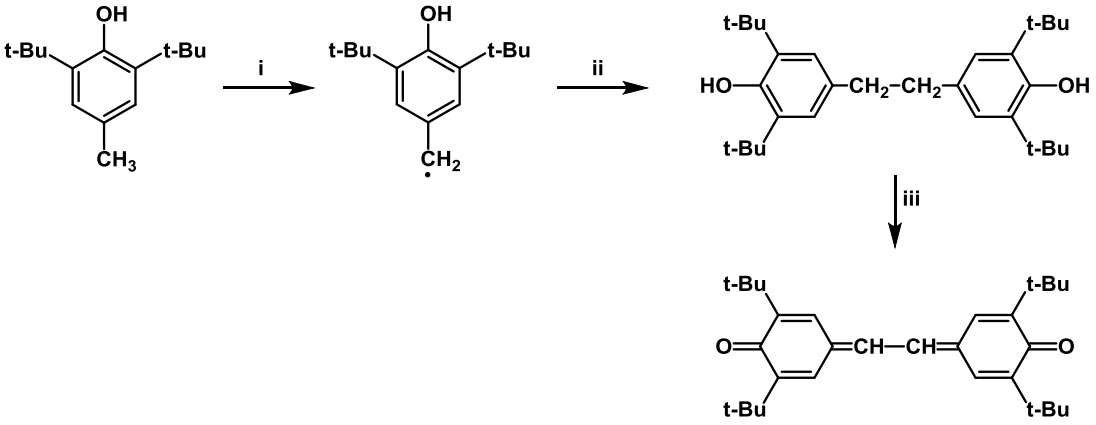

Figure 1.19: The suggested mechanism for the formation of stilbene quinone from BHT through the dimerization of benzyl radicals.[213-215]

However, there is uncertainty about the possible mechanism towards the benzyl radical formation. In the case of BHT, it has been suggested[213, 216] that a benzyl radical forms as a result of side-chain attack at the *para*-methyl group, while another[215] suggests its formation is as a result of intramolecular rearrangement of the phenoxyl radical.

Nonetheless, a later study by Becconsall and co-workers[217] have reviewed the hypothesis about possible formation of benzyl radicals, and concluded that both stilbene quinone and galvinoxyl are products from the simultaneous dimerisation and rearrangement of phenoxyl radicals, as proposed in Figure 1.20. Their conclusion is based on the absence of spectral evidence for the formation of the benzyl radical or even the benzyl phenyl ether from the reaction of BHT.[217] However, absence of evidence of benzyl radical cannot be taken as evidence of absence, it may, for instance, be due to limitations in the spectroscopy technique used.

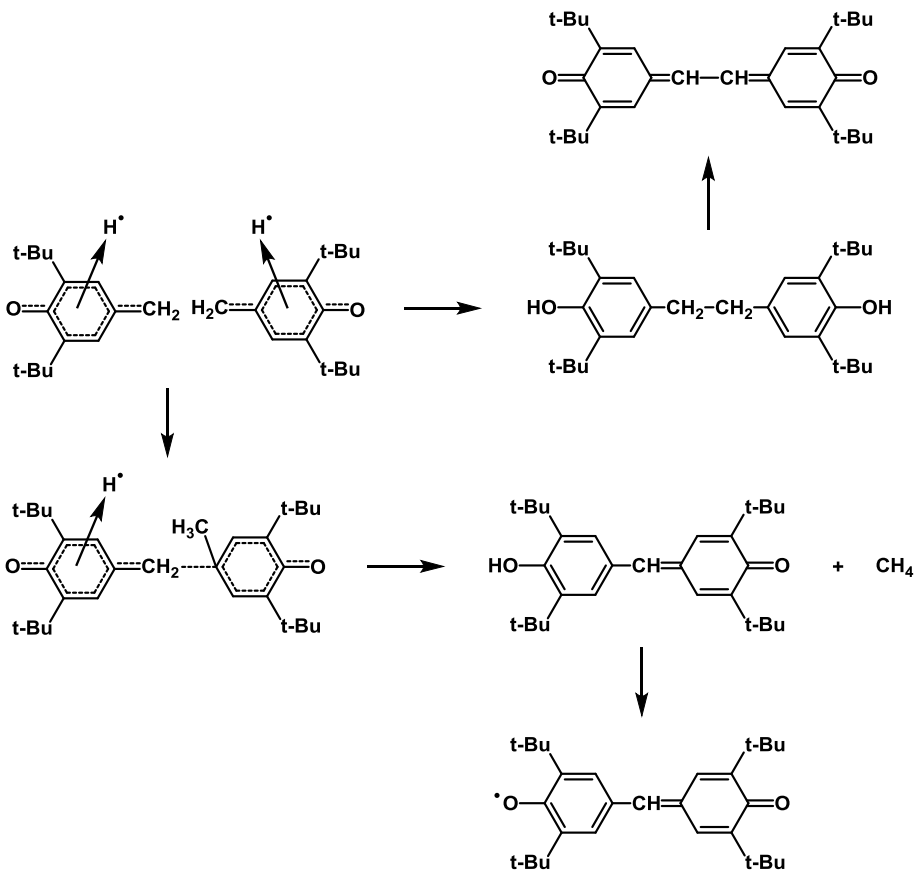

Figure 1.20: Proposed mechanisms of the formation of stilbene quinone and galvinoxyl from the simultaneous dimerisation and rearrangement of 2,6-di-*tert*-butyl-4-methylphenoxyl radicals.[217]

Other reported mechanistic path way for the formation of stilbene quinone is through the formed methylenequinone that is described earlier in Figure 1.17. Methylene-quinones are known for their high chemical activity and, when formed from BHT, they spontaneously dimerise to form stilbene quinone and ethylene bisphenol,[218, 219] as shown in Figure 1.21.

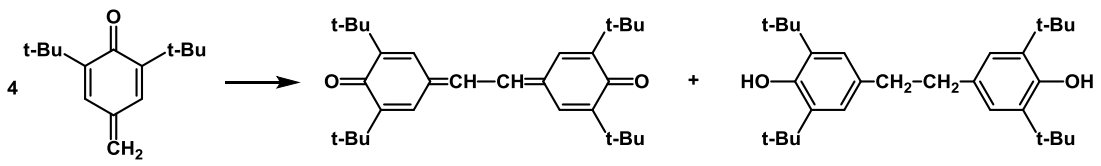

Figure 1.21: The dimerization of methylenequinone to stilbene quinone and ethylene bisphenol.[218]

1.8.2 Breaking the oxidation chains by the reaction with alkyl ($R^{\bullet}$) radicals

This class of antioxidants includes quinones, iminoquinones and methylenequinones. These are oxidising agents,[187] which can terminate the autoxidation chain reactions by readily accepting alkyl ($R^{\bullet}$) radicals.[186] These are more efficient at comparatively low concentration of O_2 and in solid polymers.[186, 187] In addition to the low O_2 concentration requirement for a good activity for this class of antioxidants, the structure of the autoxidising substrate is also important.[220] The more stable the alkyl radical generated during the autoxidation chain reactions, the better will be the chance of this type of antioxidant to break the oxidation chain *via* deactivating these stable alkyl radicals under O_2 deficient conditions.[220]

Quinones are well known for their tendency to effectively inhibit polymerization by trapping alkyl ($R^{\bullet}$) radicals, as shown in reactions ia and iia of Figure 1.22.[187] However, quinones can only act as efficient antioxidants if they can compete with oxygen for the reaction with alkyl radicals (as ib of Figure 1.22) and, hence, the important requirement of low oxygen concentration in the system.[187]

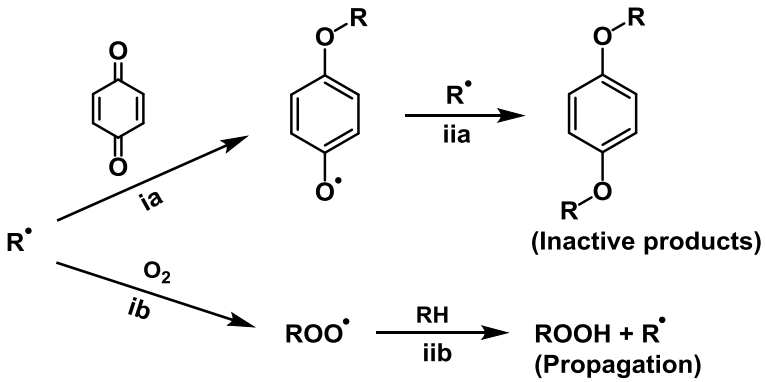

Figure 1.22: The reactions of alkyl radical with: ia) benzoquinone; ib) dioxygen.[221-223]

1.8.3 Reducing the rate of chain branching by the reaction of hydroperoxides with peroxide decomposing antioxidants

This class of peroxide decomposing antioxidants includes phosphites and sulfides which can decompose hydroperoxides (ROOH) *via* a process that does not give rise to free radicals.[187] Hydroperoxides are believed to be the major source of further free radicals in an autoxidation system and they are the most significant primary products

formed during the cyclical autoxidation process (as discussed earlier in section 1.7).[187]

Phosphite esters and sulfur-containing compounds are the two main classes of peroxide decomposers.[187] Phosphite esters, can generally decompose hydroperoxides (ROOH) stoichiometrically, while sulfur-containing compounds, can act by catalytically decomposing hydroperoxides.[187] Simple phosphite esters, such as triaryl or trialkyl phosphites, are widely used as inhibitors of oxidation.[186] They function mainly by reducing hydroperoxides to alcohols by the following stoichiometric reaction (1.10):[187]

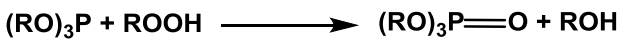

Furthermore, the sulfur-containing compounds, such as simple aliphatic sulfides and some metal-sulfur complexes, are widely used to inhibit the oxidation of lubricants. The metal-sulfur complex antioxidants have the ability to function well even at very high temperatures (>150 °C) and, hence, most modern lubricating oils contain zinc dialkyl dithiophosphate (ZDDP, Figure 1.23), which is an important stabilizing component.[186, 224]

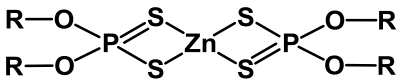

Figure 1.23: The chemical structure of zinc dialkyl dithiophosphate (ZDDP).

The mechanism of action of these sulfur-containing antioxidants primarily involves their reactions with hydroperoxide (ROOH). The chemistry of this is complex, however, the products formed during a series of reactions, especially sulfur acids, are thought to contribute much more significantly in further destroying hydroperoxides.[224]

Nonetheless, transition metal compounds, such as copper and iron, are well known for their ability to accelerate oxidation by increasing the rate of hydroperoxide

(ROOH) decomposition and, thus, forming additional free radicals that increases the rate of oxidation,[186] as the following reactions (1.11 and 1.12):[187]

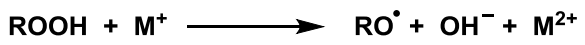

(1.11)

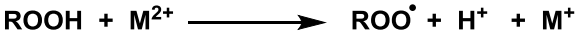

(1.12)

Therefore, this accelerated oxidation by transition metals can be prevented by the addition of what is commonly known as metal deactivators. These compounds, such as diamines, interact with metal ions to yield complexes that are inactive towards hydroperoxides.

1.9 Commercial Radical Scavenging Antioxidants

1.9.1 Phenolic antioxidants

Many researchers have found that synthetic antioxidants can be effective by increasing the oxidation stability of biodiesel.[225-228] Most antioxidants previously investigated to improve the biodiesel oxidation stability have been phenolic-type antioxidants.[174, 229, 230] Table 1.13 shows the most common reported synthetic phenolic antioxidants for use in biodiesel.

Table 1.13: Some common synthetic phenolic antioxidants previously investigated for improving the oxidation stability of biodiesel.

Name	Abbreviation	Structure	Ref.
Butylated hydroxyanisole	BHA	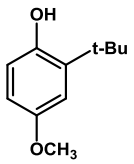	174, 229
Butyl-4-hydroxytoluene	BHT	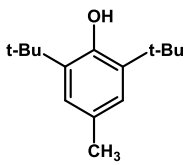	174, 229, 230

Name	Abbreviation	Structure	Ref.
Tert-butyl-hydroquinone	TBHQ	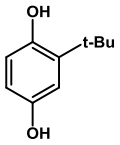	174
2,5-Di-tert-butyl-hydroquinone	DTBHQ	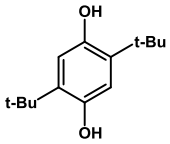	174
Propyl gallate	PG	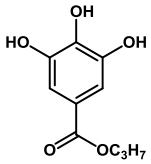	174
Pyrogallol	PY	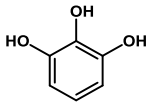	174
2,2′-Methylene-bis-(4-methyl-6-tert-butylphenol	Bis-BHT	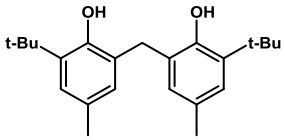	230
2,6-Di-tert-butylphenol	DTBP	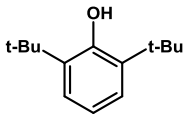	229
2,4,6-Tri-tert-butylphenol	TTBP	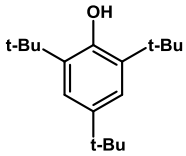	229

Tang *et al.*[174] have evaluated the effectiveness of different synthetic antioxidants, such as butylated hydroxyanisole (BHA), butylated hydroxytoluene (BHT), *tert*-butylhydroquinone (TBHQ), 2,5-di-*tert*-butylhydroquinone (DTBHQ), ionol BF200 (IB), propylgallate (PG), and pyrogallol (PY), to improve the oxidative stability of various sources of biodiesel. Soybean derived biodiesel was one biodiesel sample tested by Tangs *et al.*[174] which has significant levels of unsaturated fatty acids methyl esters (FAME), mainly methyl linoleate (C18:2) and methyl linolenate (C18:3). This high content of unsaturated FAME is believed to be the cause of making the

biodiesel more sensitive to oxidation than petroleum-derived diesel and hence gives low induction times (the time lag until the autoxidation starts).[231, 232] The soybean-based biodiesel seems to be the most interesting sample in Tangs *et al.*[174] work. They found that the addition of 1,000 ppm PY in the pure soybean-based biodiesel gives the highest induction period, followed by TBHQ and PG.

Furthermore, Ingendoh[230] has also used synthetic antioxidants to improve oxidation stability and shelf life of rapeseed-based biodiesel. He found that BHT has more significant effects on the induction time of rapeseed-based biodiesel than soybean-based biodiesel. The addition of 200 ppm of BHT in distilled rapeseed-based biodiesel showed an increase in induction time by four hours, and by eight hours with double dosage (400 ppm) of BHT.[230] He also noticed that the addition of BHT at higher concentrations more than 1,000 ppm did not show any increase of distilled rapeseed-based biodiesel induction time (at 14 hours). Even with 2,000 or 3,000 ppm BHT he did not noticed any increase with induction times more than 14 hours.

Souza *et al.*[229] have also investigated the effects of three antioxidants (butylated hydroxyl anisole (BHA), 2,6–di-*tert*-butyl-4–methylphenol (BHT) and the mixture 2,6–di-*tert*-butylphenol (DTBP) + 2,4,6–tri-*tert*-butylphenol (TTBP) on the oxidative stability of soybean biodiesel. According to Souza *et al.*,[229] the addition of these three antioxidants (at 500 ppm) improved the thermo-oxidative stability of soybean biodiesel, and with increasing the dosage of antioxidant (to 1000 ppm), they also observed an increase of biodiesel oxidative stability. Between the three investigated antioxidants using the Rancimat method,[233] the BHT antioxidant addition showed the highest oxidative stability followed by BHA and the mixture DTBP + TTBP.

1.9.2 Aminic antioxidants

The other well-known type of antioxidant is the aminic-type antioxidant. The aminic-type antioxidants can act similarly to the phenolic-type antioxidants in hindering the oxidation cycle of biodiesel, however, these aminic antioxidants are less common for use in biodiesel than the phenolic-type antioxidants.[234] Table 1.14 shows some common reported aminic antioxidants for use in biodiesel.

Table 1.14: Some synthetic aminic antioxidants previously investigated for use in biodiesel.

Name	Abbreviation	Structure	Ref.
Octylated/butylated diphenylamine	O/BDPA	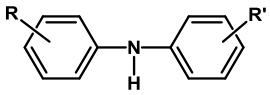	235
N,N′-di-sec-butyl-*p*-phenylenediamine	PDA	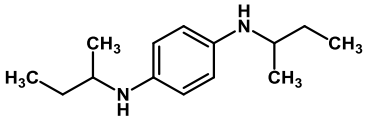	236, 237
N-Phenyl-1-naphthylamine	PANA	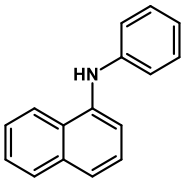	237
Ethoxyquin	EQ	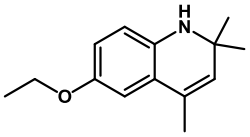	237

Sarin *et al.*[235] have investigated the effect of an aminic antioxidant (octylated butylated diphenyl amine) for improving the oxidation stability of biodiesel derived from variety of feedstocks. Based on Sarin *et al.*[235] work, a dosage of 200 ppm of the aminic antioxidant was doped in Jatropha, Karanjia, Sunflower and Soybean based biodiesels and tested in Rancimat to evaluate the effectiveness of the aminic antioxidant. According to Sarin *et al.*,[235] the aminic antioxidant was partially effective with Jatropha based biodiesel, however, interestingly, not effective with Soybean based biodiesel.

Furthermore, Chen and Luo[236] have also studied the effect of another aminic antioxidant (N,N′-di-sec-butyl-*p*-phenylenediamine (PDA)) on the oxidation stability of biodiesel derived from free fatty acids (FFAs) using Rancimat standard (EN 14112). According to Chen and Luo,[236] the effectiveness of the aminic antioxidant (PDA) at 1000 ppm on the oxidation stability of the FFA-based biodiesel was similar to a phenolic antioxidant (BHA).

Subroto *et al.*[237] have investigated the effect of a number of antioxidants (including the aminic-type) on the oxidation stability of oils extracted from Jatropha seeds by an accelerated oxidation test described as EN 14112 using the Rancimat equipment.[233] According to Subroto *et al.*,[237] pure Jatropha oil without an antioxidant added has an induction period (IP) of 1.6 hours, however, after the addition of three aminic-type antioxidants, namely N,N′-di-sec-butyl-*p*-phenylenediamine (PDA), *N*-Phenyl-1-naphthylamine (PANA), and Ethoxyquin (EQ), at a concentration of 500 ppm, the results by Subroto *et al.*[237] showed that the oxidative stability of the pure Jatropha oil increased to the IPs of 5.8, 3.7 and 2.7 hours, respectively. Nonetheless, the effects of these three aminic-type antioxidants on the pure Jatropha oil were insignificant in the investigation of Subroto *et al.*.[237] According to Subroto *et al.*,[237] the effects of two phenolic-type antioxidants, Pyrogallol (PY) and Propyl gallate (PG), were more significant, where remarkably their addition at the concentration of 500 ppm in Jatropha oil increased its IP to 27.3 and 22.5 hours, respectively.

1.10 Biomass-Derived Antioxidants

Most currently used antioxidants are derived or synthesised from petroleum which is expensive and its reserves are limited and gradually being exhausted. Thus, this situation led some research groups to be interested in finding low cost antioxidants derived from cheap renewable resources.[238] Therefore, to impose reorientation of antioxidants from fossil fuels to renewable resources, more investigation is needed on antioxidants from easily accessible biomass that does not compete with food use. To date, limited studies have investigated antioxidants from natural resources for use in fuels, in particular biodiesel.[239, 240] But, on the other hand, numerous papers have been published on the investigation of synthetic antioxidants, such as butylated hydroxytoluene (BHT), for preventing the oxidative degradation of biodiesel.[174, 225, 226, 229, 230, 241-243] Table 1.15 summarizes some previous investigations on renewable antioxidants from natural resources for use in fuels or lubricants.

Table 1.15: Some previous investigations on renewable antioxidants from biomass for use in fuels or lubricants.

Sector	Antioxidant name	Antioxidant structure	Source	Ref.
Fuel & lubricant (gasoline and lubricating materials)	Mixture of: 2-methoxyphenol;	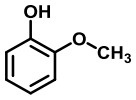	Waste product from wood hydrolysis	244
	2.6-dimethoxy-phenol;	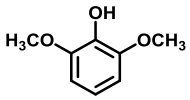		
	3-hydroxy-4-methoxy-benzaldehyde (vanillin) and	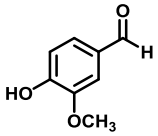		
	1-(4-hydroxy-3-methoxyphenyl) ethanone	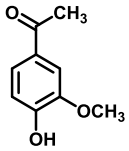		
Fuel (biodiesel)	α-tocopherol	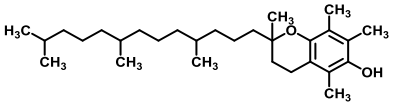	Sigma-Aldrich (derived from vegetable oil)	174, 240
Lubricant (mineral oils)	Thio-phosphorylated cardol	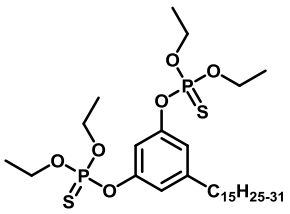	Synthesised from CNSL cardol	245
Fuel (methyl linoleate)	Ferulic acid,	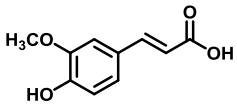	Models for phenolics in softwood and hardwood	246
	Syringaldehyde,	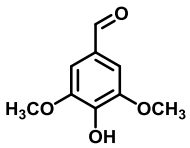		
	Vanillin alcohol	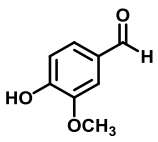		

Sector	Antioxidant name	Antioxidant structure	Source	Ref.
Fuel (biodiesel)	Mixed-phenolics	N/A[a]	Jatropha extracted with methanol	[240]
Fuel (biodiesel)	Curcumin	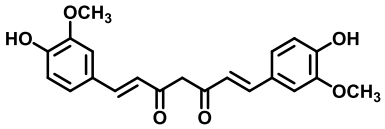	N/A	[239]
Polymers (also, for use in lubricating and diesel oil)	Ester derivatives of rosmarinic acid	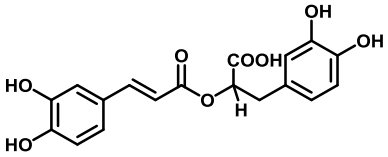	Commercial rosemary extract (93% rosmarinic acid)	[247]

[a] Not available from the source.

Vasileva *et al.*[244] have investigated a phenolic antioxidants mixture, produced by alkaline destruction of lignin, for use in gasoline and lubricating materials. The phenolic mixture is believed to be consisting of 2-methoxyphenol; 2.6-dimethoxyphenol; 3-hydroxy-4-methoxybenzaldehyde (vanillin) and 1-(4-hydroxy-3-methoxyphenyl) ethanone (their structures are presented in Table 1.15). According to Vasileva *et al.*,[244] the anti-oxidation test is carried out at 120 °C by the investigation of oxygen adsorption in a laboratory manometric installation. The anti-oxidation effect of the methoxyphenolic mixture is compared to the commercial antioxidant butylated hydroxytoluene (BHT). According to their results, the methoxyphenolic mixture antioxidant effect on liquid paraffin is comparable to the commercial antioxidant BHT at the concentration of 10 ppm.

Tang *et al.*[174] have also included one natural antioxidant (α-tocopherol) in their investigation of various synthetic antioxidants to improve the oxidation stability of biodiesel. According to Tang *et al.*,[174] the stability tests are determined according to the biodiesel industrial testing standard Rancimat method (EN 14112).[233] The selected antioxidants are added to four different feedstock-based biodiesel (soybean oil, cottonseed oil, poultry fat and yellow grease) at varying concentrations between 250 and 1,000 ppm. According to their results, the natural antioxidant α-tocopherol

addition has the least effect in increasing the induction time of the all different types of biodiesel when compared to the other synthetic antioxidant.

Maia *et al.*[245] have synthesised a new thiophosphorylated compound from cardol: long-chain phenolic compounds extracted from cashew nut shell liquid (CNSL). They investigated this compound for its antioxidant activity in mineral oil by using an accelerated oxidation experiment (PetroOXY, Germany) at 140 °C to measure the induction time. According to their results, the addition of this new compound to mineral naphthenic oil at a concentration of 1% (w/w) increased the induction time to approximately 20 hours, whereas the same concentration addition of the commercial antioxidant BHT increased the mineral oil induction time to about 13 hours.

Salehi *et al.*[246] have studied the oxidation process of methyl linoleate at 70 °C alone and in combination with 20% (w/w) of lignin model compounds. The effects of these compounds on methyl linoleate are monitored by NMR (both ^{13}C and ^{1}H) and FT-IR. According to their results, the phenolic lignin models (ferulic acid, syringaldehyde and vanillin alcohol) are capable of slowing down the methyl linoleate oxidation cycle by acting as radical scavengers.

El Diwani *et al.*[240] have also investigated the protection of Jatropha biodiesel from oxidative degradation by adding natural antioxidants. According to their work, α-tocopherol and natural Jatropha root extract were investigated using thermal oxidation at 60 °C and analysed using 2,2-diphenyl-1-picrylhydrazyl (DPPH) radical method, and the results compared to the synthetic antioxidant BHT. According to their results, by using 2,2-diphenyl-1-picrylhydrazyl (DPPH) radical method for oxidation analysis, the addition of natural Jatropha root extract at 400 ppm (of BHT equivalent, measured by Folin-Ciocalteu assay) to Jatropha biodiesel is capable to hold the biodiesel degradation up to 6 hours, whereas, in comparison, α-tocopherol and the synthetic antioxidant (BHT) are less effective in stabilising the Jatropha biodiesel at 60 °C.

Leanne de Sousa *et al.*[239] have also used a natural phenolic compound (curcumin) to study its antioxidant activity in soybean biodiesel. According to their study, samples of soybean biodiesel are doped with curcumin at three concentrations (500, 1000, and 1500 ppm) and stored at 25 °C in dark glass to monitor their oxidative process

by the industrial testing standard Rancimat method every 30 days for 180 days. According to de Sousa *et al.*,[239] the addition of curcumin at the concentration of 1500 ppm to soybean biodiesel increased the induction period to 83%, and curcumin addition at the concentration of 1000 ppm is enough to keep the oxidation induction time of soybean biodiesel above the minimum requirement by law (6 hours at 110 °C) for at least 180 days at the storage temperature of 25 °C.

Doudin *et al.*[247] have introduced several ester derivatives (rosmarinates) of rosmarinic acid derived from rosemary plant for use as antioxidants to stabilise polymers. According to Doudin *et al.*,[247] the new rosmarinates esters were synthesised from a rosmarinic acid (its chemical structure is presented in Table 1.13) obtained from a commercial rosemary extract (AquaROX 80; 93.4% pure rosmarinic acid). The investigation of these new synthesised antioxidants in polyethylene and polypropylene indicated that they are very efficient antioxidants under both melt processing and long term thermo-oxidative conditions (by contrast, the commercial hindered phenol antioxidants Irganox 1076 and Irganox 1010 showed lower antioxidancy effect than that of the new synthesised rosmarinates esters). Furthermore, the free radical scavenging activity of the rosmarinates esters antioxidants were also investigated in Doudin *et al.*[247] published work using DPPH (2,2-diphenyl-1-picrylhydrazyl radical) assay test at 90 °C. Their results showed that the DPPH scavenging activity of the synthesised rosmarinates esters is significantly higher than that of the commercial antioxidants Irganox 1010 and Irganox 1076.

In spite of the above discussed literature on the antioxidants derived from different renewable resources, the information in the open literature on effective renewable phenolic antioxidants for use to stabilise a model biodiesel autoxidation, in particular, at high temperature (~120 °C) is still limited. Therefore, the aim of this project was to extract (and characterise) a crude bio-oil from spruce woodchips (*picea abies*) using microwave-enhanced pyrolysis, and then to investigate the spruce-derived phenolic species in the crude bio-oil for their potential application as antioxidants for enhancing a model biodiesel oxidation stability by examining methyl linoleate autoxidation in 1 bar of oxygen at 120 °C.

1.11 Contextualization of Thesis

Chapter 2 explains in details the experimental procedures, apparatus and materials used for the work for this thesis.

Chapter 3 describes the microwave-enhanced pyrolysis of a woody biomass (spruce woodchips) for the production of pyrolysis liquids (crude bio-oil and aqueous fractions), char and gas. In order to understand in depth the chemical alteration of the spruce woodchips and the pyrolysis products from it (excluding the gas fraction), the spruce woodchips and its pyrolysis products were characterized further *via* proximate and ultimate analysis (proximate analysis parameters include moisture, volatile matter, fixed carbon and ash, and ultimate analysis elements include carbon, hydrogen, nitrogen and oxygen), Karl Fischer titration, as well as *via* ICP-MS analysis. Furthermore, ATR-IR analysis, NMR analysis, and GC-MS characterization were employed for the analysis of the pyrolysis liquid products: the crude bio-oil and the aqueous fractions.

Chapter 4 illustrates the isolation and characterization of phenols from the crude bio-oil produced by the microwave-enhanced pyrolysis of spruce woodchips. In order to isolate the phenolic species from the crude bio-oil, the crude bio-oil was subjected to two significant multi-solvent fractionation procedures; water-insoluble phase fractionation of crude bio-oil, and water-soluble phase fractionation of crude bio-oil. Furthermore, another fractionation was also carried out using supercritical CO_2 to investigate further the isolation of phenolic species from the crude bio-oil, using this greener alternative to more conventional solvent fractionation.

Chapter 5 investigates the potential application of using crude bio-oil produced from the microwave-enhanced pyrolysis of spruce woodchips as a source of renewable phenolic antioxidants to stabilize a model biodiesel and prevent autoxidation. The effects of the crude bio-oil phenolic content and a commercial synthetic antioxidant (BHT) on a significant biodiesel component (methyl linoleate) were investigated using static oxidation test, as well as a biodiesel industry standard Rancimat test (EN 14112). In order to understand the antioxidancy of the crude bio-oil, further investigations were also carried out on the effects of different isolated extracts from

the crude bio-oil, as well as three significant phenolic species identified in the crude bio-oil, and a mixed phenolic standard on methyl linoleate autoxidation using the static oxidation test.

Chapter 6 highlights the conclusions for the thesis projects, and the suggested directions for future work.

Chapter 2: Experimental

2.1 Microwave-Assisted Pyrolysis

The microwave-assisted pyrolysis of spruce woodchips was carried out in a Milestone ROTO SYNTH Rotative Solid Phase Microwave Reactor (Milestone Srl., Italy). The microwave was fitted with a vacuum pump to allow *in-situ* separation and collection of the generated pyrolysis liquids from the microwaved woodchips, see Figure 2.1.

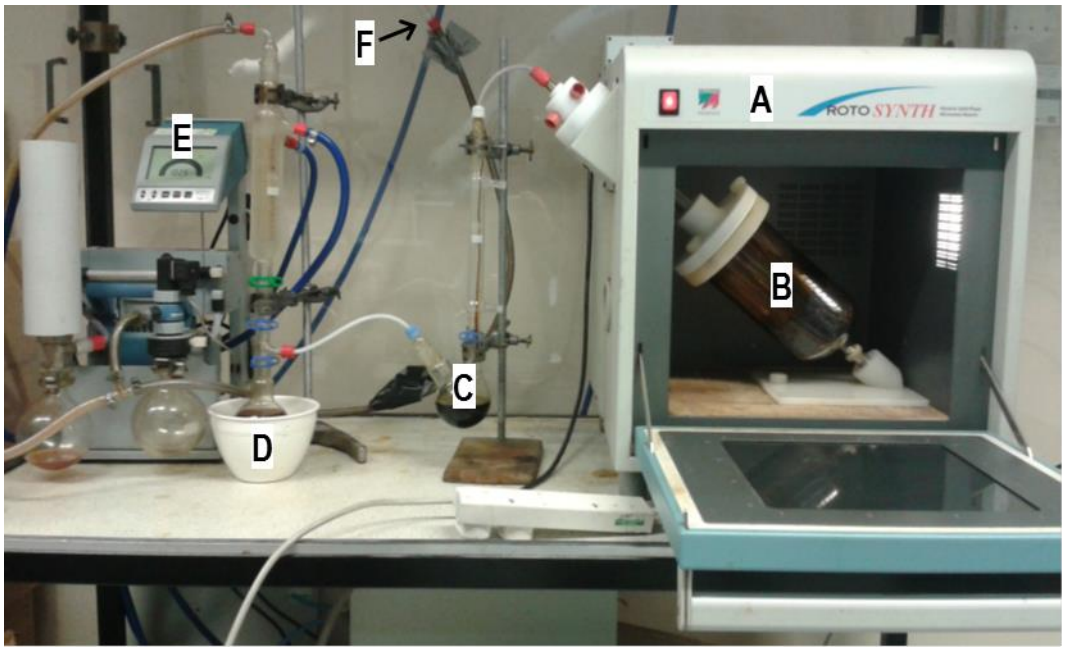

Figure 2.1: The microwave pyrolysis set-up: A) Milestone ROTO SYNTH microwave reactor; B) Rotative 2 dm^3 microwave glass flask; C) Crude bio-oil collection point; D) Aqueous collection point; E) Vacuum pump; F) Pyrolysis gas release point.

Samples of spruce woodchips (approximately 150 g per run) were placed in a 2 dm^3 glass flask (B in Figure 2.1) and attached to the microwave tube within the microwave cavity. Then, the samples were exposed to a maximum microwave power of 1200 W with a microwave frequency of 2.45 GHz (wavelength 12.2 cm, multimode). The pyrolysis was carried out under partial vacuum with an initial pressure of approximately 11 mbar absolute, and the maximum pyrolysis temperature was controlled at below 200 $^{\circ}$C. During pyrolysis, the microwave cavity temperature was monitored *via* an infrared detector, and the reaction was terminated (after approximately 10 minutes) which is the point at which the pyrolysis liquids (crude

bio-oil and aqueous) had stopped emerging from the microwave cavity. At the end of each pyrolysis experiment, three fractions were collected, a crude bio-oil, an aqueous phase and a char fraction. The gas fraction was not captured for further analysis in this study and was continuously released from the vacuum pump outlet to the external atmosphere *via* the laboratory fume extraction system.

During the duration of the work described in this thesis, two independent microwave-enhanced pyrolysis experiments were carried out. This was mainly due to the need of producing more bio-oil to carry on with experiments and not to test reproducibility. More information about the two microwave-enhanced pyrolysis experiments can be found in Appendix D.

2.2 Crude Bio-oil Fractionation

2.2.1 Solvent fractionation

The microwave enhanced pyrolysis crude bio-oil was subjected to two liquid-liquid fractionation procedures, and they were classified here as water-insoluble phase and water-soluble phase fractionation procedures.

2.2.1.1 Water-insoluble phase fractionation of crude bio-oil

The fractionation procedure of crude bio-oil was performed using a method previously patented to isolate phenols from lignocellulosic materials,[248] and previously described in literature.[249, 250] The crude bio-oil (30 g) was first mixed with 100 ml ethanol and filtered to remove solid contents, as shown in Figure 2.2. After removing ethanol by vacuum distillation, the remaining bio-oil was added to 75 ml distilled water with stirring for 30 min. The upper water-soluble phase formed was separated from the lower water-insoluble phase. Then a solution of 2.5 mol/L NaOH was gradually added to the water-insoluble phase with stirring until obtaining a black mixture having a pH of approximately 12 (monitored using a benchtop pH meter; Jenway 3505 pH Meter). At pH > 12, the water-insoluble phase was mostly dissolved in the NaOH solution, then, 100 ml of dichloromethane (DCM) was used twice for the extraction of neutral extract. The remaining DCM-insoluble alkaline solution was acidified with 1 mol/L HCl to a pH of approximately 6 (as indicated by the benchtop pH meter), and then, phenolic extract was extracted with 100 ml DCM

twice. The remaining DCM-insoluble acidic solution was further acidified with 1 mol/L HCl to a pH of approximately 2 (as indicated by the benchtop pH meter), and organic acids extract was then extracted with 100 ml DCM twice. Finally, the remaining acidic solution was filtered to collect the solid precipitate. The water-soluble extract, neutral extract, phenolic extract, and organic acids extract all had the solvent removed using a rotary evaporator under partial vacuum.

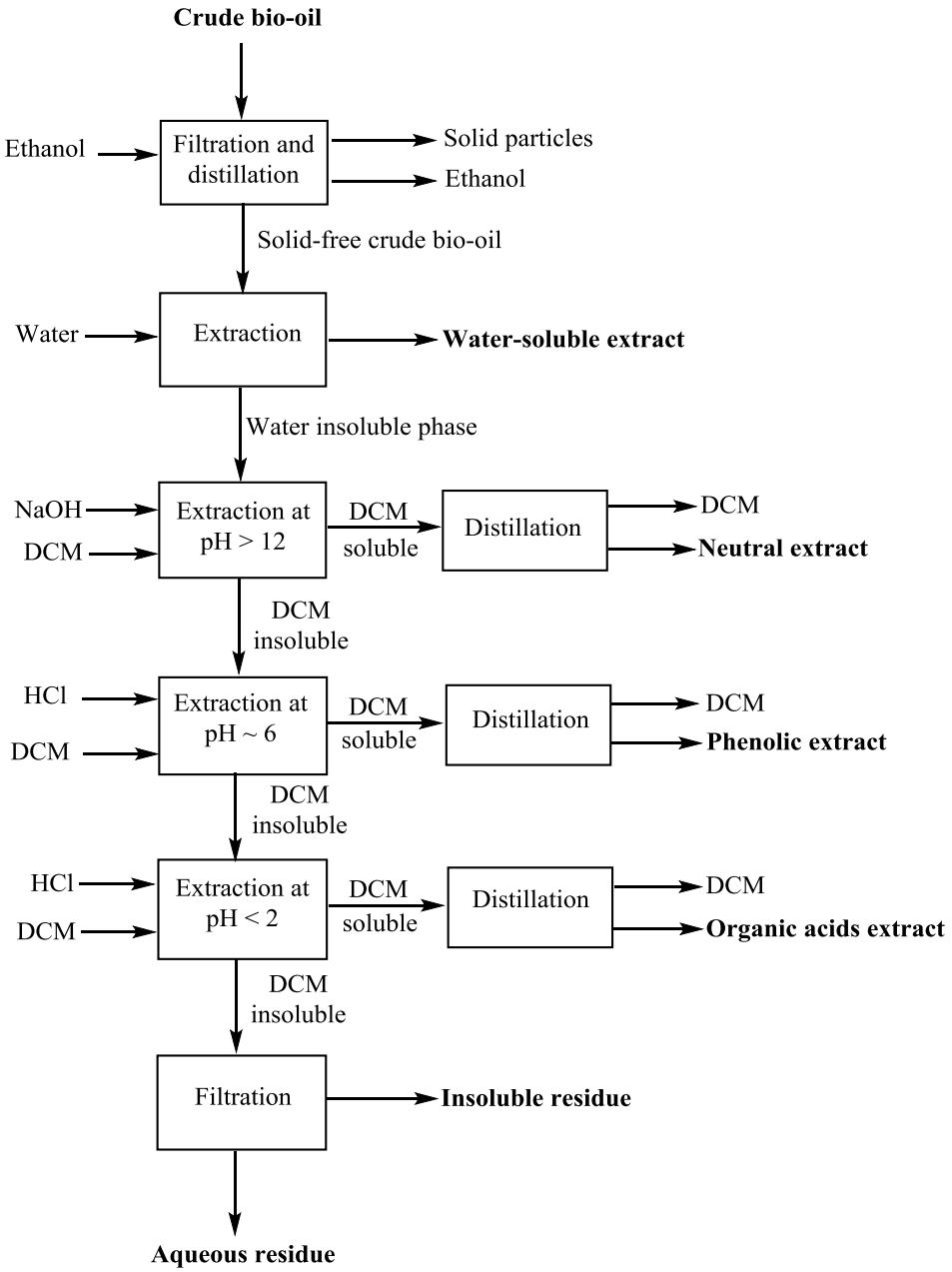

Figure 2.2: Schematic diagram of water-insoluble phase fractionation steps.

2.2.1.2 Water-soluble phase fractionation of crude bio-oil

The crude bio-oil was also further fractionated according to another method previously reported to separate phenolic antioxidants from bio-oil.[251] The crude bio-oil (30 g) was first mixed with 100 ml ethanol and filtered to remove solid contents, as shown in Figure 2.3. After removing ethanol by vacuum distillation, the remaining bio-oil was added to 75 ml distilled water with stirring for 30 min. Next, the mixture was allowed to stand for another 30 min, and then the lower water-insoluble phase formed was separated from the upper water-soluble phase. The water-soluble phase was further extracted with diethyl ether (3 x 50 ml) and then with DCM (3 x 50 ml). The solvents in the obtained extracts, including the aqueous residue, were removed by a rotary evaporator under vacuum at a temperature of 35 °C. The three obtained solvent-free extracts were labelled as a diethyl ether extract, a DCM extract and a residue extract, and stored in a fridge for future analysis.

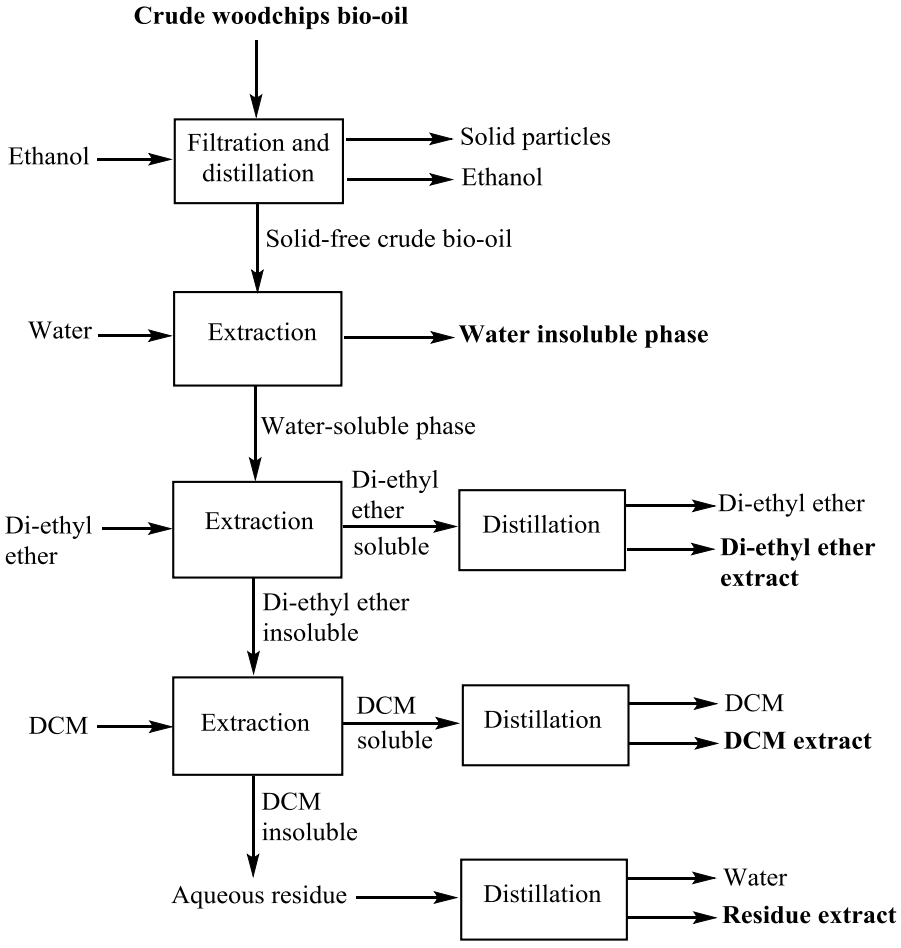

Figure 2.3: Schematic diagram of water-soluble phase fractionation steps.

2.2.2 Supercritical CO_2 fractionation

The woodchips crude bio-oil was further fractionated using a supercritical CO_2 unit system (SFE-500) supplied by Thar technology. The crude bio-oil (11 g) was dissolved in (600 ml) methanol, then mixed with (~400 ml) Celite® 545 coarse and taken to a rotary evaporator to remove the solvent. Then, the formed dry sample was placed in the unit extractor to nearly its full volume (~500 ml). The supercritical CO_2 extraction was carried out at a temperature of 50 °C and a pressure of 350 bars with a CO_2 flow rate of 40 g/min. The total run time was 3 hours, and four fractions were collected in four collecting points. Each collecting point was set with different pressure level of 200, 100, 75 and 1 bar absolute, and also with controlled temperature set at 50, 50, 35 and 35 °C, respectively.

2.3 Analysis

2.3.1 Thermogravimetric analysis

The thermogravimetric (TG) analysis of spruce woodchips and the microwave enhanced pyrolysis products (crude bio-oil, aqueous and char) was carried out using a Netzsch 409 simultaneous thermal analyser (STA). The TG analysis data was used to determine proximate analysis as of moisture, volatile matter, fixed carbon and ash contents of the spruce woodchips and its microwave enhanced pyrolysis products, according to a previous published method by Donahue and Rais.[252] Samples of 100 mg were each heated under nitrogen (100 ml/min) and heated again under atmospheric air (100 ml/min), as the following temperature programmes.

Heating programme under nitrogen (100 ml/min):

1. Heating from 30 to 105 °C at a heating rate of 10 °C per min.
2. Isotherming for 10 min at 105 °C.
3. Heating from 105 to 900 °C at a heating rate of 50 °C per min.
4. Isotherming for 1 hour at 900 °C.

Heating programme under atmospheric air (100 ml/min):

1. Heating from 30 to 900 °C at a heating rate of 50 °C per min.
2. Isotherming for 1 hour at 900 °C.

Figure 2.4 shows an illustration of measuring proximate analysis data (moisture, volatile matter, fixed carbon and ash contents) in a single sample. The moisture content was measured from the sample mass difference in nitrogen between 30 and 105 °C. The volatile matter content was determined from the sample mass difference between 105 and 900 °C under nitrogen. For fixed carbon content, it was calculated from the difference between the remained mass under nitrogen and the remained mass under atmospheric air at 900 °C. Finally, the ash content was determined as the remaining mass after isotherming samples for 1 hour at 900 °C under atmospheric air.

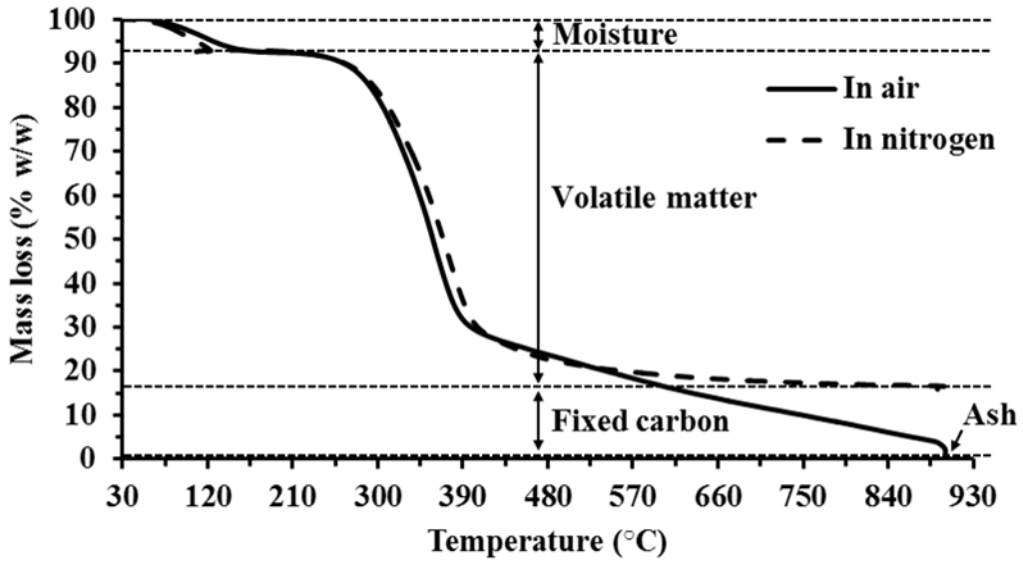

Figure 2.4: Illustration of proximate analysis (moisture, volatile matter, fixed carbon and ash contents) determination from spruce woodchips TG analysis data.

2.3.2 Carbon-Hydrogen-Nitrogen analysis

The elemental percentage distribution of carbon, hydrogen and nitrogen for pyrolysis fractions were evaluated using a carbon-hydrogen-nitrogen (CHN) analyser CE440 (Exeter Analytical, Warwick, UK).

2.3.3 Karl Fischer titration

The water content of crude bio-oil and aqueous fraction were determined by volumetric Karl Fisher (KF) titration using a Metrohm KF titrator (Metrohm 903

Titrando, with an integrated Metrohm 803 Titration Stand and a Reagent Organizer) supplied by Metrohm UK Ltd. (Runcorn, Cheshire, UK). Approximately 300 mg of each crude bio-oil sample was placed in the titration vessel, which pre-filled with approximately 30 ml of HYDRANAL-Solvent and titrated to dryness (conditioned) with the HYDRANAL-Titrant until a constant drift of approximately 10-20 µL/min is achieved. This pre-titration step assures removal of any residual water content that was in the solvent, and also removes adherent moisture in the cell, on the walls of the cell and the electrode. HYDRANAL-Composite 5K was used as the titrant and HYDRANAL-KetoSolver was used as the solvent. All samples were measured in triplicate. The results were processed and stored using ***tiamo*** titration software (Version 2.4), which allows the simultaneous collection and storing of the results from several instruments at the same time.

2.3.4 Inductively coupled plasma-mass spectrometry analysis

The inductively coupled plasma-mass spectrometry (ICP-MS) analysis of microwave enhanced pyrolysis liquid products (crude bio-oil and aqueous fractions) were performed using the Agilent 7700x ICP-MS spectrometer for the determination of metal content in each sample according to an environmental calibration method.

A 0.5 g of each sample was dissolved in 5 ml Nitric acid (69 %, TraceSELECT®) then heated at 50 °C for 10 minutes. The mixture was then diluted with ultrapure water till 100 ml and heated again at 50 °C for 30 minutes. After resting for 30 minutes, the final solution was filtered with a micro syringe filter and submitted for the analysis. Nitric acid concentration in the final solution is approximately 3.7 %.

The sampling and skimmer cones used were Ni, which is suitable for a wide variety of samples. The analysis was carried out in He mode. The sample uptake was 60 seconds, stabilise 40 seconds and wash time 60 seconds (using 5 % HCl and 2 % HNO_3 (30 seconds in each)).

It should be noted that relative standard deviation (RSD) values were calculated using three replicate data points measured for each element. Concentration values with an RSD greater than 10% will be reported as approximate values between brackets.

2.3.5 Gas chromatography

2.3.5.1 Gas chromatography-mass spectrometry

Gas chromatography-mass spectrometric (GC-MS) analysis was performed using a Perkin Elmer Clarus 500 gas chromatograph (GC) attached to a Perkin Elmer Clarus 560s mass spectrometer (MS). The GC was fitted with a DB-5HT column ((5%-phenyl)-methylpolysiloxane column; length: 30 m; internal diameter: 0.25 mm; film thickness: 0.25 μm; by J&W Scientific, Agilent Technologies), which the carrier gas used was helium and operated at constant pressure of 22.4 psi. The injector temperature was 300 °C and the flow rate was set to be 1 ml/min. The oven temperature was maintained at 60 °C for 1 minute then to 360 °C at a rate of 8 °C per minute and then set to hold for 10 minutes at 360 °C. The Perkin Elmer Clarus 560s mass spectrometer was operated in the electron ionisation mode (EI) at 70 eV, a source temperature of 300 °C and quadrupole in the scan range of 30 – 1200 amu per second.

The data was collected using the Perkin Elmer enhanced Turbomass (Ver5.4.2) chemical software and the compounds were identified by comparing their mass spectrum with NIST Mass Spectral Database (v. 2.2) 2008.

It should be noted that another oven method was also used for the analysis of water-soluble phase extracts presented in Chapter 4, where the oven initially set at 45 °C for 3 minutes and increased to 280 °C at a rate of 4 °C per minute and then set to hold for 20 minutes at 280 °C, which gives a total analysis time of 81.75 minutes.

2.3.5.2 Gas chromatography-flame ionisation detector

Gas chromatographic analysis was performed using a Shimadzu GC-17A gas chromatograph (GC) fitted with a Zebron™ ZB-5HT column (5% phenyl-95% dimethylpolysiloxane column; length: 30 m; internal diameter: 0.25 mm; film thickness: 0.25 μm; by Phenomenex Torrance, CA, USA) and a flame ionisation detector (FID). The injector and detector temperature was 360 °C. The oven was set to be heated from 50 to 350 °C at a rate of 5 °C per minute and then set to hold for 20 minutes at 350 °C, which gives a total analysis time of 80 minutes.

It should be noted that another GC-FID equipment was used for the analysis of water-soluble phase extracts presented in Chapter 4. The GC-FID apparatus was an Agilent Technologies 6890N Network gas chromatograph system equipped with a 7638B series Agilent injector. The column used was a Zebron™ ZB-5HT column (5% phenyl-95% dimethylpolysiloxane column; length: 30 m; internal diameter: 0.25 mm; film thickness: 0.25 μm; by Phenomenex Torrance, CA, USA). The injector temperature was 250 °C and the detector temperature was 340 °C. The oven was initially set at 45 °C for 3 minutes and increased to 280 °C at a rate of 4 °C per minute and then set to hold for 20 minutes at 280 °C, which gives a total analysis time of 81.75 minutes.

External standard calibration and evaluation of standard error

Quantitative data for individual phenolic compounds in crude bio-oil and its extracts were determined by GC-FID using BHT as a representative phenolic standard and the effective carbon number (ECN, described in the next section) technique was then used to obtain calibration factor for the other phenolic compounds detected. For the main GC used for the majority of this work, repeated GC calibrations were similar, within 7% over the course of this work, while the individual response versus concentration gradients used to obtain calibration factors had standard errors for their gradients of up to 5%. Therefore, the effective accuracy (standard error) of the concentration of phenolic species quoted later in this thesis is taken as ± 7% of the concentration, as an upper limit. It should be also noted that data were reported to one decimal place (1dp) figures, and this is consistent with the estimated accuracy of the concentration of phenolic species quoted in the thesis.

2.3.5.3 Effective carbon number technique

In order to give quantitative analysis for the quantification of phenolic compounds *via* GC-FID, the effective carbon number (ECN) method can be applied for the calculation of relative response factors (RRF) in cases where pure chemical standards are not accessible for GC-FID calibration. The ECN method indicates the relative response of an ionization detector (FID) to a compound in comparison with other compounds.

The ECNs for the identified phenolic compounds including the standard (BHT) were calculated according to a previous published literature,[253-255] and can be found in Appendix B. Then, the RRFs were determined using the following equation:

$$\text{RRF of compound A} = \frac{\text{MW of compound A x ECN of standard}}{\text{MW of standard x ECN of compound A}}$$

Finally, the corrected peak area (CPA) for the detected phenolic compounds was calculated according to Jung *et al.*[256] by multiplying the primary peak area (PPA) with the obtained RRF from the previous equation, as the following equation:

$$\text{CPA of compound A} = \text{PPA of compound A x RRF of compound A}$$

2.3.6 Folin-Ciocalteu assay

The Folin-Ciocalteu assay was used for the evaluation of total phenolic content in the microwave enhanced pyrolysis crude bio-oil and in its extracts. The preparation of stock solutions and samples, as well as the Folin-Ciocalteu procedure were carried out according to the literature,[257, 258] with the variation that mono-phenol 4-allyl-2-methoxyphenol (eugenol) was used instead of the poly-phenol gallic acid as a standard for calibration as most species identified by GC-MS were mono-phenols in crude bio-oil as will be demonstrated later in Chapter 4.

2.3.6.1 Preparation of stock solutions

Eugenol calibration standards

500 mg of eugenol was dissolved in 10 ml and then diluted to 100 ml with distilled water to create 5000 mg/dm^3 concentration. Then 1, 2, 5, 10 and 20 ml were diluted with distilled water in 100 ml volumetric flasks to create standards with 50, 100, 250, 500 and 1000 mg/dm^3 concentrations, respectively.

Sodium carbonate solution

100 g of anhydrous sodium carbonate was dissolved in 500 ml distilled water and let to sit 24 hours at room temperature. The final solution was filtered through filter paper and stored at room temperature.

2.3.6.2 Preparation of samples

25 mg of each crude sample was dissolved in 25 ml ethanol to create a solution with 1000 mg/dm^3 concentration. The samples then were filtered and kept in fridge for future analysis.

2.3.6.3 Folin-Ciocalteu procedure

1) 0.5 ml sample, eugenol calibration standard, or blank (distilled water) was placed in 50-ml volumetric flask.
2) 35 ml distilled water was added, followed by 2.5 ml FC reagent. Then the solution was swirled to mix and incubated 1 and not more 8 min at room temperature.
3) 7.5 ml sodium carbonate solution was added, then distilled water was added to the 50-ml line and the solution was mixed and incubated 2 hours at room temperature.
4) 2 ml was transferred to 2-ml glass cuvette and the absorbance was measured at 758 nm in a spectrophotometer.

After recording all the absorbance reading for the calibration standards, a calibration curve was created to determine the corresponding eugenol concentration in the analysed samples. The standard error for this gradient was evaluated to be 3%. Therefore, the effective accuracy (standard error) of the total content of phenolics quoted later in this thesis is taken as ± 3% of the total content. Total phenolic content values will be reported in eugenol equivalents (EE) using units of mg/dm^3.

2.3.7 Ultraviolet-visible spectrophotometry

The ultraviolet-visible spectrophotometry (UV-Vis) was performed using a Jasco model V–550 double beam UV-Vis spectrophotometer with 1.0 cm matching quartz

cells and operated by Spectra Manager software. Table 2.1 shows further parameters used with the analysis.

Table 2.1: General parameters applied for the UV-Vis spectrophotometry.

Photometric mode	Abs
Wavelength range	200 ~ 900 nm
Response	Medium
Band width	1.0 nm
Scanning speed	400 nm min^{-1}
Data pitch	1.0 nm

2.3.8 Attenuated total reflectance-Fourier transform infrared spectroscopy

The attenuated total internal reflection Fourier transform infrared (ATR-FTIR) spectroscopy analysis of crude bio-oil and its extracts were performed using a Bruker Vertex 70 FTIR spectrometer (Bruker Optics, Germany) equipped with a deuterated triglycine sulfate (DTGS) detector with potassium bromide (KBr)-window and a Golden Gate™ Single Reflection Diamond ATR accessory system (GS10500 Series; Specac Ltd., UK). The angular incidence of light at the ATR crystal sample interface is set at 45°. The beam condensing lenses used in the optical unit of the Golden Gate™ ATR are Zinc Selenide (ZnSe) lenses which fully absorb wide spectral transmission range to *ca.* 550 cm^{-1}. The spectra were recorded by averaging 128 scans in the mid-IR (4000-600 cm^{-1}) wavenumber range at a resolution of 2 cm^{-1}. The data were recorded and analyzed with OPUS software (version 5.5) from Bruker Optics.

2.3.9 Nuclear magnetic resonance spectroscopy

The nuclear magnetic resonance (NMR) spectroscopic analysis for crude bio-oil and its extracts were carried out on a JEOL ECS 400 NMR spectrometer. Each sample of 120-130 mg was dissolved in 1 ml of deuterated dimethyl sulfoxide (99.9 % DMSO-d_6, Sigma-Aldrich, UK) or in deuterated methanol (99.8% methanol-d_4, Sigma-

Aldrich, UK), filtered and submitted for ^{13}C as well as ^{1}H NMR analysis. All NMR spectra were recorded under room temperature (25 $^{\circ}C$), which at100 MHz (1024 scans) and 400 MHz (16 scans) for ^{13}C and ^{1}H, respectively.

2.3.10 High performance liquid chromatography

High performance liquid chromatography (HPLC) for the analysis of sugars in the water-soluble phase was carried out using a Hewlett Packard Series 1100 with both diode array (DAD) and evaporating light scattering (ELSD) detectors. The column used was a Luna® 5 µm NH_2 100 Å (250 mm x 4.6 mm I.D., 5 µm particle size) from Phenomenex (Torrance, CA, USA). The column was operated at a temperature of 40 $^{\circ}C$. The mobile phase consisted of acetonitrile:water (82.5:17.5, v/v). Each run was completed within 24 minutes. The flow rate was 1 ml/min and the injection volume for all samples was 20 µl. All samples and standards were filtered through 0.45 µm Millipore membrane before analysis. The DAD detects organic compounds that can absorb ultraviolet or visible light. On the other hand, the ELSD detect compounds that do not absorb light like sugars and lipids. Thus, ELSD was used for the detection and quantification of sugars in the water-soluble phase. The important parameters used for optimising ELSD condition were the nitrogen gas flow rate at 1.3 L/min and the drift tube temperature at 45 $^{\circ}C$. The electronic data capture and analysis was performed using the DataApex Clarity software.

2.3.11 Gel permeation chromatography

The gel permeation chromatography (GPC) analysis of the water soluble phase and its extracts were performed on a Hewlett Packard Series 1100 fitted with an evaporating light scattering detector (ELSD). The column used was a TSKgel GMPWXL (7.8 mm x 300 mm) purchased from TOSOH Bioscience GmbH (Griesheim, Germany). The mobile phase consisted of 0.1 mol/L NH_4OAc. The operating flow rate was 0.5 ml/min and all analyses were performed at room temperature. All crude samples were dissolved in distilled water to a final concentration of 5mg/ml, and all were subjected to filtration using a 0.22 µm syringe filter prior to GPC analysis. For calibration, the gel permeation column was calibrated with 10 different polyethylene glycol/polyethylene oxide standards with

Mp range from ~232-1015000 Daltons, which were supplied by Fluka (Sigma-Aldrich, Buchs, Switzerland).

2.4 Oxidation Tests

2.4.1 Static oxidation

The oxidation experiments of methyl linoleate and its blends with antioxidants and bio-oil extracts were carried out using a stainless steel (BS 304) bench top reactor, which was previously described by Alfahdl,[259] Stark *et al.*,[260] Dugmore and Stark,[261] and Dugmore.[262] The oxidation reactions were carried out with 2 cm^3 of substrate and 1 bar absolute of oxygen were sealed inside the stainless steel reactor. A schematic diagram of the reactor in a sealed mode is given in Figure 2.5 and the reaction conditions are given in Table 2.2.

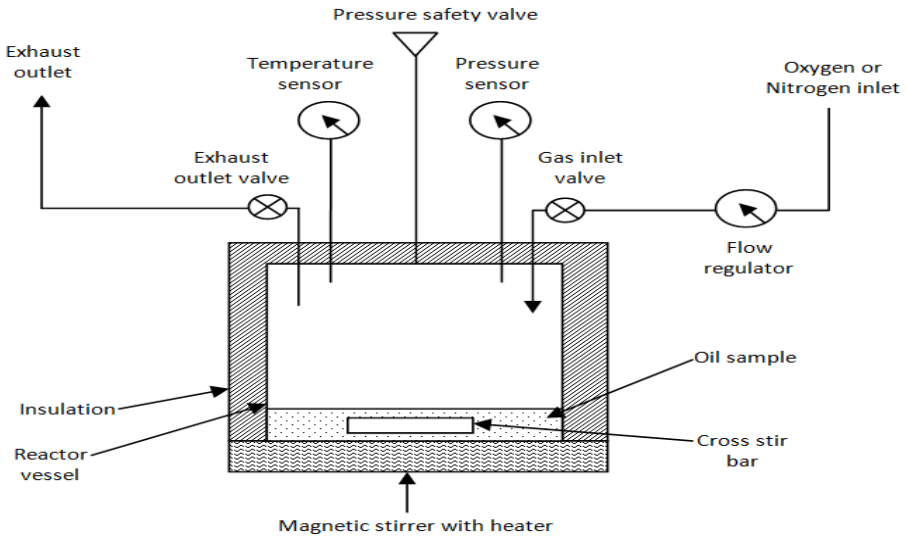

Figure 2.5: A schematic diagram of the oxidation test reactor in a sealed mode used in this study.

Table 2.2: Reaction specification for all oxidation experiments carried out in sealed mode.

Reactor volume	42 cm^3
Sample volume	2 cm^3
Temperature	120 $^{\circ}C$
Stirring rate	250 rpm
Oxygen pressure	1.00 bar absolute

For each single oxidation experiment, the reactor was pre-heated to 120 $^{\circ}C$, then nitrogen gas was passed through the reactor at a rate of 1.7 cm^3 s^{-1} to remove atmospheric oxygen, and 2 cm^3 of substrate was then injected into the reactor with a syringe through the rubber septum. The temperature was monitored by inserting a stainless steel coated, 0.5 mm diameter x 250 mm long, Type K thermocouple directly into the reactor. When the sample reached the desired temperature (120 $^{\circ}C$), the nitrogen gas flow was then switched to oxygen and after ca. 5 minutes (to allow the oxygen sensor to reach 100% in the system) the gas inlet and outlet were sealed to trap oxygen inside at 1 bar absolute. Then, the magnetic stirrer was switched on at a rate of 250 rpm to ensure the headspace gas was well mixed into the liquid. The internal pressure was then recorded every two seconds during the reaction on a PC using an analogue to digital converter (Picotec ADC-20). With the time of the reaction, the pressure began to drop, as oxygen started to be consumed by the substrate, until the pressure reached a minimum indicating the oxygen was consumed. Finally, the reaction was stopped when the pressure started rising noticeably.

Typically, in the presence of an antioxidant in the substrate inside a sealed reactor, the consumption of oxygen will be delayed by a period, defined here as the "Induction Time" (IT), where the substrate will start reacting substantially with the oxygen inside the sealed reactor, see Figure 2.6.

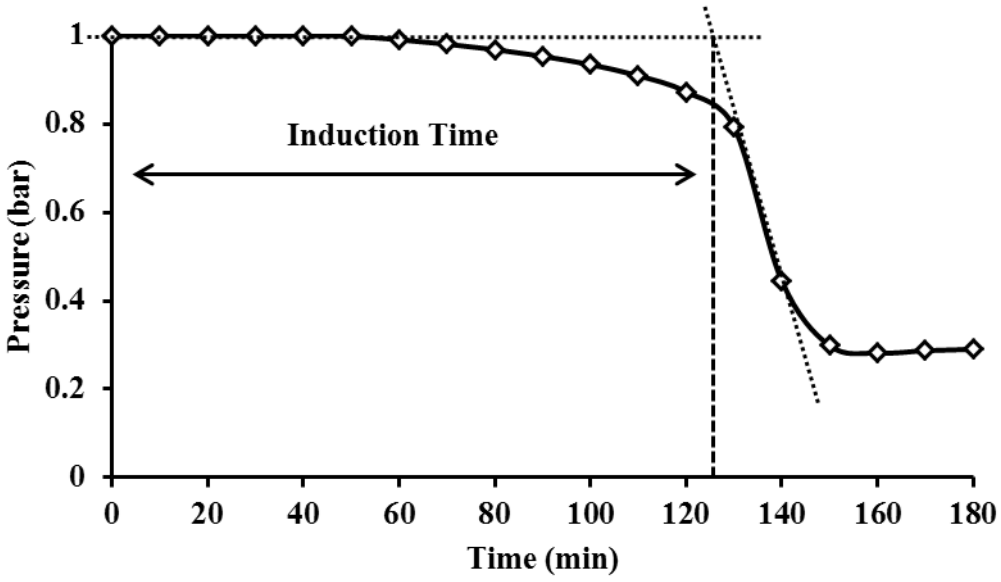

Figure 2.6: Diagrammatic illustration of induction time (IT) determination in a typical pressure trace of an oxidation experiment carried out in sealed reactor.

The induction time (IT) can be understood as a measure of the effectiveness of an antioxidant, and this is evaluated in this work by finding the time at which the tangent at the point of maximum gradient crosses the initial pressure, see for further illustration Figure 2.6. The reproducibility of induction time results was examined for repeated oxidation experiments using catechol as an antioxidant (presented in Chapter 5) and they were reproducible within 9%.

2.4.2 Rancimat test

The determination of the oxidation stability of the pure methyl linoleate, with the addition of commercial antioxidant (BHT) and with the addition of crude bio-oil was also performed on a Rancimat instrument model 743 (Metrohm, Herisau, Switzerland) to provide a comparison with this industry standard test. The evaluation was based on the determination of induction times (IT) using a Rancimat method according to the standard EN 14112.[233] Table 2.3 shows further general parameters used for this analysis.

Table 2.3: General parameters associated with Rancimat test.

Temperature	110 °C
Air flow	10 L/h
Evaluation	Induction time (IT)
Evaluation sensitivity	1
Stop criteria	End points
Sample amount	3 g
Measuring solution	60 ml distilled water

The procedure of this measurement started with passing a stream of air through the methyl linoleate sample in a sealed and heated reaction vessel at 110 °C. The oxidation reaction can oxidise alkyl ester molecules in the sample, which enhances the formation of peroxides as primary oxidation products. The methyl linoleate peroxides can decompose to form secondary oxidation products including volatile low molecular weight organic acids, for example, acetic acid and formic acid, as well as other volatile organic compounds. These formed volatile acids transport with the airstream by a connecting tube to a second vessel that contains distilled water, where the conductivity is measured constantly. The detection of the passed organic acids is achieved by the increase in conductivity. Therefore, the induction time (IT) here can be measured from the time that elapses until the appearance of these secondary reaction products, as indicated by an increase in conductivity.

2.5 Chemical Materials and Reagents

Table 2.4 summarises the biomass, chemical materials and reagents that have been used in this study.

Table 2.4: Description of biomass, chemical materials and reagents.

Category	Name	CAS Num.	Purity (%)	Supplier/Source
Biomass	Spruce woodchips	N/A	N/A	Norway (harvested in southern Sweden)
Chemical materials	Methyl linoleate	112-63-0	95+	TCI UK Ltd.
	Butylated hydroxytoluene (BHT)	128-37-0	99+	Sigma-Aldrich
	Eugenol	97-53-0	99	Fisher Scientific
	Catechol	120-80-9	99+	Fisher Scientific
	Guaiacol	90-05-1	99+	Fisher Scientific
	2-Methoxy-4-methylphenol	93-51-6	99	Fisher Scientific
	Isoeugenol	97-54-1	99	Fisher Scientific
	4-Ethylguaiacol	2785-89-9	98	Sigma-Aldrich
	4-Hydroxy-3-methoxyphenylacetone	2503-46-0	96	Sigma-Aldrich
	Ethanol	64-17-5	99.97	VWR Chemicals
	Tetrahydrofuran (THF)	109-99-9	99.7	VWR Chemicals
	Diethyl ether	60-29-7	99.99	Fisher Scientific
	Methanol-d_4	811-98-3	99.8 atom D	Sigma-Aldrich
	Dichloromethane (DCM)	75-09-2	99.9+	VWR Chemicals
	Acetonitrile	75-05-8	99.9	VWR Chemicals
	Dimethyl sulfoxide-d_6	2206-27-1	99.9 atom D	Sigma-Aldrich
	Hydrochloric acid	N/A	3	Fisher Scientific
	Nitric acid	7697-37-2	69	Sigma-Aldrich

Category	Name	CAS Num.	Purity (%)	Supplier/Source
	Sodium hydroxide	1310-73-2	98.8	Fisher Scientific
	Sodium carbonate	497-19-8	99.5	Fisher Scientific
	Ammonium acetate	631-61-8	99	Fisher Scientific
	Celite® 545	68855-54-9	89 (SiO_2)	Sigma-Aldrich
	Oxygen	7782-44-7	99.5+	BOC
	Nitrogen	7727-37-9	99.9	BOC
	Helium	7440-59-7	99.9	BOC
	Carbon dioxide	124-38-9	99.9	BOC
Reagents	Folin & Ciocalteu's phenol reagent	N/A	N/A	Sigma-Aldrich
	HYDRONAL-KetoSolver	N/A	N/A	Sigma-Aldrich
	HYDRANAL-Composite 5K	N/A	N/A	Sigma-Aldrich

Chapter 3: Extraction of Crude Bio-oils *via* Microwave-Enhanced Pyrolysis and Identification of Components

3.1 Introduction

The thermal conversion of biomass to solid, liquid and gas by means of microwave enhanced pyrolysis has been studied with great interest to explore a possible route of many potential applications to alternate energy sources and chemical raw materials.[263, 264] Most processes convert renewable solid biomass into liquid fuels using pyrolysis, which is a thermal decomposition of biomass in the absence of oxygen, and this pyrolysis treatment is believed to be the first process discovered for biomass conversion into liquid fuels.[16] The thermal breakdown of many renewable biomasses, including spruce woodchips, typically produces a large number of chemical substances. Therefore, it is reasonable and interesting to examine the potential use of some of these pyrolysis chemicals as substitutes for conventional fuels or chemicals. The understanding of the chemical composition of pyrolysis liquids, including the identification and characterization of its chemical contents, is highly important and an initial step during the investigation and applications of such fuel or chemicals. The chemical composition is a unique fundamental code that characterizes and determines the properties, quality, potential applications and any environmental issues related to any pyrolysis product. For this purpose, this chapter will cover a wide range of chemical analysis techniques that have been used for the characterization of spruce woodchips and its pyrolysis products (crude bio-oil, aqueous, char, but excluding gas) produced *via* microwave enhanced pyrolysis of spruce woodchips. For example, proximate analysis, namely moisture, volatile matter, fixed carbon, and ash contents; ultimate analysis (C, H, N, O and water content); ICP-MS analysis for trace metal contents; ATR-IR analysis for functional group assignments; ^{13}C NMR analysis for carbon assignments; and GC-MS analysis for identification of major volatile compounds have been combined to give as comprehensive picture as possible.

3.2 Microwave Pyrolysis of Spruce Woodchips

As described in Section 2.1 (Chapter 2), the microwave enhanced pyrolysis of spruce woodchips was carried out in a Milestone ROTO SYNTH Rotative Solid Phase Microwave Reactor (Milestone Srl., Italy). The microwave pyrolysis was performed under vacuum (~11 mbar absolute) to allow *in-situ* separation and collection of generated pyrolysis liquids (crude bio-oil and aqueous fraction) from the microwaved woodchips.

The spruce woodchips samples were exposed to the maximum microwave power of 1200 W using a special rotating microwave vessel (2 L), to allow an even microwave irradiation distribution within the woodchips sample inside the microwave cavity.[112] The operation under vacuum allowed *in-situ* the fractionation of the pyrolysis liquids into two forms of volatiles (a crude bio-oil and an aqueous phase), see for further illustration Figure 3.1.

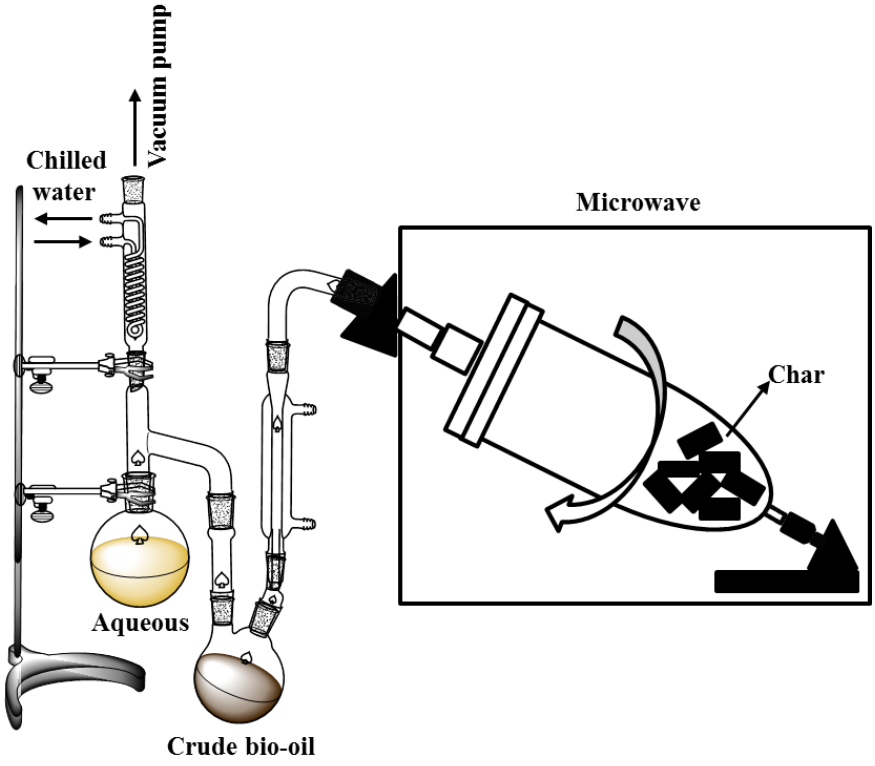

Figure 3.1: Schematic diagram of the microwave set-up, including an illustration of the obtained products (char, crude bio-oil and aqueous extracts) after the pyrolysis experiment.

During the microwave pyrolysis, an aqueous rich-fraction emerged first and was collected within the round-bottomed flask attached to the water chilled condenser. Then, a crude bio-oil fraction was produced and collected within a second round–bottomed flask attached to a room temperature condenser. The crude bio-oil fraction was dark brown, homogenous, and from previous work typically consists of a mixture of sugars and phenolics.[122] On the other hand, the aqueous fraction was light brown and typically contains water, acids and aldehydes.[122]

The distribution of yields from the microwave enhanced pyrolysis experiments (150 g of wood per run) of spruce woodchips are shown in Table 3.1. The gas fraction yield was measured by mass difference as in the current work the gaseous fractions during the microwave pyrolysis experiments of spruce woodchips were not captured for further analysis and were released from the microwave system to the air extractor system by the vacuum pump.

Table 3.1: The microwave enhanced pyrolysis fraction yields distribution per run (150 g) and the average yields distribution per 6 runs (900 g) of spruce woodchips.

	Crude bio-oil	Aqueous	Char	Gas[a]	Total
Total recovered amount per 6 runs (g)	166.2	265.7	335.8	132.3	900
Average recovered amount per run (g)	27.7	44.3	55.9	22.1	150
Fraction Recovery (% w/w)	18.5	29.5	37.3	14.7	100

[a] Calculated by difference

The microwave enhanced pyrolysis of spruce woodchips under vacuum has yielded 18.5 % crude bio-oil, 29.5 % aqueous, 37.3 % char and 14.7 % gas fractions (the gas measured by mass difference). The yields distribution obtained from spruce woodchips under these microwave enhanced pyrolysis conditions were typical and approximately similar to other previously investigated woody biomass, for instant wheat straw.[73]

3.3 Proximate and Ultimate Analysis of Spruce Woodchips and its Microwave-Enhanced Pyrolysis Products

For a better understanding of the thermal conversion processes by the microwave enhanced pyrolysis of spruce woodchips for the production of potentially high value materials, the proximate and ultimate analysis data of spruce woodchips, as well as its microwave-enhanced products (crude bio-oil, aqueous, char fractions, and excluding gas fraction) were obtained and summarized in Table 3.2. The proximate analysis of moisture, volatile matter, fixed carbon and ash contents were measured from thermogravimetric analysis (TGA) data of each sample that has been analysed under both nitrogen and air atmospheres, which is described in detail in the experimental section 2.3.1 (chapter 2).

Table 3.2: Proximate and ultimate analysis data of spruce woodchips and its microwave enhanced pyrolysis products.

Analysis type	Fraction/Element name	Spruce woodchips	Crude bio-oil	Aqueous	Char
Proximate % (w/w)	Moisture	7.5	/[a]	/	3.6
	Volatile matter	76.6	/	/	49.7
	Fixed carbon	15.0	/	/	45.6
	Ash	0.9	<0.1	1.4	1.1
Ultimate % (w/w)	C	46.52	55.57	20.34	61.88
	H	6.16	6.62	6.84	4.94
	N	N.D.[b]	0.12	N.D.	N.D.
	O[c]	47.32	37.69	72.82	33.18
	Water content	/	4.7	43.8	/

[a] Not available
[b] Not detected
[c] Calculated by difference

Figure 3.2 shows the TGA curves of spruce woodchips under both nitrogen and air atmospheres (Figure 3.2 B) and spruce char (Figure 3.2 A), including an illustration of measuring moisture, volatile matter, fixed carbon and ash contents from these curves.

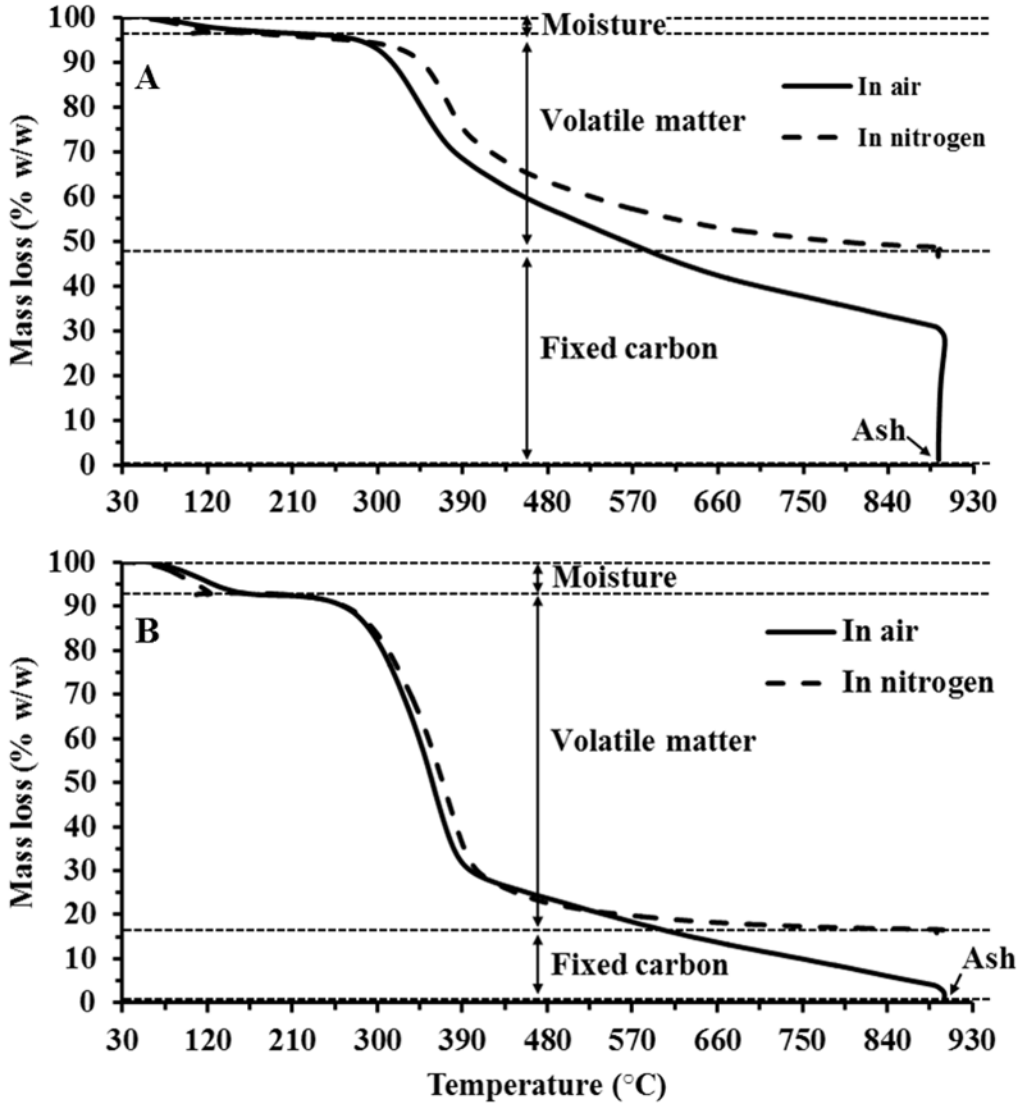

Figure 3.2: The TG analysis curves and an illustration of proximate analysis (moisture, volatile matter, fixed carbon, and ash contents) determination of: A) spruce char; B) spruce woodchips.

TGA can be defined as a technique in which the mass of a substance is monitored as a function of temperature or time as the sample is subjected to either isothermal or dynamic temperature program under controlled atmosphere.[265] Typically, most TGA data are represented by TGA curves that display mass losses, which are associated with a dynamic temperature program, and the dynamic rate usually lies between 0.5 and 50 °C/min, which depends on the type of analysis required. The starting temperature is usually at room temperature (≤ 30 °C) in order to monitor possible drying of the analysed sample. On the other hand, the final temperature is typically

relatively high (up to 1000 °C) for analysing organic materials. The reduction in the sample mass during TG analysis is typically caused by chemical reactions, for instance decomposition or combustion, or by physical transitions like desorption, evaporation or drying. In a small number of cases, it is also possible to observe an increase (mass gain) in the sample mass, which is possibly as a result of chemical reactions, for example, reactions with gaseous substances in the atmospheric air such as O_2 or CO_2, or even likely as a result from physical transitions such as adsorption of gaseous substances on the analysed sample.

It is noteworthy that when TGA was performed under air, it was noticed that the residual mass (ash content) of some samples appeared slightly negative. This also happened even after cleaning TGA crucible by heating-up to red hot (> 1000 °C). Therefore, it was necessary to measure ash content for all samples by weighing the ash residue independently after each TGA run using an analytical balance. By this way, the accuracy of ash content measurement was greatly improved.

The proximate analysis of moisture, volatile matter, fixed carbon and ash contents of spruce woodchips were 7.5, 76.6, 15.0, and 0.9% (w/w), respectively. These values are in reasonable agreement with previous works carried out by Demirbas.[19, 266] For spruce char produced from the microwave enhanced pyrolysis of spruce woodchips, the moisture, volatile matter, fixed carbon and ash contents were 3.6, 49.7, 45.6, and 1.1% (w/w), respectively, which indicates a noticeable increase in the fixed carbon content (~3 fold) in comparison to its fixed carbon content before pyrolysis. Interestingly, the lowest ash content was observed in the crude bio-oil sample (<0.1% w/w), however, on the other hand, the highest ash content was measured in the aqueous fraction (1.4% w/w).

For the ultimate analysis, the carbon, hydrogen, nitrogen and oxygen content of spruce woodchips and its pyrolysis products (excluding the pyrolysis gas fraction) were evaluated, and the instrument used is described in the experimental chapter (Chapter 2; section 2.3.2). Furthermore, the water content of the pyrolysis liquids (crude bio-oil and aqueous fraction) was also measured using Karl Fisher Titration, which is also described in the experimental chapter (Chapter 2; section 2.3.3). The water contents of crude bio-oil and aqueous fraction were 4.7, and 43.8% (w/w),

respectively, indicating that most water vapour produced during the microwave enhanced pyrolysis of spruce woodchips was condensed and collected into the aqueous fraction. Furthermore, this also can be seen as an evidence of producing crude bio-oils with low water content by using the microwave set-up illustrated in the experimental chapter (Chapter 2; section 2.1).

3.4 ICP-MS Analysis of Spruce Woodchips and its Microwave-Enhanced Pyrolysis Products

Inductively coupled plasma mass spectrometry (ICP-MS) was used for the determination of metal contents in spruce woodchips and in its microwave enhanced pyrolysis products (crude bio-oil, aqueous, char, and excluding gas fraction). A detailed experimental procedure for samples preparation, apparatus, and ICP-MS analysis parameters are fully described in section 2.3.4 (Chapter 2). Table 3.3 summarises the elements detected in spruce woodchips and in its microwave enhanced pyrolysis products (excluding gas fraction). The results from the ICP-MS analysis of the raw material (spruce woodchips) indicate a relatively high concentration of calcium (~1616 ppm) and potassium (~715 ppm), followed by sodium (~544 ppm), magnesium (~364 ppm) and iron (~256 ppm). The top two concentrated elements are typical in most woody biomass and approximately in agreement with what has been reported previously in literature by Azeez *et al.*[267] and by Werkelin *et al.*[268] for the mineral content of spruce wood. Furthermore, after the microwave enhanced pyrolysis of spruce woodchips, the top five concentrated elements (Ca, K, Na, Mg and Fe) in the spruce woodchips remained in great quantity in the microwave pyrolysis residue (the char fraction). Therefore, the ICP-MS analyses of collected pyrolysis liquids (crude bio-oil and aqueous fraction) show lower concentrations of Ca, K, Na, Mg and Fe, which indicates the difficulty for these elements to leave the microwave cavity during the microwave pyrolysis.

Table 3.3: Mineral contents of spruce woodchips and its microwave enhanced pyrolysis products.

Element (ppm)[a]	Spruce woodchips	Crude bio-oil	Aqueous	Char
Na	543.7	268.1	248.2	302.9
Mg	363.7	11.0	10.2	945.0
Al	74.1	22.1	(16.1)[b]	149.4
K	715.2	57.7	49.0	1785.8
Ca	1616.2	(93.1)	(61.8)	4410.8
Ti	(6.9)	N.D.[c]	N.D.	(10.2)
V	0.3	N.D.	(0.0)	(0.1)
Cr	0.8	0.5	0.1	0.7
Mn	62.8	0.8	(0.2)	172.6
Fe	255.9	N.D.	3.2	647.0
Co	0.2	N.D.	0.0	(0.0)
Ni	(0.5)	0.0	0.3	0.7
Cu	1.9	3.7	0.7	3.8
Zn	17.0	32.2	19.7	29.0
As	5.9	2.0	(4.4)	3.3
Se	N.D.	N.D.	N.D.	N.D.
Pd	1.0	0.7	0.2	0.9
Ag	1.0	N.D.	0.1	0.2
Cd	0.4	N.D.	(0.0)	0.3
Ba	45.7	16.0	15.5	62.5
U	0.1	N.D.	0.0	0.0

[a] In mg/L.

b Values between brackets are approximate values as their relative standard deviation (RSD) greater than 10%.

[c] Not detected.

3.5 ATR-IR Analysis of Spruce Woodchips and its Microwave-Enhanced Pyrolysis Products

Fourier transform-infrared spectroscopy in attenuated total reflectance (ATR) mode was used for the characterization of the chemical composition of crude bio-oil and aqueous fraction that were produced during the microwave enhanced pyrolysis of spruce woodchips. The experimental details and instrument used for ATR-IR analysis are described in section 2.3.8 (Chapter 2).

The ATR-IR spectra of crude bio-oil and aqueous fraction are shown in Figure 3.3. The wavenumbers with their band assignments of most absorption peaks in the crude bio-oil and aqueous fraction are summarized in Table 3.4.

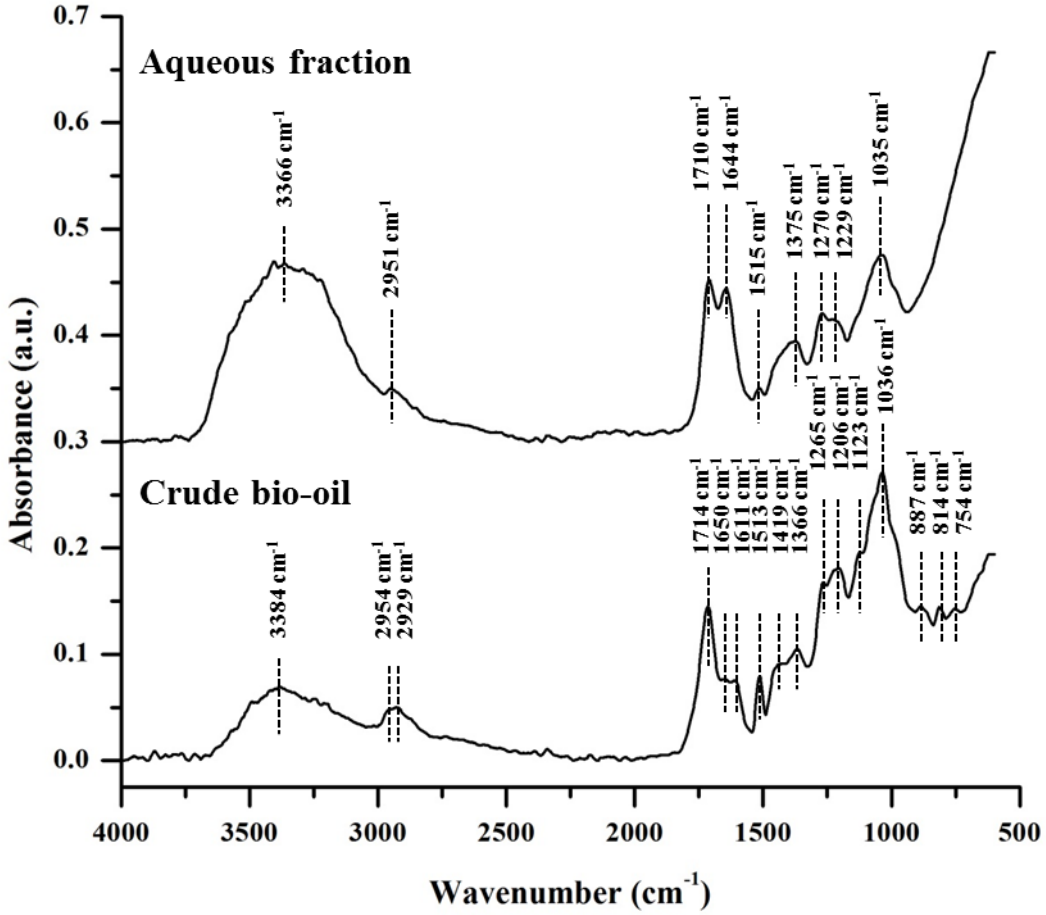

Figure 3.3: ATR-IR spectra of crude bio-oil and the aqueous fraction generated from the microwave enhanced pyrolysis of spruce woodchips. (Spectra offset vertically for clarity)

Table 3.4: ATR-IR data of functional groups and compound classes for crude bio-oil and aqueous fraction.[250, 269-271]

Wavenumber (cm^{-1})[a]		Functional group	Compound classes
Crude bio-oil	Aqueous fraction		
3384	3366	O-H stretching vibration	Phenols, alcohols, water, carboxylic acids
2954	2951	C-H stretching vibration	Alkanes, alkyl groups
2929		C-H stretching vibration	Alkanes, alkyl groups
1714	1710	Carbonyl C=O stretching vibration	Aldehydes, ketones, carboxylic acids, esters
1650	1644	C=O stretching vibration	Hydroxy unsaturated ketones, aldehydes
		+ H-O-H bending vibration	Water
1611		Aromatic C=C ring breathing	Aromatics with various types of substitution
1513	1515	Aromatic C=C ring breathing	Aromatics with various types of substitution
1419		C-H bending vibration	Aromatics, alkanes, alkyl groups
1366	1375	Aliphatic C-H bending vibration	Alkanes, alkyl groups
		+ O-H bending vibration	Alcohols, phenols
1265	1270	C-O stretching vibration in guaiacyl units	Phenols with guaiacyl substitution
1206	1229	C-O stretching vibration	Aromatics
1123		C-O stretching vibration	Secondary alcohols, cyclic ethers, sugars
		+ C-H bending vibration in syringyl units	Phenols with syringyl substitution

Wavenumber (cm^{-1})		Functional group	Compound classes
Crude bio-oil	Aqueous fraction		
1036	1035	Aliphatic ether and alcohol C-O stretching vibration	Primary alcohols, aliphatic ethers, sugars
		+ C-H bending vibration in plain in guaiacyl units	Phenols with guaiacyl substitution
887		Aromatic and alkenes C-H bending vibration	Aromatics, alkenes
814		Aromatic and alkenes C-H bending vibration	Aromatics, alkenes
754		Aromatic and alkenes C-H bending vibration	Aromatics, alkenes

[a] As allocated in Figure 3.3.

From the infrared spectrum of crude bio-oil, the absorbed broad peak at *ca.* 3384 cm^{-1} was due to hydroxyl group (-OH) presence in the crude bio-oil, indicating the possible presence of phenols, alcohols, carboxylic acids, and residual water. The C-H stretching vibrations of symmetric and asymmetric bonds were observed in the crude bio-oil infrared spectrum at *ca.* 2929 cm^{-1} and *ca.* 2954 cm^{-1}, respectively. These bands suggest the existence of alkanes and alkyl groups, which was further confirmed by the appearance of the low intensity C-H bending vibration bands at *ca.* 1419 and *ca.* 1366 cm^{-1}. The sharp medium intensity peak appeared at *ca.* 1714 cm^{-1} was associated with the presence of compounds with carbonyl C=O group, and this carbonyl stretching vibration band mostly corresponds to aldehydes, ketones, carboxylic acids and esters compounds. However, the assignment to mainly carboxylic acids compounds is more appropriate rather than ketones and aldehydes, as these compounds generally exist in smaller concentrations compared to carboxylic acids.[272-274] Moreover, the carboxylic acid carbonyl group has much more absorbance intensity in comparison to the absorbance intensity of ketones and aldehydes.[269] Therefore, carboxylic acids compounds are possibly the highest contributors to *ca.* 1714 cm^{-1} band in the infrared spectra of crude bio-oil. The low intensity absorbed band at *ca.* 1650 cm^{-1} in the crude bio-oil infrared spectrum was also due to either carbonyl groups C=O stretching vibration of possibly hydroxy

unsaturated aldehyde and ketones or the bending vibration of water (H-O-H). The presence of hydroxyl group (-OH) on unsaturated aldehydes or ketones decreases the C=O stretching vibration to *ca.* 1670-1645 cm^{-1} and *ca.* 1655-1540 cm^{-1}, respectively.[275] The sharp low intensity absorbed band appeared at *ca.* 1513 cm^{-1} in the crude bio-oil infrared spectrum was due to the aromatic C=C ring breathing vibrations, and this is associated with aromatic compounds with various substitutions in crude bio-oil. For the medium intensity absorbed band appeared at *ca.* 1265 cm^{-1}, it was due to C-O stretching vibration in guaiacyl units, indicating the presence of phenolic compounds with guaiacyl substitution.[250] In addition, the presence of aromatic compounds can be also confirmed with the appearance of the medium intensity absorbed band at *ca.* 1206 cm^{-1} in the crude bio-oil infrared spectrum, as this was due to the C-O stretching vibration in aromatic compounds. For the medium intensity absorbed band appeared at *ca.* 1123 cm^{-1}, it might be associated with C-O stretching vibration in secondary alcohols and cyclic ethers. However, this band can be also assigned as C-H bending vibration in syringyl units, indicating the presence of phenolic compounds with syringyl substitution. The high intensity band appearing at *ca.* 1036 cm^{-1} was related to C-O stretching vibration of primary alcohols and aliphatic ethers. However, this band can be also assigned as C-H bending vibration in guaiacyl units, consistent with the presence of phenolic compounds with guaiacyl substitution. Furthermore, the appearance of the last two absorption bands (*ca.* 1123 cm^{-1} and 1036 cm^{-1}) can also be due to C-O stretching vibration in carbohydrate sugars, as previously suggested by Nimlos and Evans.[276] The several medium intensity adsorbed bands between 890 and 750 cm^{-1} were due to C-H bending vibration of aromatics and alkenes.

On the other hand, the infrared spectrum of the aqueous fraction produced during the microwave enhanced pyrolysis of spruce woodchips shows some significant difference in its chemical composition in comparison to the crude bio-oil infrared spectrum. Similar to the crude bio-oil, an absorption band was observed in the aqueous fraction at *ca.* 3366 cm^{-1}, indicating O-H stretching vibration, but, however, with higher intensity than the one observed in the crude bio-oil, which might attribute mainly to the high carboxylic acids and water contents present in the aqueous fraction. The suggestion of the presence of excessive carboxylic acids and

water contents in the aqueous faction can be also enhanced with the appearance of high intensity absorption bands at *ca.* 1710 and *ca.* 1644 cm^{-1}, respectively.[277] The presence of aromatic compounds in low quantities in the aqueous fraction can be confirmed by the appearance of low intensity absorption band at *ca.* 1515 cm^{-1}, which was due to C=C ring breathing associated with aromatics with various types of substitution. The medium intensity absorption band at *ca.* 1035 cm^{-1} in the aqueous fraction indicates the existence of alcohols and ethers, as this band appearance could be associated with C-O stretching vibration in primary alcohols and aliphatic ethers.

3.6 NMR Analysis of Crude Bio-oil

The fact that pyrolysis bio-oils produced from various types of biomasses have a complex chemical nature, a complete chemical characterization of these bio-oils is, and always will be, a challenging task. As a result, many researchers tend to use a variety of analysis techniques to understand the physical and chemical properties of bio-oil's complex nature. For instance, analysis techniques based on gas chromatography (GC) were commonly used to identify and quantify individual components in pyrolysis bio-oils.[278-281] However, just approximately 25-40% of the bio-oil components could be detected by GC, as a great portion of these bio-oils contains carbohydrate and lignin oligomers that are not volatile enough to pass through GC columns.[16, 282, 283] Furthermore, other applicable analysis techniques, such as high-performance liquid chromatography (HPLC) can be used to quantify minor water-soluble components (≤15%), and gel permeation chromatography (GPC) can be also used to estimate molecular weight distributions of higher molecular weight species in bio-oils.[16, 282, 283] Despite the usefulness that these chromatographic methods could contribute to the characterization of bio-oils, again all these can only characterize a small fraction of the bio-oil. In addition, spectroscopic methods, such as infrared (IR) can be useful to know functional groups existed in bio-oils, however, this is can only provide an indication of the main functional groups in the bio-oil.[284, 285] With respect to all analysis techniques mentioned above, as explained each one has its own limitation, and may be nuclear magnetic resonance spectroscopy (NMR) has the potential to provide additional detailed characterization of the bio-oil.[286]

The ^{13}C NMR analysis of crude bio-oil and aqueous fraction was performed based on the procedure described in experimental section 2.3.9 (Chapter 2). Due to the high water content presented in the aqueous fraction, both crude bio-oil and aqueous fractions produced from the microwave enhanced pyrolysis of spruce woodchips were dissolved in methanol-d_4 (MeOD-d_4) and submitted for ^{13}C NMR analysis. As a result of the complex nature of crude bio-oil and aqueous fraction, varieties of resonance signals were recorded in each ^{13}C NMR spectrum. Therefore, the carbon assignments for both spectra were broadly grouped into a chemical shift range according to a previous published work in literature.[286]

Figure 3.4 shows the ^{13}C NMR spectra of crude bio-oil and aqueous fraction derived from the microwave enhanced pyrolysis of spruce woodchips, and the typical carbon assignments relative to their chemical shift regions are summarized in Table 3.5. The determination of exact chemical composition of crude bio-oil and aqueous fraction was difficult, or even was impossible, due to their complex mixture of components. However, it was possible to demonstrate in general the nature and the types of chemical functional groups that were presented in the assigned regions of crude bio-oil and aqueous fraction ^{13}C NMR spectra. As illustrated in the spectra, it was clear that there were many differences in the whole chemical composition of the crude bio-oil and the aqueous fraction formed during the microwave enhanced pyrolysis of spruce woodchips.

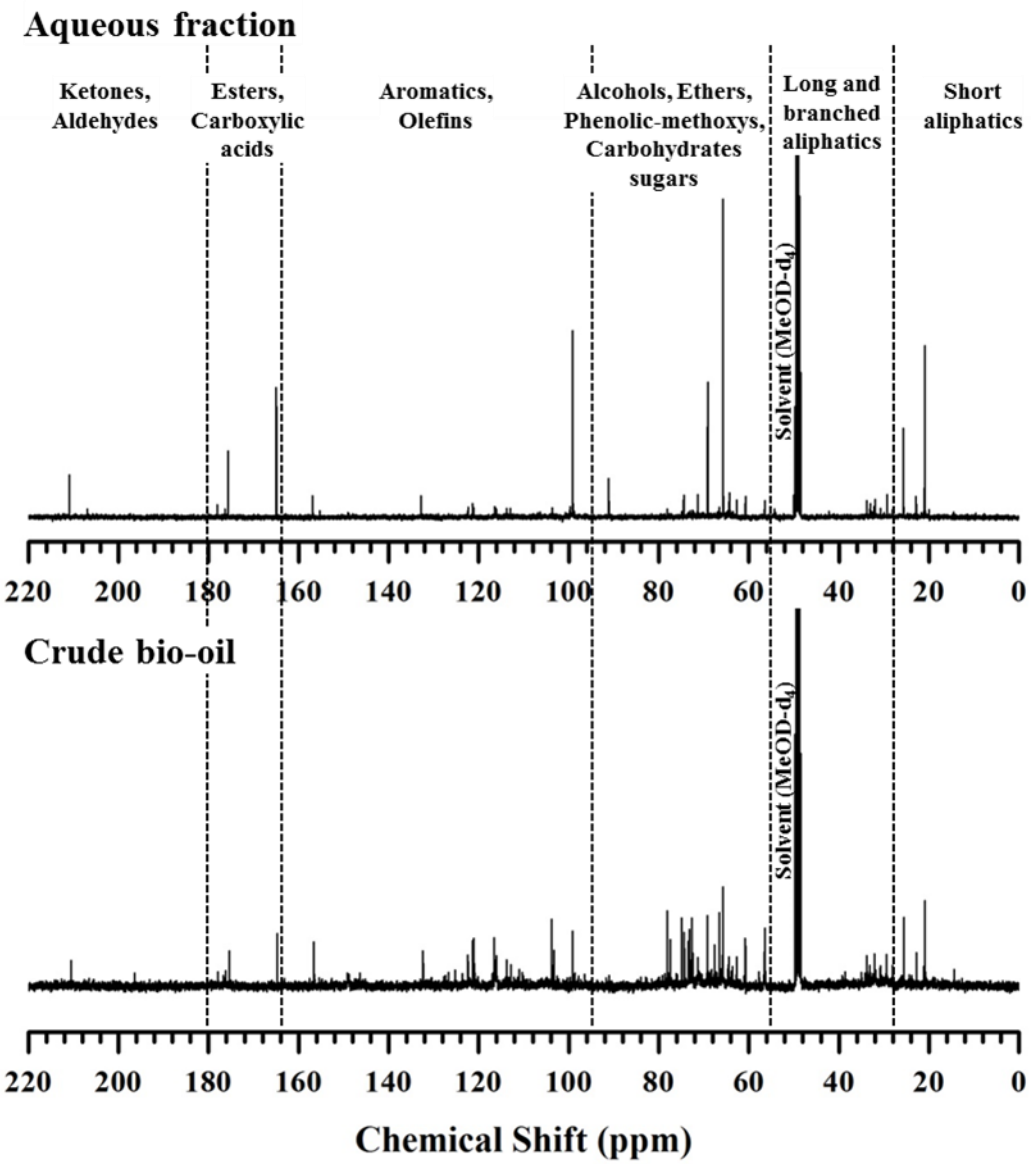

Figure 3.4: ^{13}C NMR spectra of crude bio-oil and aqueous fraction produced from the microwave enhanced pyrolysis of spruce woodchips. (spectra offset vertically for clarity)

Table 3.5: Carbon assignments based on ^{13}C NMR analysis of bio-oil and aqueous fraction produced from the microwave enhanced pyrolysis of spruce woodchips, and the assignments arranged according to chemical shift range. (reproduced from[286])

Carbon assignments	Relative structures	Chemical shifts (ppm)
Short aliphatics	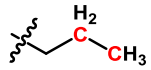	0-28
Long and branched aliphatics	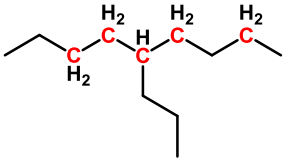	28-55
Alcohols, ethers, phenolic-methoxys, carbohydrate sugars	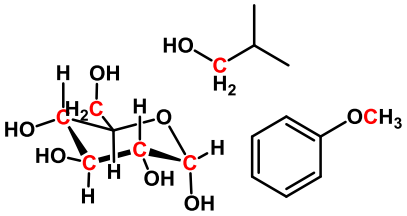	55-95
Aromatics, olefins, furans	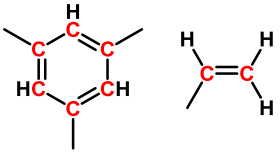	95-165
Esters, carboxylic acids		165-180
Ketones, aldehydes		180-215

Resonance signals in the 0-55 ppm region of ^{13}C NMR spectra of crude bio-oil and aqueous fraction were due to aliphatic carbon atoms. The most resonance signals appeared on the upfield region from 0 to 28 ppm of the ^{13}C NMR spectra of crude bio-oil and aqueous fraction consisted of methyl groups ($-CH_3$), which were assigned as short aliphatic chains. For example, the appearance of sharp resonance signal at ~21 ppm of crude bio-oil and aqueous fraction ^{13}C NMR spectra was likely due to the methyl group ($-CH_3$) of acetic acid compound.[287] On the other hand, the resonance signals (excluding the methanol solvent) on the region from 28 to 55 ppm of the ^{13}C NMR spectra of crude bio-oil and aqueous fraction were dominated by

methylene carbons (-CH_2-), and they were assigned as part of long aliphatic chains. Furthermore, methine carbon (CH) signals can also appear in the 28-55 ppm region, as the appearance of these signals indicates the presence of branched aliphatic groups within the chains. Overall, comparing the entire aliphatic region (0-55 ppm) of ^{13}C NMR spectra of the crude bio-oil and the aqueous fraction, they were approximately similar, as both have the possibility of containing short and long aliphatic. However, the aqueous fraction ^{13}C NMR spectrum showed more intense signals in the 0-28 ppm region, suggesting that the aqueous fraction contains higher amounts of short aliphatic chains than the crude bio-oil.

From the ^{13}C NMR spectrum of crude bio-oil, several carbohydrate sugars, such as levoglucosan derived from the thermal degradation of cellulose, existed in the crude bio-oil, which was confirmed by the appearance of complex signals in the typical carbohydrate sugars region from 55 to 95 ppm. In comparison, the ^{13}C NMR spectrum of the aqueous fraction displays fewer and much less complex signals in the same region from 55 to 95 ppm, indicating the possibility of just small quantities of carbohydrate sugars that had been collected into the aqueous fraction during the microwave enhanced pyrolysis of spruce woodchips. Furthermore, the presence of alcohols and ethers in the crude bio-oil as well as the aqueous fraction were also possible, as these could contribute to the appearance of the complex resonance signals in the same region from 55 to 95 ppm. However, the intense resonance signals appeared at ~66 ppm and ~69 ppm in the aqueous fraction ^{13}C NMR spectrum could be related more to alcohol compounds rather than ethers.[287] Moreover, it is noteworthy that the presence of methoxy groups on phenolic compounds, such as guiaicol and syringol derivatives was also observed, as the sharp resonance signal at ~56 ppm confirms the existence of small amounts of these species in the aqueous fraction and much higher amounts in the crude bio-oil.[286, 288]

The resonance signals which appeared in the region between 95 and 165 ppm in the ^{13}C NMR spectrum of crude bio-oil were due to the aromatic portion of the crude bio-oil, including carbon atoms in heteroaromatics that contain O such as furans, as well as any olefinic carbons, which can also contribute to the resonance signals appeared in this region. In comparison with the ^{13}C NMR spectra of the aqueous fraction, the resonance signals appeared in the same region were fewer and much less

complex, suggesting the possibility of containing lower aromatics than the crude bio-oil.

The resonance signals on the far downfield end of the ^{13}C NMR spectra of crude bio-oil and aqueous fraction from 165 to 215 ppm were due to carbonyl carbons, as the 165-180 ppm region represents carboxylic acids and esters, and the 180-215 ppm region represents ketones and aldehydes. Comparing the ^{13}C NMR spectra of crude bio-oil and aqueous fraction for the carbonyl carbons region, they both show approximately similar signals, suggesting the possibility of containing carboxylic acids, esters, ketones and aldehydes in each. However, the signals were more intense in the aqueous fraction, especially at the 165-180 ppm region, which indicates the presence in significant concentrations of possibly simple carboxylic acids related compounds, such as formic and acetic acids, as the sharp resonance signals at ~165 and ~175 ppm appearance in the aqueous fraction ^{13}C NMR spectrum were likely due to carboxyl group of formic and acetic acids, respectively.[287]

3.7 GC-MS Characterization of Spruce Pyrolysis Liquids

3.7.1 Results

The identification of major compounds in crude bio-oil and in aqueous fraction produced from the microwave enhanced pyrolysis of spruce woodchips was achieved by the use of gas chromatography-mass spectroscopy (GC-MS). Details of the GC-MS analysis method, apparatus and column used are fully described in the experimental section 2.3.5.1 (Chapter 2). The identification of compounds in crude bio-oil and aqueous fraction was achieved by comparison with the 2008 mass spectral library of National Institute of Standard and Technology (NIST 2008). The NIST database of mass spectra can help to predict chemical structures of unknown GC-MS peaks through the comparison of mass fragmentation. The mass spectra of the identified compounds in crude bio-oil and aqueous fraction and their matching mass spectra from NIST database are presented in Appendix A.

The complex chemical composition of the crude bio-oil and the aqueous fraction makes it difficult, or even impossible, to perform a complete chemical characterization using single or even a combination of analysis techniques.

Therefore, the characterization of crude bio-oil and aqueous fraction by GC-MS will only detect a portion, mainly, lower molecular weight components that are volatile enough to pass through the GC column. Furthermore, despite the small detectable portion of the crude bio-oil and the aqueous fraction, many peaks were detected in GC-MS traces of both fractions, which also cause a very difficult task to identify them all. Thus, just major and identifiable peaks were identified in both GC-MS traces of the crude bio-oil and the aqueous fraction.

Figure 3.5 shows the GC-MS trace of crude bio-oil derived from the microwave enhanced pyrolysis of spruce woodchips. The major identified compounds in the crude bio-oil according to the NIST 2008 mass spectral database are summarised in Table 3.6.

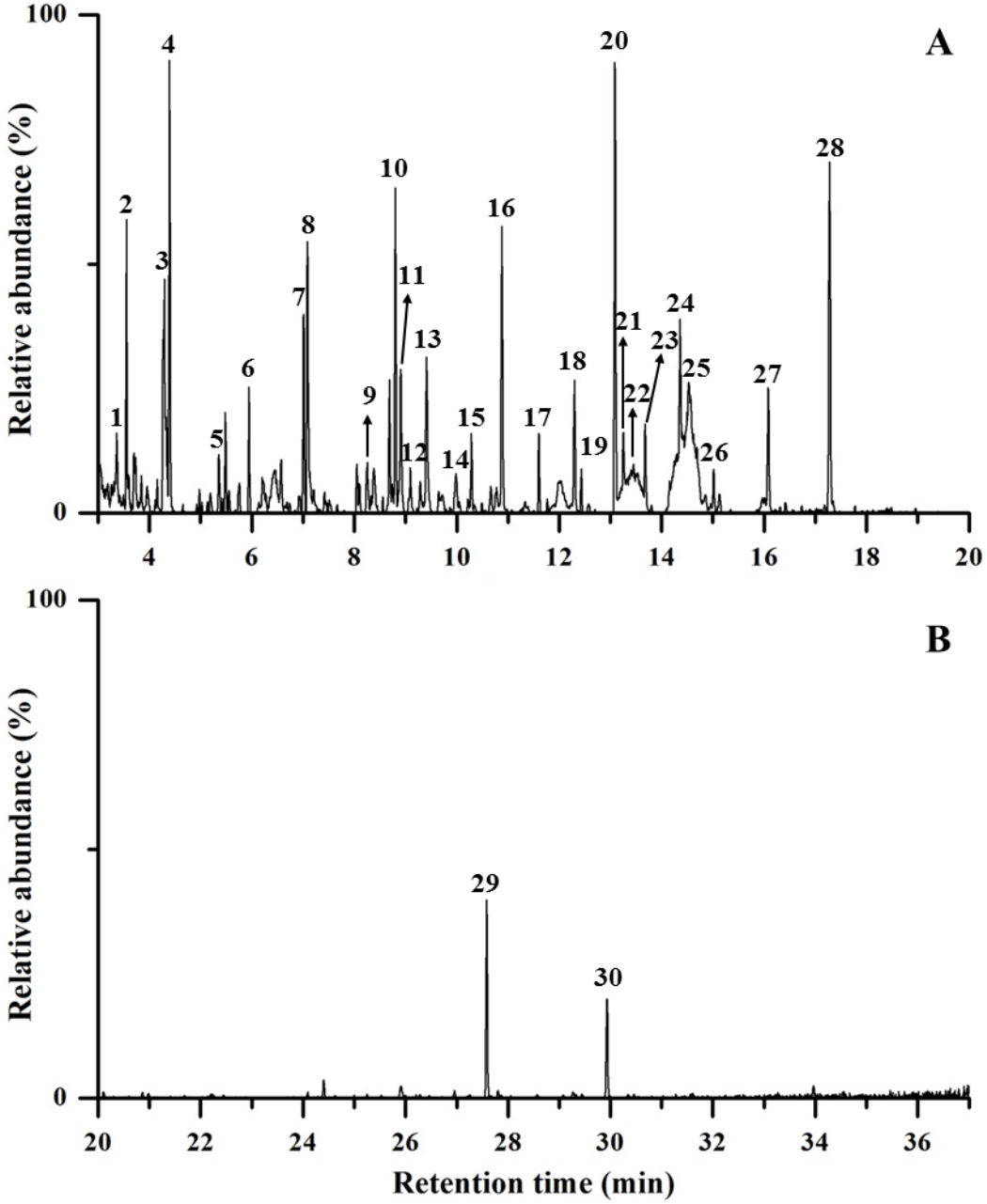

Figure 3.5: GC-MS spectrum of crude bio-oil derived from the microwave enhanced pyrolysis of spruce woodchips; A) Spectrum retention time from 3 to 20 min, B) The follow-up of spectrum retention time from 20 to 37 min.

Table 3.6: Major identified compounds in crude bio-oil derived from the microwave enhanced pyrolysis of spruce woodchips.

Identified compound[a]	Structure	Peak number[b]	Retention time (min)
Furfural	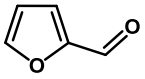	1	3.37
2-Furanmethanol	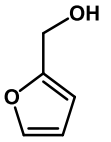	2	3.55
2(5H)-Furanone	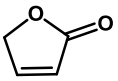	3	4.30
1,2-Cyclopentanedione	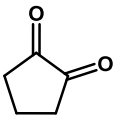	4	4.40
2-Hydroxy-gamma-butyrolactone	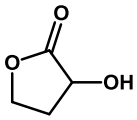	5	5.36
1,2-Cyclopentanedione, 3-methyl-	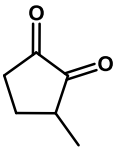	6	5.94
Phenol, 2-methoxy-	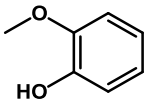	7	7.01
Cyclopropyl carbinol	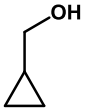	8	7.09
2(3H)-Furanone, dihydro-4-hydroxy-	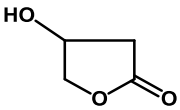	9	8.25
Phenol, 2-methoxy-4-methyl-	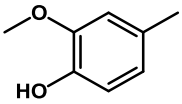	10	8.80
1,2-Benzenediol	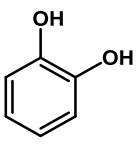	11	8.90

Identified compound[a]	Structure	Peak number[b]	Retention time (min)
1,4:3,6-Dianhydro-α-d-glucopyranose	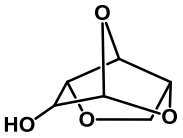	12	9.09
2-Furancarboxaldehyde, 5-(hydroxymethyl)-	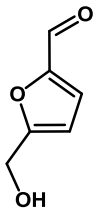	13	9.41
1,2-Benzenediol, 4-methyl-	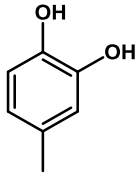	14	9.98
Phenol, 4-ethyl-2-methoxy-	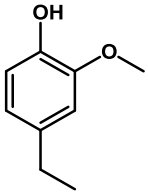	15	10.29
2-Methoxy-4-vinylphenol	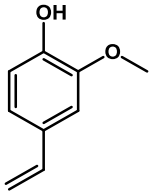	16	10.87
3-Allyl-6-methoxyphenol	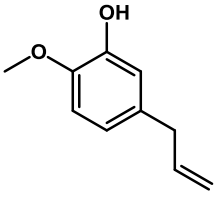	17	11.60
Benzaldehyde, 3-hydroxy-4-methoxy-	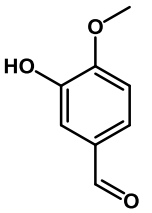	18	12.30

Identified compound[a]	Structure	Peak number[b]	Retention time (min)
Phenol, 2-methoxy-4-(1-propenyl)-	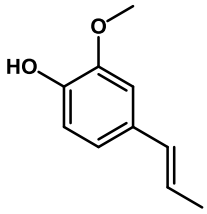	19	12.44
Phenol, 2-methoxy-4-(1-propenyl)-, (Z)-	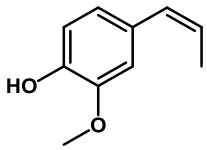	20	13.09
Phenol, 2-methoxy-4-propyl-	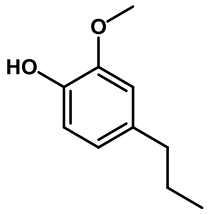	21	13.25
β-D-Glucopyranose, 1,6-anhydro-	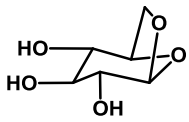	22	13.45
Ethanone, 1-(4-hydroxy-3-methoxyphenyl)-	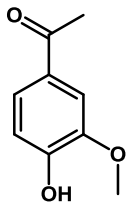	23	13.68
2-Propanone, 1-(4-hydroxy-3-methoxyphenyl)-	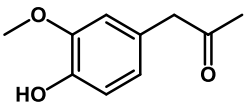	24	14.36
β-D-Glucopyranose, 1,6-anhydro-[c]	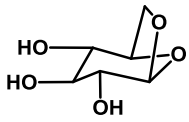	25	14.54
Phenol, 4-(3-hydroxy-1-propenyl)-2-methoxy-	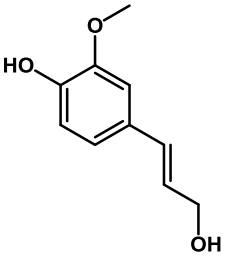	26	15.02

Identified compound[a]	Structure	Peak number[b]	Retention time (min)
Benzeneacetic acid, 4-hydroxy-3-methoxy-	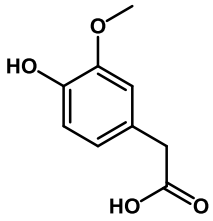	27	16.08
4-Hydroxy-2-methoxycinnamaldehyde	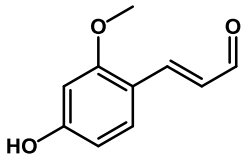	28	17.28
10,11-Dihydro-10-hydroxy-2,3-dimethoxydibenz(b,f)oxepin	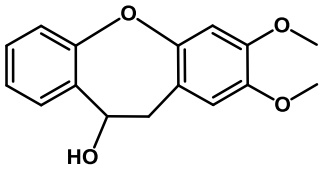	29	27.58
Unknown	Unknown	30	29.94

[a] According to NIST 2008 mass spectral database.
[b] As marked in Figure 3.5.
[c] Peak 25 is possibly an isomer of 1,6-anhydro-β-D-glucopyranose.

Overall, 29 major compounds have been identified *via* the GC-MS in the crude bio-oil, and the majority of these identified compounds were phenols, followed by furans and carbohydrate sugars.

Figure 3.6 shows the GC-MS trace of aqueous fraction derived from the microwave enhanced pyrolysis of spruce woodchips. The major identified compounds in the aqueous fraction according to the NIST 2008 mass spectral database are summarised in Table 3.7.

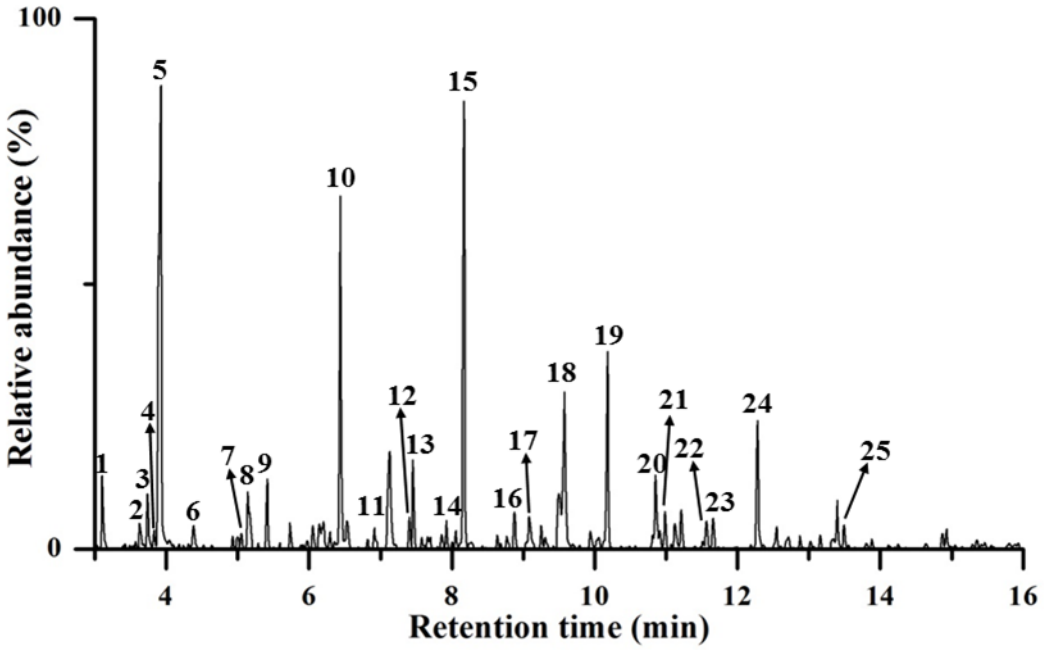

Figure 3.6: GC-MS spectrum of aqueous fraction obtained from the microwave enhanced pyrolysis of spruce woodchips.

Table 3.7: Major identified compounds in aqueous fraction obtained from the microwave enhanced pyrolysis of spruce woodchips.

Identified compound[a]	Structure	Peak number[b]	Retention time (min)
2-Furanmethanol	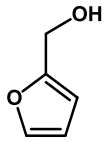	1	3.11
Butanoic acid, 4-hydroxy-	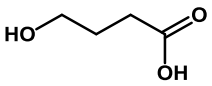	2	3.63
2(5H)-Furanone	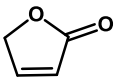	3	3.74
2-Cyclohexen-1-ol	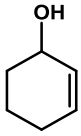	4	3.83
Ethanol, 2,2-diethoxy-	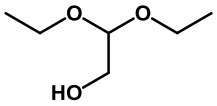	5	3.93

Identified compound[a]	Structure	Peak number[b]	Retention time (min)
2-Furancarboxaldehyde, 5-methyl-	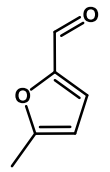	6	4.39
Phenol	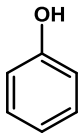	7	5.05
Furan, 2,5-diethoxytetrahydro-	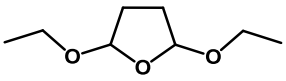	8	5.14
1,2-Cyclopentanedione, 3-methyl-	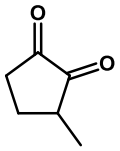	9	5.41
Phenol, 2-methoxy-	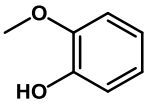	10	6.43
2-Cyclopenten-1-one, 3-ethyl-2-hydroxy-	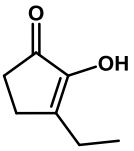	11	6.91
cis-3-Hexenal diethyl acetal	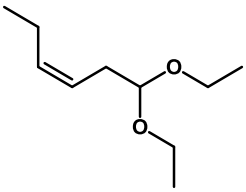	12	7.40
Cyclohexanone, 2,3-dimethyl-	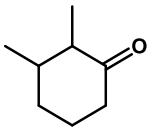	13	7.45
1,3-Benzenediol, 4-ethyl-	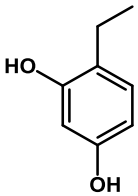	14	7.92
Phenol, 2-methoxy-4-methyl-	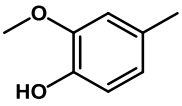	15	8.17

Identified compound[a]	Structure	Peak number[b]	Retention time (min)
3,4-Dimethoxytoluene	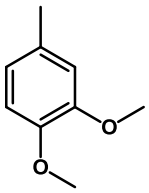	16	8.87
1,2-Benzenediol	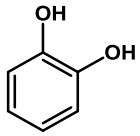	17	9.08
Phenol, 4-ethyl-2-methoxy-	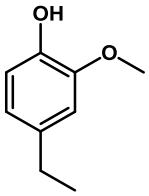	18	9.57
2-Methoxy-4-vinylphenol	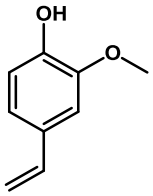	19	10.18
3-Allyl-6-methoxyphenol	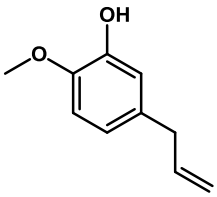	20	10.85
Phenol, 2-methoxy-4-propyl-	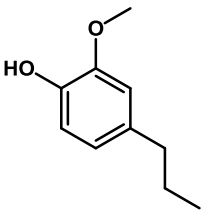	21	10.99
Benzaldehyde, 3-hydroxy-4-methoxy-	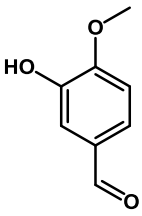	22	11.57

Identified compound[a]	Structure	Peak number[b]	Retention time (min)
Phenol, 2-methoxy-4-(1-propenyl)-	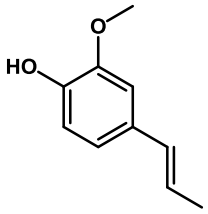	23	11.66
Phenol, 2-methoxy-4-(1-propenyl)-, (Z)-	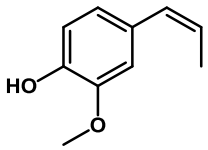	24	12.28
2-Propanone, 1-(4-hydroxy-3-methoxyphenyl)-	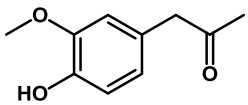	25	13.50

[a] According to NIST 2008 mass spectral database.
[b] As marked in Figure 3.6.

Generally, 25 major compounds were identified in the aqueous fraction, and the majority of these were phenols, followed by furans and ketones, including simple carboxylic acid compounds (formic and acetic acids) as the GC-MS cuts of the first 3 minutes of the run to preserve the MS from solvent.

3.7.2 Discussion

All the identified phenols appeared in the region between 7 and 18 minutes on the crude bio-oil GC-MS trace (Figure 3.5), and they are typical compounds derived from the breakdown of lignin during the microwave enhanced pyrolysis of spruce woodchips.[289] Most of these detected phenols were guaiacol (methoxy phenols) derivatives, such as (Z)-2-methoxy-4-(1-propenyl)-phenol (peak marked 20 in Figure 3.5 A), which is the highest intensity chromatographic peak observed in the crude bio-oil. Other non-guaiacol phenolic compounds were also detected in the GC-MS trace of crude bio-oil, for example 1,2-benzenediol and 4-methyl-1,2-benzenediol (peaks marked 11 and 14 in Figure 3.5 A, respectively). The formation of 1,2-benzenediol (catechol) is believed as a result of the further decomposition of guaiacols during pyrolysis,[290] as shown in Figure 3.7.

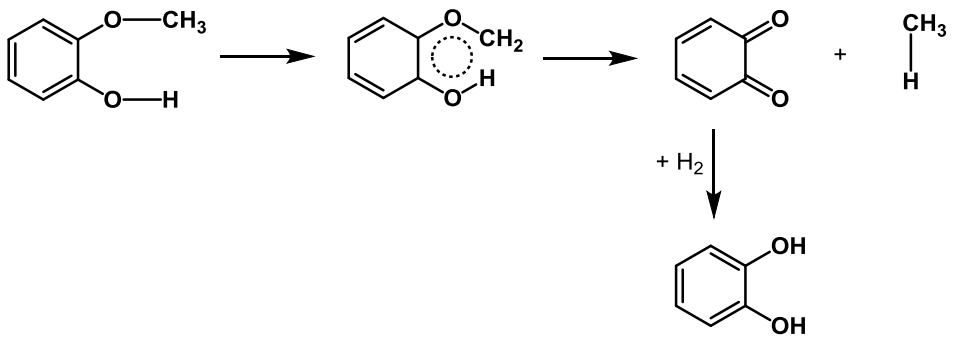

Figure 3.7: The suggested mechanism of 1,2-benzenediol formation from guaiacol during pyrolysis.[290]

The compounds identified in the region between 3 and 6 minutes in Figure 3.5 were mostly furans and their derivatives, for instance furfural (peak marked 1 in Figure 3.5 A) and 2-furanmethanol (peak marked 2 in Figure 3.5 A). In addition, 5-hydroxymethyl-2-furancarboxaldehyde (peak marked 13 in Figure 3.5 A) was also observed at *ca.* 9.41 minutes in the crude bio-oil GC-MS trace. The appearance of these furans and their derivatives was probably due to the thermal degradation of cellulose and hemi-cellulose during the microwave enhanced pyrolysis of spruce woodchips. Furthermore, the broad chromatographic peaks appeared at *ca.* 13.45 and *ca.* 14.54 minutes were identified as 1,6-anhydro-β-D-glucopyranose (peaks marked 22 and 25 in Figure 3.5 A), which is a carbohydrate sugar, and it is considered as the most important primary degradation product of cellulose.[267] The second peak (peak marked 25) is possibly an isomer of 1,6-anhydro-β-D-glucopyranose, however, a definite assignment of this isomer could not be confirmed by MS. 1,4:3,6-dianhydro-α-D-glucopyranose was also another significant identified sugar in the crude bio-oil (peak marked 12 in Figure 3.5 A), which is a dehydrated form of 1,6-anhydro-β-D-glucopyranose.[267] The chromatographic peak detected at the far end in the GC-MS trace of crude bio-oil (peak marked 29 in Figure 3.5 B) was identified as 10,11-dihydro-10-hydroxy-2,3-dimethoxydibenz(b,f)oxepin (mass of *ca.* 272 Da), which is possibly a product derived from the thermal degradation of lignin. The last chromatographic peak appeared at the far end in the GC-MS trace of the crude bio-oil (peak marked 30 in Figure 3.5 B) could not be identified using the NIST database of mass spectra, as none of the mass spectra hits sufficiently matches its mass spectrum (the highest mass detected for this unknown peak was *ca.* 344 Da).

However, a previous study was carried out by Takada *et al.*[291] under the title of "gas chromatographic and mass spectrometric (GC-MS) analysis of lignin-derived products from *Cryptomeria japonica* treated in supercritical water" have detected similar mass fragment peaks to peak 30 (in Figure 3.5 B), and they have assigned this peak as a lignin-derived dimeric product. Therefore, it is reasonable to assume that peak 30 (in Figure 3.5 B) is also a lignin-derived dimeric compound.

The appearances of phenols in the aqueous fraction GC-MS trace (Figure 3.6) were due to the thermal degradation of the lignin fraction in the spruce woodchips. As with the bio-oils, most of these detected phenols were guaiacols (methoxy phenols) and their derivatives, for example 2-methoxy-phenol, 2-methoxy-4-methyl-phenol, 4-ethyl-2-methoxy-phenol, 2-methoxy-4-vinylphenol, and (Z)-2-methoxy-4-(1-propenyl)-phenol (peaks marked 10, 15, 18, 19, and 24, respectively, in Figure 3.6). Furans were also detected in the aqueous fraction GC-MS trace, such as 2-furanmethanol (peak marked 1 in Figure 3.6), and 2(5H)-furanone (peak marked 3 in Figure 3.6). Cyclic ketones as well were present in the aqueous fraction, such as 3-methyl-1,2-cyclopentanedione (peak marked 9 in Figure 3.6), and 2,3-dimethyl-cyclohexanone (peak marked 13 in Figure 3.6), which are believed to be typical products derived from the thermal breakdown of cellulose fraction that probably occurred during the microwave enhanced pyrolysis of spruce woodchips.[292]

By comparing crude bio-oil GC-MS trace (Figure 3.5 A) with aqueous fraction (Figure 3.6), the crude bio-oil contained more complex species than the aqueous fraction, with many more chromatographic peaks, and also with greater intensities, appeared in the crude bio-oil GC-MS trace. This also further suggests that the crude bio-oil possibly has higher concentrations of organic species than the aqueous fraction. Interestingly, some of the pyrolysis products appeared in both GC-MS traces (the crude bio-oil and the aqueous fraction), such as 2-furanmethanol (peak marked 2 in Figure 3.5 A and peak marked 1 in Figure 3.6), 2(5H)-furanone (Peak marked 3 in Figure 3.5 A and Figure 3.6), 3-methyl-1,2-cyclopentanedione (peak marked 6 in Figure 3.5 A and peak marked 9 in Figure 3.6), 2-methoxy-phenol (peak marked 7 in Figure 3.5 A and peak marked 10 in Figure 3.6), 2-methoxy-4-methyl-phenol (peak marked 10 in Figure 3.5 A and peak marked 15 in Figure 3.6), 1,2-benzenediol (peak marked 11 in Figure 3.5 A and peak marked 17 in Figure 3.6), 4-

ethyl-2-methoxy-phenol (peak marked 15 in Figure 3.5 A and peak marked 18 in Figure 3.6), 2-methoxy-4-vinylphenol (peak marked 16 in Figure 3.5 A and peak marked 19 in Figure 3.6), and (Z)-2-methoxy-4-(1-propenyl)-phenol (peak marked 20 in Figure 3.5 A and peak marked 24 in Figure 3.6). However, in terms of their chromatographic peak intensity, all those species were more intense in the crude bio-oil GC-MS trace, except 2-methoxy-phenol (peak marked 7 in Figure 3.5 A and peak marked 10 in Figure 3.6) and 2-methoxy-4-methyl-phenol (peak marked 10 in Figure 3.5 A and peak marked 15 in Figure 3.6), which they were slightly less intense than that in the GC-MS trace of aqueous fraction (Figure 3.6). Surprisingly, carbohydrate sugars, for example 1,6-anhydro-β-D-glucopyranose, were not detected in the aqueous fraction, indicating all carbohydrate sugars were collected into the crude bio-oil, although the earlier ^{13}C NMR analysis results (in section 3.6) suggested the possibility of their presence in the aqueous fraction.

3.8 Conclusion

The work described in this chapter demonstrates the success of thermally converting a renewable biomass (spruce woodchips) into liquids (crude bio-oil and aqueous fraction), char and gas *via* the microwave enhanced pyrolysis technique. The product distribution obtained from the microwave enhanced pyrolysis of spruce woodchips were 18.5 % (w/w) for crude bio-oil, 29.5 % (w/w) for aqueous, 37.3 % (w/w) for char and 14.7 % (w/w) for gas (measured by mass difference).

The further study of these products by multiple analytical techniques allows a detailed understanding of their chemical nature to be developed, which is an important step to explore the many possible routes of potential applications. Among the three obtained pyrolysis fractions (crude bio-oil, aqueous and char), the crude bio-oil was found to be the most important pyrolysis fraction that could be an interesting source to many potential applications.

The microwave set-up that has been used in this study helped to separate (*in-situ*) most pyrolysis water from the crude bio-oil, and the water content in the crude bio-oil was found to be just 4.7 % (w/w). The ash content was low in the crude bio-oil and found to be <0.1 % (w/w). The ICP-MS analysis of the metal contents of spruce

woodchips and its pyrolysis products revealed that the spruce woodchips contain high levels of calcium (~1616 ppm) and potassium (~715 ppm), and after pyrolysis, these minerals were at greater levels in the char fraction, indicating the difficulty for these minerals to leave the microwave cavity during the pyrolysis.

From the ATR-IR analysis of crude bio-oil and aqueous fraction, the results indicated that the crude bio-oil contains aromatics and sugars, whereas the aqueous fraction contains mainly water and carboxylic acids. In addition, ^{13}C NMR analysis added more characterization information into the crude bio-oil and aqueous fraction. The result from the ^{13}C NMR analysis confirms the presence of carbohydrate sugars, as well as the high aromatic content in crude bio-oil. Large portion of the aromatic content in the crude bio-oil is probably phenols, with mostly methoxy group attached to the phenol ring. Carbonyl carbon related compounds, such as simple carboxylic acids compounds, existed in great concentrations in the aqueous fraction. The results by ^{13}C NMR analysis would also suggest the likelihood of the presence of acetic and formic acids in aqueous fraction. The presence of alcohols in the aqueous fraction was also possible, as the ^{13}C NMR spectrum showed some intense signals that could be related to alcohol compounds.

The GC-MS analysis of crude bio-oil and aqueous fraction identified the major volatile compounds. The results showed that the crude bio-oil contain more complex volatile organic species than the aqueous fraction. The majority of the identified compounds *via* the GC-MS were phenols, furans and carbohydrate sugars in the crude bio-oil. In contrast, in the aqueous fraction, the majority of the identified compounds were phenols, furans and ketones, although acetic and formic acid elute with the solvent and therefore are excluded from the MS. However, the phenol concentration in the aqueous fraction is low, as their peaks were less intense in comparison to the same phenolic peaks intensity in the crude bio-oil GC-MS trace.

Chapter 4: Extraction and Characterisation of Phenols from Spruce-Derived Bio-oils

4.1 Introduction

In chemistry, separation methods are very important and fundamental in many analytical investigations, for example, in purifying synthetic products, and in isolating natural products from renewable sources. Therefore, for a chemist, it can be quite challenging to separate a product, especially from a complex mixture of hundreds or more of compounds within different chemical families. This challenge starts with choosing a separation method, and typically choosing an organic solvent, as most laboratory-scale separation techniques involve one or more of organic solvents.

The common laboratory-scale techniques used for separating chemicals are not all suitable for use to separate key chemicals in crude bio-oils.[293] The thermal and chemical instability of crude bio-oils and the richness of components with similar boiling points narrow the choice of separation techniques.[293]

This chapter will demonstrate the possibility of fractionating crude bio-oils into chemically valuable extracts *via* laboratory accessible techniques, such as supercritical CO_2 extraction technique. The main aim of carrying out these fractionation procedures was to isolate phenolic species from the crude bio-oil and, as will be demonstrated in Chapter 5, study their effect as a renewable antioxidants for use in fuels (biodiesel). Each fractionation procedure was supported with detailed characterization of the extracted components *via* GC-MS and GC-FID, as well as other techniques, for example, ATR-IR, ^{13}C NMR and total phenols by Folin-Ciocalteu assay.

4.2 Identification and Quantification of Phenolic Compounds in Crude Bio-oil Extracts

The identification of phenolic compounds in crude bio-oils generated from microwave enhanced pyrolysis of spruce woodchips was carried out by the use of gas chromatography-mass spectroscopy (GC-MS). The details on the GC-MS analysis method, apparatus and column used are described in the experimental chapter (section 2.3.5.1, Chapter 2). The identification of phenolic compounds separated by GC in crude bio-oils was based on the best match with the 2008 mass spectral library

of National Institute of Standard and Technology (NIST 2008) and a consideration of potential biomass decomposition pathways.

Two microwave enhanced pyrolysis experiments of the spruce woodchips were carried out at different stages during this study, and both crude bio-oil yields have been analysed *via* GC-MS, named here as 1st and 2nd extracts of crude bio-oil.

After the GC-MS analysis of the 1st crude bio-oil extract; 13 phenolic compounds were identified as shown in Figure 4.1 (A). However, for the 2nd crude bio-oil extract, 18 phenolic compounds were identified as shown in Figure 4.1 (B) (note that the retention time differ slightly between run A and B, due to slightly different GC conditions, particularly column length). The mass spectra for the identified phenolics in both crude bio-oil extracts and their best NIST library match of mass spectrum are shown in Appendix A.

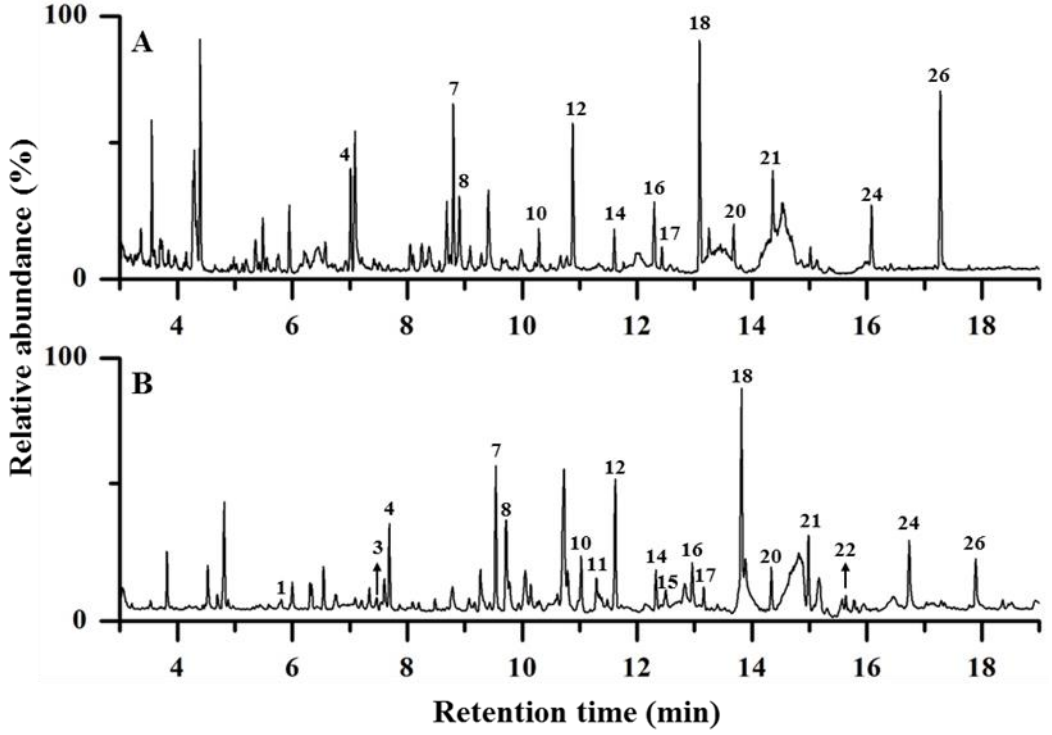

Figure 4.1: The GC-MS chromatograms of: (A) identified phenolic compounds in 1st extract of crude bio-oil; (B) identified phenolic compounds in 2nd extract of crude bio-oil (some phenolic peaks were identified later in Table 4.3, therefore, for consistency the phenolic peaks numbering were labeled here according to the phenolic peak retention times of Table 4.3).

The quantification of the phenolic compounds identified by GC-MS in the 1st and 2nd crude bio-oil extracts were achieved by the use of gas chromatography-flame ionization detector (GC-FID). The details on the GC-FID analysis method, apparatus and column used are also described in the experimental chapter (section 2.3.5.2, Chapter 2). The quantification of phenolic compounds in crude bio-oil extracts using GC-FID was based on a method associated with a concept of an effective carbon number (ECN).[256] Further information of the ECN concept is explained in the experimental chapter (section 2.3.5.3, Chapter 2).

The quantification results by GC-FID of the identified phenolic compounds in 1st and 2nd extracts of crude bio-oil by GC-MS are presented in Table 4.1 in terms of w/w of component (obtained using BHT as a representative phenolic standard and the effective carbon number (ECN) technique).

Table 4.1: The quantification and identification of GC detectable phenolic compounds in 1st and 2nd extracts of crude bio-oil.

Compound	Structure	Peak Num.	Ret. Time [a] (min)	Quantity (mg/g)[b]	
				1st extract	2nd extract
Phenol		1	5.81	/[c]	0[d]
Phenol, 4-methyl-	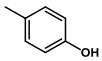	3	7.47	/	0
Phenol, 2-methoxy-		4	7.69	8.8	7.5
Phenol, 2-methoxy-4-methyl-	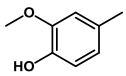	7	9.53	10.2	6.3
1,2-Benzenediol		8	9.72	6.2	9.4
Phenol, 4-ethyl-2-methoxy-	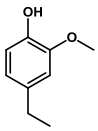	10	11.03	4.6	1.8

Compound	Structure	Peak Num.	Ret. Time [a] (min)	Quantity (mg/g)[b]	
				1st extract	2nd extract
1,2-Benzenediol, 4-methyl-	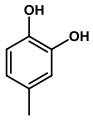	11	11.30	/	2.4
2-Methoxy-4-vinylphenol	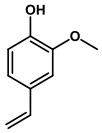	12	11.62	7.3	4.6
3-Allyl-6-methoxyphenol	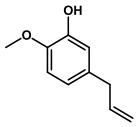	14	12.33	3.0	1.3
Phenol, 2-methoxy-4-propyl-	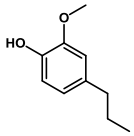	15	12.50	/	0.2
Benzaldehyde, 3-hydroxy-4-methoxy-	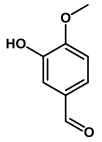	16	12.96	7.4	2.8
Phenol, 2-methoxy-4-(1-propenyl)-	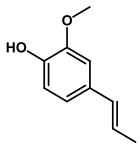	17	13.16	2.0	0.4
Phenol, 2-methoxy-4-(1-propenyl)-, (Z)-	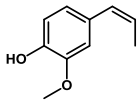	18	13.82	8.7	8.7
Ethanone, 1-(4-hydroxy-3-methoxyphenyl)-	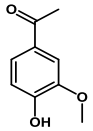	20	14.34	4.4	2.0
2-Propanone, 1-(4-hydroxy-3-methoxyphenyl)-	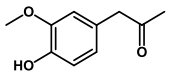	21	14.98	10.9	6.5
Phenol, 4-(3-hydroxy-1-propenyl)-2-methoxy-	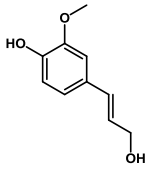	22	15.63	/	0.8

Compound	Structure	Peak Num.	Ret. Time [a] (min)	Quantity (mg/g)[b]	
				1st extract	2nd extract
Benzeneacetic acid, 4-hydroxy-3-methoxy-	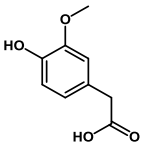	24	16.74	2.4	4.1
4-Hydroxy-2-methoxycinnamaldehyde	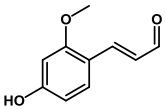	26	17.89	6.5	2.5

[a] Retention times according to detection in 2nd crude bio-oil extract.
[b] The standard error is ± 7% of the quantities quoted in this table, as described in section 2.3.5.2.
[c] Not detected.
[d] Detected but too small to quantify reliably.

1-(4-hydroxy-3-methoxyphenyl)-2-propanone (peak number 21), 2-methoxy-4-methylphenol (peak number 7), 2-methoxy-phenol (peak number 4), and (Z)-2-methoxy-4-(1-propenyl)phenol (peak number 18) are the most abundant phenolic components in 1st crude bio-oil extract present at 10.9, 10.2, 8.8, and 8.7 mg g^{-1}, respectively. The total content of identified phenols in the 1st crude bio-oil extract, as quantified by GC-FID, was 8.2% (w/w).

For the 2nd extract of crude bio-oil, 1,2-benzenediol (peak number 8), (Z)-2-methoxy-4-(1-propenyl)phenol (peak number 18), 2-methoxy-phenol (peak number 4), and 1-(4-hydroxy-3-methoxyphenyl)-2-propanone (peak number 21) are the most abundant phenolic components in 2nd crude bio-oil extract presented at 9.4, 8.7, 7.5, and 6.5 mg g^{-1}, respectively. The total content of identified phenols in the 2nd crude bio-oil extract, as quantified by GC-FID, was 6.1% (w/w).

It is noteworthy that all phenolic species identified in the 1st crude bio-oil extract were identified again in the 2nd crude bio-oil extract, however, their concentrations vary slightly, which could be attributed to the degree of the thermal degradation of lignin in spruce woodchips during the microwave pyrolysis experiment. This also could explain the appearance of more phenolic peaks in the 2nd crude bio-oil extract. However, the concentrations of these new phenolic species are mostly low.

Therefore, the reproducibility of the majority of these phenolic species is reasonable, while their individual and total concentration might vary slightly.

The phenolic content in pyrolysis crude bio-oils can be influenced by multi-factors, including pyrolysis temperature, heating rate, reactor pressure and holding time.[294, 295] However, pyrolysis temperature and heating rate are the most significant factors that affect the phenolic content in pyrolysis crude bio-oils.[294]

Garcia-Perez *et al.*[296] have carried out an investigation on the effects of temperature on the formation of lignin-derived oligomers during the fast pyrolysis of Mallee woody biomass. Within their discussion, they have linked the changes in the contents of the most significant compounds in the crude pyrolysis bio-oils (*e.g.*, phenolic compounds) to the function of pyrolysis temperature. This was observed when they have carried out a number of fast pyrolysis experiments at different temperatures between 350-580 $^{\circ}$C, and they have found that phenols content (according to GC-MS) in the crude bio-oil were at maximum at the pyrolysis temperature of *ca.* 450 $^{\circ}$C, but not at higher pyrolysis temperatures. Their interpretation of this was that the increase in the yield/content of the phenolic compounds with increasing pyrolysis temperature (< 500 $^{\circ}$C) was a result of the intensification of the primary thermochemical reactions with temperature. However, the decrease in their yield/content at higher temperatures (> 500 $^{\circ}$C) indicates that the rates of the secondary thermochemical decomposition reactions surpassed the rates of primary thermochemical reactions that responsible for the formation of phenolic compounds that detectable by GC-MS.

Similar observations of the effect of pyrolysis temperature on the phenolic content were also reported when producing crude bio-oils using microwave-assisted pyrolysis of woody biomass.[297, 298] Therefore, the interpretation that the pyrolysis temperature has the most significant effect on the phenolic concentration in crude bio-oils could support the previous suggestion that the degree of the thermal degradation of lignin during the microwave pyrolysis of spruce woodchips has caused the changes in the individual phenolic concentration, as well as the appearance of new phenolic peaks in the 2nd crude bio-oil extract.

4.3 Multi-Solvent Fractionation of Crude Bio-oil

The 2nd crude bio-oil extract was subjected to two significant multi-solvent fractionation procedures. Each fractionation procedure was based on work that has been previously reported to fractionate phenolic species from bio-oils obtained by pyrolysis of lignocellulosic materials.[248-251] Both procedures have used water as the first step to fractionate crude bio-oil into water-insoluble phase and water-soluble phase. For the following steps reported here, one procedure used the water-insoluble phase, while the other used the water-soluble phase. Therefore, it was interesting to combine the two procedures to study in-depth each fraction produced from these two multi-solvent fractionation procedures. However, for clarity, each procedure is presented here under two subheadings: water-insoluble phase fractionation, and water-soluble phase fractionation.

4.3.1 Water-insoluble phase fractionation

Further fractionation of the 2nd crude bio-oil extract was carried out for the isolation of phenolics according to a previous reported method,[248-250] and fully described in the experimental chapter (section 2.2.1.1, Chapter 2) which produced a water-soluble extract, a neutral extract, a phenolic extract and an organic acids extract, as well as an insoluble and an aqueous residues that were not studied further. Approximately 57% (w/w) of the crude bio-oil was soluble in water and described as water-soluble extract after removing water by distillation. A total of 16.6% (w/w of the crude bio-oil) was recovered from the remaining water-insoluble phase by DCM extraction at three different pH levels. The phenolic extract extracted at pH ~ 6 had the highest extract amount of 11.2% (w/w) of the crude bio-oil, which was approximately equivalent to 2.1% (w/w) of the original woodchips. The quantities recovered of each fraction are shown in Table 4.2.

Table 4.2: Fractional weight distribution recovered from crude bio-oil *via* the water-insoluble phase fractionation experiment and its equivalent recovery percentage from the original woodchips.

Fraction	Recovery (% w/w) of crude bio-oil	Recovery (% w/w) of woodchips
Water-soluble extract	57	10.5
Neutral extract	2.7	0.5
Phenolic extract	11.2	2.1
Organic acids extract	2.7	0.5
Insolubles & aqueous residue [a]	26.4	4.9
Total (crude bio-oil)	100	18.5

[a] Calculated by difference.

Figure 4.2 shows the total identified phenolic peaks in GC traces. The analysis by GC-MS identified 18 phenolic compounds in the crude bio-oil. For the isolated fractions, 8 phenolic compounds were identified in the water-soluble extract, 12 phenolic compounds in the neutral extract, 18 phenolic compounds in the phenolic extract, and 15 phenolic compounds in the organic acids extract. The mass spectra and assignments are provided in Appendix A. Some new phenolic compounds were detected after the fractionation of the crude bio-oil on the GC-MS. The likely explanation for this could be the low phenolic compound concentration in the crude bio-oil or overlap with other peaks in GC-MS chromatogram.

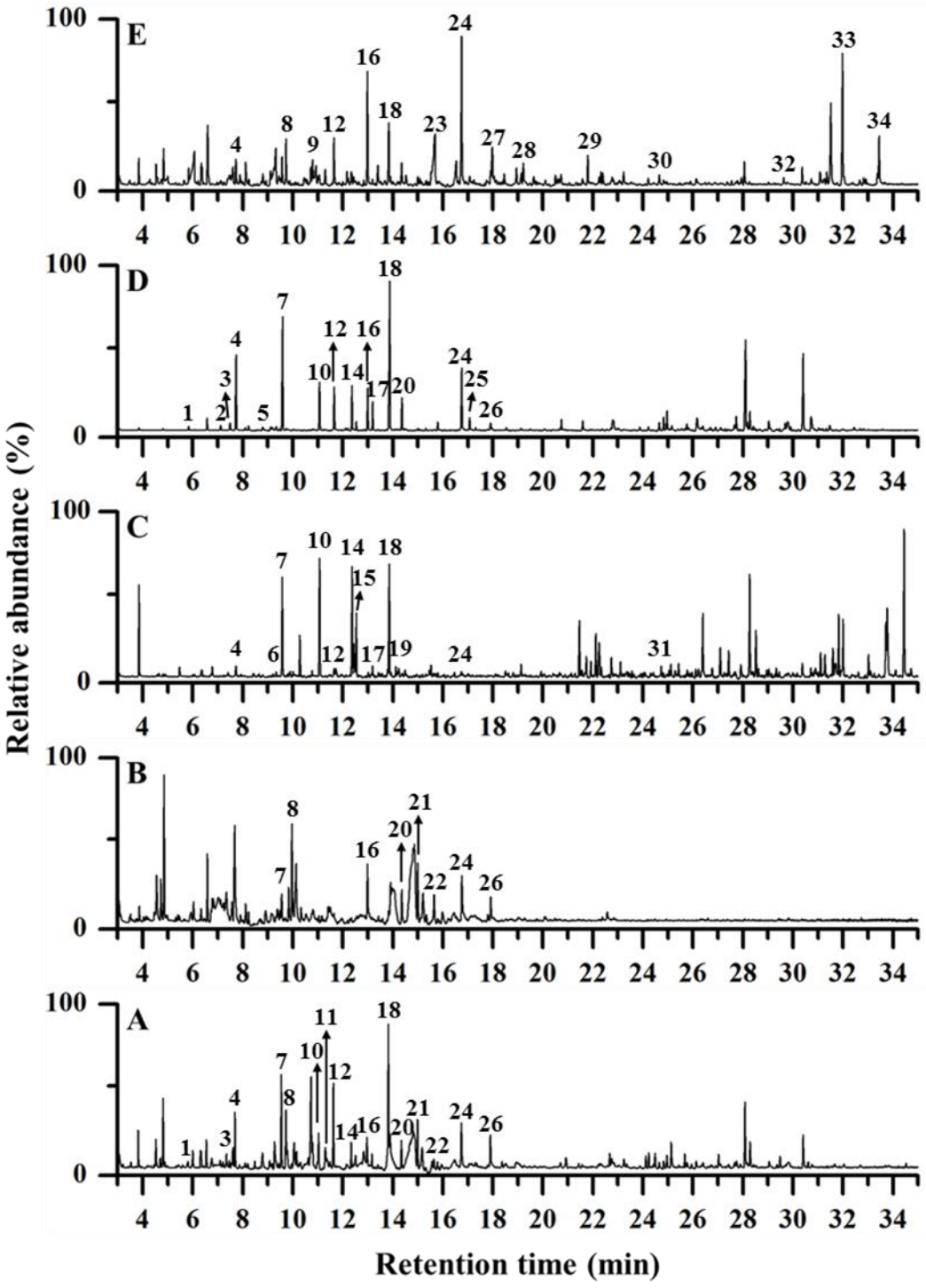

Figure 4.2: The GC-MS chromatograms of the identified phenolic compounds in: A) 2nd extract of crude bio-oil; B) Water-soluble extract; C) Neutral extract; D) Phenolic extract; and E) Organic acids extracts.

The quantification results by GC-FID of the identified phenolics by GC-MS are presented in Table 4.3 in terms of w/w of component.

Table 4.3: Identification and quantification of phenolic compounds in 2nd extract of crude bio-oil and in its extracted fractions.

Compound	Structure	Peak num.	Ret. time [a] (min)	Quantity (mg/g)[b]				
				2nd crude bio-oil ex.	Water-soluble ex.	Neutral ex.	Phenolic ex.	Organic acids ex.
Phenol		1	5.81	0[c]	/[d]	/	0.9	/
Phenol, 2-methyl-		2	7.12	/	/	/	0.5	/
Phenol, 4-methyl-	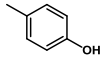	3	7.47	0	/	/	1.7	/
Phenol, 2-methoxy-		4	7.69	7.5	/	1.0	21.3	3.4
Phenol, 2,5-dimethyl-		5	8.79	/	/	/	0.1	/
1,3-Benzenediol, 4-ethyl-		6	9.33	/	/	0.5	/	/
Phenol, 2-methoxy-4-methyl-	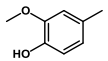	7	9.53	6.3	0.7	14.0	35.2	/

Compound	Structure	Peak num.	Ret. time [a] (min)	Quantity (mg/g)[b]				
				2nd crude bio-oil ex.	Water-soluble ex.	Neutral ex.	Phenolic ex.	Organic acids ex.
1,2-Benzenediol		8	9.72	9.4	7.2	/	/	4.6
1,2-Benzenediol, 3-methyl-		9	10.79	/	/	/	/	0.9
Phenol, 4-ethyl-2-methoxy-		10	11.03	1.8	/	13.5	8.4	/
1,2-Benzenediol, 4-methyl-		11	11.30	2.4	/	/	/	/
2-Methoxy-4-vinylphenol	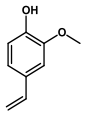	12	11.62	4.6	/	0.4	8.7	1.6
Phenol, 4-(2-propenyl)-	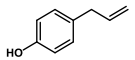	13	12.10	/	/	/	0.5	/
3-Allyl-6-methoxyphenol	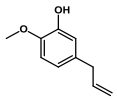	14	12.33	1.3	/	15.0	8.6	/

Compound	Structure	Peak num.	Ret. time [a] (min)	Quantity (mg/g)[b]				
				2nd crude bio-oil ex.	Water-soluble ex.	Neutral ex.	Phenolic ex.	Organic acids ex.
Phenol, 2-methoxy-4-propyl-	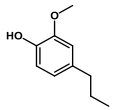	15	12.50	0.2	/	6.1	1.2	/
Benzaldehyde, 3-hydroxy-4-methoxy-	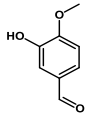	16	12.96	2.8	2.2	/	13.6	7.8
Phenol, 2-methoxy-4-(1-propenyl)-	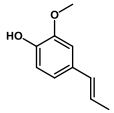	17	13.16	0.4	/	0.8	5.5	/
Phenol, 2-methoxy-4-(1-propenyl)-, (Z)-	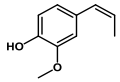	18	13.82	8.7	/	15.7	37.9	2.2
3,7-Benzofurandiol, 2,3-dihydro-2,2-dimethyl-		19	14.12	/	/	1.4	/	/
Ethanone, 1-(4-hydroxy-3-methoxyphenyl)-	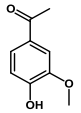	20	14.34	2.0	0.6	/	8.1	/

Compound	Structure	Peak num.	Ret. time [a] (min)	Quantity (mg/g)[b]				
				2nd crude bio-oil ex.	Water-soluble ex.	Neutral ex.	Phenolic ex.	Organic acids ex.
2-Propanone, 1-(4-hydroxy-3-methoxyphenyl)-	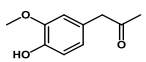	21	14.98	6.5	1.4	/	/	/
Phenol, 4-(3-hydroxy-1-propenyl)-2-methoxy-	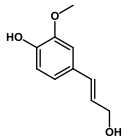	22	15.63	0.8	0.2	/	/	/
Benzoic acid, 4-hydroxy-3-methoxy-	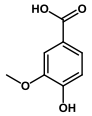	23	15.68	/	/	/	/	9.6
Benzeneacetic acid, 4-hydroxy-3-methoxy-	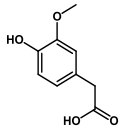	24	16.74	4.1	1.6	0	17.4	9.9
4-((1E)-3-Hydroxy-1-propenyl)-2-methoxyphenol	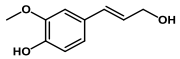	25	17.06	/	/	/	2.8	/
4-Hydroxy-2-methoxycinnamaldehyde	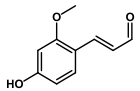	26	17.89	2.5	0.6	/	1.3	/

Compound	Structure	Peak num.	Ret. time [a] (min)	Quantity (mg/g)[b]				
				2nd crude bio-oil ex.	Water-soluble ex.	Neutral ex.	Phenolic ex.	Organic acids ex.
Benzeneacetic acid, 4-hydroxy-3-methoxy-, methyl ester	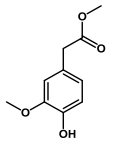	27	17.97	/	/	/	/	2.6
Phenylacetylformic acid, 4-hydroxy-3-methoxy-	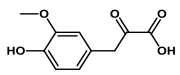	28	19.22	/	/	/	/	1.3
Naphtho[2,3-c]furan-1,4-dione, 3,3a,9,9a-tetrahydro-6-hydroxy-7-methoxy-	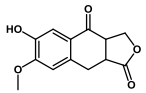	29	21.80	/	/	/	/	1.5
2H-1-Benzopyran-7-ol, 3,4-dihydro-3-(4-hydroxy-2-methoxyphenyl)-	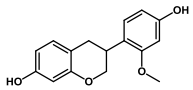	30	24.66	/	/	/	/	0
Podocarpa-8,11,13-triene-7β,13-diol, 14-isopropyl-	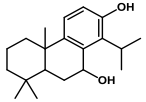	31	24.73	/	/	0.5	/	/
Phenol, 4-[2,3-dihydro-7-methoxy-3-methyl-5-(1-propenyl)-2-benzofuranyl]-2-methoxy-	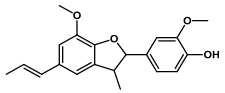	32	29.63	/	/	/	/	0

Compound	Structure	Peak num.	Ret. time [a] (min)	Quantity (mg/g)[b]				
				2nd crude bio-oil ex.	Water-soluble ex.	Neutral ex.	Phenolic ex.	Organic acids ex.
2(3H)-Furanone, dihydro-3,4-bis[(4-hydroxy-3-methoxyphenyl)methyl]-, (3R-trans)-	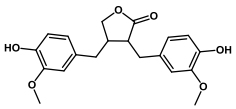	33	31.98	/	/	/	/	4.5
Naphtho[2,3-c]furan-1(3H)-one, 3a,4,9,9a-tetrahydro-6-hydroxy-4-(4-hydroxy-3-methoxyphenyl)-7-methoxy-, [3aR-(3aα,4α,9aβ)]-	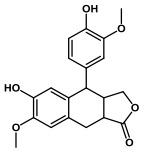	34	33.44	/	/	/	/	1.4

[a] Retention times according to detection in crude bio-oil GC-MS spectrum, some according to GC-MS detection in the other extracts.

[b] The standard error is ± 7% of the quantities quoted in this table, as described in section 2.3.5.2.

[c] Detected but too small to quantify reliably.

[d] Not detected.

1,2-Benzenediol (peak number 8) and (Z)-2-methoxy-4-(1-propenyl)phenol (peak number 18), are the most abundant phenolic components in the 2nd crude bio-oil extract present at 9.4 and 8.7 mg/g, respectively. The total content of phenols in crude bio-oil, as identified and determined by GC-FID, was 6.1% (w/w), while of the extracts, the phenolic had the highest total phenolic content of 17.4% (w/w), with (Z)-2-Methoxy-4-(1-propenyl)phenol (peak number 18) and 2-methoxy-4-methylphenol (peak number 7) being the most abundant phenolic components at 37.9 and 35.2 mg/g, respectively. In comparison with their quantity before fractionation, they are 4.3 and 5.6 times higher, respectively.

The heaviest phenolic species identified by GC had a mass of ca. 350 Da (equivalent to $C_{20}O_6H_{18}$), however, as it was suspected that larger polyaromatic species could be in the samples, but were not volatile enough to pass through the GC column, another phenolic quantification method was also carried out by Folin-Ciocalteu (FC) assay. The total phenolic determination by means of Folin-Ciocalteu (FC) assay showed a higher phenolic content for the crude bio-oil and the extracted fractions in comparison with GC-FID results. Table 4.4 shows the total phenolic content estimated by GC-FID and by Folin-Ciocalteu (FC) assay. In the phenolic extract, the phenolic content quantified by GC-FID was 17.4% (w/w), whereas by FC assay was 49.6% (w/w of eugenol equivalent). The large difference between the two methods could be consistent with the presence of phenolic compounds with high molecular weights, such as phenolic dimers, trimers or other larger phenolics, being too large to be detectable by GC due to being involatile at the maximum operating temperature of the GC column, but however detectable by the FC method.

Table 4.4: Summary of the phenols content estimated by GC-FID and by Folin-Ciocalteu (FC) assay, and the ratio of these.

Sample ID	Total phenolic content by GC-FID (% w/w)[a]	Total phenols by FC assay (% w/w)[b]	Proportion of phenolic species detected by GC-FID (% w/w)[c]
2nd crude bio-oil extract	6.1	23	26.5
Water-soluble extract	1.5	13.7	10.9
Neutral extract	6.9	11.3	61.1
Phenolic extract	17.4	49.6	35.1
Organic acids extract	5.2	38.3	13.6

[a] Mass ratio of phenolics to the mass of total sample detected by GC-FID.
[b] Mass ratio of phenolics to the mass of total sample detected by Folin-Ciocalteu reagent, using eugenol as standard.
[c] Ratio of phenolic content by GC-FID to total phenols by FC assay.

ATR-IR spectra of the 2nd crude bio-oil extract and the extracted fractions are shown in Figure 4.3, along with the band assignments of the major absorption peaks, also summarized in Table 4.5. The broad absorption peak at *ca.* 3380 cm^{-1} was due to hydroxyl groups (-OH) present in the crude bio-oil and the extracted fractions. After fractionation, most of hydroxyl-containing molecules remained in the water-soluble phase, which is consistent with the crude bio-oil containing a high content of alcohol groups for instance, sugars. Furthermore, the strong absorbance peak at *ca.* 1043 cm^{-1} in the water-soluble phase spectrum is consistent with a C-O stretching of primary alcohols, which reinforces the suggestion that most of the alcohols stayed in the water-soluble phase. The neutral extract spectrum shows the lowest hydroxyl absorbance band of the hydroxyl groups suggesting that it has the lowest hydroxyl-containing molecules. According to the GC-FID results, the phenolic extract contains the highest amount of mono-phenolics, and hence, the hydroxyl absorbance band in the phenolic extract might be from phenols. The sharp absorbance peak at *ca.* 1517 cm^{-1} in the phenolic extract was attributed to aromatic C=C ring stretching, which also supports the presence of phenols. The C=O stretching band at the position of *ca.* 1716 cm^{-1} was due to carbonyl and/or carboxyl groups. This peak was intense in the

water-soluble phase and in the organic acids extract. The appearance of this band in the water-soluble phase could be from aldehydes, ketones, carboxylic acids and esters. However, in the organic acids extract, the majority of the absorbance could be from carboxylic acids and esters rather than aldehydes and ketones due to the low pH extraction level (< 2) when this fraction was extracted.

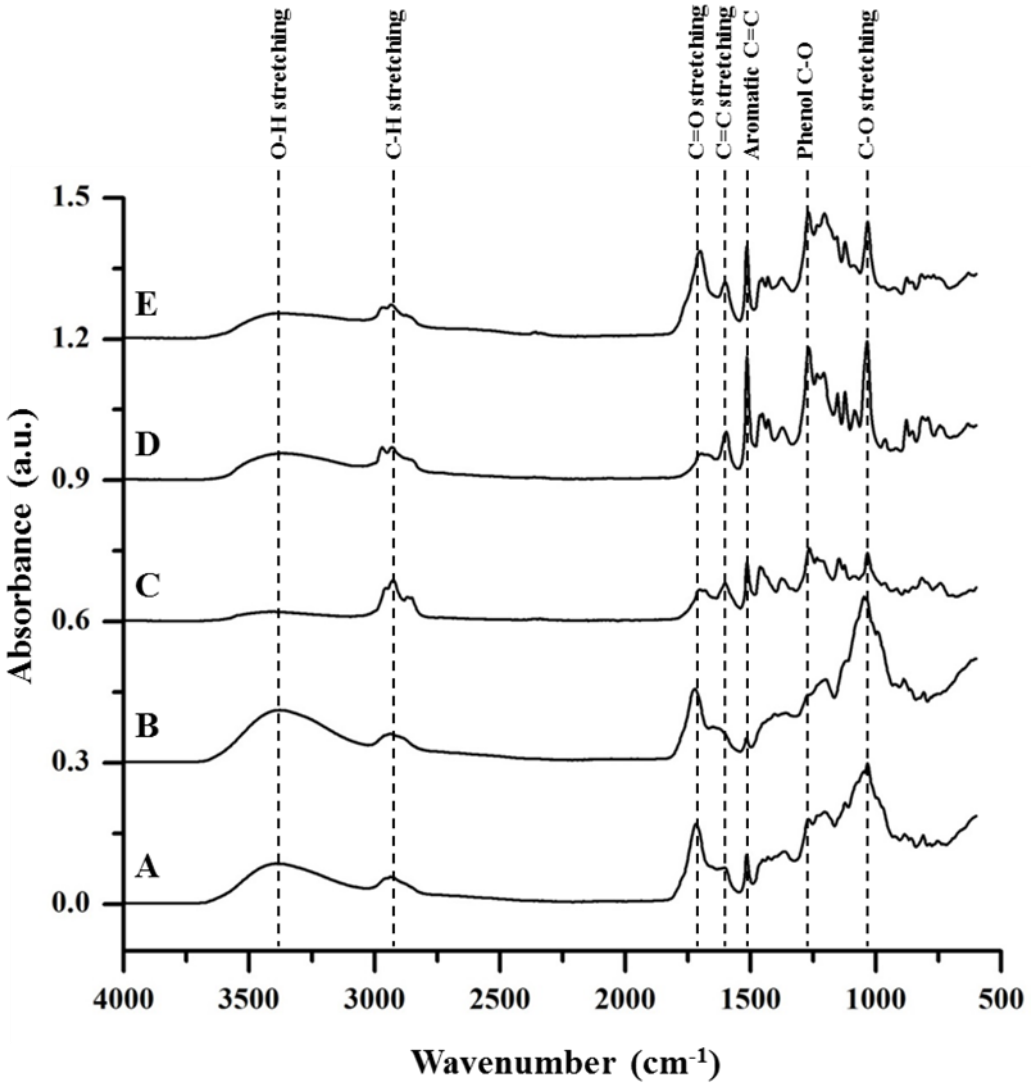

Figure 4.3: ATR-IR spectra of: A) Crude bio-oil; B) Water-soluble extract; C) Neutral extract; D) Phenolic extract; and E) Organic acids extract.

Table 4.5: ATR-IR data of functional groups and compound class.[250]

Wave numbers (cm^{-1})	Functional groups	Compound class
3380	O-H stretching vibration	phenol, alcohols, water, carboxylic acids
2940	C-H stretching vibration	alkanes
1716	Carbonyl/carboxyl C=O stretching	aldehydes, ketones, carboxylic acids, esters
1601	C=C stretching vibration	aromatics
1517	Aromatic C=C ring stretching	aromatics
1272	Phenol C-O	phenol
1043	Aliphatic ether C-O and alcohol C-O stretching	alcohols, ethers

^{13}C NMR spectroscopy was also employed for the characterization of the 2nd crude bio-oil and the extracted fractions, and their spectra are shown in Figure 4.4. The typical ^{13}C assignments relative to their chemical shift regions are summarized in Table 4.6 and also provide information on the typical chemical functional groups that appeared in the spectra.[286] From comparing the extracted fractions' spectra to the unfractionated crude bio-oil spectrum, it was obvious that the multi-solvent extraction interestingly fractionated the crude bio-oil into two major families; sugars and phenols. Carbohydrates sugars typically appear from 55 to 95 ppm on ^{13}C NMR spectra, which mostly appeared in the water-soluble extract. On the other hand, phenolic extract contains the most phenols fraction that usually lay between 95 to 165 ppm. The majority of these phenols in the phenolic extract may have a methoxy ($-OCH_3$) substitution due to the sharp peak appearance at ~56 ppm.

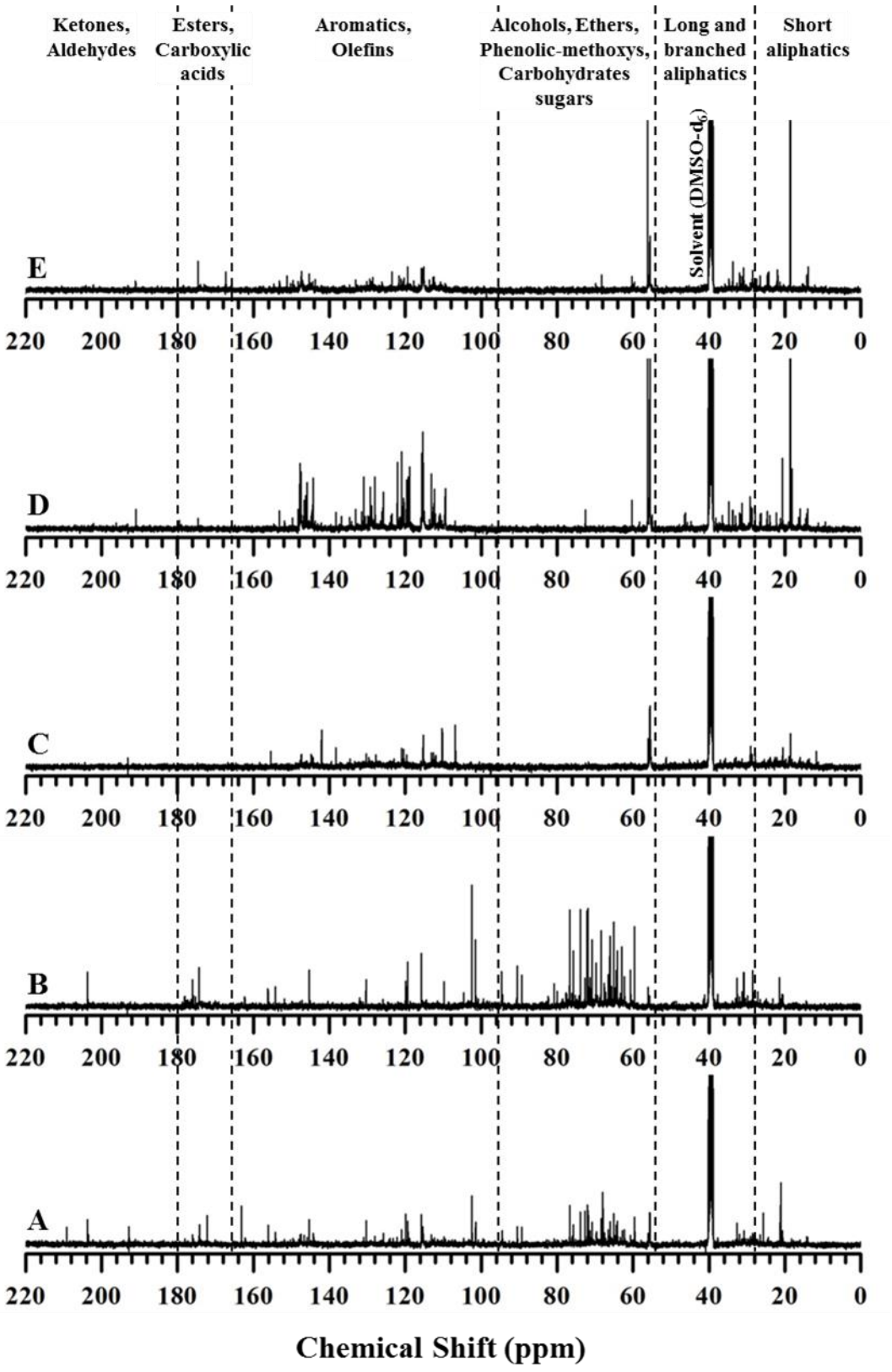

Figure 4.4: ^{13}C NMR spectra of: A) 2nd extract of crude bio-oil; B) Water-soluble extract; C) Neutral extract; D) Phenolic extract; and E) Organic acids extract.

Table 4.6: Peak assignments for ^{13}C NMR spectra.[286]

Chemical Shifts (ppm)	Carbon assignments
0-28	Short aliphatics
28-55	Long and branched aliphatics
55-95	Alcohols, ethers, phenolic-methoxys, carbohydrates sugars
95-165	Aromatics, olefins
165-180	Esters, carboxylic acids
180-215	Ketones, aldehydes

Further analysis of sugars in the water-soluble extract was carried out using High Performance Liquid Chromatography (HPLC). The details about this technique and apparatus used are explained in the experimental chapter (section 2.3.10, Chapter 2). The HPLC spectra of sugars standards and the water-soluble extract are shown in Figure 4.5. As can be seen from water-soluble extract trace (red trace in Figure 4.5), only levoglucosan was identified in the sample. The estimated concentration of levoglucosan in water-soluble extract was approximately 31 mg/g (equivalent to 3.1% w/w).

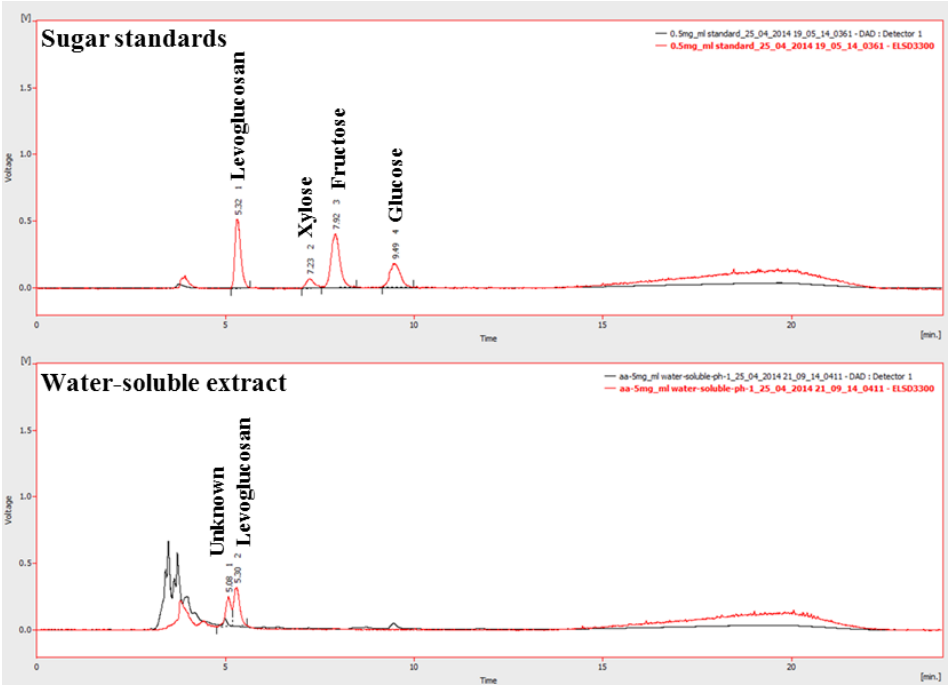

Figure 4.5: HPLC spectra of sugars standards and water-soluble extract (red trace: ELSD detector, and black trace: DAD detector).

4.3.2 Water-soluble phase fractionation

Further fractionation to the water-soluble phase of the 2nd crude bio-oil extract was also carried out for further investigation on the water-soluble phenolics. The fractionation procedure was carried out according to a previous reported study,[251] and fully described in the experimental chapter (section 2.2.1.2, Chapter 2). This fractionation procedure was based on a liquid-liquid extraction method, and produced a diethyl ether extract, a DCM extract, and a water-soluble residue. Approximately 16.7% (w/w) of the water-soluble extract was soluble in diethyl ether and described as diethyl ether extract after removing diethyl ether by distillation. The remaining water-soluble phase was also subjected to another solvent (DCM) extraction, and approximately 9.6% (w/w) was recovered and described as DCM extract after removing DCM by distillation. A water-soluble residue (73.7% w/w) of the remaining water-soluble phase was stored for further analysis after removing water by vacuum distillation. The quantities recovered of each fraction and their equivalent recoveries of the original woodchips are shown in Table 4.7.

Table 4.7: Fractional weight distribution recovered from crude bio-oil *via* the water-soluble phase fractionation experiment and its equivalent recovery percentage from the original woodchips.

Fraction	Recovery (% w/w) of crude bio-oil	Recovery (% w/w) of woodchips
Water-insoluble phase	43	7.9
Diethyl ether extract	9.5	1.8
DCM extract	5.5	1.0
Water-soluble residue [a]	42	7.8
Total (crude bio-oil)	100	18.5

[a] Calculated by difference.

Figure 4.6 shows the total identified phenolic peaks in the GC-FID traces of the 2nd extract of crude bio-oil, water soluble extract, diethyl ether extract, DCM extract, and water-soluble residue.

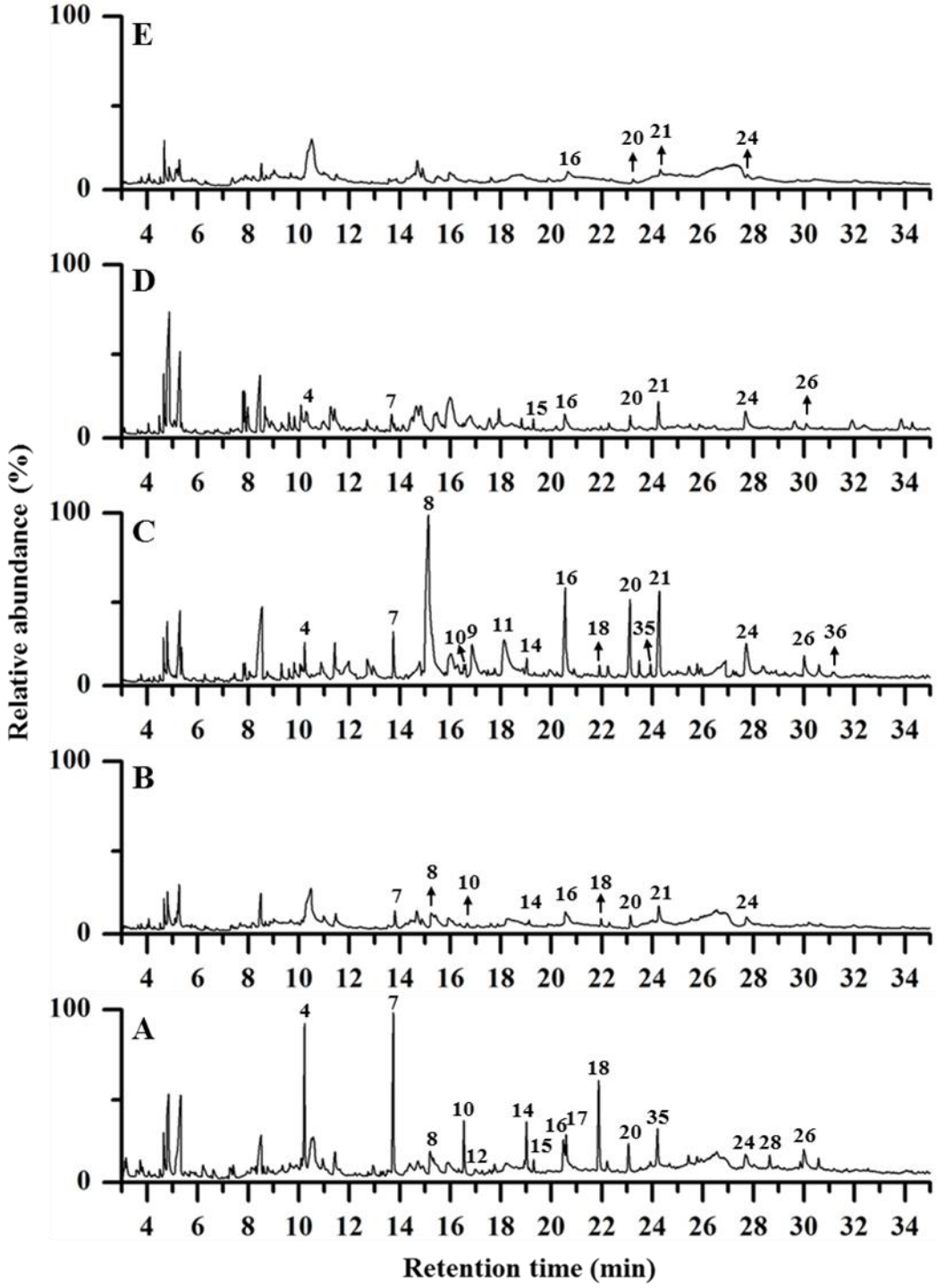

Figure 4.6: The GC-FID chromatograms of the identified phenolic compounds in: A) 2nd extract of crude bio-oil; B) Water-soluble extract; C) Diethyl ether extract; D) DCM extract; and E) Water-soluble residue. (For consistency, the 2nd crude bio-oil and the water soluble extracts were reanalyzed again together with the rest of extracts *via* another GC-FID apparatus with different programmed method at the point of this experiment. Therefore, the retention time of phenolic peaks differ from previous GC-MS chromatograms in Figure 4.2).

The analysis by GC-MS identified 15 phenolic compounds in the 2nd extract of crude bio-oil, and for the isolated fractions, 9 phenolic compounds were identified in the water-soluble extract, 15 phenolic compounds in the diethyl ether extract, 8 phenolic compounds in the DCM extract, and 4 phenolic compounds in the water-soluble residue. The mass spectra and assignments are provided in Appendix A (excluding DCM extract and water-soluble residue, as the assignments of their phenolic compounds were based on the retention time of phenolic compounds in the other extracts). It is noteworthy that the numbers and the retention times of the identified phenolics here in the 2nd crude bio-oil and in the water-soluble extracts are different when compared to Figure 4.2, and this is due to different GC-MS programmed method that was used at the point of carrying out this experiment.

Interestingly, four new phenolic compounds have appeared in the diethyl ether extract (peaks numbered 9, 11, 35, and 36 in Figure 4.6). This again could be due to the low concentration of these phenolic compounds in the 2nd crude bio-oil extract or overlap with other peaks in the 2nd crude bio-oil extract GC trace.

The quantification results by GC-FID of the identified phenolics by GC-MS are presented in Table 4.8 in terms of w/w of component. Due to different GC-MS and GC-FID programmed method used in this section, and for consistency, 2nd crude bio-oil and water-soluble extract identified phenols (with the new GC method) were quantified again and presented in Table 4.8.

Table 4.8: Identification and quantification of phenolic compounds in 2nd crude bio-oil extract and in its water-soluble phase extracted fractions.

Compound	Structure	Peak num.	Ret. time [a] (min)	Quantity (mg/g)[b]				
				2nd crude bio-oil ex.	Water-soluble ex.	Diethyl ether ex.	DCM ex.	Water-soluble re.
Phenol, 2-methoxy-	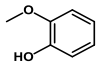	4	10.23	6.2	/[c]	2.7	3.0	/
Phenol, 2-methoxy-4-methyl-	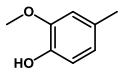	7	13.74	7.0	2.0	3.0	2.3	/
1,2-Benzenediol		8	15.19	3.3	2.6	24.4	/	/
Phenol, 4-ethyl-2-methoxy-	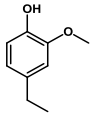	10	16.53	3.1	1.6	1.8	/	/
1,2-Benzenediol, 3-methyl-	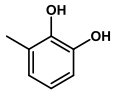	9	16.85	/	/	5.6	/	/
2-Methoxy-4-vinylphenol	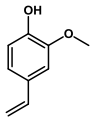	12	16.99	1.8	/	/	/	/

Compound	Structure	Peak num.	Ret. time [a] (min)	Quantity (mg/g)[b]				
				2nd crude bio-oil ex.	Water-soluble ex.	Diethyl ether ex.	DCM ex.	Water-soluble re.
1,2-Benzenediol, 4-methyl-	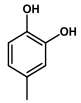	11	18.12	/	/	8.9	/	/
3-Allyl-6-methoxyphenol	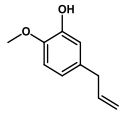	14	19.02	2.9	1.6	2.1	/	/
Phenol, 2-methoxy-4-propyl-	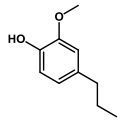	15	19.30	1.8	/	/	1.7	/
Benzaldehyde, 3-hydroxy-4-methoxy-	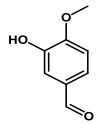	16	20.48	3.3	3.0	8.8	3.0	2.5
Phenol, 2-methoxy-4-(1-propenyl)-	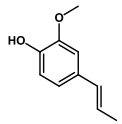	17	20.59	2.8	/	/	/	/
Phenol, 2-methoxy-4-(1-propenyl)-, (Z)-	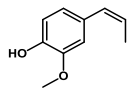	18	21.88	4.8	1.7	1.8	/	/

Compound	Structure	Peak num.	Ret. time [a] (min)	Quantity (mg/g)[b]				
				2nd crude bio-oil ex.	Water-soluble ex.	Diethyl ether ex.	DCM ex.	Water-soluble re.
Ethanone, 1-(4-hydroxy-3-methoxyphenyl)-	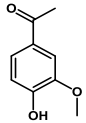	20	23.06	2.9	2.1	5.8	2.1	1.6
Benzoic acid, 4-hydroxy-3-methoxy-, methyl ester	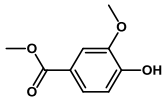	35	23.93	/	/	2.0	/	/
2-Propanone, 1-(4-hydroxy-3-methoxyphenyl)-	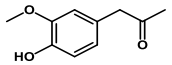	21	24.21	3.2	2.4	7.0	2.9	1.8
Benzeneacetic acid, 4-hydroxy-3-methoxy-	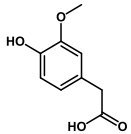	24	27.68	3.1	2.2	5.6	3.4	1.7
Phenylacetylformic acid, 4-hydroxy-3-methoxy-	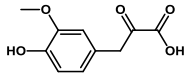	28	28.64	2.2	/	/	/	/
4-Hydroxy-2-methoxycinnamaldehyde	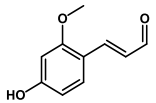	26	29.99	2.8	/	3.1	1.8	/

Compound	Structure	Peak num.	Ret. time [a] (min)	Quantity (mg/g)[b]				
				2nd crude bio-oil ex.	Water-soluble ex.	Diethyl ether ex.	DCM ex.	Water-soluble re.
β-(4-Hydroxy-3-methoxyphenyl)propionic acid	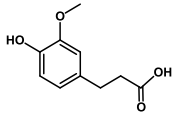	36	31.19	/	/	2.0	/	/

[a] Retention time according to detection in 2nd crude bio-oil extract GC-FID spectrum, some according to GC-FID detection in the other extracts.

[b] The standard error is ± 7% of the quantities quoted in this table, as described in section 2.3.5.2.

[c] Not detected.

2-methoxy-phenol (peak number 4) and 2-methoxy-4-methyl-phenol (peak number 7) are the most abundant phenolic components in crude bio-oil presented at 6.2 and 7.0 mg g^{-1}, respectively. The total content of phenols in crude bio-oil, as determined by GC-FID, was 5.1% (w/w), while of the extracts, the diethyl ether extract had the highest total phenolic content of 8.5% (w/w), with 1,2-benzenediol (peak number 8) and 4-methyl-1,2-benzenediol (peak number 11) being the most abundant phenolic components at 24.4 and 8.9 mg g^{-1}, respectively. Interestingly, 1,2-benzenediol quantity is 7.4 times higher in the diethyl ether extract when compared to its quantity before fractionation (3.3 mg g^{-1}).

The heaviest phenolic species identified by GC had a mass of *ca.* 210 Da (equivalent to $C_{10}H_{10}O_5$), however, as it was suspected that larger polyphenolic species could be in the sample, but were not volatile enough to pass through the GC column, another phenolic quantification method was also carried out by Folin-Ciocalteu (FC) assay. The total phenolic determination by this method showed a higher phenolic content for the crude bio-oil and the extracted fractions when compared to their GC-FID results. Table 4.9 shows the total phenolic content estimated by GC-FID and by Folin-Ciocalteu (FC) assay. In the diethyl ether extract, the phenolic content quantified by GC-FID was 8.5% (w/w), whereas by FC assay was 55.7% (w/w of mono-phenol equivalent). The great disagreement between these two methods could be again due to the presence of high molecular weights of phenolic species that were not detected by GC, but however detectable by the FC method.

Table 4.9: Summary of the phenolic content estimated by GC-FID and by Folin-Ciocalteu (FC) assay, and the ratio of these.

Sample ID	Total phenolic content by GC-FID[a] (% w/w)	Total phenols by FC assay[b] (% w/w)	Proportion of phenolic species detected by GC-FID (% w/w)[c]
2nd crude bio-oil	5.1[d]	23	22.2
Water-soluble extract	1.9[d]	13.7	13.9
Diethyl ether extract	8.5	55.7	15.3
DCM extract	2	12.8	15.6
Water-soluble residue	0.8	1.4	57.1

[a] Mass ratio of phenolics to the mass of total sample detected by GC-FID.
[b] Mass ratio of phenolics to the mass of total sample detected by Folin-Ciocalteu reagent, using eugenol as standard.
[c] Ratio of phenolic content by GC-FID to total phenols by FC assay.
[d] Quantified using another GC method, hence the difference in comparison with Table 4.4.

ATR-IR spectra of the 2nd crude bio-oil and the extracted fractions from the water-soluble phase are shown in Figure 4.7. The band assignments of the major absorption peaks are summarized earlier in Table 4.5, as most absorption peaks appeared in Figure 4.7 are similar to absorption peaks appeared in the ATR-IR spectra of extracts from the water-insoluble phase (Figure 4.3).

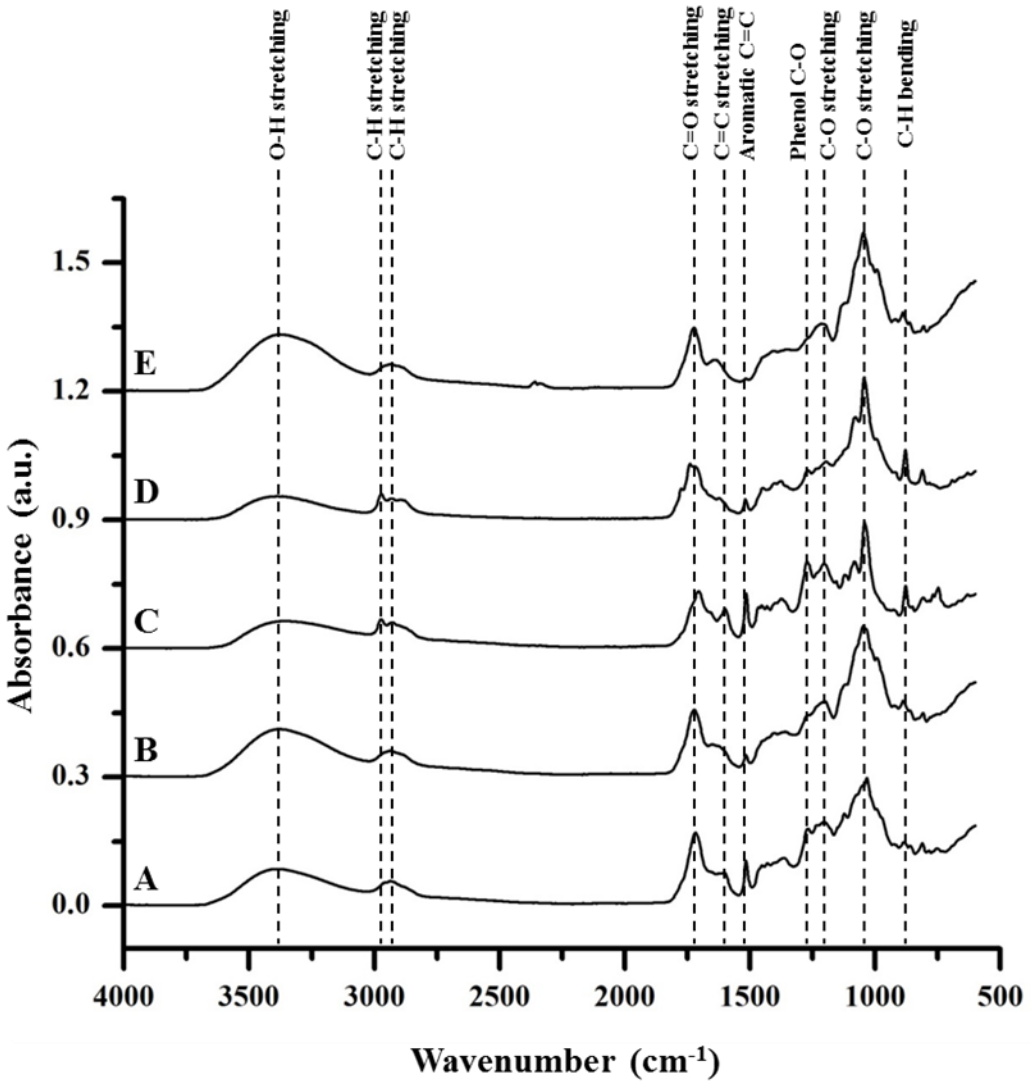

Figure 4.7: ATR-IR spectra of: A) Crude bio-oil; B) Water-soluble extract; C) Diethyl ether extract; D) DCM extract; and E) Water-soluble residue.

The interesting finding according to ATR-IR spectra of extracts from the water-soluble phase are that the water-soluble residue spectrum (spectrum E in Figure 4.7) is almost identical to the water-soluble extract (spectrum B in Figure 4.7). The solvent extraction by diethyl ether and the following extraction by DCM seems not significantly changed the overall ATR-IR spectrum of the water-soluble extract. The only minuscule observations when thoroughly comparing the ATR-IR spectrums of the water-soluble extract to the water-soluble residue are the absorption peaks of *ca.* 1515, 1270, and 1043 cm^{-1}.

The absorption peaks of *ca.* 1515 and 1270 cm^{-1} were due to aromatic C=C ring and phenol C-O stretching, respectively. These absorption peaks appeared less intense in the ATR-IR spectrum of water-soluble residue, suggesting that most aromatic species, in particular phenols, were extracted into diethyl ether and DCM extracts. In fact, the spectrum of the diethyl ether extract (spectrum C in Figure 4.7) shows the most strong absorption peaks of *ca.* 1515 and 1270 cm^{-1} when compared to the other ATR-IR spectra. Thus, the aromatic species were mostly extracted into the diethyl ether extract from the water-soluble extract. This ATR-IR observation agree with results presented earlier in Table 4.9, which showed that diethyl ether extract has the highest concentrations of phenolic species, present at 55.7% (w/w) as estimated by Folin-Ciocalteu (FC) assay.

Moreover, the strong absorption peak at *ca.* 1043 cm^{-1} in the water-soluble extract spectrum was due to C-O stretching vibration of primary alcohols, and this strong peak appeared slightly more intense in the water-soluble residue, which could be because of the concentration of primary alcohols were slightly increased after the solvent extraction by diethyl ether and DCM.

^{13}C NMR spectroscopy was also employed for the characterization of extracts from the water-soluble phase, and their spectra are shown in Figure 4.8. The typical ^{13}C assignments relative to their chemical shift regions are summarized earlier in Table 4.6, including information on the typical chemical functional groups that appeared in the spectra. When comparing the crude bio-oil spectrum with the other extracts, it can be seen that significant changes occurred to each fractionated extract. For instance, the complex peaks appeared in the chemical shift region between 55 and 95 ppm of the crude bio-oil spectrum remained in the water-soluble extract, but however, mostly disappeared in the diethyl ether extract as well as in the DCM extract, suggesting that the majority of these peaks could be related to carbohydrate sugars. Furthermore, the peaks appeared in the chemical shift region between 95 and 165 ppm of the crude bio-oil spectrum mostly disappeared in the water-soluble residue, but however, mostly appeared in the diethyl ether extract as well as in the DCM extract, indicating that the majority of these peaks could be related to aromatic compounds, particularly phenolic species.

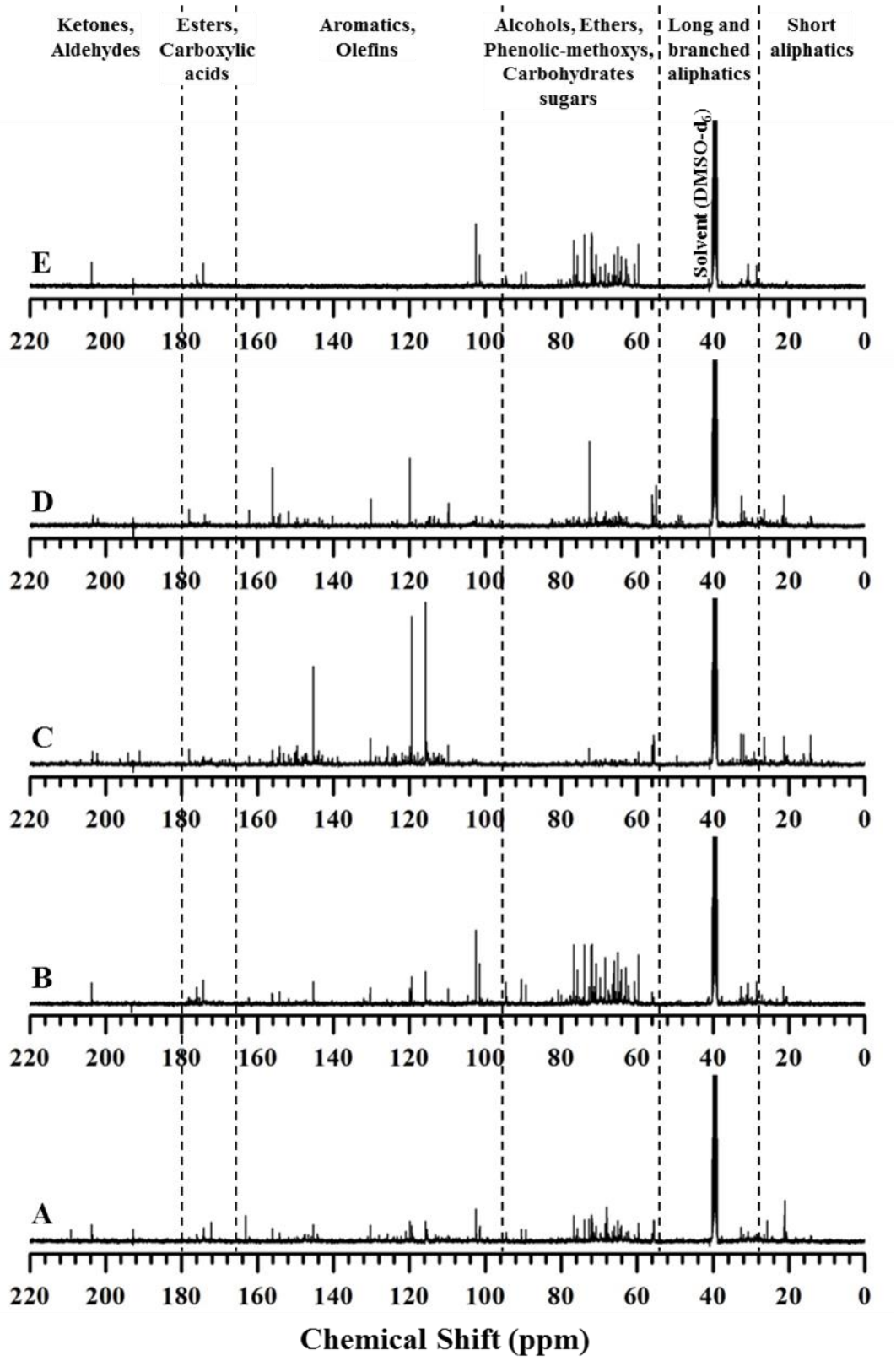

Figure 4.8: ^{13}C NMR spectra of: A) Crude bio-oil; B) Water-soluble extract; C) Diethyl ether extract; D) DCM extract; and E) Water-soluble residue.

According to GC-FID quantification results, 1,2-Benzenediol (catechol) was identified in the diethyl ether extract at a concentration of 24.4 mg g^{-1}, which is high when compared to other concentrations of identified phenolic species. Therefore, the three sharp peaks appeared in the aromatic region of the diethyl ether spectrum could be related to catechol presence in a relatively higher concentration in comparison to other phenolic species concentrations. In fact, after comparing these sharp peaks with a ^{13}C NMR spectrum of a catechol standard, it was confirmed that these peaks are indeed derived from the catechol molecule, see Figure 4.9.

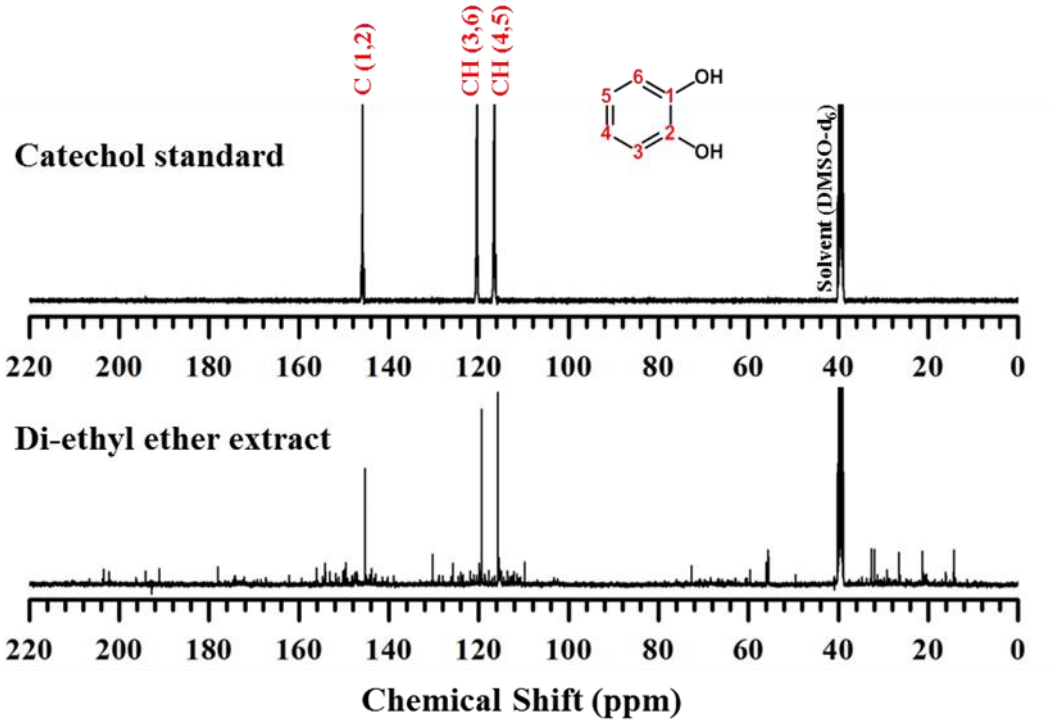

Figure 4.9: ^{13}C NMR spectra of diethyl ether extract and catechol standard.

The weight average molecular weights (Mw) of organic species in water-soluble extract and in its extracts were estimated by gel permeation chromatography with an evaporative light scattering detector (GPC-ELSD). The details of the apparatus, column used, sample preparation, and GPC standards are described in the experimental chapter (section 2.3.11, Chapter 2). The GPC-ELSD spectra of these extracts are shown in Figure 4.10, and the estimated molecular weights in each extract are presented in Table 4.10.

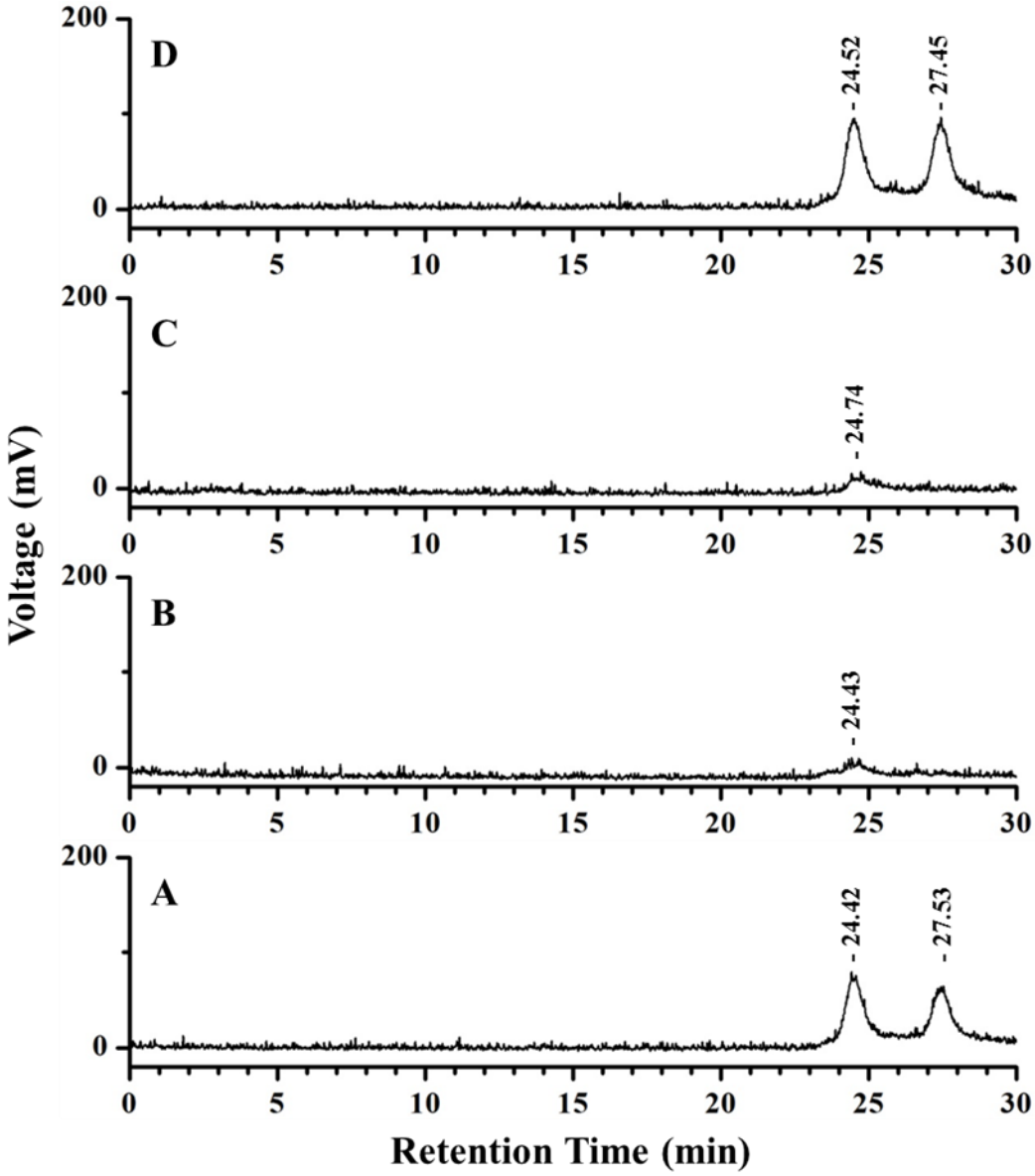

Figure 4.10: GPC-ELSD spectra of: A) water-soluble extract; B) di-ethyl ether extract; C) DCM extract; and D) water-soluble residue.

Table 4.10: The weight average molecular weight (Mw) of water-soluble extract and its fractions estimated by GPC-ELSD.

Extract ID	Retention time (min)	Mw (Da)
Water-soluble extract	24.42	715
	27.53	53
Diethyl ether extract	24.43	709
DCM extract	24.74	547
Water-soluble residue	24.52	657
	27.45	57

From the results presented in Table 4.10, the weight average molecular weights of organic species in water-soluble extract were estimated to be *ca.* 715 and 53 Da. For the diethyl ether and DCM extracts, they were estimated to be *ca.* 709 and 547 Da, respectively. The water-soluble residue has approximately similar weight average molecular weights (Mw) of organic species to the water-soluble extract, which were estimated to be *ca.* 657 and 57 Da. The low average molecular weight (Mw) of *ca.* 55 Da estimated in water-soluble extract and in water-soluble residue could be attributed to the presence of high content of light carboxylic acid compounds, *e.g.*, formic and acetic acids, and possibly light alcohols. Whereas, the high average molecular weight (Mw) of *ca.* 700 Da estimated in all samples could be related to the presence of polyaromatic species.

4.4 Supercritical CO_2 Extraction

4.4.1 Overview

When a fluid is described as supercritical, this means that the fluid is forced into a pressure and temperature beyond its critical point, see Figure 4.11.[299] Therefore, under these conditions, the properties of this fluid are positioned between those of a liquid and those of a gas.[299]

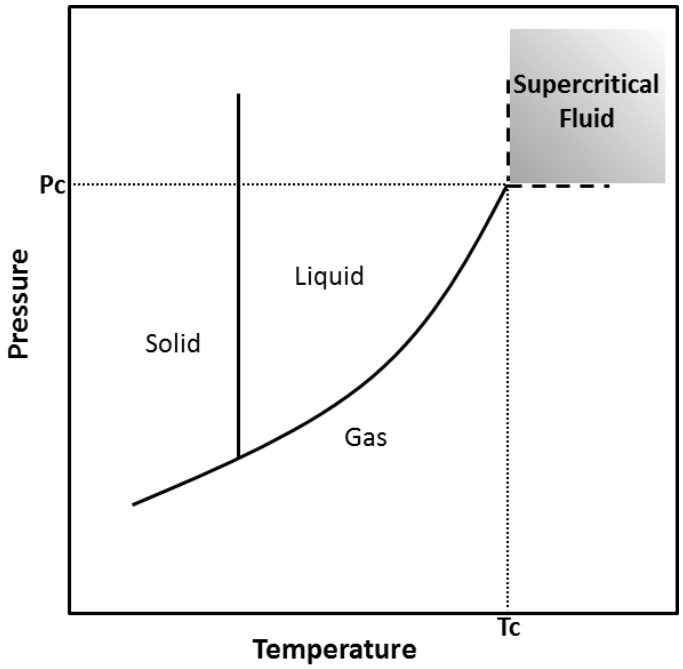

Figure 4.11: Typical pressure-temperature phase diagram of supercritical fluid.[299]

The diffusivity of a supercritical fluid is intermediate between the two states (liquid and gas), however, its density is comparable to a liquid and its viscosity is comparable to a gas, see Table 4.11.[299] Thus, the definition of the supercritical state of a fluid is a state in which liquid and gas are indistinguishable from each other, or a state in which the fluid becomes compressible as a gas even though having a density comparable to a liquid and, hence, comparable solvating power.[299]

Table 4.11: Range values of some physicochemical properties of gases, liquids and supercritical fluids.[299]

Fluid state	Density (ρ, g/cm^3)	Diffusivity (D_{AB}, cm^2/s)	Viscosity (μ, g/s cm)
Gas [a]	10^{-3}	10^{-1}	10^{-4}
Liquid [b]	1	$<10^{-5}$	10^{-2}
Supercritical [c]	0.3-0.8	10^{-3}-10^{-4}	10^{-4}-10^{-3}

[a] p = 1 bar; T = 21 °C. [b] p = 1 bar; T = 15-30 °C. [c] $p = p_c$; $T = T_c$.

Due to these different physicochemical properties, the extraction and/or fractionation *via* supercritical fluids offer several operational advantages over traditional extraction methods.[300] For instance, supercritical fluids have better diffusion properties than liquids.[300] This is because of their relatively high diffusivity and low viscosity, where they can diffuse easily through solid materials and, hence, can provide faster extraction yields when compared to liquids.[300] Furthermore, one of the key characteristics of a supercritical fluid is the option of manipulating its solvation power by altering pressure and/or temperature.[301] This is particularly useful for achieving high selectivity, especially when extracting and/or fractionating complex samples such as plant materials.[301] Also, the extraction by a supercritical fluid is usually conducted at relatively low temperatures, thus, it could be the most suitable technique to investigate thermally unstable compounds, where many undesirable reactions, such as oxidation, hydrolysis, rearrangement and degradation, could be effectively prevented.[300, 302]

The other advantages, in comparison with other extraction techniques, are the use of no or significantly few amount of organic solvents, the elimination of potential contamination of the product by extraction solvents, and the possibility of direct coupling with analytical chromatographic techniques, such as gas chromatography (GC) or supercritical fluid chromatography (SFC), which can be substantially practical for extraction and direct quantification of highly volatile compounds.[300, 303]

A wide range of solvents can be used as supercritical fluids.[303] Table 4.12 shows some of these solvents as well their critical properties.

Table 4.12: Critical properties of some selected solvents used in supercritical fluid extraction.[303]

Solvent	T_c (°C) [a]	P_c (bar) [b]
Ethene	9.4	50.4
Carbon dioxide	31.1	73.8
Ethane	32.3	48.7
Nitrous oxide	36.6	72.6

Solvent	T_c (°C) [a]	P_c (bar) [b]
Propane	96.8	42.5
n-Hexane	234.5	30.1
Acetone	235.1	47.0
Methanol	239.6	80.9
Ethanol	240.9	61.4
Ethyl acetate	250.2	38.3
Water	374.1	220.6

[a] T_c: critical temperature.

[b] P_c: critical pressure (values are converted from MPa (megapascal): 1 MPa = 10 bar).

The most common used solvent in supercritical fluid extraction and/or fractionation technology is carbon dioxide due to its low critical temperature (31.1 °C) and low critical pressure (73.8 bar).[301] Also, it is non-flammable, relatively cheap, readily obtainable in large quantities with high purity, and has lower toxicological effects than some of the conventional volatile organic solvents.[302, 304]

Additionally, there are a number of operational advantages that make carbon dioxide a popular choice over the wide range of solvents.[305] For instance, carbon dioxide is a gas at room temperature, thus, a complete elimination of carbon dioxide is achieved without any residues when the system is decompressed after an extraction process, leaving a solvent-free extract.[305] Another advantage is the possibility of recycling carbon dioxide internally when using this technology at an industrial scale.[303]

The negative side, however, of using pure supercritical carbon dioxide is its inefficiency in extracting more polar compounds from plant materials.[299] This is due to its low polarity. Therefore, to resolve this issue, highly polar compounds called 'modifiers' (also known as co-solvents) are commonly added in small quantities, which can make significant changes to the solvent properties of pure supercritical carbon dioxide.[300, 303] The most commonly used modifier in supercritical carbon dioxide extraction of plant materials is methanol because it is an effective polar modifier and is up to 20% miscible with carbon dioxide.[300] Another commonly used

modifier of supercritical carbon dioxide extraction is ethanol, especially when extracting natural products due to its lower toxicity in comparison with methanol.[300]

Another critical factor that can affect the extraction of natural products using supercritical fluid extraction technology is sample particle size.[300, 306, 307] Large particles could result in prolonged extraction as the process can become diffusion-controlled.[300, 307] Therefore, pulverizing the sample until it becomes a fine powder can improve the process efficiency by speeding up the extraction.[300, 306, 307] However, this may also cause a problem in keeping a good flow rate.[300, 307] Thus, an effective way to avoid this potential problem is by packing the sample with rigid inert materials such as glass beads or sea sand to prevent the samples from pressing into solid impermeable plugs and, hence, maintaining a smooth flow rate.[300]

To conclude, it is obvious that supercritical fluid extraction technology has immediate advantages over traditional extraction techniques. However, from an industrial point of view, the only serious drawback of scaling up this technology to a commercial scale is the higher investment costs when compared to the existing traditional extraction techniques.[307] Indeed, this will most likely be the case when supercritical fluid extraction technology is considered as an alternative to a single extraction step. It should, however, be developed as an integrated process for biomass processing, probably as part of a larger biorefinery.[308] Without such an integrated approach, the feasibility and the full potential of supercritical fluid technology cannot be recognized.[308]

4.4.2 Results and discussion

A further fractionation of the 1st crude bio-oil was carried out using a supercritical CO_2 extraction method. The detailed experimental procedure for sample preparation, apparatus, and supercritical CO_2 extraction parameters are described in the experimental chapter (section 2.2.2, Chapter 2). The crude material was separated by using four vessels set with different pressure levels of 200, 100, 75, and 1 bar, and with controlled temperature at 50, 50, 35, and 35 $^{\circ}$C, respectively. Therefore, the extraction procedure produced four extracts, named here CO_2-1, CO_2-2, CO_2-3, and CO_2-4.

The quantities recovered of each fraction are shown in Table 4.13. A total of 33.4% (w/w of the crude bio-oil) was extracted from the crude bio-oil into the four extraction systems, and the weight distribution of extracts was 5.6, 8.8, 1.5 and 17.5% (w/w) in CO_2-1, CO_2-2, CO_2-3 and CO_2-4, respectively. As can be seen, CO_2-4 has the highest extract amount of 17.5% (w/w), whereas, CO_2-3 has the lowest extract amount of 1.5% (w/w).

Table 4.13: Fractions weight distribution recovered from crude bio-oil *via* supercritical CO_2 fractionation experiment at 350 bar and 50 °C.

Fraction	Recovery (% w/w) of crude bio-oil	Recovery (% w/w) of woodchips
CO_2-1	5.6	0.8
CO_2-2	8.8	1.3
CO_2-3	1.5	0.2
CO_2-4	17.5	2.6
Residue [a]	66.6	10.1
Total (crude bio-oil)	100	15

[a] Calculated by difference.

From the previous results of the analysis of the 1st extract of crude bio-oil by GC-MS presented in Figure 4.1, the GC-MS had identified 13 phenolic species in the 1st crude bio-oil extract. Therefore, after the fractionation of the 1st extract of crude bio-oil into four extracts using the supercritical CO_2 technique, the analysis by GC-MS of the CO_2 extracts identified 12 phenolic species in the CO_2-1 extract, and 13 phenolic species in the rest of extracts (CO_2-2, CO_2-3, and CO_2-4), see Figure 4.12. The mass spectra and assignments for the identified phenolic peaks in all four CO_2 extracts are shown in Appendix A.

The quantification results by GC-FID of the identified phenolic species in the four CO_2 extracts by GC-MS are presented in Table 4.14 in terms of w/w of component.

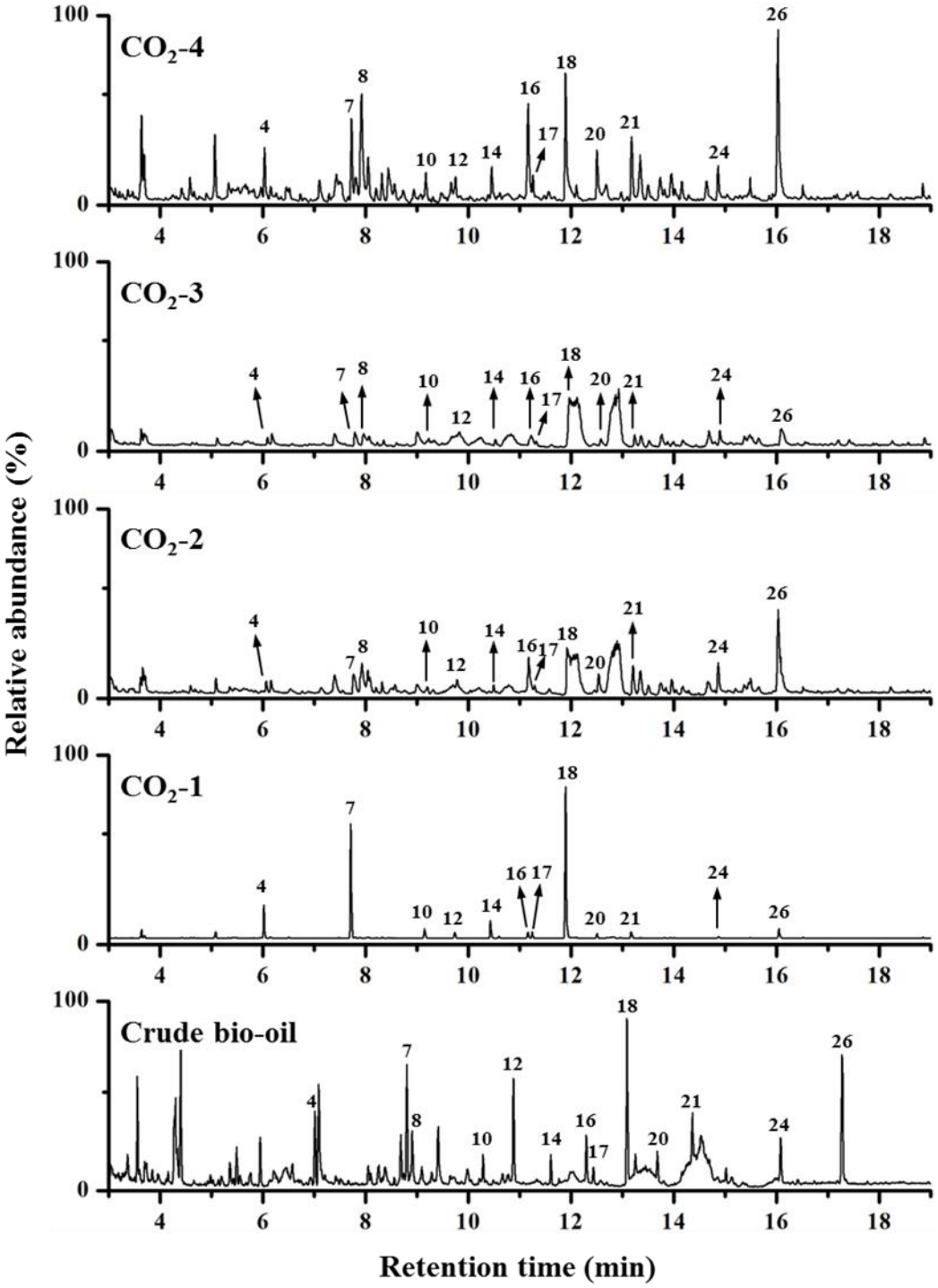

Figure 4.12: The GC-MS chromatograms of the identified phenolic compounds in 1st crude bio-oil extract and in CO_2 isolated fractions.

Table 4.14: The identification and quantification of GC detectable phenolic compounds in crude bio-oil and in the CO_2 isolated fractions.

Compound	Structure	Peak num.	Ret. time[a] (min)	Quantity (mg/g)[b]				
				1st crude bio-oil ex.	CO_2-1 ex.	CO_2-2 ex.	CO_2-3 ex.	CO_2-4 ex.
Phenol, 2-methoxy-		4	6.19	8.8	20.6	3.3	2.9	8.7
Phenol, 2-methoxy-4-methyl-	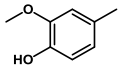	7	7.91	10.2	28.2	2.3	2.6	7.8
1,2-Benzenediol		8	8.07	6.2	/[c]	8.4	5.1	19.8
Phenol, 4-ethyl-2-methoxy-	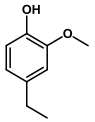	10	9.35	4.6	10.2	2.4	2.8	2.6
2-Methoxy-4-vinylphenol	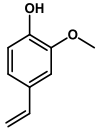	12	9.93	7.3	8.1	1.8	1.6	2.3

Compound	Structure	Peak num.	Ret. time[a] (min)	Quantity (mg/g)[b]				
				1st crude bio-oil ex.	CO_2-1 ex.	CO_2-2 ex.	CO_2-3 ex.	CO_2-4 ex.
3-Allyl-6-methoxyphenol	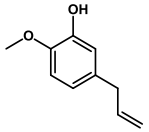	14	10.65	3.0	10.7	0.8	1.6	5.0
Benzaldehyde, 3-hydroxy-4-methoxy-	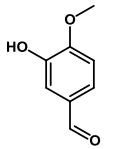	16	11.34	7.4	7.3	6.9	4.3	7.3
Phenol, 2-methoxy-4-(1-propenyl)-	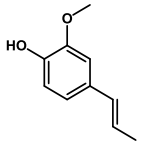	17	11.46	2.0	5.6	0.8	1.3	3.7
Phenol, 2-methoxy-4-(1-propenyl)-, (Z)-	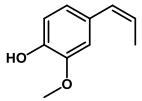	18	12.10	8.7	26.6	3.6	3.8	9.6
Ethanone, 1-(4-hydroxy-3-methoxyphenyl)-	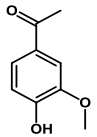	20	12.70	4.4	4.8	9.1	11.6	6.2

Compound	Structure	Peak num.	Ret. time[a] (min)	Quantity (mg/g)[b]				
				1st crude bio-oil ex.	CO_2-1 ex.	CO_2-2 ex.	CO_2-3 ex.	CO_2-4 ex.
2-Propanone, 1-(4-hydroxy-3-methoxyphenyl)-	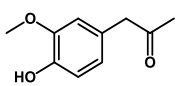	21	13.37	10.9	8.5	4.6	7.2	6.3
Benzeneacetic acid, 4-hydroxy-3-methoxy-	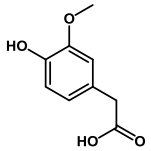	24	15.06	2.4	3.8	2.7	2.4	4.6
4-Hydroxy-2-methoxycinnamaldehyde	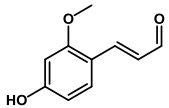	26	16.23	6.5	7.7	9.3	3.5	14.1

[a] Retention times according to detection in 1st extract of crude bio-oil.

[b] The standard error is ± 7% of the quantities quoted in this table, as described in section 2.3.5.2.

[c] Not detected.

1-(4-hydroxy-3-methoxyphenyl)-2-propanone (peak number 21) and 2-methoxy-4-methylphenol (peak number 7), were the most abundant phenolic components in the 1st extract of crude bio-oil presented at 10.9 and 10.2 mg g^{-1}, respectively. However, after supercritical CO_2 extraction, the distribution of concentrations of the phenolic species quantified in the 1st extract of crude bio-oil has changed with all four CO_2 extracts. For instance, in CO_2-1 extract, 2-methoxy-4-methylphenol (peak number 7) and (Z)-2-methoxy-4-(1-propenyl)phenol (peak number 18) are the most abundant phenolic components present at 28.2 and 26.6 mg g^{-1}, respectively. Therefore, in comparison with their quantity before extraction, they are 2.8 and 3.1 times higher, respectively.

It is noteworthy that 1,2-benzenediol (peak number 8) was not detected in the CO_2-1 extract, however, it was detected in the other CO_2 extracts, which indicate that 1,2-benzenediol is not stable under the supercritical CO_2 extraction pressure of 200 bar and at the temperature of 50 °C. This phenolic species was the most abundant phenolic component in the CO_2-4 extract presented at 19.8 mg g^{-1}, and in comparison with its quantity before extraction, it is 3.2 times higher.

Table 4.15 shows the total phenolic content estimated by GC-FID in the 1st extract of crude bio-oil and its supercritical CO_2 extracts. Therefore, according to GC-FID quantification results, the CO_2-1 extract has the highest total content of phenols at 14.2% (w/w), followed by CO_2-4 extract at 9.8% (w/w).

Table 4.15: Summary of the phenolic content estimated by GC-FID for 1st crude bio-oil extract and its supercritical CO_2 extracts.

Extract ID	Total phenolic content by GC-FID (% w/w)
1st crude bio-oil extract	8.2
CO_2-1 extract	14.2
CO_2-2 extract	5.6
CO_2-3 extract	5.1
CO_2-4 extract	9.8

ATR-IR spectra of the 1st extract of crude bio-oil and the supercritical CO_2 extracted fractions are shown in Figure 4.13. The band assignments of the major absorption peaks were summarized earlier in Table 4.5, as most significant absorption peaks appeared in ATR-IR spectra of Figure 4.13 are mostly similar to Figure 4.3.

The absorbed broad peak at *ca.* 3380 cm^{-1} was associated with hydroxyl groups (-OH) present in the crude bio-oil and supercritical CO_2 extracts. After supercritical CO_2 extraction, the absorption band intensity of hydroxyl groups noticeably decreased in CO_2-3 and CO_2-4 extracts, suggesting that both have the lowest hydroxyl-containing molecules. However, in the other hand, in CO_2-2 extract, the absorption band intensity of hydroxyl groups is almost identical to the absorption band intensity of hydroxyl groups in crude bio-oil, suggesting that CO_2-2 extract has the highest hydroxyl-containing molecules. The strong absorption band at *ca.* 1123 cm^{-1} in the crude bio-oil spectrum is consistence with a C-O stretching vibration of secondary alcohols and cyclic ethers. This absorption band is less intense in CO_2-3 and CO_2-4 extracts, which indicates a low content of secondary alcohols and cyclic ethers. Furthermore, the strong absorption band at *ca.* 1055 cm^{-1} in the crude bio-oil spectrum is also consistence with a C-O stretching vibration, but however, of primary alcohols and aliphatic ethers. This absorption band is sharp in CO_2-3 and CO_2-4 extracts, indicating the possibility of containing a high concentration of either primary alcohols or aliphatic ethers. It is noteworthy that the absorption bands at *ca.* 1123 and *ca.* 1055 cm^{-1} in the crude bio-oil spectrum could also be consistent with a C-O stretching vibration of sugars, suggesting the possibility of sugars presence in crude bio-oil, however, in CO_2-3 and CO_2-4 extracts, the sugars concentration could be very low because of the low intensity of the absorption band at *ca.* 1123 cm^{-1}.

The presence of phenols in the crude bio-oil was confirmed by GC-FID, therefore, the sharp band appeared at *ca.* 1515 cm^{-1} in the crude bio-oil spectrum is attributed to the aromatic C=C ring stretching, which also confirms the presence of phenols. Moreover, in supercritical CO_2 extracts, the same sharp band appeared in each spectrum, however, in CO_2-1 and CO_2-2 extracts, the sharp band is more intense than the other extracts, indicating the possibility of phenolic presence at higher concentrations. The appearance of the absorption band at *ca.* 898 cm-1 in CO_2-3 and CO_2-4 extracts is due to C-H bending vibration of either aromatics or alkenes.

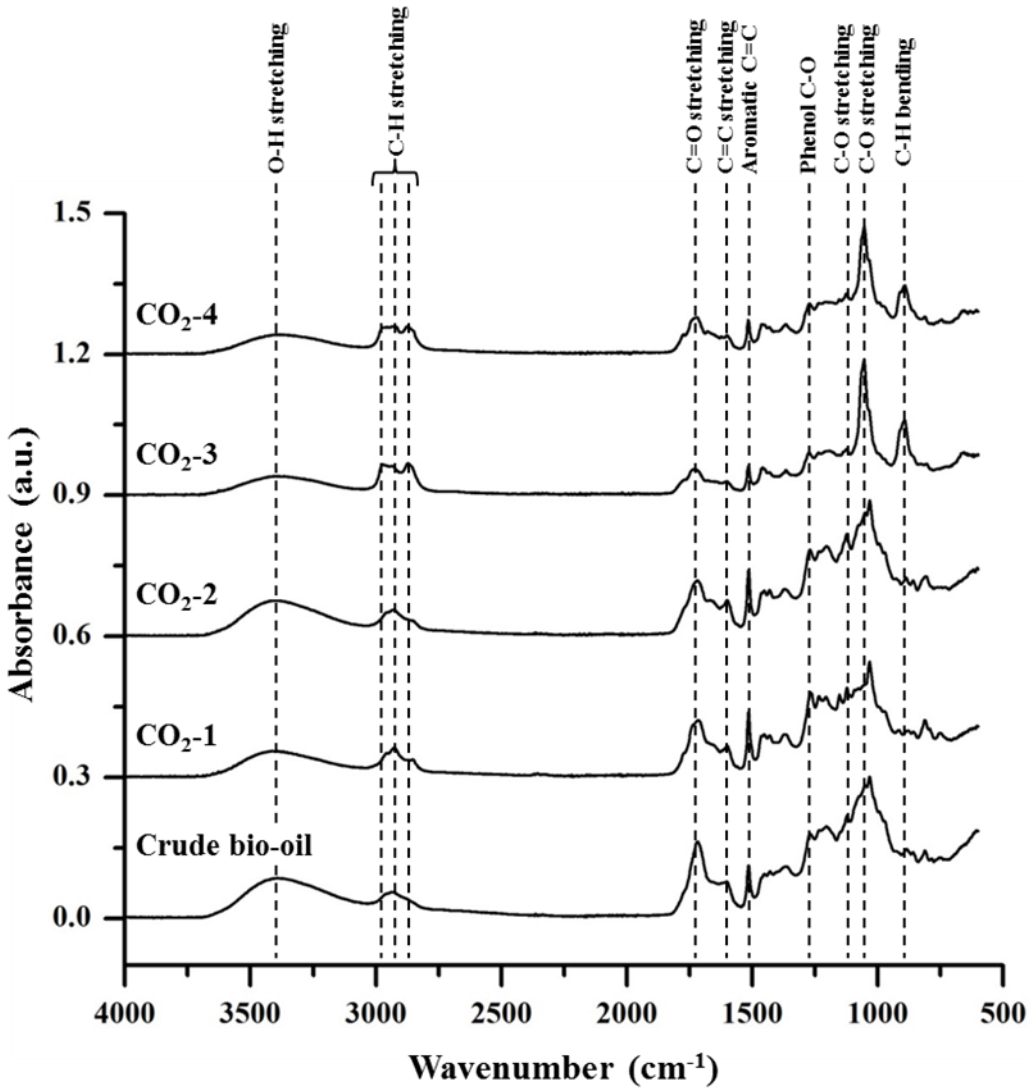

Figure 4.13: ATR-IR spectra of crude bio-oil and its supercritical CO_2 isolated extracts (spectra offset vertically for clarity).

4.5 Discussion of the Phenolic Separation and Quantification

Bio-oils derived from biomass pyrolysis contain hundreds of compounds with relatively high amount of oxygen-containing organic species. The quantities of these various components in the bio-oil are strongly dependent on the biomass feedstock, as well as the production method and reaction conditions.[128] Lately, increasing attention has been paid to the recovery of high-value chemicals from bio-oil, more specifically, the recovery of oxygen-containing organic compounds, such as alcohols and phenols, which are value-added chemicals used in industry and in many other applications.[309] Currently, most oxygen-containing chemicals are synthesized from

crude oil *via* hydration or oxidation of alkenes to introduce oxygen-containing functional groups.[309] Fortunately, these functional groups are also found in bio-oil. Therefore, separating high-value chemicals from bio-oil is a potential approach for efficiently utilizing biomass.

Typically, phenolic compounds found in bio-oils are simple phenols containing an aromatic ring bearing one hydroxyl group (-OH), with aldehyde or carboxylic acid side groups, and also found are oligomeric polyphenols having large multiples of phenol structural units.[128] All of the phenolic compounds found in bio-oils are products of lignin decomposition, which is one of the primary components of dry wood and generally accounts for 18-40% (w/w) of the total wood mass, depending on the wood species.[290]

Table 4.16 summarizes some of the previous work on phenolic separation from bio-oil by liquid-liquid extraction technique.

Table 4.16: Summary of some previous work on phenolic separation from bio-oil by liquid-liquid extraction.

Bio-oil source	Solvents[a]	Species isolated	Ref.
Eucalyptus wood	Ethyl acetate, NaOH and HCl aqueous solutions	Phenols	310
Cotton stalk	DCM, NaOH and HCl aqueous solutions	Phenol, cresols, guaiacol, 4-methyl guaiacol and syringol	311
Pine wood and forest residue	Methyl isobutyl ketone and NaOH aqueous solution	Phenols	293
Salix viminalis wood	Diethyl ether, DCM and water	Phenols	251
Douglas fir sawdust pellets	Chloroform and water	Phenols and guaiacols	312
Lauan sawdust	DCM, water, NaOH and HCl aqueous solutions	Phenols and guaiacols	250
Coal[b]	Methanol, DCM and water	Phenols	313

[a] Just recommended solvents by the authors were stated.

[b] For comparison.

As it can be seen from Table 4.16, different types of biomass were used to obtain the pyrolysis bio-oil and varieties of solvents were investigated to separate phenolic compounds from the bio-oil. All of these studies appear to claim that their solvent extraction method and the choice of solvents associated with this method is the optimum way to extract the phenols from bio-oils. However, it is not straightforward to establish which one may be optimal for the phenolic separation from a particular bio-oil.

Olejniczak *et al.*[251] have investigated phenolic components of *Salix viminalis* derived pyrolysis bio-oil for their potential application as antioxidants of synthetic lubricating oils. According to their study, a solvent extraction method was performed to isolate the phenolic species from the bio-oil, generating two phenolic fractions, extract A and extract B. Their results showed that extract A was the richest in monomeric phenols when compared to extract B, which, according to their results, found to be respectively 47.5% and 16.8% (w/w) by GC-FID. The major phenolic components of the extract A were syringol (2,6-dimethoxyphenol) and its *para*-substituted derivatives, whereas in extract B, the major phenolic components were mainly syringol and syringyl acetone. Interestingly, they determined the total phenolic content of extract A *via* another method, namely the Folin-Ciocalteu (FC) assay. According to their results, this quantification method revealed a higher content of total phenols, at 97% (w/w of the extract), in comparison to the GC-FID result. This was more than 2 times higher than their reported GC-FID concentration value of 47.5% (w/w). Their attribution for the higher total phenolic content was that extract A contain phenolic compounds with large molecular weights. Unfortunately, they have not determined the total phenolic content for extract B by the Folin-Ciocalteu assay which could be interesting to compare with its GC-FID concentration value.

By comparing the work of Olejniczak *et al.*[251] with the work described in this chapter, a similar separation method of phenolics was carried out for the 2nd crude bio-oil extract as presented earlier in section 4.3.2. The results of total phenolic content by FC assay were in approximate agreement with the work of Olejniczak *et al.*,[251] where the total phenolic content of diethyl ether extract was higher (55.7% w/w) than that of DCM extract. However, in comparison with Olejniczak *et al.*,[251] this total phenolic content of diethyl ether extract is lower than their reported value

of 97% (w/w). This is probably because of the different species of wood used to obtain the bio-oil, as well as the different pyrolysis technique.

Wang *et al.*[250] have also investigated the separation of monophenols and pyrolytic lignins from the water-insoluble phase of lauan sawdust derived bio-oil. According to their study, a multi-step separation procedure was carried out to fractionate the bio-oil by a solvent extraction method. Three fractions were generated by Wang *et al.*,[250] namely fraction A (FA), fraction B (FB) and fraction C (FC). According to their results, FB was rich in phenolic compounds and its phenolic concentration was reported to be approximately 94% (based on % of total area in GC analyses of the compounds eluting by GC). Unfortunately, Wang *et al.*[250] did not mention in their published work the total phenolic concentration of the original sample of bio-oil before fractionation for comparison. In addition, Wang *et al.*[250] have evaluated the phenolic concentration using GC-MS peak area normalization. The accuracy of this quantification technique is unlikely to be as good as that achievable using GC-FID technique, as, for example, used in the work reported here. Besides, from other work, including that reported here, it is very unlikely that all the phenolic species in their bio-oil sample are volatile in nature, many will be involatile polyphenolics. Therefore, their reported concentration of phenols may not be reliable. The same separation method of phenolics was also carried out for the 2nd crude bio-oil extract as presented earlier in section 4.3.1, with results being similar to the work of Wang *et al.*,[250] where the phenolic extract (FB in Wang *et al.*[250] work) was indeed rich in phenolic compounds.

Recently, an alternative green technology, supercritical fluid extraction (SFE), has been applied for the separation of bio-oil components.[128] This new extraction technology has many advantages in comparison to solvent extraction. For instance, it eliminates the possible contamination by organic solvents and it can avoid additional costs of removing these solvents from the extracts.[307] A number of solvents have been investigated for use as a SFE solvent.[128] However, CO_2 is found to be the ideal SFE solvent, most likely due to its low critical temperature (31.1 $^{\circ}$C) and low critical pressure (73.8 bar).[301]

Mudraboyina *et al.*[314] have demonstrated the use of supercritical CO_2 to selectively extracting single ring phenolic components from lignin microwave-pyrolysis oil. The extraction method that they have used was supercritical fluid rectification (SFR), a variation system of supercritical fluid extraction (SFE), where a rectifier column is included after the supercritical CO_2 extractor to increase the selectivity for some compounds over others during the extraction process. According to Mudraboyina *et al.*,[314] the extraction was carried out at temperature of 35 $^{\circ}$C and 80 bar pressure on a 4 g bio-oil sample using a CO_2 flow rate of 10 mL/min. The mass of the extract recovered was 0.47 g and its total single ring phenolic concentration was found to be 68% (w/w). According to their results, the extract was selectively enriched with all major single ring phenols except catechols. The most two concentrated single ring phenols in the extract were creosol and guaiacol at 18.5 and 17.0% (w/w), respectively. Interestingly, these two phenolic compounds were also the most abundant phenolic species in their bio-oil sample before supercritical rectification, at 4.9 and 3.9% (w/w), respectively.

A similar result to Mudraboyina *et al.*[314] was observed for the supercritical CO_2 extraction of bio-oil that was presented earlier in section 4.4.2. Creosol (2-methoxy-4-methylphenol), one of the most abundant phenolic species in the 1st extract of bio-oil, was also found to be the most concentrated phenolic compound in the CO_2-1 extract. However, unlike Mudraboyina *et al.*,[314] catechol (1,2-benzenediol) was successfully extracted *via* supercritical CO_2, which was found to be the most concentrated phenolic compound in the CO_2-4 extract. This is probably due to the different extraction condition that was used, where the extraction was performed at temperature of 50 $^{\circ}$C and 350 bar pressure using a CO_2 flow rate of 40 g/min.

4.6 Conclusion

The identification of phenolic compounds in two extracts of crude bio-oil extracted using microwave enhanced pyrolysis of spruce woodchips was carried out by the use of gas chromatography-mass spectroscopy (GC-MS). The GC-MS identified 13 phenolic species in the 1st extract of crude bio-oil, and the total quantification of these phenolic species were 8.2% (w/w) that achieved by the use of gas chromatography-flame ionization detector (GC-FID). For the 2nd extract of crude

bio-oil, the analysis by GC-MS identified 18 phenolic species, and the total quantification of these phenolic species were 6.1% (w/w) that achieved also by the use of GC-FID. The variation between crude bio-oil extracts in the total concentration and the number of phenolic species is attributed to differ in degrees of the thermal degradation of lignin during the microwave pyrolysis of spruce woodchips. However, all the 13 phenolic species identified in the 1st crude bio-oil extract were identified again in the 2nd crude bio-oil extract. Therefore, the reproducibility of the majority of these phenolic species is comparatively high, though the concentrations may vary slightly.

The 2nd extract of crude bio-oil was subjected to two multi-solvent fractionation procedures; water-insoluble phase fractionation, and water-soluble phase fractionation.

The water-insoluble phase fractionation procedure produced a water-soluble extract, a neutral extract, a phenolic extract and an organic acids extract, as well as an insoluble and an aqueous residue that was not studied further. The analysis by GC-MS identified 8 phenolic compounds in the water-soluble extract, 12 phenolic compounds in the neutral extract, 18 phenolic compounds in the phenolic extract, and 15 phenolic compounds in the organic acids extract. Phenolic extract was the richest in phenolic species, and the phenolic content quantified by GC-FID was 17.4% (w/w), whereas by Folin-Ciocalteu (FC) assay was 49.6% (w/w of eugenol equivalent).

For the water-soluble phase fractionation procedure, it produced a diethyl ether extract, a DCM extract, and a water-soluble residue. The analysis by GC-MS identified 15 phenolic compounds in the diethyl ether extract, 8 phenolic compounds in the DCM extract, and 4 phenolic compounds in the water-soluble residue. Diethyl ether extract was the richest with phenolic species, and the phenolic content quantified by GC-FID was 8.5% (w/w), whereas by FC assay was 55.7% (w/w of mono-phenol equivalent).

The greater quantities of phenolic compounds detected using FC assay, in comparison with GC-FID, is consistent with the presence of phenolic species with high molecular weights (> 350 Da). These heavier phenolic species are too large to

be detectable by GC due to being involatile at the maximum operating temperature of the GC column, but however can still be detectable by the FC method.

Further fractionation of the 1st extract of crude bio-oil was carried out using a supercritical CO_2 extraction method. The extraction procedure produced four extracts that extracted at different controlled pressures and temperatures, and the four extracts were named as CO_2-1, CO_2-2, CO_2-3, and CO_2-4. The analysis carried out by GC-MS of each extract identified 12 phenolic species in CO2-1 extract, and 13 phenolic species in each of the other CO_2 extracts, which are identical, but vary in their individual concentration. According to GC-FID quantification results of the phenolic species, the CO_2-1 extract was the highest in the total content of phenols at 14.2% (w/w), followed by the CO_2-4 extract at 9.8% (w/w).

Chapter 5: Effect of Spruce-Derived Phenols on Oxidative Stability of Methyl Linoleate

5.1 Introduction

Biodiesel is treated with chemicals known as additives that function to help the biodiesel when used as a road transportation fuel by improving several negative properties, for instance higher viscosity, sensitivity to hydrolysis (corrosion), cold filter plugging point (CFPP), low cetane number, storage problems, and oxidation stability.[315-318]

Fuel stability is a key characteristic of fuel quality and it can be defined as the fuel's resistance to degradation processes that can change the fuel properties and form undesirable species.[319] When focusing on stability of the biodiesel fuel, different terms of stabilities can be associated to biodiesel. For example, the term "oxidation stability" is a common term used in relation to the capability of fuels to react with oxygen at ambient temperatures, or in other words, to describe relatively the tendency of fuels to degradation *via* autoxidation.[319] However, these reactions are considerably slower than those that would take place at higher temperatures.[319]

The term "thermal stability" can also be used to address susceptibility to degradation as a result of very high temperatures.[319] This term was associated to biodiesel usage since the possibility of being exposed to elevated temperatures at environments encountered in engine fuel injection systems, specifically when biodiesel fuel is re-circulated *via* the injection system and back to the fuel tank.[319]

The term "storage stability" is another commonly used term that refers to the stability of fuels during the long-term storage.[319] One of the primary problems related to this term could be the oxidative degradation, however, storage stability can also involve other issues like water contamination and microbial growth.[320] Microbial growth can be promoted by water that leads to tank corrosion, participate in the formation of emulsions, and cause hydrolysis or hydrolytic oxidation.[321]

With respect to different uses of the terms above, the term "oxidation stability" could be the most appropriate one for use in general with biodiesel, as oxidation can occur during biodiesel production, storage and end-use.[322]

The poor oxidation stability of pure biodiesel (B100) could be the most undesirable feature that prevents the use of B100 biodiesel as a transportation fuel from being widespread in the marketplace. Therefore, to solve this with other negative matters, the biodiesel industry add additives to biodiesel, and one of the most important group of additives in the biodiesel industry could be the antioxidants – chemicals added, usually less than or equal to 1000 ppm (w/w), to prevent autoxidation of the product.[323, 324]

Antioxidants are well recognised for use to control biodiesel oxidation by inhibiting the oxidation process. Generally, there are two types of antioxidants used to prevent autoxidation: hydroperoxide decomposers and chain breakers, with most reported papers within the biodiesel development sector focused on the chain breaking type, and the two well-known chain breaking types are phenolic and amine antioxidants.[325]

5.1.1 Methyl linoleate autoxidation mechanism

The autoxidation reactions (as discussed in Chapter 1) of saturated lipids are comparatively straight forward. They produce hydroperoxides as the primary product in a noticeably quantitative yield at moderate temperature and low conversion.[326] Therefore, according to a previous published work,[326] the quantitative results, under these conditions, of oxygen uptake, substrate disappearance, and hydroperoxide formation are all agree well with the autoxidation mechanism. The autoxidation reactions of unsaturated lipids can be more complicated.[326] An addition reaction to the double bond could occur, and this can compete with the allylic hydrogen abstraction reaction by peroxyl radicals.[326] The addition mechanism can produce polyperoxides and epoxide, whereas the abstraction mechanism produces hydroperoxides as a major product.[327]

Similar oxidation reactions can occur in biodiesel major components, which are generally described as fatty acid methyl esters (FAME). The unsaturated FAMEs in biodiesel are known to be the source of biodiesel's low oxidation stability, and this instability is fundamentally due to the presence of carbon double bonds (C=C) in the FAME chain.[325] The instability is critically exacerbated if a higher number of carbon double bonds (two or more) is present in the FAME chain, and therefore, the

biodiesel with higher concentrations of polyunsaturated fatty acids (PUFA) is relatively less stable.[328]

In the oxidation process of PUFA, unsaturated sites of a FAME chain undergo free radical attack, which results in a hydrogen atom abstraction from the FAME chain.[319] Ambient oxygen then freely reacts at the site, subsequently forming hydroperoxides, see for example Figure 5.1.[319, 329]

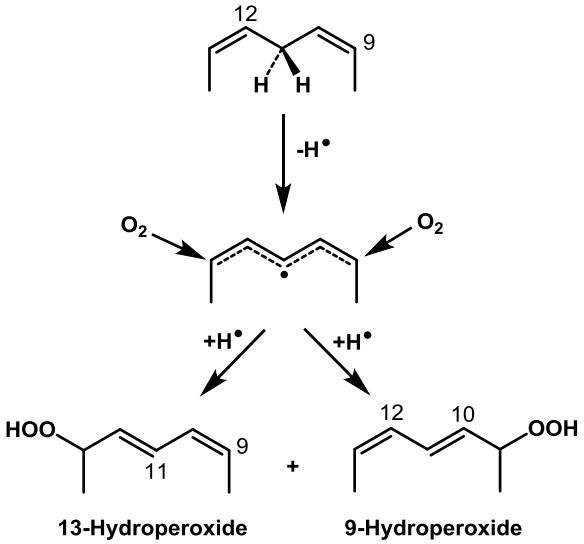

Figure 5.1: Initial stages of the mechanism of methyl linoleate autoxidation.[329]

The FAME unsaturated sites in biodiesel generally contain allylic or doubly allylic C-H bonds that are lower in their bond dissociation energy (BDE) than FAME saturated sites,[330] see Table 5.1. Thus, the oxygen-centred radicals will tend to react more rapidly with the FAME unsaturated sites.[330]

Table 5.1: The BDEs of major types of C-H bonds in biodiesel FAME chains and their rate constants (k) at 30 °C for hydrogen-atom abstraction.

Compound	Structure	BDE (KJ/mol)	Ref.	k (M^{-1} s^{-1})	Ref.
Methyl stearate	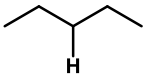	416.3	[331]	/[a]	/
Methyl oleate	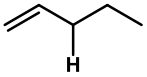	359.8	[331]	0.22	[332]
Methyl linoleate	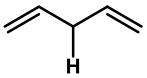	320.5 ± 2.5	[333]	31	[332]
Methyl linolenate	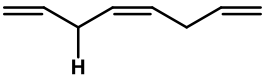	320.5 ± 2.5	[333]	59	[332]

[a] Not available.

Most typical biodiesel fuels consist of a mixture of FAMEs that have structural characteristics as summarised in Table 5.2. As can be seen from Table 5.2, most of the FAMEs in biodiesel consist of hydrocarbon chains with 18 carbon atoms and mostly have between one and three C=C bonds in their hydrocarbon chain. The proportions of these FAMEs in biodiesel can vary depending on the feedstock.[334] In the United States, biodiesel is commonly derived from soybean feedstock, however, in Europe, rapeseed-derived biodiesel is more common.[334] Therefore, Table 5.2 also shows the proportions of major FAMEs in biodiesel derived from both feedstocks.

Table 5.2: Major FAMEs in biodiesel and their typical concentrations in soybean and rapeseed derived biodiesel.[335]

Common name	IUPAC name	No. of C: no. of C=C	% in biodiesel (w/w)	
			Soybean	Rapeseed
Methyl palmitate	Methyl hexadecanoate	16:0	10-12	2-6
Methyl stearate	Methyl octadecanoate	18:0	3-5	4-6
Methyl oleate	Methyl (*E*)-octadec-9-enoate	18:1	18-26	52-65
Methyl linoleate	Methyl (9*E*,12*E*)-octadeca-9,12-dienoate	18:2	49-57	18-25
Methyl linolenate	Methyl (9*E*,12*E*,15*E*)-octadeca-9,12,15-trienoate	18:3	6-9	10-11

5.1.2 Antioxidant mechanism by phenols

Phenolic antioxidants interrupt the radical chain by transferring a hydrogen atom to the propagating peroxyl radicals ($ROO^{\bullet}$) to form a hydroperoxide (ROOH),[336] see Reaction 5.1.

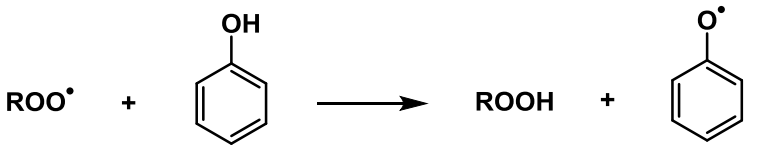

(5.1)

In order for this reaction to be successful, the hydrogen atom donation by the phenolic antioxidant must proceed at a rate much faster than that in the chain-propagating step of the hydrocarbon peroxidation.[336]

For the antioxidant derived radical ($A^{\bullet}$) formed in Reaction 5.1, it should ideally react further to produce non-radical products by reacting with another peroxyl radical ($ROO^{\bullet}$) to be more efficient,[336] see Reaction 5.2.

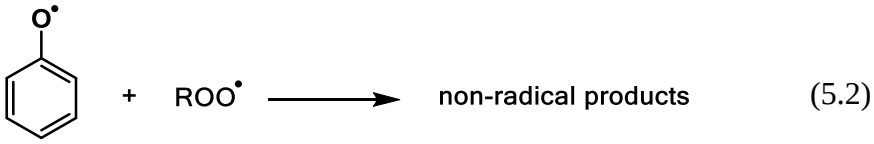

(5.2)

This reaction (Reaction 5.2) has not been studied in depth,[186] however, it is thought that the $ROO^{\bullet}$ addition to the benzene ring of a phenoxyl radical is *via* the *ortho*- and *para*- positions to produce alcohol and *ortho*- and *para*-quinones,[186] see for example Figure 5.2.

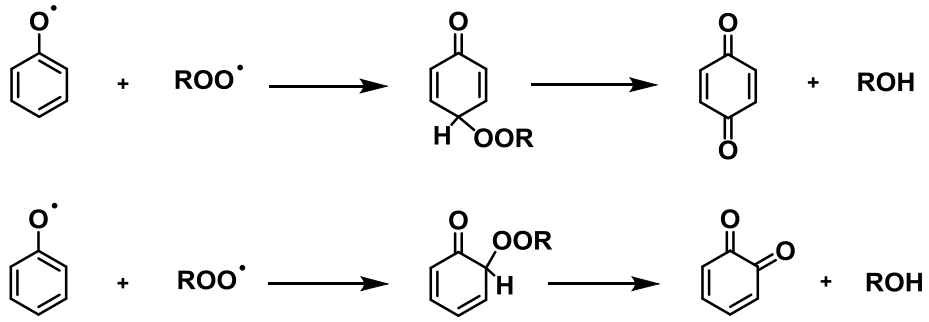

Figure 5.2: Proposed reactions of the phenoxyl radical with peroxyl radical to produce alcohol and *ortho*- and *para*-quinones.[186]

The antioxidant power of phenols depends on various structural factors, including the reaction conditions of the oxidation (*e.g.*, solvent and temperature).[186] However, the greatest factor is usually the rate constant for its reaction with peroxyl radicals, which, in turn, depending on the O-H bond strength of the phenol.[186] During the antioxidant reaction with a peroxyl radical, the O-H bond of a phenolic antioxidant is cleaved, and a hydroperoxide (ROOH) is formed.[186] Therefore, in order to achieve the phenolic O-H bond cleavage, an amount of energy is required, which is often described as the bond dissociation energy (BDE).[186] The BDE of the O-H bond of various types of phenols were investigated intensively in the past years and gathered in data books.[337, 338] These investigations revealed that the substituents in a phenolic ring have strong influence on the BDE value of the phenolic O-H bond, see for example Figure 5.3.

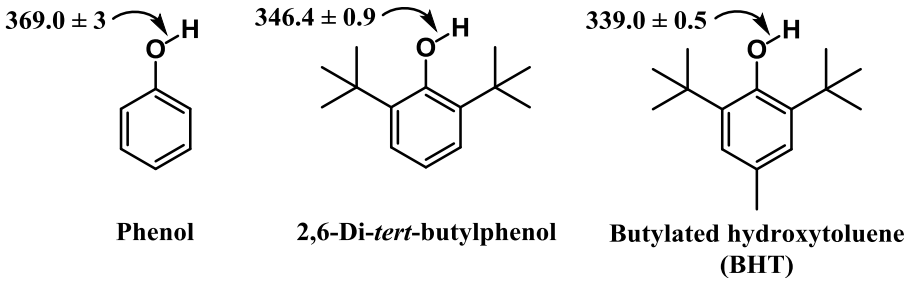

Figure 5.3: Examples of phenolic species and their experimental BDE values (kJ mol^{-1}).[339]

The BDE value of the phenolic O-H bond can be noticeably lowered when specific substituent groups are attached in the phenolic ring.[340] The character of substitution group (mostly alkyl, alkoxyl, or hydroxyl groups) and its position (*ortho*, *meta*, or *para* position) in the phenolic ring play an important role in reducing the BDE value of the phenolic O-H bond.[340]

5.2 Results

5.2.1 Effect of crude bio-oil derived phenols on methyl linoleate

5.2.1.1 Static oxidation test

To examine the effect of the crude bio-oil in preventing the autoxidation of methyl linoleate, a number of high-temperature static oxidation tests were carried out. The experimental details of the oxidation test (under static mode, *i.e.*, a sealed reactor with no flowing oxygen) are explained in the experimental chapter (Chapter 2, section 2.4.1).

The exposure of methyl linoleate to high temperature (120 $^{\circ}$C) and oxygen pressure at 1 bar absolute gives rapid methyl linoleate autoxidation, which could be delayed by adding an antioxidant. For example Figure 5.4 shows the effect of the crude bio-oil on the inhibition of methyl linoleate autoxidation, where the antioxidant concentrations quoted (from 0 to 69.5 x 10^{-3} mol dm^{-3}) correspond to the amount of total phenolics added to the methyl linoleate, expressed as the equivalent molar concentration of a mono-phenol (eugenol) as determined by the Folin-Ciocalteu (FC) assay.

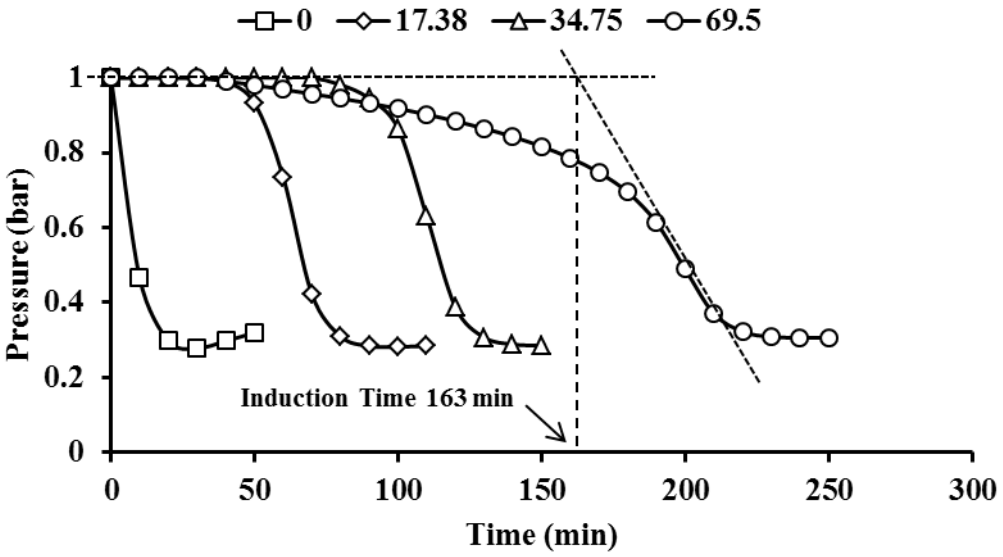

Figure 5.4: Oxidation pressure traces of 2 ml methyl linoleate with concentrations of crude bio-oil from 0 to 69.5 x 10^{-3} (mol dm^{-3}) at 120 °C and 1 bar of oxygen (phenolic concentrations determined by FC assay that assume only mono-phenolic present).

The traces in Figure 5.4 show that the crude bio-oil greatly extended the methyl linoleate induction period at the addition of three investigated total phenolic concentrations (17.4, 34.8 and 69.5 x 10^{-3} mol/dm^3).

Figure 5.5 shows the oxidation pressure traces of methyl linoleate with concentrations of butylated hydroxytoluene (BHT) from 0 to 80 x 10^{-3} (mol/dm^3). This common commercial petroleum derived antioxidant was used as a reference species to which the bio-derived extract could be compared.

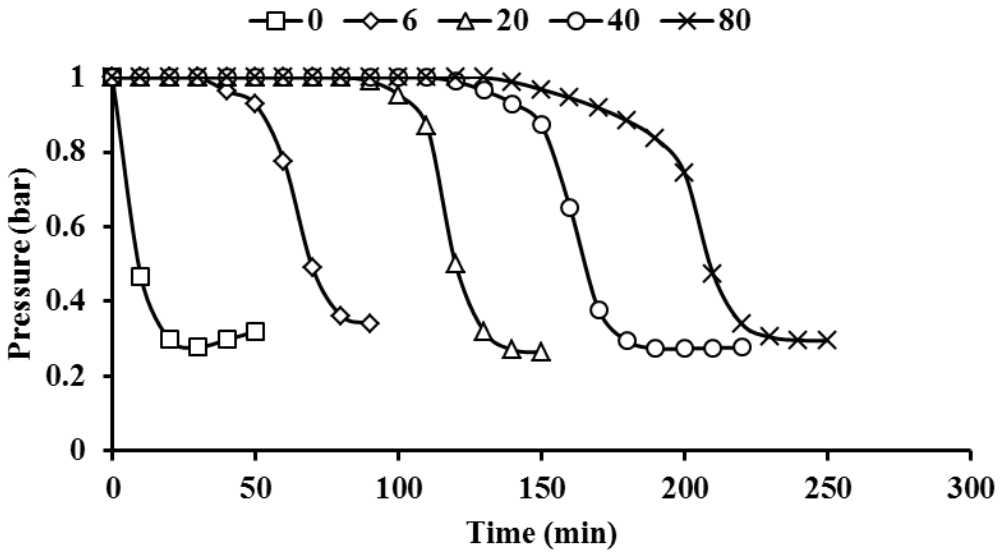

Figure 5.5: Oxidation pressure traces of 2 ml methyl linoleate with concentrations of BHT from 0 to 80 x 10^{-3} (mol dm^{-3}) at 120 °C and 1 bar of oxygen.

The traces in Figure 5.5 show that the commercial antioxidant BHT extended the induction period (IP) of methyl linoleate at the addition of four investigated BHT concentrations (6, 20, 40 and 80 x 10^{-3} mol/dm^3). When comparing this commercial antioxidant with the crude bio-oil (as in Figure 5.4), it is noteworthy that the crude bio-oil is clearly an effective antioxidant at approximately comparable molar phenolic concentrations to the commercial antioxidant BHT.

5.2.1.2 Rancimat test

Tests were also carried out using the industry standard Rancimat test (EN 14112), which uses a temperature of 110 °C for testing the oxidation stability of biodiesel. More details on the Rancimat test, including sample preparation, test condition and the apparatus used were explained in the experimental chapter (Chapter 2, section 2.4.2).

Figure 5.6 show the obtained induction times (IT) of methyl linoleate alone, and with the addition of: 20 x 10^{-3} mol dm^{-3} of the commercial antioxidant BHT, and 35 x 10^{-3} mol dm^{-3} phenol (eugenol) equivalent of crude bio-oil, separately, by using the industry standard Rancimat test (EN 14112). The concentration quoted for the crude bio-oil corresponds to the amount of total phenolics added to the methyl linoleate,

which is the equivalent molar concentration of a mono-phenol (eugenol) as determined by the Folin-Ciocalteu (FC) assay.

These tests were conducted to provide confirmation of the comparatively high antioxidant power of the crude bio-oil in an industry standard test and to demonstrate its potential competitiveness in comparison with the commercial antioxidant BHT.

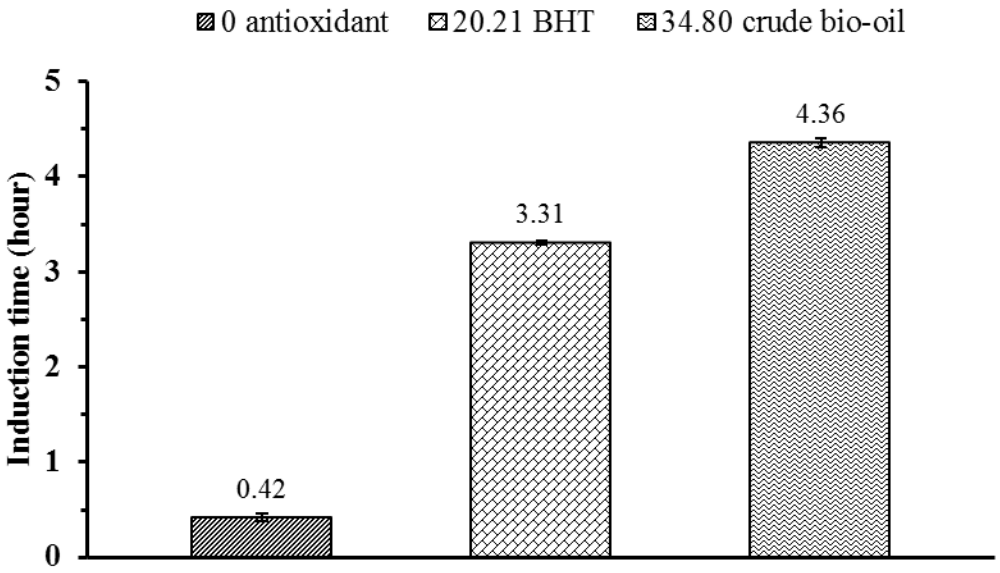

Figure 5.6: The average Rancimat test (EN 14112) induction times of 3 g methyl linoleate without antioxidant, and with concentrations of 20.21 and 34.80 ($x10^{-3}$ mol dm^{-3}) respectively of BHT and crude bio-oil at 110 °C (the induction times here are the average of four independent runs and the error bars are ±standard deviation. the phenolic concentration quoted for the crude bio-oil was determined by FC assay that assume only mono-phenolic present).

The results in Figure 5.6 show that the crude bio-oil greatly extended the methyl linoleate induction time to ~4.4 hours at the addition of the molar phenolic concentration of *ca.* 35 x 10^{-3} mol dm^{-3}. Therefore, in comparison with BHT, the crude bio-oil can be comparable at approximately similar molar phenolic concentrations.

5.2.2 Effect of Isolated Extracts on Methyl linoleate

5.2.2.1 Water-insoluble phase isolated extracts

Figure 5.7 shows a schematic diagram of the crude bio-oil's water-insoluble phase fractionation steps. The extraction procedure, condition and solvents used are described in detail in the experimental chapter (Chapter 2, section 2.2.1.1).

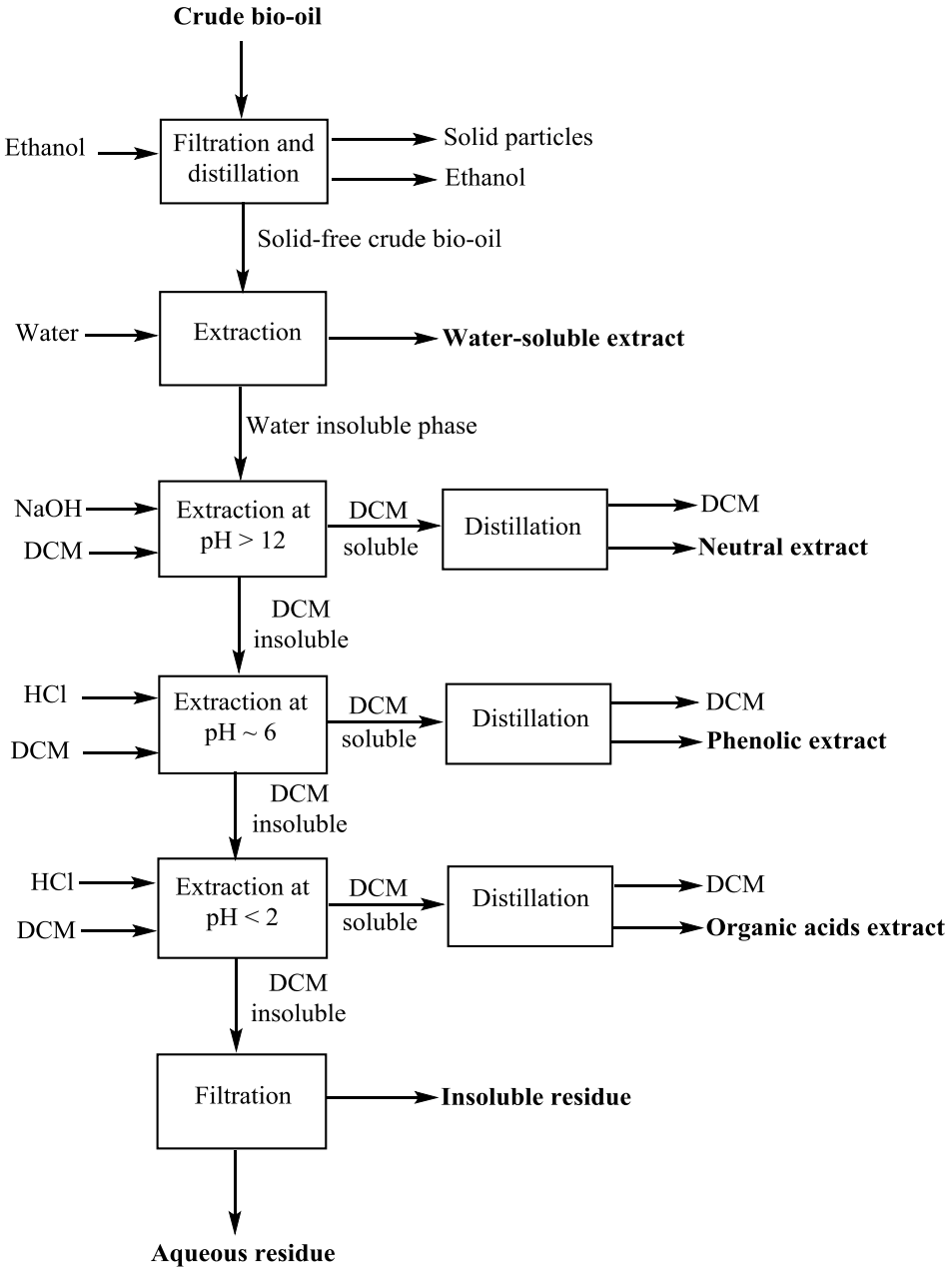

Figure 5.7: Schematic diagram of water-insoluble phase fractionation steps.

Figure 5.8 shows the effect on methyl linoleate autoxidation of four extracts from the crude bio-oil, the water-soluble (A), neutral (B), phenolic (C) and organic acids (D) extracts. The concentrations quoted here again correspond to the total phenolics added to the methyl linoleate, which is the equivalent molar concentration of a mono-phenol as determined by the Folin-Ciocalteu (FC) assay.

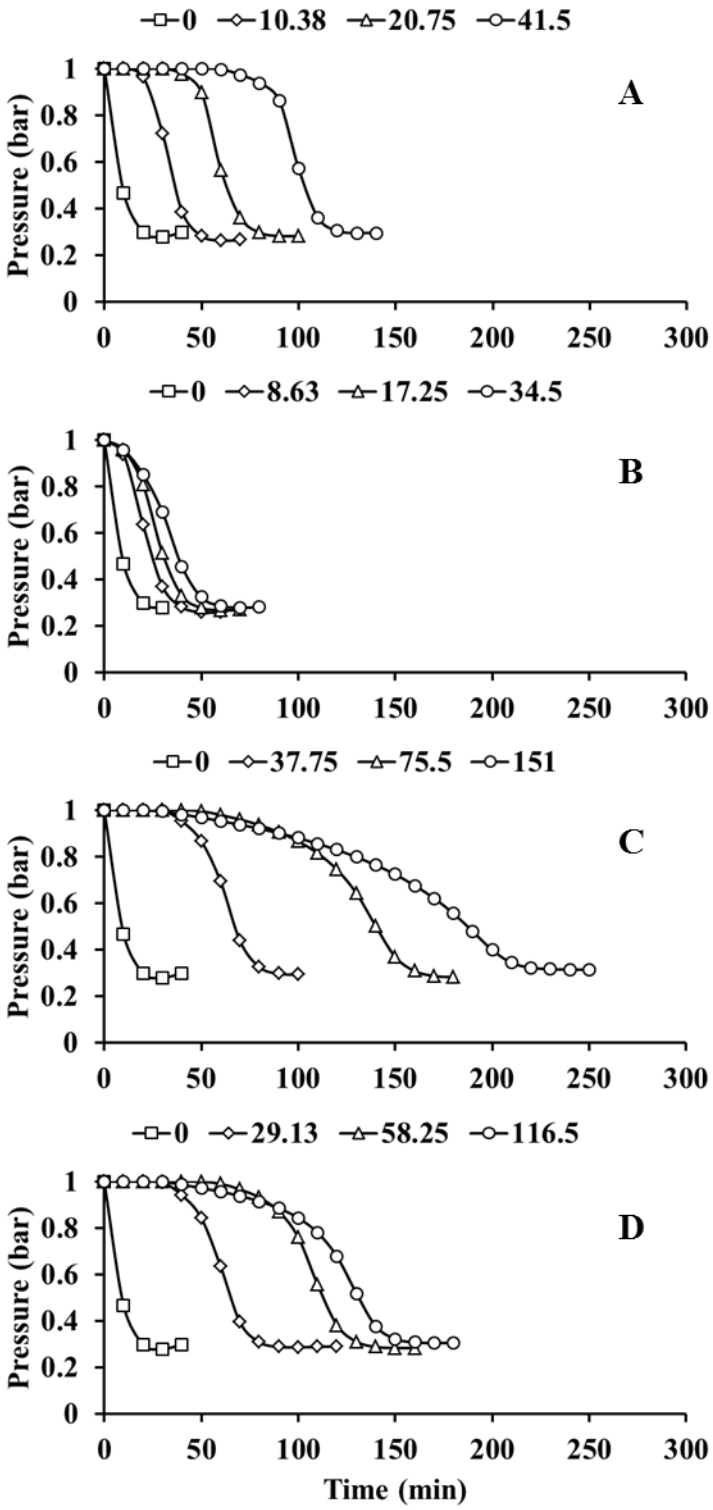

Figure 5.8: Oxidation pressure traces of 2 ml methyl linoleate with concentrations of: (A) water-soluble extract from 0 to 41.5 x 10^{-3} mol dm^{-3}; (B) neutral extract from 0 to 34.5 x 10^{-3} mol dm^{-3}; (C) phenolic extract from 0 to 151 x 10^{-3} mol dm^{-3}; (D) organic acids extract from 0 to 116.5 x 10^{-3} mol dm^{-3}, at 120 $^{\circ}$C and 1 bar of oxygen. (Phenolic concentrations determined by FC assay assuming only mono-phenolic present).

These oxidation experiments (in Figure 5.8) were conducted to see how extracts with higher contents of phenolics than the crude bio-oil (*e.g.*, the phenolic extract) would behave as antioxidants when added to methyl linoleate.

It is noteworthy that all four isolated fractions gave lower induction times than the crude bio-oil when compared at similar molar phenolic concentrations, indicating that the crude bio-oil was better than the isolated extracts in delaying the methyl linoleate autoxidation reaction at 120 $^{\circ}$C.

5.2.2.2 Water-soluble phase isolated extracts

Further oxidation tests were performed on another extracts isolated from the water-soluble phase of the crude bio-oil. Figure 5.9 shows a schematic diagram of the crude bio-oil's water-soluble phase fractionation steps. The extraction procedure, condition and solvents used are described in detail in the experimental chapter (Chapter 2, section 2.2.1.2).

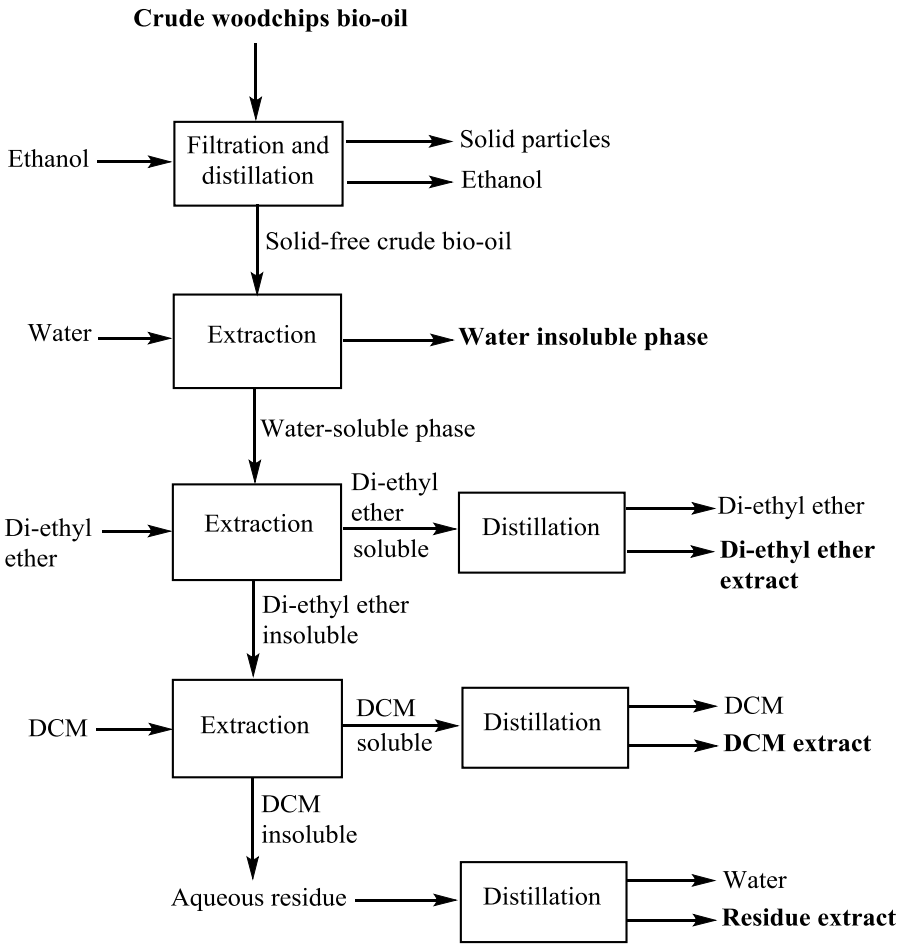

Figure 5.9: Schematic diagram of water-soluble phase fractionation steps.

Figure 5.10 shows the effect on methyl linoleate autoxidation of four extracts from the crude bio-oil, the water-soluble extract (A), diethyl ether extract (B), DCM extract (C) and water-soluble residue (D). The concentrations quoted here again correspond to the total phenolics added to the methyl linoleate, which is the equivalent molar concentration of a mono-phenol (eugenol) as determined by the Folin-Ciocalteu (FC) assay.

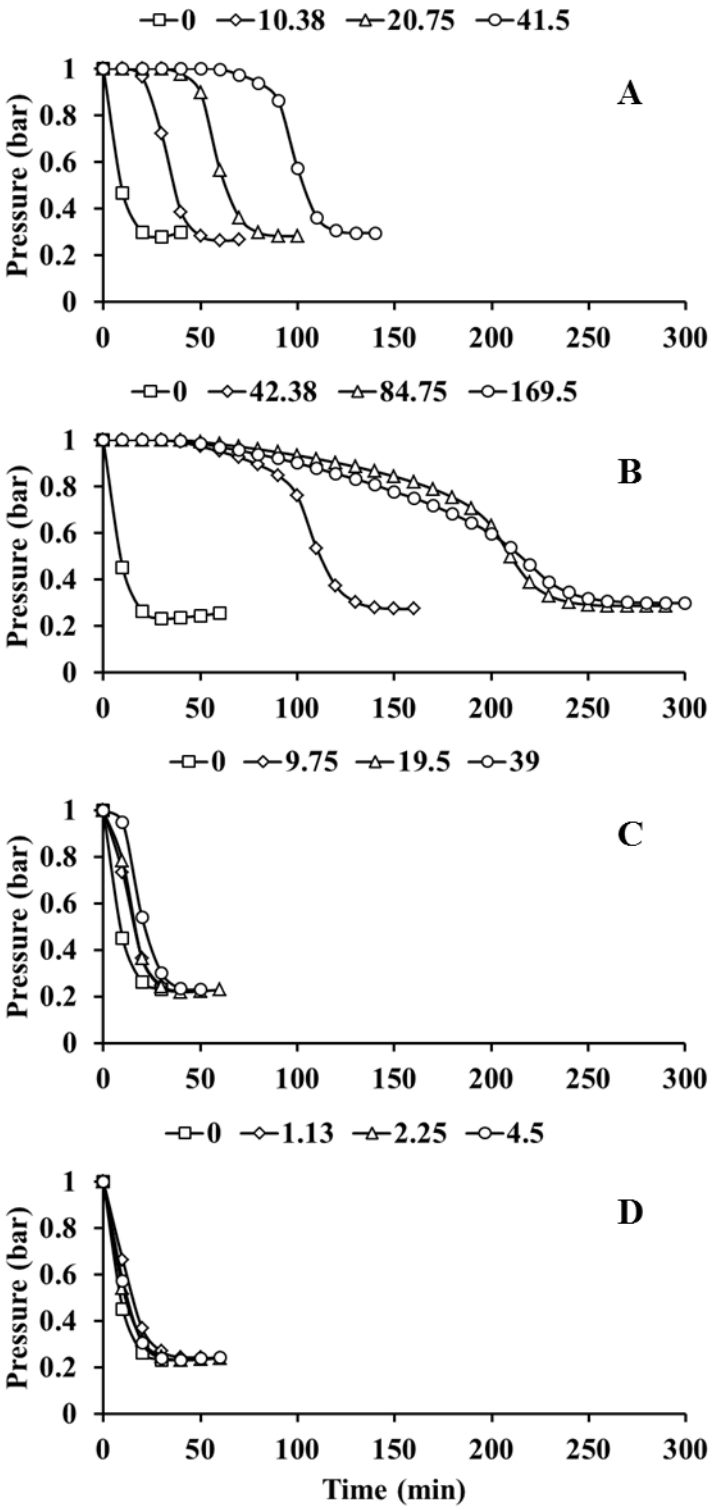

Figure 5.10: Oxidation pressure traces of 2 ml methyl linoleate with concentrations of: (A) water-soluble extract from 0 to 41.5 x 10^{-3} (mol dm^{-3}); (B) diethyl ether extract from 0 to 169.5 x 10^{-3} (mol dm^{-3}); (C) DCM extract from 0 to 39 x 10^{-3} (mol dm^{-3}); (D) water-soluble residue extract from 0 to 4.5 x 10^{-3} (mol dm^{-3}), at 120 °C and 1 bar of oxygen. (Phenolic concentrations determined by FC assay assume only mono-phenolic present).

The oxidation tests in Figure 5.10 were carried out to investigate further the effect of the water-soluble phenolic species on the autoxidation of methyl linoleate.

It is noteworthy that the effect of diethyl ether extract on methyl linoleate induction time was the same as the water-soluble extract when compared at similar molar phenolic concentrations. However, both extracts were slightly less effective than the crude bio-oil in hindering methyl linoleate oxidation at 120 °C.

5.2.3 Effect of phenolic standards on methyl linoleate

5.2.3.1 Effect of single phenolic standard on methyl linoleate

The antioxidancy of three significant phenolic components of the crude bio-oil as identified during analysis (described in Chapter 4, section 4.2) were also examined, and Figure 5.11 shows their chemical structures.

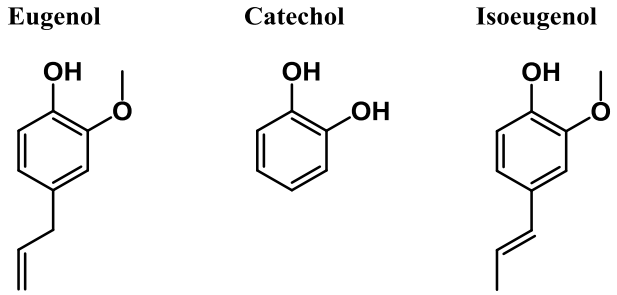

Figure 5.11: Chemical structures of eugenol, catechol and trans-isoeugenol.

Eugenol, isoeugenol and catechol were chosen as they are commercially available, and their structures, chemical formulas and masses were known, allowing accurate molar concentration values to be calculated. Also, their O-H BDE values were previously measured, and more importantly, their chemical structures are similar to most of those mono-phenolic species identified by GC-MS in the crude bio-oil as described in Chapter 4.

Figure 5.12 to Figure 5.15 show the effect of eugenol, catechol (two experimental runs) and isoeugenol on methyl linoleate oxidation at 120 °C and 1 bar of oxygen.

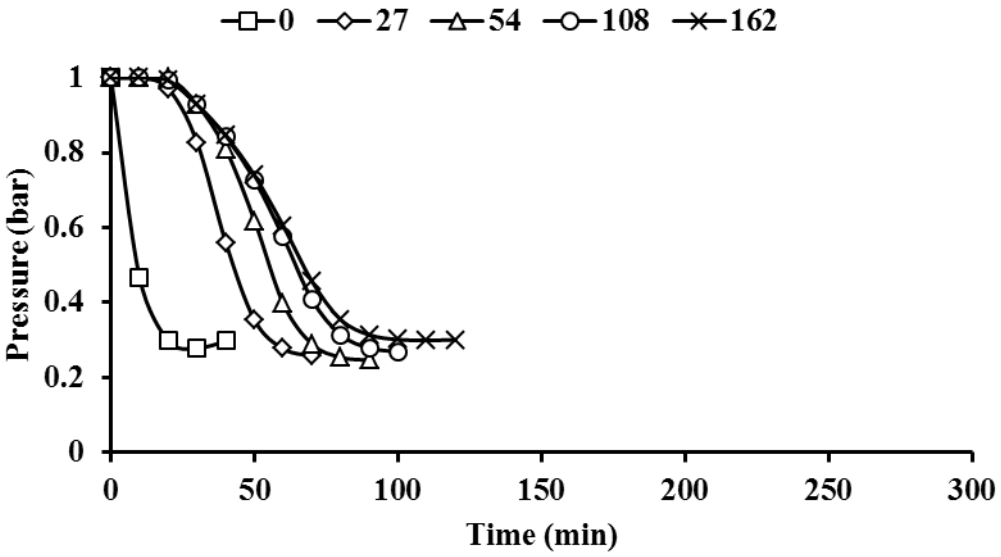

Figure 5.12: Oxidation pressure traces of 2 ml methyl linoleate with concentrations of 4-allyl-2-methoxyphenol (eugenol) from 0 to 162 x 10^{-3} (mol dm^{-3}) at 120 °C and 1 bar of oxygen.

The traces in Figure 5.12 show that eugenol poorly extended the methyl linoleate induction period at 120 °C and 1 bar of oxygen.

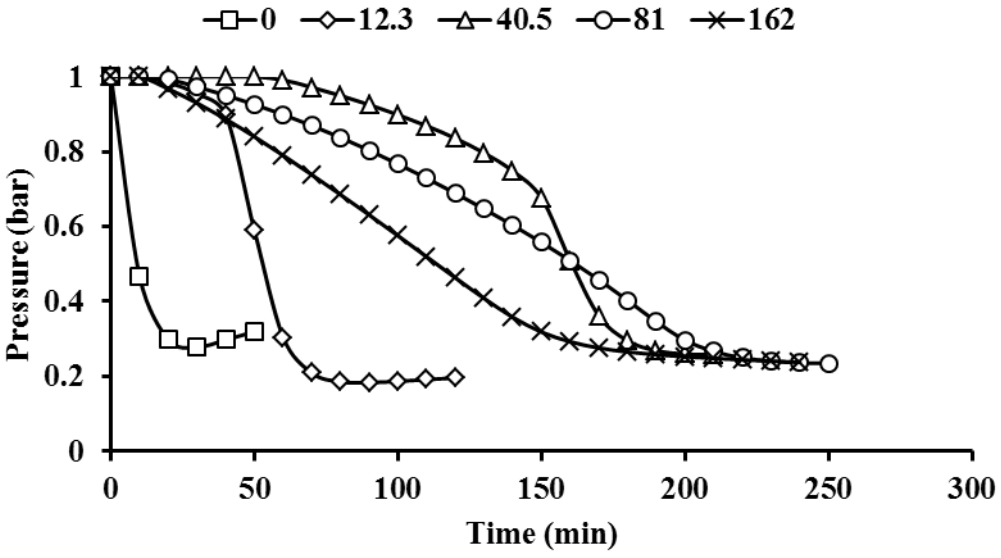

Figure 5.13: Oxidation pressure traces of 2 ml methyl linoleate with concentrations of 1,2-benzenediol (catechol) from 0 to 162 x 10^{-3} (mol dm^{-3}) at 120 °C and 1 bar of oxygen (catechol here was a 1st experimental run)

The traces in Figure 5.13 show that catechol greatly extended the methyl linoleate induction time, however, when higher molar concentrations of catechol (> 40 x 10^{-3} mol/dm^3) were added, its effect on methyl linoleate induction time were noticeably reduced.

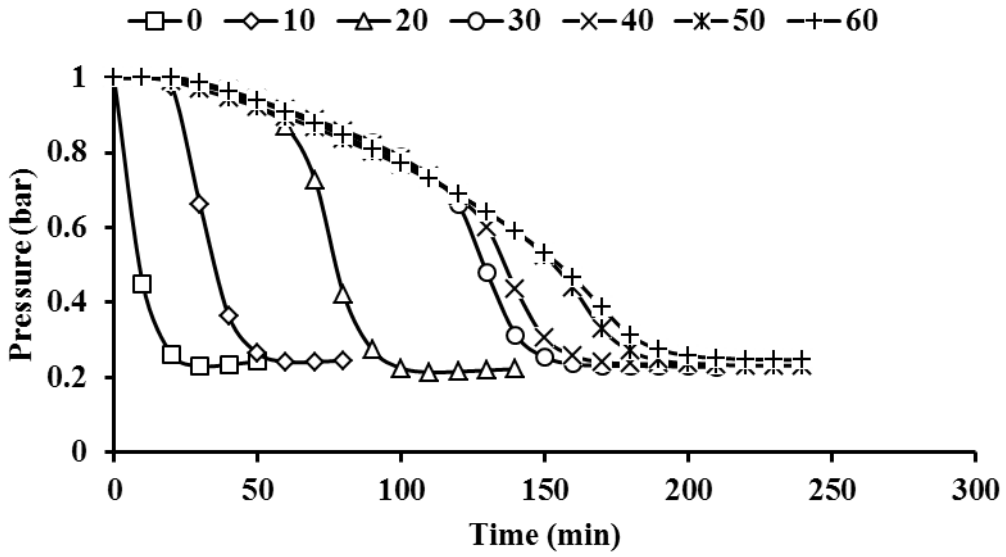

Figure 5.14: Oxidation pressure traces of 2 ml methyl linoleate with concentrations of 1,2-benzenediol (catechol) from 0 to 60 x 10^{-3} (mol dm^{-3}) at 120 °C and 1 bar of oxygen (catechol here was a 2nd experimental run).

The traces in Figure 5.14 show a 2nd experimental oxidation tests of catechol addition to methyl linoleate at 120 °C and 1 bar of oxygen. These oxidation tests were carried out to confirm the high antioxidant activity of catechol in methyl linoleate as observed in the previous figure (Figure 5.13).

It is clear from the traces in Figure 5.13 and Figure 5.14 that catechol can be a powerful antioxidant, however, when molar concentrations greater than *ca.* 40 x 10^{-3} mol/dm^3 of catechol were added, the effect of any additional catechol in extending the methyl linoleate induction time were very limited or negative.

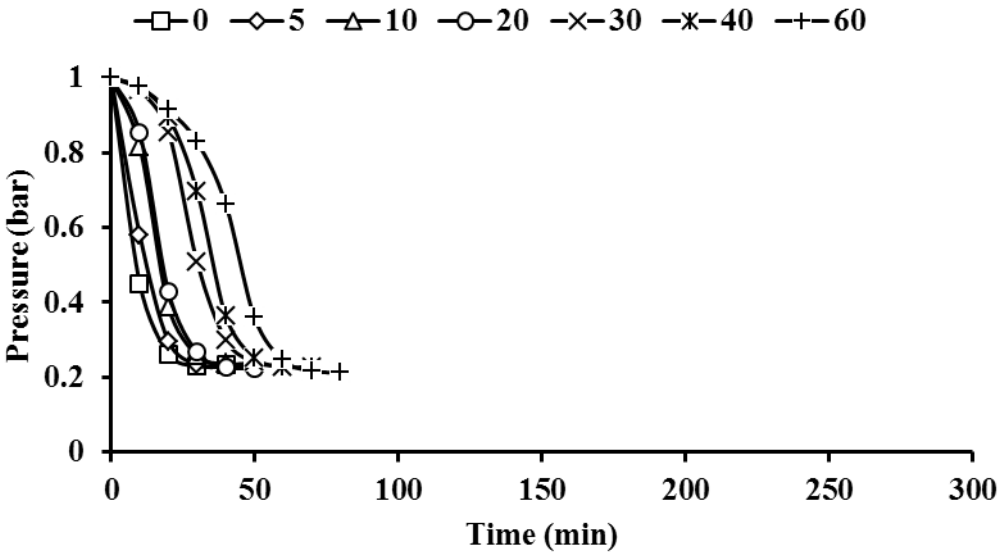

Figure 5.15: Oxidation pressure traces of 2 ml methyl linoleate with concentrations of isoeugenol from 0 to 60 x 10^{-3} (mol dm^{-3}) at 120 °C and 1 bar of oxygen.

The traces in Figure 5.15 show that isoeugenol extended the methyl linoleate induction time, but its antioxidant effect was very low.

5.2.3.2 Effect of mixed phenolic standard on methyl linoleate

The antioxidant effect of a mixed phenolic standard on methyl linoleate was also examined. The standard consists of 6 phenolic components: guaiacol, catechol, 2-methoxy-4-methylphenol, isoeugenol, 4-ethylguaiacol and 4-hydroxy-3-methoxyphenylacetone. Their molar concentrations in methyl linoleate samples before oxidation tests are shown in Table 5.3.

Table 5.3: The phenolic composition of mixed phenolic standard and their molar concentrations in methyl linoleate samples before oxidation.

Phenolic standard	Structure	Concentration (x 10^{-3} mol dm^{-3})				
		Sa. 1	Sa. 2	Sa. 3	Sa. 4	Sa. 5
Guaiacol	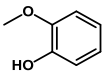	0.76	3.04	6.08	12.16	24.32
Catechol	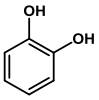	1.10	4.40	8.80	17.60	35.20
2-methoxy-4-methylphenol	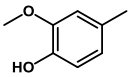	0.57	2.28	4.56	9.12	18.24
Isoeugenol	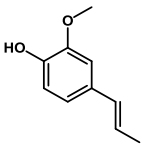	0.69	2.76	5.52	11.04	22.08
4-ethylguaiacol	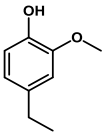	0.15	0.60	1.20	2.40	4.80
4-hydroxy-3-methoxyphenylacetone	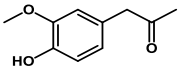	0.45	1.80	3.60	7.20	14.40
Total		3.72	14.88	29.76	59.52	119.04

It is noteworthy that these 6 phenolic standards were the highest mono-phenolic components in the crude bio-oil, and their molar concentrations in the mixed phenolic stock (as in Sa. 1, Table 5.3) were chosen to be approximately similar to their GC-FID estimated molar concentrations in crude bio-oil, specifically, the concentrations of the 6 phenolic standards (as in Sa. 1, Table 5.3) are equivalent to their molar concentrations in 25 mg of crude bio-oil as estimated *via* GC-FID. Their equivalent molar concentrations in 100 mg are presented in Appendix C, along with other identified phenolic species in the crude bio-oil.

Figure 5.16 shows the oxidation pressure traces of methyl linoleate with increasing molar concentrations of the mixed phenolic standard.

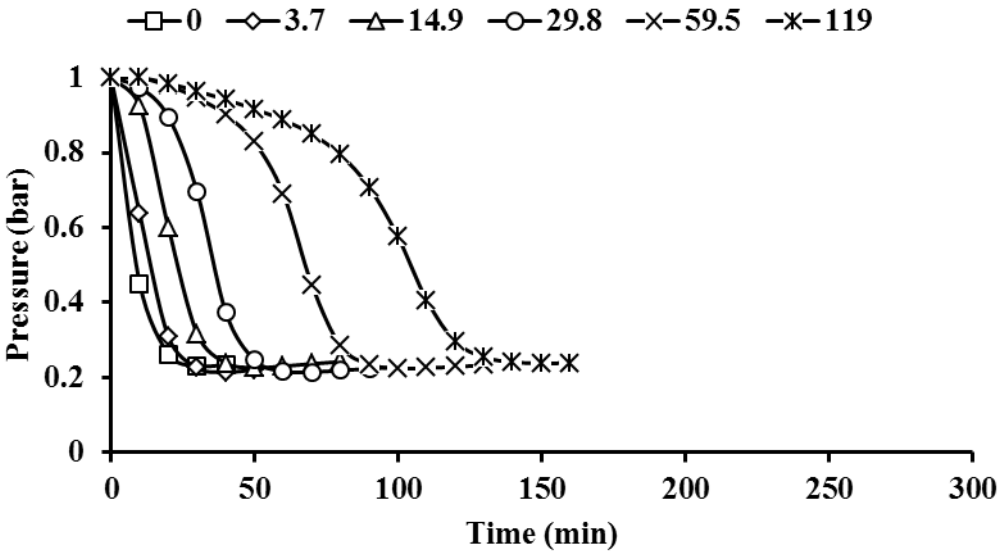

Figure 5.16: Oxidation pressure traces of 2 ml methyl linoleate with concentrations of mixed phenolic standard from 0 to 119 x 10^{-3} (mol dm^{-3}) at 120 °C and 1 bar of oxygen.

The oxidation tests in Figure 5.16 were carried out to see how the antioxidant activity of mixed phenolics will compare with the antioxidant activity of the crude bio-oil when examined with methyl linoleate at 120 °C and 1 bar of oxygen. It is clear from Figure 5.16 that the mixed phenolic standard addition was effective in extending the methyl linoleate induction time at 120 °C and 1 bar of oxygen.

5.3 Discussion

5.3.1 Effect of isolated extracts total weight addition on induction time

5.3.1.1 Effect of water-insoluble phase isolated extracts

To allow a comparison of the antioxidancy imparted to methyl linoleate by crude bio-oil (Figure 5.4), and with water-soluble, neutral, phenolic and organic acids extracts (Figure 5.8) at 120 °C and 1 bar of oxygen, the induction times determined for the above figures are given in Figure 5.17.

Induction time is a measure of the effectiveness of an antioxidant, and this was evaluated for this work by determining the time at which the tangent at the point of maximum rate gradient crosses the initial pressure, see for example Figure 5.4.

Figure 5.17 shows methyl linoleate induction times with total weight addition percentages (w/w) of the crude bio-oil and its extracts from the water-insoluble phase. The concentration added for each extract and their corresponding induction times are given in Appendix C.

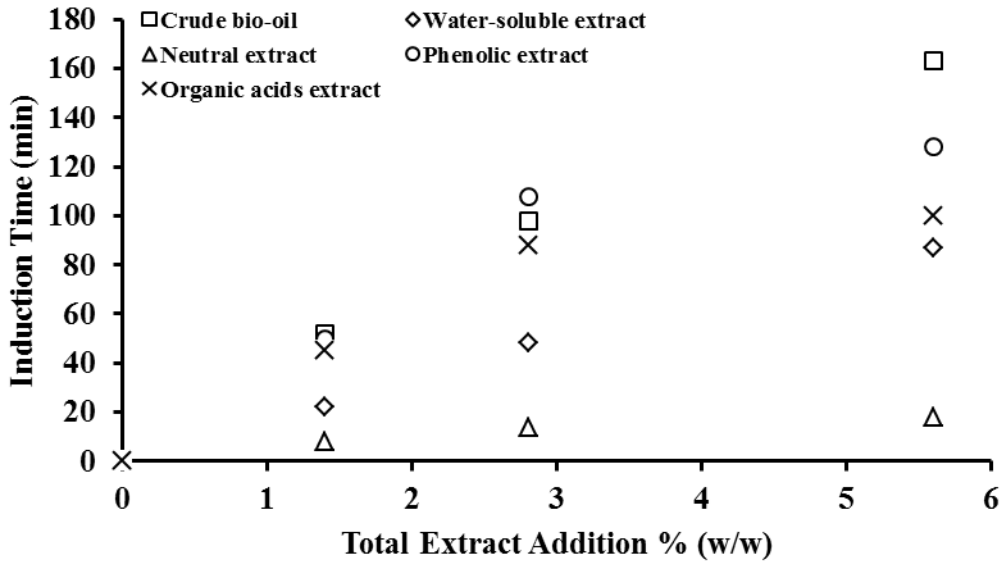

Figure 5.17: The induction time of 2 ml methyl linoleate at three total weight addition % (w/w) of crude bio-oil, water-soluble extract, neutral extract, phenolic extract and organic acids extract at 120 $^{\circ}$C and 1 bar of oxygen.

The results in Figure 5.17 illustrate the variation of inhibition activity by each extract and the crude bio-oil at three total weight addition percentages (1.4, 2.8 and 5.6% w/w). The crude bio-oil, phenolic and organic acids extracts gave approximately similar induction times with the addition of 1.4 and 2.8% (w/w). However, with the addition of 5.6% (w/w), the crude bio-oil gave the highest induction time (163 min) in comparison with the other extracts. Moreover, neutral extract gave the lowest induction times at the three investigated addition percentages followed by the water-soluble extract.

5.3.1.2 Effect of water-soluble phase isolated extracts

To allow also a comparison of the antioxidancy examined of methyl linoleate with crude bio-oil (Figure 5.4), and with water-soluble, diethyl ether, DCM and water-

soluble residue extracts (Figure 5.10) at 120 °C and 1 bar of oxygen, the induction times determined for the above figures are given in Figure 5.18.

Figure 5.18 shows methyl linoleate induction times with total weight addition percentages (w/w) of the crude bio-oil and the extracts from the water-soluble phase. The concentration added for each extract and their corresponding induction times can be found in Appendix C.

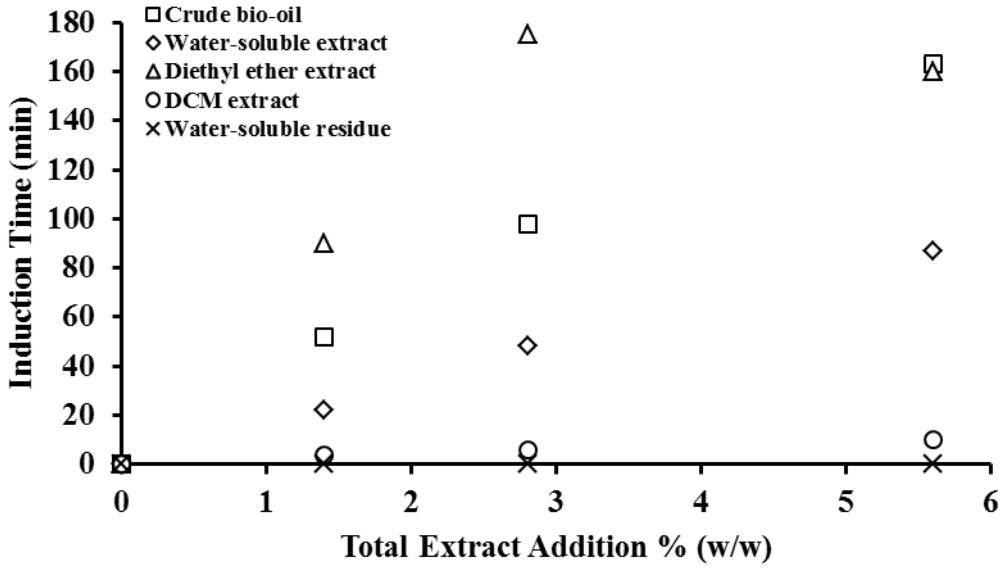

Figure 5.18: The induction times of 2 ml methyl linoleate at three total weight addition % (w/w) of crude bio-oil, water-soluble extract, diethyl ether extract, DCM extract and water-soluble residue at 120 °C and 1 bar of oxygen (crude bio-oil and water-soluble extract results are presented here again for ease of comparison).

The results in Figure 5.18 demonstrate the variation of inhibition activity by each isolated extract and the crude bio-oil at three total weight addition percentages of 1.4, 2.8 and 5.6% w/w. Remarkably, the diethyl ether extract shows the highest induction times at the addition of 1.4 and 2.8% (w/w). However, at the addition of 5.6% (w/w), the diethyl ether extract effect on methyl linoleate induction time was noticeably decreased, but still the highest when compared to the rest of the other isolated extracts. Moreover, the water-soluble residue addition to methyl linoleate was essentially ineffective at the addition of 1.4% (w/w) or even after increasing its addition fourfold. This suggests that most of the antioxidant effective components in the water-soluble extract were successfully extracted into the diethyl ether phase.

DCM extract addition has very low effect on methyl linoleate induction time, and it was approximately similar to the water-soluble residue at the two total weight additions of 1.4 and 2.8% (w/w).

5.3.2 Effect of isolated extracts total phenols on induction time

5.3.2.1 Effect of water-insoluble isolated extracts

To allow a comparison of the antioxidancy of methyl linoleate with the additions of crude bio-oil (Figure 5.4); commercial antioxidant BHT (Figure 5.5); water-soluble, neutral, phenolic and organic acids extracts (Figure 5.8); eugenol (Figure 5.12); and catechol (Figure 5.13 and Figure 5.14) at 120 $^{\circ}$C and 1 bar of oxygen, the induction times determined for the above figures are given in Figure 5.19. The phenolic concentrations, as determined by the Folin-Ciocalteu technique, and the induction times are given in Appendix C.

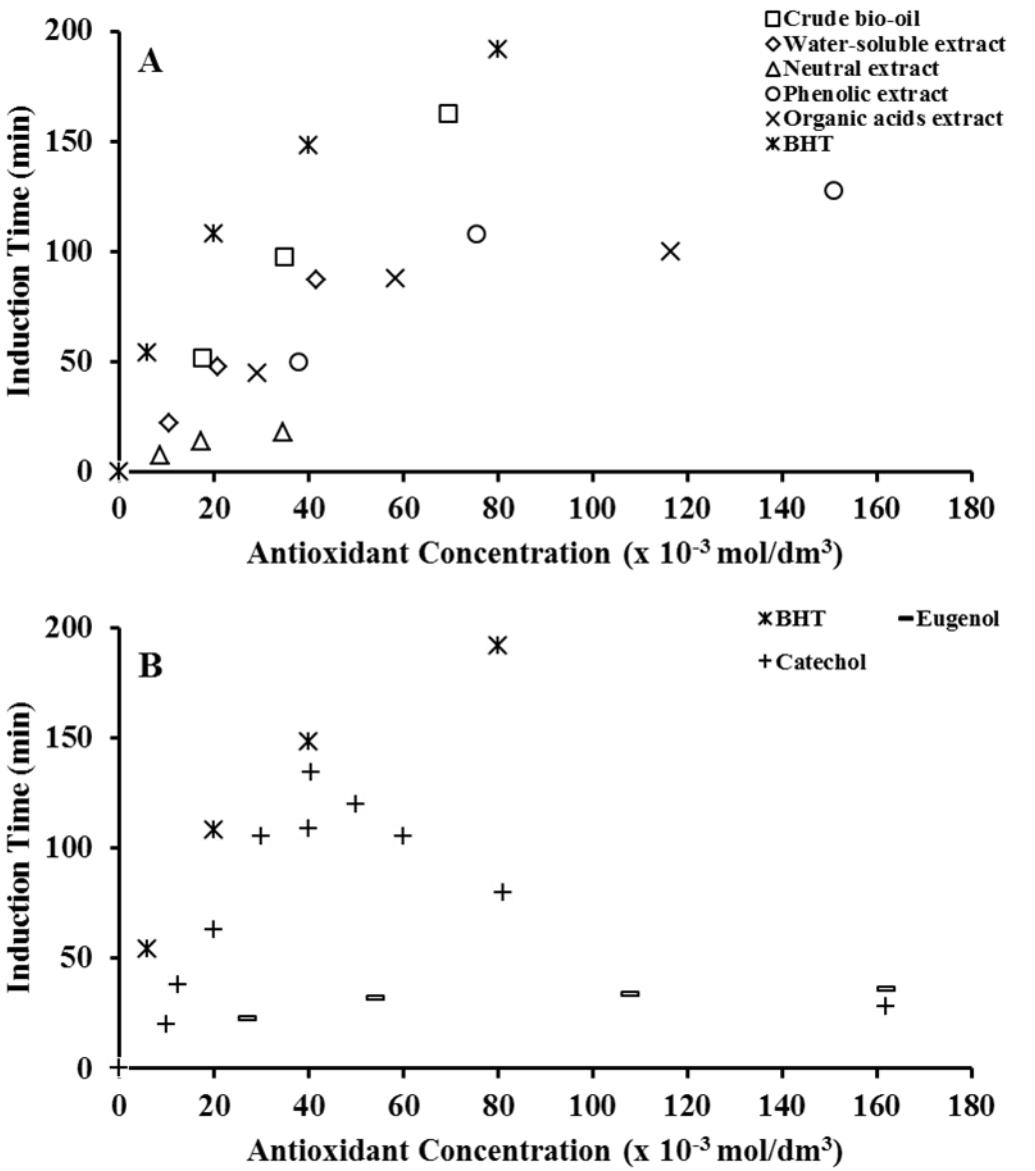

Figure 5.19: The induction times of 2 ml methyl linoleate with increasing concentrations of: (A) crude bio-oil, water-soluble, neutral, phenolic and organic acids extracts; (B) BHT, eugenol and catechol at 120 $^{\circ}$C and 1 bar of oxygen.

The results from Figure 5.19 indicated that the addition of the commercial phenolic antioxidant BHT increased methyl linoleate induction time from 0 to 192 minutes at a concentration of 80 x 10^{-3} mol/dm^3. BHT, along with the other standard antioxidants show "saturation" effect whereby it is less effective the more is added, most strikingly for eugenol where the induction time was essentially unchanged (~34 minutes) when its concentration increased threefold from 54 to 162 x 10^{-3} mol/dm^3.

The inhibition difference between BHT and eugenol could be attributed to many factors. However, generally, phenolic antioxidants can be evaluated for their antioxidant power by the bond dissociation energy (BDE) of the phenol O-H bond and by the kinetic rate constant for inhibition (k_{inh}), and from a thermodynamic point of view, the O-H BDE value of the phenolic antioxidant has to be lower than the O-H BDE value of the ROO-H (368.2 kJ/mol) formed in the inhibition mechanism in order to give a more favorable reaction.[341] Therefore, comparison of the O-H BDE values for BHT (339.0 kJ/mol) and eugenol (351.5 kJ/mol), as presented in Table 5.4 with other O-H BDE values of some selected phenols, indicate that BHT provide more exothermic reactions towards peroxy radicals ($ROO^{\bullet}$) than eugenol, thus better antioxidant power.

Table 5.4: Bond dissociation energies (BDE) of some selected phenols O-H bond (kJ mol^{-1}) and their rate constant (M^{-1} s^{-1}) at 30 °C for H abstraction by peroxy radicals ($ROO^{\bullet}$).

Compound	Structure	BDE (kJ/mol)	Ref.	k_{inh} (x 10^4 M^{-1} s^{-1})	Ref.
Phenol		369 ± 3	339	0.6	342
BHT	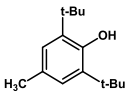	339.0 ± 0.5	339	1.4	343
Catechol		342.25	344	55	341
2-Methoxyphenol	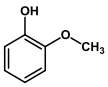	354.4 ± 0.8	342	0.47	342
2-Methoxy-4-methylphenol	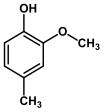	346.4 ± 0.9	342	1.2	342
Eugenol	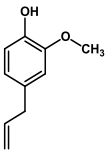	351.5	345	\[a]	\

Compound	Structure	BDE (kJ/mol)	Ref.	k_{inh} (x 10^4 M^{-1} s^{-1})	Ref.
Isoeugenol	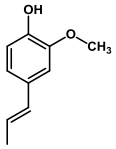	347.1	345	\	\

[a] Not available.

The results in Figure 5.19 also show that the separate addition of the four isolated extracts from the crude bio-oil extended the methyl linoleate induction time at varying molar phenolic concentrations. However, the relative induction time extension to the total molar phenolic content was not identical between the four isolated extracts. This finding suggests that the phenolic species in the crude bio-oil have differing antioxidant effects on methyl linoleate. This was clearly obvious when comparing the antioxidancy effects of water-soluble and neutral extracts on methyl linoleate. An induction time of ~22 minutes was achieved when adding a *ca.* 10 x 10^{-3} mol/dm^3 of total molar phenolics from the water-soluble extract, whereas an induction time of just ~18 minutes was achieved when adding more than threefold (at *ca.* 35 x 10^{-3} mol/dm^3) of total molar phenolics from the neutral extract.

Furthermore, the results from Figure 5.19 clearly show that the crude bio-oil addition to methyl linoleate increased its induction time from 0 to 163 minutes at the total molar phenolic concentration of *ca.* 70 x 10^{-3} mol/dm^3. In comparison with the other extracts, crude bio-oil has the best inhibition performance, and the overall ranking order was as follows: crude bio-oil > water-soluble extract > organic acids extract > phenolic extract > neutral extract. Surprisingly, the water-soluble extract showed comparable induction times to the crude bio-oil at similar molar phenolic concentration, and neither showed any saturation effect when increasing their concentration in methyl linoleate.

Strangely, the phenolic extract did not show a better inhibition performance than the crude bio-oil, as had been expected. However, the phenolic extract had a better inhibition performance than eugenol, especially at high molar concentrations (> 27 x 10^{-3} mol/dm^3). The inhibition difference between the crude bio-oil and the phenolic

extract could be attributed to the absence of other phenolic components which are either better antioxidants or able to create a synergistic effect with the phenols in the phenolic extract for a stronger inhibition performance.

From the GC-FID quantification results presented in Chapter 4 (section 4.3.1), 1,2-benzenediol (catechol) is the phenolic with the highest concentration in the water-soluble extract, and also in the crude bio-oil. Consequently, catechol could potentially be a key phenolic component that plays a significant role as a powerful inhibitor among the other identified phenols in spruce crude bio-oil. Therefore, Figure 5.19 also shows the induction times of catechol towards methyl linoleate autoxidation at varying concentrations. Remarkably, the results indicated that catechol showed similar induction times with the crude bio-oil at below *ca.* 40 x 10^{-3} mol/dm^3. However, catechol shows a reduction in its effectiveness at higher concentrations, greater than *ca.* 40 x 10^{-3} mol/dm^3, where, unexpectedly, catechol somehow acted as a retarder of methyl linoleate autoxidation rather than an effective antioxidant.

A retarder decreases the autoxidation rate, but does not eliminate visible oxidation early in the reaction (similar to that observed with the addition of 162 x 10^{-3} mol/dm^3 of catechol standard to 2 ml methyl linoleate in Figure 5.13).[346] An effective antioxidant, however, prevents visible oxidation up to a certain time (as observed with the addition of 80 x 10^{-3} mol/dm^3 of BHT to 2 ml methyl linoleate in Figure 5.5), and when this certain time ends, the autoxidation begins with a rate that is essentially the same as that for the reaction without an antioxidant added (as observed when oxidizing 2 ml methyl linoleate alone, as in for example Figure 5.5).[346]

When comparing crude bio-oil inhibition performance with BHT (as in Figure 5.19), the crude bio-oil did not show a saturation effect like BHT, and the crude bio-oil induction times were approximately comparable with BHT at an approximately similar molar phenolic concentration in methyl linoleate. Remarkably, BHT and catechol inhibition performances were similar at the molar concentration of *ca.* 40 x 10^{-3} mol/dm^3. However, at molar concentrations above *ca.* 40 x 10^{-3} mol dm^{-3}, BHT addition to methyl linoleate was better in achieving higher induction times. The

inhibition performance agreement between BHT and catechol at low molar concentrations (< 40 x 10^{-3} mol/dm^3) could be attributed to the approximately comparable O-H BDE values for catechol (342.3 kJ/mol) and BHT (339.0 kJ/mol).

5.3.2.2 Effect of water-soluble isolated extracts

To allow a comparison of the antioxidancy of methyl linoleate with, individually, the additions of crude bio-oil (Figure 5.4); the commercial antioxidant BHT (Figure 5.5); water-soluble, diethyl ether, DCM extracts, and water-soluble residue (Figure 5.10); catechol (Figure 5.13 and Figure 5.14); and isoeugenol (Figure 5.15) at 120 $^{\circ}$C and 1 bar of oxygen, the induction times determined for the above figures are given in Figure 5.20. The measured total phenolic concentrations and the induction times are given in Appendix C.

Figure 5.20 (A) shows the induction times of methyl linoleate with isolated extracts from the water-soluble phase of crude bio-oil (diethyl ether, DCM and water-soluble residue), including the induction times results of crude bio-oil and water-soluble extract for ease of comparison. The antioxidant concentrations quoted again correspond to the amount of total phenolics added to the methyl linoleate, which is the equivalent molar concentration of a mono-phenol as determined by the Folin-Ciocalteu (FC) assay.

Figure 5.20 (B) shows the induction times of methyl linoleate with the commercial antioxidant BHT, isoeugenol and catechol. BHT and catechol are presented again for ease of comparison.

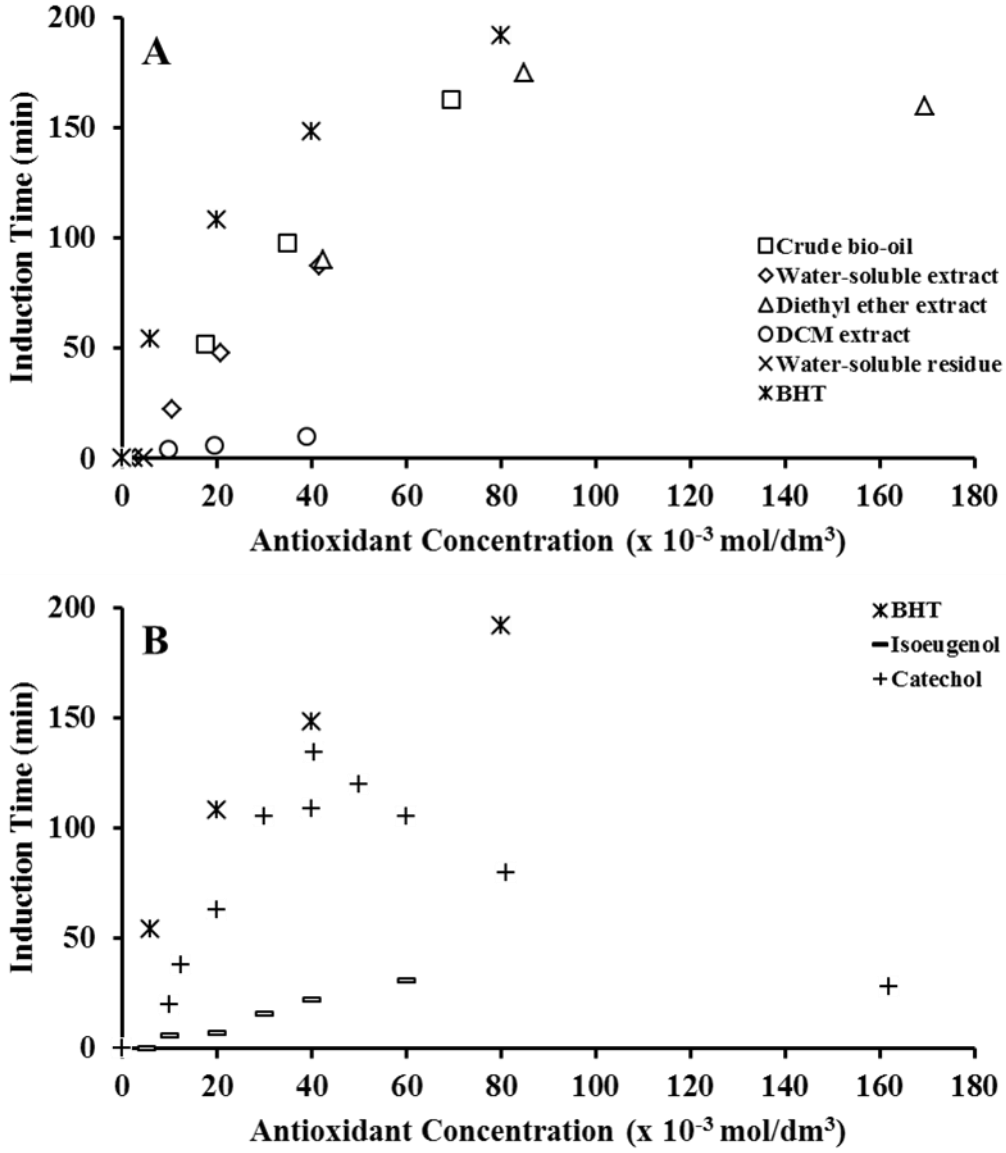

Figure 5.20: The induction times of 2 ml methyl linoleate with increasing concentrations of: (A) crude bio-oil, water-soluble, diethyl ether, DCM and water-soluble residue extracts; (B) BHT, isoeugenol and catechol, at 120 $^{\circ}$C and 1 bar of oxygen (crude bio-oil, water-soluble extract, BHT and catechol are presented again for ease of comparison).

The results in Figure 5.20 (A) indicated that the addition of the diethyl ether extract increased methyl linoleate induction time from 0 to 175 minutes at the total phenolic concentration of 85 x 10^{-3} mol dm^{-3}. However, at the total phenolic concentration of 170 x 10^{-3} mol dm^{-3}, the effect of diethyl ether extract on methyl linoleate induction time was slightly decreased.

Moreover, the concentration of catechol in the diethyl ether extract was significantly higher to the extent that it was possible to observe it *via* ^{13}C NMR spectroscopy after the addition to methyl linoleate. After the oxidation experiment of the linoleate-extract sample at 120 $^{\circ}C$ and 1 bar of oxygen, the ^{13}C NMR resonance signals of catechol molecule disappeared from the linoleate medium, indicating the reaction of catechol (in diethyl ether extract) with the free radicals generated during the oxidation experiment of methyl linoleate. Figure 5.21 shows the ^{13}C NMR spectra of catechol standard and the linoleate-extract sample before and after the oxidation experiment at 120 $^{\circ}C$ and 1 bar of oxygen.

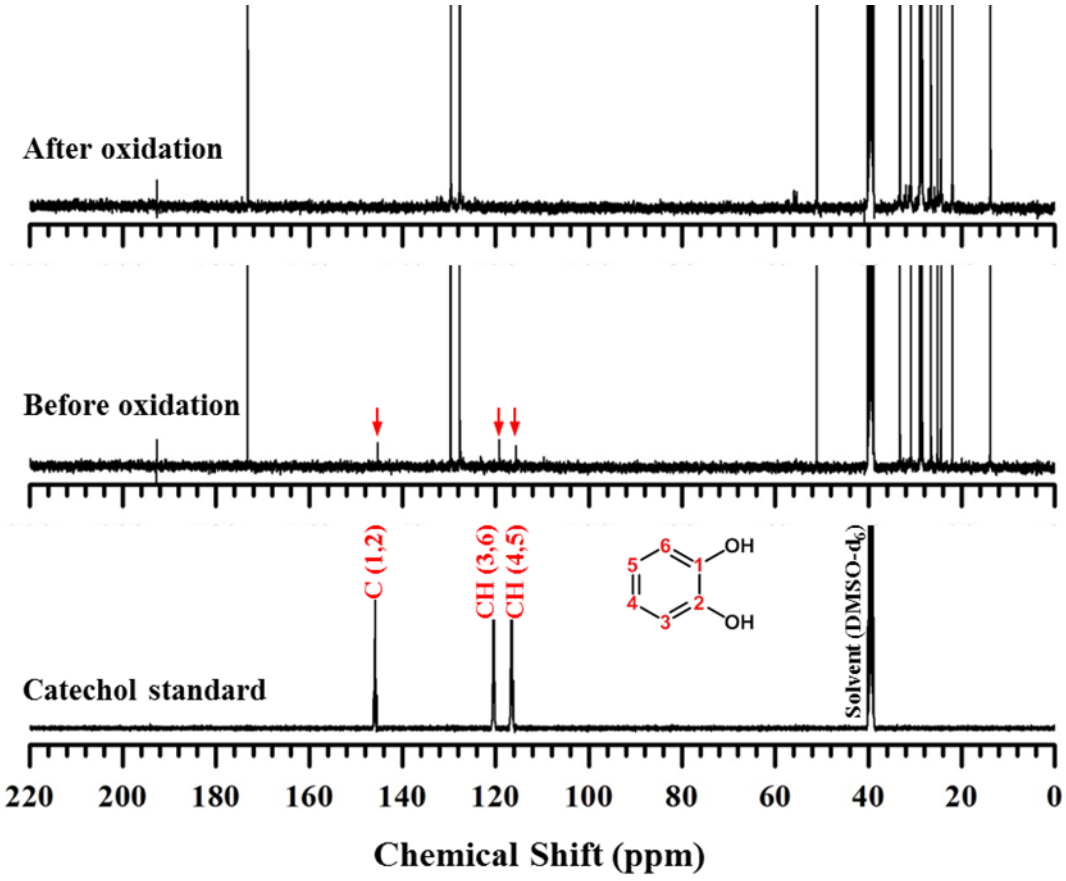

Figure 5.21: The ^{13}C NMR spectrum of catechol standard and the ^{13}C NMR spectra of methyl linoleate with the addition of 170 x 10^{-3} mol dm^{-3} of diethyl ether extract before and after oxidation at 120 $^{\circ}C$ and 1 bar oxygen.

The ^{13}C NMR resonance signals of the catechol from the diethyl ether extract in methyl linoleate before oxidation (in Figure 5.21) was the same as the ^{13}C NMR resonance signals of a catechol standard in methyl linoleate before the oxidation test,

see Figure 5.22. After the oxidation test of the linoleate-catechol sample at 120 °C and 1 bar of oxygen, the ^{13}C NMR resonance signals of the catechol standard (in Figure 5.22) also disappeared from the linoleate medium, evidencing the catechol reaction (as the catechol in the diethyl ether extract) with the free radicals generated during the oxidation experiment of methyl linoleate at 120 °C and 1 bar of oxygen.

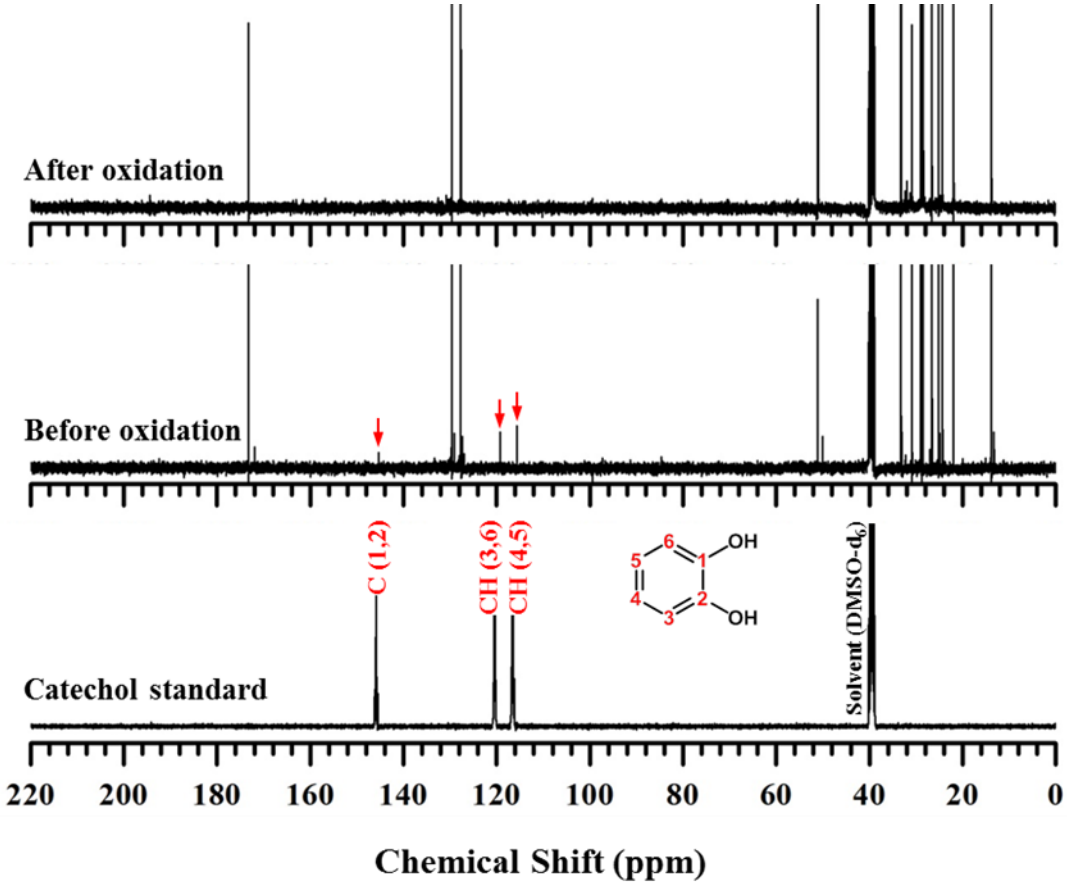

Figure 5.22: The ^{13}C NMR spectrum of catechol standard and the ^{13}C NMR spectra of methyl linoleate with the addition of 20 x 10^{-3} mol dm^{-3} of catechol standard before and after oxidation at 120 °C and 1 bar oxygen.

In comparison with the crude bio-oil, the addition of diethyl ether extract to methyl linoleate surprisingly showed comparable induction times to the crude bio-oil at approximately similar molar phenolic concentrations. This important finding suggests that the highly phenolic antioxidant active species in the crude bio-oil were soluble in the water phase, and were successfully extracted further by diethyl ether.

For the other isolated extracts from the water-soluble phase, DCM extract addition to methyl linoleate showed poor inhibition effects, even though at the addition of the molar phenolic concentration of *ca.* 40 x 10^{-3} mol dm^{-3}, the methyl linoleate induction time was very low (~10 minutes), whereas, by contrast, the addition of approximately similar molar phenolic concentration of the diethyl ether extract to methyl linoleate has extended the methyl linoleate induction time to ~90 minutes. Furthermore, the water-soluble residue addition to methyl linoleate did not show any inhibition effect, and this was expected as the phenolic concentration in the water-soluble residue was extremely low (~1.4% w/w, as determined by FC assay).

In summary, crude bio-oil, water-soluble extract and diethyl ether extract additions to methyl linoleate were comparable in their induction times at approximately similar molar phenolic concentrations, and the overall ranking order of the water-soluble phase isolated extracts including water-soluble extract and crude bio-oil can be as follows: crude bio-oil > diethyl ether extract > water-soluble extract > DCM extract > water-soluble residue.

From the results in Figure 5.20 (B), isoeugenol addition to methyl linoleate gave low inhibition activity, where just ~31 minutes induction time was achieved at the molar concentration of 60 x 10^{-3} mol dm^{-3}, whereas, by contrast, BHT addition to methyl linoleate gave much better inhibition activity when compared at similar molar concentrations. This low inhibition activity by isoeugenol could be related to its high O-H BDE value (347.1 kJ mol^{-1}) when compared to the O-H BDE value for BHT (339.0 kJ mol^{-1}).

5.3.3 Effect of mixed phenolic standard on induction time

To allow a comparison of the antioxidancy examined of methyl linoleate with 6 mixed phenolic standard (Figure 5.16; their composition are discussed in section 5.2.3.2), with crude bio-oil (Figure 5.4), with the commercial antioxidant BHT (Figure 5.5), with eugenol (Figure 5.12), with catechol (Figure 5.13 and Figure 5.14), and with isoeugenol (Figure 5.15) at 120 $^{\circ}$C and 1 bar of oxygen, the induction times determined for these figures are given in Figure 5.23. The phenolic concentrations and the induction times are given in Appendix C.

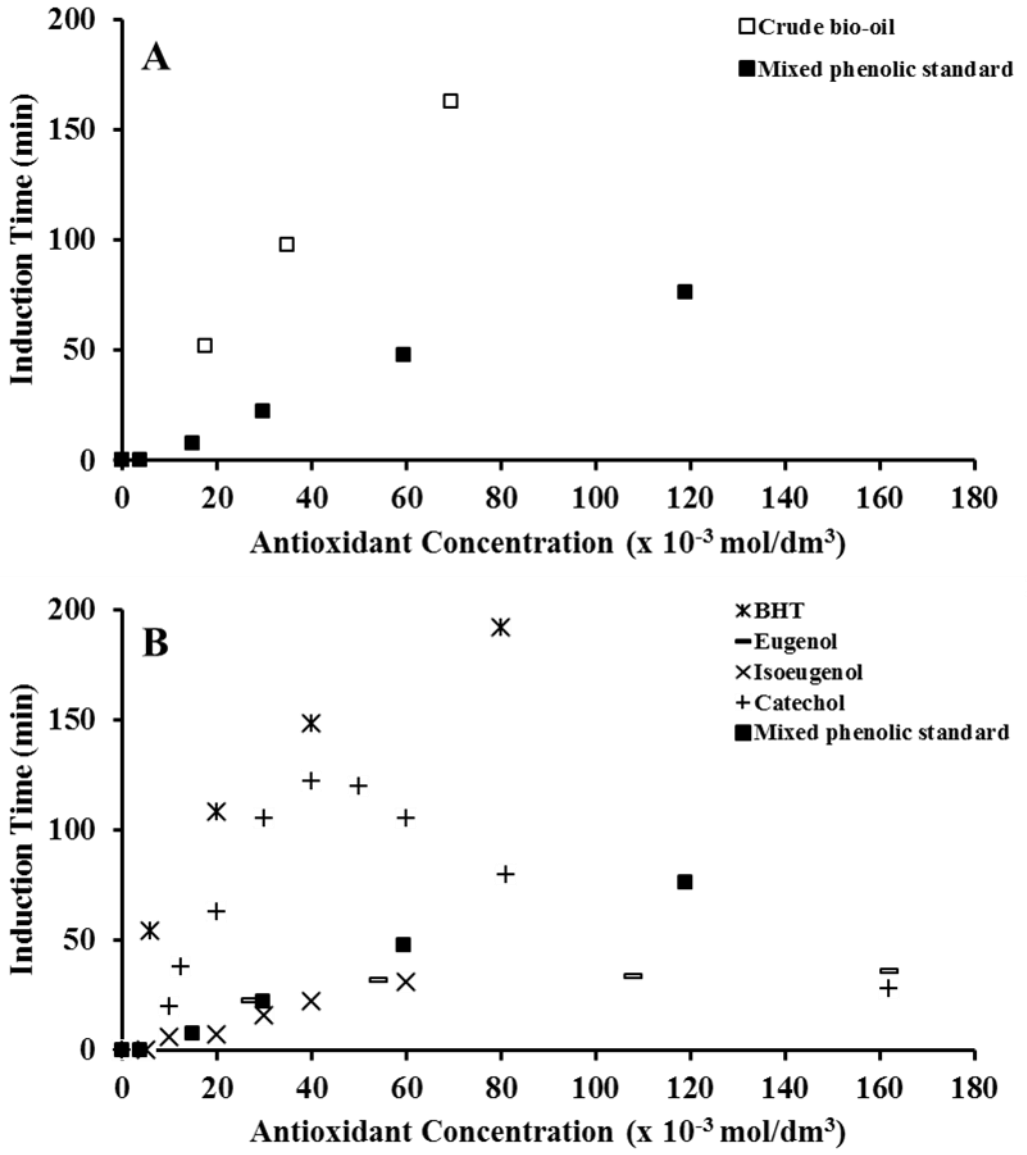

Figure 5.23: The induction times of 2 ml methyl linoleate with increasing concentrations of: (A) crude bio-oil and mixed phenolic standard; (B) BHT, eugenol, isoeugenol, catechol and mixed phenolic standard at 120 °C and 1 bar of oxygen (the induction time of catechol at 40 x 10^{-3} mol/dm^3 presented here is the average of two independent experiments).

The results from Figure 5.23 show that the mixed phenolic standard increased methyl linoleate induction time from 0 to 76 minutes at the total molar phenolic concentration of *ca.* 119 x 10^{-3} mol dm^{-3}. At molar concentrations below *ca.* 60 x 10^{-3} mol dm^{-3}, the antioxidant effect of the mixed phenolic standard was comparable with eugenol and isoeugenol, indicating no improvement in the antioxidant power. However at molar concentrations above *ca.* 60 x 10^{-3} mol dm^{-3}, the antioxidant effect

of the mixed phenolic standard was better than eugenol and isoeugenol, indicating higher antioxidant power, and this could be from the presence of catechol.

When comparing the antioxidancy of the mixed phenolic standard with catechol, catechol was noticeable much better at low phenol concentrations, below *ca.* 40 x10^{-3} mol dm^{-3}. Of note when the total phenolic concentration of *ca.* 119 x 10^{-3} mol dm^{-3} of the mixed phenolic standard was added to methyl linoleate. This was striking because this linoleate-phenolic mixture contained a relatively high molar concentration of catechol (35.2 x 10^{-3} mol dm^{-3}), but it did not show a better or even similar induction time to the antioxidant activity of catechol alone (at *ca.* 40 x 10^{-3} mol dm^{-3}). It did show however a lower induction time of ~76 minutes, where the expected induction time should be more than ~105 minutes (based on previous result for the addition of *ca.* 30 x 10^{-3} mol dm^{-3} of catechol standard to methyl linoleate).

From comparing the mixed phenolic standard with the crude bio-oil, it is clear that the crude bio-oil has noticeably a better antioxidant activity than the mixed phenolic standard. The crude bio-oil increased methyl linoleate induction time from 0 to 163 minutes at the molar phenolic concertation of *ca.* 70 x 10^{-3} mol dm^{-3}, whereas the mixed phenolic standard increased the methyl linoleate induction time from 0 to just 76 minutes at the molar concentration of 119 x 10^{-3} mol dm^{-3}. The mixed phenolic standard was approximately three times less active than the crude bio-oil in methyl linoleate at the equivalent molar phenolic concentrations. This suggests that the identified mono-phenolic species in the crude bio-oil could possibly not have a dominant contribution towards the total antioxidant activity of the crude bio-oil in methyl linoleate. Therefore, the source of two-thirds of the total antioxidants activity of the crude bio-oil remains unknown. Although catechol was found to be the most active phenolic antioxidant in the crude bio-oil, it did not show a comparable antioxidant performance to the crude bio-oil or even to itself when mixed with other phenolic standards. This finding would benefit from further future investigation to examine the possibilities behind the strong antioxidant activity of the crude bio-oil.

5.3.4 Discussion of the mechanism of antioxidant activity of bio-oil

Plant extracts, generally used in food applications, are known to possess strong H-donating activity thus making them extremely effective antioxidants.[347] This antioxidant activity is most often because of particular components within the plant extracts, such as phenolic acids (*e.g.*, protocatechuic, caffeic, and gallic acids), phenolic diterpenes (*e.g.*, carnosol, and carnosic acid), flavonoids (*e.g.*, quercetin, catechin, and kaempferol), and volatile oils (*e.g.*, eugenol, carvacrol, and thymol).[347]

In a similar manner, the crude bio-oil produced in this study from the microwave-enhanced pyrolysis of spruce woodchips was found to be an effective antioxidant towards the methyl linoleate autoxidation at 120 $^{\circ}$C and 1 bar of oxygen. This high antioxidant activity in the crude bio-oil is most likely as a result of its phenolic content as discussed earlier in Chapter 4 (section 4.2). These phenolic species within the crude bio-oil have strong H-donating activity and hence can scavenge free radicals formed during methyl linoleate autoxidation, as previously demonstrated from the consumption of catechol in Figure 5.21 and Figure 5.22. However, individual phenols can vary in their antioxidant activity. This is most likely due to their different chemical structures as identified *via* GC-MS in Chapter 4 (section 4.2).

In principal, the phenols in the bio-oil would expected to behave like typical phenolic antioxidants as previously discussed in Chapter 1 (section 1.8), where the initial mechanism of action by the phenol is the donation of hydrogen to a peroxyl radical ($ROO^{\bullet}$) formed during the autoxidation reactions. However, when the phenoxyl radical is formed, the subsequent mechanisms can be more complex and, depending on the structural conformation of the phenolic compound, the latter mechanisms could involve trapping more free radicals.[348] For instance, eugenol, which has a chemical structure similar to most of those monophenols identified in the bio-oil, is found to reduce nearly two free radicals even though it has only one hydrogen on a hydroxyl group thus, initially, cannot reduce more than one free radical unless more complex reactions are involved after the phenoxyl radical formation.[348]

To explain this antiradical efficiency for eugenol, Brand-Williams and co-workers[349] have suggested three hypotheses that could take place following eugenol donation of

the first hydrogen to a free radical (reaction i in Figure 5.24). Their first hypothesis is that the product phenoxyl radical donate a second hydrogen after electron delocalization onto the *para*-substituted group (reaction ii in Figure 5.24). In the second hypothesis, another free radical reacts with the phenoxyl radical after electron delocalization onto the free *ortho*- position (reaction iii in Figure 5.24). The third hypothesis is the dimerization of two phenoxyl radicals (reaction iv in Figure 5.24) followed by regeneration of two hydroxyl groups (reaction v in Figure 5.24) *via* an intramolecular transfer of $H^{\bullet}$ and, thus, this new formed bisphenol could contribute by further reacting with one or more free radicals.

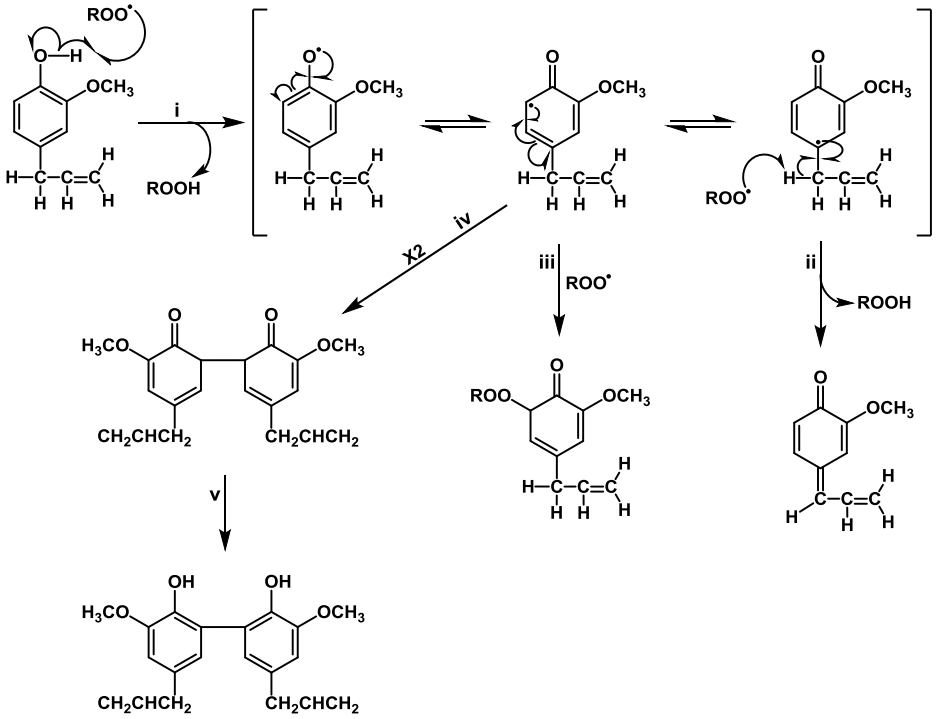

Figure 5.24: Potential reaction mechanism and oxidation products of eugenol.[349]

This suggested mechanism of eugenol is possible for the majority of the monophenolic compounds identified in the crude bio-oil. However, some other identified monophenolic compounds in the crude bio-oil are expected to be less efficient than eugenol because of their different structural conformation. In fact, compounds such as isoeugenol, which is one of the significant identified compound in the crude bio-oil, was found to reduce just one free radical during autoxidation reactions.[348] This different antiradical behavior of isoeugenol, as interpreted by

Brand-Williams and his co-workers,[349] is possibly as a result of the conjugated group in its *para*- position which would enter into resonance with the phenoxyl's aromatic ring. Thus, the chances of a dimerization or even complexation with a second free radical by the isoeugenol-drived phenoxyl radical would be lower as, preferably, the radical would be stabilized outside of the phenoxyl's aromatic ring, as shown in Figure 5.25.

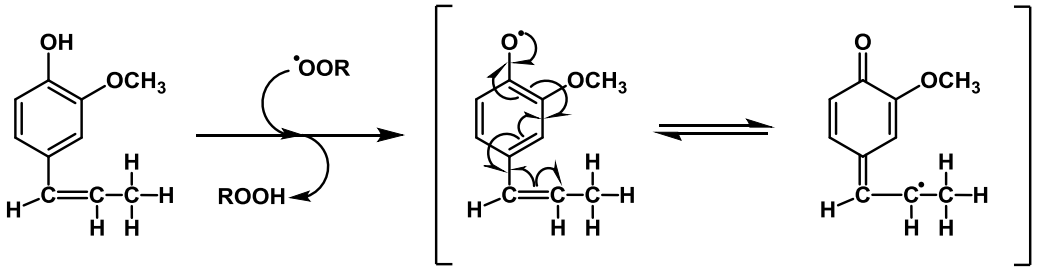

Figure 5.25: The formation of isoeugenol-derived phenoxyl radical and its radical stabilization.

Polyphenols are compounds with more than one hydroxyl group attached to the phenol ring, and are also present in the crude bio-oil and generally known to be more efficient antioxidants than the monophenols.[350, 351] For instance, Brand-Williams and co-workers[349] have found that caffeic acid, a diphenol, can reduce four or more free radicals, whereas coumaric acid, the caffeic acid monophenol counterpart, can reduce nearly one free radical. Likewise, the triphenol gallic acid was found to be more effective than its diphenol counterpart, protocatechuic acid, where the former can reduce six or more free radicals and the latter can just reduce three or more free radicals.[349] The chemical structures of these acids are provided in Figure 5.26.

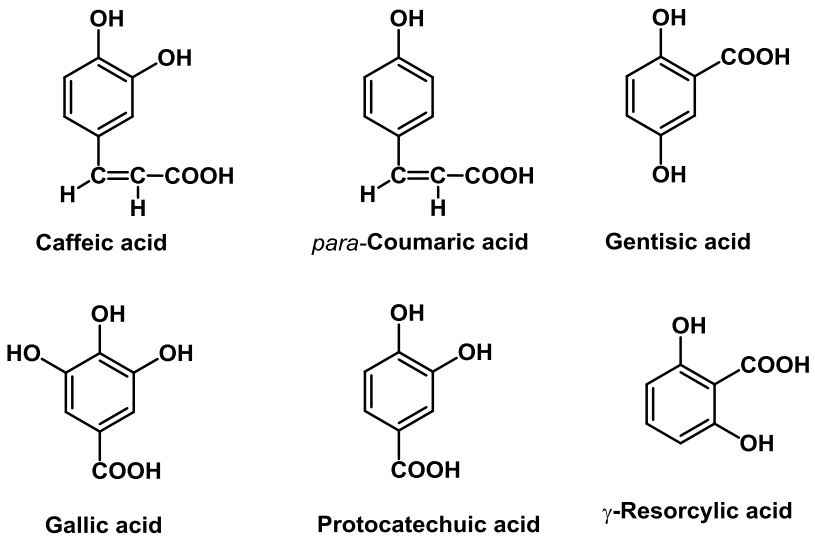

Figure 5.26: The chemical structures of caffeic, *p*-coumaric, gallic, protocatechuic, gentisic and γ-resorcylic acids.

Furthermore, the position of the other hydroxyl groups on the ring is also important.[352] According to Brand-Williams and his co-workers,[349] those compounds whose second hydroxyl group is in *meta*- position possess a lower activity than when it is *ortho*- or *para*-, as they found for γ-resorcylic acid which can reduce just one free radical in comparison with three or more and five or more free radicals reduction for respectively protocatechuic acid and gentisic acid (their chemical structures are provided in Figure 5.26).

The antiradical efficiency of *ortho*- and *para*- diphenols is possibly due to the additional stabilization of the formed phenoxyl radical by an intramolecular hydrogen bonding (reaction i in Figure 5.27),[341, 349] or by the possibility of the diphenol phenoxyl radical to either further react with a second free radical to form an *ortho*-quinone (reaction iia in Figure 5.27) or to regenerate another diphenol molecule by the reaction with another diphenol phenoxyl radical (reaction iib in Figure 5.27).[349, 353, 354]

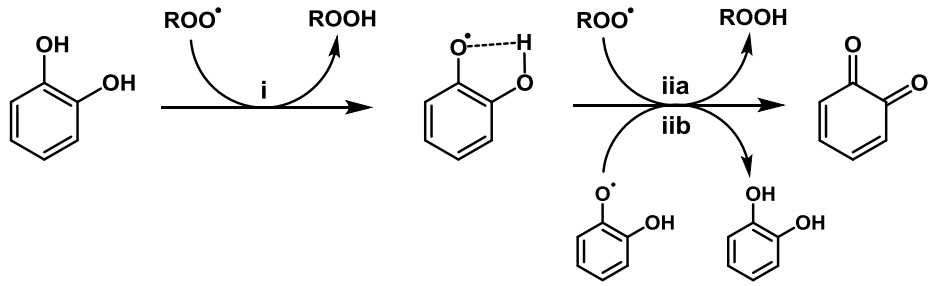

Figure 5.27: The formation of intramolecular hydrogen bond in the catechol-derived phenoxyl radical, and the formation *ortho*-quinone by either the reaction of the formed phenoxyl radical with a second peroxyl radical or by the regeneration mechanism of a catechol.[341, 349, 354]

This proposed antioxidant mechanism of *ortho*-diphenols shown in Figure 5.27 is quite reasonable to explain the reduction of two or more free radicals. However, in the case of caffeic acid, an *ortho*-diphenol, it is reported by Brand-Williams and his co-workers[349] to reduce four or more free radicals. Therefore, there are probably more complex reactions being involved as the mechanism in Figure 5.27 does not explain the further two or more free radicals reduction in the case of caffeic acid. Unfortunately, the literature is lacking in information about these further free radical trapping mechanisms by *ortho*-diphenols. However, there are a few studies that discuss possible formation of *ortho*-diphenol dimers during autoxidation reactions.[355, 356]

According to these studies,[355, 356] these new diphenol dimers could form *via* two possible pathways: (a) two phenoxyl radicals, the intermediate oxidation products of *ortho*-diphenols, dimerize after electron delocalization onto the *para*- position (reaction iia in Figure 5.28) followed by regeneration of two hydroxyl groups by an intramolecular transfer of $H^{\bullet}$ (reaction iiia in Figure 5.28); or (b) the *ortho*-quinone, the primary oxidation product of an *ortho*-diphenol, is unstable and undergo further reaction with the starting *ortho*-diphenol to finally produce a new *ortho*-diphenol dimer (reaction iib in Figure 5.28).

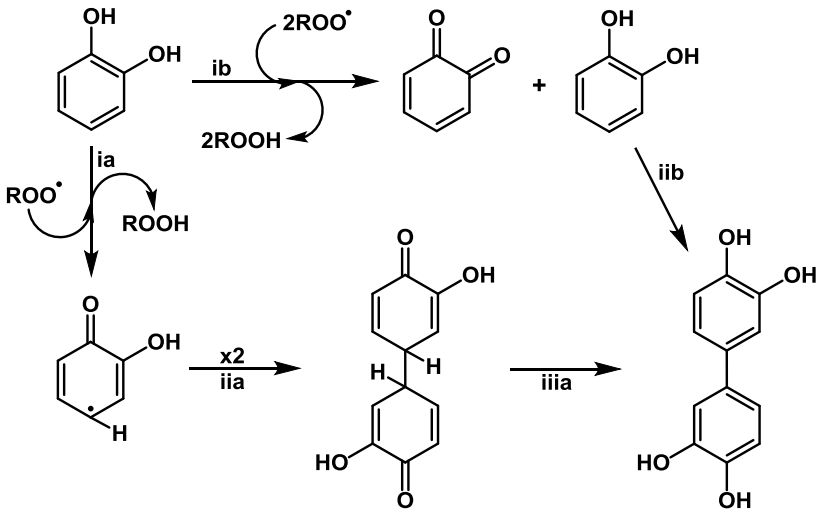

Figure 5.28: The formation of diphenol dimer by either the reaction between two phenoxyl radicals or the reaction between an *ortho*-quinone and a diphenol.[355, 356]

In fact, Ryan and his co-workers[357] have investigated the electrochemical oxidation of catechol and substituted catechols. They found that catechol and all of its studied derivatives are initially oxidized to *ortho*-quinones, and the latter can react with the starting material to form a dimer. However, they could not identify this formed dimer due to its poor stability and the great tendency of the quinones to polymerize. Therefore, according to their study, the identity of this dimer can only be inferred. Thus, two general types of the dimer are visualized by them to form either by C-O coupling (reaction ia in Figure 5.29) or C-C coupling (reaction ib in Figure 5.29).

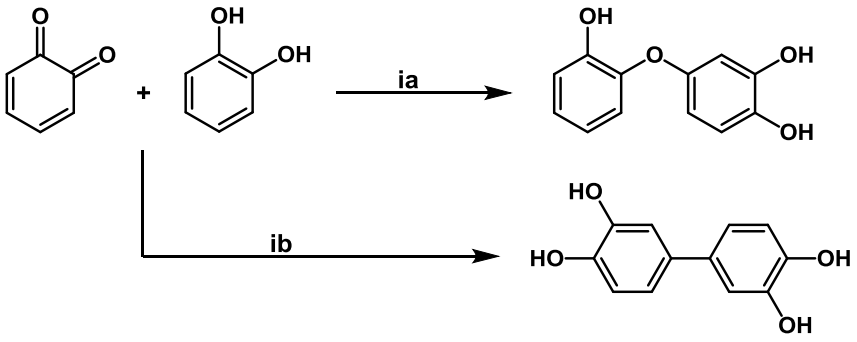

Figure 5.29: Two possible types of dimer formation from the reaction of *ortho*-quinones with *ortho*-diphenols.[357]

The formation of either dimer, as shown in Figure 5.29, can eventually participate in the further reduction of more free radicals during autoxidation reactions and, thus, their additional antiradical activity might explain the reduction of four or more free radicals in the case of caffeic acid as is found by Brand-Williams and his co-workers.[349] According to Ryan and his co-workers,[357] if the dimer is formed by C-O coupling, then it could potentially further trap two free radicals as the reaction in Figure 5.30.

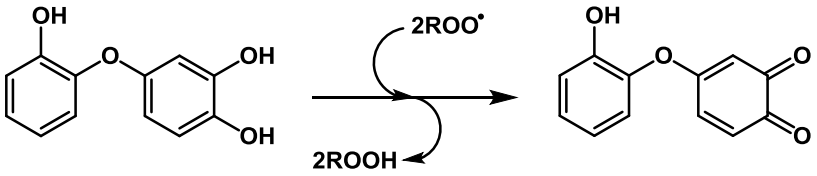

Figure 5.30: The trapping of two peroxyl radicals by the formed C-O dimer of *ortho*-diphenol.[357]

However, if the dimer is formed by C-C coupling, then this new C-C dimer could potentially further trap the total of four free radicals as reaction i and reaction ii in Figure 5.31.

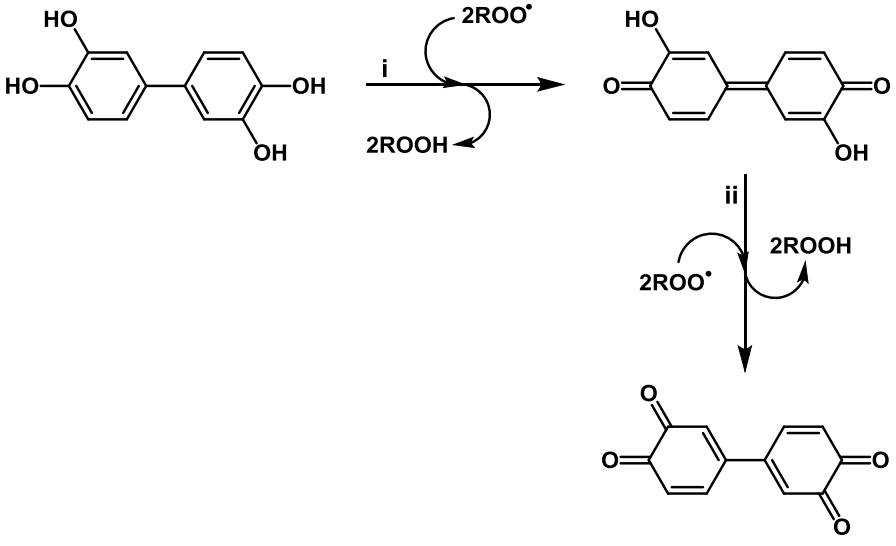

Figure 5.31: The trapping of four peroxyl radicals by the formed C-C dimer of *ortho*-diphenol.[357]

In addition, there are possible interactions between the phenolic species within the crude bio-oil, where a potent regeneration of an antioxidant by another one can increase or decrease the total activity of a mixture of antioxidants. This regeneration phenomenon is generally descried in literature as synergistic (positive) or antagonistic (negative) effects. According to Peyrat-Maillard *et al.*,[358] three scenarios could happen between two phenolic antioxidants in a mixture: (1) a synergistic effect, where the less effective antioxidant regenerates the more effective one; (2) an antagonistic effect, where the more effective phenolic molecule regenerates the less effective one; or (3) no effect, where both antioxidants have the same effectiveness.

The first scenario was found by Peyrat-Maillard *et al.*[358] to occur between quercetin and rosmarinic acid which, according to their results, the former is less efficient antioxidant than the latter one, thus, part of quercetin regenerates rosmarinic acid creating a synergistic effect. The second scenario was found by Peyrat-Maillard *et al.*[358] to be occurring between α-tocopherol and caffeic acid where, according to their results, the former is a less efficient antioxidant than the latter, thus, part of caffeic acid regenerates α-tocopherol creating an antagonistic effect. Figure 5.32 shows the chemical structures of quercetin, rosmarinic acid, α-tocopherol, and caffeic acid.

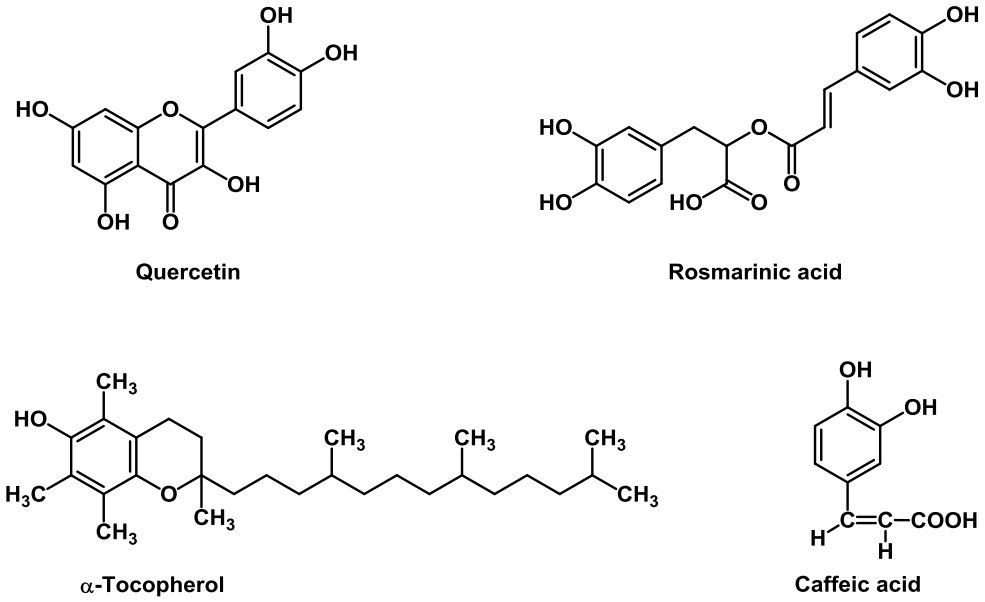

Figure 5.32: The chemical structures of quercetin, rosmarinic acid, α-tocopherol, and caffeic acid.

The regeneration of an antioxidant by another one in a given mixture is suggested to occur by the mechanism presented in Figure 5.33, where the first antioxidant (A_1OH) is only acting as a hydrogen donor to free radicals, while the second antioxidant (A_2OH) is acting as hydrogen donor to free radicals and a regenerator of first antioxidant.[359]

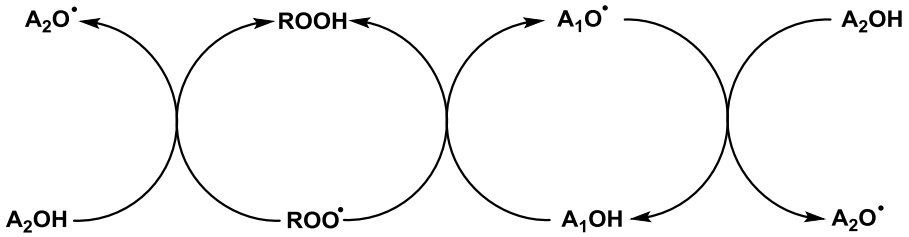

Figure 5.33: The suggested regeneration mechanism of an antioxidant by another one in a mixture.[359]

This regeneration mechanism of an antioxidant by another one is possibly occurring between the phenolic species in the crude bio-oil. However, it is difficult to specifically determine the ones that undergo this regeneration mechanism as the crude bio-oil contains many types of phenols. In fact, catechol, an *ortho*-diphenol identified in the crude bio-oil, was found to be a very efficient antioxidant when tested alone in the autoxidation of methyl linoleate at 120 $^{\circ}$C and 1 bar of oxygen (as illustrated earlier in Figure 5.23). However, when catechol is mixed with other phenolic standard (as discussed earlier in section 5.2.3.2 and section 5.3.3), its antioxidant power was noticeably reduced, which suggests that part of catechol in the mixed phenolic standard is possibly acting as a regenerator of the other mixed phenols thus creating an antagonistic effect.

5.3.5 The reduction of catechol antioxidancy at higher concentrations

Three hypotheses are suggested to explain the reduction of catechol antioxidancy at concentrations above *ca.* 40 x 10^{-3} mol/dm^3 during methyl linoleate autoxidation at 120 $^{\circ}$C and 1 bar of oxygen.

The first hypothesis is that introducing high concentration of catechol in the system could affect antioxidancy due to the initial formed phenoxyl radicals being more

likely to undergo coupling reactions to form a dimer (reactions iib and iiib in Figure 5.34) over trapping a second free radical (reaction iia in Figure 5.34), due to the phenoxyl being at higher concentration so the self-reaction being more likely.

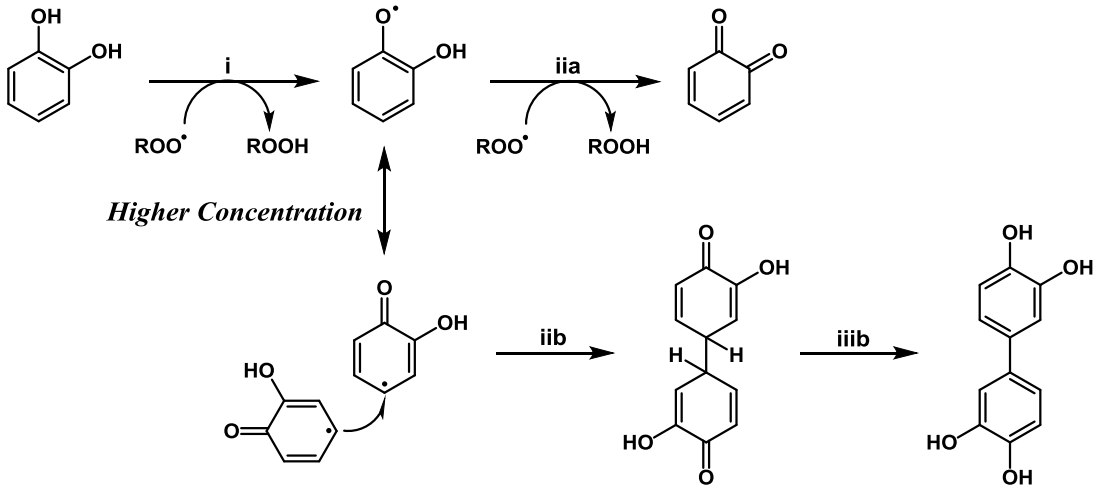

Figure 5.34: Proposed change in antiradical mechanism of catechol at higher concentration during autoxidation reaction.

This change in the mechanism of action by phenoxyl radicals when a higher concentration of an antioxidant being introduced in the system was previously reported by Masuda *et al.*[360] after they have identified new curcumin dimers that formed during the autoxidation of ethyl linoleate in the presence of curcumin. According to Masuda *et al.*,[360] the rate of the dimer formation is significantly dependent on curcumin concentration, while the formation of the peroxide, a product formed from the reaction of lipid-derived peroxyl radical and the curcumin-derived phenoxyl radical, remained constant regardless of curcumin concentration. Therefore, increasing the concentration of curcumin in ethyl linoleate, according to Masuda *et al.*,[360] will eventually lead to the formation of larger amount of dimers in addition to the constantly produced curcumin-lipid peroxides.

The second hypothesis is that increasing the concentration of catechol could result in the formation of less soluble catechol-derived oligomers in the autoxidation reaction medium. Voisin and Williams[361] have shown that the following structures (1 and 2 in Figure 5.35) can be formed from catechol when chemically or electrochemically oxidized.

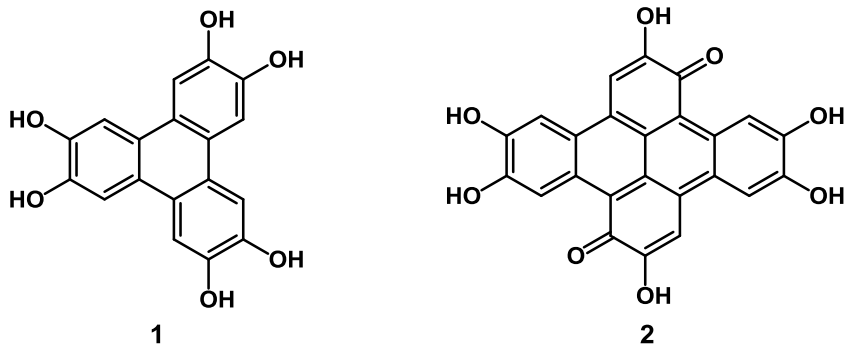

Figure 5.35: The proposed oxidation products of catechol during oxidation reactions.[361]

According to Voisin and Williams,[361] the formation of the first oxidation product (triphenylene; product 1 in Figure 5.35) from catechol can be by the oxidative reaction pathway shown in Figure 5.36.

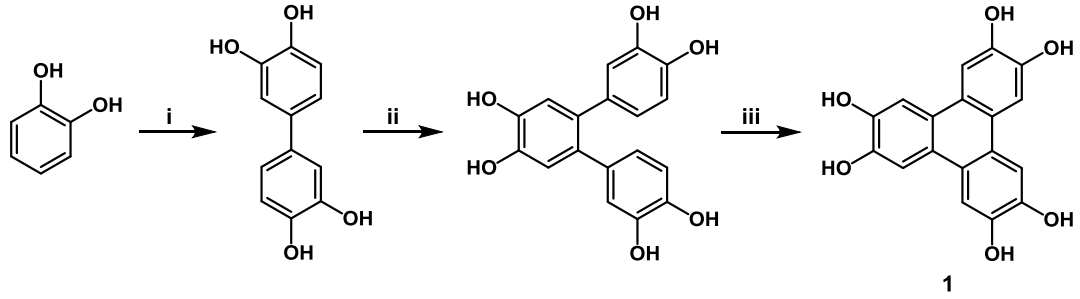

Figure 5.36: Proposed oxidative reaction pathway for the formation of triphenylene (product 1) from catechol.[361-363]

Figure 5.37 provides more detailed mechanistic steps that were not given explicitly by Voisin and Williams[361] for the formation of triphenylene (product 1). As can be seen in Figure 5.37, the first oxidation product of catechol (triphenylene; product 1) can be formed by first the dimerization of initial catechol-derived phenoxyl radicals to form biphenyls (reactions ii and iii in Figure 5.37). In the second stage, these biphenyls, after their donation of hydrogen to a free radical, they preferentially react with the starting material (catechol) derived phenoxyl radicals, possibly forming *ortho*-terphenyls (reactions v and vi in Figure 5.37), the latter of which, according to

Voisin and Williams,[361] would efficiently undergo intramolecular cyclization to form triphenylenes (reaction vii in Figure 5.37).

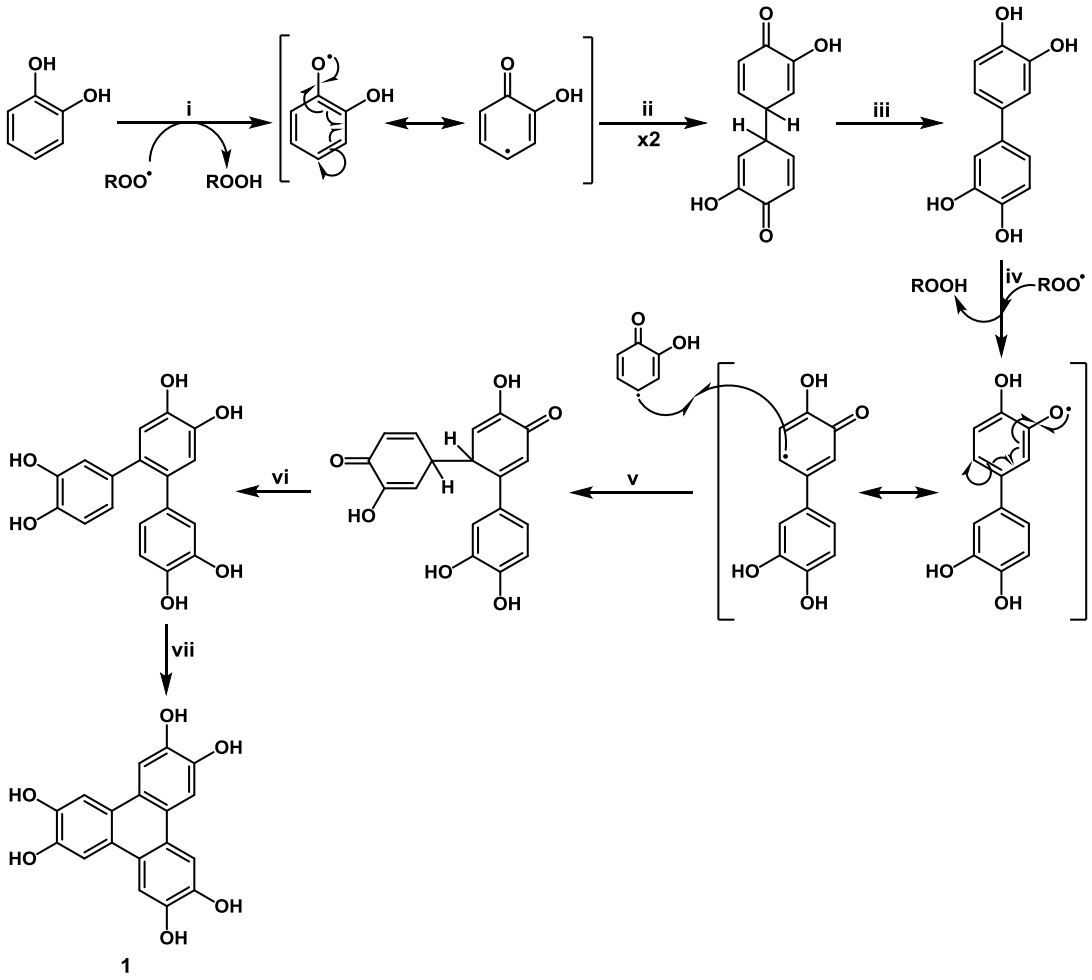

Figure 5.37: Proposed mechanism for the formation of triphenylene (product 1) from catechol during oxidation reactions.

As for the second oxidation product of catechol (polycyclic quinone; product 2 in Figure 5.35), Voisin and Williams[361] did not explain the full mechanistic details of its formation. However, they suggest that the formation of this polycyclic quinone structure is possibly *via* tetraphenyl oligomers, products of the dimerization of biphenyl-derived phenoxyl radicals (reaction i in Figure 5.38).

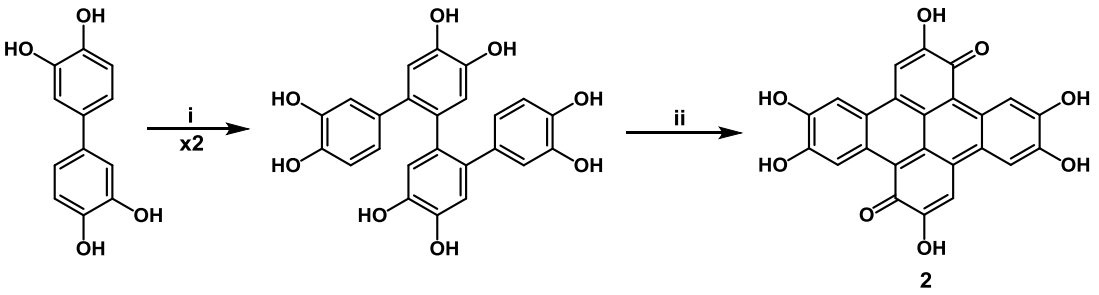

Figure 5.38: Proposed mechanistic pathway for the formation of polycyclic quinone (product 2) from catechol-derived biphenyl during oxidation reactions.[361]

A similar polycyclic quinone compound, namely 2,5,6,9,12,13-hexamethoxy-1,8-quinone (Figure 5.39), was previously prepared by Musgrave and Webster.[364, 365] According to their observations, this polycyclic quinone compound is involatile and virtually insoluble in most solvents except boiling chloroform which dissolves only *ca.* 0.2 g/l. Thus, their finding supports the suggestion that the formation of a polycyclic quinone (product 2 in Figure 5.35) during the autoxidation reaction of methyl linoleate could be responsible for the catechol antioxidancy reduction at higher concentrations due to this oxidation product being insoluble in the reaction medium.

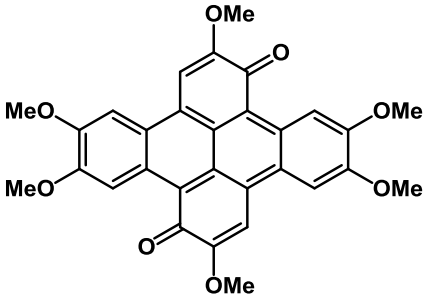

Figure 5.39: The chemical structure of 2,5,6,9,12,13-hexamethoxy-1,8-quinone.

The third hypothesis is related to the effect of polarity of the medium on catechol efficiency. The antioxidant activity of catechols is known to be very strongly affected by the polarity of the medium in which it functions, for instance, 3,5-di-tert-butylcatechol at 30 °C, is 1.2 x 10^3 times less active in acetone than hexane (by contrast, BHT is comparatively unaffected by the polarity of the medium, being just 7 times less effective in acetone than hexane).[366]

The polarity of methyl linoleate is low, in comparison with the antioxidants used for this work. As the initial antioxidant concentration is increased this will give a corresponding (relatively small) increase in polarity of the linoleate-antioxidant medium. From the work of Barclay *et al.*[366] this would be expected to have little effect on the activity of BHT, but it is suggested here that the small amount of added catechol could be increasing the polarity of the medium sufficient to have a substantial effect on the activity of the catechol, due to the exceedingly high sensitivity of catechol antioxidancy to the polarity of the medium.

This effect could also be exacerbated by the catechol used in this work having no alkyl groups to aid with solubilizing the antioxidant (by comparison, Barclay *et al.*[366] used the di-alkyl substituted di-tert-butylcatechol, which would be much more soluble in non-polar media than unsubstituted catechol).

By contrast, the unsubstituted catechol used in this work would be expected to be less soluble, and that above a threshold saturation concentration further addition of catechol would result in the catechol molecule aggregating together, so that they are no longer homogeneously distributed throughout the medium. This would have two effects, the bulk of the medium would have a lower catechol concentration than expected from the amount added, and further, where catechol molecules have aggregated to an extent, these would be in much more polar surroundings, so, from the work of Barclay *et al.*[366] these molecules would be substantially less effective and would contribute little antioxidancy. This explanation could be a topic for future investigation.

Tichonov *et al.*[367] have also investigated the effect of the polarity of the medium on the activity of 15 natural and synthetic antioxidants. According to Tichonov *et al.*,[367] most of the investigated antioxidants were also strongly affected by the polarity of the medium in which they function. For example, catechol at 37 $^{\circ}$C, is 12 times less active in methyl linoleate than styrene.[367] However, by contrast, BHT is essentially unaffected by the polarity of the medium.[367]

Furthermore, according to Tichonov *et al.*,[367] when reducing the concentration of methyl linoleate in chlorobenzene, the antioxidant activity of catechol is progressively increased, and when the methyl linoleate concentration in

chlorobenzene is zero, the antioxidant activity of catechol is the same as its activity in styrene. Therefore, their finding supports the suggestion that catechol is possibly less soluble in methyl linoleate, and increasing its amount above the threshold saturation concentration will most likely result in catechol molecule aggregating together in methyl linoleate.

5.4 Conclusion

The potential use of spruce crude bio-oil phenols as antioxidants for protecting biodiesel from autoxidation at elevated temperature has been investigated by examining methyl linoleate autoxidation in 1 bar of oxygen at 120 $^{\circ}$C. Blending small concentrations of crude bio-oil (1.4-5.6% w/w) with methyl linoleate significantly increased the methyl linoleate induction time, with an induction time of ~163 minutes achieved when methyl linoleate was blended with 5.6% (w/w) of crude bio-oil.

In comparison to the commercial antioxidant BHT, crude bio-oil gave approximately comparable induction times to BHT when blended with methyl linoleate at approximately similar molar concentrations of total phenols.

The antioxidancy tests of several isolated extracts (from the crude bio-oil) with methyl linoleate were also conducted. The results revealed that the effect of the isolated extracts were lower than the effect of the crude bio-oil on methyl linoleate autoxidation at approximately equivalent molar phenolic concentrations. However, when comparing these isolated extracts in terms of total weight addition to methyl linoleate, the results showed that the diethyl ether extract addition was much better than the crude bio-oil, especially at the total addition of 2.8% (w/w), which gave almost two times higher induction time (~175 minutes) than the crude bio-oil (~98 minutes).

Further antioxidancy tests were also carried out on three selected phenolic standards: catechol, eugenol and isoeugenol (model of phenolic compounds identified in the crude bio-oil). Remarkably, catechol was found to be very effective, comparable with the crude bio-oil, in hindering methyl linoleate autoxidation cycle at least at low concentrations. However, eugenol and isoeugenol were very much less effective in

methyl linoleate than either catechol or the crude bio-oil when treated at equivalent molar concentrations of phenols. Furthermore, the antioxidant activity of catechol in methyl linoleate at high molar concentrations, higher than *ca.* 40 x 10^{-3} mol dm^{-3}, was found to be progressively decreasing. The most likely explanation for this reduction at higher concentrations is that the initial formed catechol-derived phenoxyl radicals undergo coupling reactions to form a dimer rather than scavenging more free radicals during the autoxidation reaction of methyl linoleate.

Moreover, a mixed phenolic standard (a model of the crude bio-oil phenols) was examined for its antioxidant effect on methyl linoleate. The results indicated that the mixed phenolic standard addition to methyl linoleate increased its induction time, but this increase was not significant in comparison to the crude bio-oil at approximately equivalent molar phenolic concentrations. This suggests that the identified mono-phenolic species in the crude bio-oil could possibly not have a dominant contribution towards the total antioxidant activity of the crude bio-oil in methyl linoleate. Therefore, the source of approximately two-thirds of the crude bio-oil antioxidant power still remains unknown.

In addition, the antioxidancy effect of the mixed phenolic standard was even lower than the effect of catechol alone on methyl linoleate, which was significant because the mixed phenolic standard contained a relatively higher concentration of catechol. This suggests that part of catechol in the mixed phenolic standard is probably acting as a regenerator of the other phenols thus creating an antagonistic effect.

Chapter 6: Conclusions and Future Work

6.1 Concluding Remarks

The development of more powerful and efficient antioxidants for use in biodiesel is a continually ongoing process. This is essentially because of the significant well-known downside of pure biodiesel, which being unstable, and can easily be degraded by autoxidation reactions. To date, most antioxidants investigated for use in biodiesel are synthesized from petroleum, such as butylated hydroxy toluene (BHT). The synthetic antioxidants derived from petroleum are non-renewable and their prices in the marketplace are not stable as a result of the current volatility of petroleum prices. Therefore, the need to find and develop alternative antioxidants that are renewable and can easily be extracted from low-cost reliable resources is essential.

Within the scope of this project, a new potential route for the extraction of renewable antioxidants using microwave technology and their potential application in protecting a model biodiesel (methyl linoleate) from autoxidation have been demonstrated and discussed in depth. The pyrolysis of spruce woodchips using microwave heating under vacuum successfully converted the spruce woodchips into liquids (crude bio-oil and aqueous fraction), char and gas within ~10 minutes and without any pretreatments. The further study of the pyrolysis products by multiple analytical techniques indicated that the obtained crude bio-oil (18.5% w/w of the woodchips) has complex chemical feature and has the potential to be a good source of many value-added chemicals. The water and ash contents in the crude bio-oil were very low, at approximately below 5 and 0.1% (w/w), respectively. The characterization by ATR-IR, ^{13}C NMR and GC-MS indicated that the crude bio-oil contains aromatic compounds (mostly furans & phenols) and carbohydrate sugars.

The spruce crude bio-oil holds great potential to be used as a source of renewable antioxidants, in particular the phenolic-type antioxidants. The phenolic content within the crude bio-oil's complex chemical nature was high as evidenced by GC-MS, GC-FID and Folin-Ciocalteu (FC) assay. The phenolic content was estimated to be *ca.* 6 and 23% (w/w) *via* GC and FC assay, respectively. The separation of the relatively high phenolic content from the crude bio-oil was conducted by means of laboratory accessible techniques, most extensively by the liquid-liquid extraction method. Two multi-solvent fractionation procedures were chosen to help with the

phenolic separation, and named as water-insoluble and water-soluble phase fractionation procedures. The main investigated extracts from the water-insoluble phase fractionation procedure were water-soluble, neutral, phenolic and organic acids extracts, while the main investigated extracts from the water-soluble phase fractionation procedure were diethyl ether, DCM and water-soluble residue extracts.

The phenolic and the diethyl ether extracts from the two fractionation procedures were relatively the highest in the phenolic content as evidenced by GC-FID (and GC-MS), respectively at 17.4 and 8.5% (w/w), and by FC assay, respectively at 49.6 and 55.7% (w/w). The greater contents of phenolic species detected using the FC assay, in comparison with GC-FID, are consistent with the presence of phenolic species with high molecular weights (> 350 Da). These heavier phenolic species are too large to be detectable by GC due to the large phenolics being involatile at the maximum operating temperature of the GC column, but can still be detectable by the FC method.

In principle, the phenols within the crude bio-oil would be expected to behave like typical commercial phenolic antioxidants, where the initial mechanism of action by the phenol is the donation of hydrogen to a free radical formed during autoxidation reactions. Thus, the potential application of spruce crude bio-oil's phenols as an antioxidant for inhibiting the biodiesel's deterioration *via* autoxidation at elevated temperature has been investigated by examining a model biodiesel (methyl linoleate) autoxidation in 1 bar of oxygen at 120 $^{\circ}$C. Blending small concentrations of crude bio-oil with methyl linoleate significantly increased its induction time, with an induction time of ~163 minutes being achieved when the methyl linoleate was blended with 5.6% (w/w) of crude bio-oil. In comparison with a commercial antioxidant, the crude bio-oil's antioxidancy effect on methyl linoleate was approximately comparable with BHT at approximately similar molar phenolic concentrations that were measured *via* the FC method.

Further antioxidancy tests of the methyl linoleate with the addition of several isolated extracts from the crude bio-oil were also conducted. From the comparison of the extract's total molar phenolic concentrations addition to the methyl linoleate with their determined induction times, the results indicated that the antioxidancy effect of

the isolated extracts on methyl linoleate accelerated autoxidation were lower than the effect of their parent the crude bio-oil. This was striking because some of the isolated extracts contained higher molar phenolic concentration than the crude bio-oil. The possible explanation for the better antioxidancy effect of the crude bio-oil over its isolated extracts with higher phenolic content is that the crude bio-oil contains phenolic species that differ in their antioxidant power, and the absence of these stronger antioxidant species in the isolated extracts, especially in those extracts with higher phenolic content than the crude bio-oil, causes a reduction of the methyl linoleate induction time in comparison with the crude bio-oil at approximately similar molar phenolic concentrations. This suggestion was further evidenced by examining individually the methyl linoleate autoxidation with three phenolic standards identified in the crude bio-oil, catechol, eugenol and isoeugenol. The antioxidancy effect of catechol, at low concentrations, on methyl linoleate autoxidation was found to be very strong and comparable with the crude bio-oil. However, eugenol and isoeugenol were much less effective than either catechol or the crude bio-oil when compared at equivalent molar phenolic concentrations.

Additionally, catechol showed reducing effectiveness when higher concentrations, higher than *ca.* 40×10^{-3} mol/dm^3, being added to methyl linoleate. Therefore, three hypotheses were suggested to try to explain this reduction of catechol antioxidancy at higher concentrations. The first was that the initial formed catechol-derived phenoxyl radicals undergo coupling reactions to form a dimer rather than scavenging more free radicals during the autoxidation reaction of methyl linoleate. The second was due to the formation of less soluble oxidation products of catechol in the reaction medium. However, the third was related to the effect of polarity of the medium on catechol efficiency, as increasing the catechol concentration will give a corresponding (relatively small) increase in polarity of the reaction medium.

A mixed phenolic standard (a chemical model of the crude bio-oil's phenols) was also examined for its antioxidancy effect on methyl linoleate autoxidation. The effect of the mixed phenolic standard, in comparison with the crude bio-oil at approximately equivalent molar phenolic concentrations, was not as effective as the crude bio-oil in hindering the methyl linoleate autoxidation. This suggests that the identified mono-phenolic species in the crude bio-oil could possibly not have a

dominant contribution towards the overall antioxidant activity of the crude bio-oil in methyl linoleate, and thus, the source of approximately two-thirds of the crude bio-oil's antioxidant power remains undiscovered.

Moreover, the effect of the mixed phenolic standard on methyl linoleate autoxidation was even lower than catechol. This was striking because the mixed standard contained a relatively high concentration of catechol. Therefore, the reduction of catechol antioxidant activity in the presence of other phenols could suggest that some of the catechol is possibly acting as a regenerator of the other less effective phenols thus creating an antagonistic effect, in the model phenolic standard.

6.2 Future Work on Biomass Pyrolysis

As the work described in this thesis is mainly based on crude bio-oils derived from one biomass feedstock (spruce woodchips), one useful and interesting future study would be to investigate bio-oils from a range of biomass feedstocks. Such a study would allow general comparison between the spruce-derived bio-oil and the other types of bio-oils. The results of this comparison could further help with the direction of future studies.

It would also be highly beneficial to investigate the production of bio-oil from spruce woodchips by conventional pyrolysis methods. This work would add useful information about the quality of conventionally produced bio-oils in comparison with crude bio-oils produced *via* microwave technology. Moreover, having demonstrated the potential of microwave pyrolysis oil, closer monitoring of variable such as moisture content of the woodchips would be valuable to optimise oil composition. This is partly due to the moisture of the woodchips being a microwave absorber, but also maybe as a hydrolytic reagent that might help break up the biomass.

6.3 Future Work on Antioxidant Testing and Antioxidants

The crude bio-oil phenolic compounds appeared to behave approximately the same as a commercial antioxidant (BHT) in stabilizing a significant biodiesel component (methyl linoleate) at 120 $^{\circ}$C and 1 bar of oxygen. Another beneficial future study therefore would be to study the antioxidancy of the crude bio-oil with a commercial

biodiesel to test whether it would show similar results to the ones carried out by methyl linoleate, and further, to test the validity of using methyl linoleate alone to represent an actual biodiesel.

In Chapter 4 (section 4.4), supercritical CO_2 extraction of bio-oil was performed and produced four extracts, each having different concentration of phenols. Therefore, another part of potential future work could be to examine the antioxidancy of these supercritical CO_2 extracts in methyl linoleate. Such a study would help to evaluate the extraction quality of supercritical CO_2 by determining which of the four extracts is more efficient in stabilizing methyl linoleate during autoxidation test, and more importantly to study the effect of their phenolic content on the induction time of methyl linoleate.

The addition of catechol in methyl linoleate at high concentrations, above 40 x 10^{-3} mol/dm^3, has been shown to reduce its overall antioxidative efficacy. Thus, it is mechanistically interesting to further investigate the cause of this uncommon behavior of an antioxidant. To try to understand this antioxidative behavior of catechol at higher concentrations, three hypotheses have been suggested here. The first was that catechol-derived phenoxyl radicals prefer to undergo coupling reactions to form a dimer rather than trapping a second free radical, due to the phenoxyl being at higher concentration. The second was associated with the formation of less soluble catechol-derived oligomers in the reaction medium, and the third was related to the effect of polarity of the medium on catechol efficiency, as increasing catechol concentration will give a corresponding (relatively small) increase in polarity of the reaction medium. However, to support these hypotheses, it would be interesting to characterize the autoxidation reaction of catechol products probably *via* liquid chromatograph coupled with a mass spectrometer (LC-MS). A completed study would help to not only understand the most likely cause of catechol antioxidancy reduction at higher concentrations during methyl linoleate autoxidation, but also to further the knowledge of antioxidant mechanisms of *ortho*-diphenols in general.

Appendix A: Mass Spectra

A.1 Mass Spectra of Major Identified Compounds in Pyrolysis Liquids

A.1.1 Mass spectra of major identified compounds in crude bio-oil

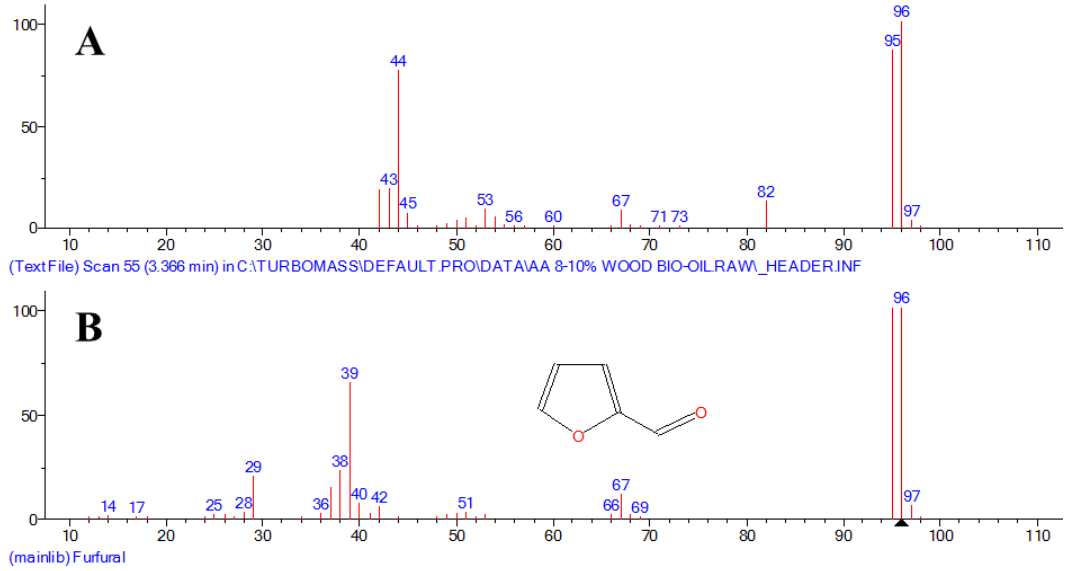

Figure A.1: Matching mass spectrum of peak number 1 in crude bio-oil GC-MS: A) MS of peak number 1 in crude bio-oil sample; B) MS of furfural according to NIST library database.

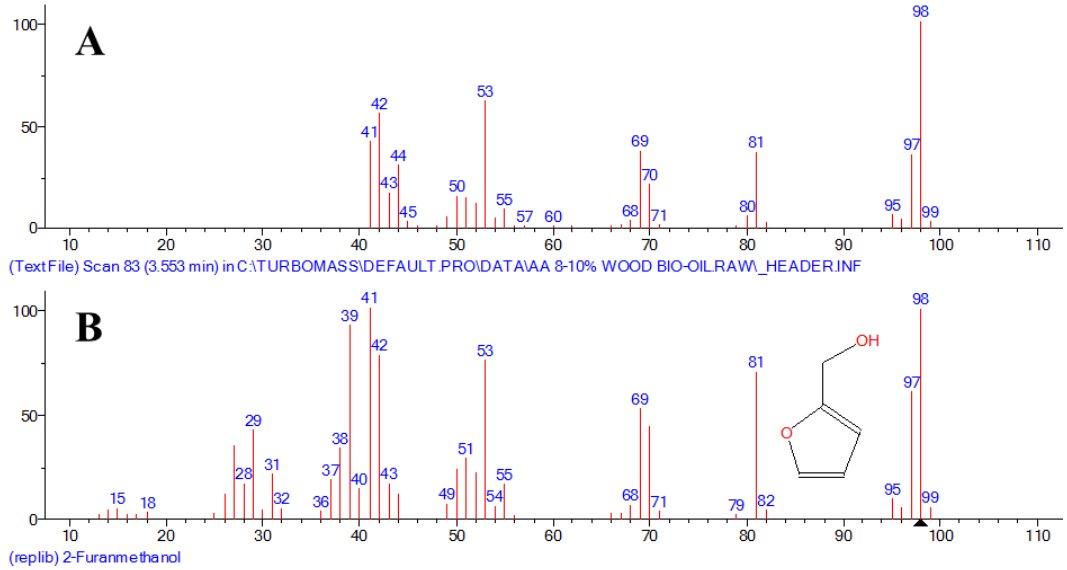

Figure A.2: Matching mass spectrum of peak number 2 in crude bio-oil GC-MS: A) MS of peak number 2 in crude bio-oil sample; B) MS of 2-furanmethanol according to NIST library database.

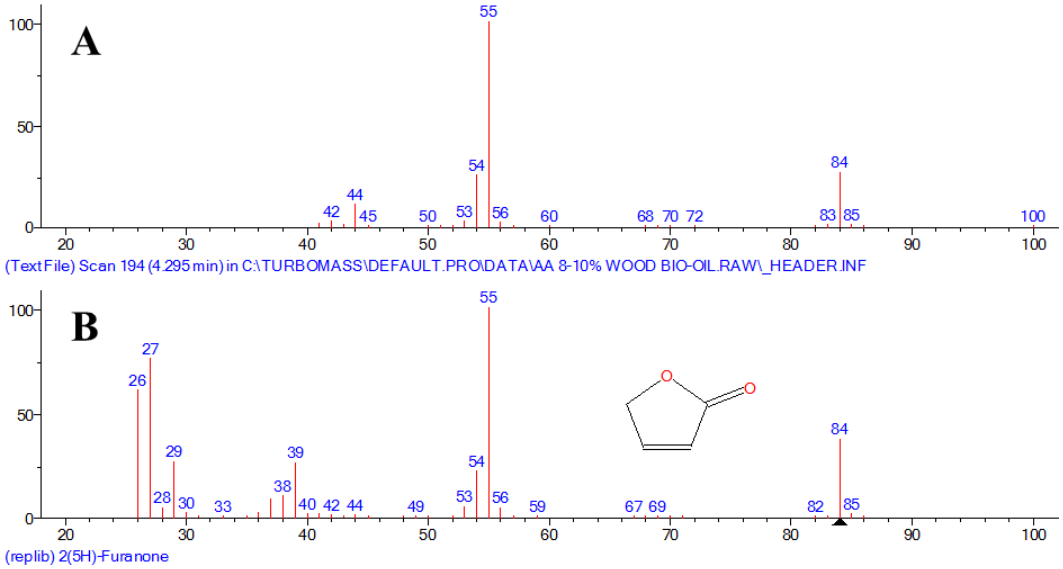

Figure A.3: Matching mass spectrum of peak number 3 in crude bio-oil GC-MS: A) MS of peak number 3 in crude bio-oil sample; B) MS of 2(5H)-furanone according to NIST library database.

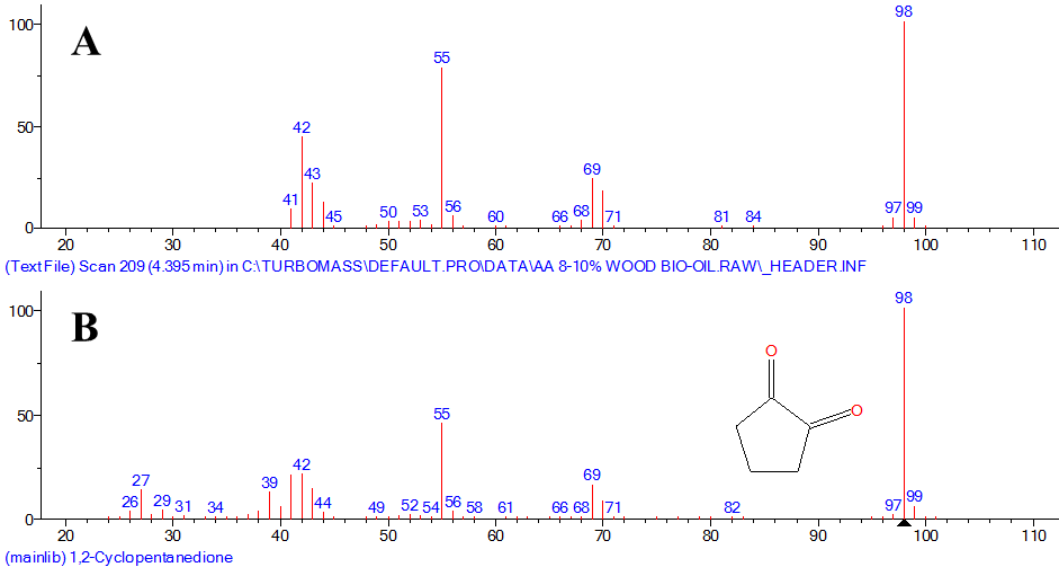

Figure A.4: Matching mass spectrum of peak number 4 in crude bio-oil GC-MS: A) MS of peak number 4 in crude bio-oil sample; B) MS of 1,2-cyclopentanedione according to NIST library database.

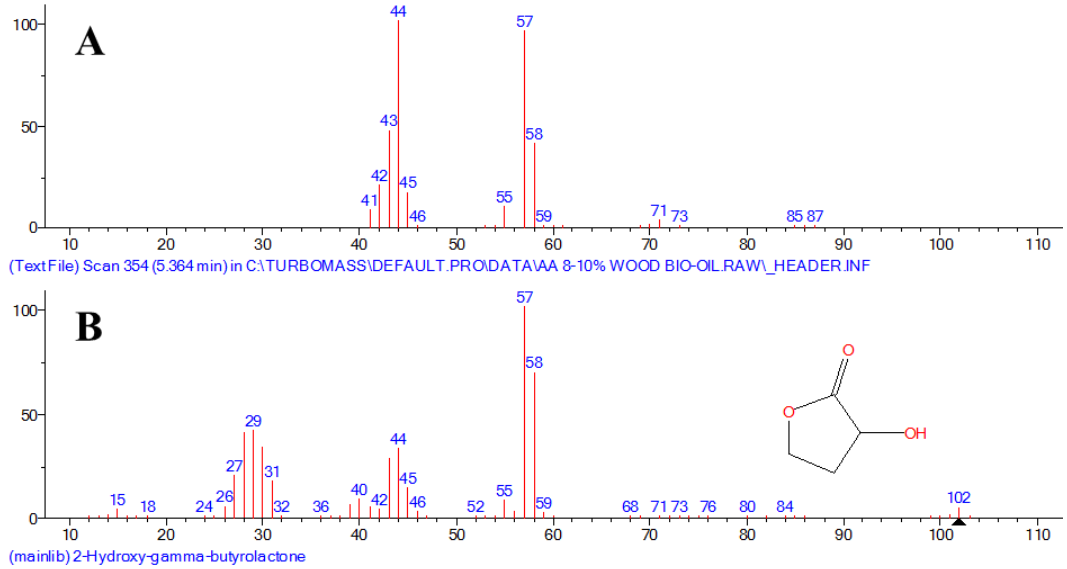

Figure A.5: Matching mass spectrum of peak number 5 in crude bio-oil GC-MS: A) MS of peak number 5 in crude bio-oil sample; B) MS of 2-hydroxy-gamma-butyrolactone according to NIST library database.

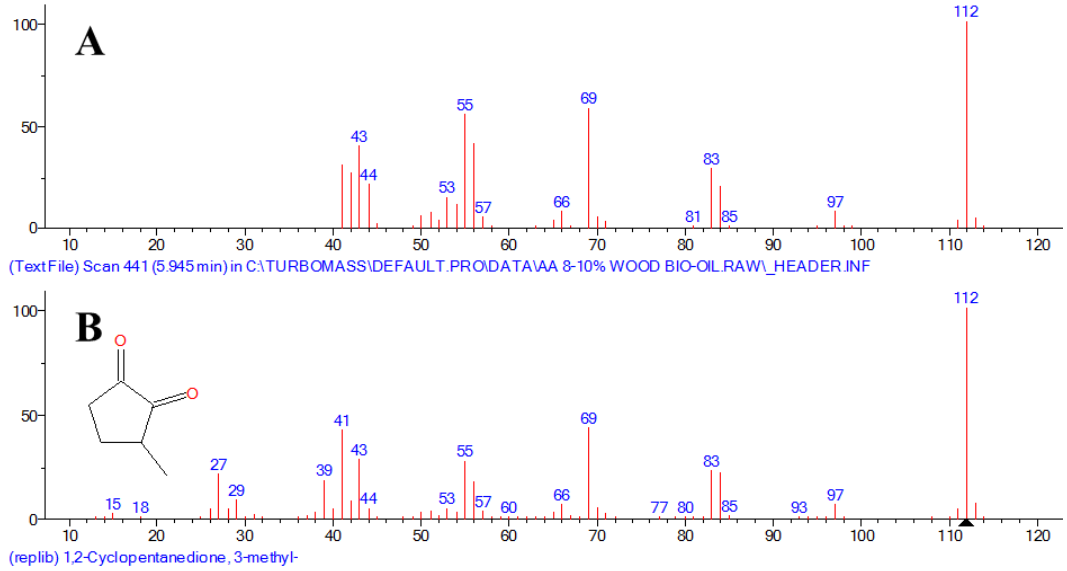

Figure A.6: Matching mass spectrum of peak number 6 in crude bio-oil GC-MS: A) MS of peak number 6 in crude bio-oil sample; B) MS of 1,2-cyclopentanedione, 3-methyl- according to NIST library database.

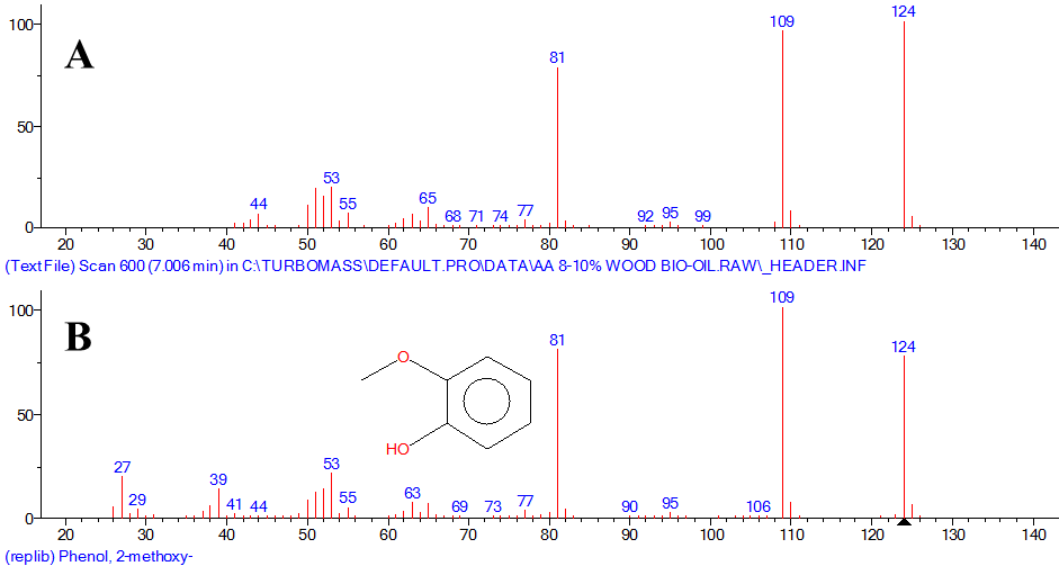

Figure A.7: Matching mass spectrum of peak number 7 in crude bio-oil GC-MS: A) MS of peak number 7 in crude bio-oil sample; B) MS of phenol, 2-methoxy- according to NIST library database.

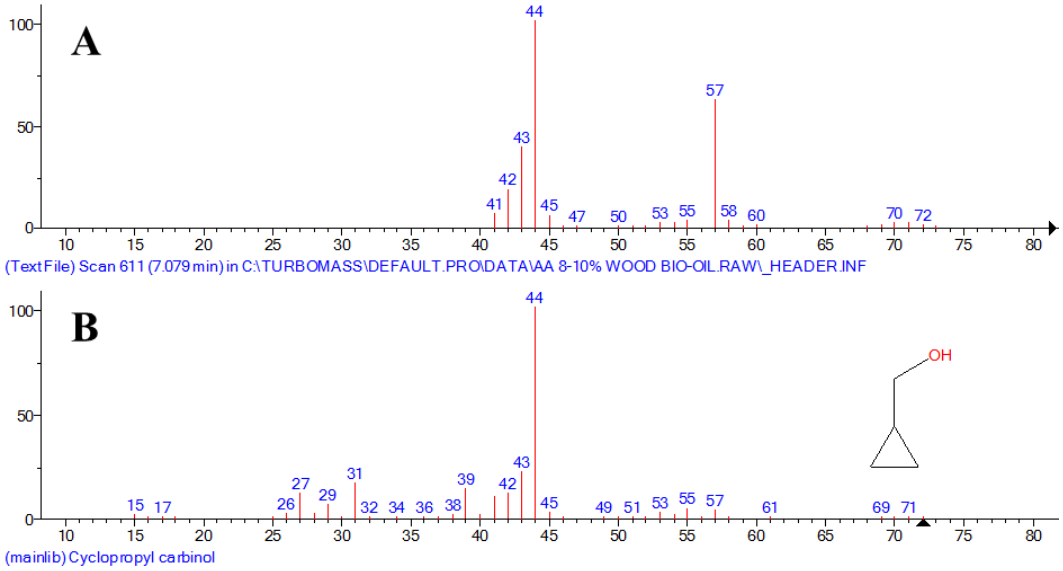

Figure A.8: Matching mass spectrum of peak number 8 in crude bio-oil GC-MS: A) MS of peak number 8 in crude bio-oil sample; B) MS of cyclopropyl carbinol according to NIST library database.

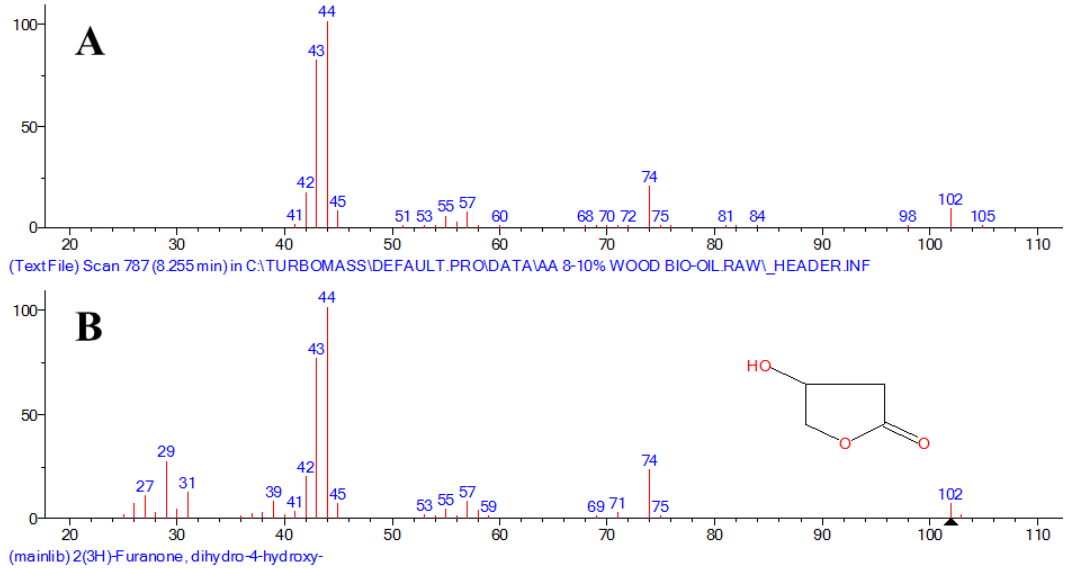

Figure A.9: Matching mass spectrum of peak number 9 in crude bio-oil GC-MS: A) MS of peak number 9 in crude bio-oil sample; B) MS of 2(3H)-furanone, dihydro-4-hydroxy- according to NIST library database.

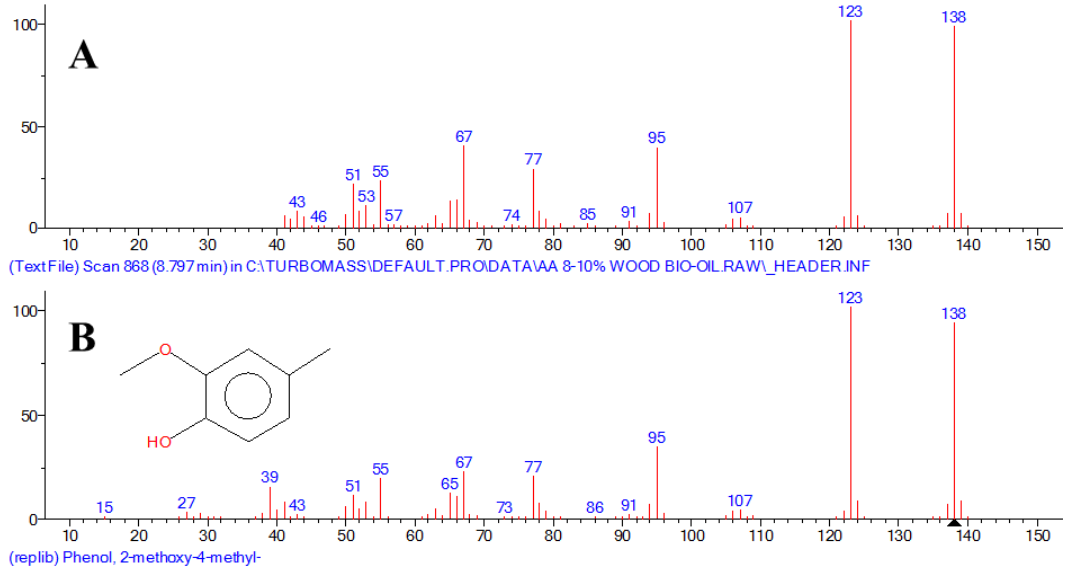

Figure A.10: Matching mass spectrum of peak number 10 in crude bio-oil GC-MS: A) MS of peak number 10 in crude bio-oil sample; B) MS of phenol, 2-methoxy-4-methyl- according to NIST library database.

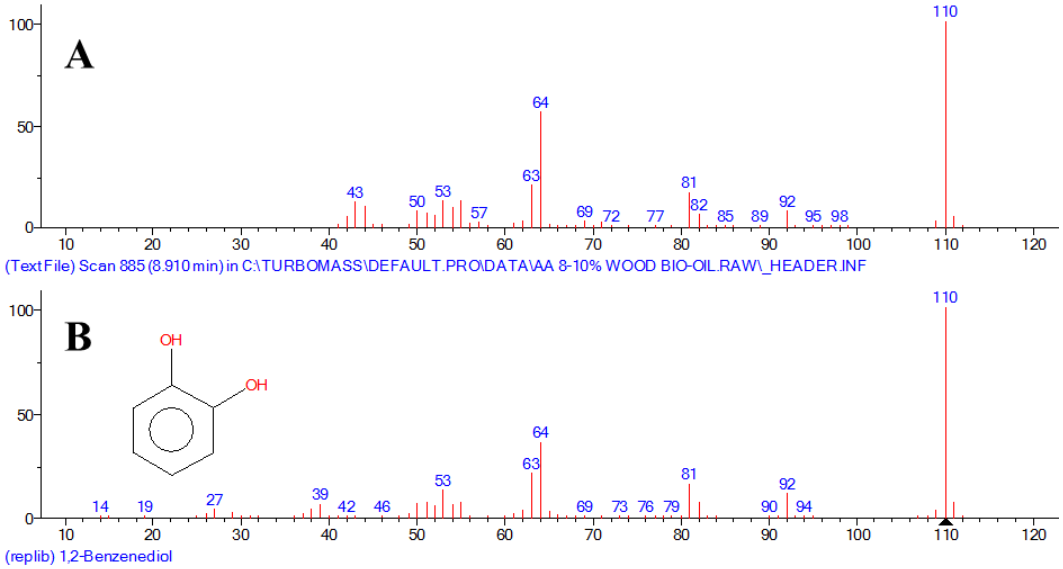

Figure A.11: Matching mass spectrum of peak number 11 in crude bio-oil GC-MS: A) MS of peak number 11 in crude bio-oil sample; B) MS of 1,2-benzenediol according to NIST library database.

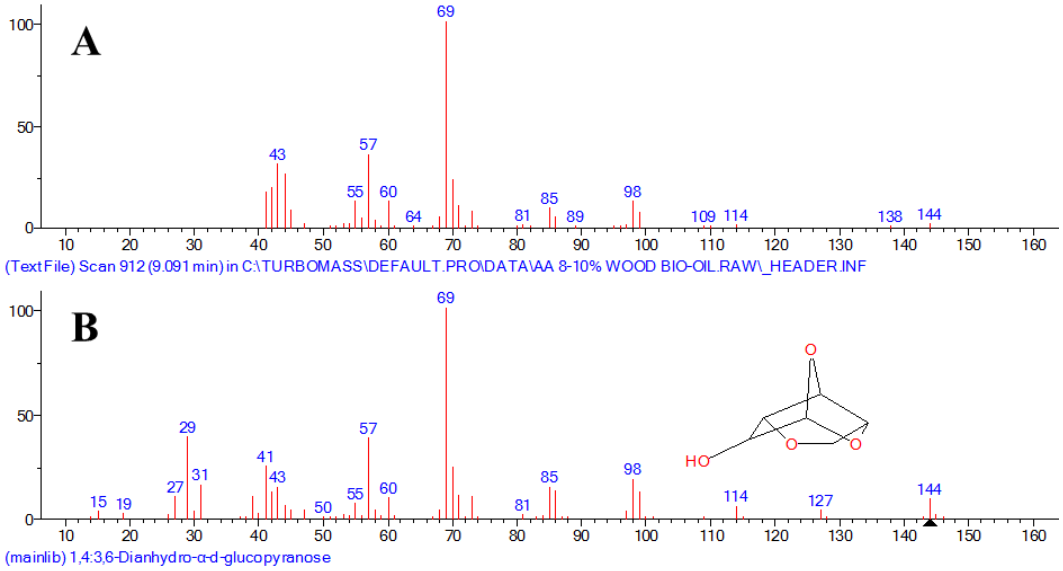

Figure A.12: Matching mass spectrum of peak number 12 in crude bio-oil GC-MS: A) MS of peak number 12 in crude bio-oil sample; B) MS of 1,4:3,6-dianhydro-α-d-glucopyranose according to NIST library database.

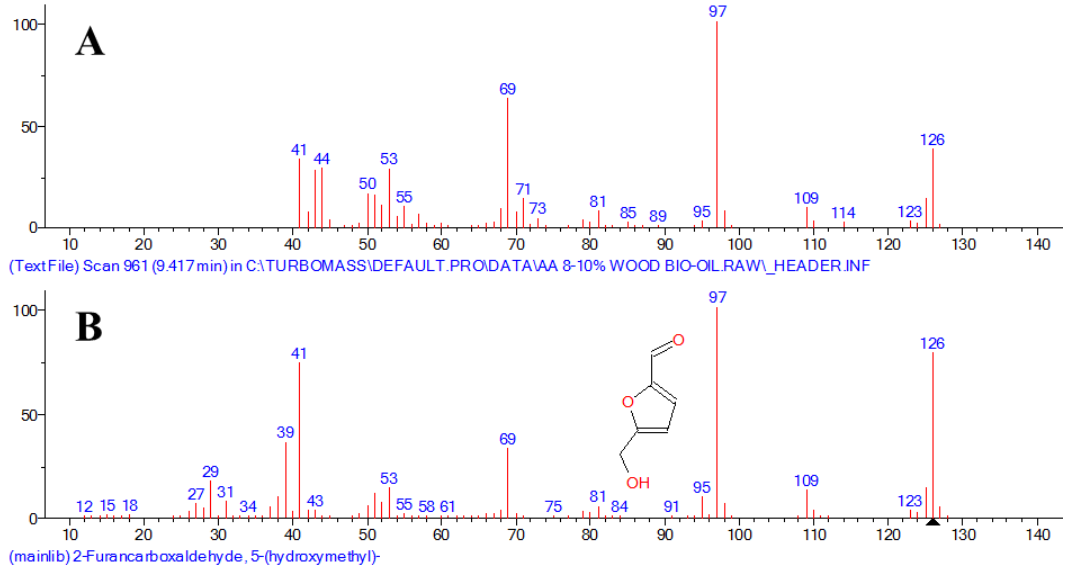

Figure A.13: Matching mass spectrum of peak number 13 in crude bio-oil GC-MS: A) MS of peak number 13 in crude bio-oil sample; B) MS of 2-furancarboxaldehyde, 5-(hydroxymethyl)- according to NIST library database.

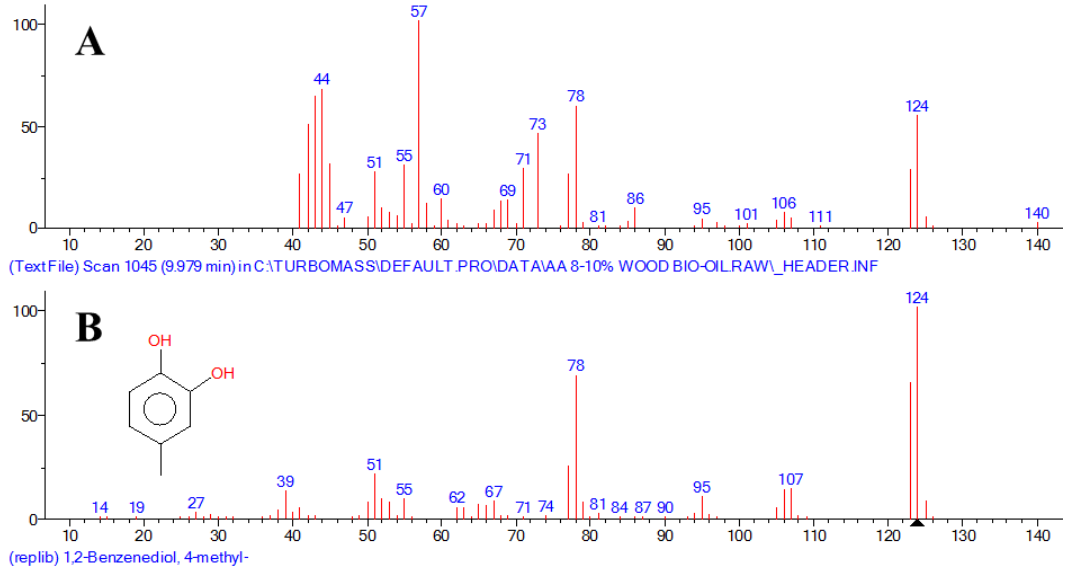

Figure A.14: Matching mass spectrum of peak number 14 in crude bio-oil GC-MS: A) MS of peak number 14 in crude bio-oil sample; B) MS of 1,2-benzenediol, 4-methyl- according to NIST library database.

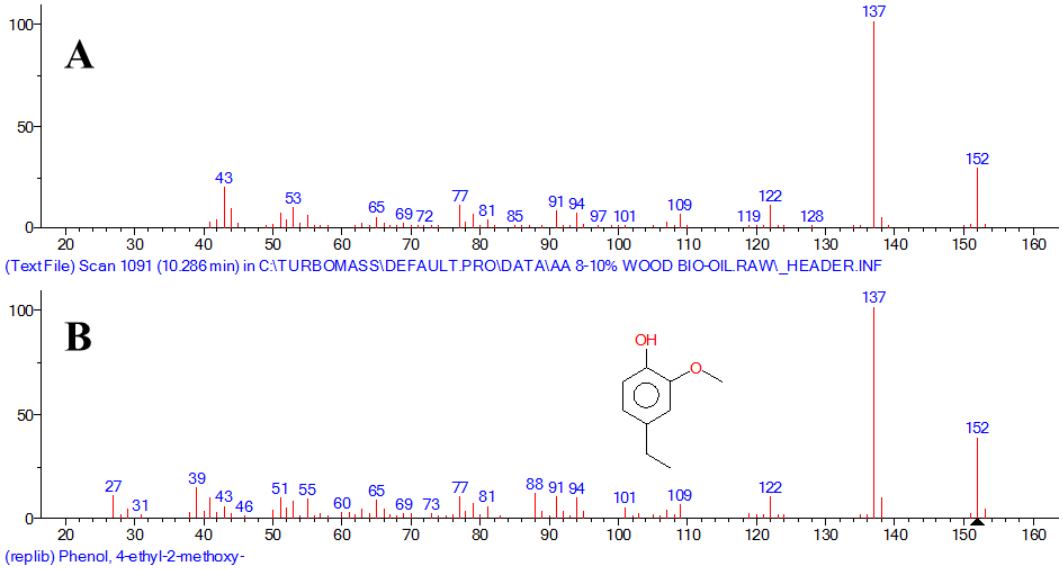

Figure A.15: Matching mass spectrum of peak number 15 in crude bio-oil GC-MS: A) MS of peak number 15 in crude bio-oil sample; B) MS of phenol, 4-ethyl-2-methoxy- according to NIST library database.

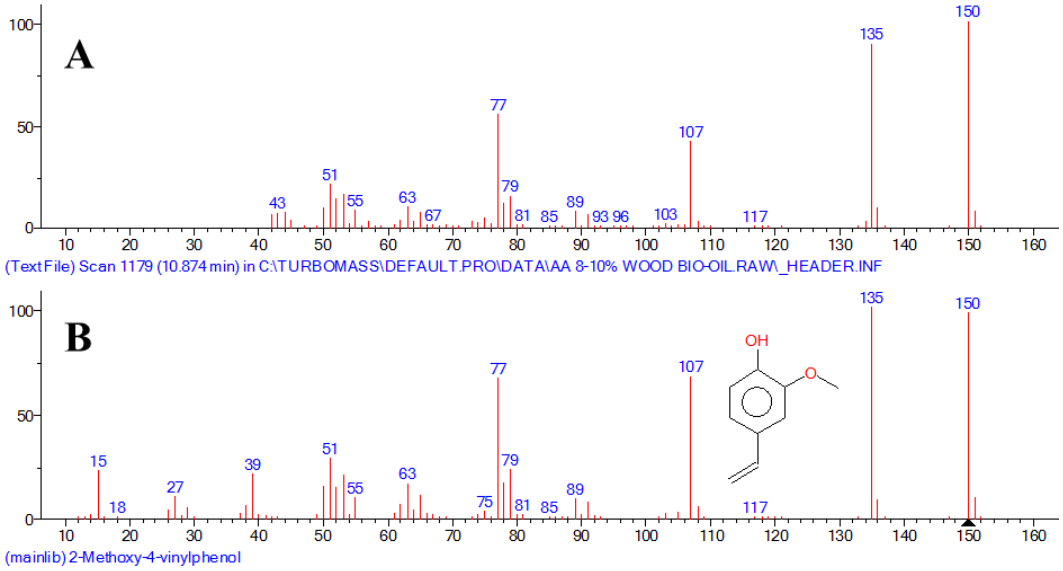

Figure A.16: Matching mass spectrum of peak number 16 in crude bio-oil GC-MS: A) MS of peak number 16 in crude bio-oil sample; B) MS of 2-methoxy-4-vinylphenol according to NIST library database.

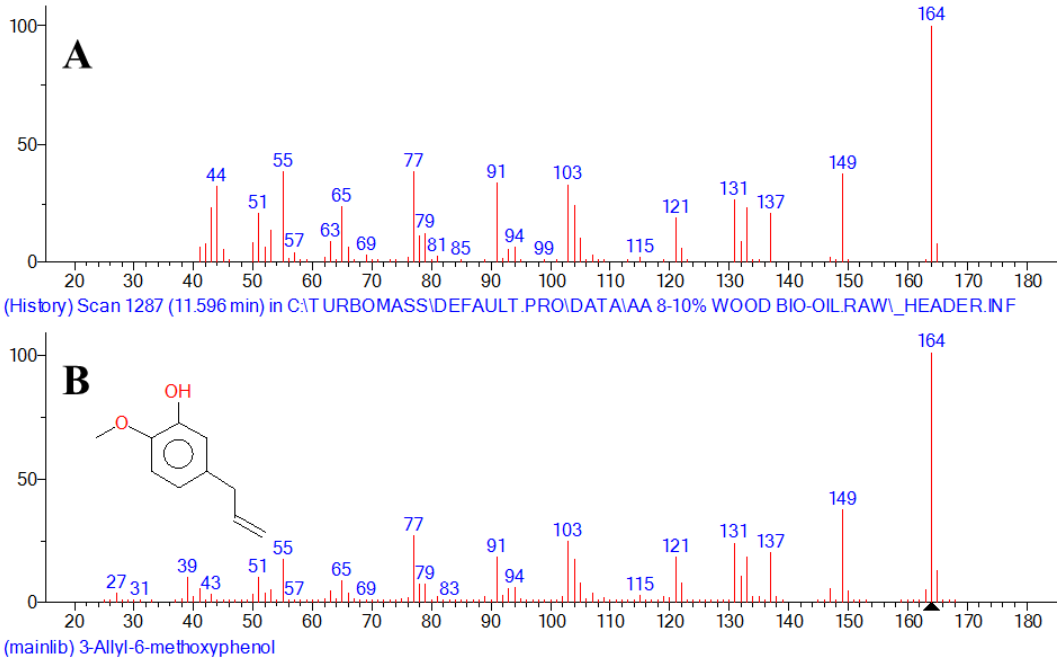

Figure A.17: Matching mass spectrum of peak number 17 in crude bio-oil GC-MS: A) MS of peak number 17 in crude bio-oil sample; B) MS of 3-allyl-6-methoxyphenol according to NIST library database.

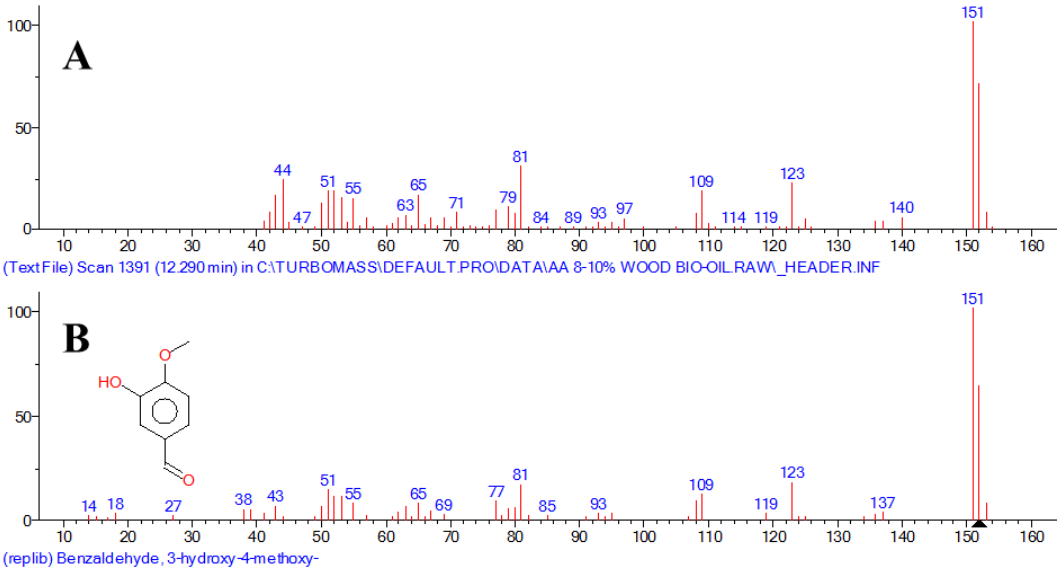

Figure A.18: Matching mass spectrum of peak number 18 in crude bio-oil GC-MS: A) MS of peak number 18 in crude bio-oil sample; B) MS of benzaldehyde, 3-hydroxy-4-methoxy- according to NIST library database.

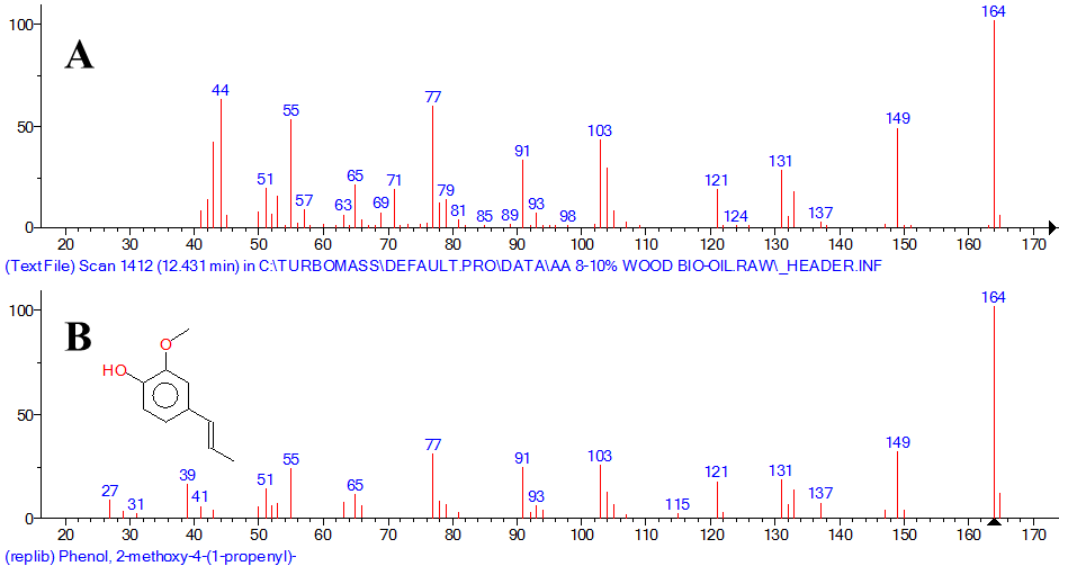

Figure A.19: Matching mass spectrum of peak number 19 in crude bio-oil GC-MS: A) MS of peak number 19 in crude bio-oil sample; B) MS of phenol, 2-methoxy-4-(1-propenyl)- according to NIST library database.

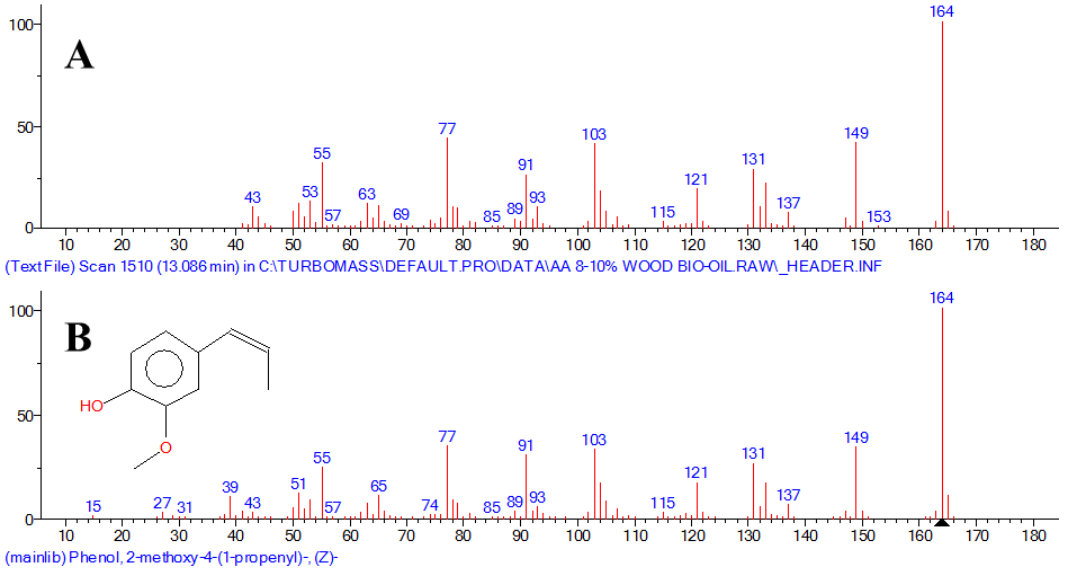

Figure A.20: Matching mass spectrum of peak number 20 in crude bio-oil GC-MS: A) MS of peak number 20 in crude bio-oil sample; B) MS of phenol, 2-methoxy-4-(1-propenyl)-, (Z)- according to NIST library database.

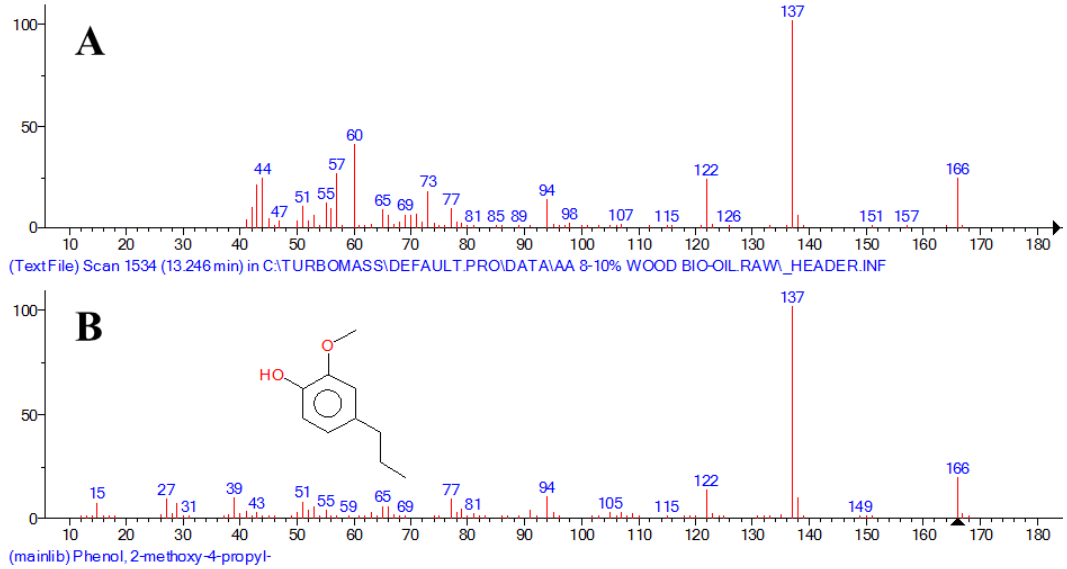

Figure A.21: Matching mass spectrum of peak number 21 in crude bio-oil GC-MS: A) MS of peak number 21 in crude bio-oil sample; B) MS of phenol, 2-methoxy-4-propyl- according to NIST library database.

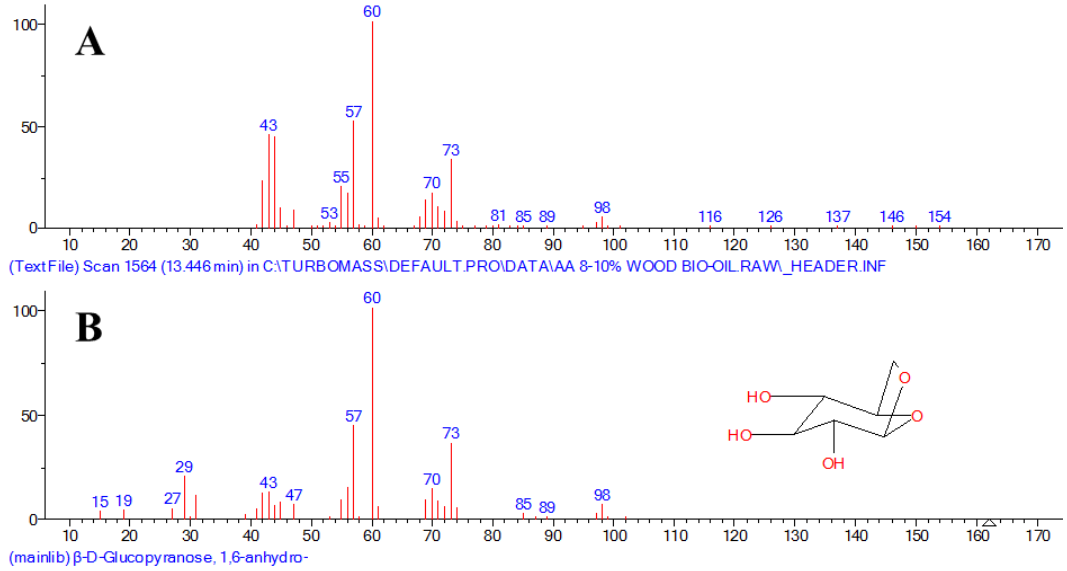

Figure A.22: Matching mass spectrum of peak number 22 in crude bio-oil GC-MS: A) MS of peak number 22 in crude bio-oil sample; B) MS of β-D-glucopyranose, 1,6-anhydro- according to NIST library database.

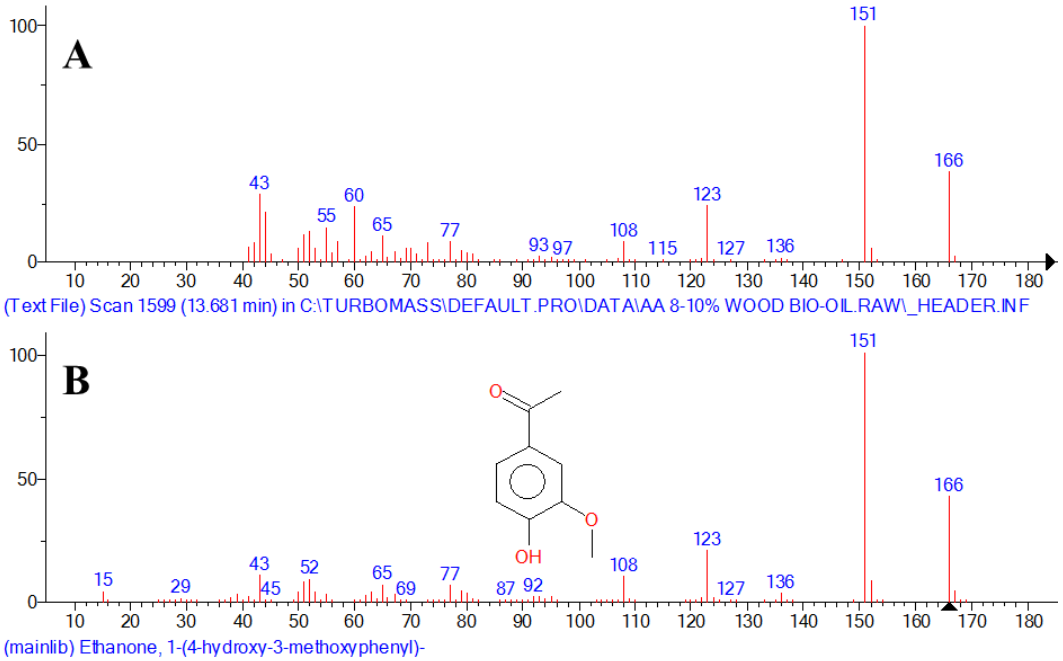

Figure A.23: Matching mass spectrum of peak number 23 in crude bio-oil GC-MS: A) MS of peak number 23 in crude bio-oil sample; B) MS of ethanone, 1-(4-hydroxy-3-methoxyphenyl)- according to NIST library database.

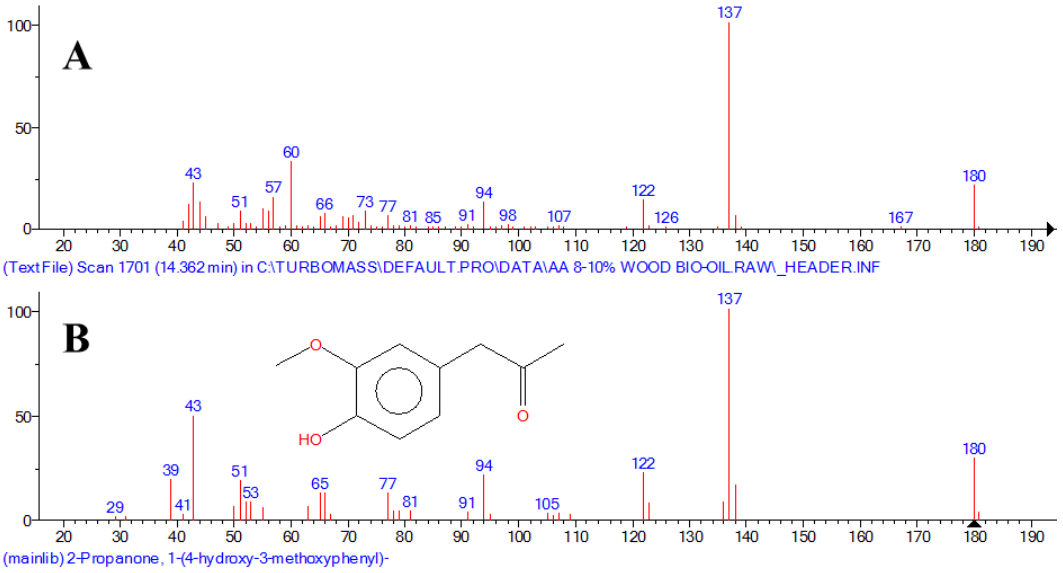

Figure A.24: Matching mass spectrum of peak number 24 in crude bio-oil GC-MS: A) MS of peak number 24 in crude bio-oil sample; B) MS of 2-propanone, 1-(4-hydroxy-3-methoxyphenyl)- according to NIST library database.

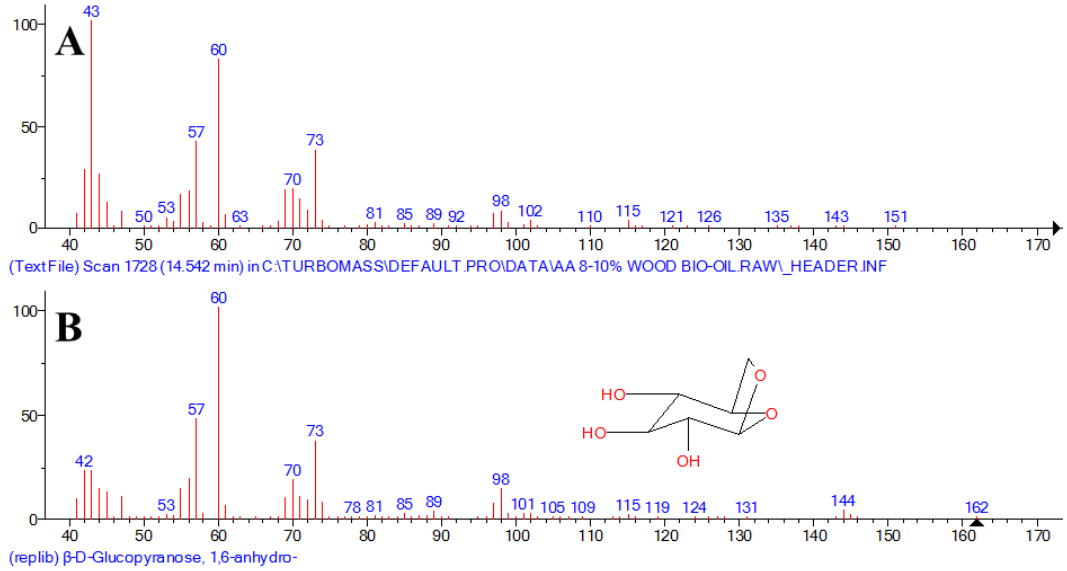

Figure A.25: Matching mass spectrum of peak number 25 in crude bio-oil GC-MS: A) MS of peak number 25 in crude bio-oil sample; B) MS of β-D-glucopyranose, 1,6-anhydro- according to NIST library database.

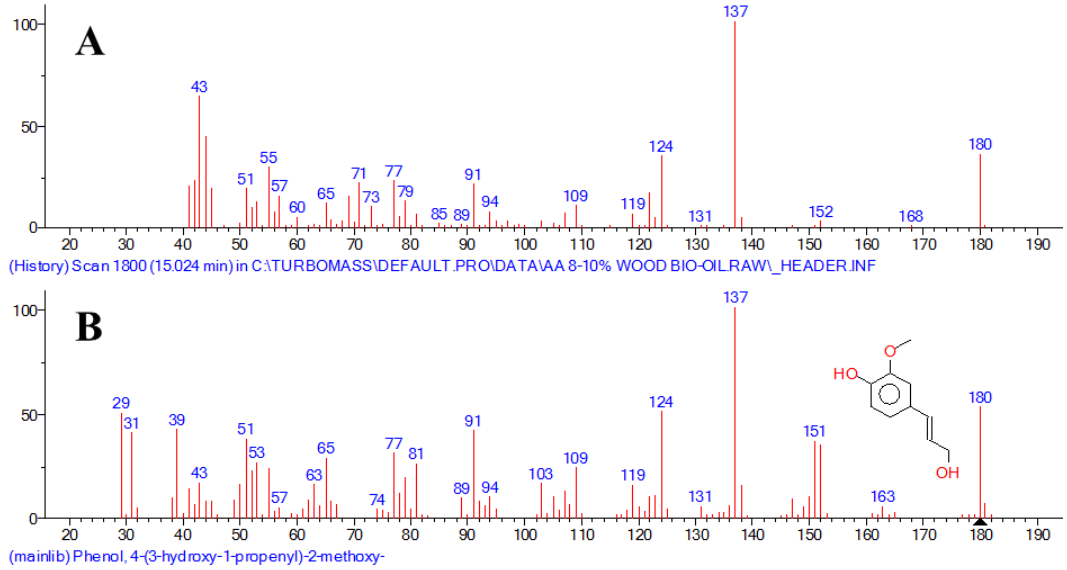

Figure A.26: Matching mass spectrum of peak number 26 in crude bio-oil GC-MS: A) MS of peak number 26 in crude bio-oil sample; B) MS of phenol, 4-(3-hydroxy-1-propenyl)-2-methoxy- according to NIST library database.

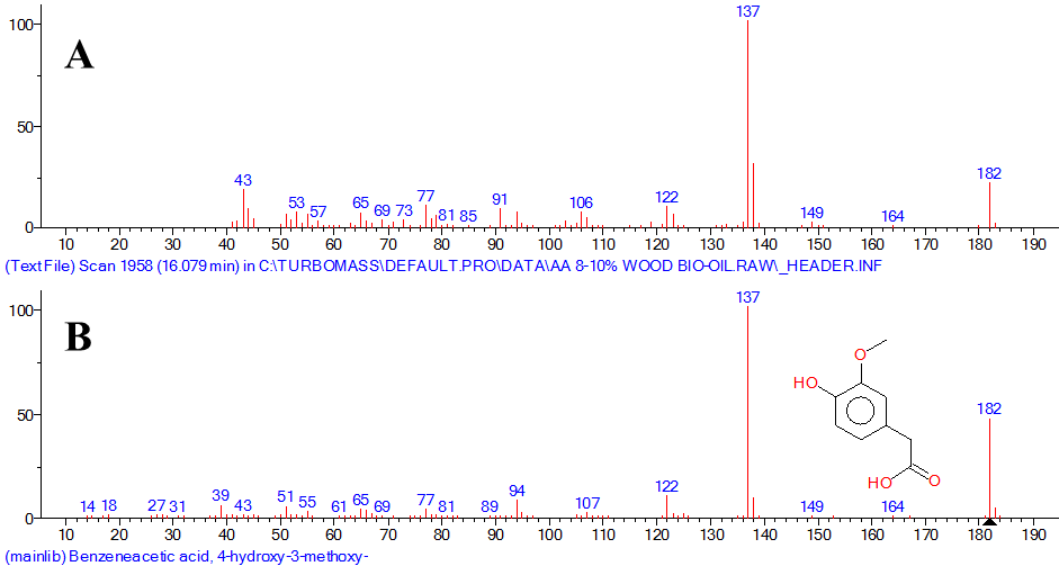

Figure A.27: Matching mass spectrum of peak number 27 in crude bio-oil GC-MS: A) MS of peak number 27 in crude bio-oil sample; B) MS of benzeneacetic acid, 4-hydroxy-3-methoxy- according to NIST library database.

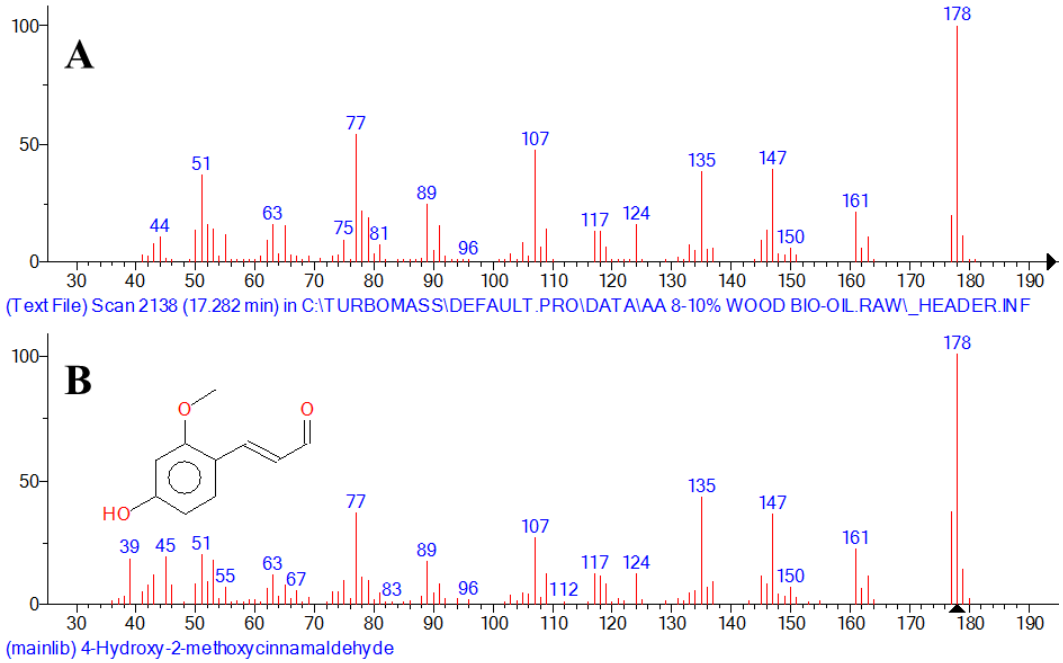

Figure A.28: Matching mass spectrum of peak number 28 in crude bio-oil GC-MS: A) MS of peak number 28 in crude bio-oil sample; B) MS of 4-hydroxy-2-methoxycinnamaldehyde according to NIST library database.

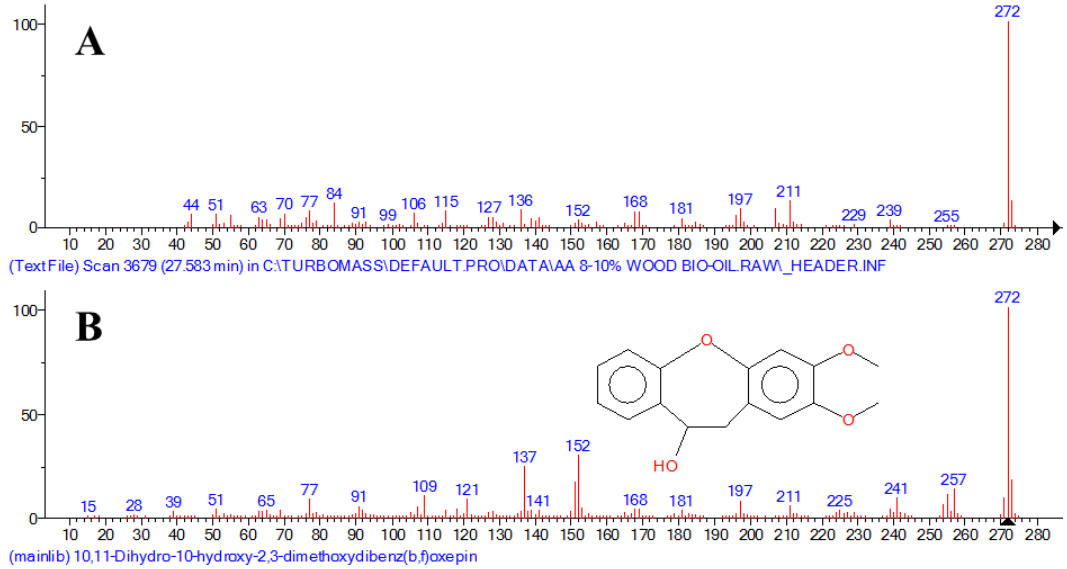

Figure A.29: Matching mass spectrum of peak number 29 in crude bio-oil GC-MS: A) MS of peak number 29 in crude bio-oil sample; B) MS of 10,11-dihydro-10-hydroxy-2,3-dimethoxydibenz(b,f)oxepin according to NIST library database.

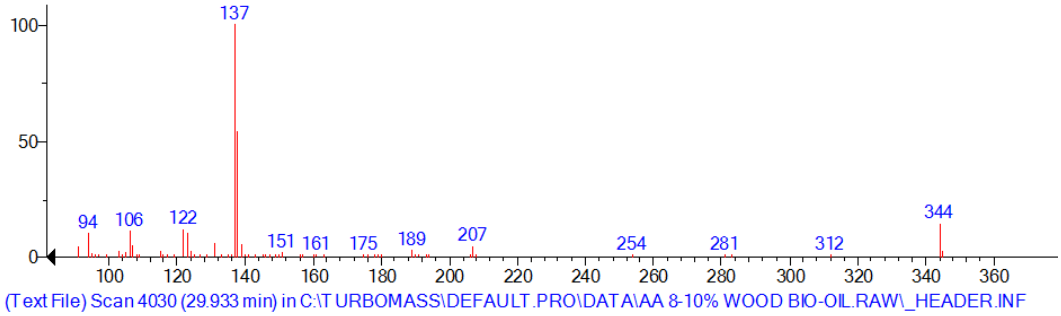

Figure A.30: Unidentified MS of peak 30 in crude bio-oil sample.

A.1.2 Mass spectra of major identified compounds in aqueous fraction

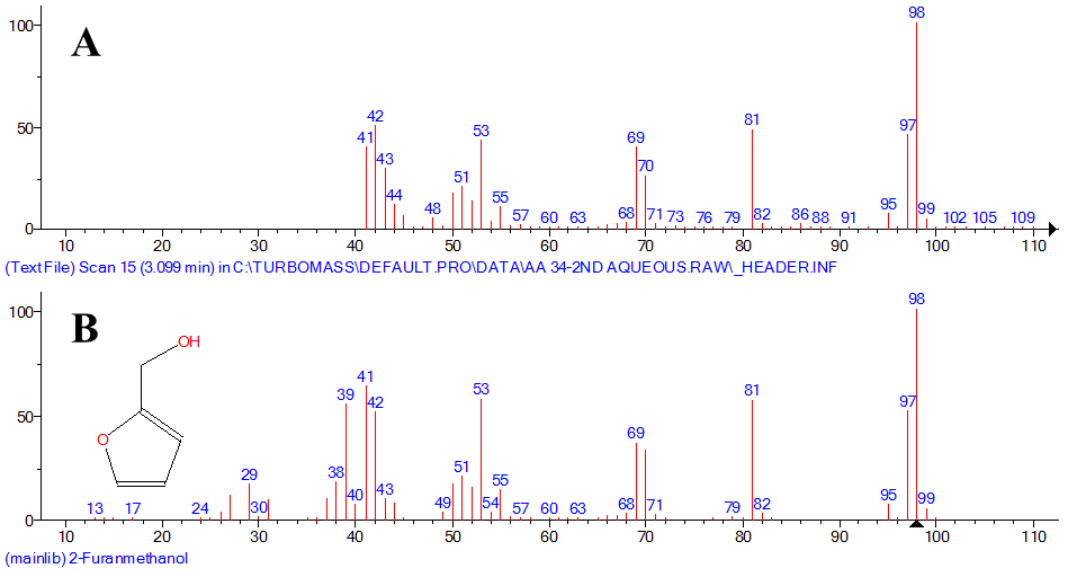

Figure A.31: Matching mass spectrum of peak number 1 in aqueous fraction GC-MS: A) MS of peak number 1 in aqueous fraction sample; B) MS of 2-furanmethanol according to NIST library database.

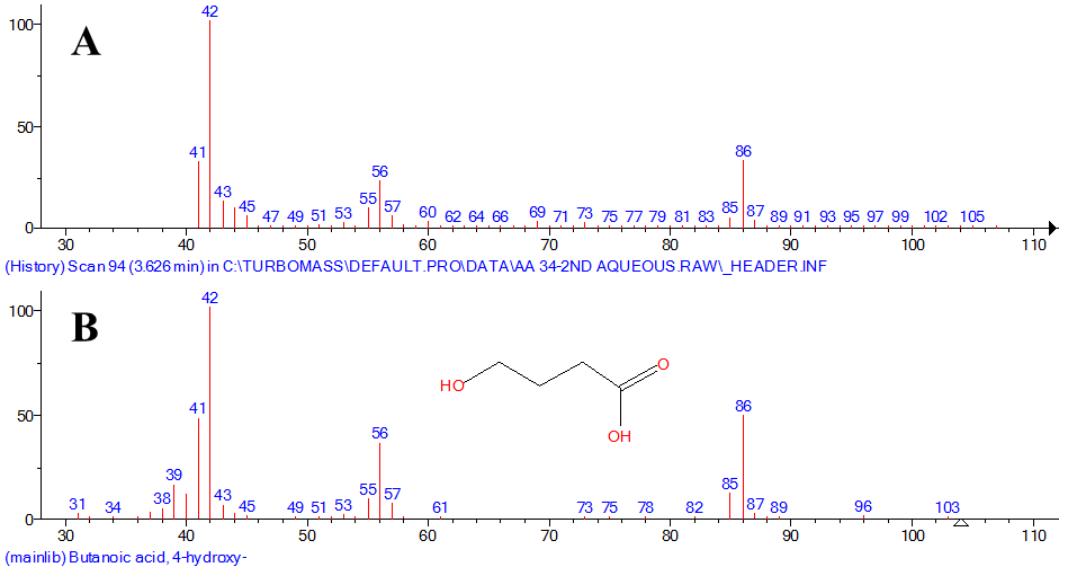

Figure A.32: Matching mass spectrum of peak number 2 in aqueous fraction GC-MS: A) MS of peak number 2 in aqueous fraction sample; B) MS of butanoic acid, 4-hydroxy- according to NIST library database.

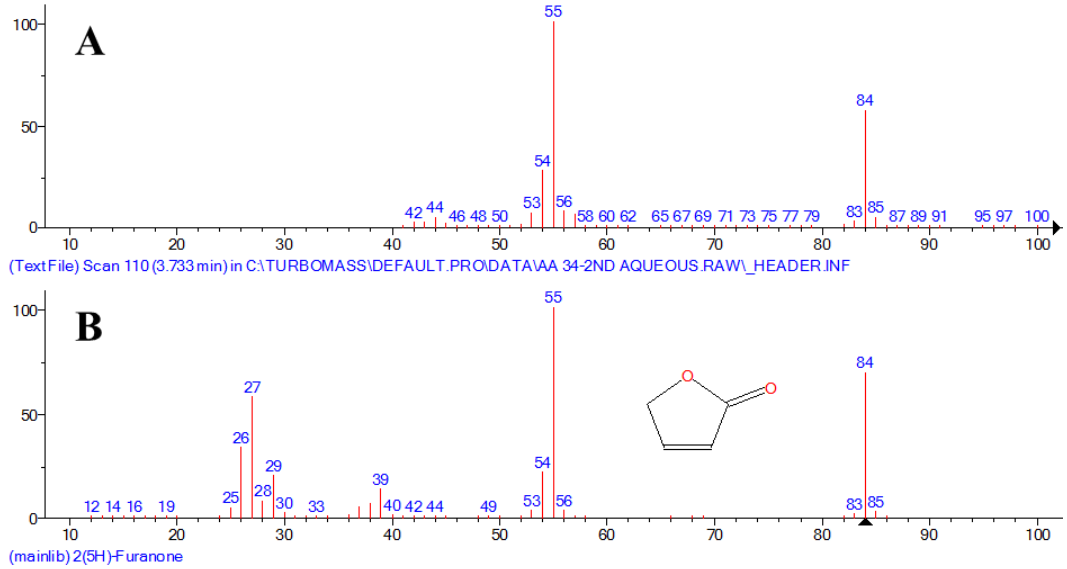

Figure A.33: Matching mass spectrum of peak number 3 in aqueous fraction GC-MS: A) MS of peak number 3 in aqueous fraction sample; B) MS of 2(5H)-furanone according to NIST library database.

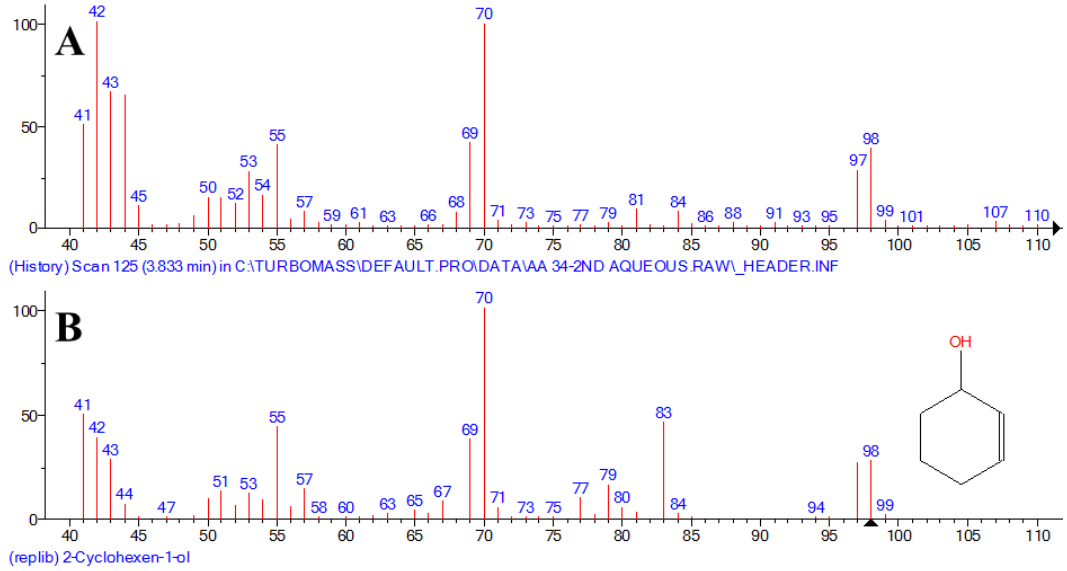

Figure A.34: Matching mass spectrum of peak number 4 in aqueous fraction GC-MS: A) MS of peak number 4 in aqueous fraction sample; B) MS of 2-cyclohexen-1-ol according to NIST library database.

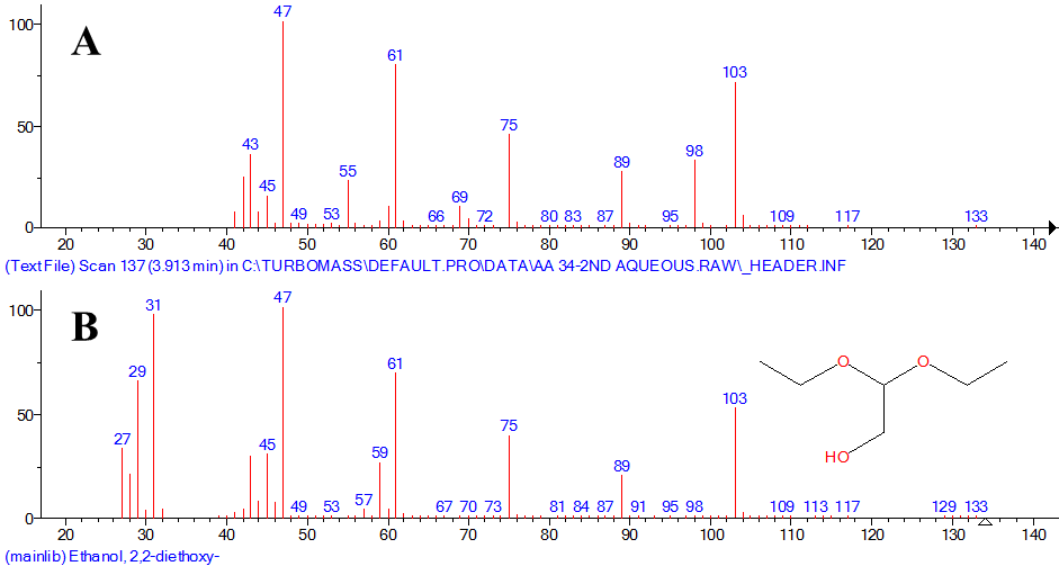

Figure A.35: Matching mass spectrum of peak number 5 in aqueous fraction GC-MS: A) MS of peak number 5 in aqueous fraction sample; B) MS of ethanol, 2,2-diethoxy- according to NIST library database.

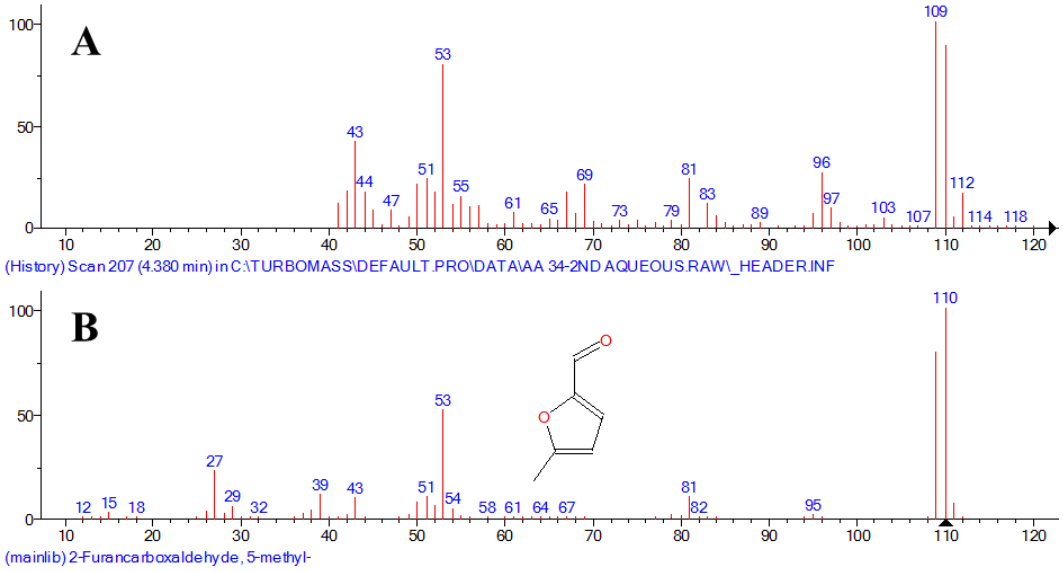

Figure A.36: Matching mass spectrum of peak number 6 in aqueous fraction GC-MS: A) MS of peak number 6 in aqueous fraction sample; B) MS of 2-furancarboxaldehyde, 5-methyl- according to NIST library database.

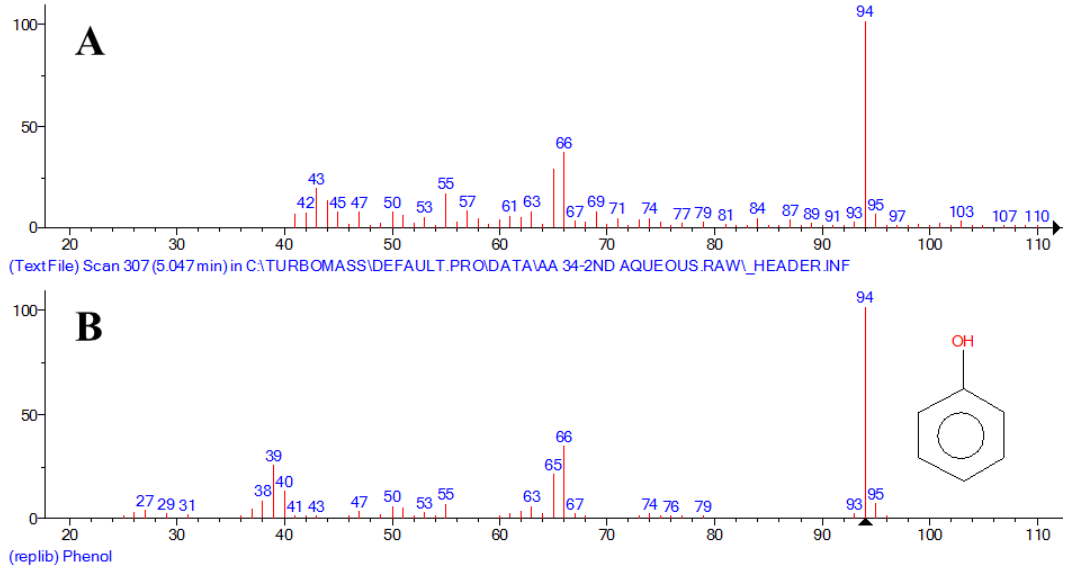

Figure A.37: Matching mass spectrum of peak number 7 in aqueous fraction GC-MS: A) MS of peak number 7 in aqueous fraction sample; B) MS of phenol according to NIST library database.

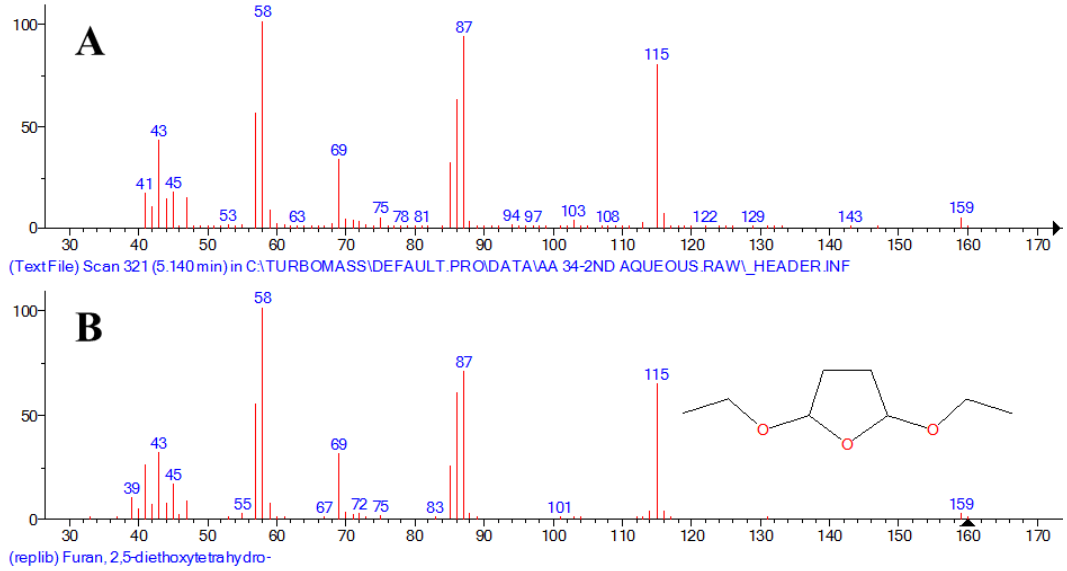

Figure A.38: Matching mass spectrum of peak number 8 in aqueous fraction GC-MS: A) MS of peak number 8 in aqueous fraction sample; B) MS of furan, 2,5-diethoxytetrahydro- according to NIST library database.

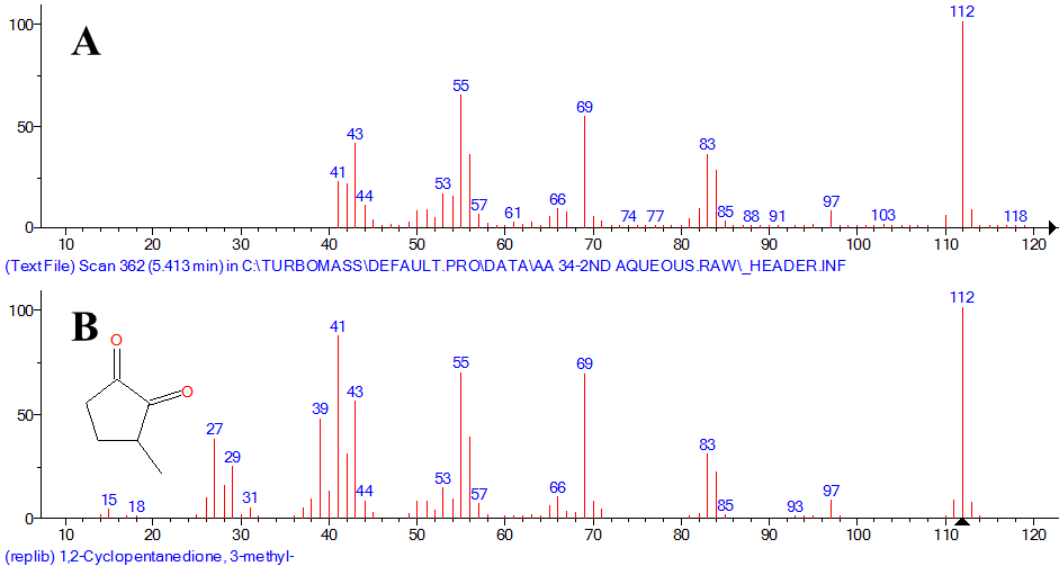

Figure A.39: Matching mass spectrum of peak number 9 in aqueous fraction GC-MS: A) MS of peak number 9 in aqueous fraction sample; B) MS of 1,2-cyclopentanedione, 3-methyl- according to NIST library database.

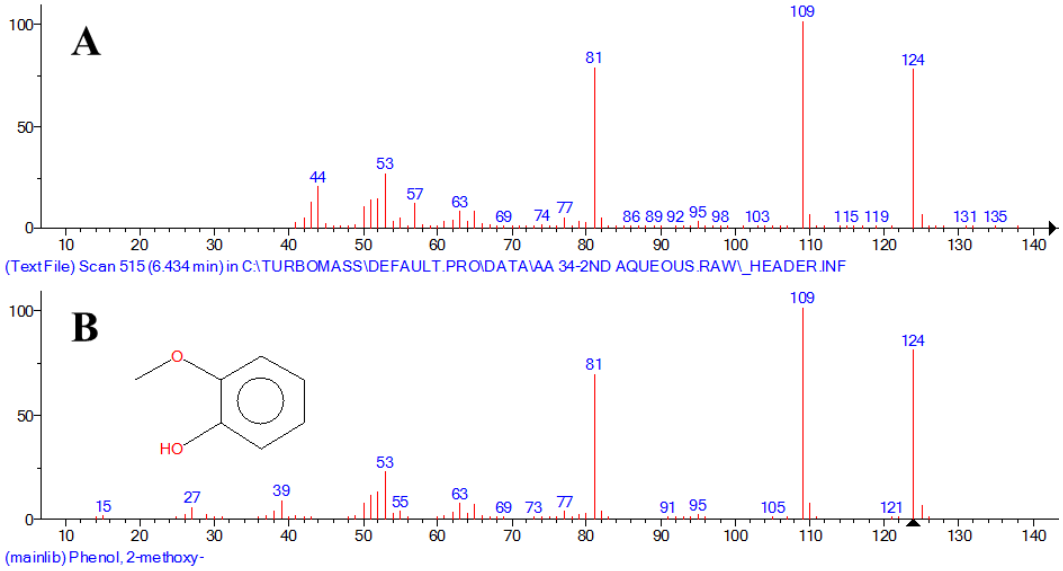

Figure A.40: Matching mass spectrum of peak number 10 in aqueous fraction GC-MS: A) MS of peak number 10 in aqueous fraction sample; B) MS of phenol, 2-methoxy- according to NIST library database.

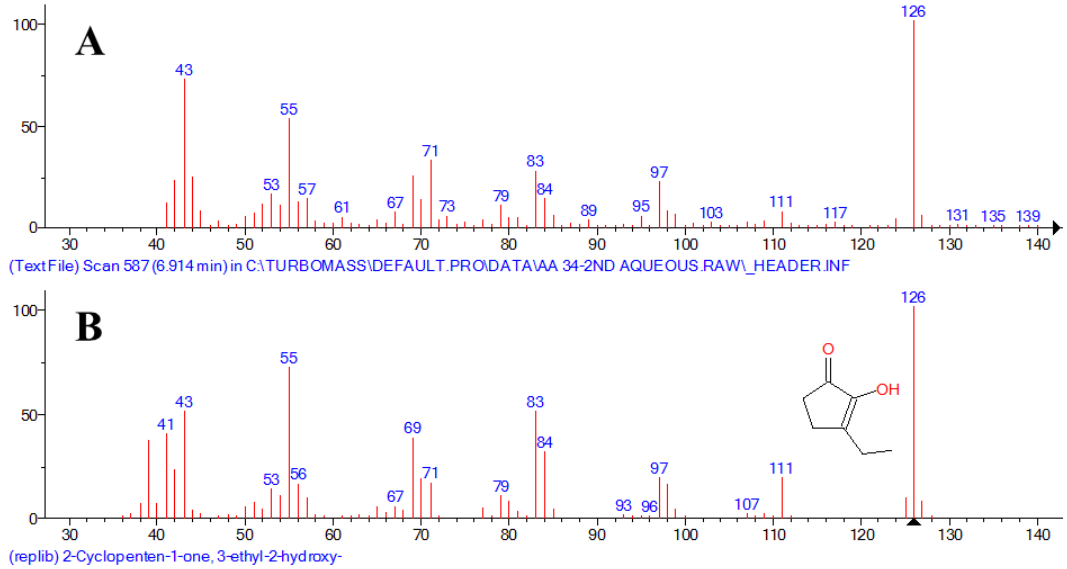

Figure A.41: Matching mass spectrum of peak number 11 in aqueous fraction GC-MS: A) MS of peak number 11 in aqueous fraction sample; B) MS of 2-cyclopenten-1-one, 3-ethyl-2-hydroxy- according to NIST library database.

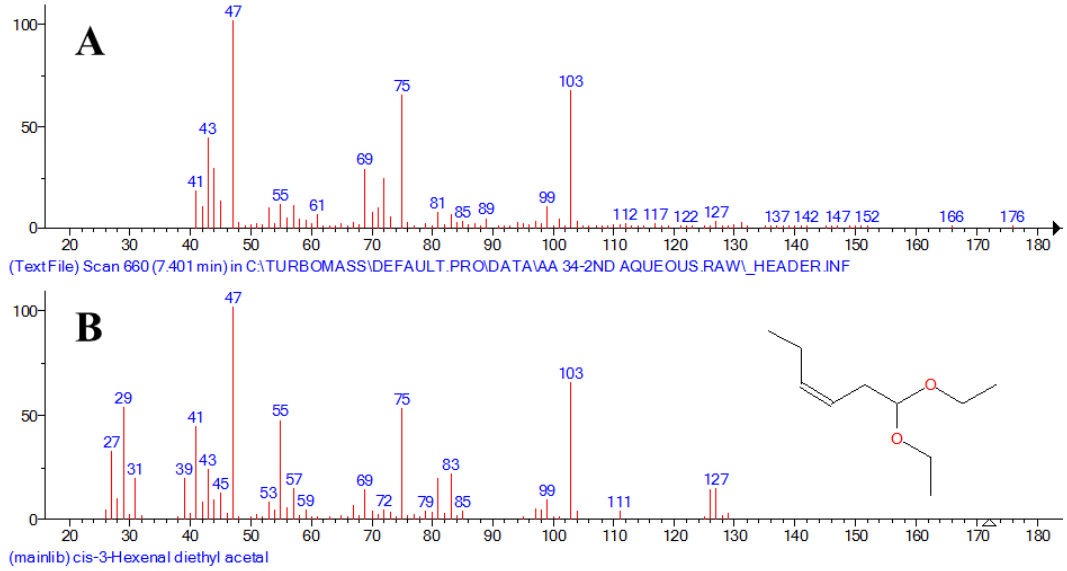

Figure A.42: Matching mass spectrum of peak number 12 in aqueous fraction GC-MS: A) MS of peak number 12 in aqueous fraction sample; B) MS of cis-3-hexenal diethyl acetal according to NIST library database.

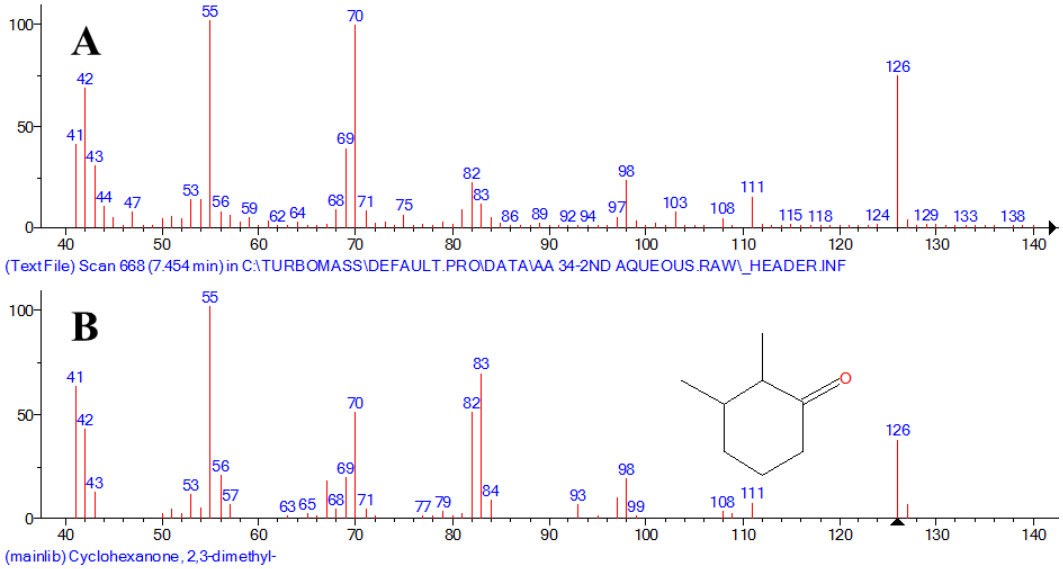

Figure A.43: Matching mass spectrum of peak number 13 in aqueous fraction GC-MS: A) MS of peak number 13 in aqueous fraction sample; B) MS of cyclohexanone, 2,3-dimethyl- according to NIST library database.

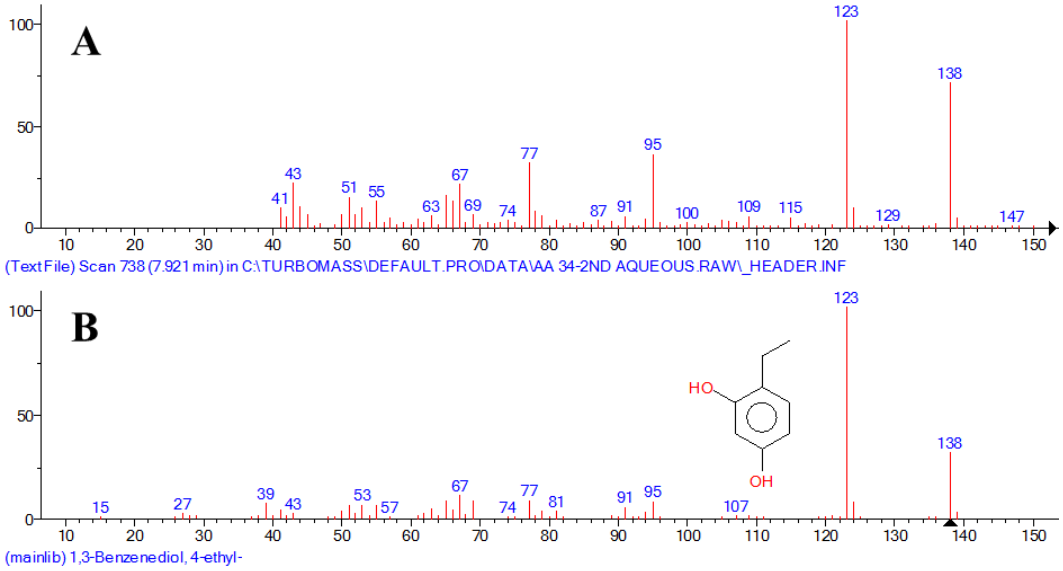

Figure A.44: Matching mass spectrum of peak number 14 in aqueous fraction GC-MS: A) MS of peak number 14 in aqueous fraction sample; B) MS of 1,3-benzenediol, 4-ethyl- according to NIST library database.

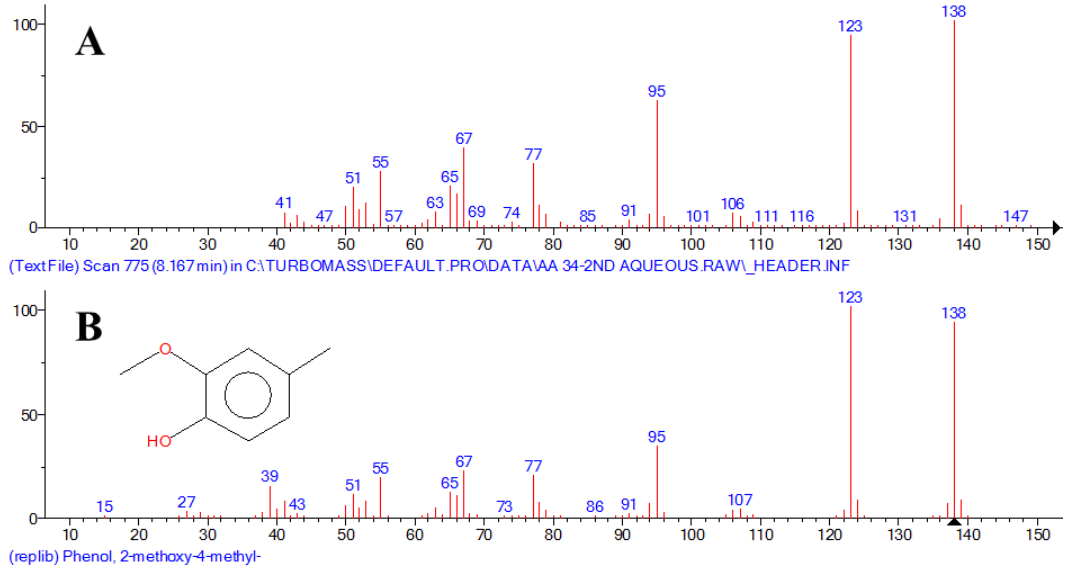

Figure A.45: Matching mass spectrum of peak number 15 in aqueous fraction GC-MS: A) MS of peak number 15 in aqueous fraction sample; B) MS of phenol, 2-methoxy-4-methyl- according to NIST library database.

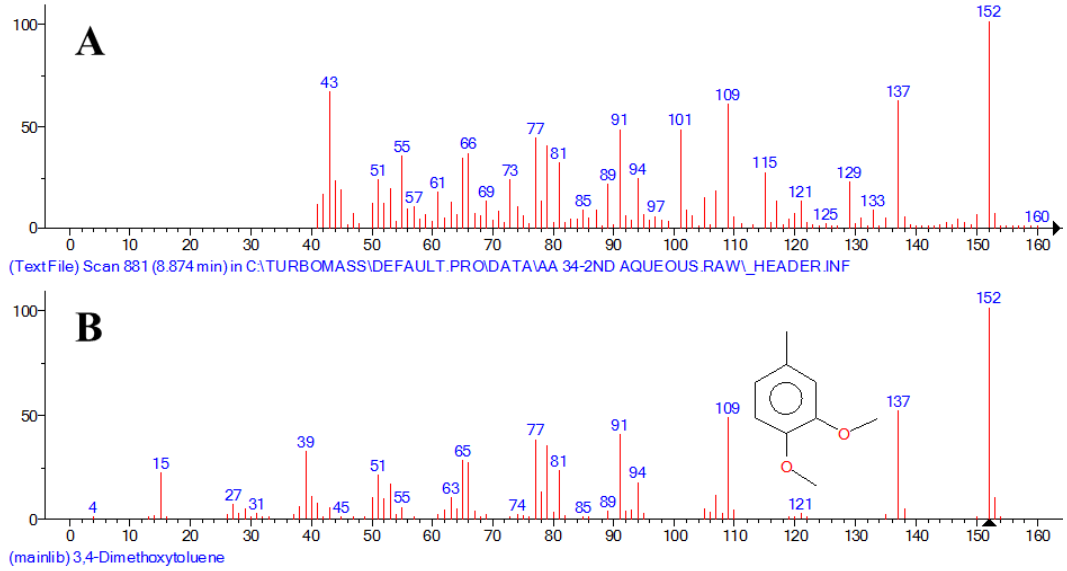

Figure A.46: Matching mass spectrum of peak number 16 in aqueous fraction GC-MS: A) MS of peak number 16 in aqueous fraction sample; B) MS of 3,4-dimethoxytoluene according to NIST library database.

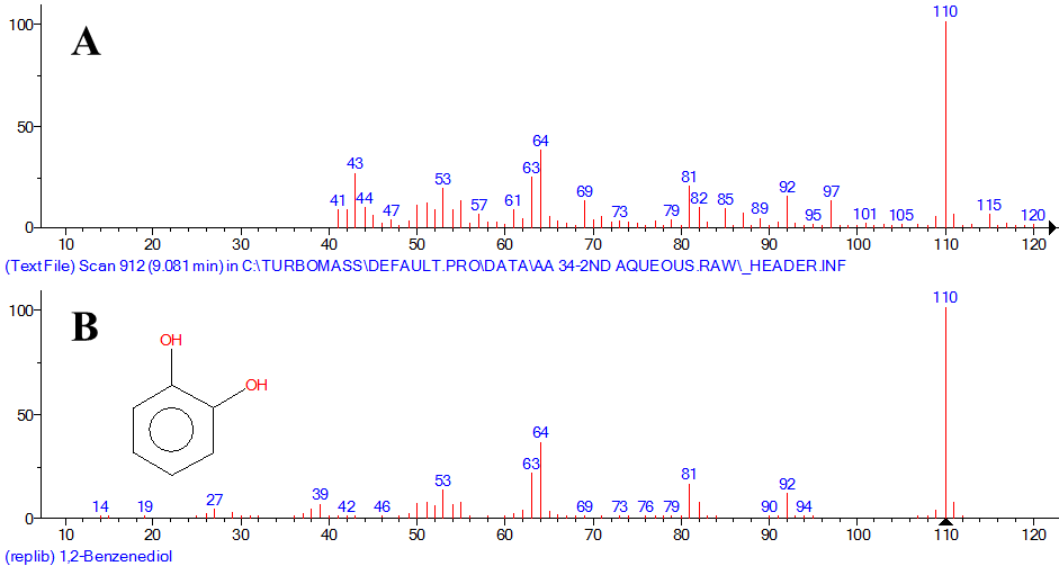

Figure A.47: Matching mass spectrum of peak number 17 in aqueous fraction GC-MS: A) MS of peak number 17 in aqueous fraction sample; B) MS of 1,2-benzenediol according to NIST library database.

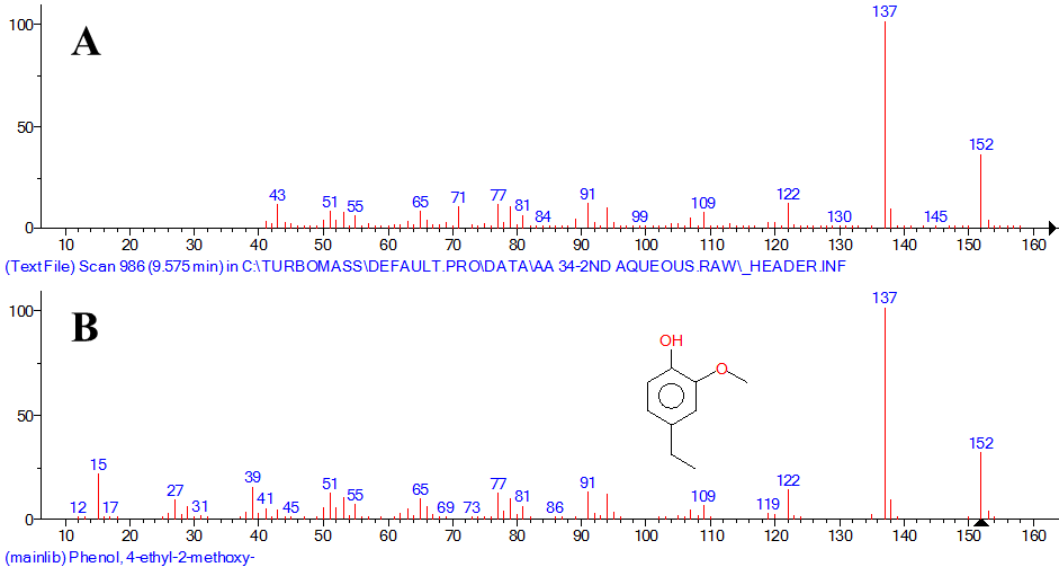

Figure A.48: Matching mass spectrum of peak number 18 in aqueous fraction GC-MS: A) MS of peak number 18 in aqueous fraction sample; B) MS of phenol, 4-ethyl-2-methoxy- according to NIST library database.

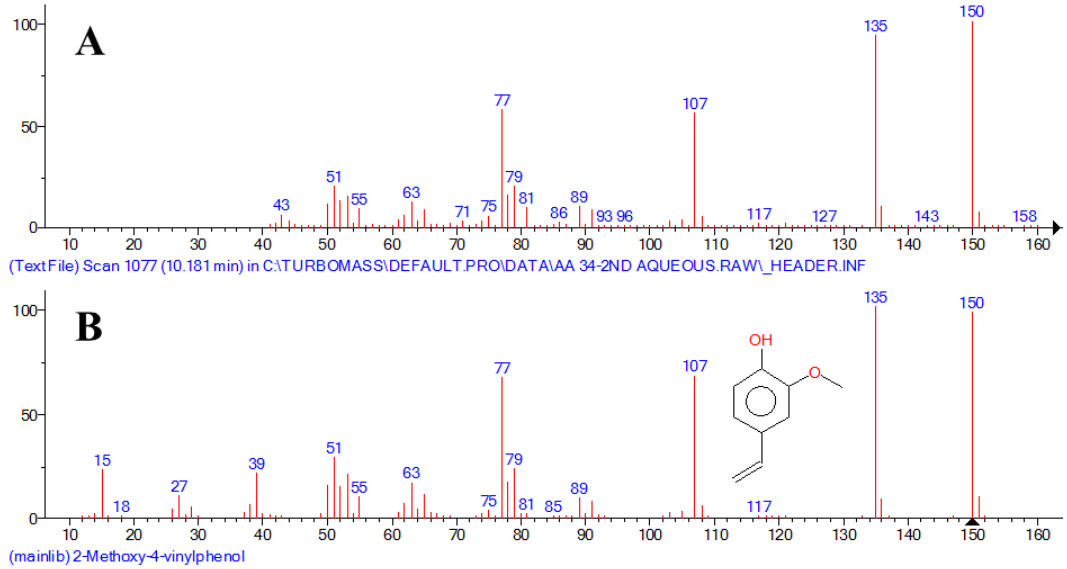

Figure A.49: Matching mass spectrum of peak number 19 in aqueous fraction GC-MS: A) MS of peak number 19 in aqueous fraction sample; B) MS of 2-methoxy-4-vinylphenol according to NIST library database.

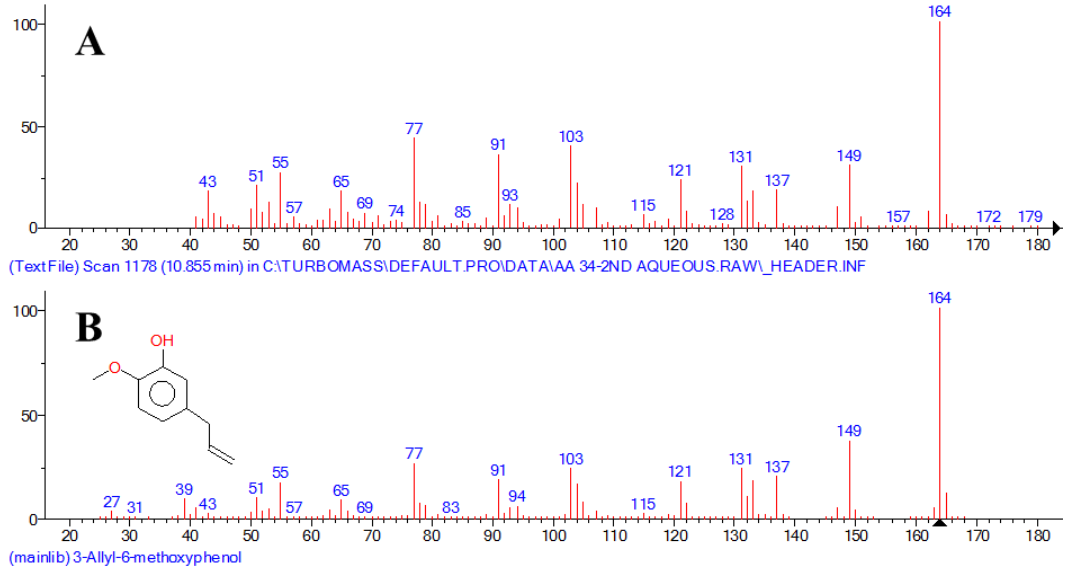

Figure A.50: Matching mass spectrum of peak number 20 in aqueous fraction GC-MS: A) MS of peak number 20 in aqueous fraction sample; B) MS of 3-allyl-6-methoxyphenol according to NIST library database.

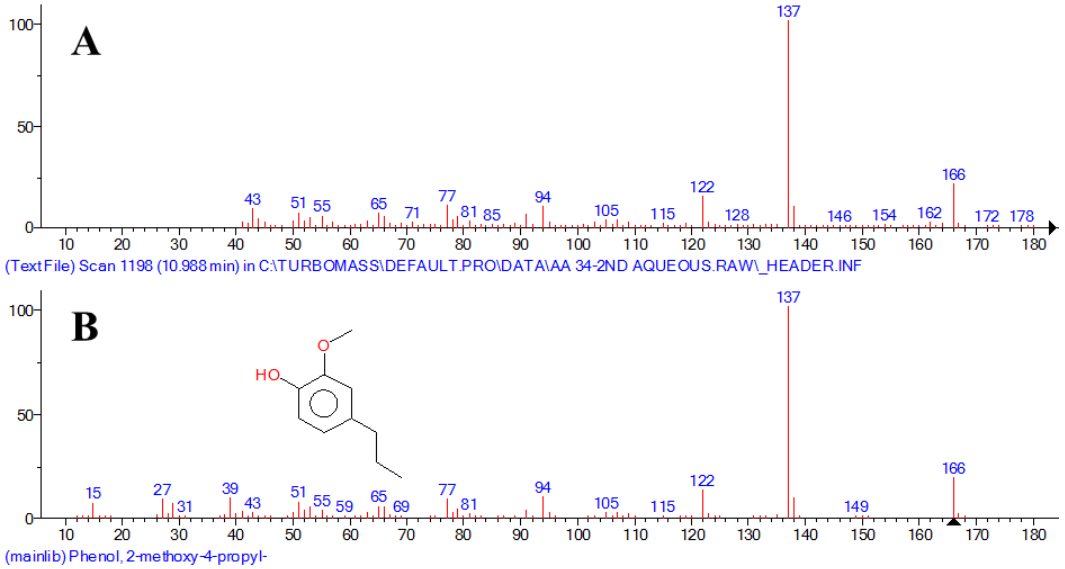

Figure A.51: Matching mass spectrum of peak number 21 in aqueous fraction GC-MS: A) MS of peak number 21 in aqueous fraction sample; B) MS of phenol, 2-methoxy-4-propyl- according to NIST library database.

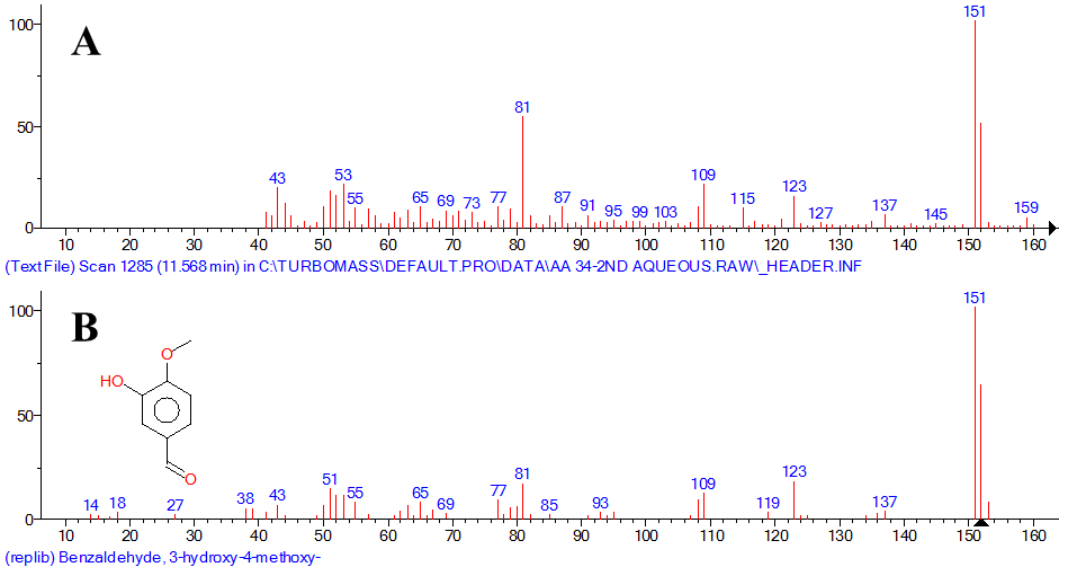

Figure A.52: Matching mass spectrum of peak number 22 in aqueous fraction GC-MS: A) MS of peak number 22 in aqueous fraction sample; B) MS of benzaldehyde, 3-hydroxy-4-methoxy- according to NIST library database.

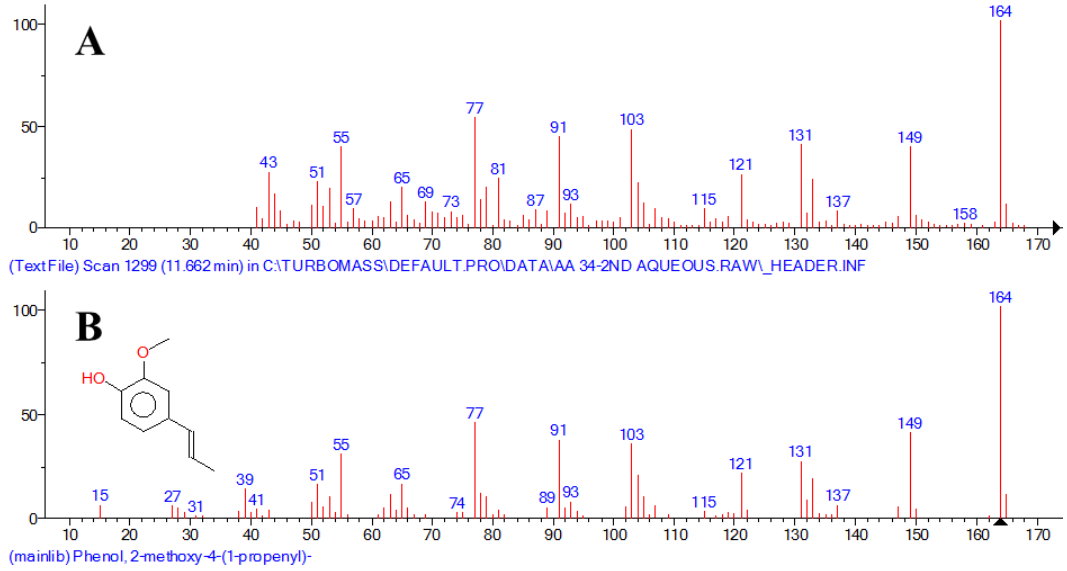

Figure A.53: Matching mass spectrum of peak number 23 in aqueous fraction GC-MS: A) MS of peak number 23 in aqueous fraction sample; B) MS of phenol, 2-methoxy-4-(1-propenyl)- according to NIST library database.

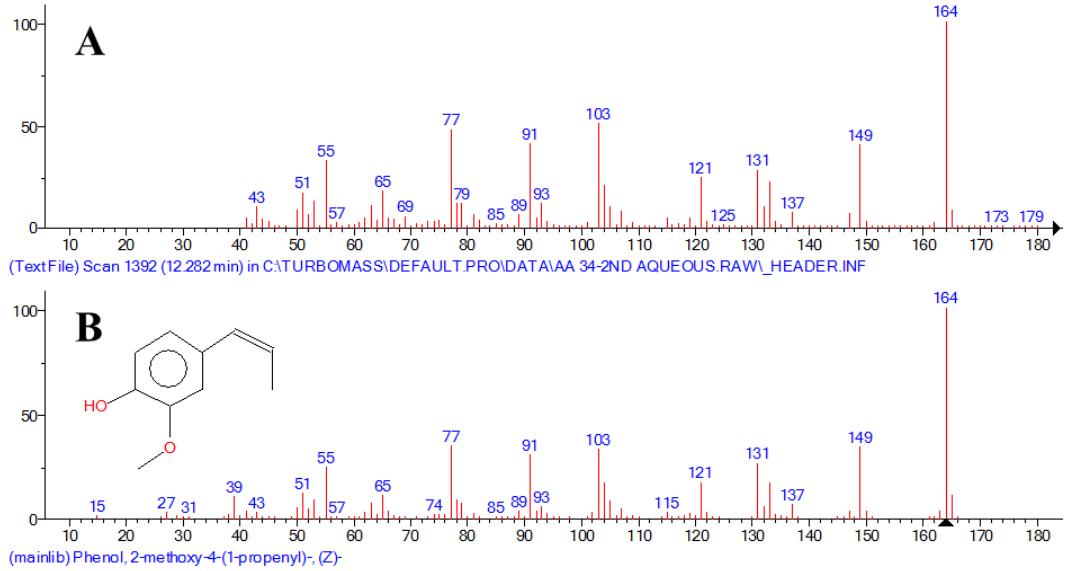

Figure A.54: Matching mass spectrum of peak number 24 in aqueous fraction GC-MS: A) MS of peak number 24 in aqueous fraction sample; B) MS of phenol, 2-methoxy-4-(1-propenyl)-, (Z)- according to NIST library database.

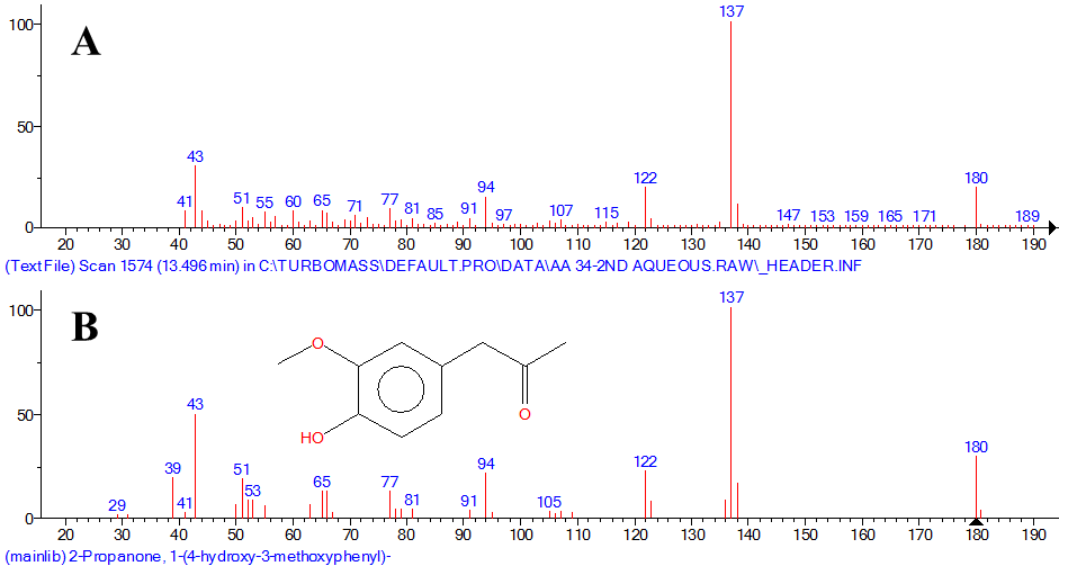

Figure A.55: Matching mass spectrum of peak number 25 in aqueous fraction GC-MS: A) MS of peak number 25 in aqueous fraction sample; B) MS of 2-propanone, 1-(4-hydroxy-3-methoxyphenyl)- according to NIST library database.

A.2 Mass Spectra of Identified Phenolic Peaks in Crude Bio-oil

A.2.1 Mass spectra of identified phenolic peaks in 1st extract of crude bio-oil and their best NIST library match

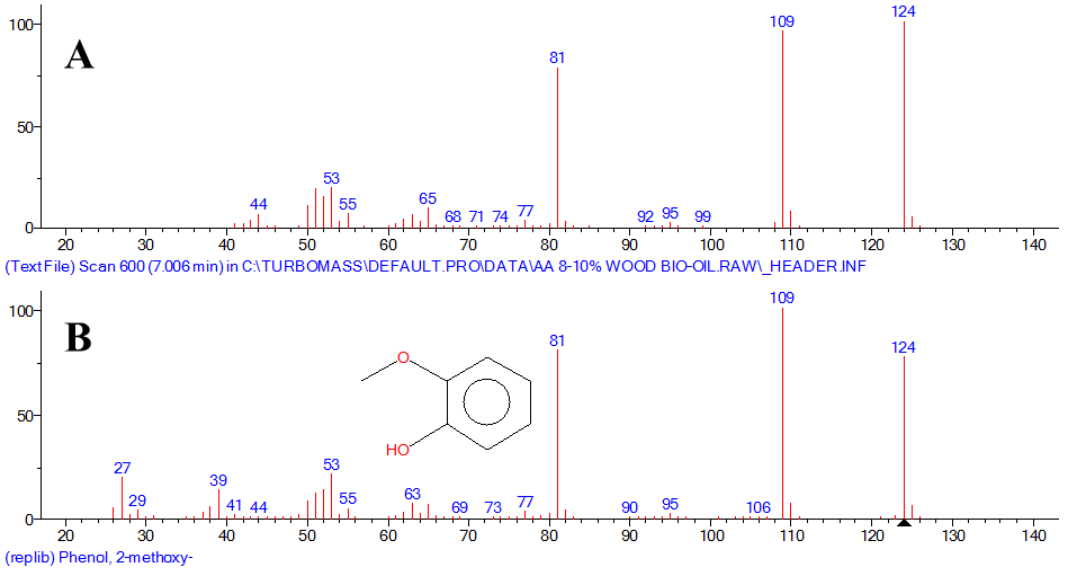

Figure A.56: Matching mass spectrum of peak number 4 in 1st extract of crude bio-oil GC-MS: A) MS of peak number 4 in 1st extract of crude bio-oil sample; B) MS of phenol, 2-methoxy- according to NIST library database.

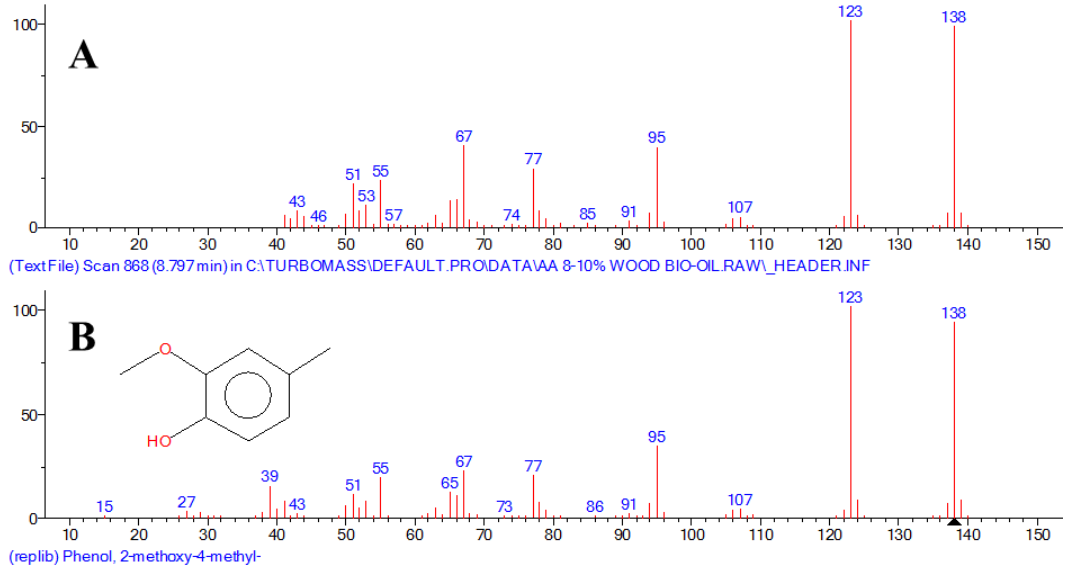

Figure A.57: Matching mass spectrum of peak number 7 in 1st extract of crude bio-oil GC-MS: A) MS of peak number 7 in 1st extract of crude bio-oil sample; B) MS of phenol, 2-methoxy-4-methyl- according to NIST library database.

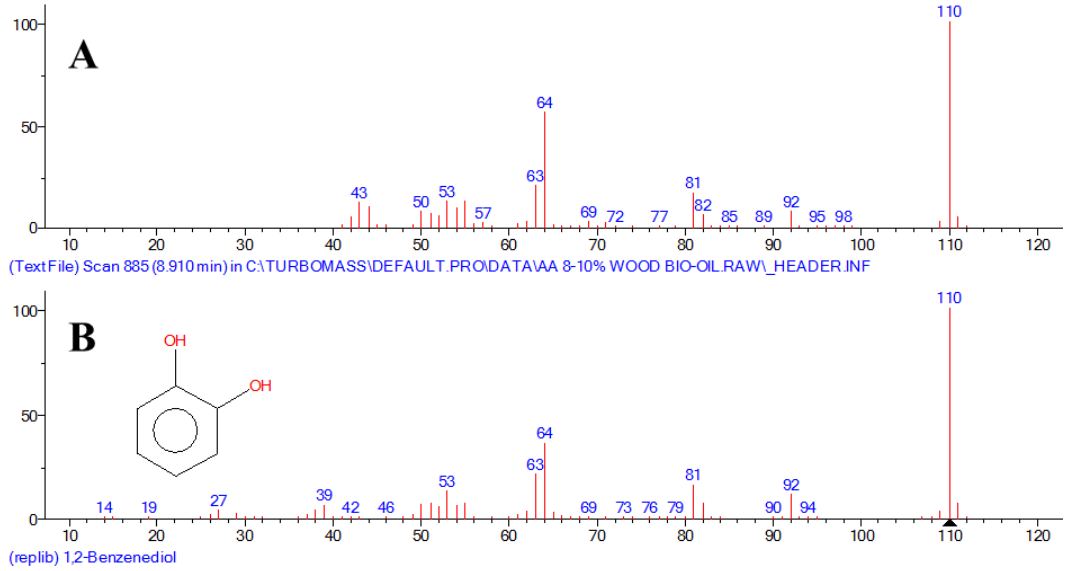

Figure A.58: Matching mass spectrum of peak number 8 in 1st extract of crude bio-oil GC-MS: A) MS of peak number 8 in 1st extract of crude bio-oil sample; B) MS of 1,2-benzenediol according to NIST library database.

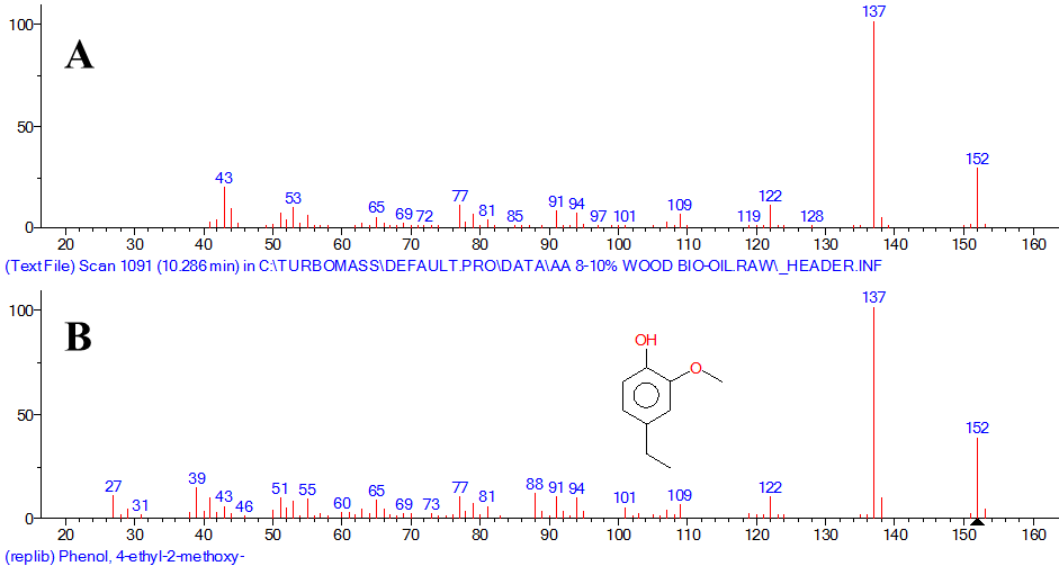

Figure A.59: Matching mass spectrum of peak number 10 in 1st extract of crude bio-oil GC-MS: A) MS of peak number 10 in 1st extract of crude bio-oil sample; B) MS of phenol, 4-ethyl-2-methoxy- according to NIST library database.

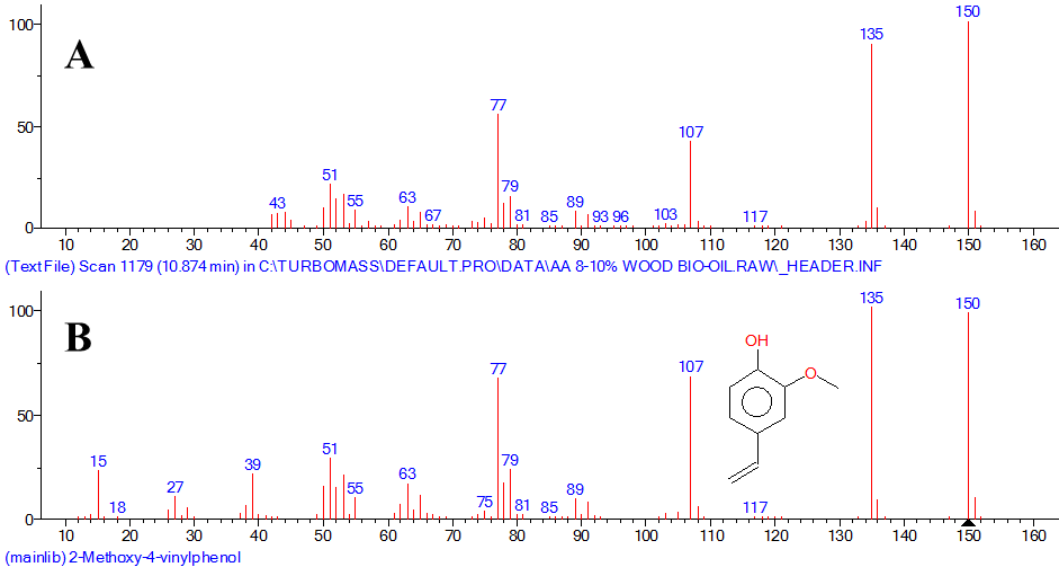

Figure A.60: Matching mass spectrum of peak number 12 in 1st extract of crude bio-oil GC-MS: A) MS of peak number 12 in 1st extract of crude bio-oil sample; B) MS of 2-methoxy-4-vinylphenol according to NIST library database.

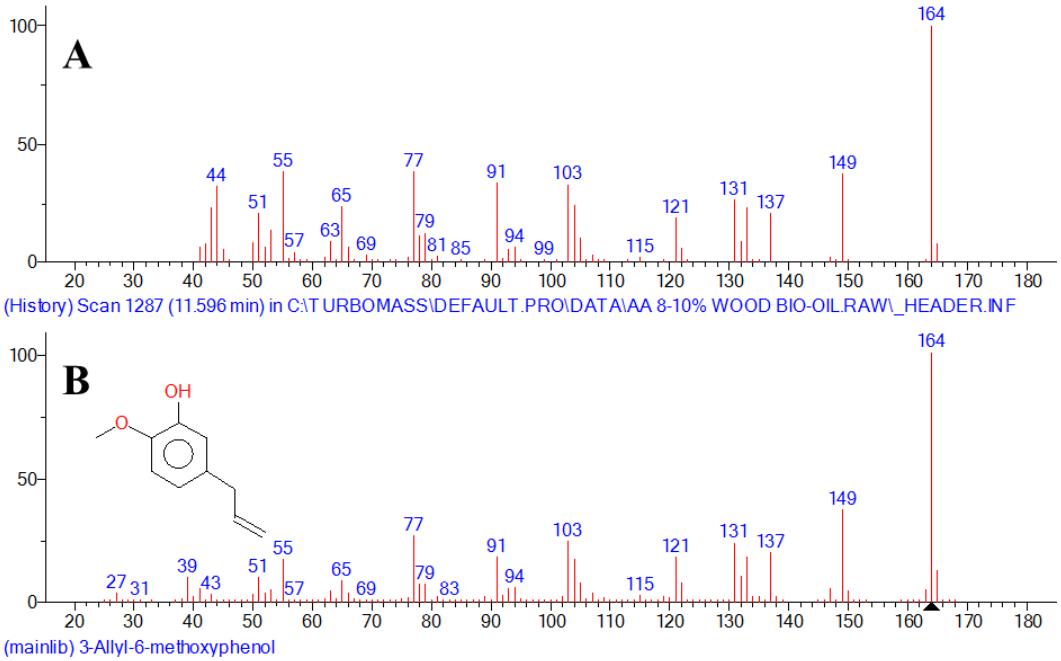

Figure A.61: Matching mass spectrum of peak number 14 in 1st extract of crude bio-oil GC-MS: A) MS of peak number 14 in 1st extract of crude bio-oil sample; B) MS of 3-allyl-6-methoxyphenol according to NIST library database.

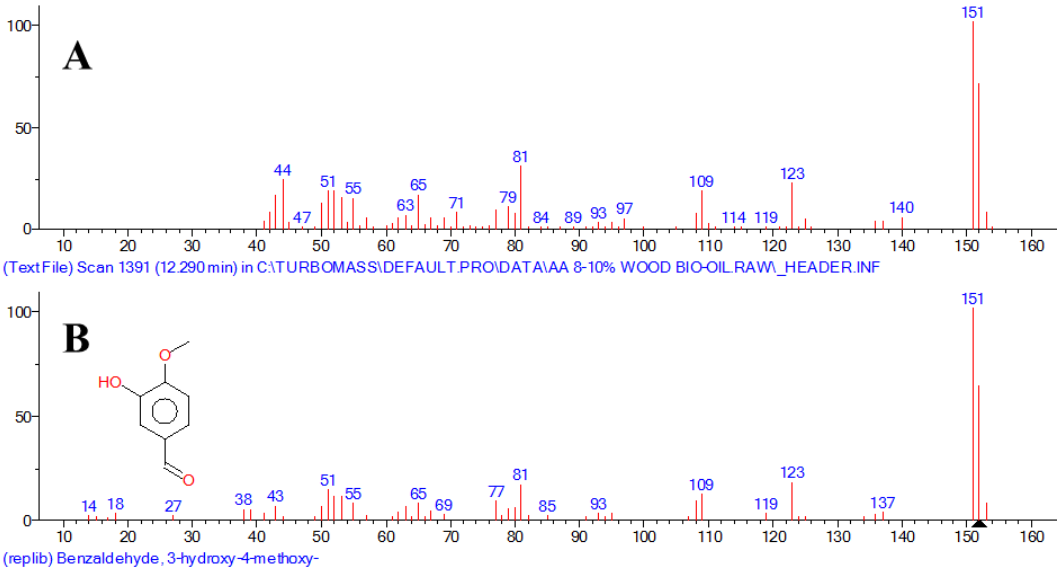

Figure A.62: Matching mass spectrum of peak number 16 in 1st extract of crude bio-oil GC-MS: A) MS of peak number 16 in 1st extract of crude bio-oil sample; B) MS of benzaldehyde, 3-hydroxy-4-methoxy- according to NIST library database.

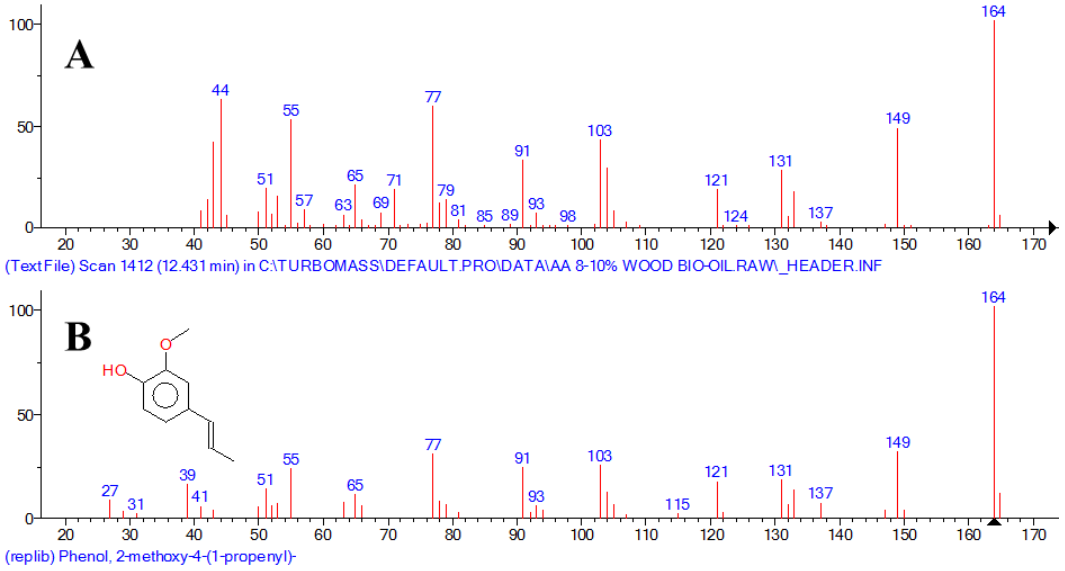

Figure A.63: Matching mass spectrum of peak number 17 in 1st extract of crude bio-oil GC-MS: A) MS of peak number 17 in 1st extract of crude bio-oil sample; B) MS of phenol, 2-methoxy-4-(1-propenyl)- according to NIST library database.

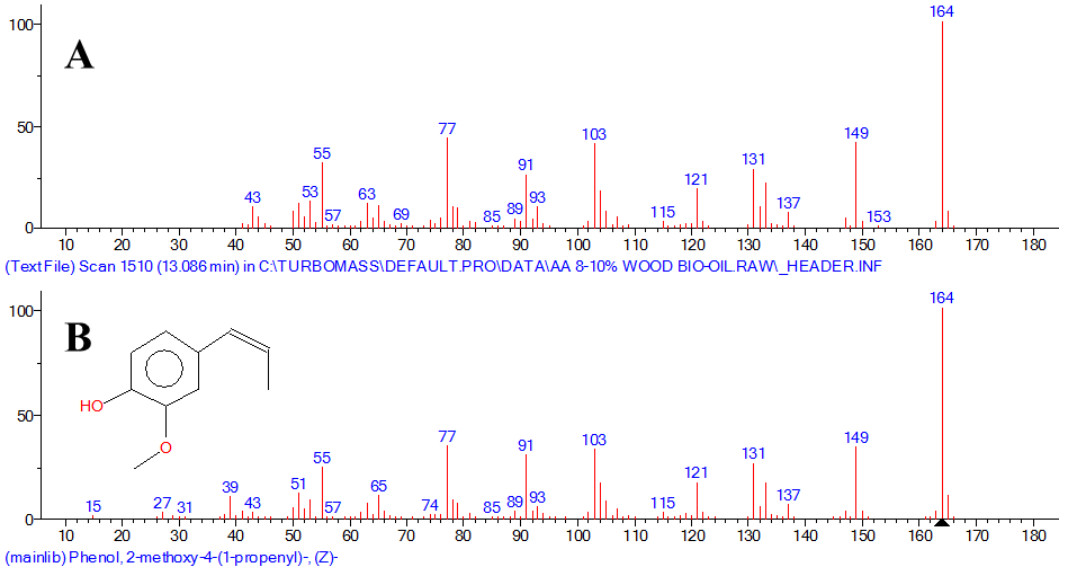

Figure A.64: Matching mass spectrum of peak number 18 in 1st extract of crude bio-oil GC-MS: A) MS of peak number 18 in 1st extract of crude bio-oil sample; B) MS of phenol, 2-methoxy-4-(1-propenyl)-, (Z)- according to NIST library database.

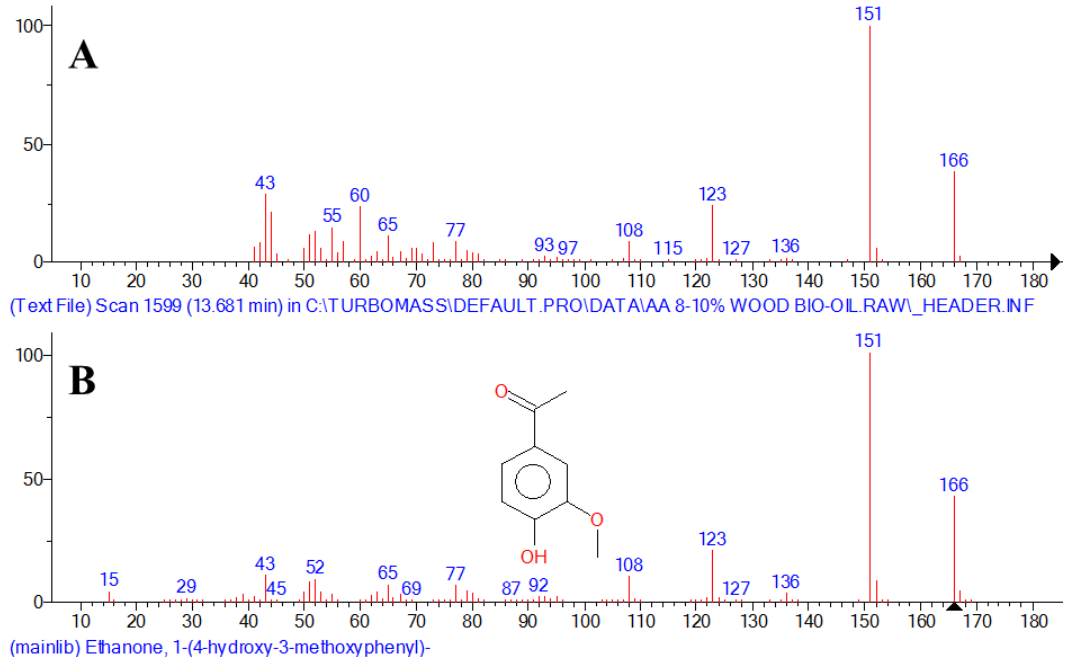

Figure A.65: Matching mass spectrum of peak number 20 in 1st extract of crude bio-oil GC-MS: A) MS of peak number 20 in 1st extract of crude bio-oil sample; B) MS of ethanone, 1-(4-hydroxy-3-methoxyphenyl)- according to NIST library database.

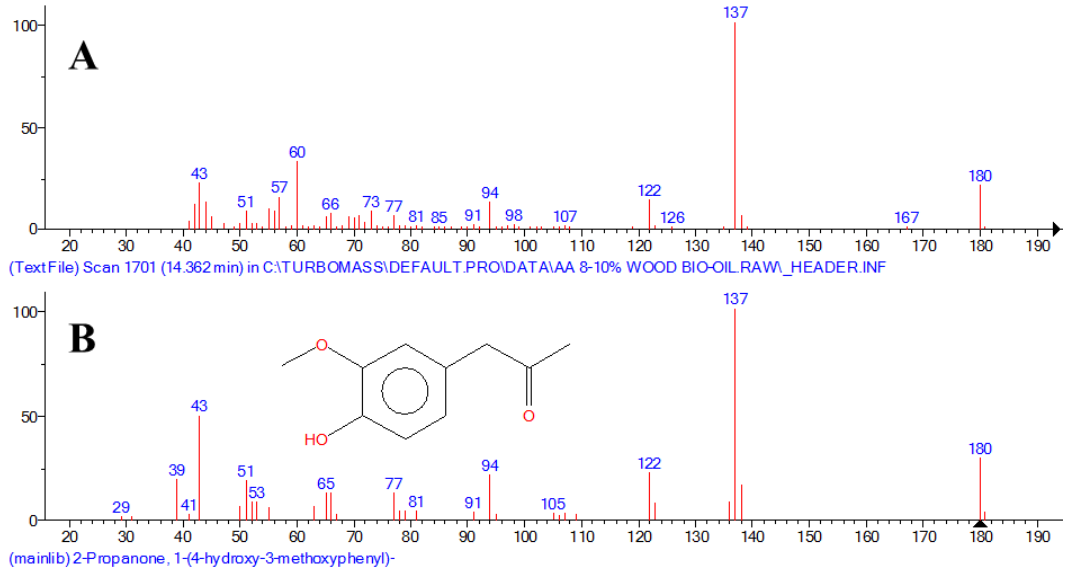

Figure A.66: Matching mass spectrum of peak number 21 in 1st extract of crude bio-oil GC-MS: A) MS of peak number 21 in 1st extract of crude bio-oil sample; B) MS of 2-propanone, 1-(4-hydroxy-3-methoxyphenyl)- according to NIST library database.

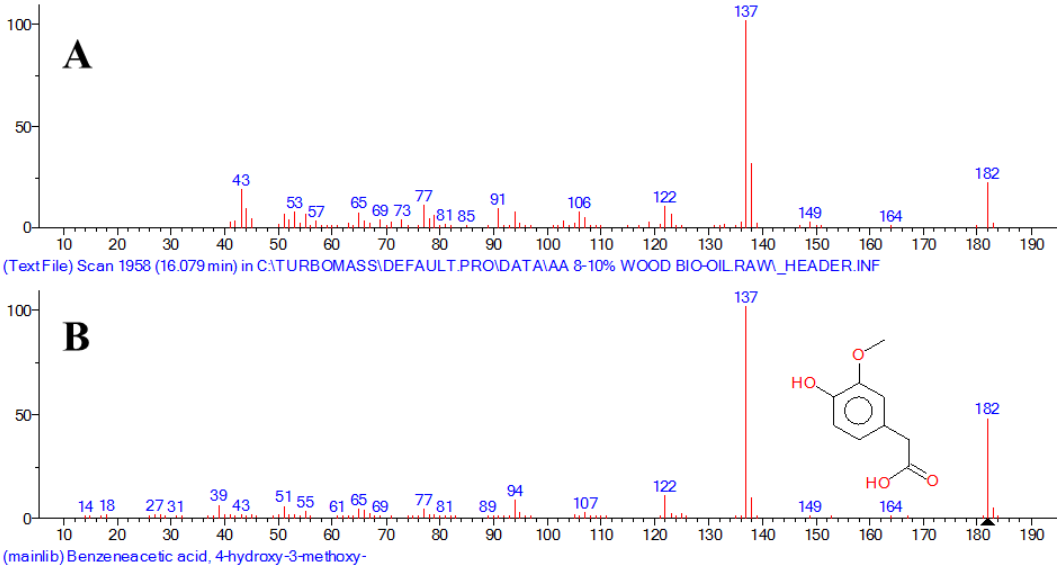

Figure A.67: Matching mass spectrum of peak number 24 in 1st extract of crude bio-oil GC-MS: A) MS of peak number 24 in 1st extract of crude bio-oil sample; B) MS of benzeneacetic acid, 4-hydroxy-3-methoxy- according to NIST library database.

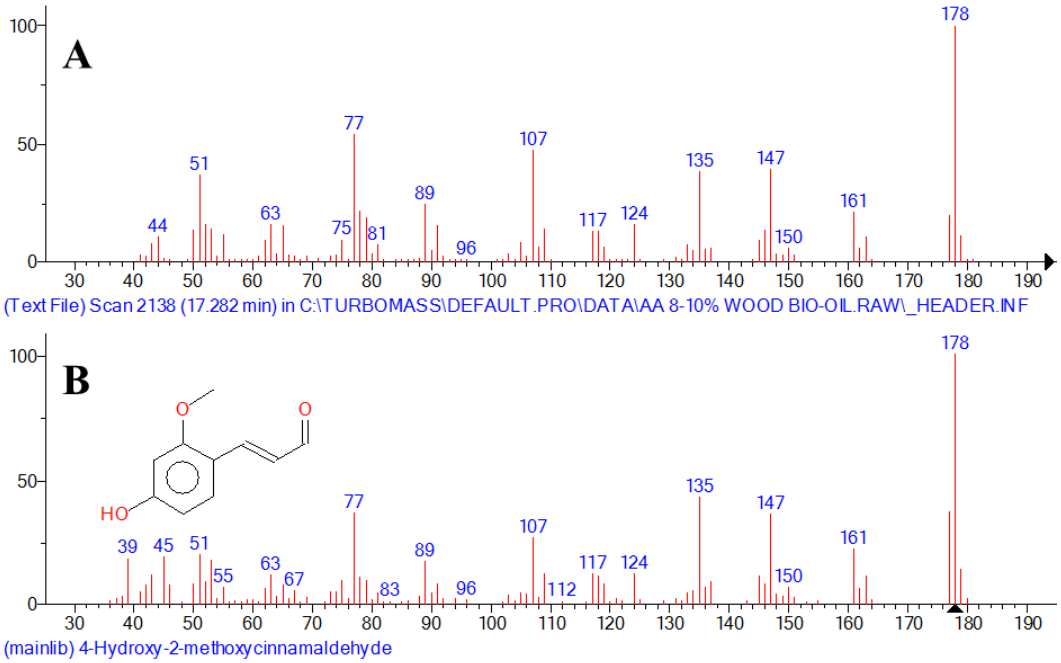

Figure A.68: Matching mass spectrum of peak number 26 in 1st extract of crude bio-oil GC-MS: A) MS of peak number 26 in 1st extract of crude bio-oil sample; B) MS of 4-hydroxy-2-methoxycinnamaldehyde according to NIST library database.

A.2.2 Mass spectra of identified phenolic peaks in 2nd extract of crude bio-oil and their best NIST library match

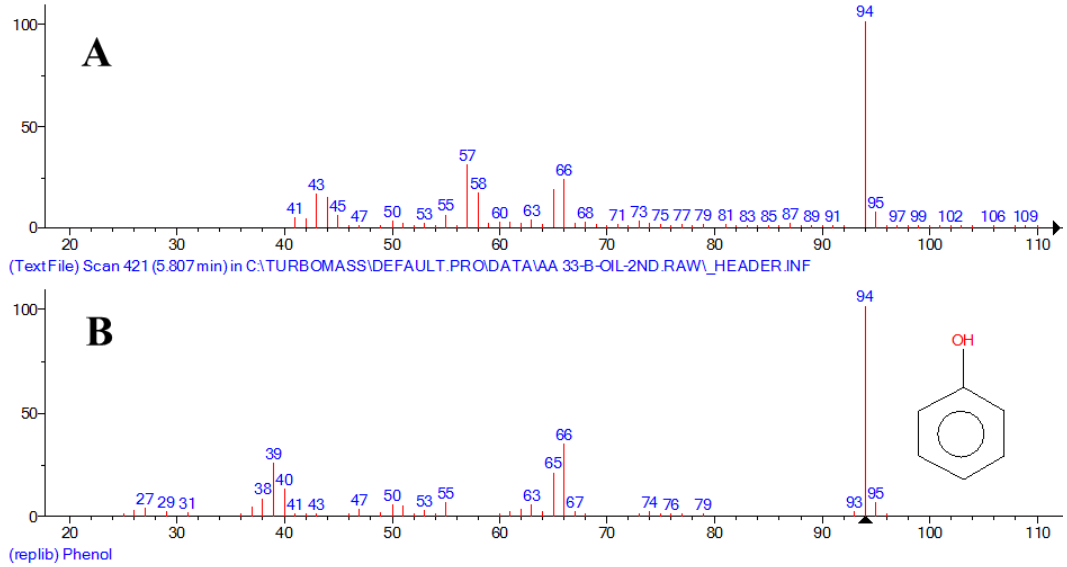

Figure A.69: Matching MS spectrum of peak number 1 MS in 2nd extract of crude bio-oil GC-MS: A) MS of Peak number 1 in 2nd extract of crude bio-oil sample; B) MS of phenol according to NIST library database.

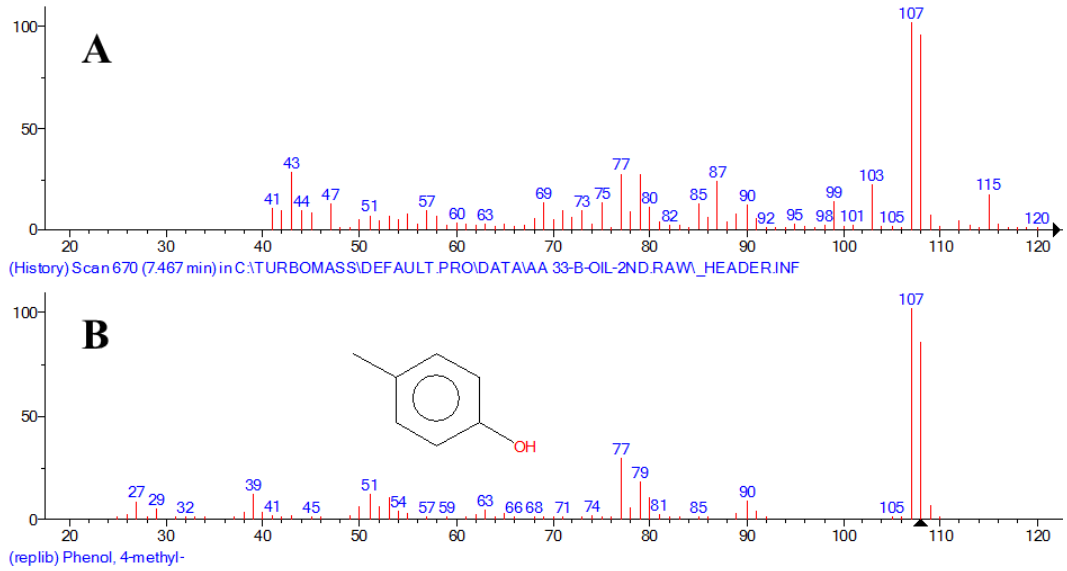

Figure A.70: Matching MS spectrum of peak number 3 MS in 2nd extract of crude bio-oil GC-MS: A) MS of peak number 3 in 2nd extract of crude bio-oil sample; B) MS of Phenol, 4-methyl- according to NIST library database.

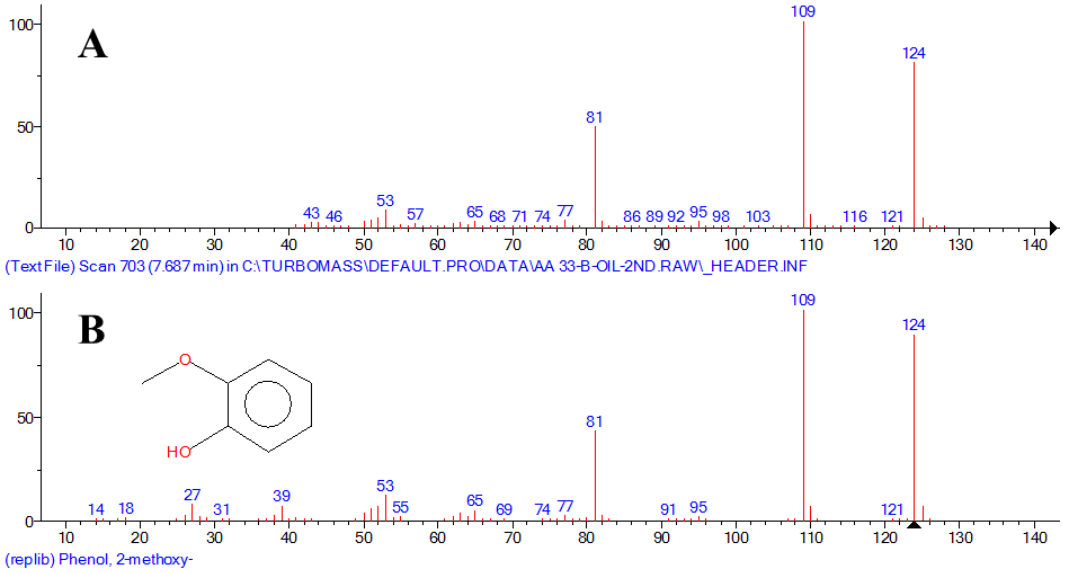

Figure A.71: Matching MS spectrum of peak number 4 MS in 2nd extract of crude bio-oil GC-MS: A) MS of peak number 4 in 2nd extract of crude bio-oil sample; B) MS of Phenol, 2-methoxy- according to NIST library database.

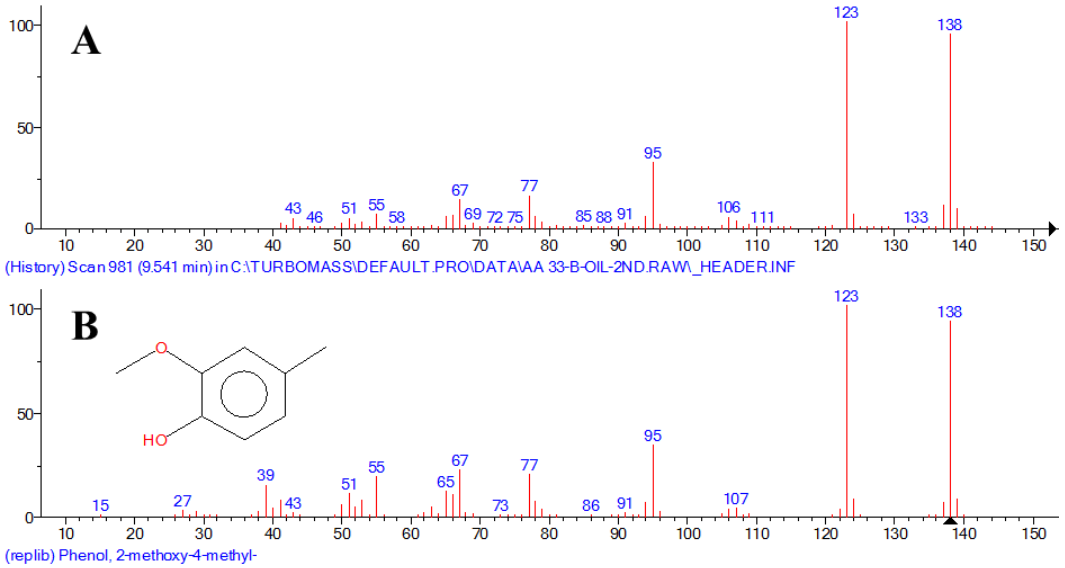

Figure A.72: Matching MS spectrum of peak number 7 MS in 2nd extract of crude bio-oil GC-MS: A) MS of peak number 7 in 2nd extract of crude bio-oil sample; B) MS of Phenol, 2-methoxy-4-methyl- according to NIST library database.

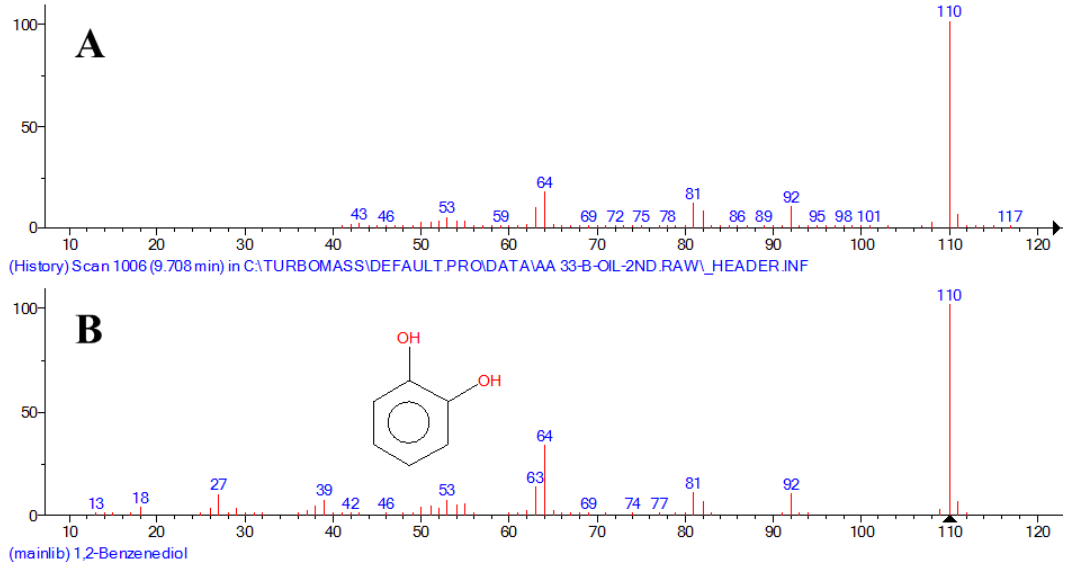

Figure A.73: Matching MS spectrum of peak number 8 MS in 2nd extract of crude bio-oil GC-MS: A) MS of peak number 8 in 2nd extract of crude bio-oil sample; B) MS of 1,2-Benzenediol according to NIST library database.

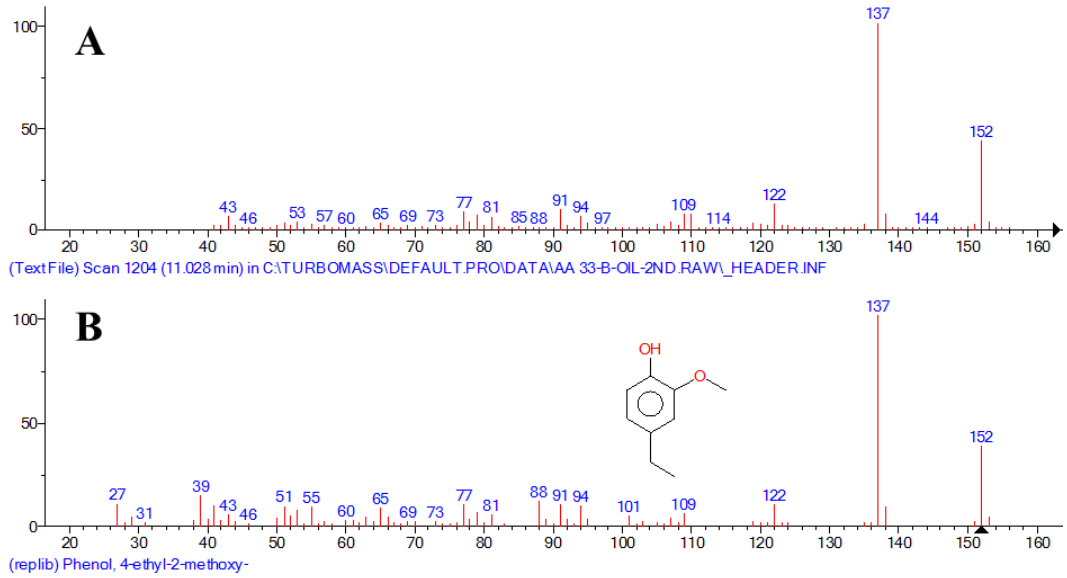

Figure A.74: Matching MS spectrum of peak number 10 MS in 2nd extract of crude bio-oil GC-MS: A) MS of peak number 10 in 2nd extract of crude bio-oil sample; B) MS of Phenol, 4-ethyl-2-methoxy- according to NIST library database.

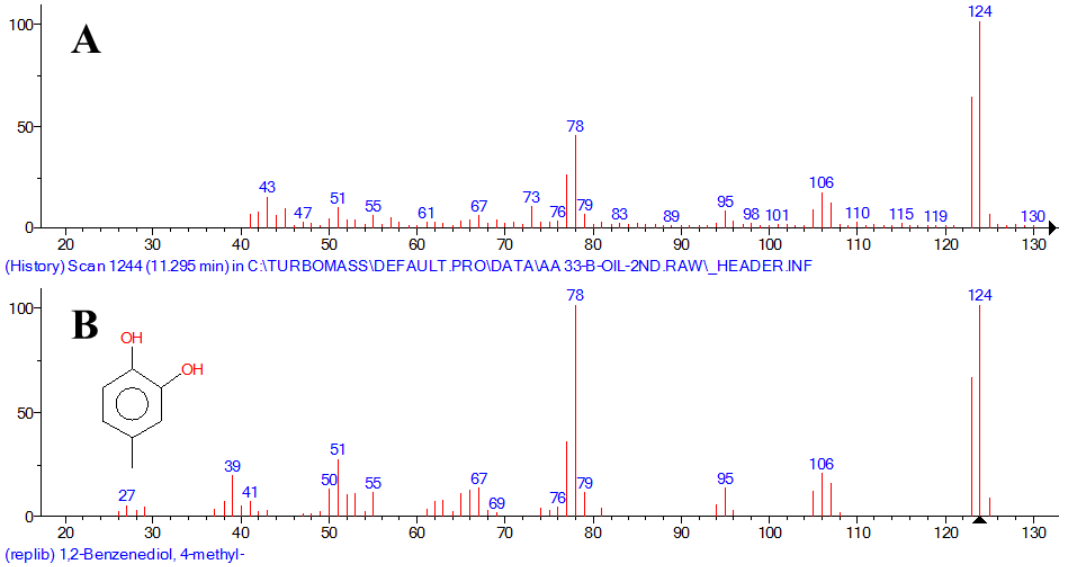

Figure A.75: Matching MS spectrum of peak number 11 MS in 2nd extract of crude bio-oil GC-MS: A) MS of peak number 11 in 2nd extract of crude bio-oil sample; B) MS of 1,2-Benzenediol, 4-methyl- according to NIST library database.

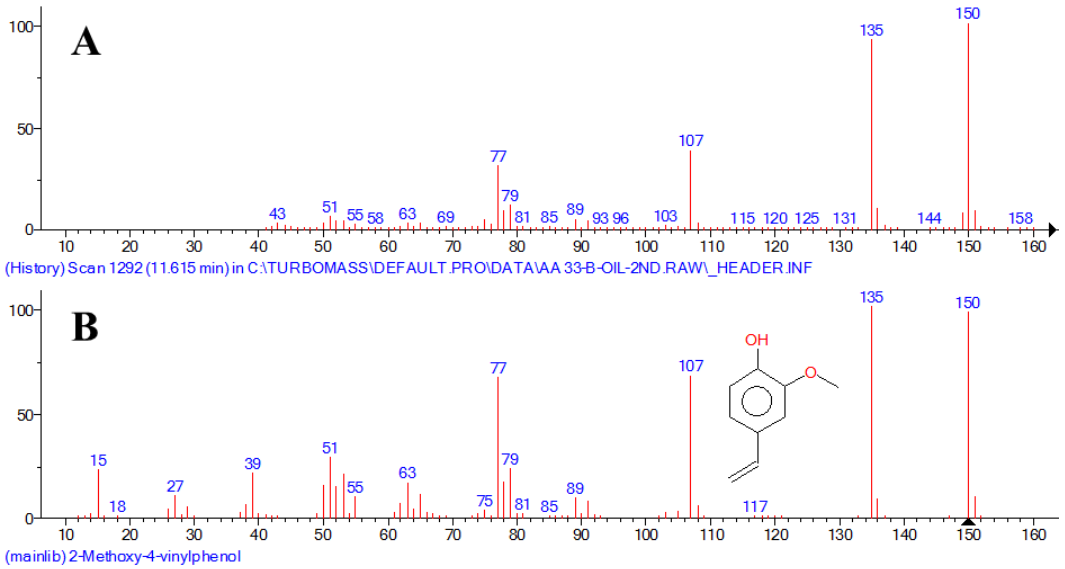

Figure A.76: Matching MS spectrum of peak number 12 MS in 2nd extract of crude bio-oil GC-MS: A) MS of peak number 12 in 2nd extract of crude bio-oil sample; B) MS of 2-Methoxy-4-vinylphenol according to NIST library database.

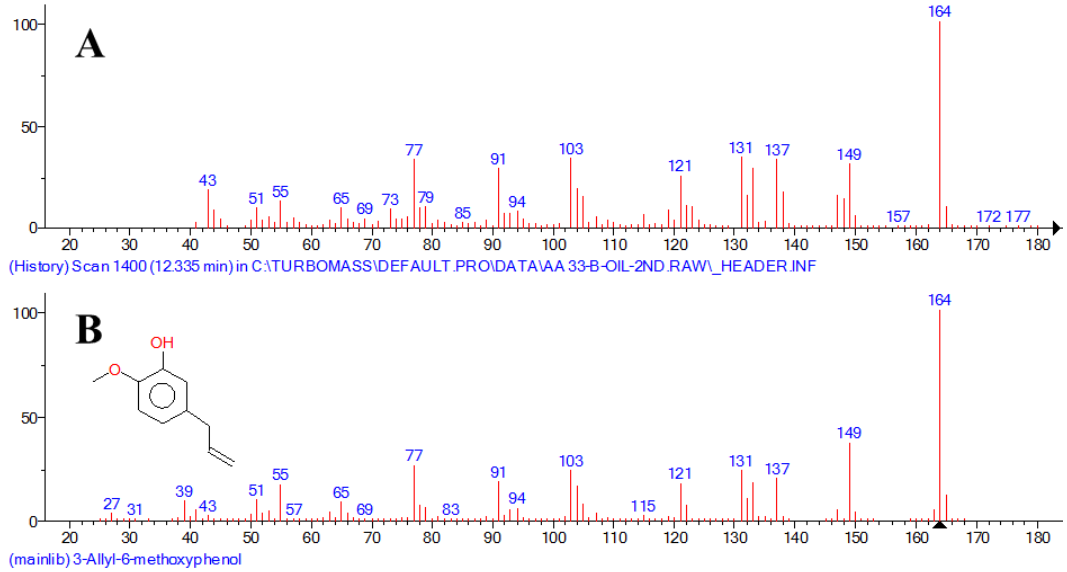

Figure A.77: Matching MS spectrum of peak number 14 MS in 2nd extract of crude bio-oil GC-MS: A) MS of peak number 14 in 2nd extract of crude bio-oil sample; B) MS of 3-Allyl-6-methoxyphenol according to NIST library database.

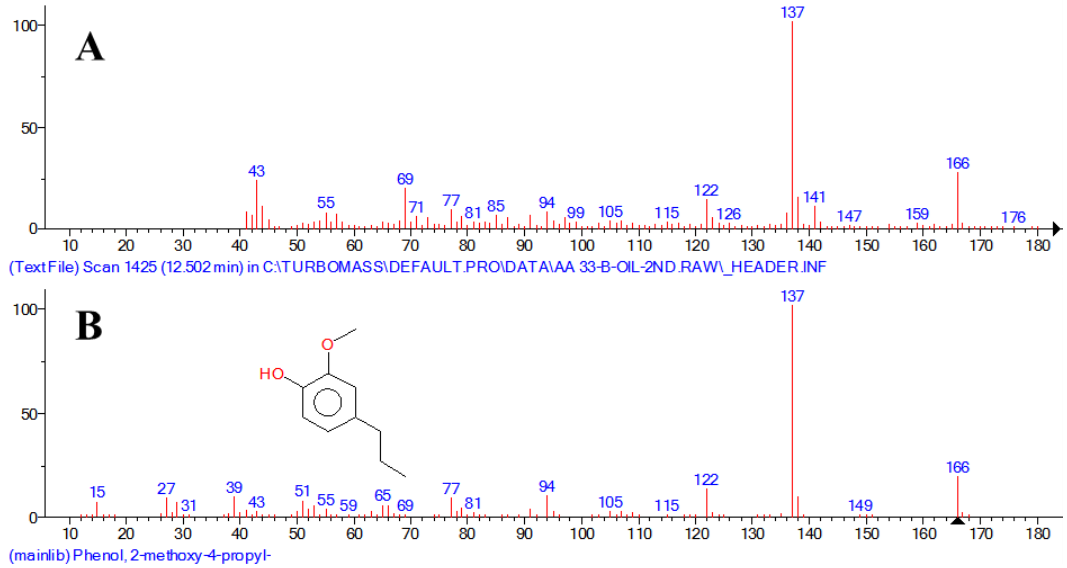

Figure A.78: Matching MS spectrum of peak number 15 MS in 2nd extract of crude bio-oil GC-MS: A) MS of peak number 15 in 2nd extract of crude bio-oil sample; B) MS of Phenol, 2-methoxy-4-propyl- according to NIST library database.

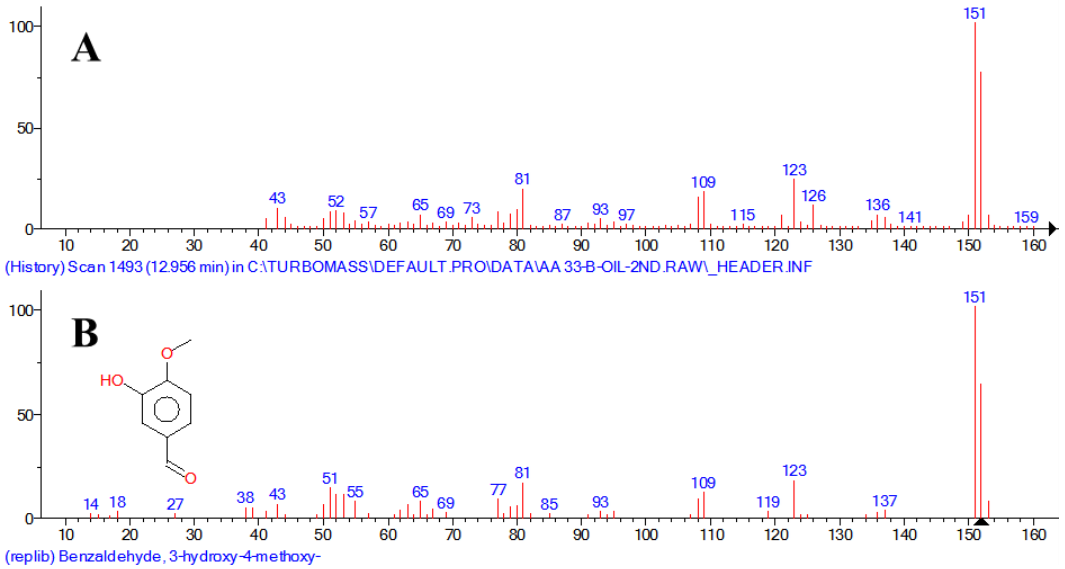

Figure A.79: Matching MS spectrum of peak number 16 MS in 2nd extract of crude bio-oil GC-MS: A) MS of peak number 16 in 2nd extract of crude bio-oil sample; B) MS of Benzaldehyde, 3-hydroxy-4-methoxy- according to NIST library database.

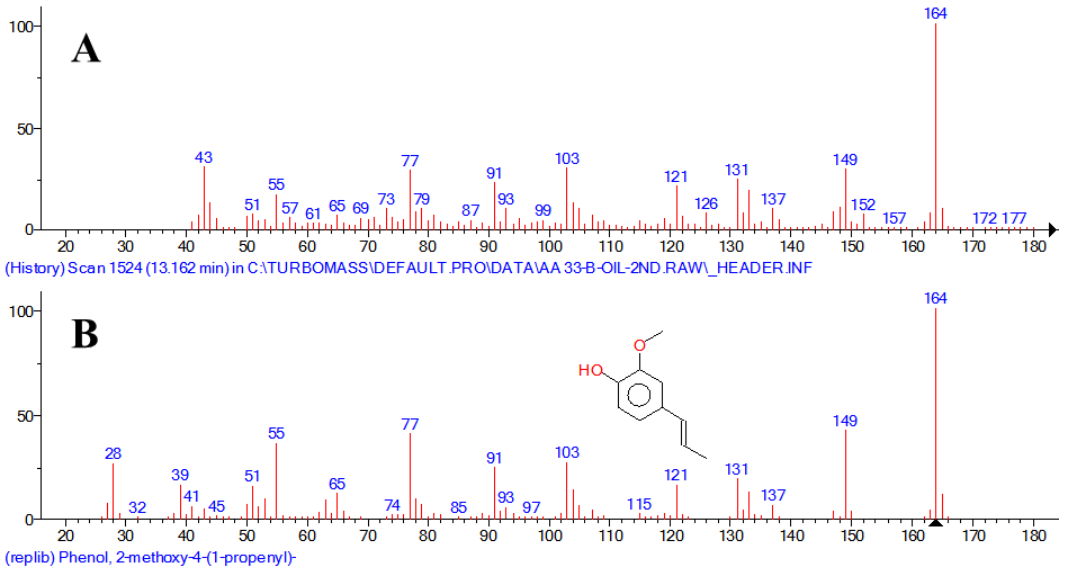

Figure A.80: Matching MS spectrum of peak number 17 MS in 2nd extract of crude bio-oil GC-MS: A) MS of peak number 17 in 2nd extract of crude bio-oil sample; B) MS of Phenol, 2-methoxy-4-(1-propenyl)- according to NIST library database.

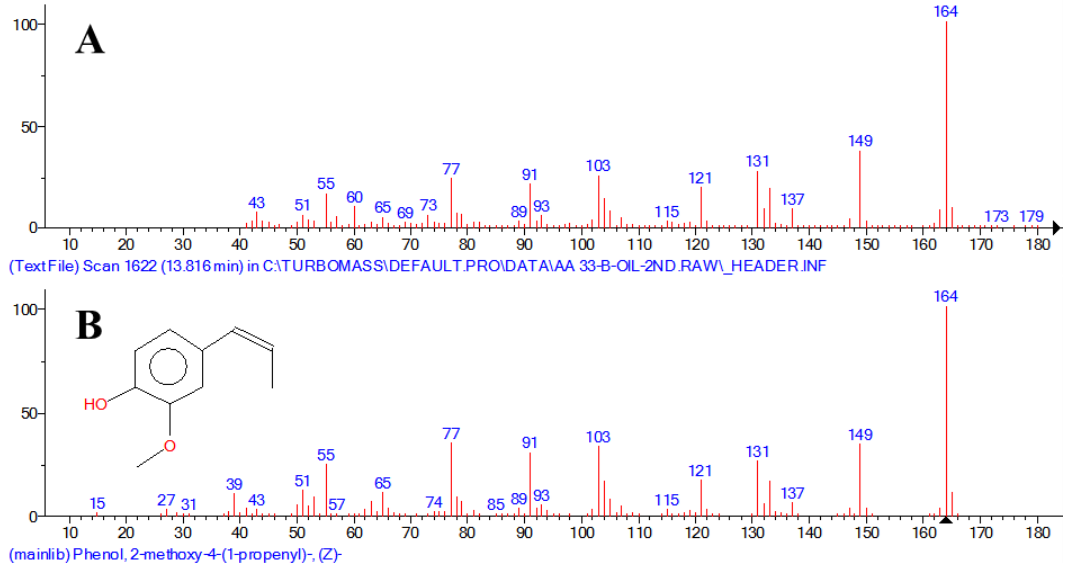

Figure A.81: Matching MS spectrum of peak number 18 MS in 2nd extract of crude bio-oil GC-MS: A) MS of peak number 18 in 2nd extract of crude bio-oil sample; B) MS of Phenol, 2-methoxy-4-(1-propenyl)-, (Z)- according to NIST library database.

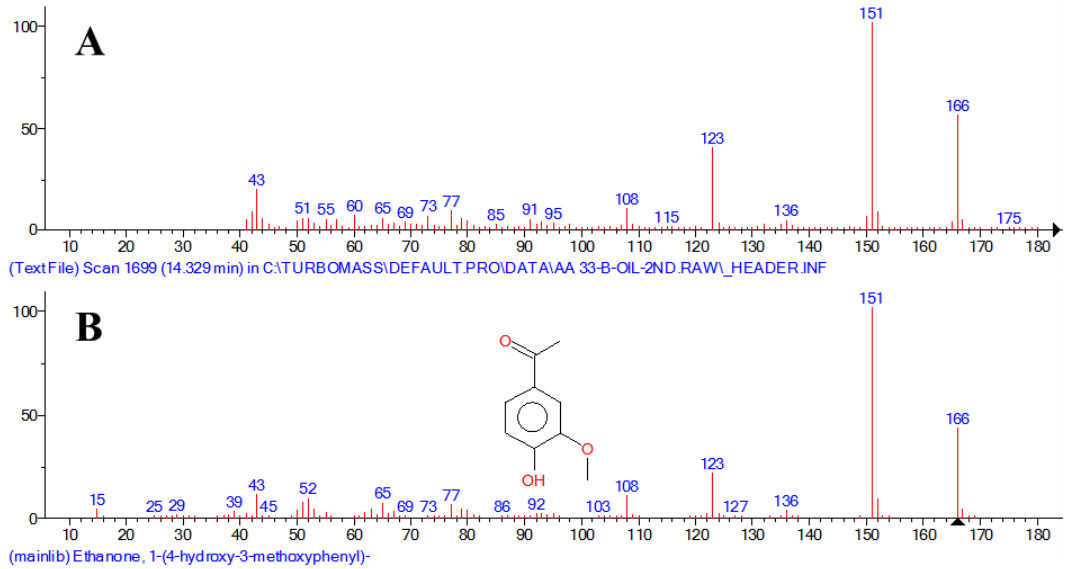

Figure A.82: Matching MS spectrum of peak number 20 MS in 2nd extract of crude bio-oil GC-MS: A) MS of peak number 20 in 2nd extract of crude bio-oil sample; B) MS of Ethanone, 1-(4-hydroxy-3-methoxyphenyl)- according to NIST library database.

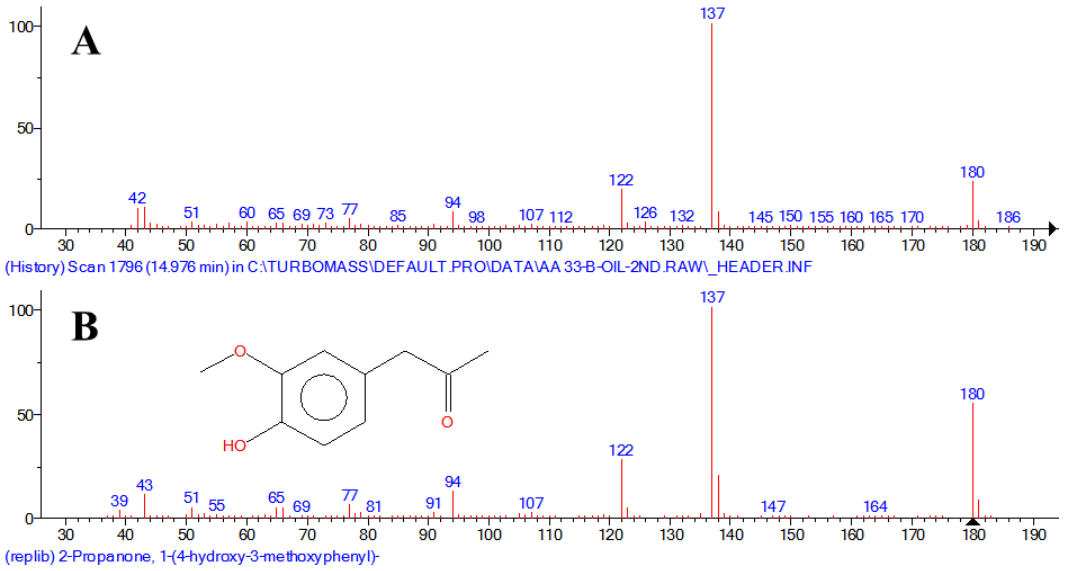

Figure A.83: Matching MS spectrum of peak number 21 MS in 2nd extract of crude bio-oil GC-MS: A) MS of peak number 21 in 2nd extract of crude bio-oil sample; B) MS of 2-Propanone, 1-(4-hydroxy-3-methoxyphenyl)- according to NIST library database.

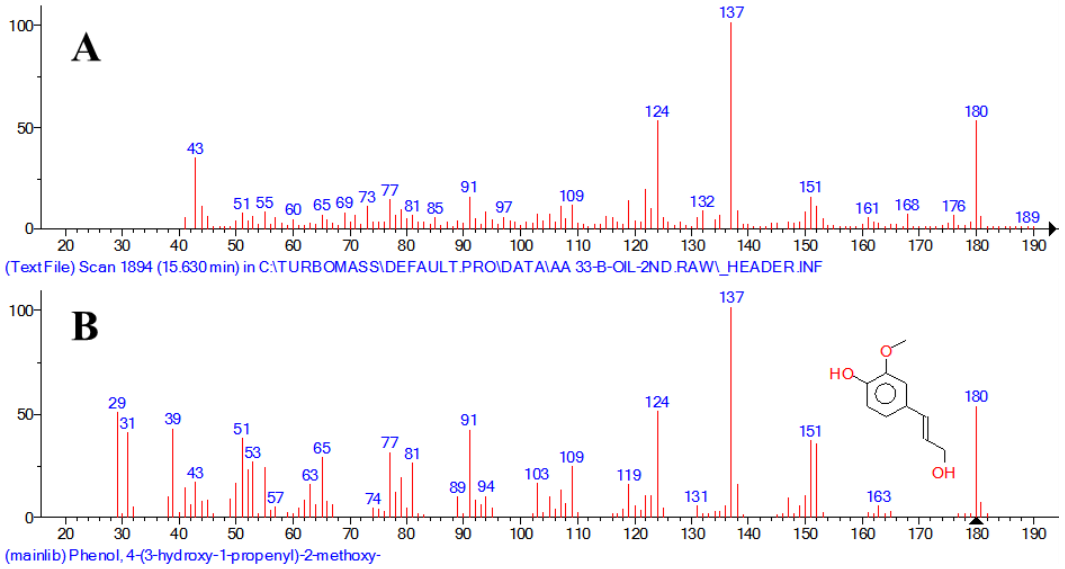

Figure A.84: Matching MS spectrum of peak number 22 MS in 2nd extract of crude bio-oil GC-MS: A) MS of peak number 22 in 2nd extract of crude bio-oil sample; B) MS of Phenol, 4-(3-hydroxy-1-propenyl)-2-methoxy- according to NIST library.

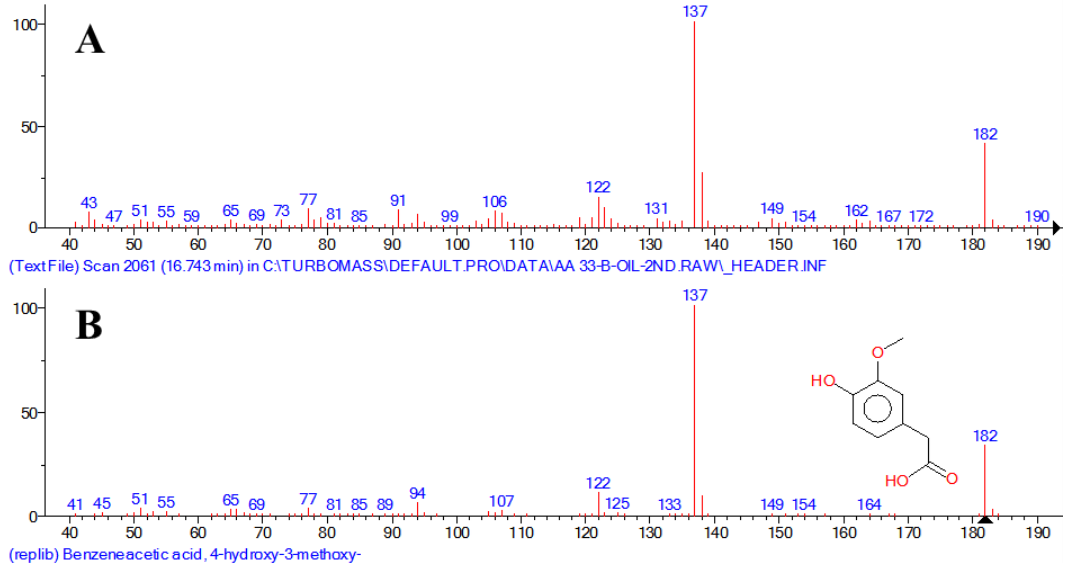

Figure A.85: Matching MS spectrum of peak number 24 MS in 2nd extract of crude bio-oil GC-MS: A) MS of peak number 24 in 2nd extract of crude bio-oil sample; B) MS of Benzeneacetic acid, 4-hydroxy-3-methoxy- according to NIST library.

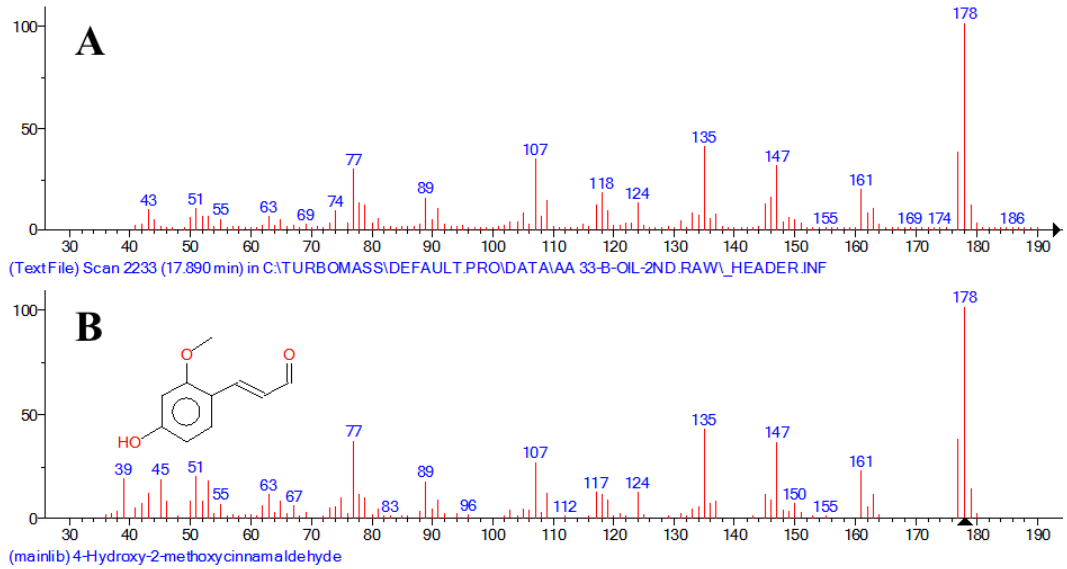

Figure A.86: Matching MS spectrum of peak number 26 MS in 2nd extract of crude bio-oil GC-MS: A) MS of peak number 26 in 2nd extract of crude bio-oil sample; B) MS of 4-Hydroxy-2-methoxycinnamaldehyde according to NIST library.

A.3 Mass Spectra of Identified Phenolic Peaks in Water-Insoluble Phase Fractionation Experiment

A.3.1 Mass spectra of identified phenolic peaks in 2nd extract of crude bio-oil and their best NIST library match

The mass spectra are the same as A.2.2.

A.3.2 Mass spectra of identified phenolic peaks in water-soluble extract and their best NIST library match

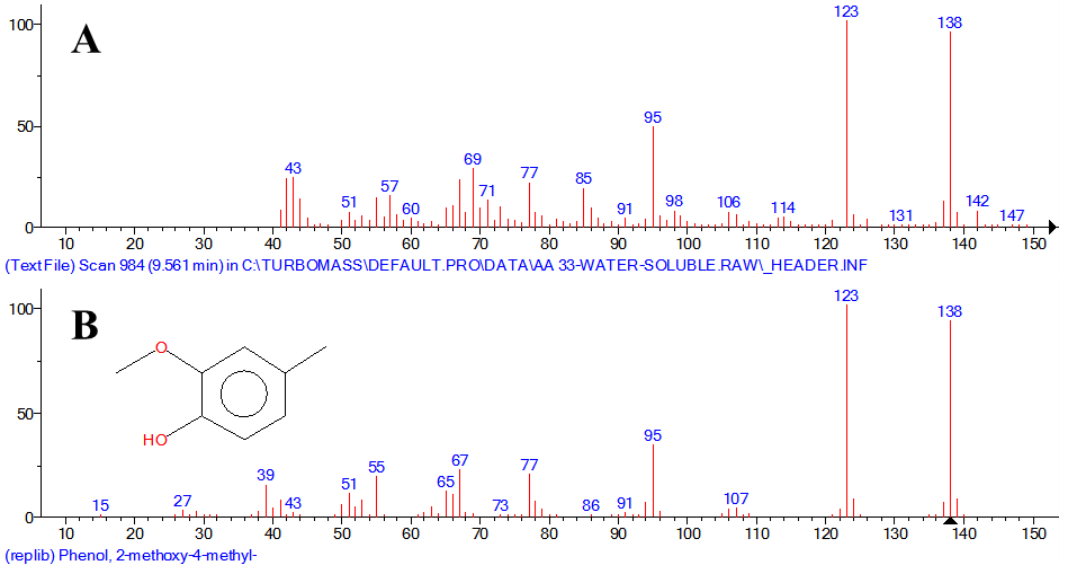

Figure A.87: Matching MS spectrum of peak number 7 MS in water-soluble extract GC-MS: A) MS of peak number 7 in water-soluble extract sample; B) MS of Phenol, 2-methoxy-4-methyl- according to NIST library.

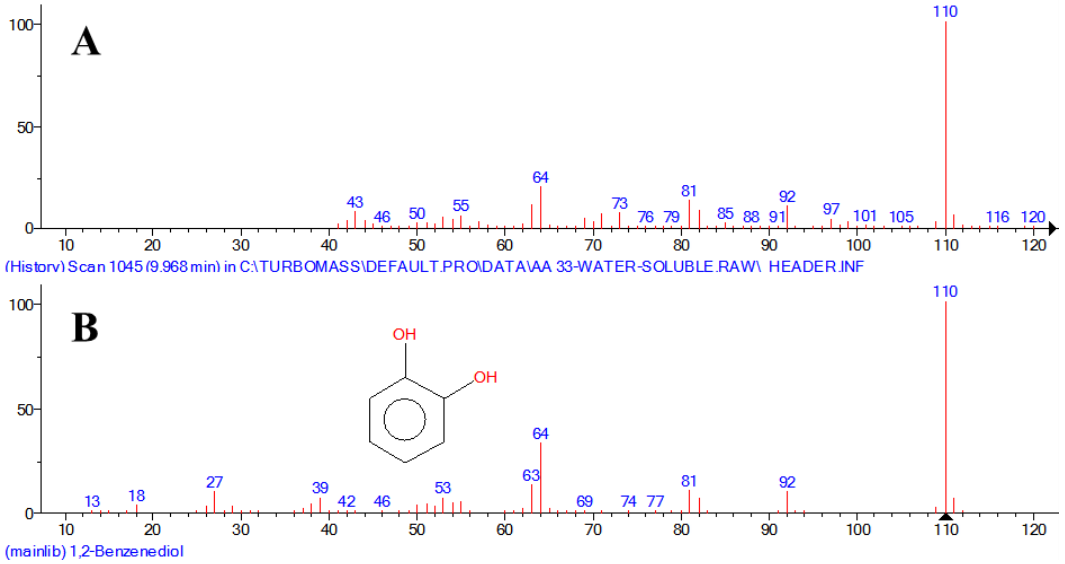

Figure A.88: Matching MS spectrum of peak number 8 MS in water-soluble extract GC-MS: A) MS of peak number 8 in water-soluble extract sample; B) MS of 1,2-Benzenediol according to NIST library.

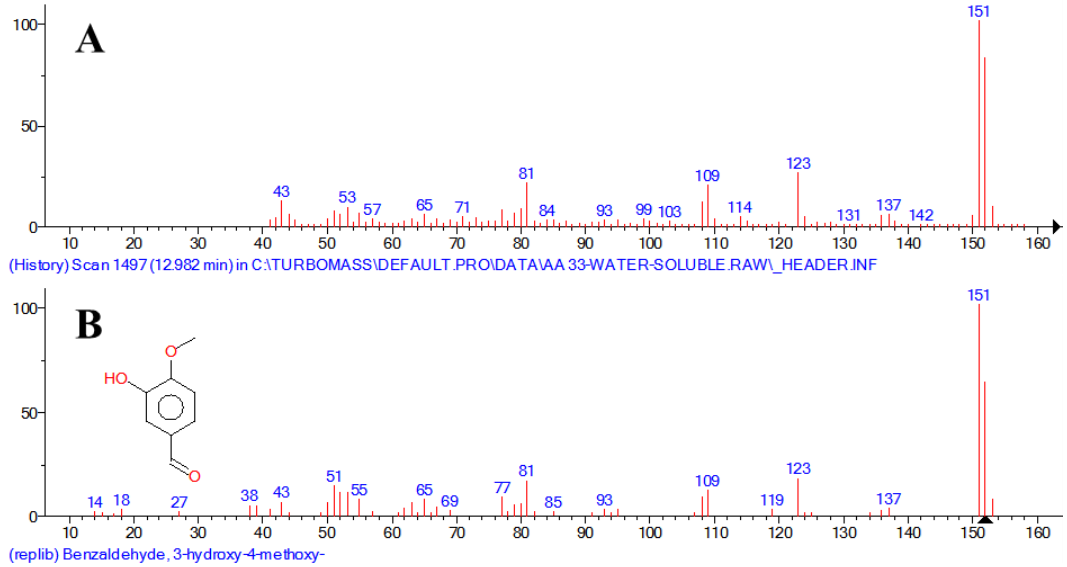

Figure A.89: Matching MS spectrum of peak number 16 MS in water-soluble extract GC-MS: A) MS of peak number 16 in water-soluble extract sample; B) MS of Benzaldehyde, 3-hydroxy-4-methoxy- according to NIST library.

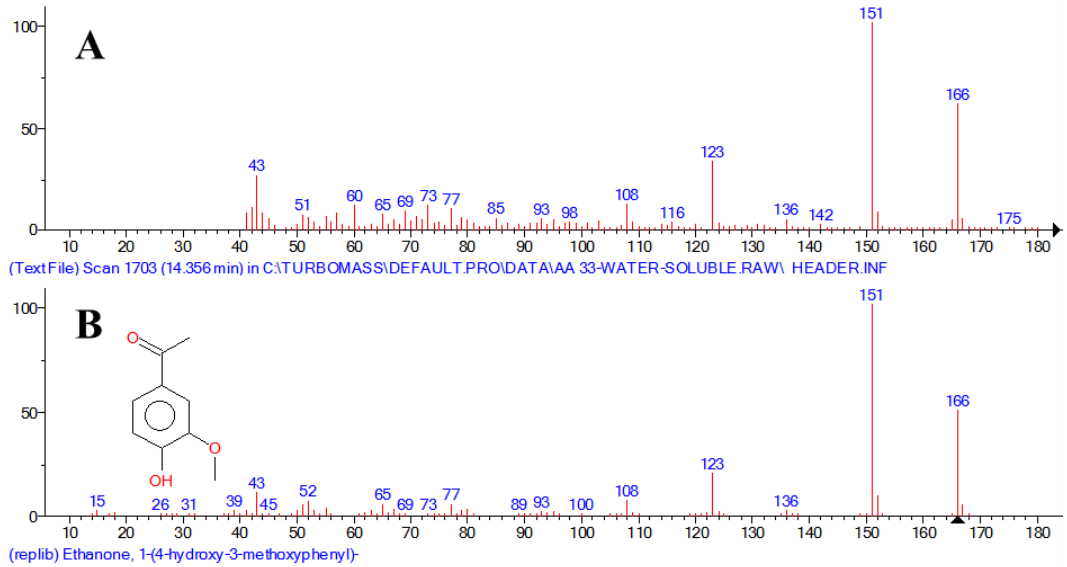

Figure A.90: Matching MS spectrum of peak number 20 MS in water-soluble extract GC-MS: A) MS of peak number 20 in water-soluble extract sample; B) MS of Ethanone, 1-(4-hydroxy-3-methoxyphenyl)- according to NIST library.

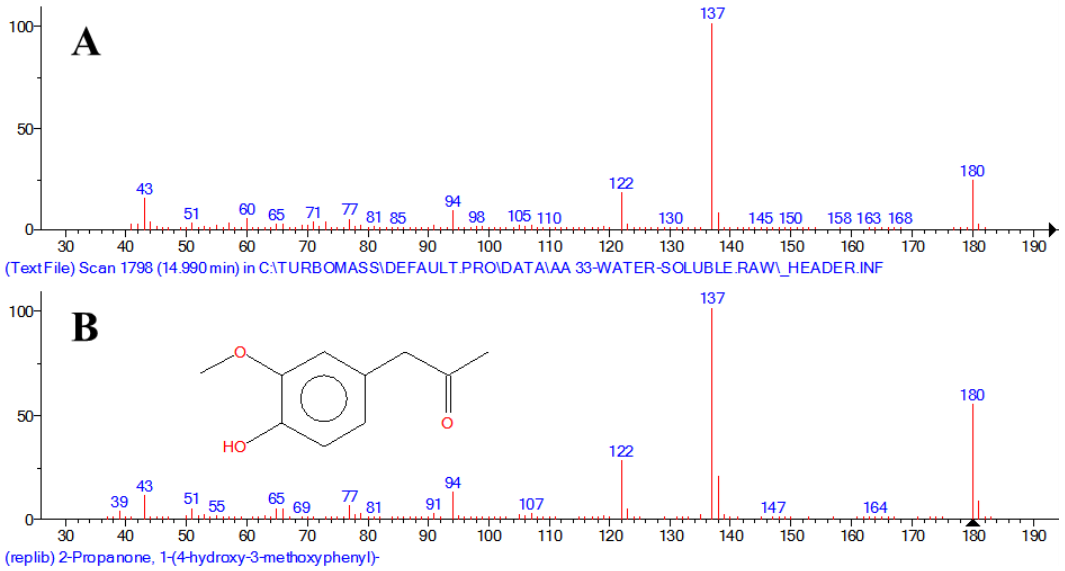

Figure A.91: Matching MS spectrum of peak number 21 MS in water-soluble extract GC-MS: A) MS of peak number 21 in water-soluble extract sample; B) MS of 2-Propanone, 1-(4-hydroxy-3-methoxyphenyl)- according to NIST library.

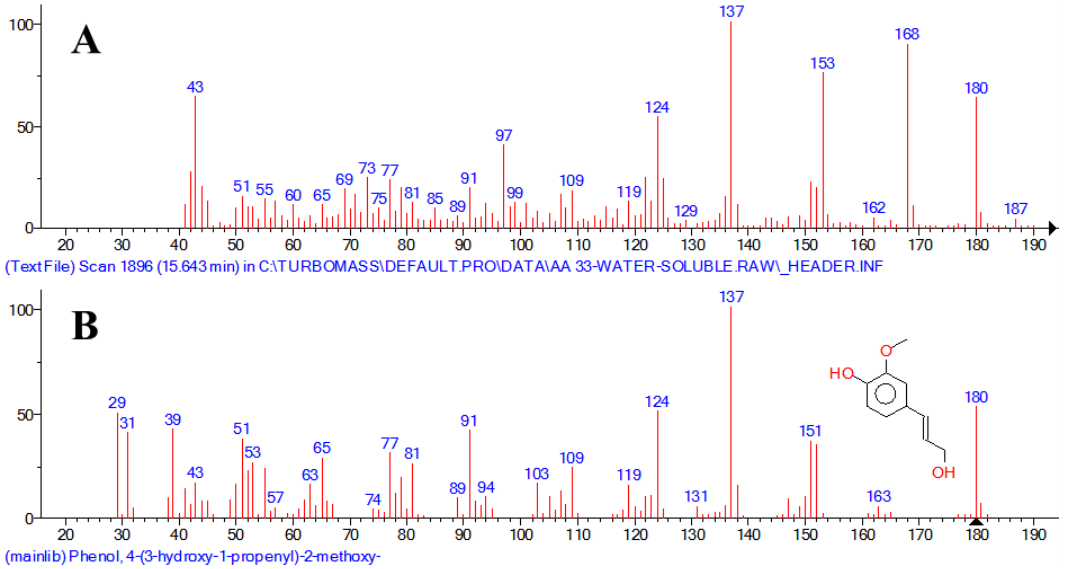

Figure A.92: Matching MS spectrum of peak number 22 MS in water-soluble extract GC-MS: A) MS of peak number 22 in water-soluble extract sample; B) MS of Phenol, 4-(3-hydroxy-1-propenyl)-2-methoxy- according to NIST library.

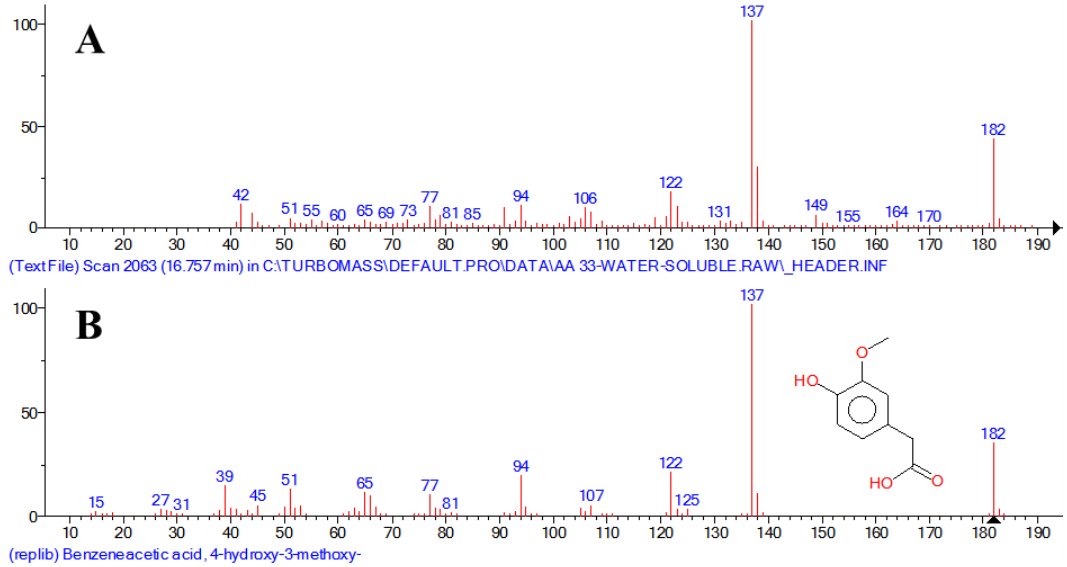

Figure A.93: Matching MS spectrum of peak number 24 MS in water-soluble extract GC-MS: A) MS of peak number 24 in water-soluble extract sample; B) MS of Benzeneacetic acid, 4-hydroxy-3-methoxy- according to NIST library.

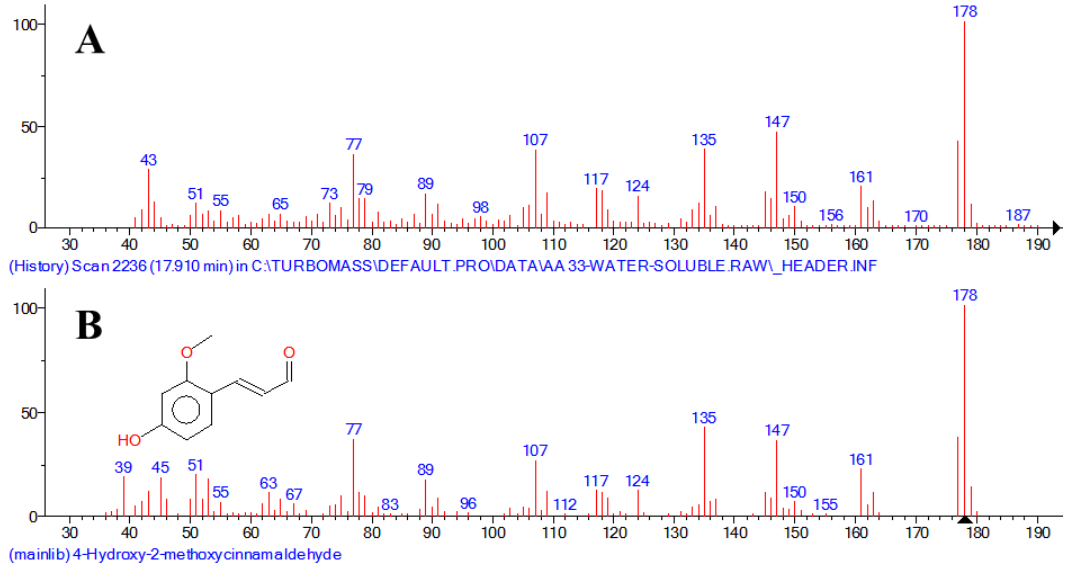

Figure A.94: Matching MS spectrum of peak number 26 MS in water-soluble extract GC-MS: A) MS of peak number 26 in water-soluble extract sample; B) MS of 4-Hydroxy-2-methoxycinnamaldehyde according to NIST library.

A.3.3 Mass spectra of identified phenolic peaks in neutral extract and their best NIST library match

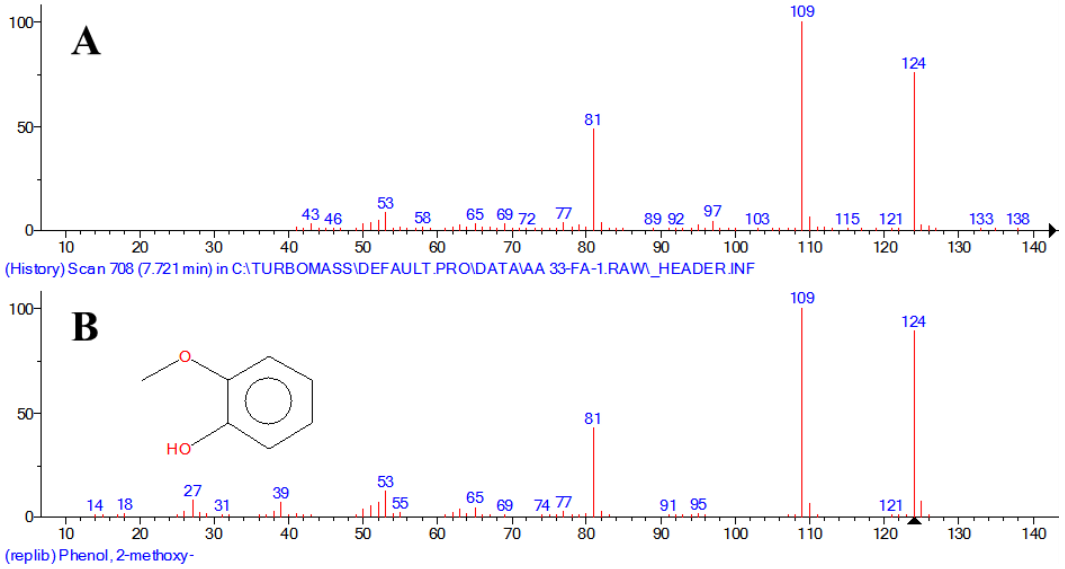

Figure A.95: Matching MS spectrum of peak number 4 MS in neutral extract GC-MS: A) MS of peak number 4 in neutral extract sample; B) MS of Phenol, 2-methoxy- according to NIST library.

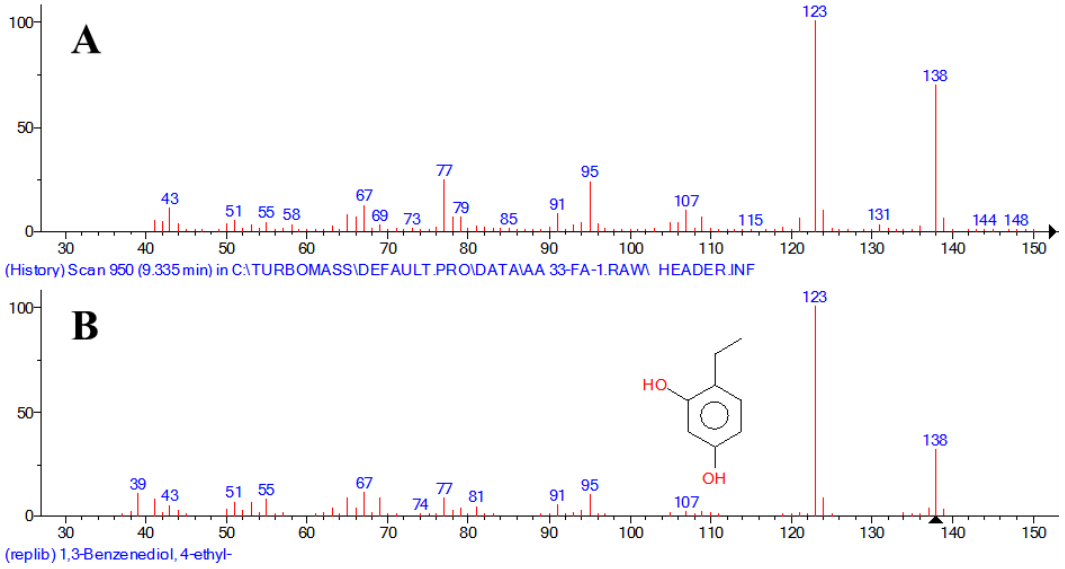

Figure A.96: Matching MS spectrum of peak number 6 MS in neutral extract GC-MS: A) MS of peak number 6 in neutral extract sample; B) MS of 1,3-Benzenediol, 4-ethyl- according to NIST library.

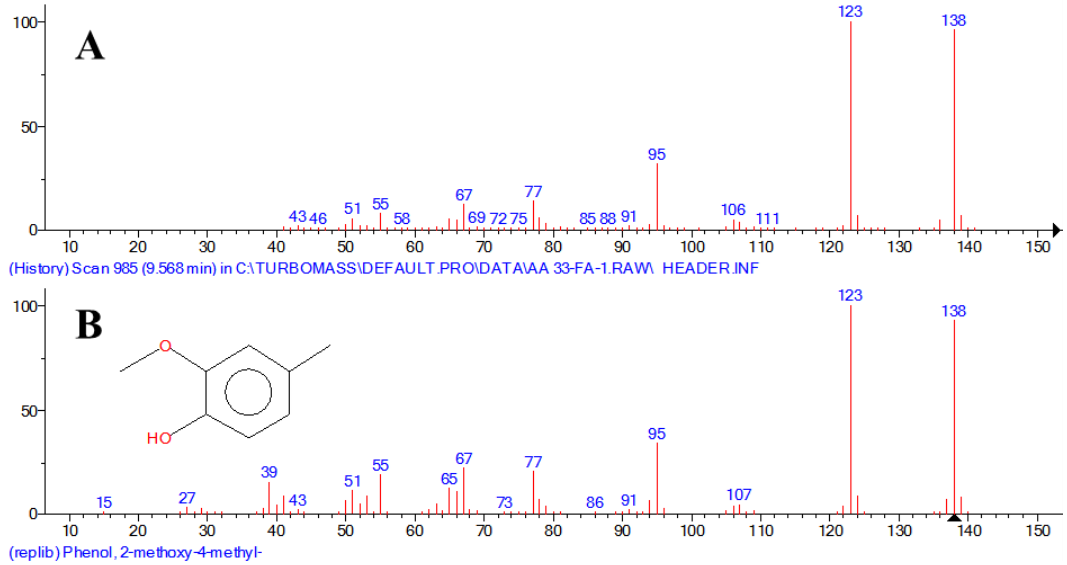

Figure A.97: Matching MS spectrum of peak number 7 MS in neutral extract GC-MS: A) MS of peak number 7 in neutral extract sample; B) MS of Phenol, 2-methoxy-4-methyl- according to NIST library.

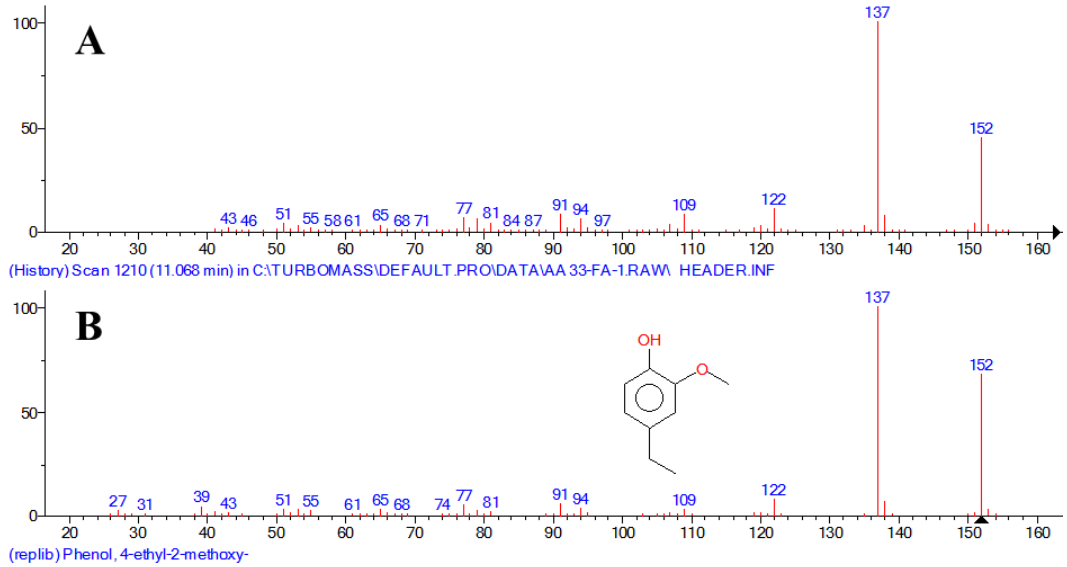

Figure A.98: Matching MS spectrum of peak number 10 MS in neutral extract GC-MS: A) MS of peak number 10 in neutral extract sample; B) MS of Phenol, 4-ethyl-2-methoxy- according to NIST library.

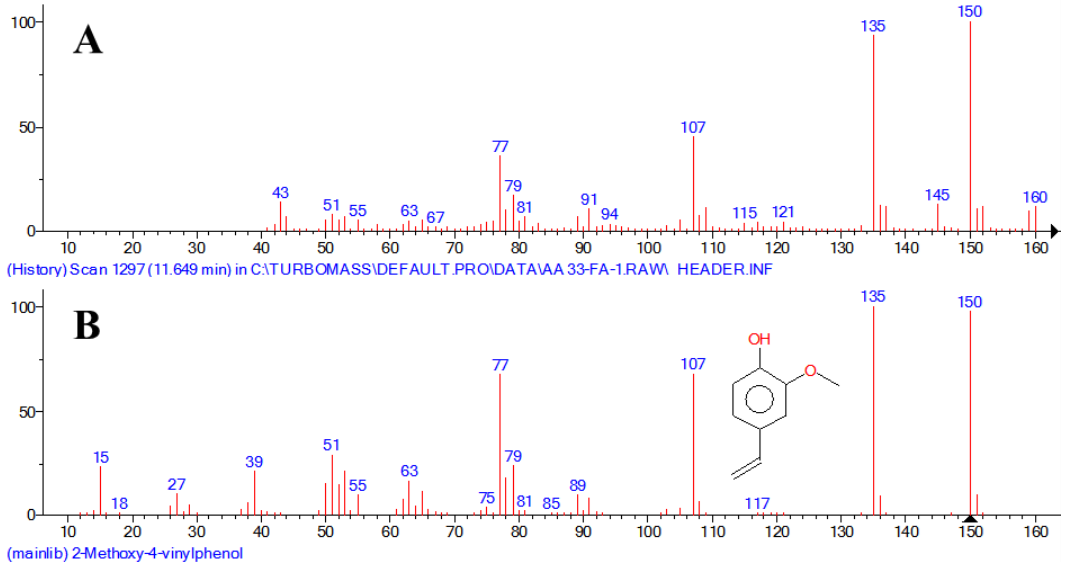

Figure A.99: Matching MS spectrum of peak number 12 MS in neutral extract GC-MS: A) MS of peak number 12 in neutral extract sample; B) MS of 2-Methoxy-4-vinylphenol according to NIST library.

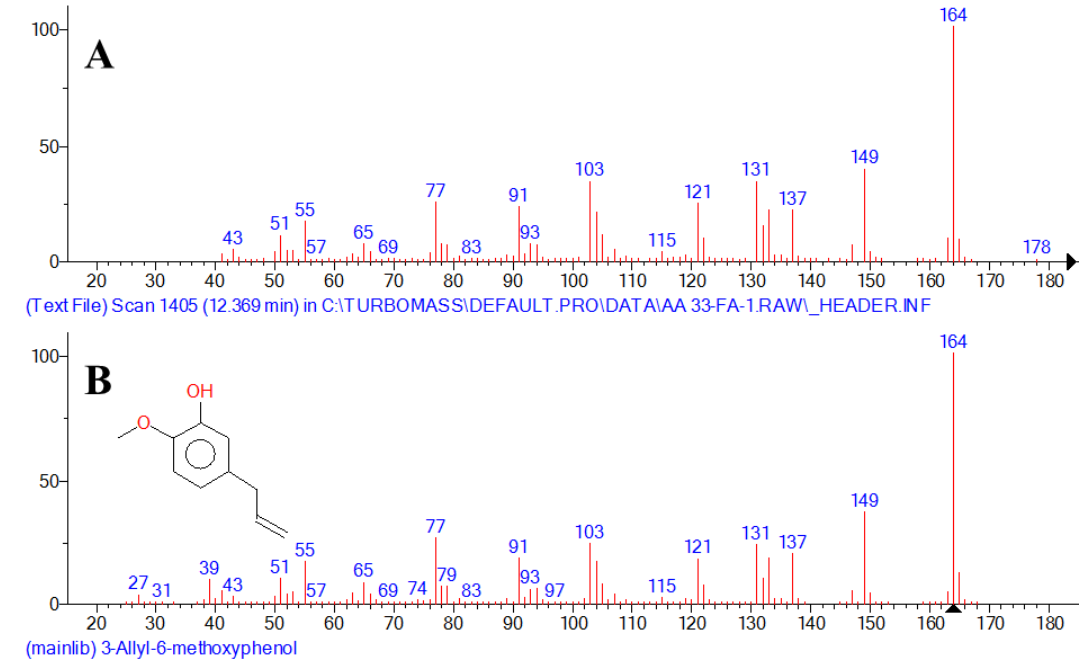

Figure A.100: Matching MS spectrum of peak number 14 MS in neutral extract GC-MS: A) MS of peak number 14 in neutral extract sample; B) MS of 3-Allyl-6-methoxyphenol according to NIST library.

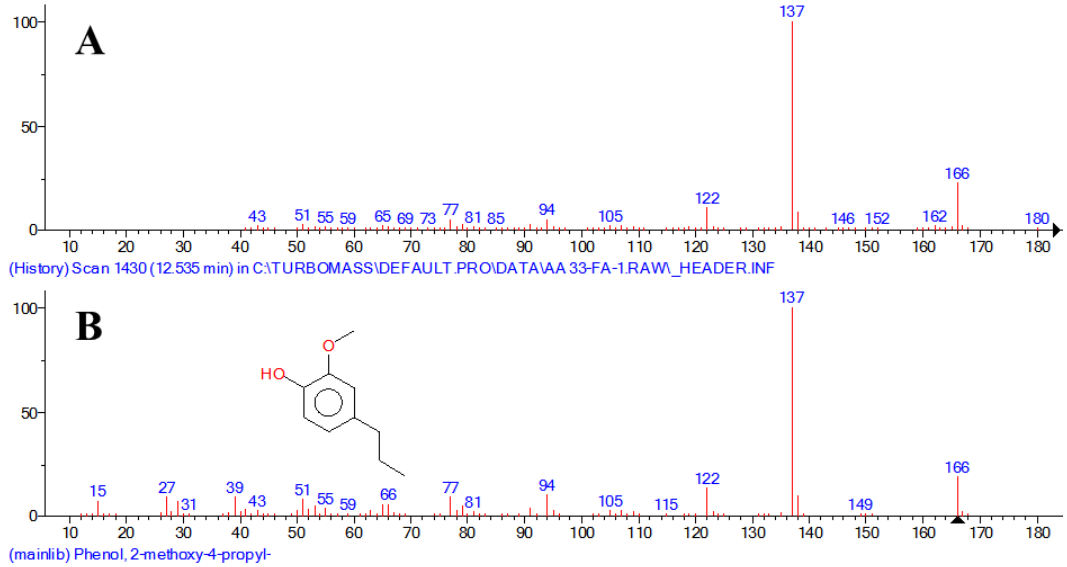

Figure A.101: Matching MS spectrum of peak number 15 MS in neutral extract GC-MS: A) MS of peak number 15 in neutral extract sample; B) MS of Phenol, 2-methoxy-4-propyl- according to NIST library.

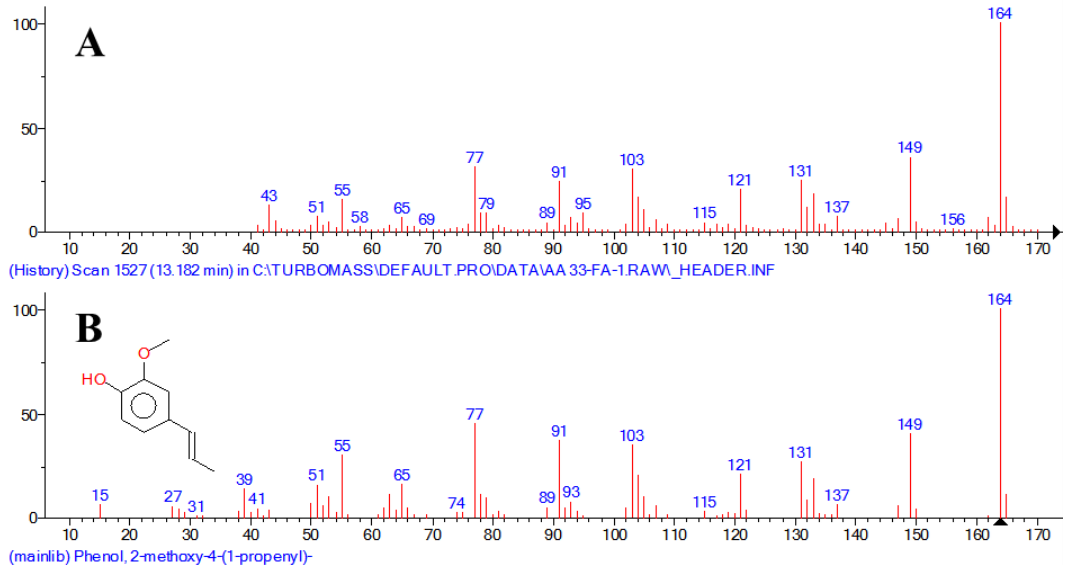

Figure A.102: Matching MS spectrum of peak number 17 MS in neutral extract GC-MS: A) MS of peak number 17 in neutral extract sample; B) MS of Phenol, 2-methoxy-4-(1-propenyl)- according to NIST library.

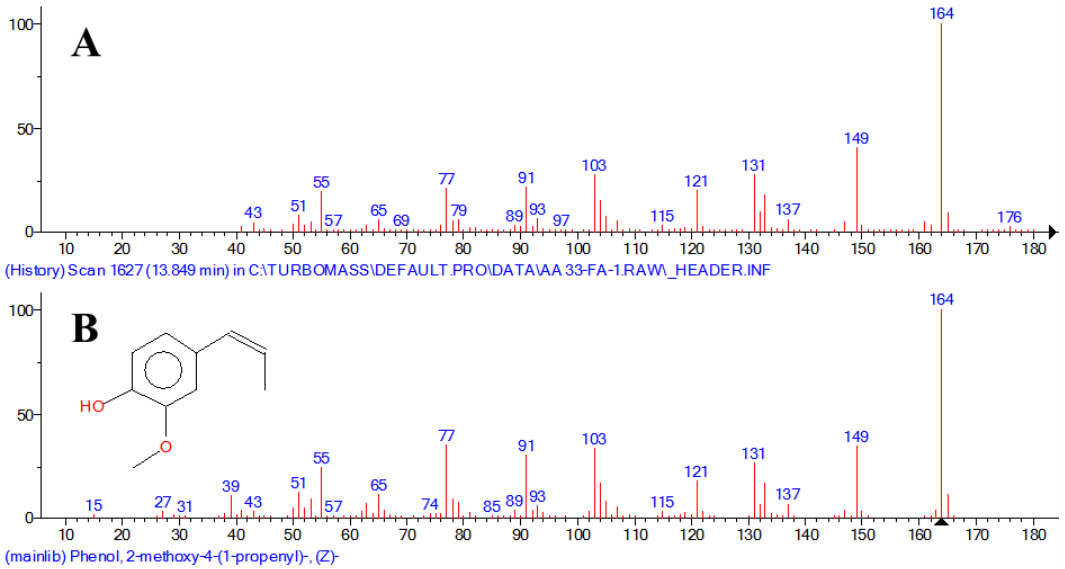

Figure A.103: Matching MS spectrum of peak number 18 MS in neutral extract GC-MS: A) MS of peak number 18 in neutral extract sample; B) MS of Phenol, 2-methoxy-4-(1-propenyl)-, (Z)- according to NIST library.

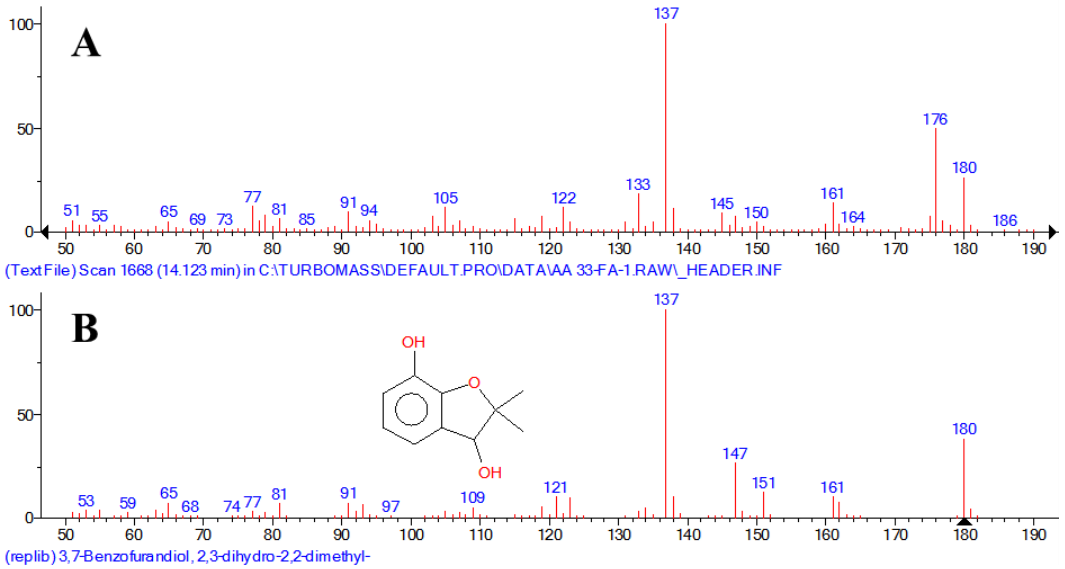

Figure A.104: Matching MS spectrum of peak number 19 MS in neutral extract GC-MS: A) MS of peak number 19 in neutral extract sample; B) MS of 3,7-Benzofurandiol, 2,3-dihydro-2,2-dimethyl- according to NIST library.

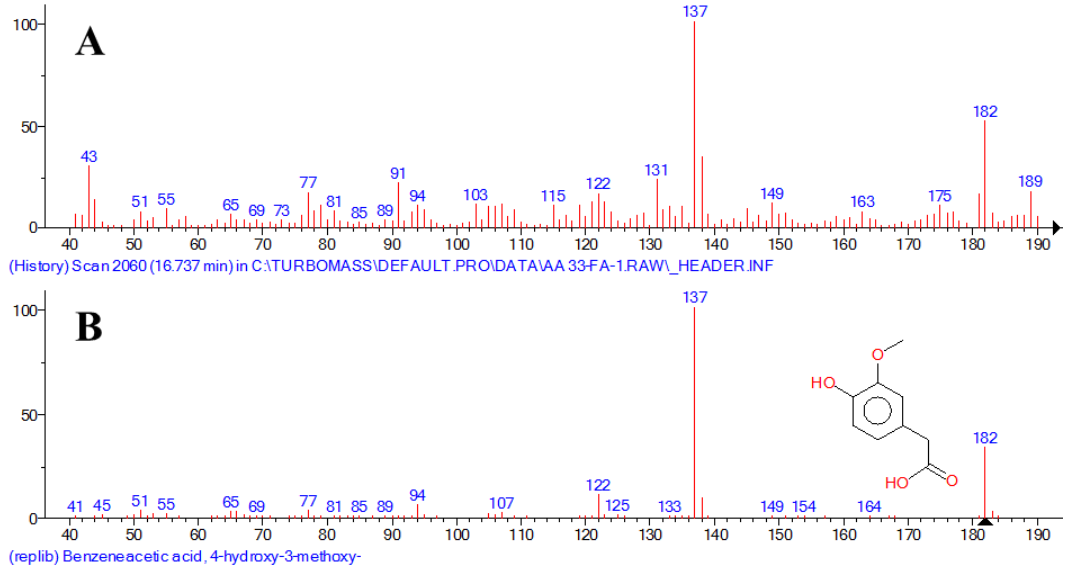

Figure A.105: Matching MS spectrum of peak number 24 MS in neutral extract GC-MS: A) MS of peak number 24 in neutral extract sample; B) MS of Benzeneacetic acid, 4-hydroxy-3-methoxy- according to NIST library.

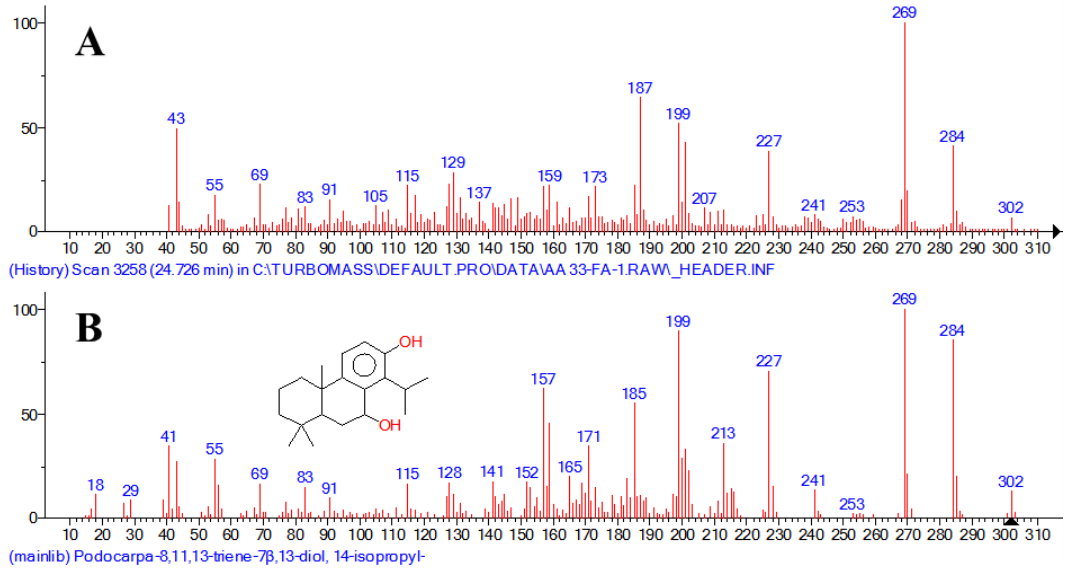

Figure A.106: Matching MS spectrum of peak number 31 MS in neutral extract GC-MS: A) MS of peak number 31 in neutral extract sample; B) MS of Podocarpa-8,11,13-triene-7β,13-diol, 14-isopropyl- according to NIST library.

A.3.4 Mass spectra of identified phenolic peaks in phenolic extract and their best NIST library match

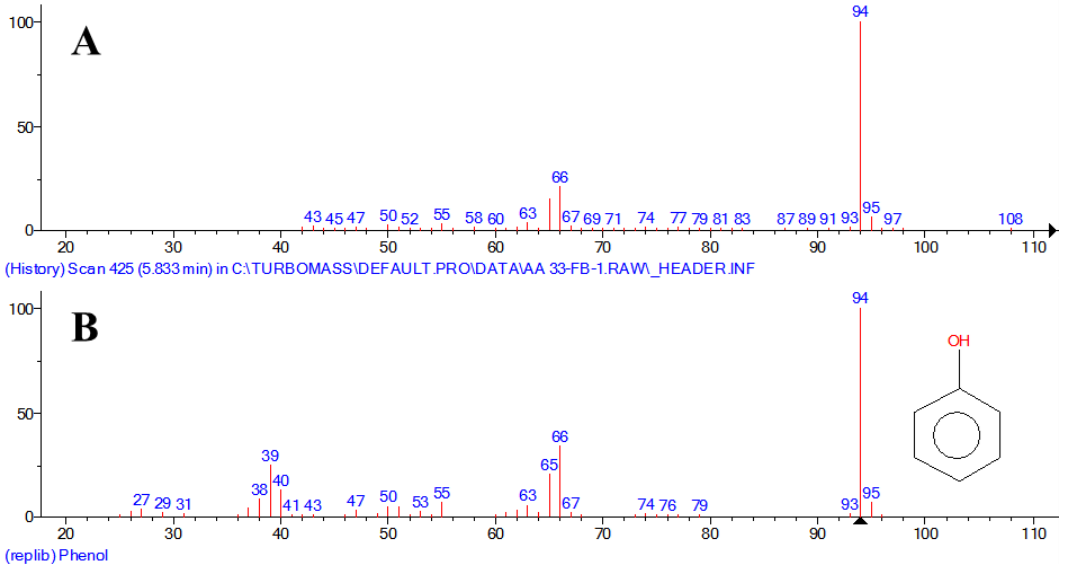

Figure A.107: Matching MS spectrum of peak number 1 MS in phenolic extract GC-MS: A) MS of peak number 1 in phenolic extract sample; B) MS of Phenol according to NIST library.

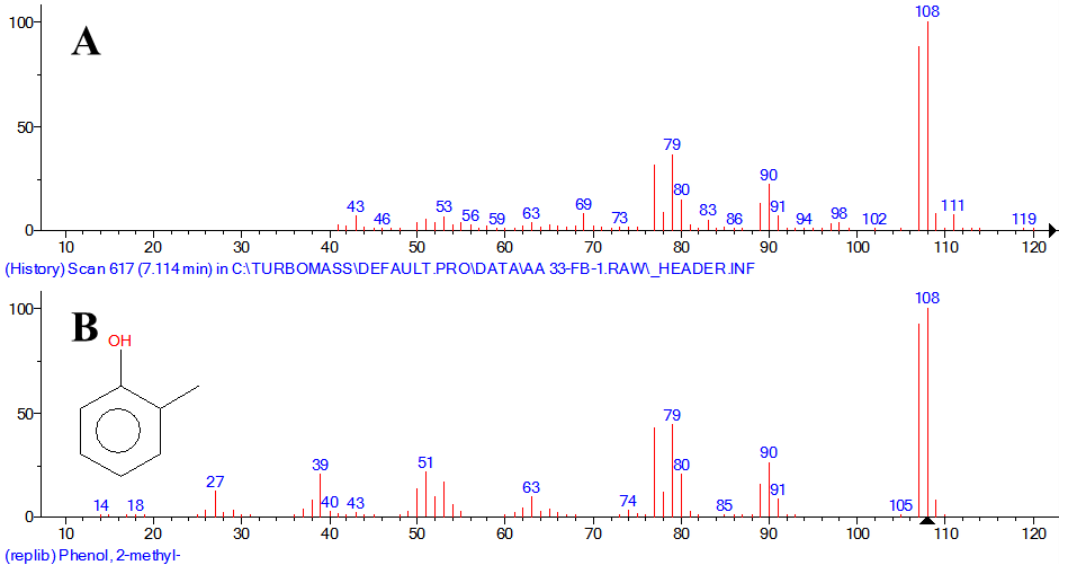

Figure A.108: Matching MS spectrum of peak number 2 MS in phenolic extract GC-MS: A) MS of peak number 2 in phenolic extract sample; B) MS of Phenol, 2-methyl- according to NIST library.

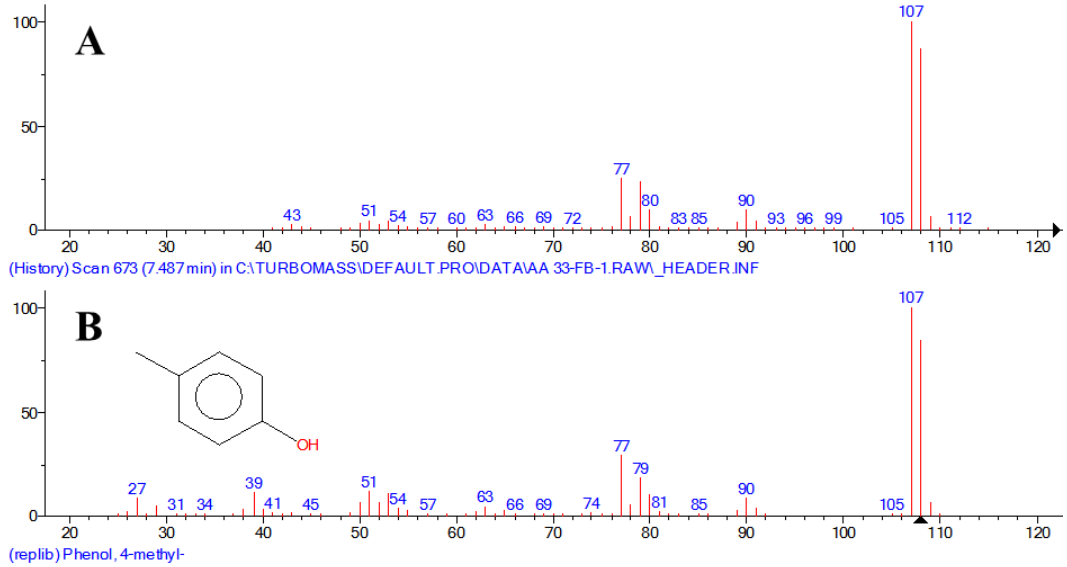

Figure A.109: Matching MS spectrum of peak number 3 MS in phenolic extract GC-MS: A) MS of peak number 3 in phenolic extract sample; B) MS of Phenol, 4-methyl- according to NIST library.

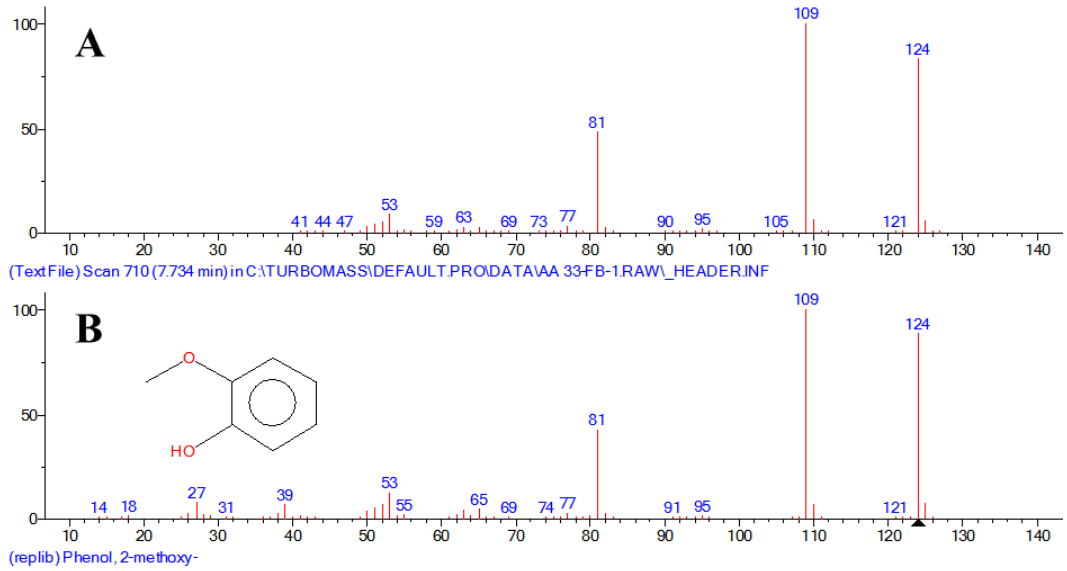

Figure A.110: Matching MS spectrum of peak number 4 MS in phenolic extract GC-MS: A) MS of peak number 4 in phenolic extract sample; B) MS of Phenol, 2-methoxy- according to NIST library.

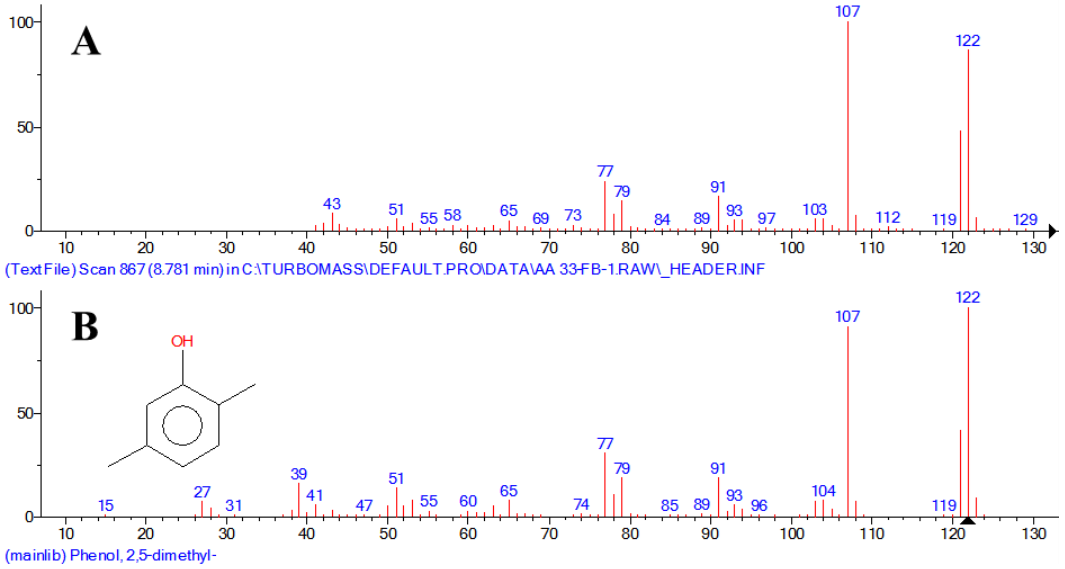

Figure A.111: Matching MS spectrum of peak number 5 MS in phenolic extract GC-MS: A) MS of peak number 5 in phenolic extract sample; B) MS of Phenol, 2,5-dimethyl- according to NIST library.

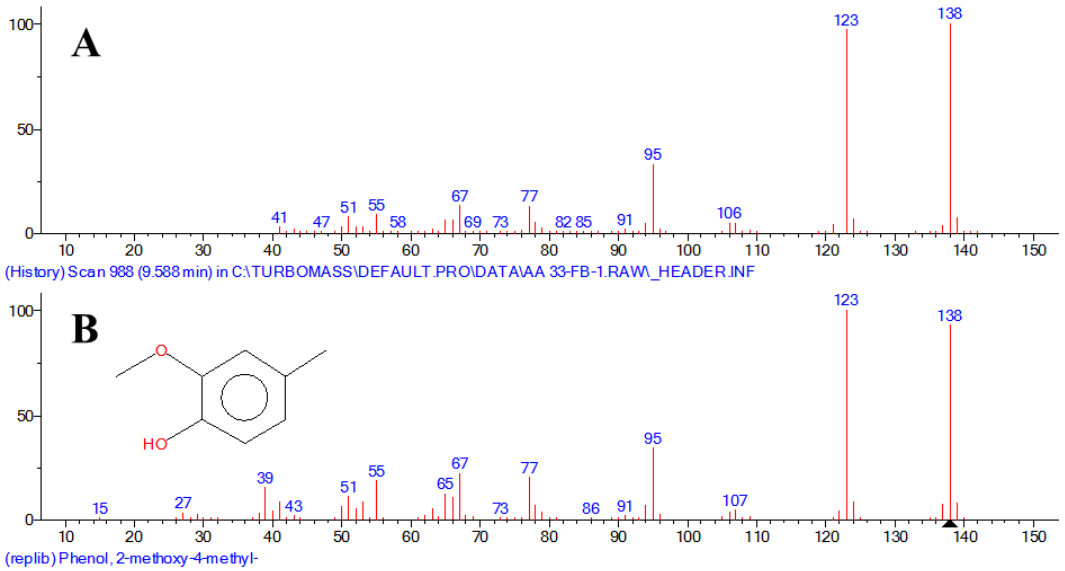

Figure A.112: Matching MS spectrum of peak number 7 MS in phenolic extract GC-MS: A) MS of peak number 7 in phenolic extract sample; B) MS of Phenol, 2-methoxy-4-methyl- according to NIST library.

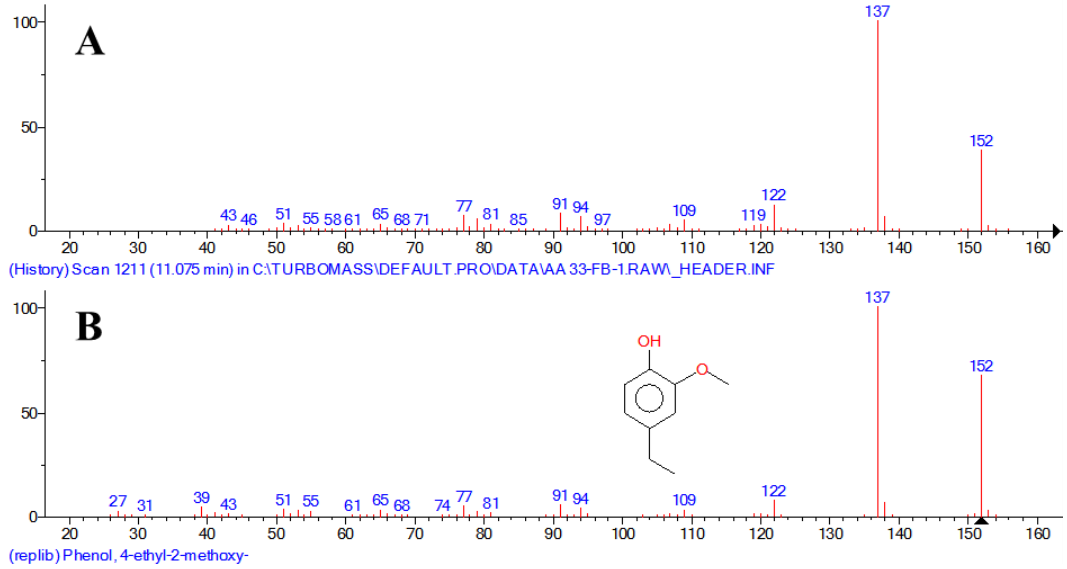

Figure A.113: Matching MS spectrum of peak number 10 MS in phenolic extract GC-MS: A) MS of peak number 10 in phenolic extract sample; B) MS of Phenol, 4-ethyl-2-methoxy- according to NIST library.

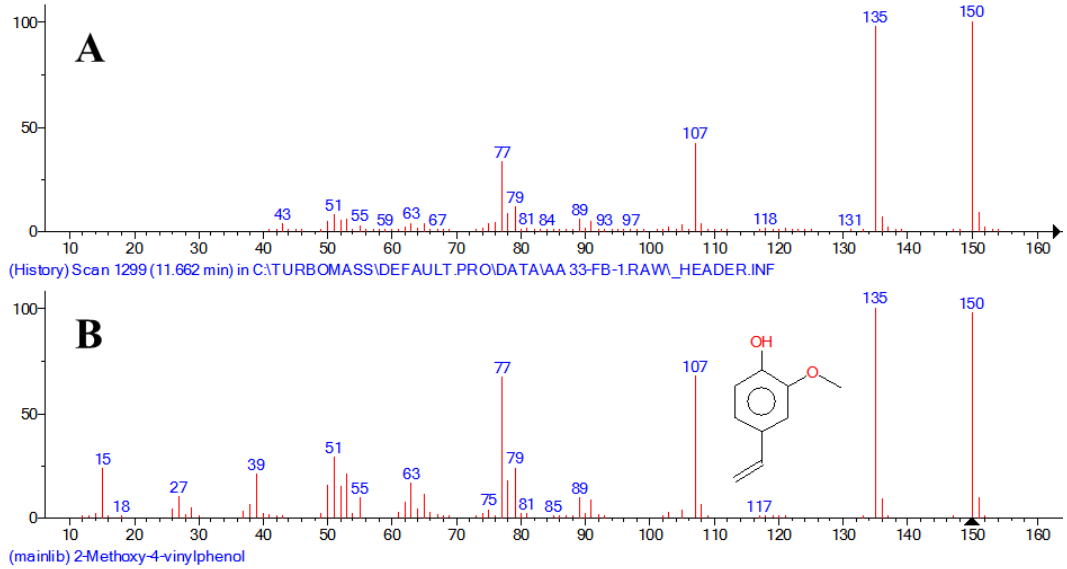

Figure A.114: Matching MS spectrum of peak number 12 MS in phenolic extract GC-MS: A) MS of peak number 12 in phenolic extract sample; B) MS of 2-Methoxy-4-vinylphenol according to NIST library.

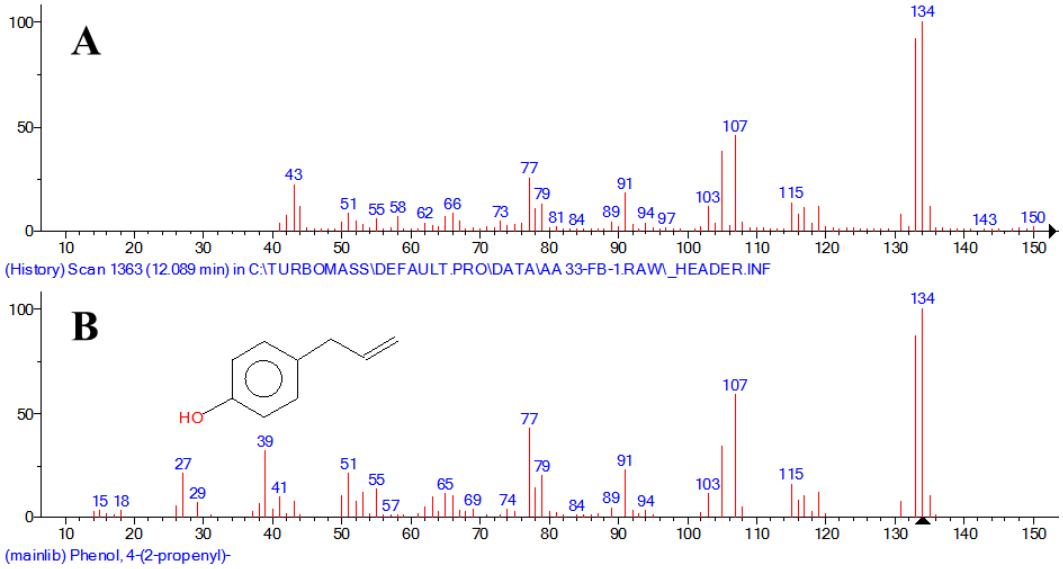

Figure A.115: Matching MS spectrum of peak number 13 MS in phenolic extract GC-MS: A) MS of peak number 13 in phenolic extract sample; B) MS of Phenol, 4-(2-propenyl)- according to NIST library.

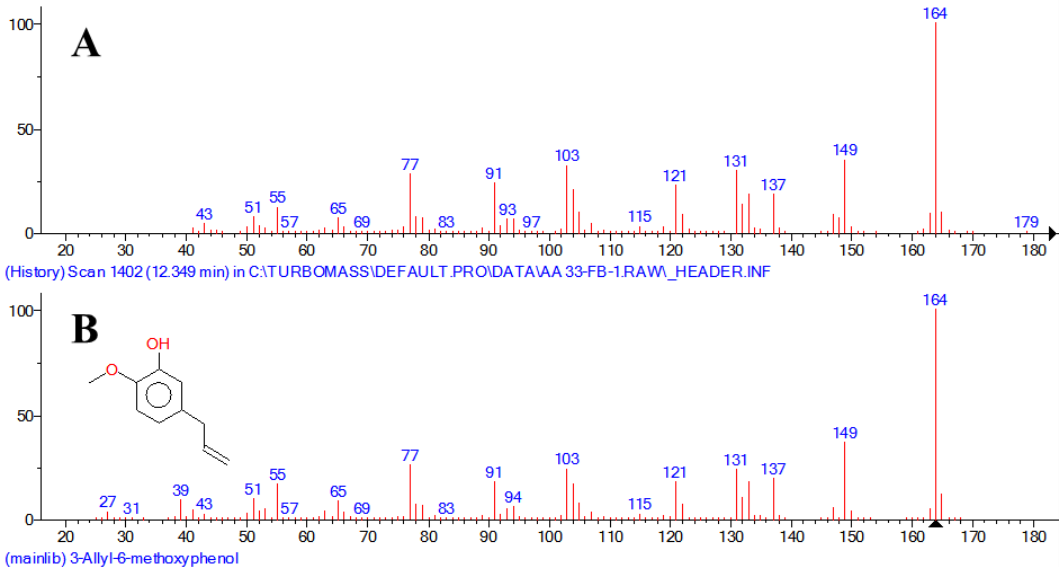

Figure A.116: Matching MS spectrum of peak number 14 MS in phenolic extract GC-MS: A) MS of peak number 14 in phenolic extract sample; B) MS of 3-Allyl-6-methoxyphenol according to NIST library.

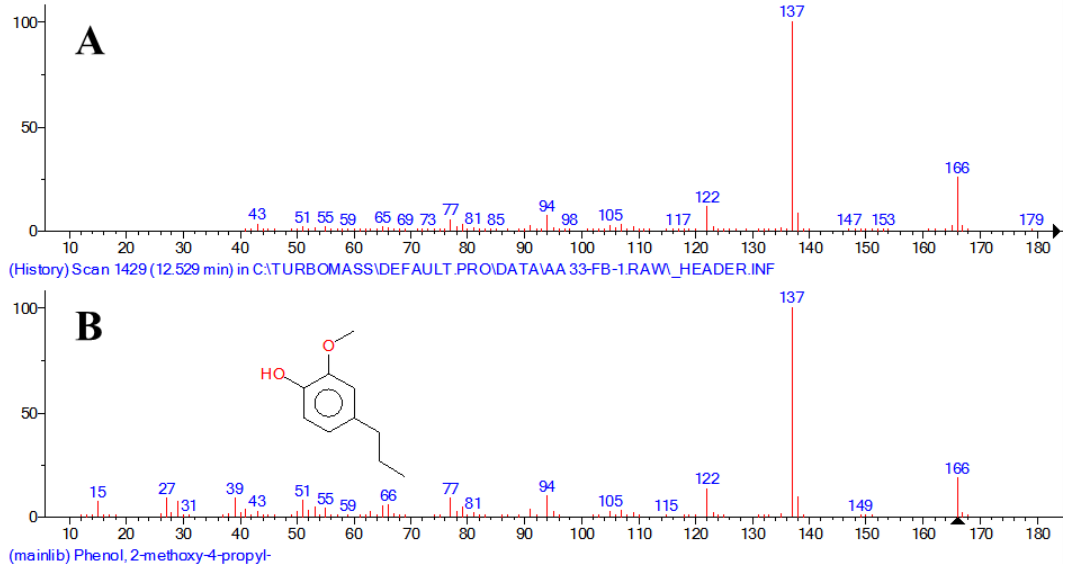

Figure A.117: Matching MS spectrum of peak number 15 MS in phenolic extract GC-MS: A) MS of peak number 15 in phenolic extract sample; B) MS of Phenol, 2-methoxy-4-propyl- according to NIST library.

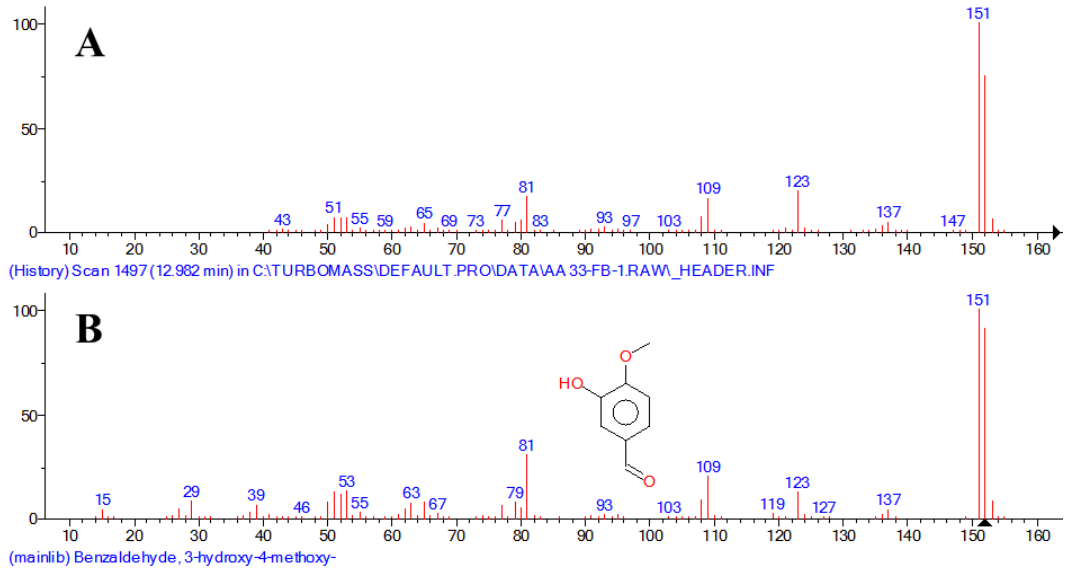

Figure A.118: Matching MS spectrum of peak number 16 MS in phenolic extract GC-MS: A) MS of peak number 16 in phenolic extract sample; B) MS of Benzaldehyde, 3-hydroxy-4-methoxy- according to NIST library.

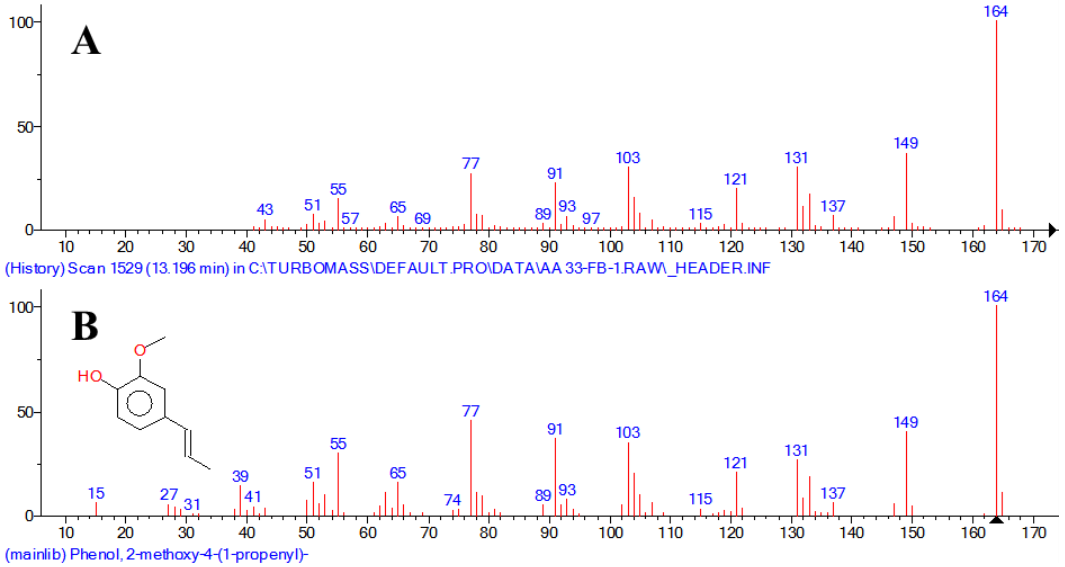

Figure A.119: Matching MS spectrum of peak number 17 MS in phenolic extract GC-MS: A) MS of peak number 17 in phenolic extract sample; B) MS of Phenol, 2-methoxy-4-(1-propenyl)- according to NIST library.

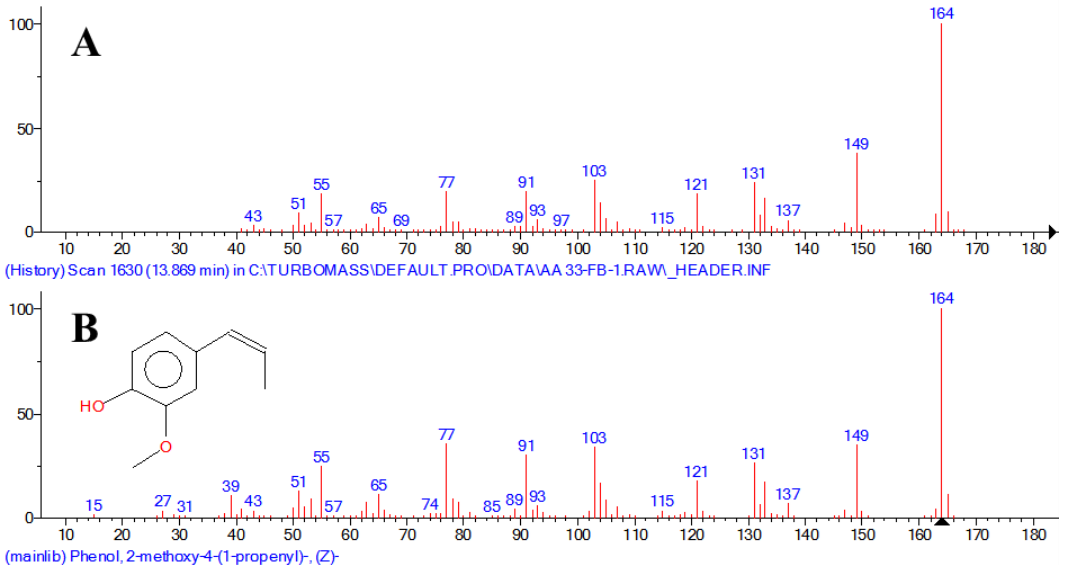

Figure A.120: Matching MS spectrum of peak number 18 MS in phenolic extract GC-MS: A) MS of peak number 18 in phenolic extract sample; B) MS of Phenol, 2-methoxy-4-(1-propenyl)-, (Z)- according to NIST library.

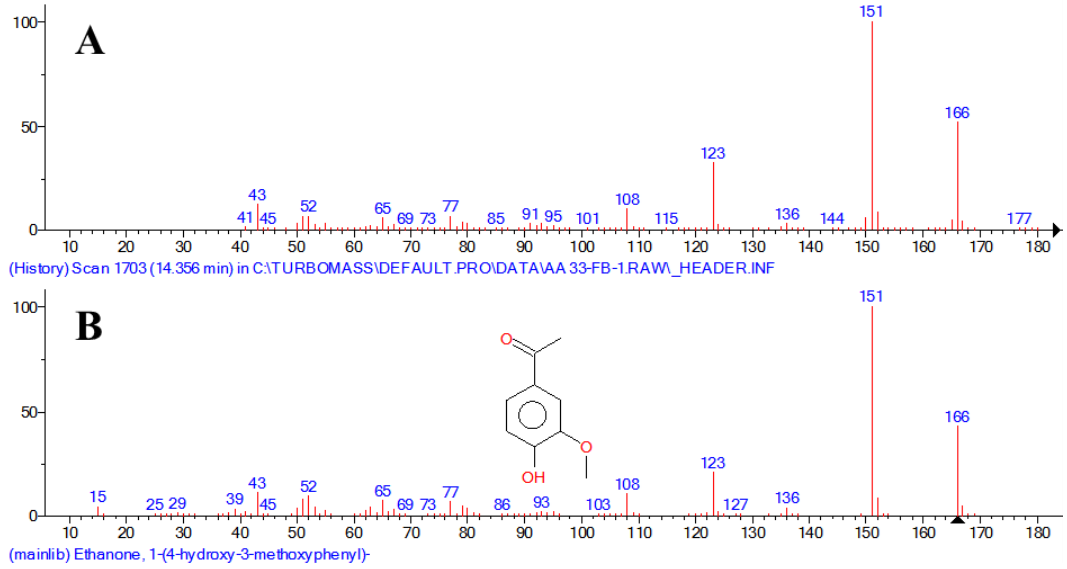

Figure A.121: Matching MS spectrum of peak number 20 MS in phenolic extract GC-MS: A) MS of peak number 20 in phenolic extract sample; B) MS of Ethanone, 1-(4-hydroxy-3-methoxyphenyl)- according to NIST library.

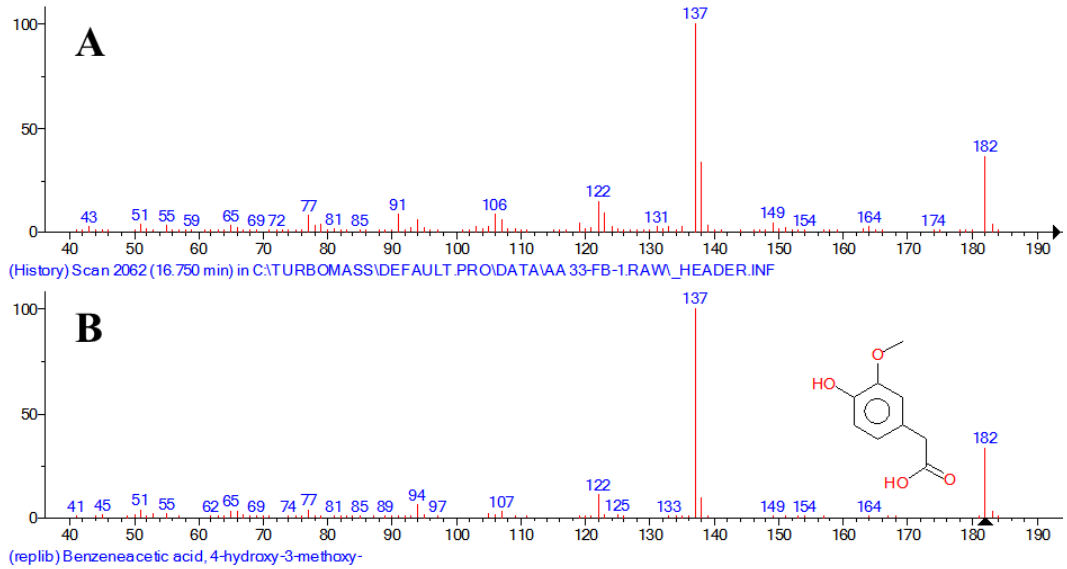

Figure A.122: Matching MS spectrum of peak number 24 MS in phenolic extract GC-MS: A) MS of peak number 24 in phenolic extract sample; B) MS of Benzeneacetic acid, 4-hydroxy-3-methoxy- according to NIST library.

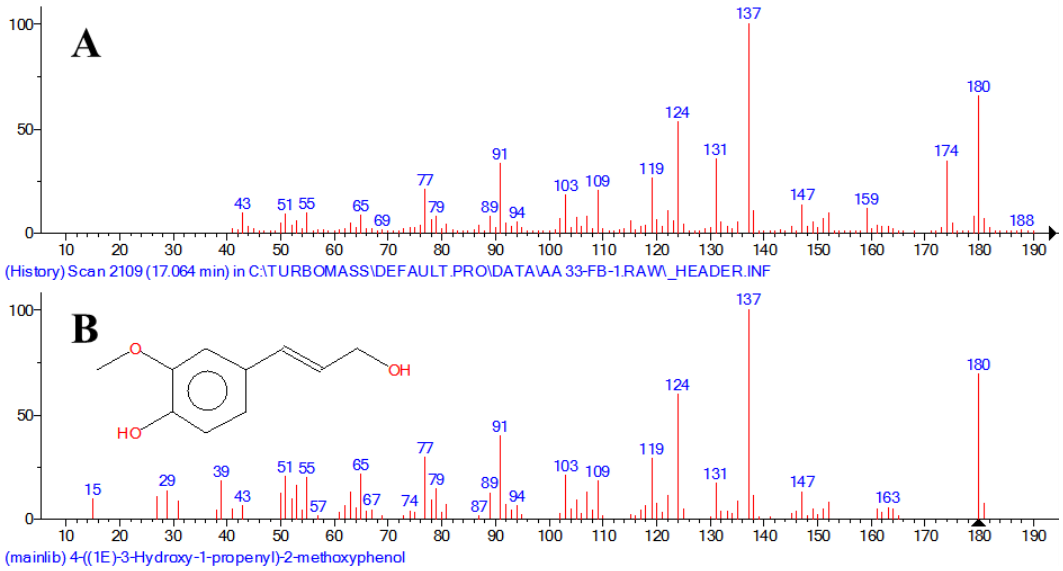

Figure A.123: Matching MS spectrum of peak number 25 MS in phenolic extract GC-MS: A) MS of peak number 25 in phenolic extract sample; B) MS of 4-((1E)-3-Hydroxy-1-propenyl)-2-methoxyphenol according to NIST library.

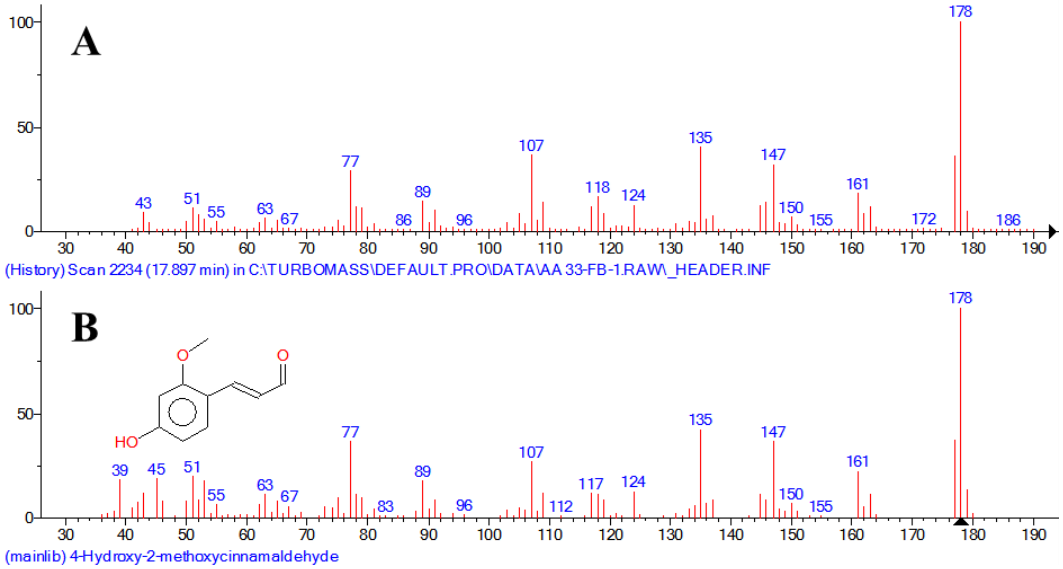

Figure A.124: Matching MS spectrum of peak number 26 MS in phenolic extract GC-MS: A) MS of peak number 26 in phenolic extract sample; B) MS of 4-Hydroxy-2-methoxycinnamaldehyde according to NIST library.

A.3.5 Mass spectra of identified phenolic peaks in organic acids extract and their best NIST library match

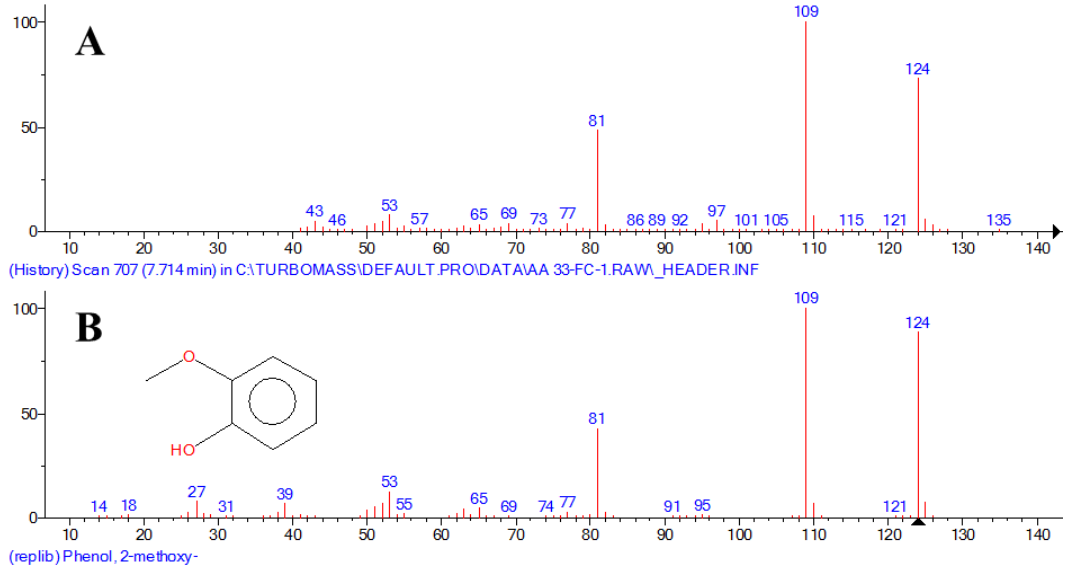

Figure A.125: Matching MS spectrum of peak number 4 MS in organic acids extract GC-MS: A) MS of peak number 4 in organic acids extract sample; B) MS of Phenol, 2-methoxy- according to NIST library.

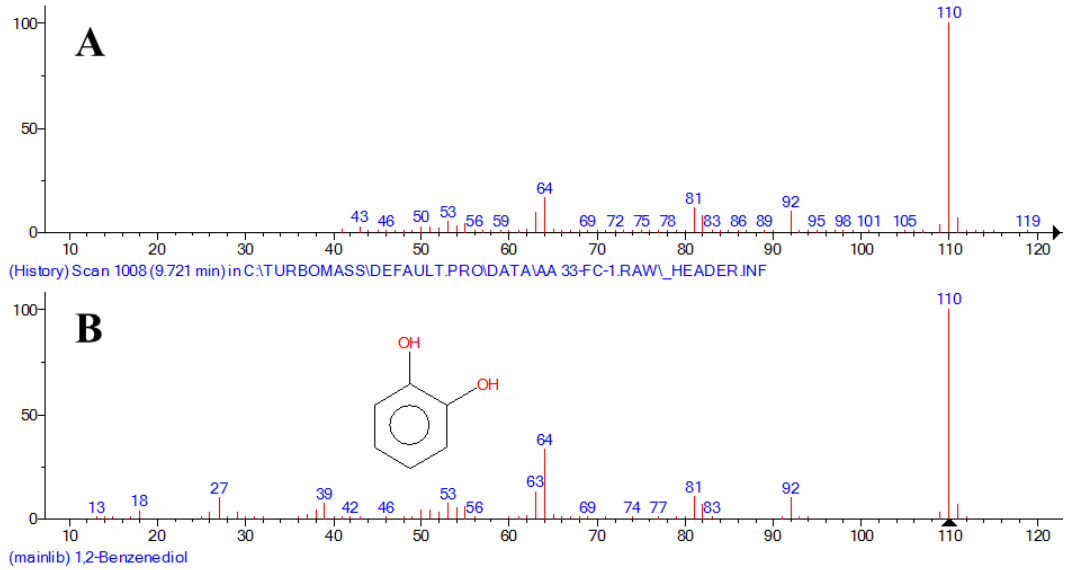

Figure A.126: Matching MS spectrum of peak number 8 MS in organic acids extract GC-MS: A) MS of peak number 8 in organic acids extract sample; B) MS of 1,2-Benzenediol according to NIST library.

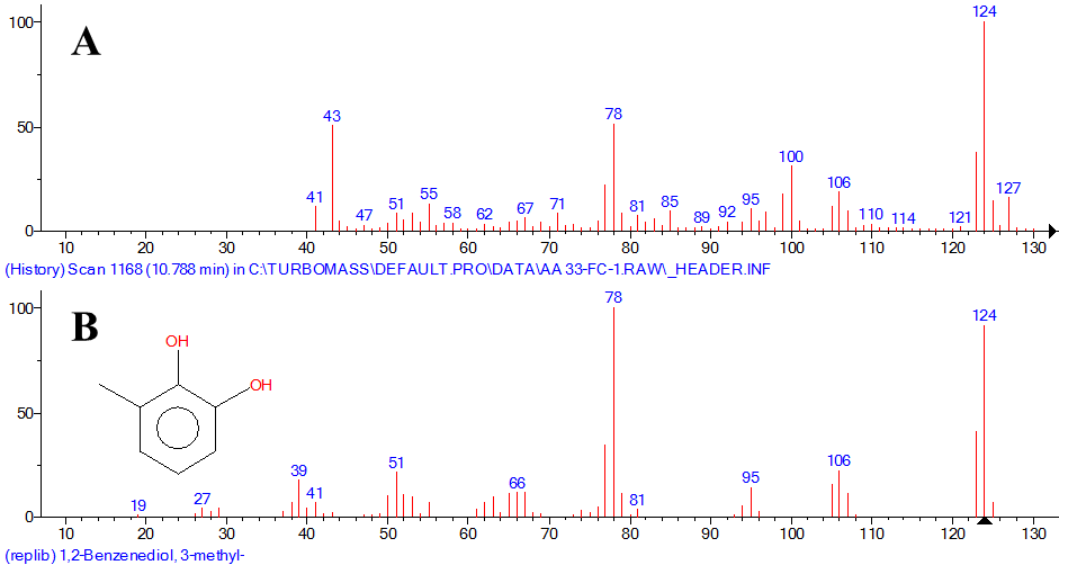

Figure A.127: Matching MS spectrum of peak number 9 MS in organic acids extract GC-MS: A) MS of peak number 9 in organic acids extract sample; B) MS of 1,2-Benzenediol, 3-methyl- according to NIST library.

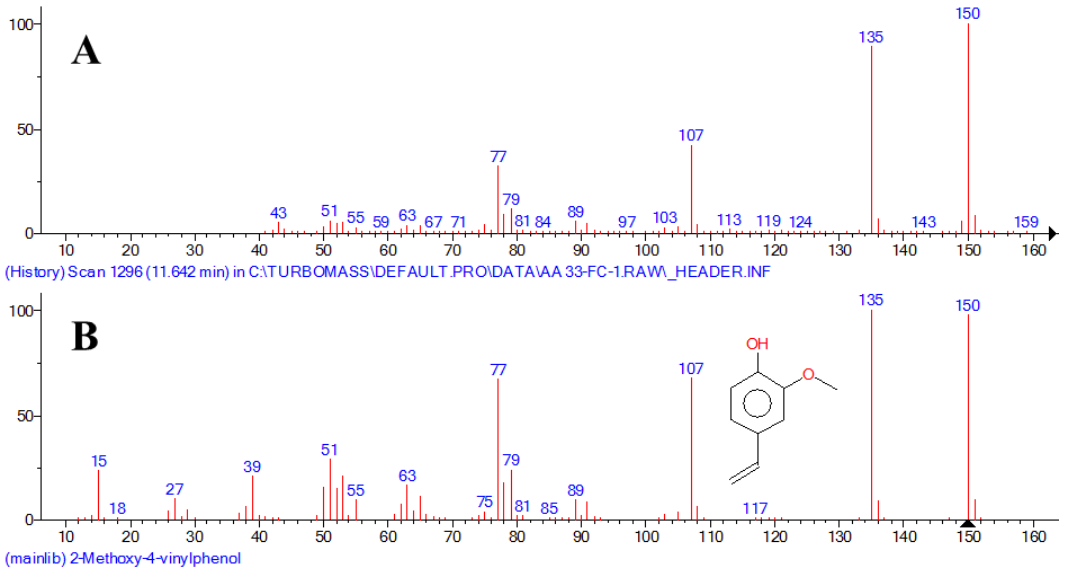

Figure A.128: Matching MS spectrum of peak number 12 MS in organic acids extract GC-MS: A) MS of peak number 12 in organic acids extract sample; B) MS of 2-Methoxy-4-vinylphenol according to NIST library.

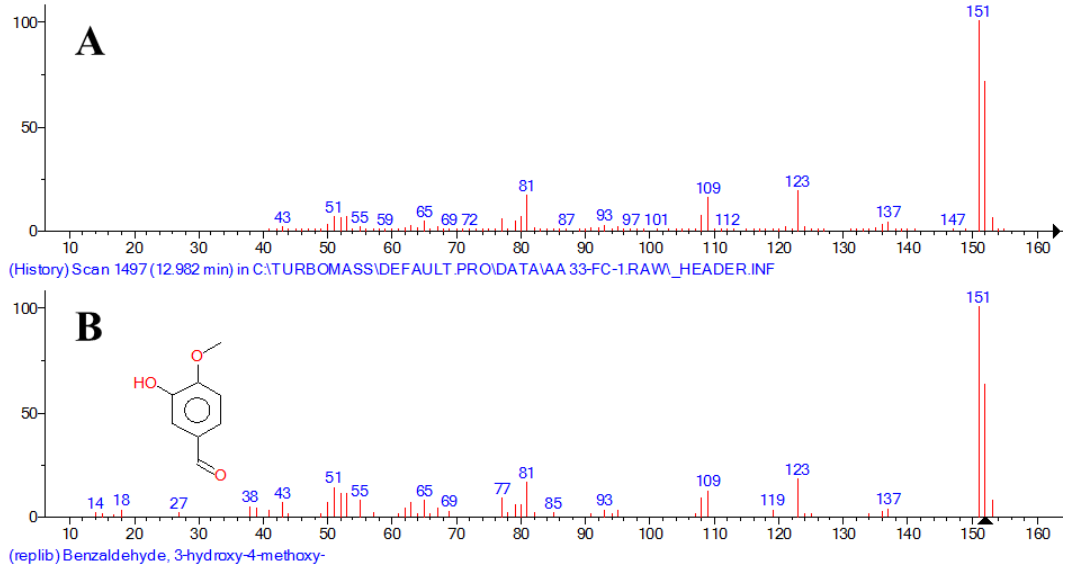

Figure A.129: Matching MS spectrum of peak number 16 MS in organic acids extract GC-MS: A) MS of peak number 16 in organic acids extract sample; B) MS of Benzaldehyde, 3-hydroxy-4-methoxy- according to NIST library.

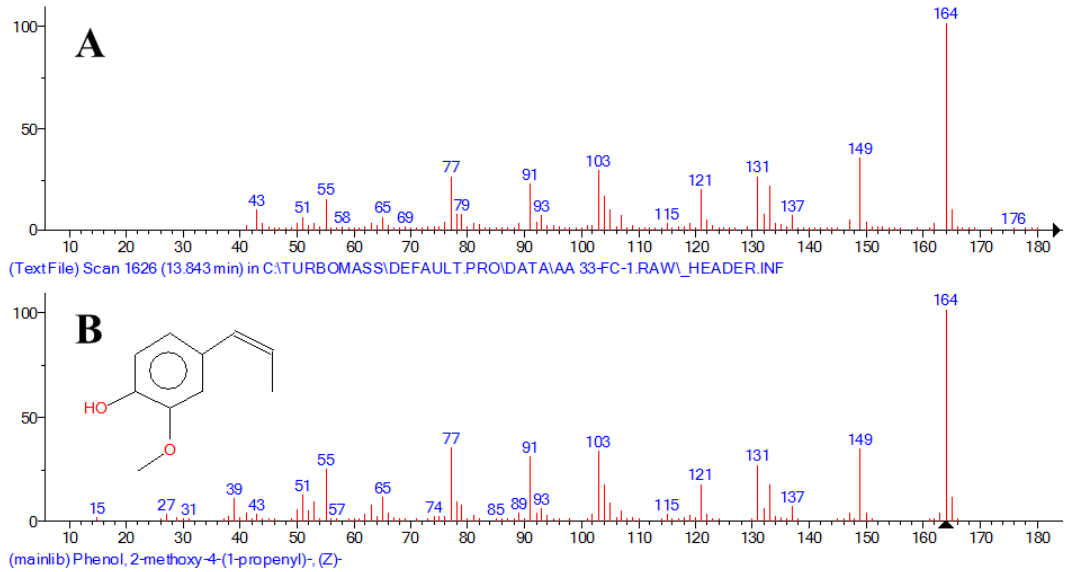

Figure A.130: Matching MS spectrum of peak number 18 MS in organic acids extract GC-MS: A) MS of peak number 18 in organic acids extract sample; B) MS of Phenol, 2-methoxy-4-(1-propenyl)-, (Z)- according to NIST library.

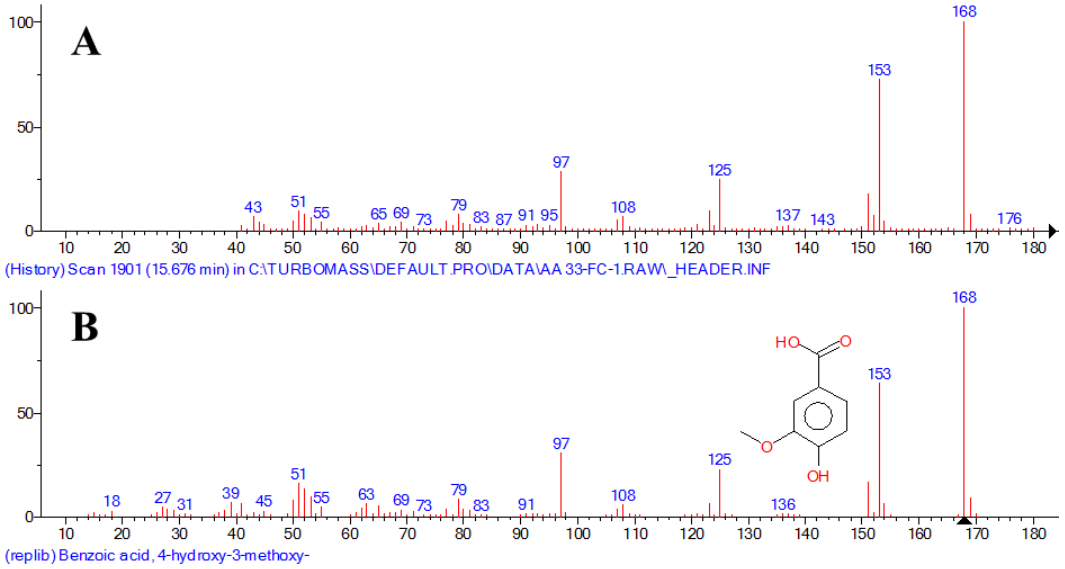

Figure A.131: Matching MS spectrum of peak number 23 MS in organic acids extract GC-MS: A) MS of peak number 23 in organic acids extract sample; B) MS of Benzoic acid, 4-hydroxy-3-methoxy- according to NIST library.

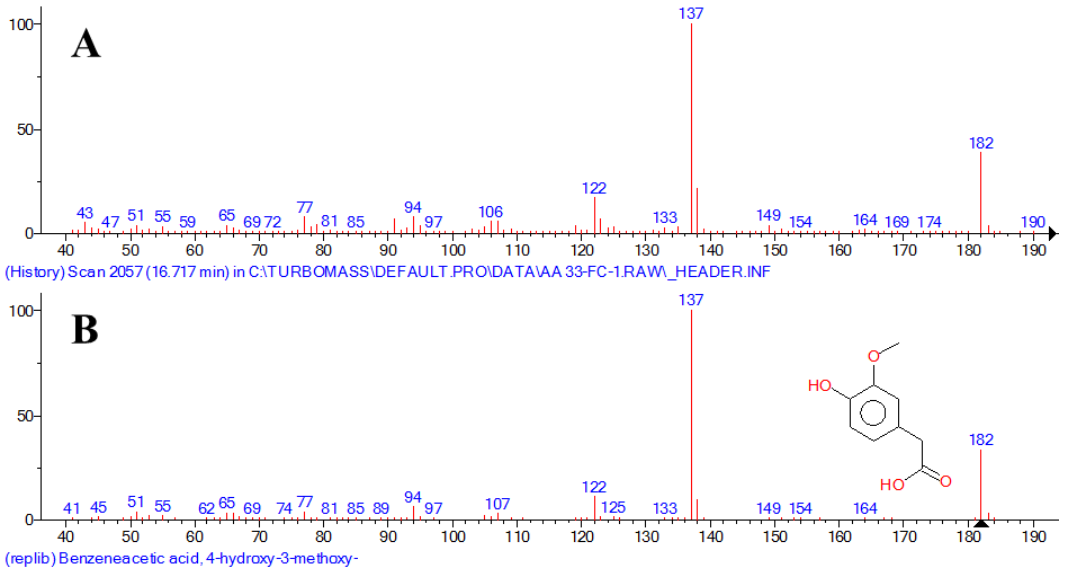

Figure A.132: Matching MS spectrum of peak number 24 MS in organic acids extract GC-MS: A) MS of peak number 24 in organic acids extract sample; B) MS of Benzeneacetic acid, 4-hydroxy-3-methoxy- according to NIST library.

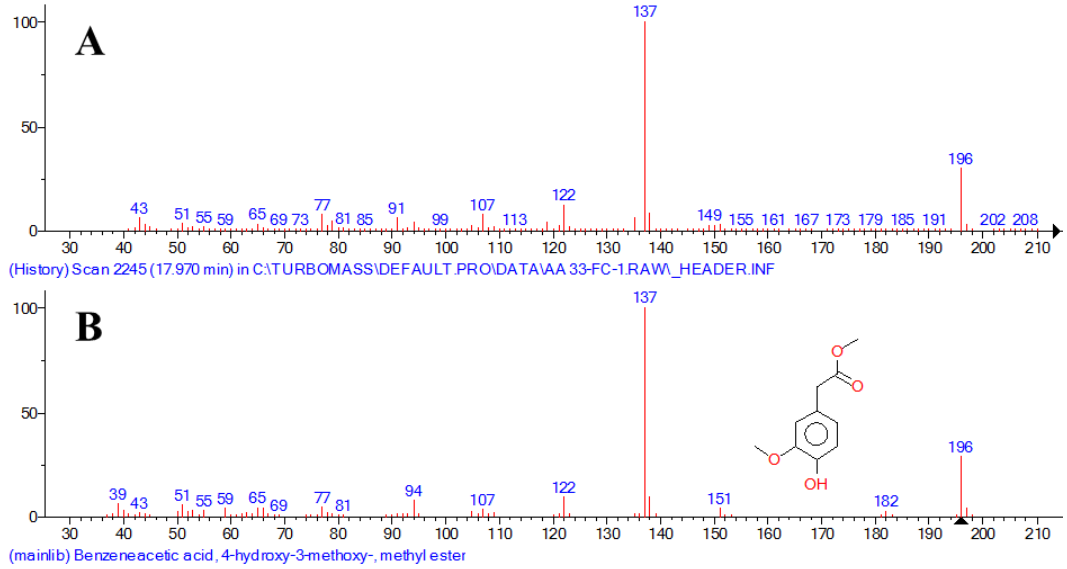

Figure A.133: Matching MS spectrum of peak number 27 MS in organic acids extract GC-MS: A) MS of peak number 27 in organic acids extract sample; B) MS of Benzeneacetic acid, 4-hydroxy-3-methoxy-, methyl ester according to NIST library.

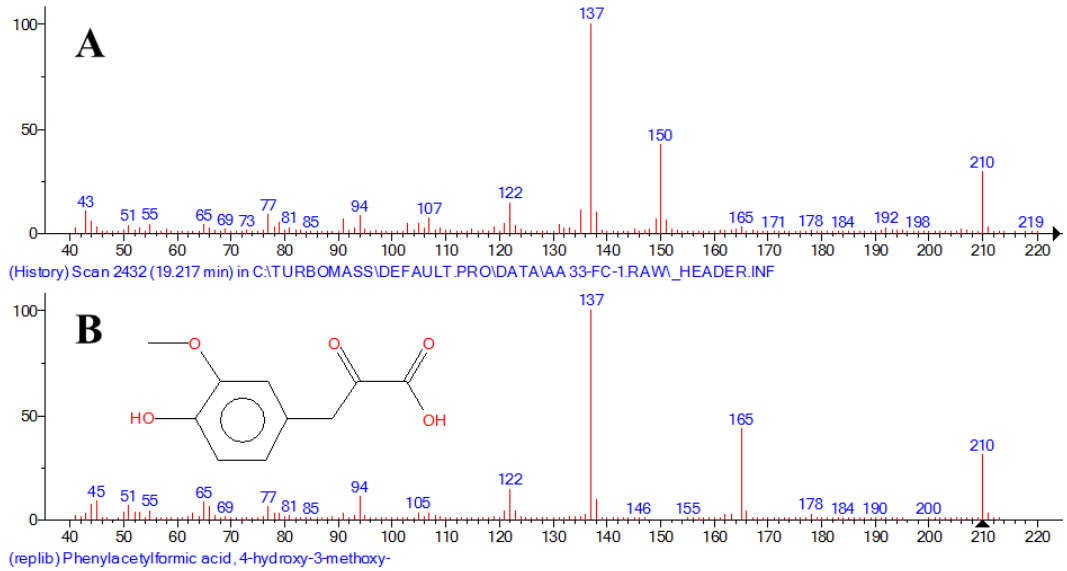

Figure A.134: Matching MS spectrum of peak number 28 MS in organic acids extract GC-MS: A) MS of peak number 28 in organic acids extract sample; B) MS of Phenylacetylformic acid, 4-hydroxy-3-methoxy- according to NIST library.

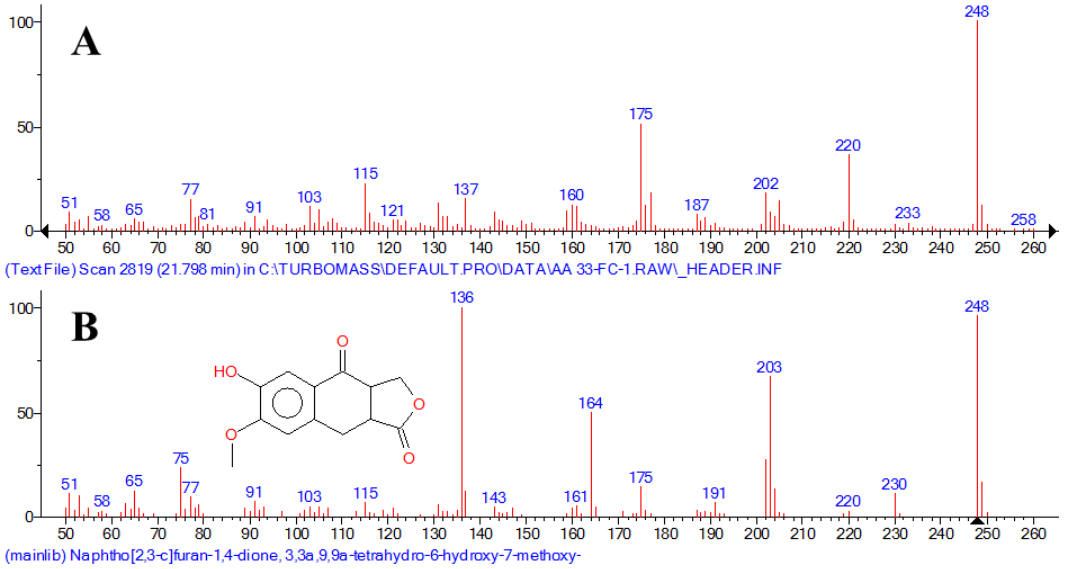

Figure A.135: Matching MS spectrum of peak number 29 MS in organic acids extract GC-MS: A) MS of peak number 29 in organic acids extract sample; B) MS of Naphtho[2,3-c]furan-1,4-dione, 3,3a,9,9a-tetrahydro-6-hydroxy-7-methoxy- according to NIST library.

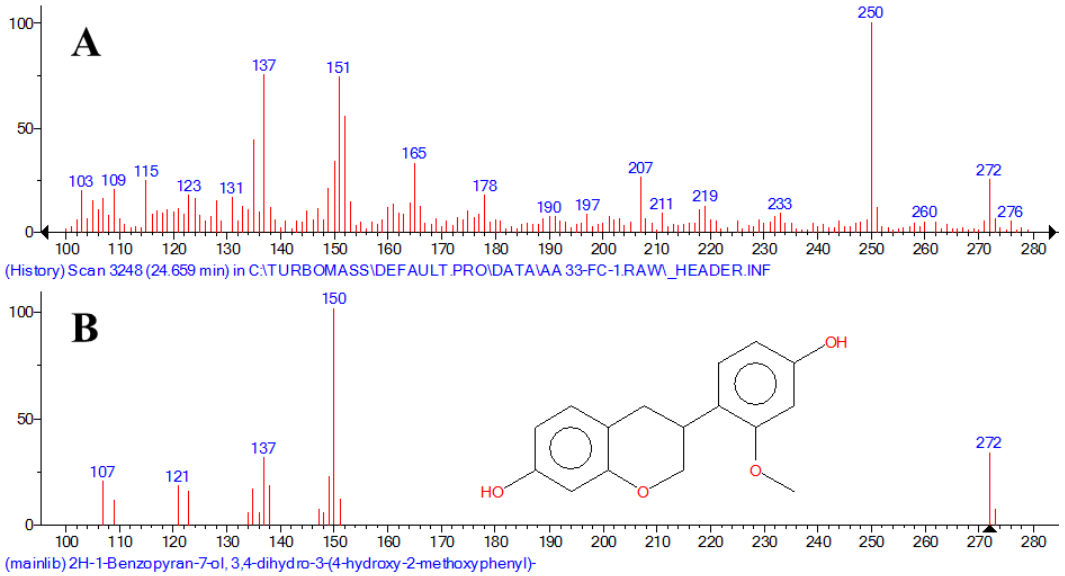

Figure A.136: Matching MS spectrum of peak number 30 MS in organic acids extract GC-MS: A) MS of peak number 30 in organic acids extract sample; B) MS of 2H-1-Benzopyran-7-ol, 3,4-dihydro-3-(4-hydroxy-2-methoxyphenyl)- according to NIST library.

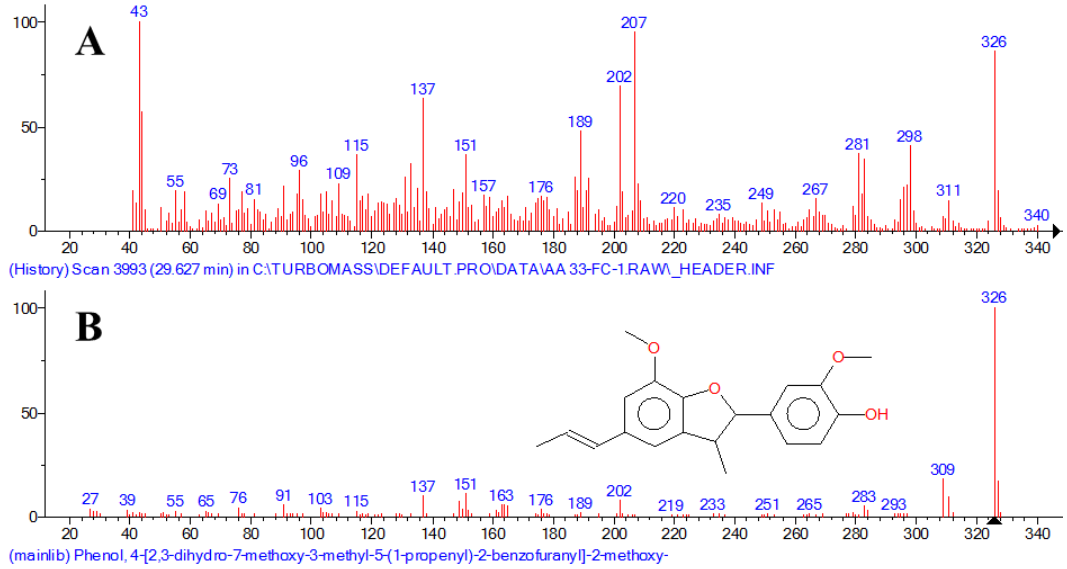

Figure A.137: Matching MS spectrum of peak number 32 MS in organic acids extract GC-MS: A) MS of peak number 32 in organic acids extract sample; B) MS of Phenol, 4-[2,3-dihydro-7-methoxy-3-methyl-5-(1-propenyl)-2-benzofuranyl]-2-methoxy- according to NIST library.

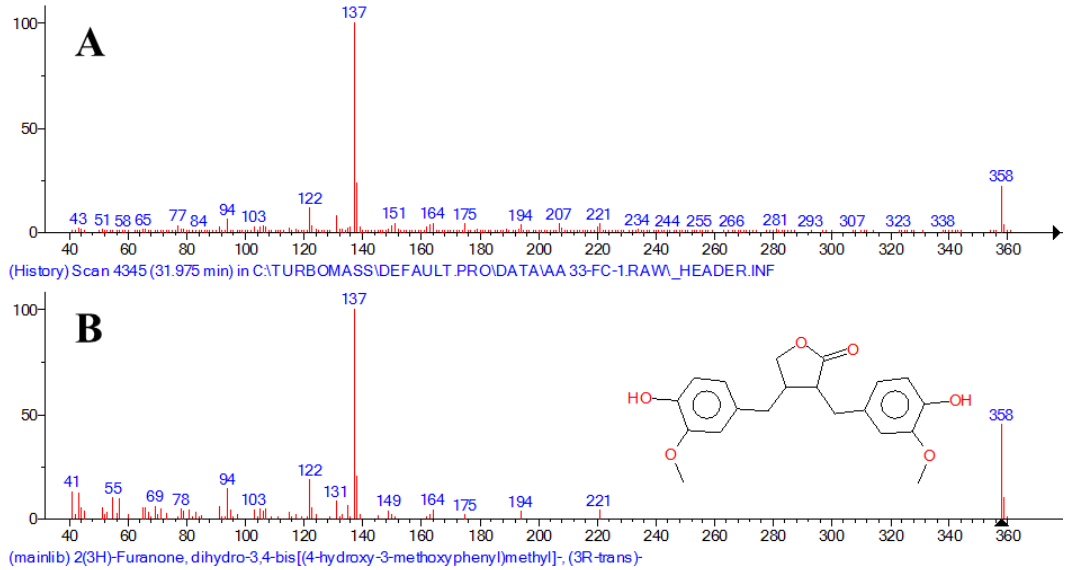

Figure A.138: Matching MS spectrum of peak number 33 MS in organic acids extract GC-MS: A) MS of peak number 33 in organic acids extract sample; B) MS of 2(3H)-Furanone, dihydro-3,4-bis[(4-hydroxy-3-methoxyphenyl)methyl]-, (3R-trans)- according to NIST library.

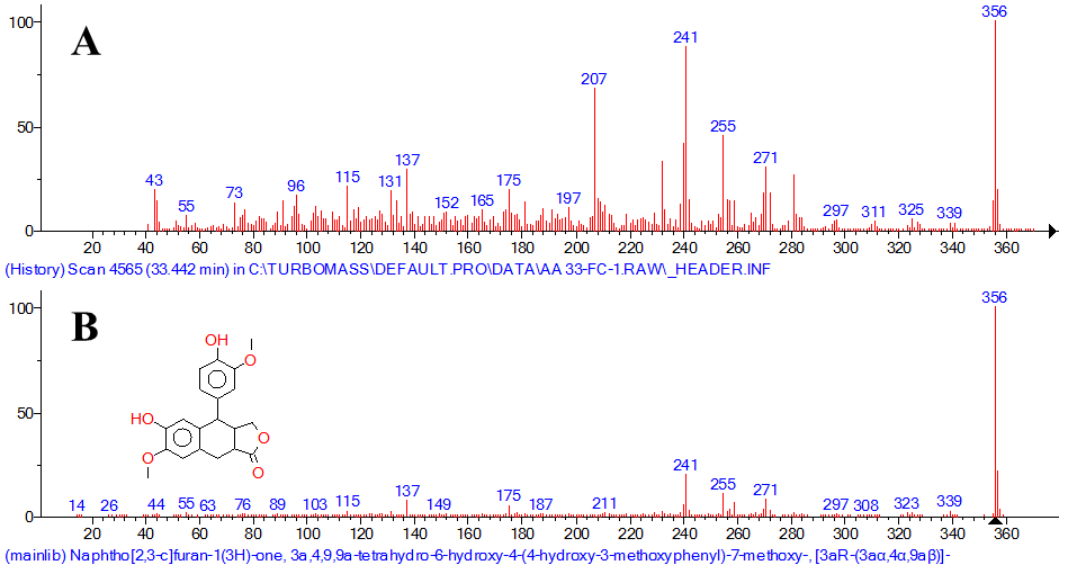

Figure A.139: Matching MS spectrum of peak number 34 MS in organic acids extract GC-MS: A) MS of peak number 34 in organic acids extract sample; B) MS of Naphtho[2,3-c]furan-1(3H)-one, 3a,4,9,9a-tetrahydro-6-hydroxy-4-(4-hydroxy-3-methoxyphenyl)-7-methoxy-, [3aR-(3aα,4α,9aβ)]- according to NIST library.

A.4 Mass Spectra of Identified Phenolic Peaks in Water-Soluble Phase Fractionation Experiment

A.4.1 Mass spectra of identified phenolic peaks in 2nd extract of crude bio-oil and their best NIST library match

The 2nd extract of crude bio-oil was re-analyzed using a different GC-MS method at the point of this experiment. Therefore, for consistency, the MS spectra of the detected phenolic peaks in the 2nd GC-MS analysis and there matching MS according to NIST library are presented here.

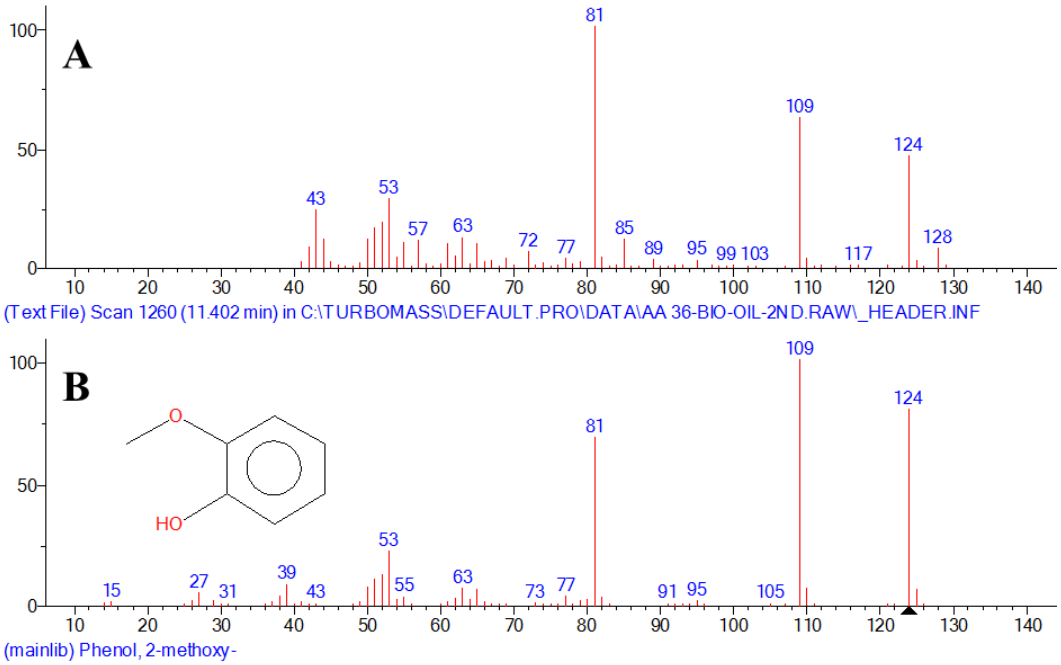

Figure A.140: Matching MS spectrum of peak number 4 MS in 2nd crude bio-oil extract GC-MS: A) MS of peak number 4 in 2nd crude bio-oil extract sample; B) MS of Phenol, 2-methoxy- according to NIST library.

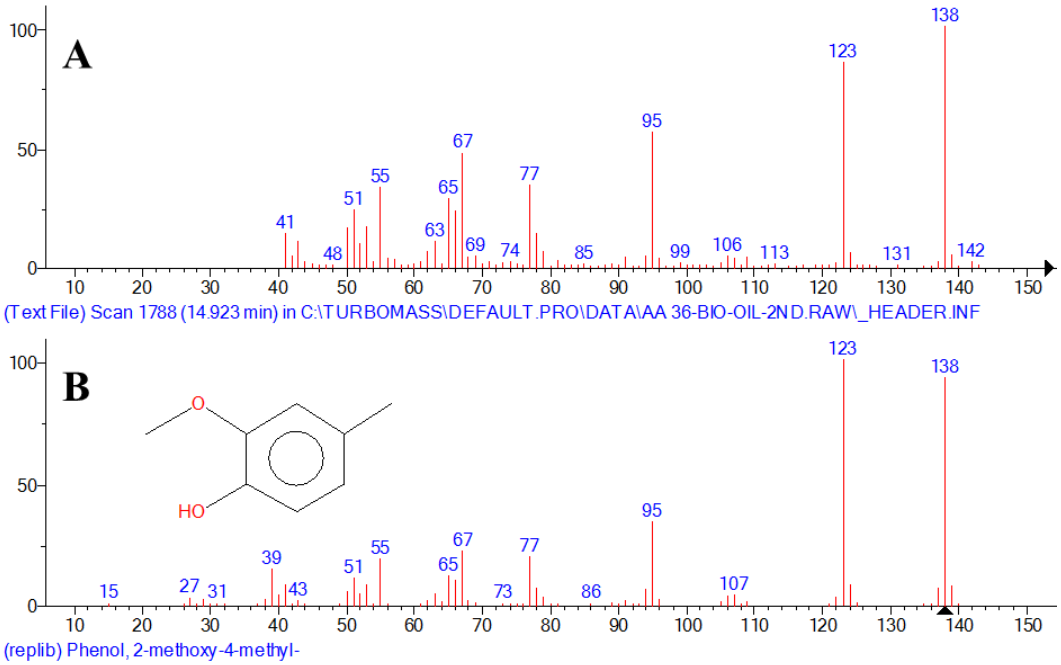

Figure A.141: Matching MS spectrum of peak number 7 MS in 2nd crude bio-oil extract GC-MS: A) MS of peak number 7 in 2nd crude bio-oil extract sample; B) MS of Phenol, 2-methoxy-4-methyl- according to NIST library.

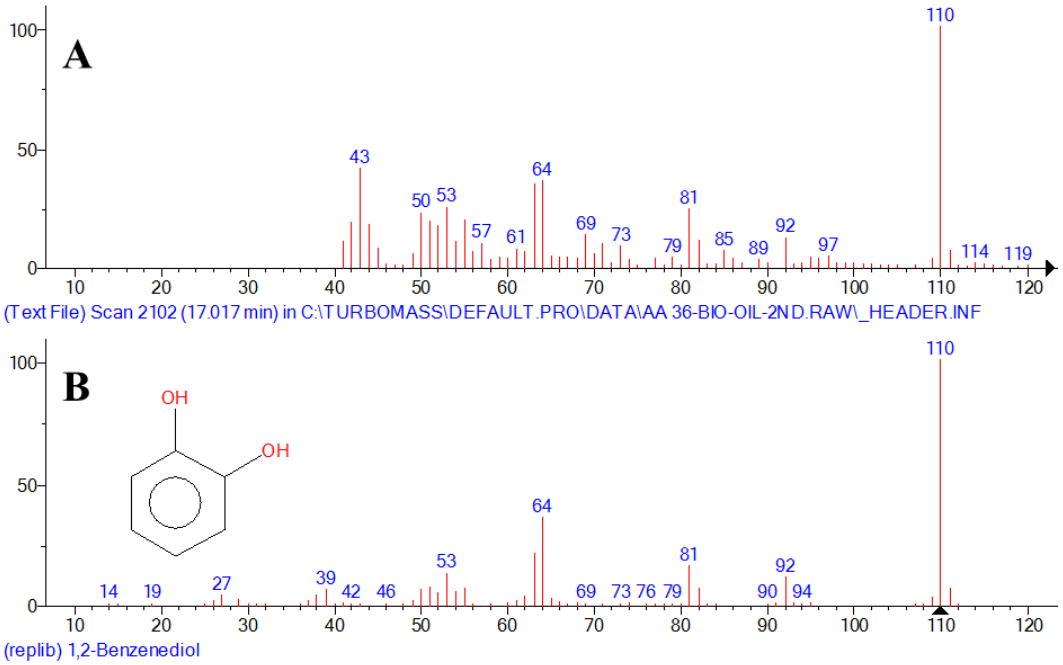

Figure A.142: Matching MS spectrum of peak number 8 MS in 2nd crude bio-oil extract GC-MS: A) MS of peak number 8 in 2nd crude bio-oil extract sample; B) MS of 1,2-Benzenediol according to NIST library.

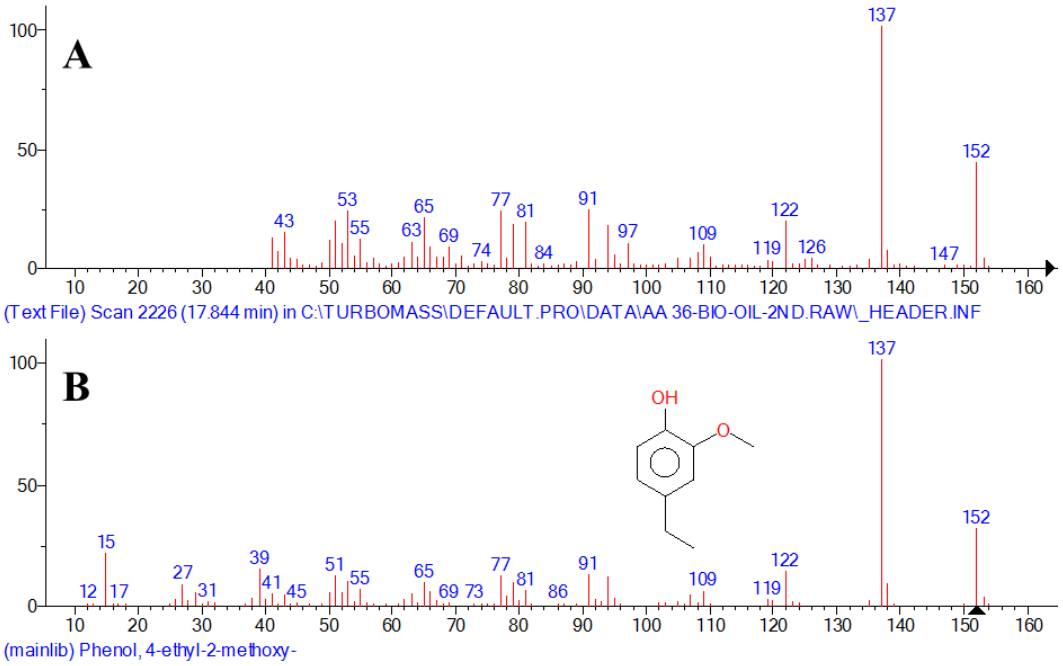

Figure A.143: Matching MS spectrum of peak number 10 MS in 2nd crude bio-oil extract GC-MS: A) MS of peak number 10 in 2nd crude bio-oil extract sample; B) MS of Phenol, 4-ethyl-2-methoxy- according to NIST library.

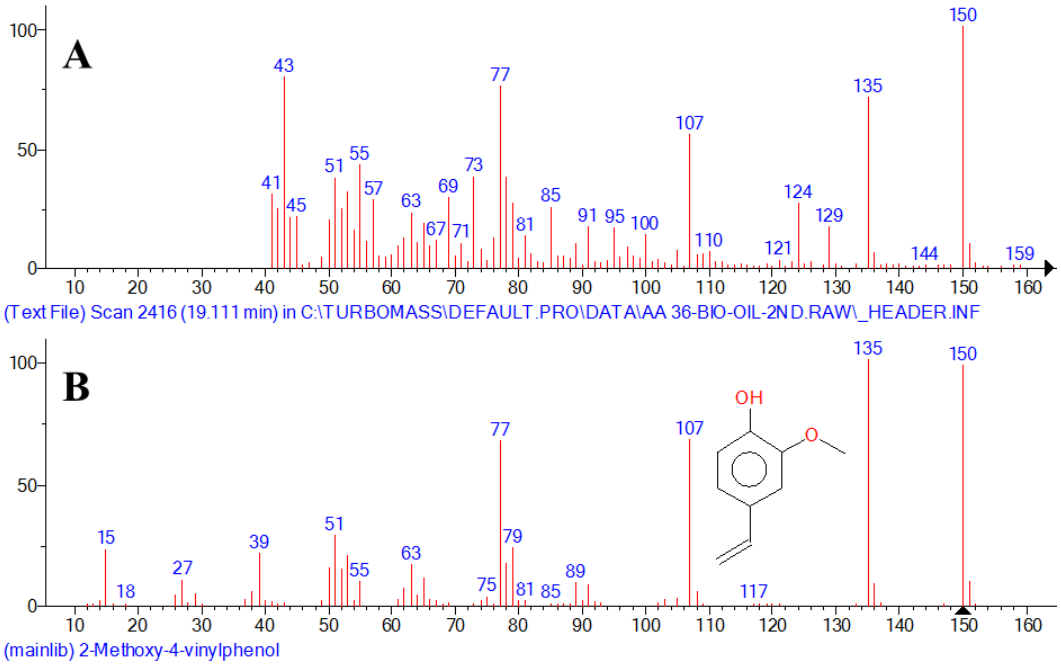

Figure A.144: Matching MS spectrum of peak number 12 MS in 2nd crude bio-oil extract GC-MS: A) MS of peak number 12 in 2nd crude bio-oil extract sample; B) MS of 2-Methoxy-4-vinylphenol according to NIST library.

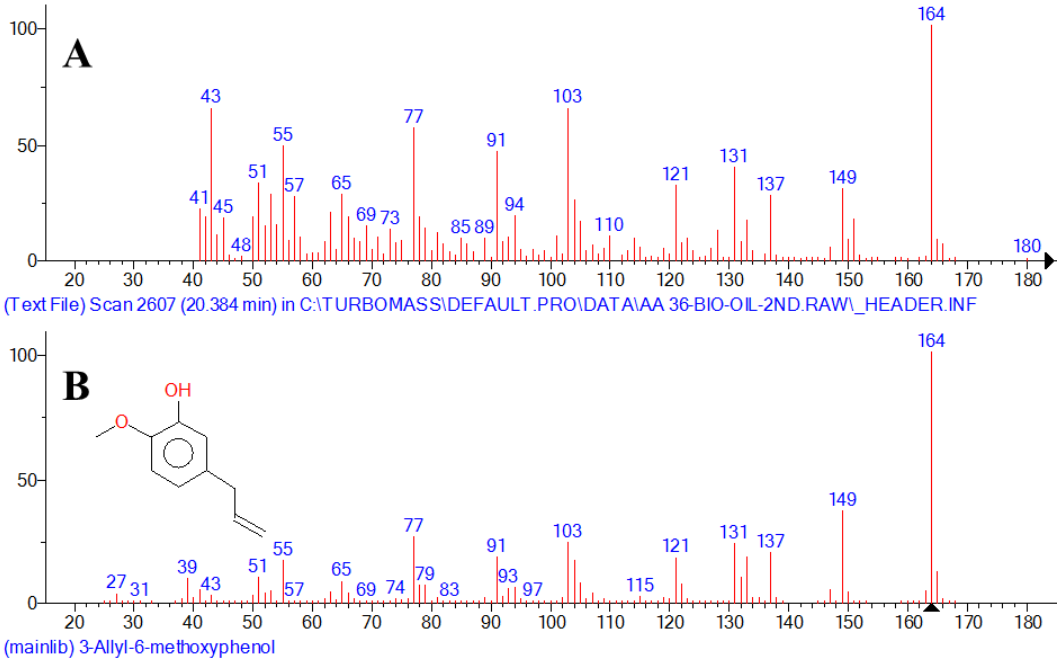

Figure A.145: Matching MS spectrum of peak number 14 MS in 2nd crude bio-oil extract GC-MS: A) MS of peak number 14 in 2nd crude bio-oil extract sample; B) MS of 3-Allyl-6-methoxyphenol according to NIST library.

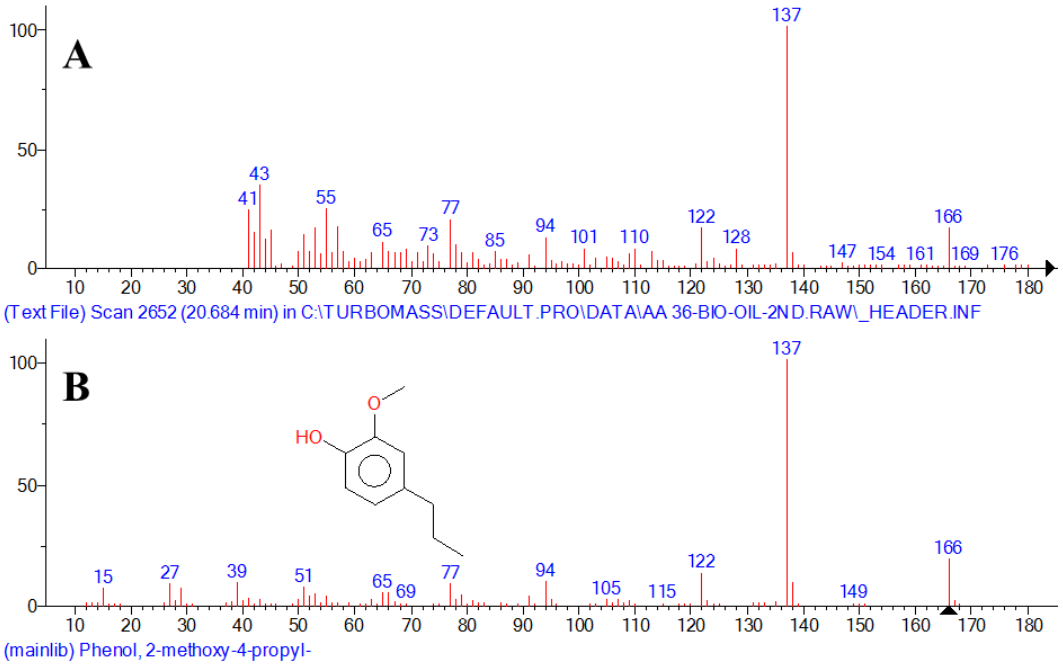

Figure A.146: Matching MS spectrum of peak number 15 MS in 2nd crude bio-oil extract GC-MS: A) MS of peak number 15 in 2nd crude bio-oil extract sample; B) MS of Phenol, 2-methoxy-4-propyl- according to NIST library.

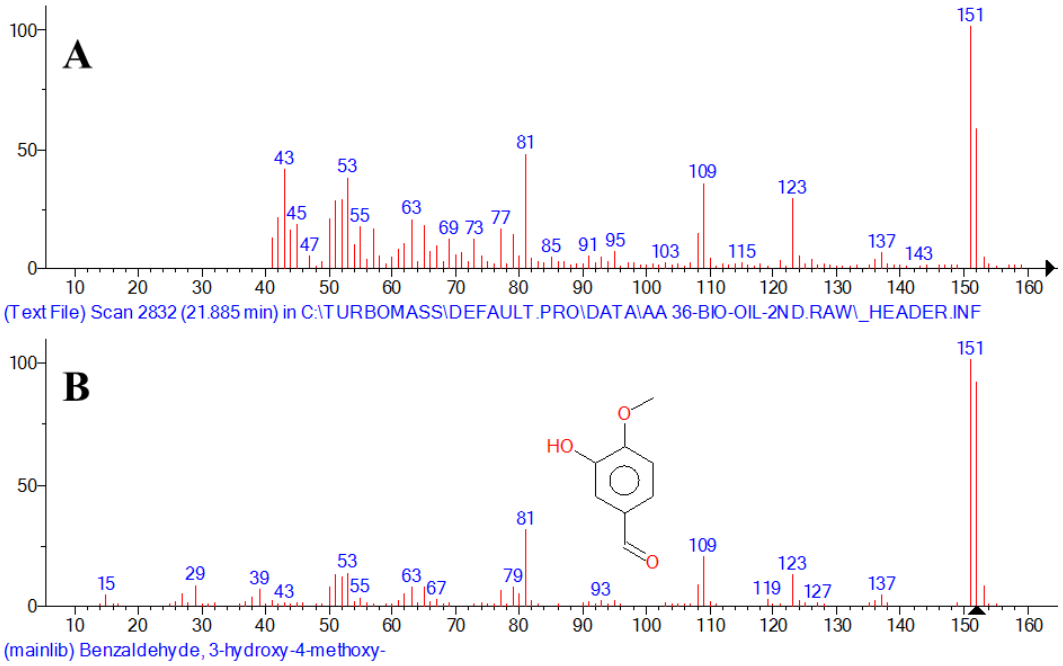

Figure A.147: Matching MS spectrum of peak number 16 MS in 2nd crude bio-oil extract GC-MS: A) MS of peak number 16 in 2nd crude bio-oil extract sample; B) MS of Benzaldehyde, 3-hydroxy-4-methoxy- according to NIST library.

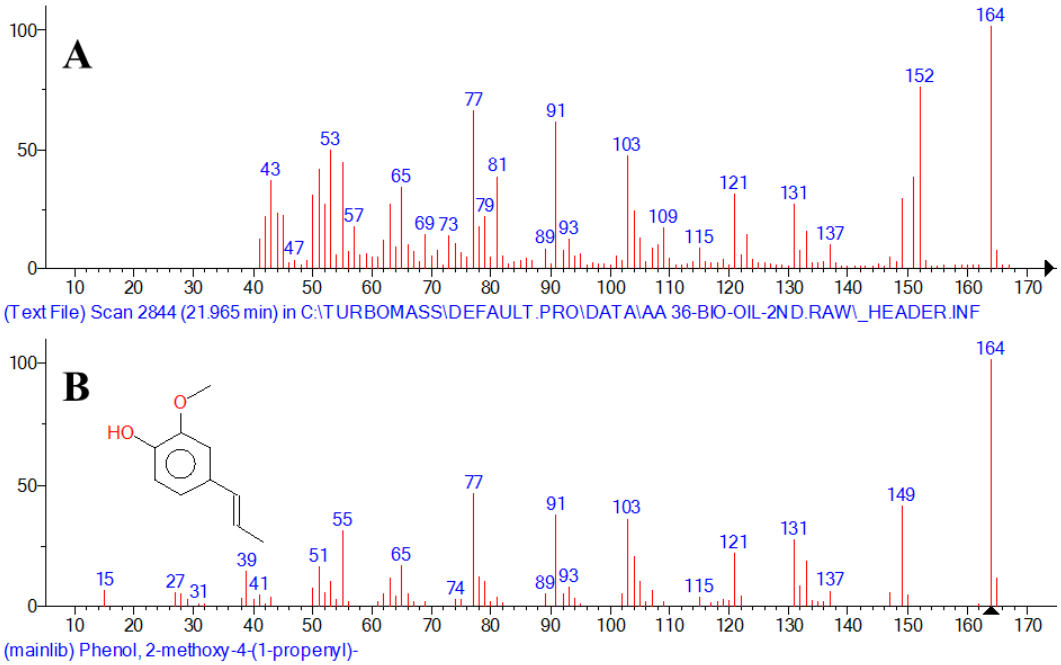

Figure A.148: Matching MS spectrum of peak number 17 MS in 2nd crude bio-oil extract GC-MS: A) MS of peak number 17 in 2nd crude bio-oil extract sample; B) MS of Phenol, 2-methoxy-4-(1-propenyl)- according to NIST library.

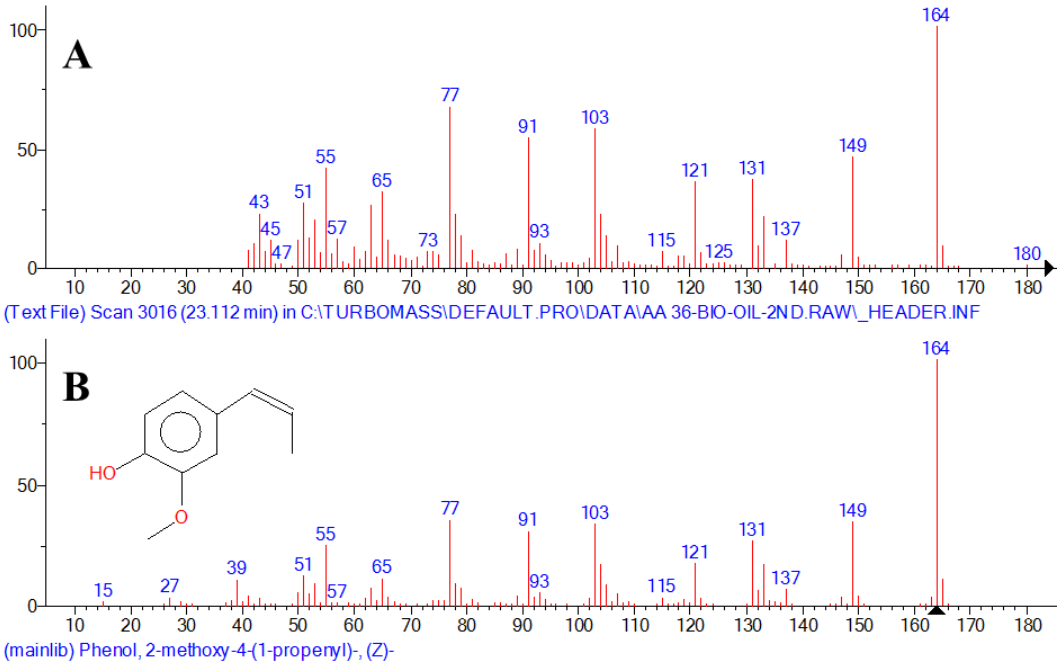

Figure A.149: Matching MS spectrum of peak number 18 MS in 2nd crude bio-oil extract GC-MS: A) MS of peak number 18 in 2nd crude bio-oil extract sample; B) MS of Phenol, 2-methoxy-4-(1-propenyl)-, (Z)- according to NIST library.

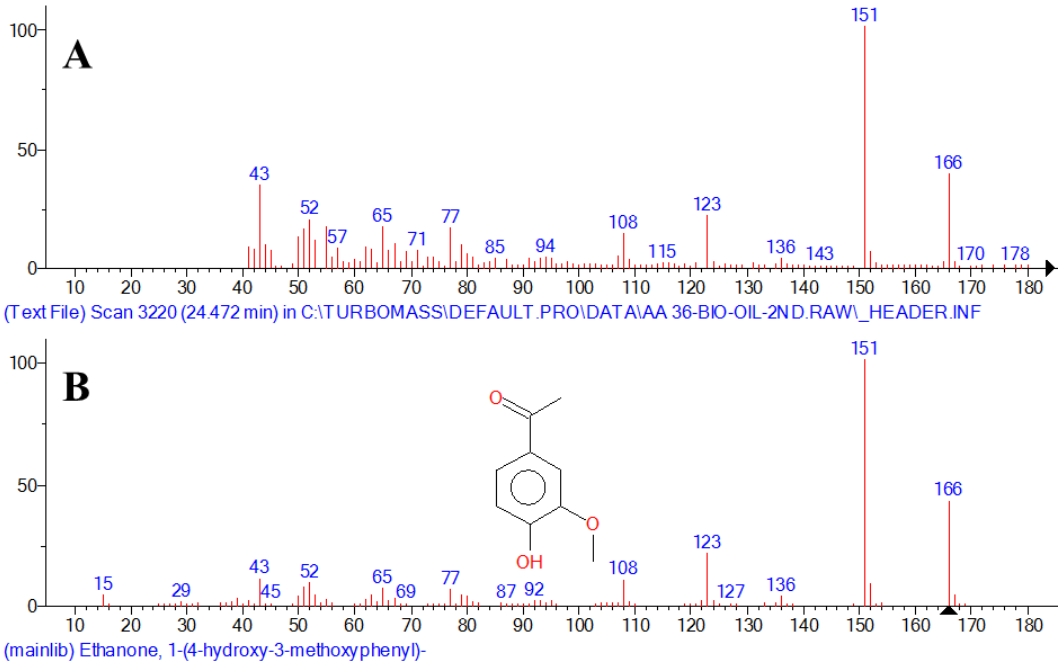

Figure A.150: Matching MS spectrum of peak number 20 MS in 2nd crude bio-oil extract GC-MS: A) MS of peak number 20 in 2nd crude bio-oil extract sample; B) MS of Ethanone, 1-(4-hydroxy-3-methoxyphenyl)- according to NIST library.

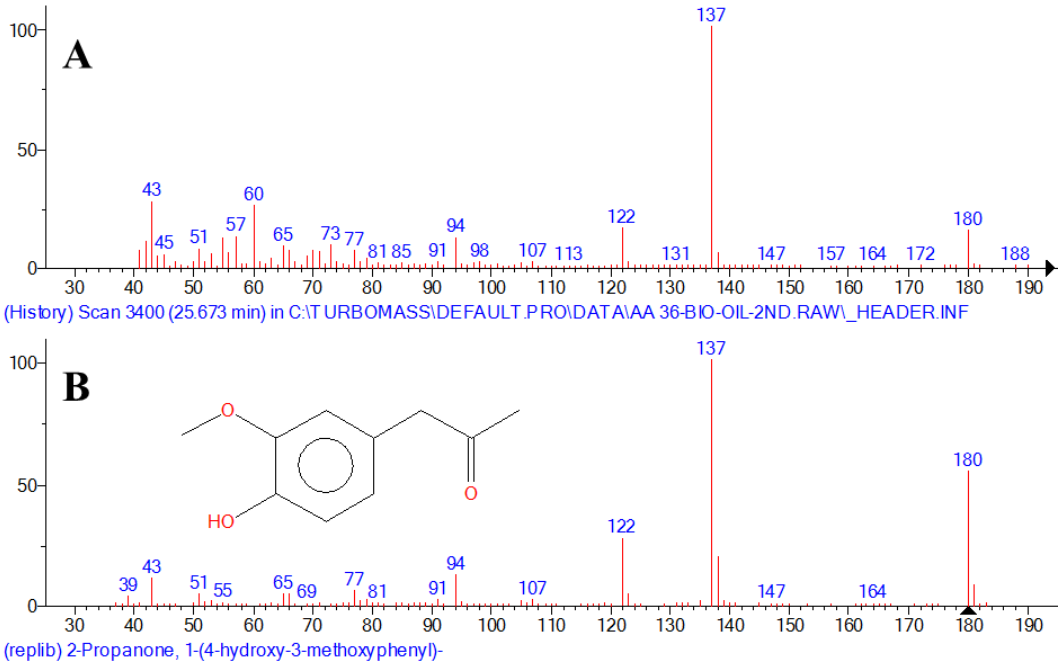

Figure A.151: Matching MS spectrum of peak number 21 MS in 2nd crude bio-oil extract GC-MS: A) MS of peak number 21 in 2nd crude bio-oil extract sample; B) MS of 2-Propanone, 1-(4-hydroxy-3-methoxyphenyl)- according to NIST library.

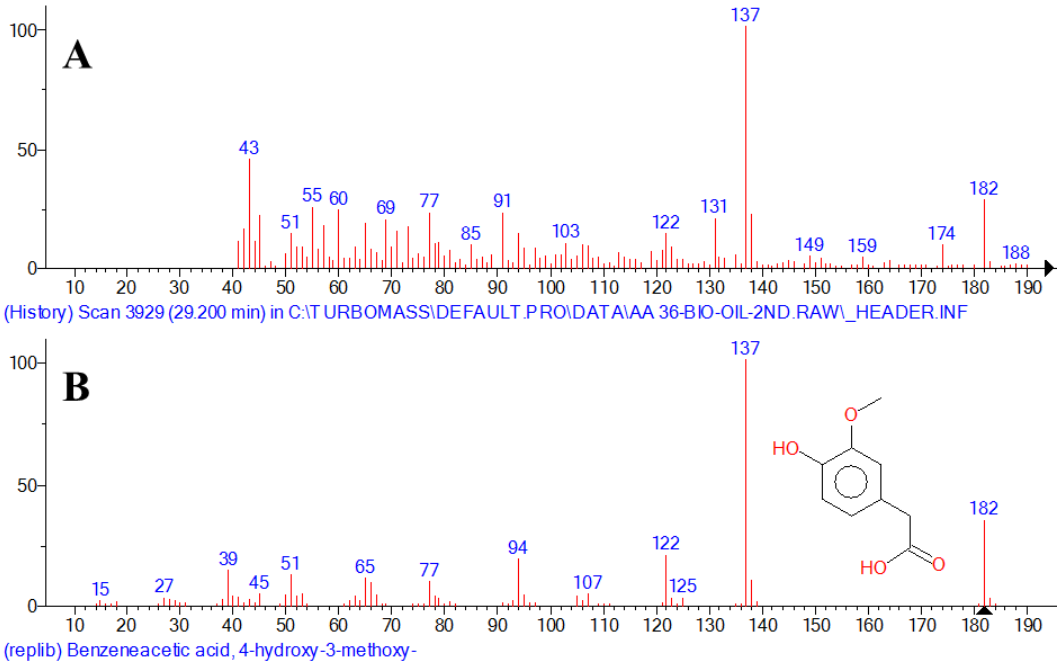

Figure A.152: Matching MS spectrum of peak number 24 MS in 2nd crude bio-oil extract GC-MS: A) MS of peak number 24 in 2nd crude bio-oil extract sample; B) MS of Benzeneacetic acid, 4-hydroxy-3-methoxy- according to NIST library.

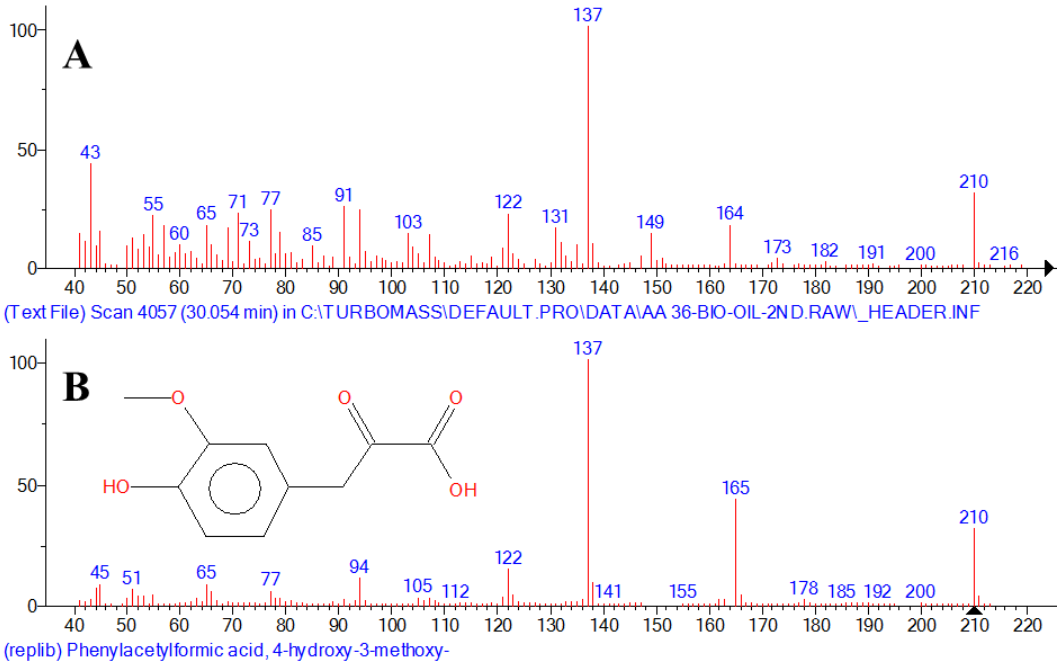

Figure A.153: Matching MS spectrum of peak number 28 MS in 2nd crude bio-oil extract GC-MS: A) MS of peak number 28 in 2nd crude bio-oil extract sample; B) MS of Phenylacetylformic acid, 4-hydroxy-3-methoxy- according to NIST library.

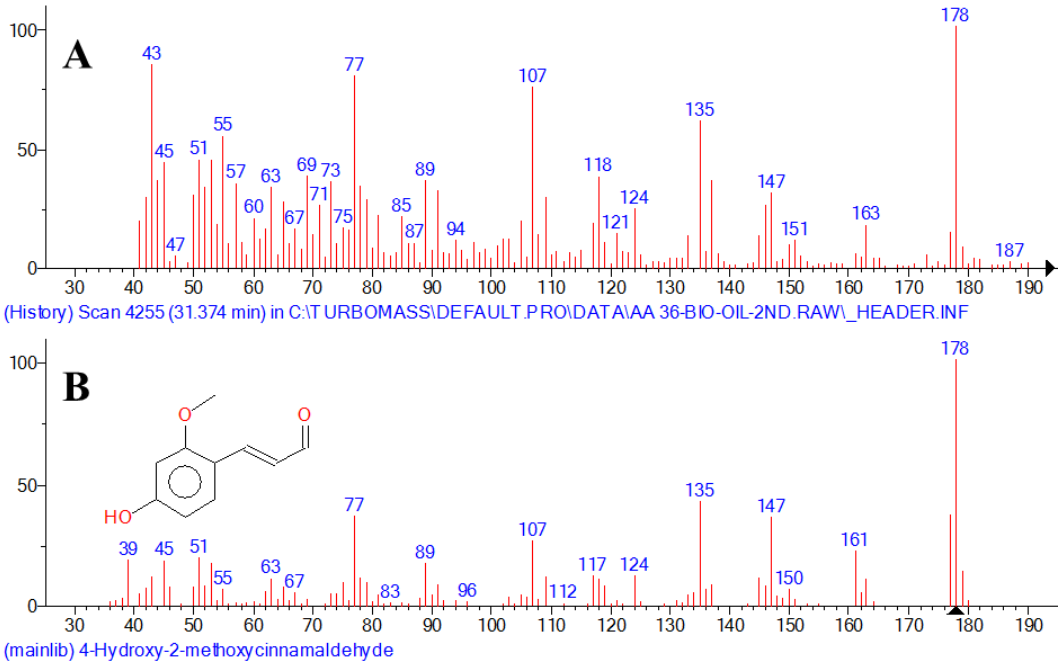

Figure A.154: Matching MS spectrum of peak number 26 MS in 2nd crude bio-oil extract GC-MS: A) MS of peak number 26 in 2nd crude bio-oil extract sample; B) MS of 4-Hydroxy-2-methoxycinnamaldehyde according to NIST library.

A.4.2 Mass spectra of identified phenolic peaks in water-soluble extract and their best NIST library match

This again was re-analyzed using another GC method.

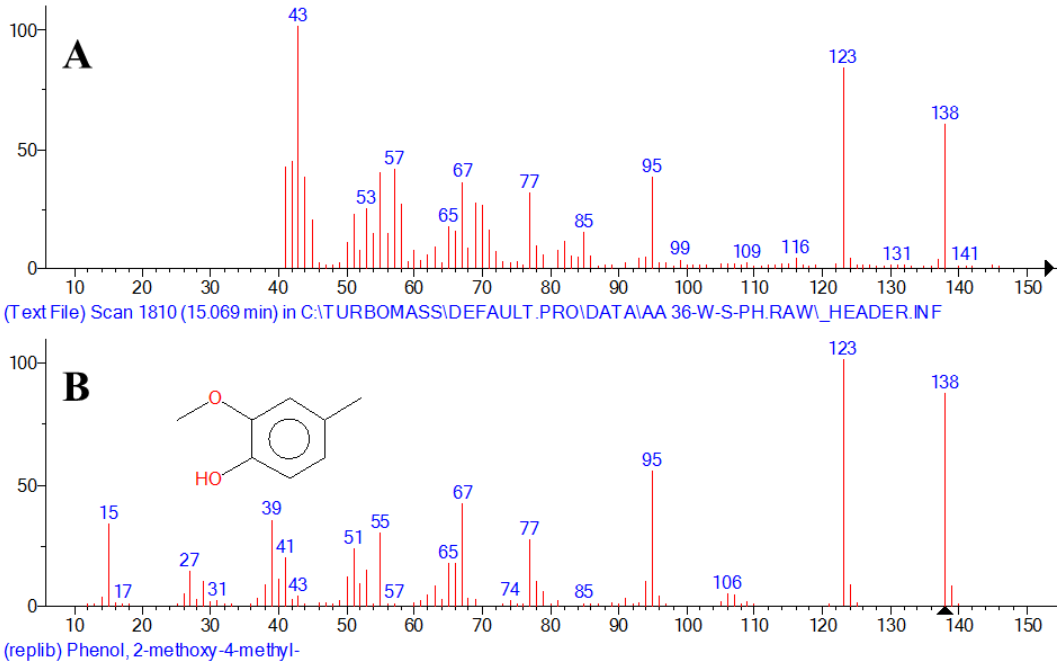

Figure A.155: Matching MS spectrum of peak number 7 MS in water-soluble extract GC-MS: A) MS of peak number 7 in water-soluble extract sample; B) MS of Phenol, 2-methoxy-4-methyl- according to NIST library.

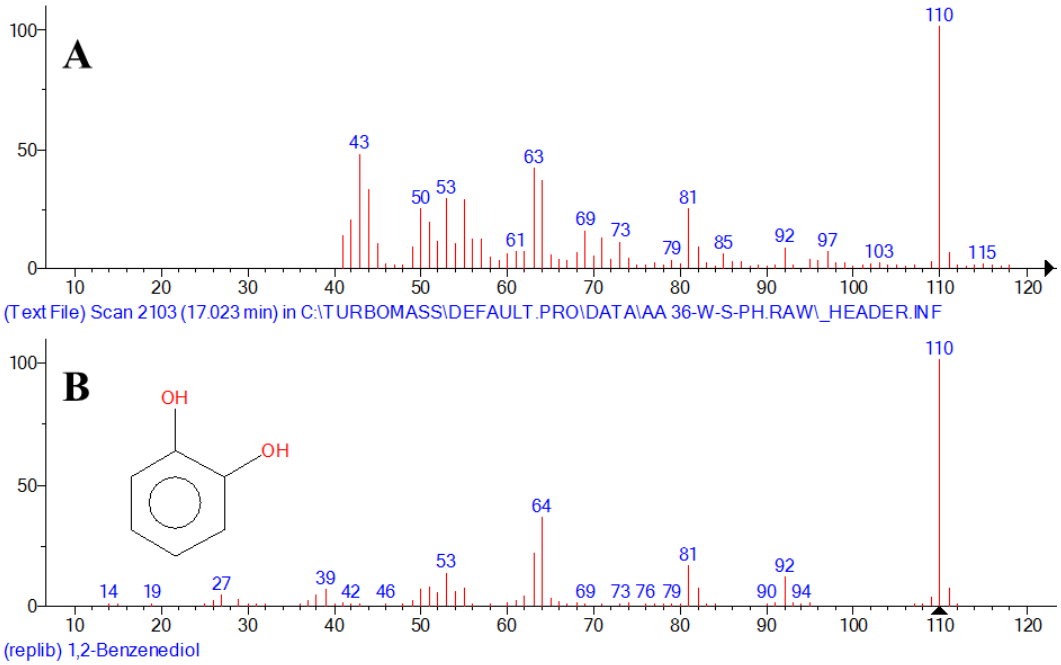

Figure A.156: Matching MS spectrum of peak number 8 MS in water-soluble extract GC-MS: A) MS of peak number 8 in water-soluble extract sample; B) MS of 1,2-Benzenediol according to NIST library.

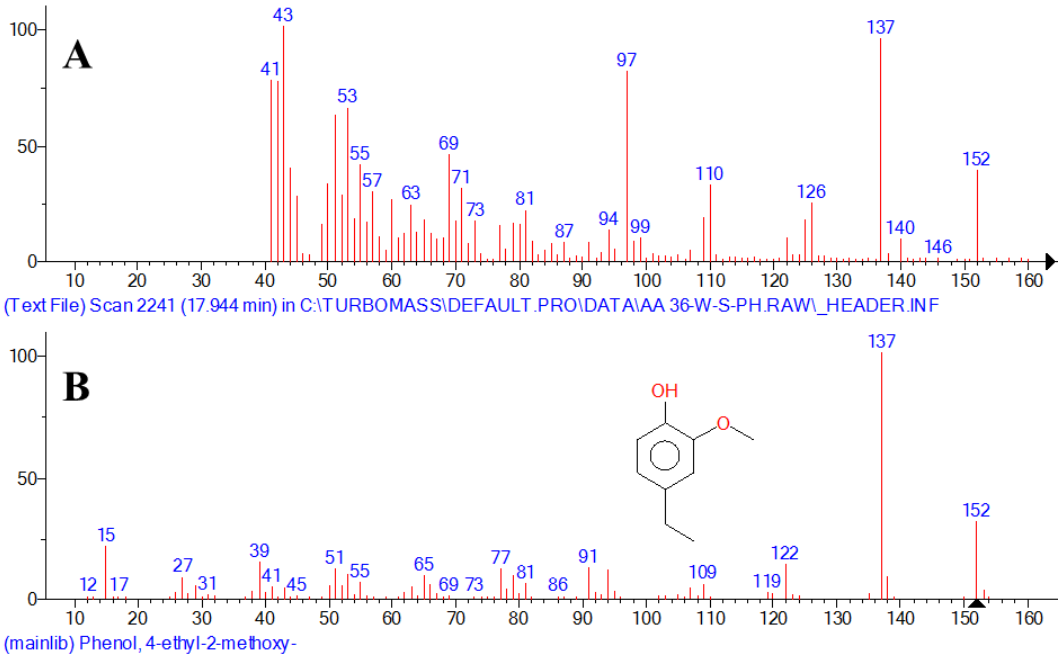

Figure A.157: Matching MS spectrum of peak number 10 MS in water-soluble extract GC-MS: A) MS of peak number 10 in water-soluble extract sample; B) MS of Phenol, 4-ethyl-2-methoxy- according to NIST library.

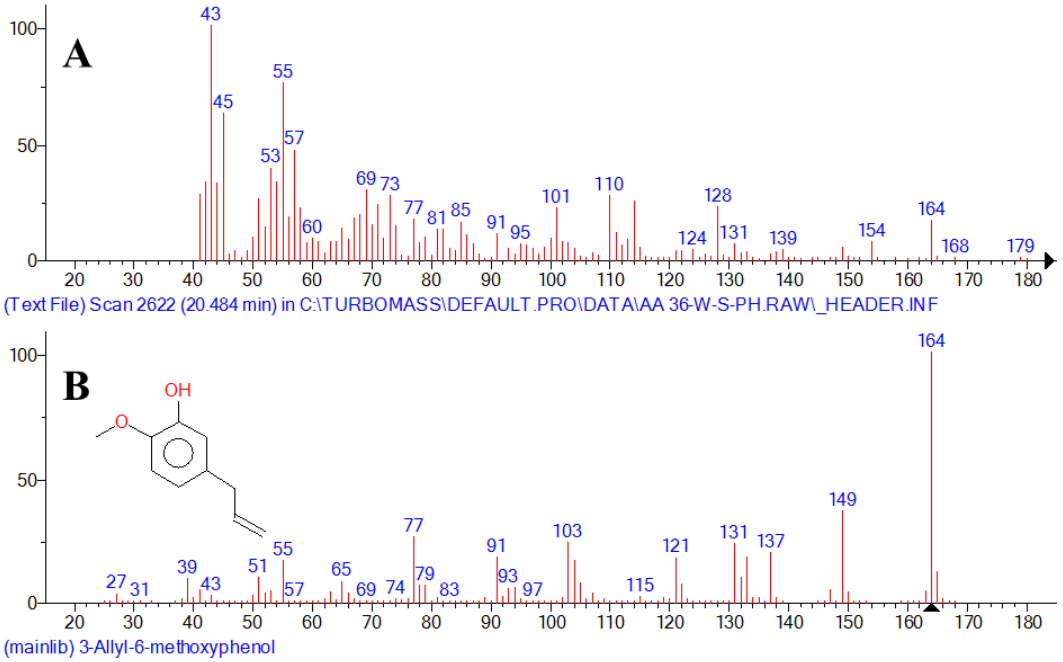

Figure A.158: Matching MS spectrum of peak number 14 MS in water-soluble extract GC-MS: A) MS of peak number 14 in water-soluble extract sample; B) MS of 3-Allyl-6-methoxyphenol according to NIST library.

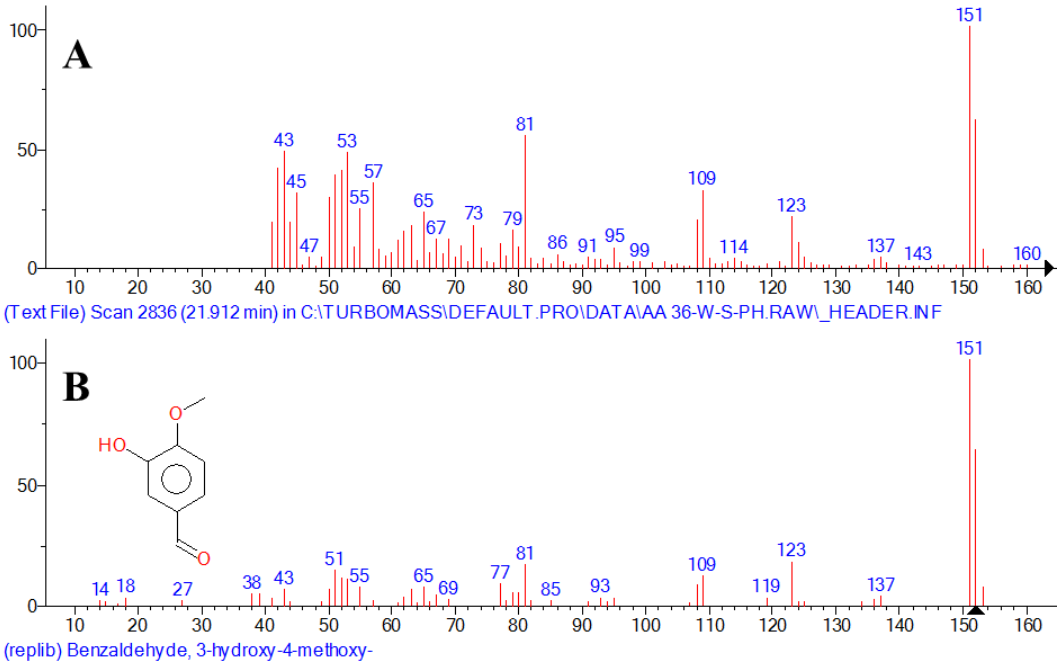

Figure A.159: Matching MS spectrum of peak number 16 MS in water-soluble extract GC-MS: A) MS of peak number 16 in water-soluble extract sample; B) MS of Benzaldehyde, 3-hydroxy-4-methoxy- according to NIST library.

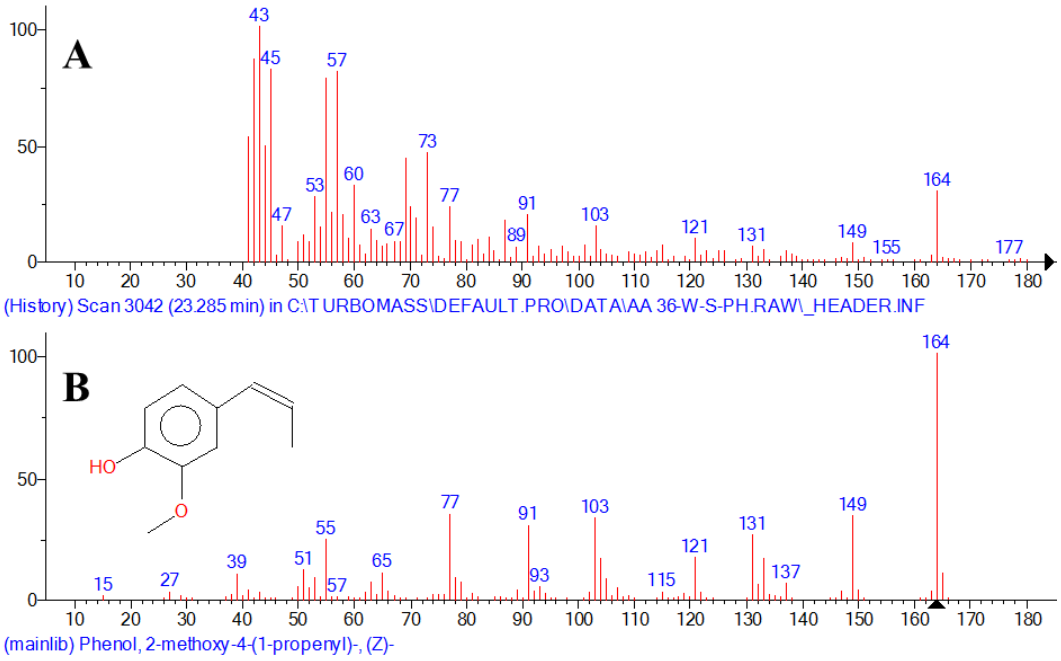

Figure A.160: Matching MS spectrum of peak number 18 MS in water-soluble extract GC-MS: A) MS of peak number 18 in water-soluble extract sample; B) MS of Phenol, 2-methoxy-4-(1-propenyl)-, (Z)- according to NIST library.

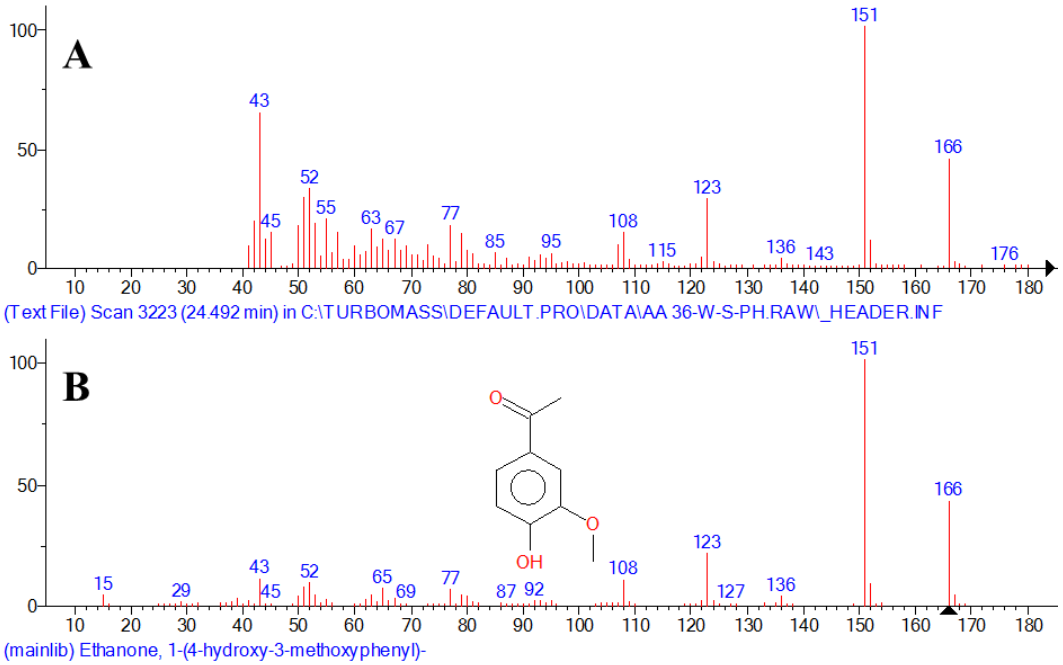

Figure A.161: Matching MS spectrum of peak number 20 MS in water-soluble extract GC-MS: A) MS of peak number 20 in water-soluble extract sample; B) MS of Ethanone, 1-(4-hydroxy-3-methoxyphenyl)- according to NIST library.

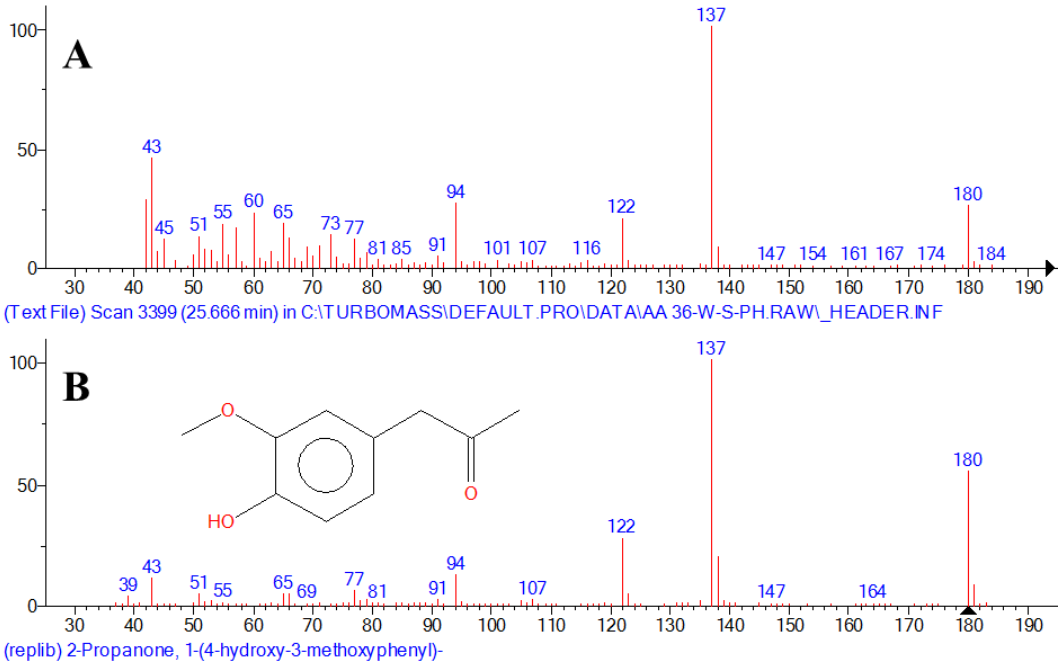

Figure A.162: Matching MS spectrum of peak number 21 MS in water-soluble extract GC-MS: A) MS of peak number 21 in water-soluble extract sample; B) MS of 2-Propanone, 1-(4-hydroxy-3-methoxyphenyl)- according to NIST library.

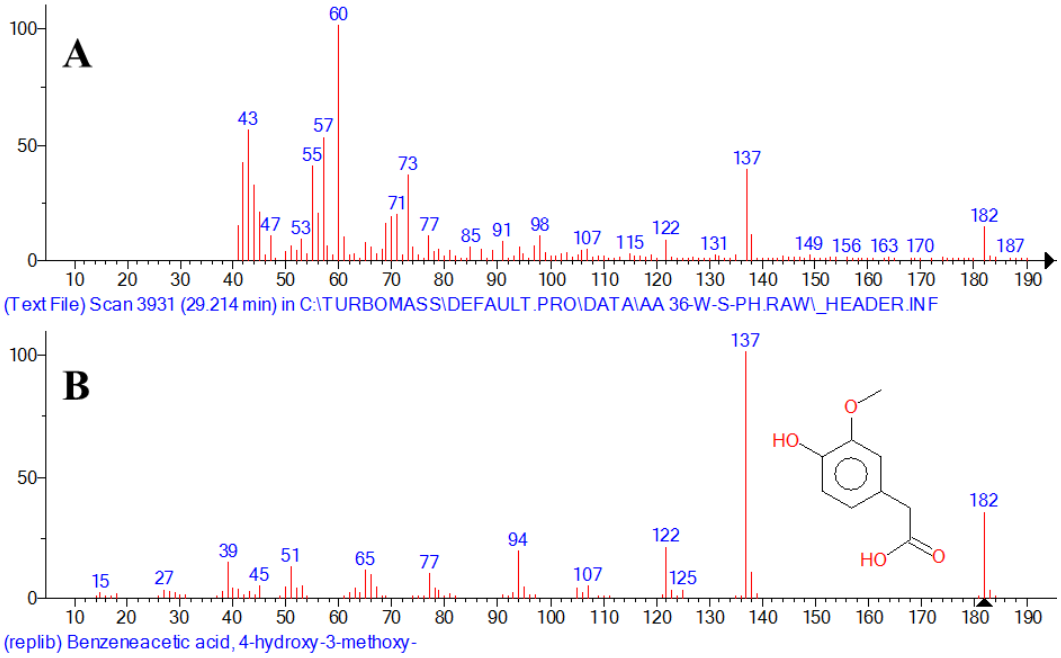

Figure A.163: Matching MS spectrum of peak number 24 MS in water-soluble extract GC-MS: A) MS of peak number 24 in water-soluble extract sample; B) MS of Benzeneacetic acid, 4-hydroxy-3-methoxy- according to NIST library.

A.4.3 Mass spectra of identified phenolic peaks in diethyl ether extract and their best NIST library match

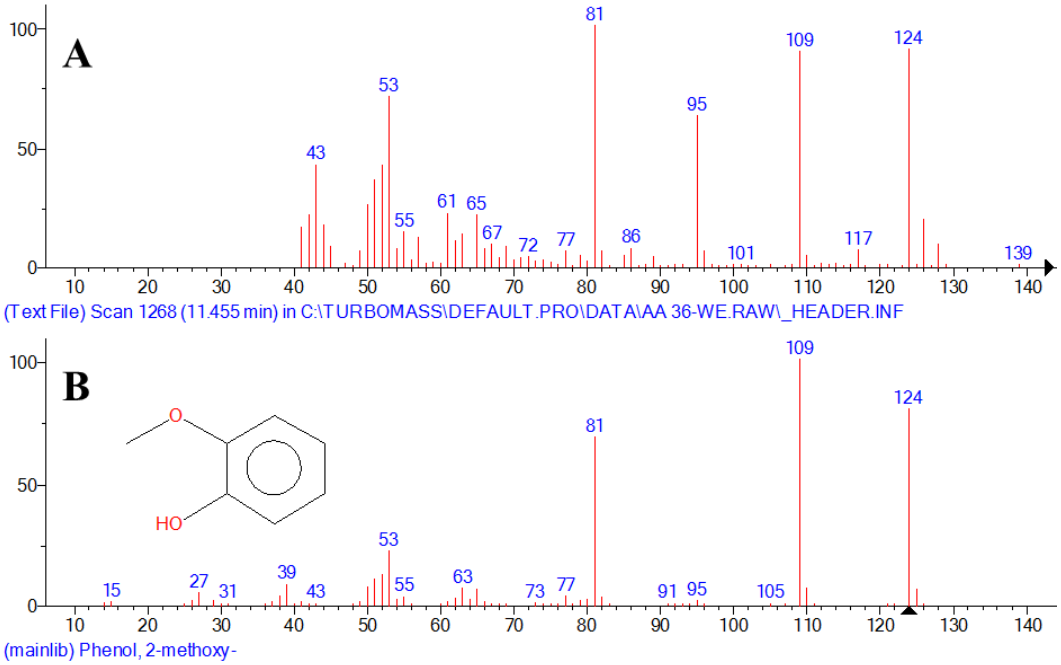

Figure A.164: Matching MS spectrum of peak number 4 MS in diethyl ether extract GC-MS: A) MS of peak number 4 in diethyl ether extract sample; B) MS of Phenol, 2-methoxy- according to NIST library.

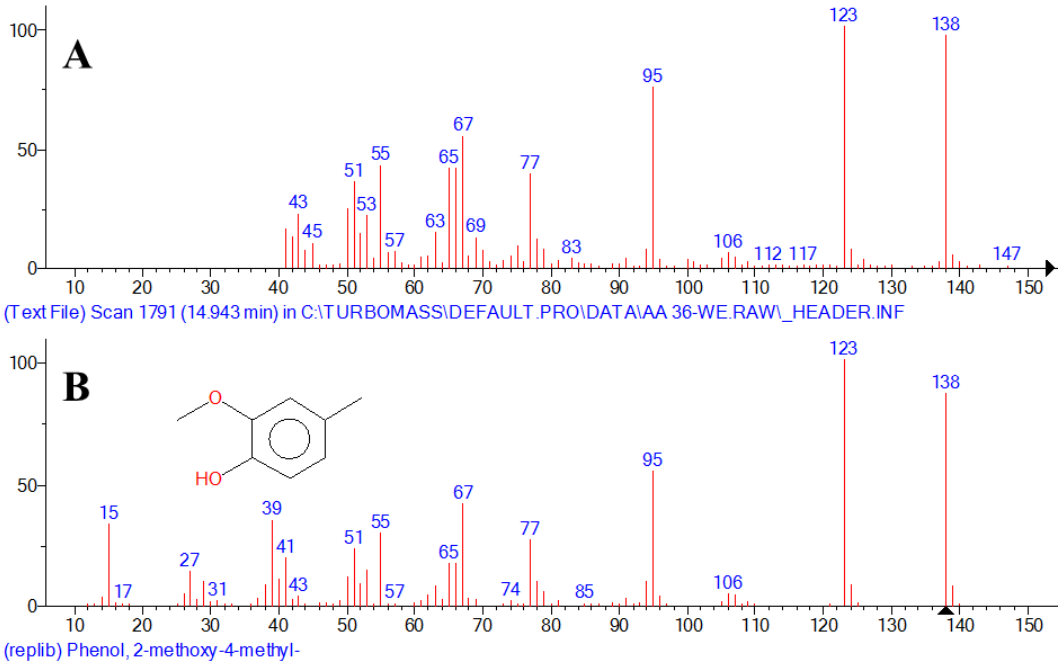

Figure A.165: Matching MS spectrum of peak number 7 MS in diethyl ether extract GC-MS: A) MS of peak number 7 in diethyl ether extract sample; B) MS of Phenol, 2-methoxy-4-methyl- according to NIST library.

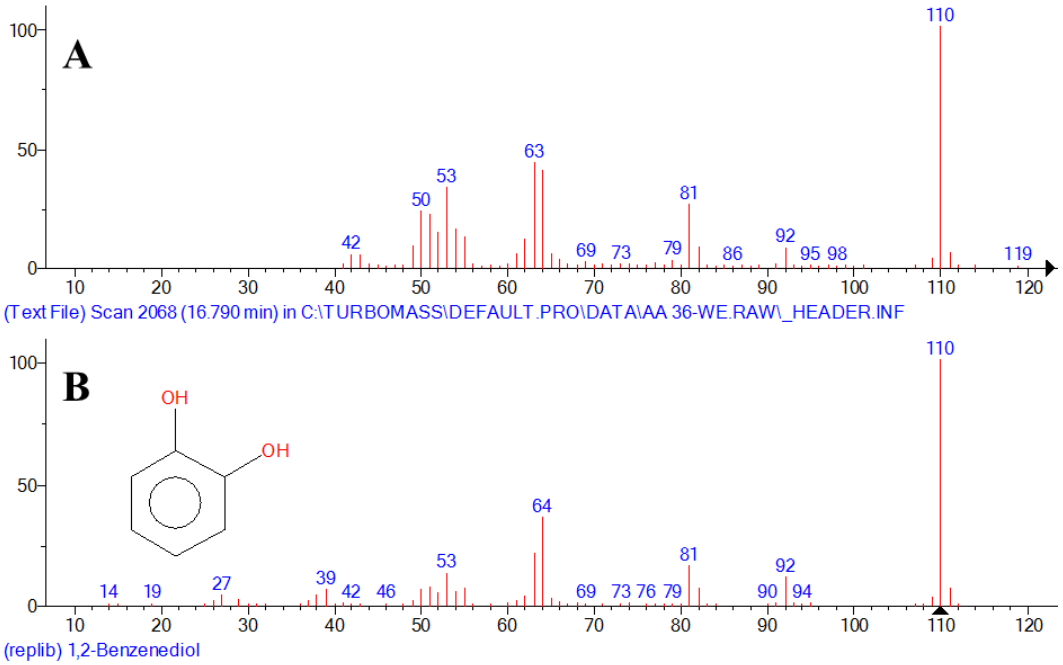

Figure A.166: Matching MS spectrum of peak number 8 MS in diethyl ether extract GC-MS: A) MS of peak number 8 in diethyl ether extract sample; B) MS of 1,2-Benzenediol according to NIST library.

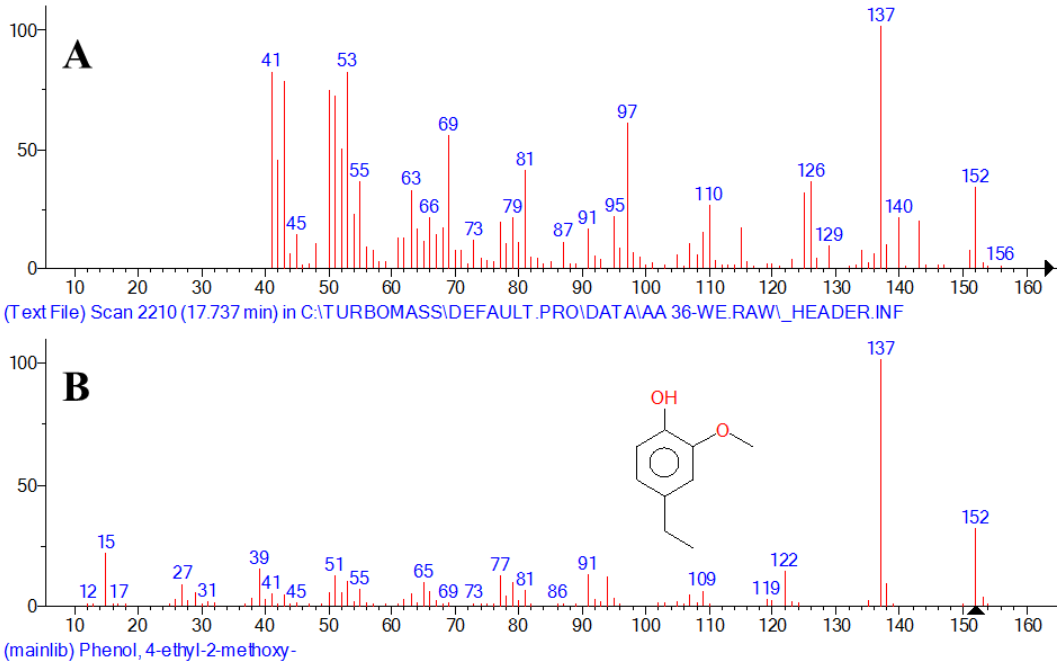

Figure A.167: Matching MS spectrum of peak number 10 MS in diethyl ether extract GC-MS: A) MS of peak number 10 in diethyl ether extract sample; B) MS of Phenol, 4-ethyl-2-methoxy- according to NIST library.

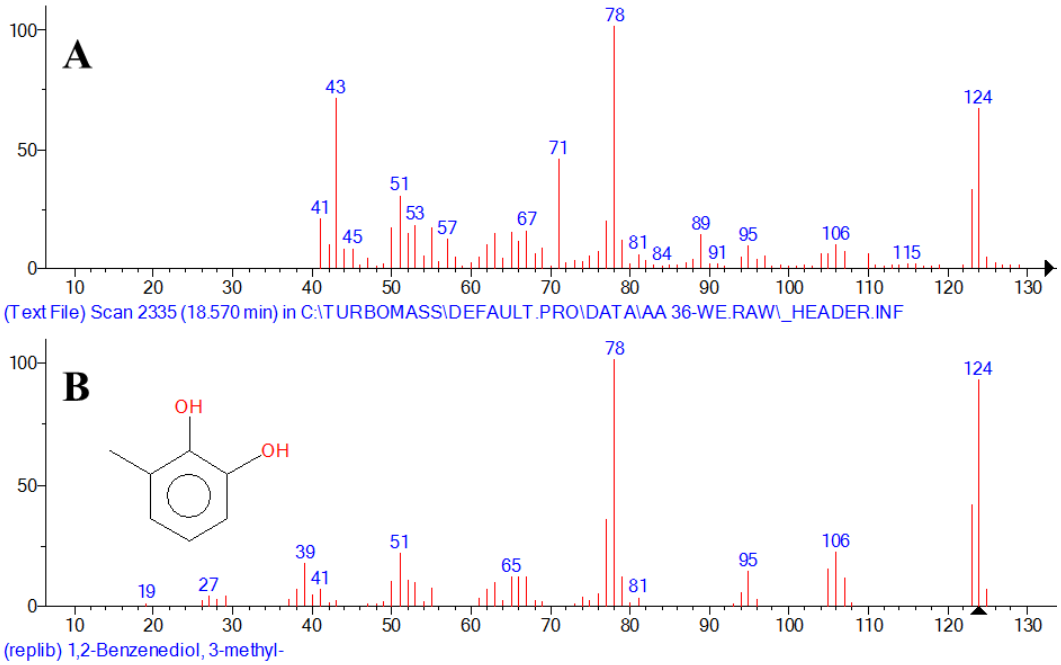

Figure A.168: Matching MS spectrum of peak number 9 MS in diethyl ether extract GC-MS: A) MS of peak number 9 in diethyl ether extract sample; B) MS of 1,2-Benzenediol, 3-methyl- according to NIST library.

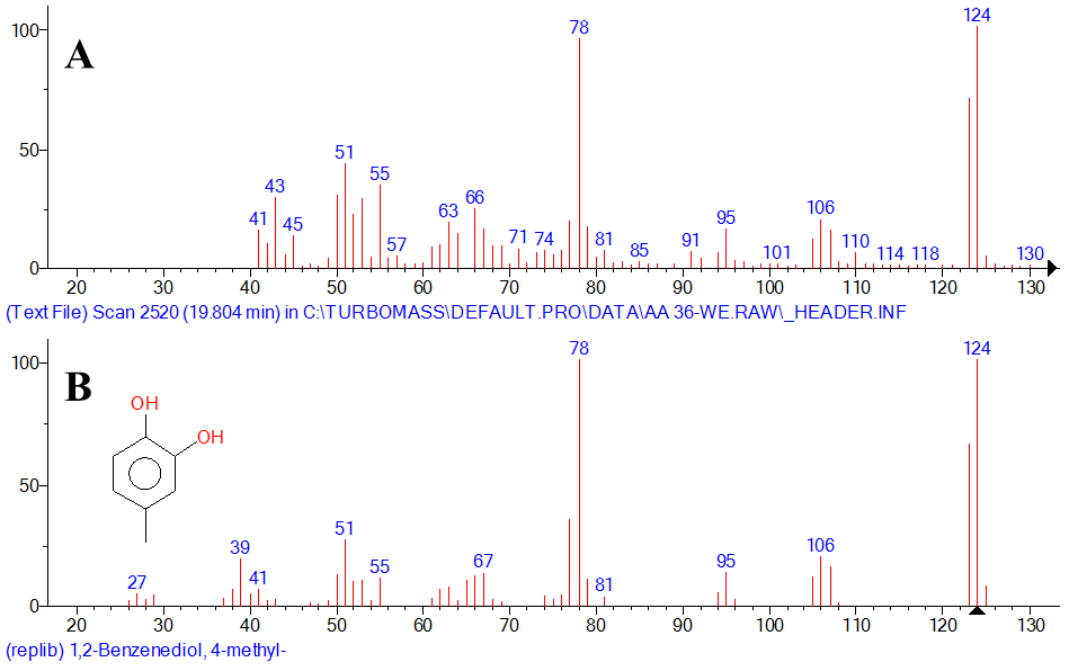

Figure A.169: Matching MS spectrum of peak number 11 MS in diethyl ether extract GC-MS: A) MS of peak number 11 in diethyl ether extract sample; B) MS of 1,2-Benzenediol, 4-methyl- according to NIST library.

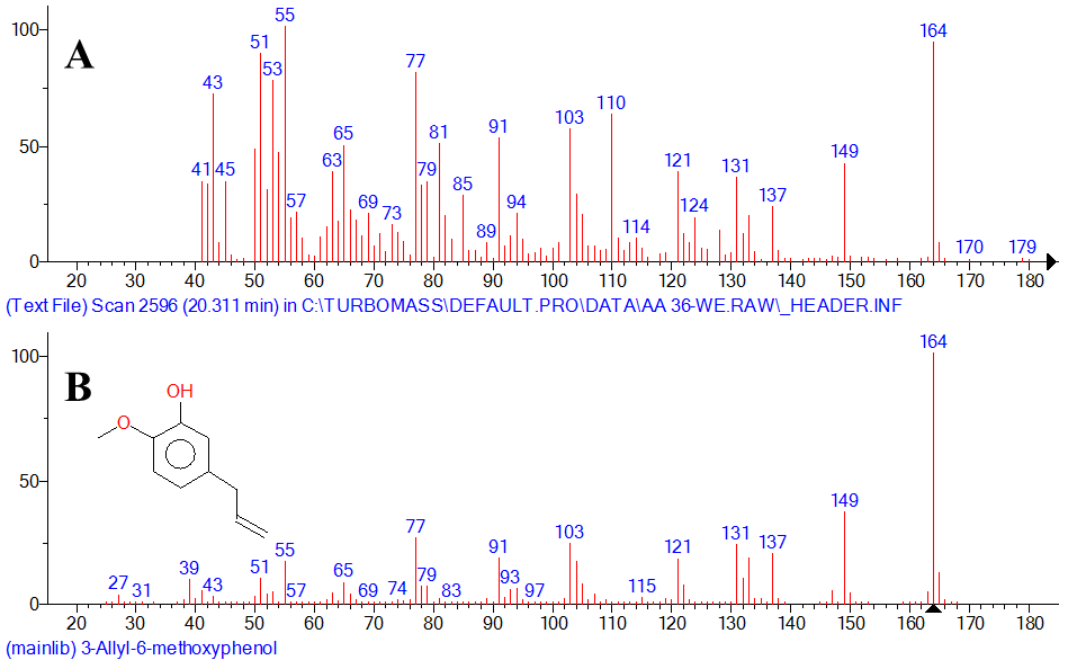

Figure A.170: Matching MS spectrum of peak number 14 MS in diethyl ether extract GC-MS: A) MS of peak number 14 in diethyl ether extract sample; B) MS of 3-Allyl-6-methoxyphenol according to NIST library.

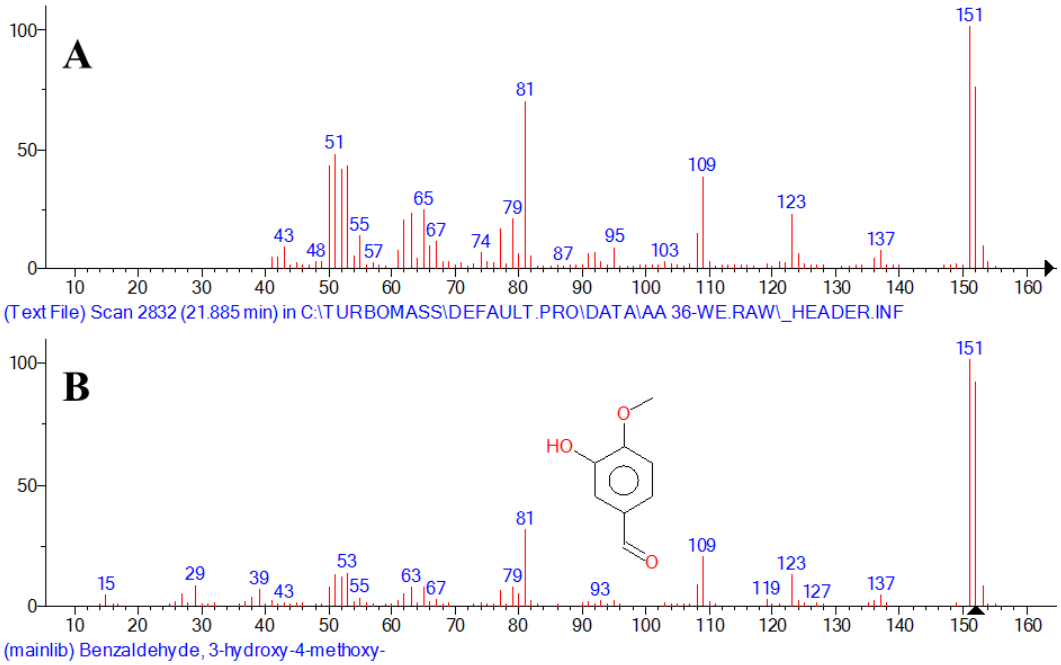

Figure A.171: Matching MS spectrum of peak number 16 MS in diethyl ether extract GC-MS: A) MS of peak number 16 in diethyl ether extract sample; B) MS of Benzaldehyde, 3-hydroxy-4-methoxy- according to NIST library.

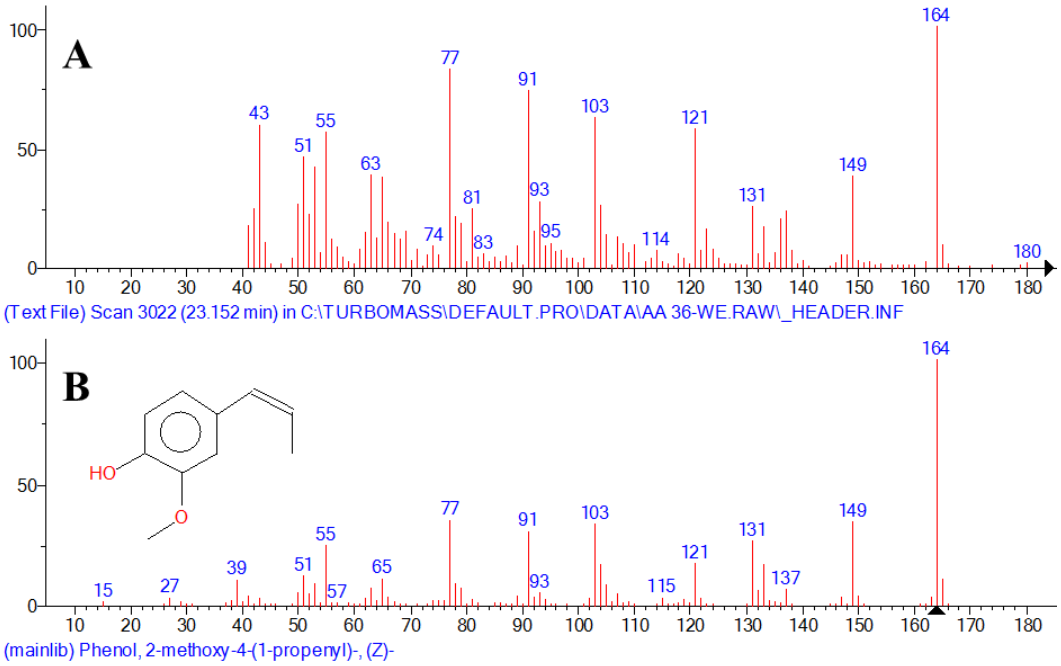

Figure A.172: Matching MS spectrum of peak number 18 MS in diethyl ether extract GC-MS: A) MS of peak number 18 in diethyl ether extract sample; B) MS of Phenol, 2-methoxy-4-(1-propenyl)-, (Z)- according to NIST library.

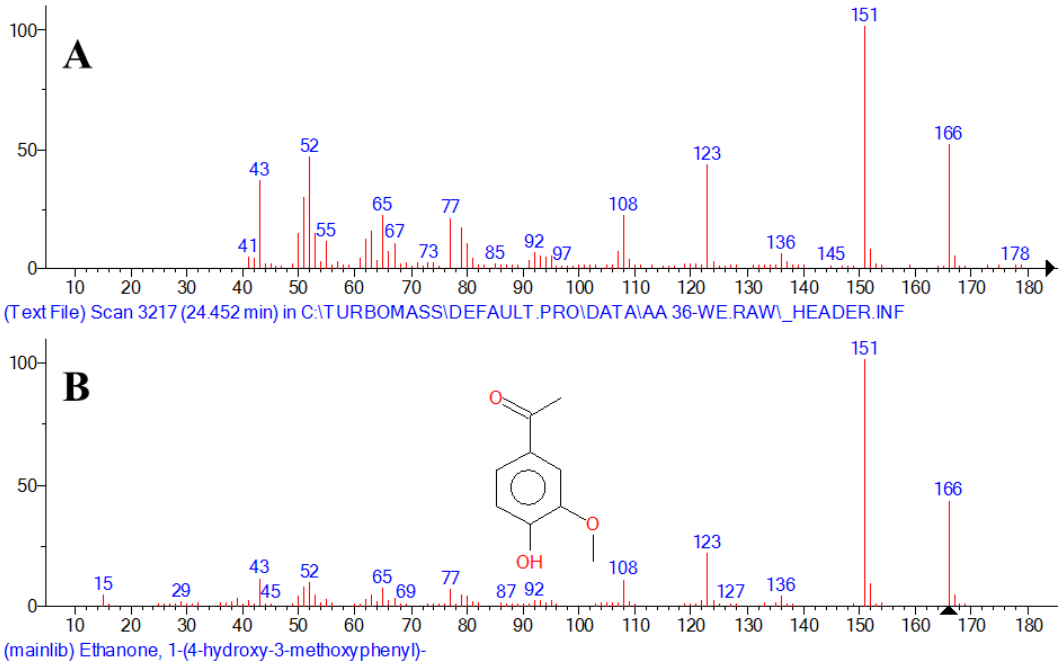

Figure A.173: Matching MS spectrum of peak number 20 MS in diethyl ether extract GC-MS: A) MS of peak number 20 in diethyl ether extract sample; B) MS of Ethanone, 1-(4-hydroxy-3-methoxyphenyl)- according to NIST library.

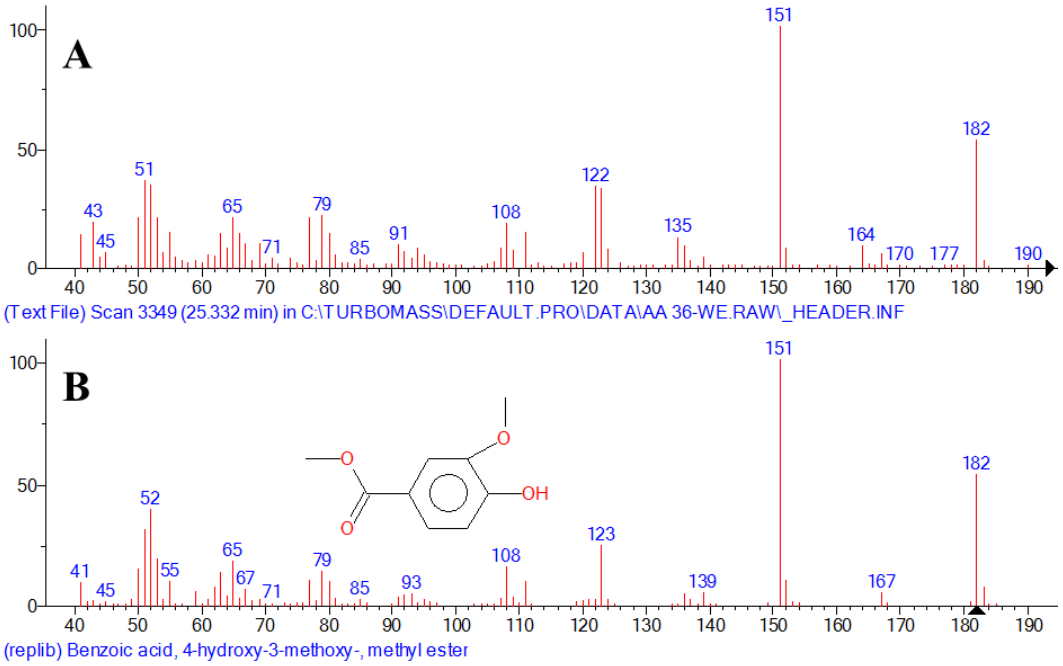

Figure A.174: Matching MS spectrum of peak number 35 MS in diethyl ether extract GC-MS: A) MS of peak number 35 in diethyl ether extract sample; B) MS of Benzoic acid, 4-hydroxy-3-methoxy-, methyl ester according to NIST library.

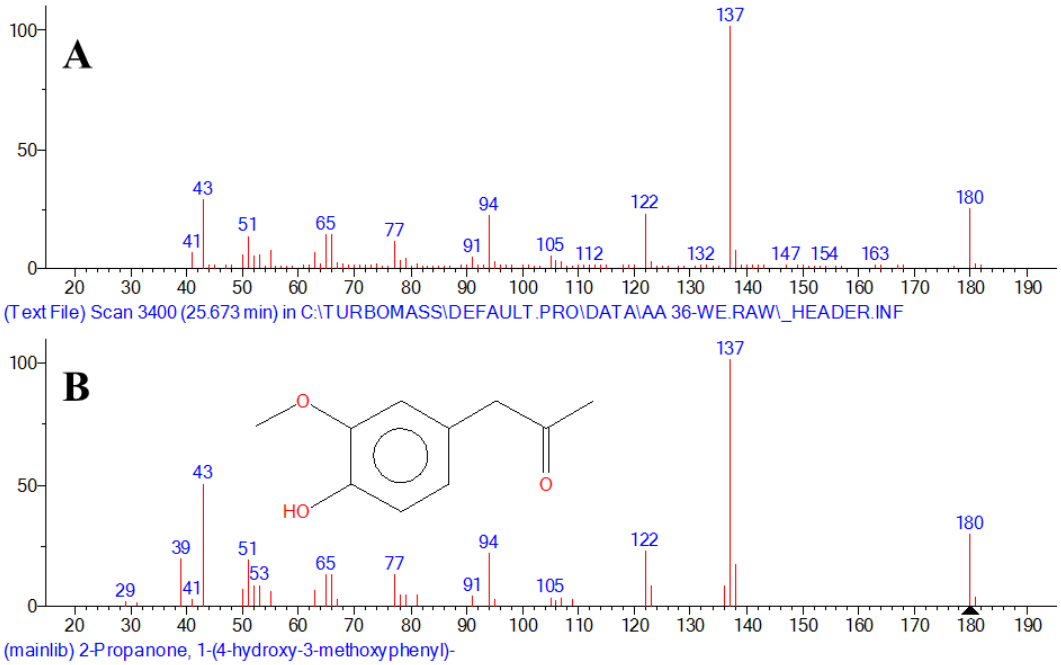

Figure A.175: Matching MS spectrum of peak number 21 MS in diethyl ether extract GC-MS: A) MS of peak number 21 in diethyl ether extract sample; B) MS of 2-Propanone, 1-(4-hydroxy-3-methoxyphenyl)- according to NIST library.

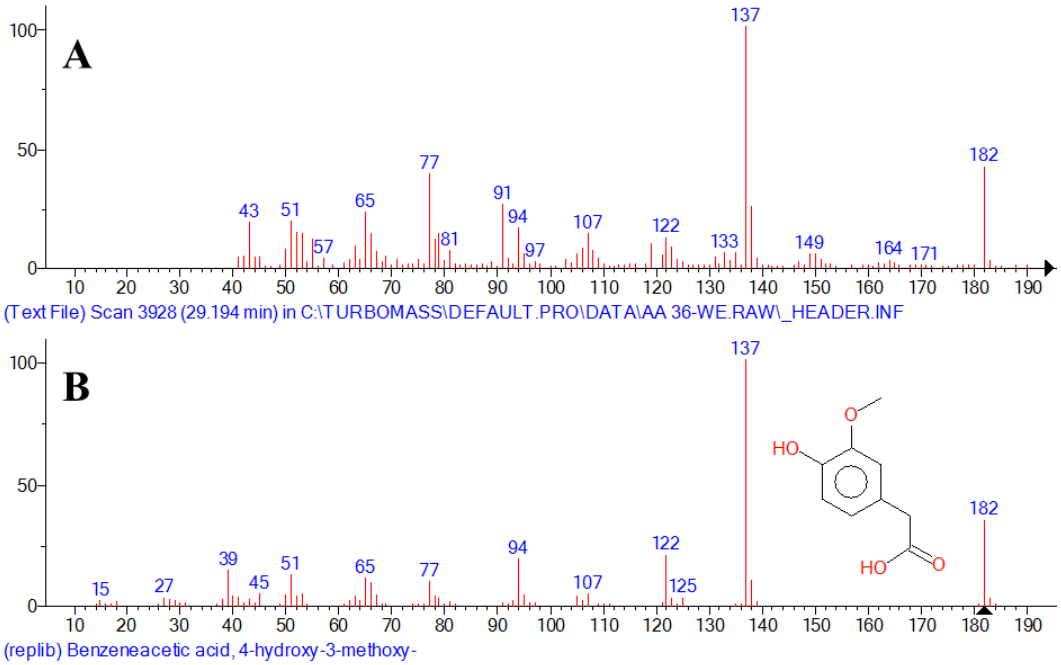

Figure A.176: Matching MS spectrum of peak number 24 MS in diethyl ether extract GC-MS: A) MS of peak number 24 in diethyl ether extract sample; B) MS of Benzeneacetic acid, 4-hydroxy-3-methoxy- according to NIST library.

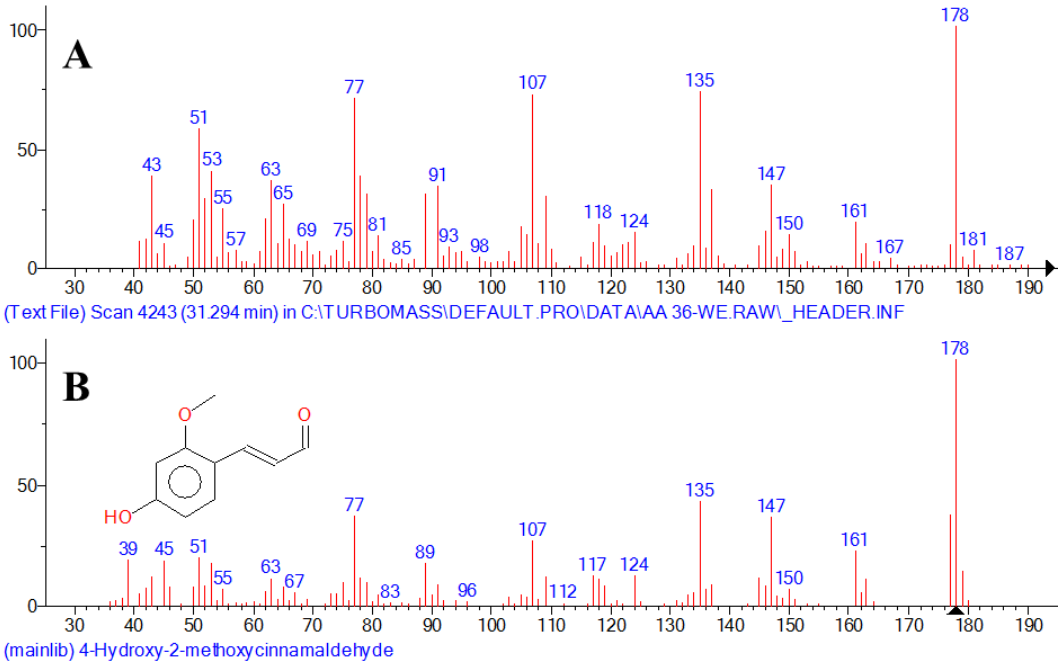

Figure A.177: Matching MS spectrum of peak number 26 MS in diethyl ether extract GC-MS: A) MS of peak number 26 in diethyl ether extract sample; B) MS of 4-Hydroxy-2-methoxycinnamaldehyde according to NIST library.

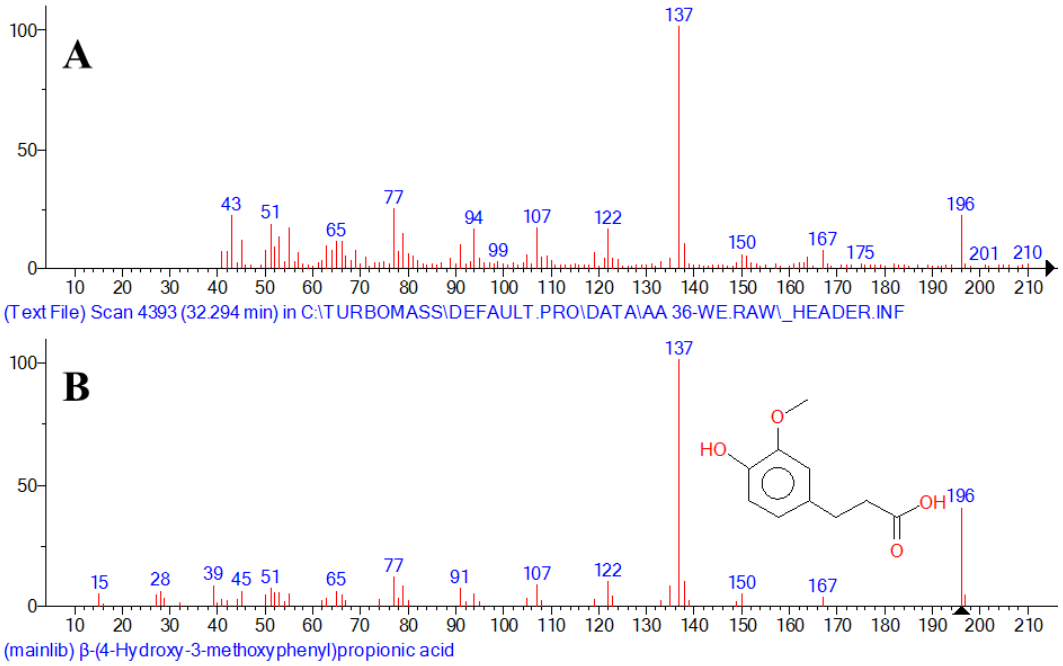

Figure A.178: Matching MS spectrum of peak number 36 MS in diethyl ether extract GC-MS: A) MS of peak number 36 in diethyl ether extract sample; B) MS of β-(4-Hydroxy-3-methoxyphenyl)propionic acid according to NIST library.

A.5 Mass Spectra of Identified Phenolic Peaks in Supercritical CO_2 Extraction Experiment

A.5.1 Mass spectra of identified phenolic peaks in 1st extract of crude bio-oil and their best library match

The mass spectra are the same as A.2.1.

A.5.2 Mass spectra of identified phenolic peaks in CO_2-1 and their best library match

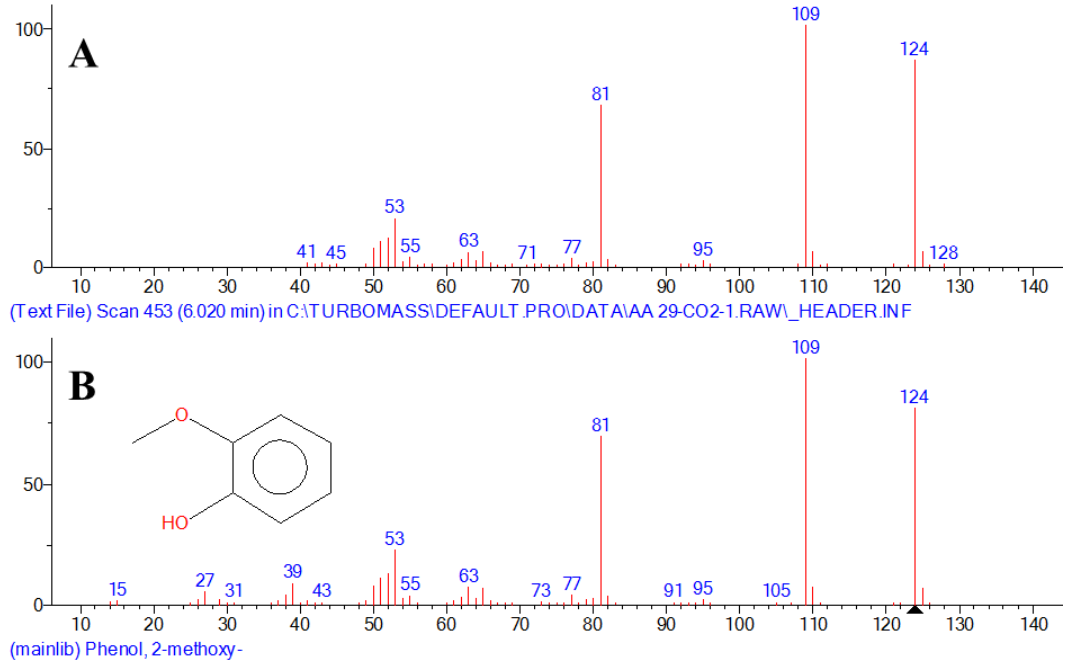

Figure A.179: Matching MS spectrum of peak number 4 MS in CO_2-1 extract GC-MS: A) MS of peak number 4 in CO_2-1 extract sample; B) MS of Phenol, 2-methoxy- according to NIST library.

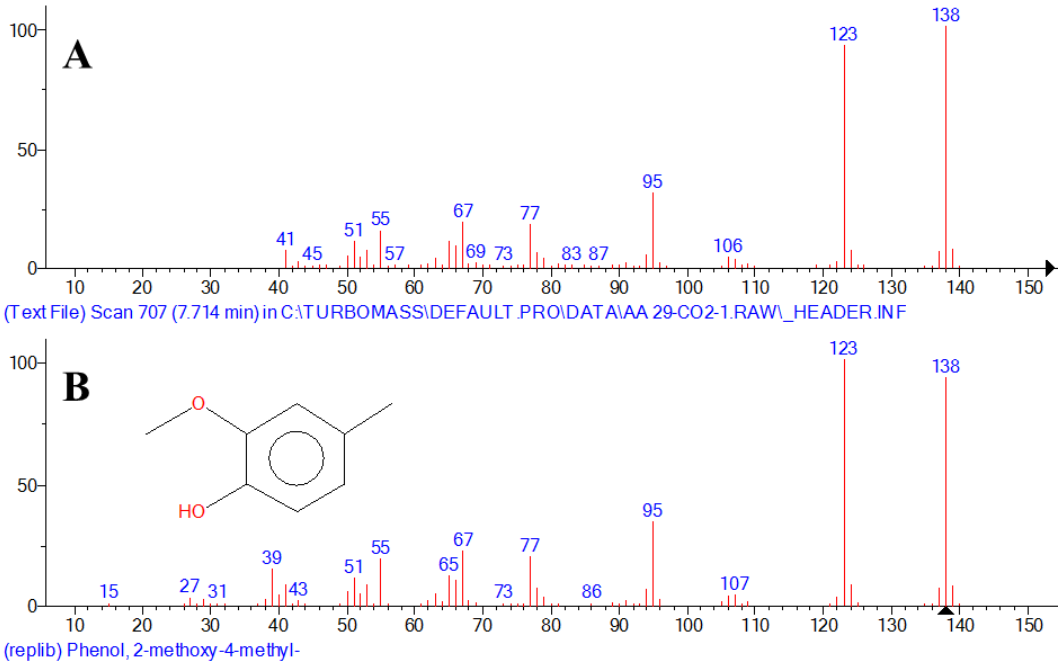

Figure A.180: Matching MS spectrum of peak number 7 MS in CO_2-1 extract GC-MS: A) MS of peak number 7 in CO_2-1 extract sample; B) MS of Phenol, 2-methoxy-4-methyl- according to NIST library.

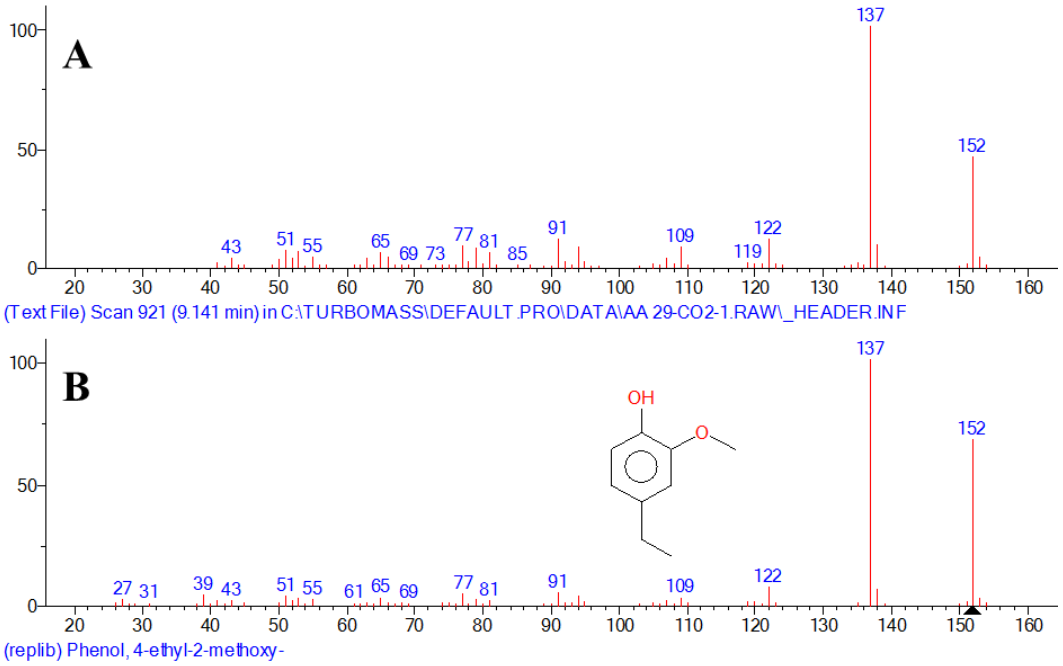

Figure A.181: Matching MS spectrum of peak number 10 MS in CO_2-1 extract GC-MS: A) MS of peak number 10 in CO_2-1 extract sample; B) MS of Phenol, 4-ethyl-2-methoxy- according to NIST library.

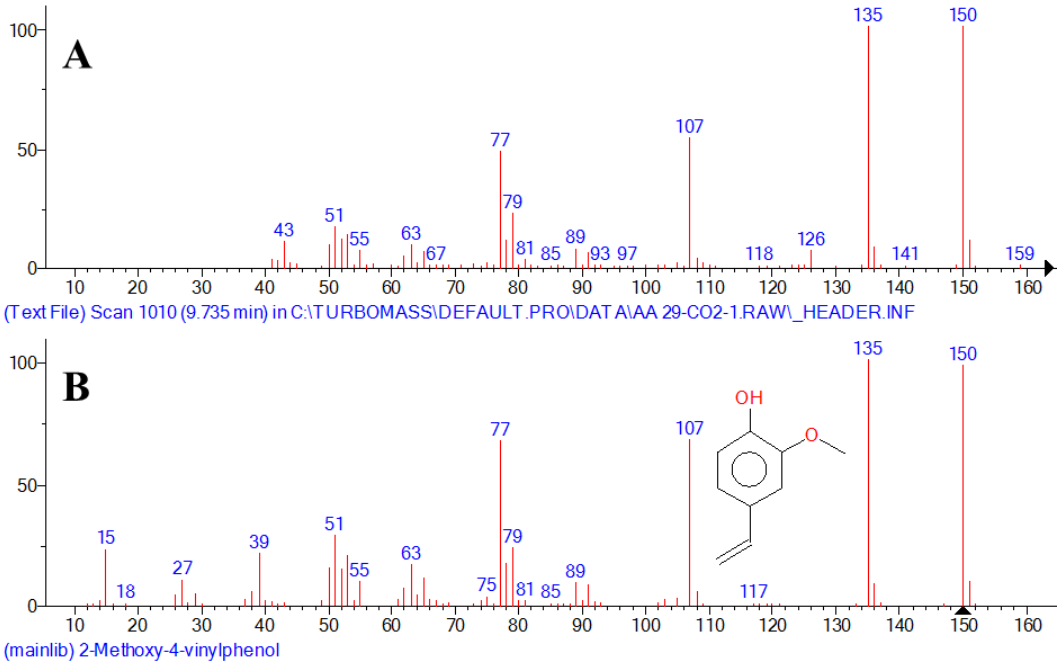

Figure A.182: Matching MS spectrum of peak number 12 MS in CO_2-1 extract GC-MS: A) MS of peak number 12 in CO_2-1 extract sample; B) MS of 2-Methoxy-4-vinylphenol according to NIST library.

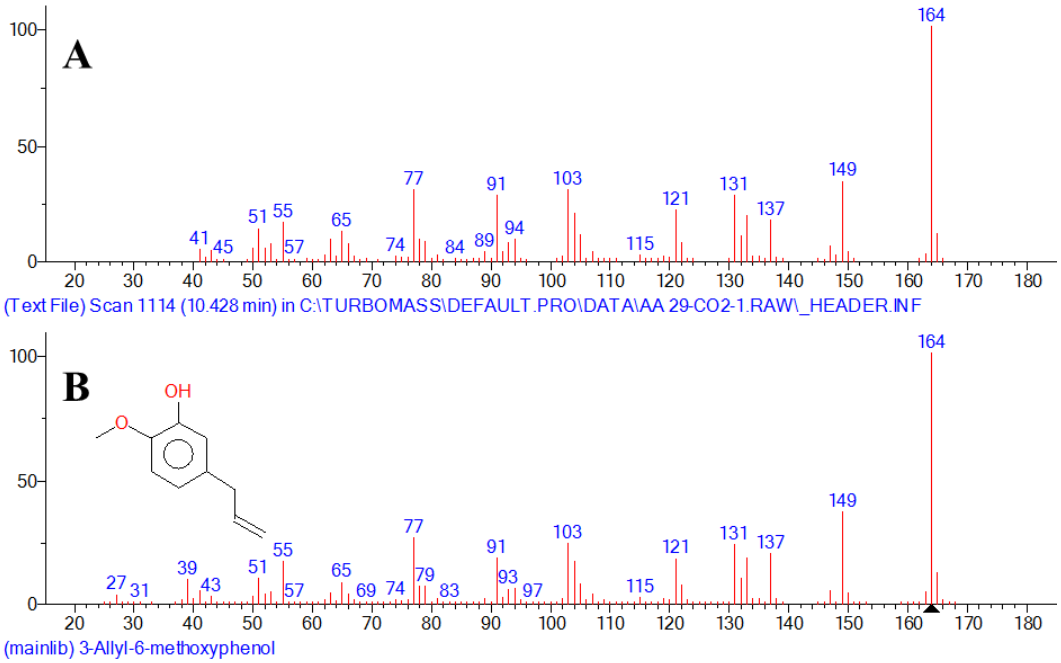

Figure A.183: Matching MS spectrum of peak number 14 MS in CO_2-1 extract GC-MS: A) MS of peak number 14 in CO_2-1 extract sample; B) MS of 3-Allyl-6-methoxyphenol according to NIST library.

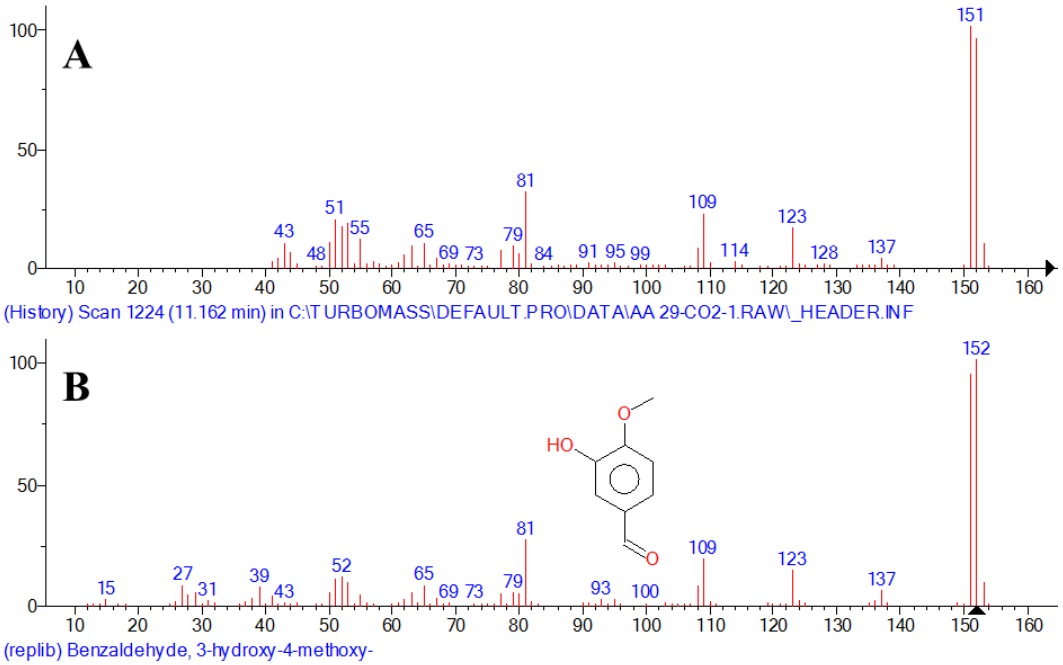

Figure A.184: Matching MS spectrum of peak number 16 MS in CO_2-1 extract GC-MS: A) MS of peak number 16 in CO_2-1 extract sample; B) MS of Benzaldehyde, 3-hydroxy-4-methoxy- according to NIST library.

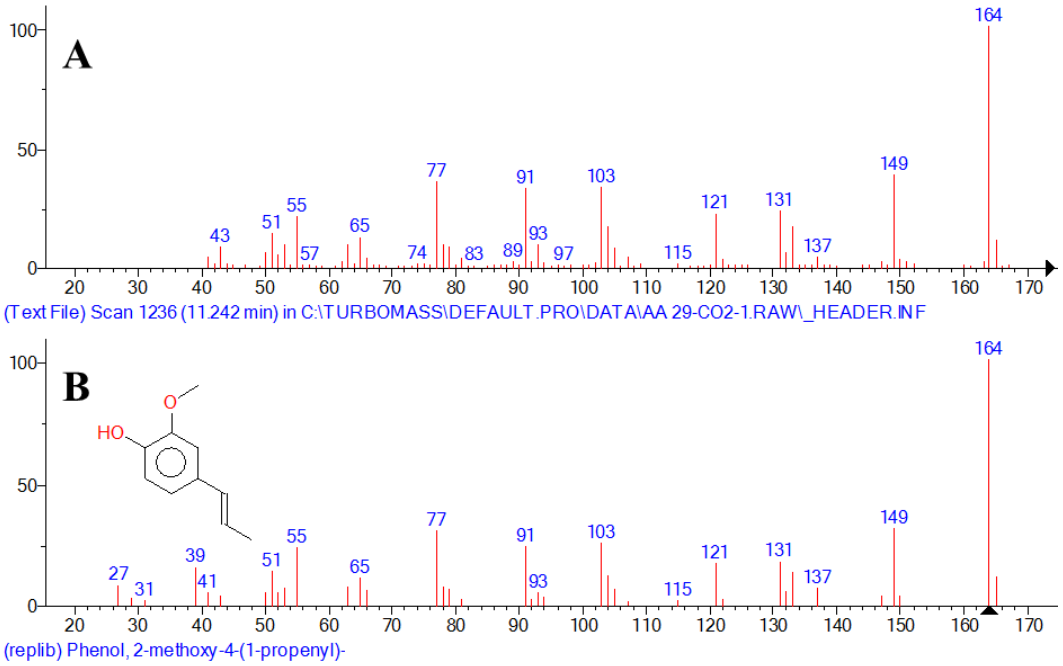

Figure A.185: Matching MS spectrum of peak number 17 MS in CO_2-1 extract GC-MS: A) MS of peak number 17 in CO_2-1 extract sample; B) MS of Phenol, 2-methoxy-4-(1-propenyl)- according to NIST library.

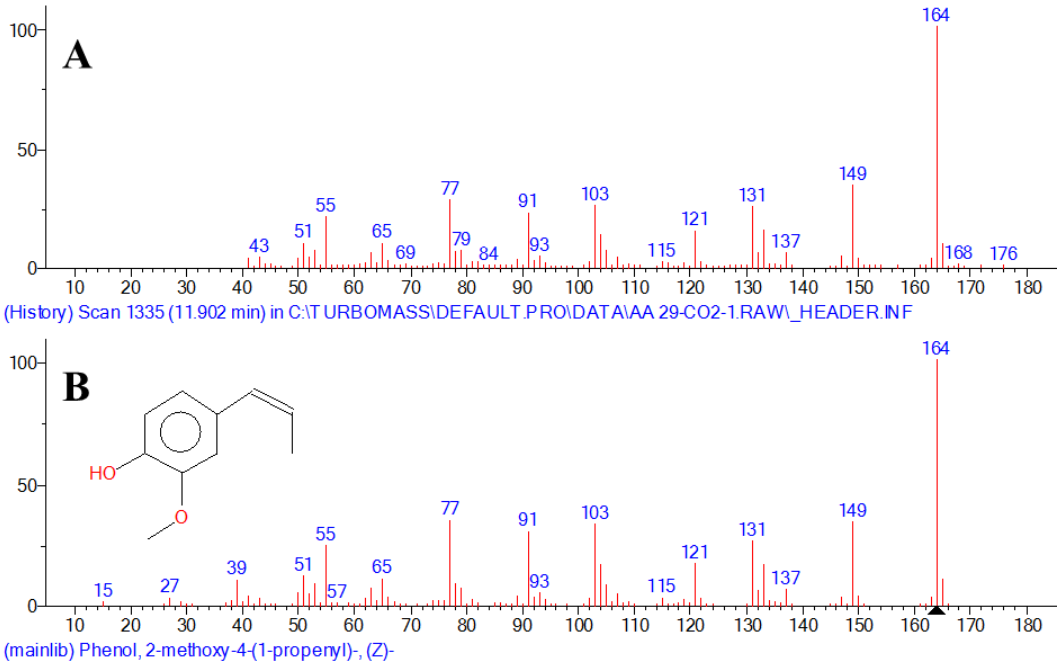

Figure A.186: Matching MS spectrum of peak number 18 MS in CO_2-1 extract GC-MS: A) MS of peak number 18 in CO_2-1 extract sample; B) MS of Phenol, 2-methoxy-4-(1-propenyl)-, (Z)- according to NIST library.

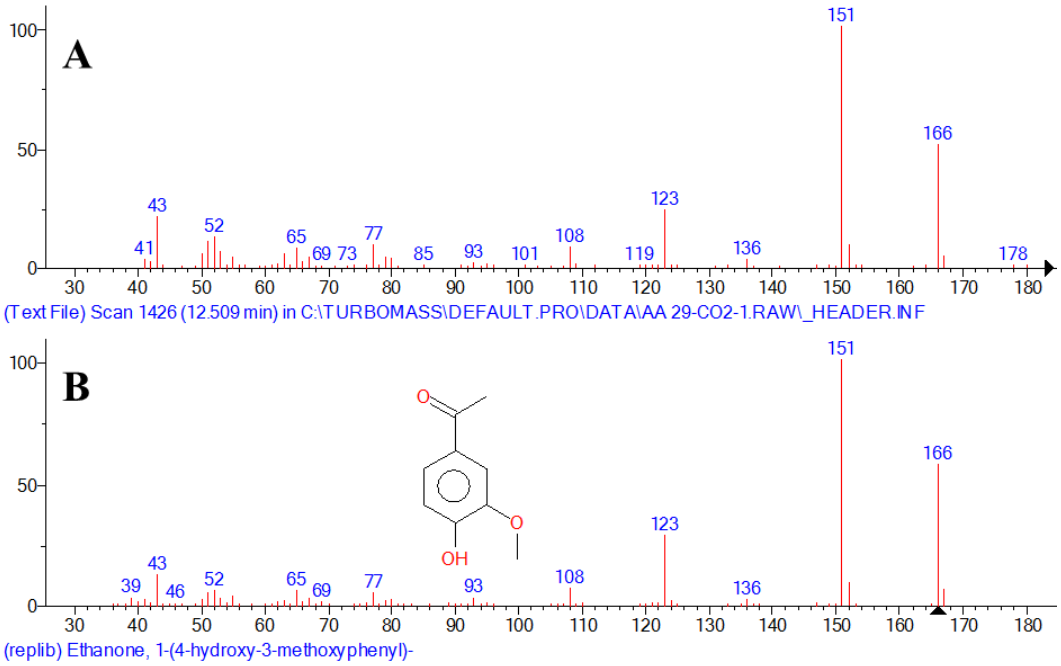

Figure A.187: Matching MS spectrum of peak number 20 MS in CO_2-1 extract GC-MS: A) MS of peak number 20 in CO_2-1 extract sample; B) MS of Ethanone, 1-(4-hydroxy-3-methoxyphenyl)- according to NIST library.

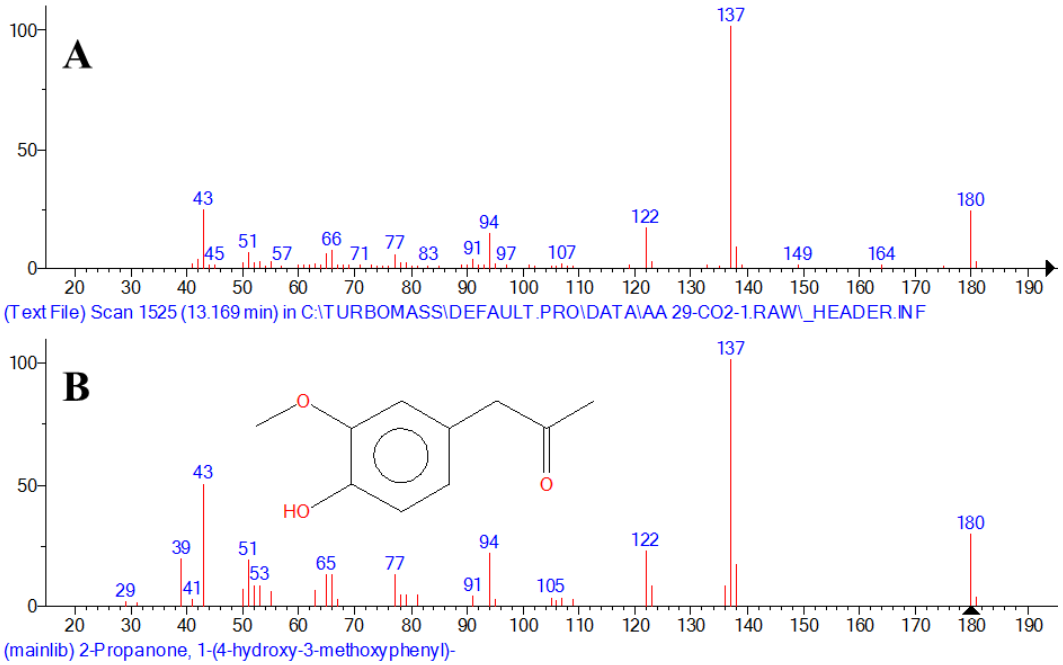

Figure A.188: Matching MS spectrum of peak number 21 MS in CO_2-1 extract GC-MS: A) MS of peak number 21 in CO_2-1 extract sample; B) MS of 2-Propanone, 1-(4-hydroxy-3-methoxyphenyl)- according to NIST library.

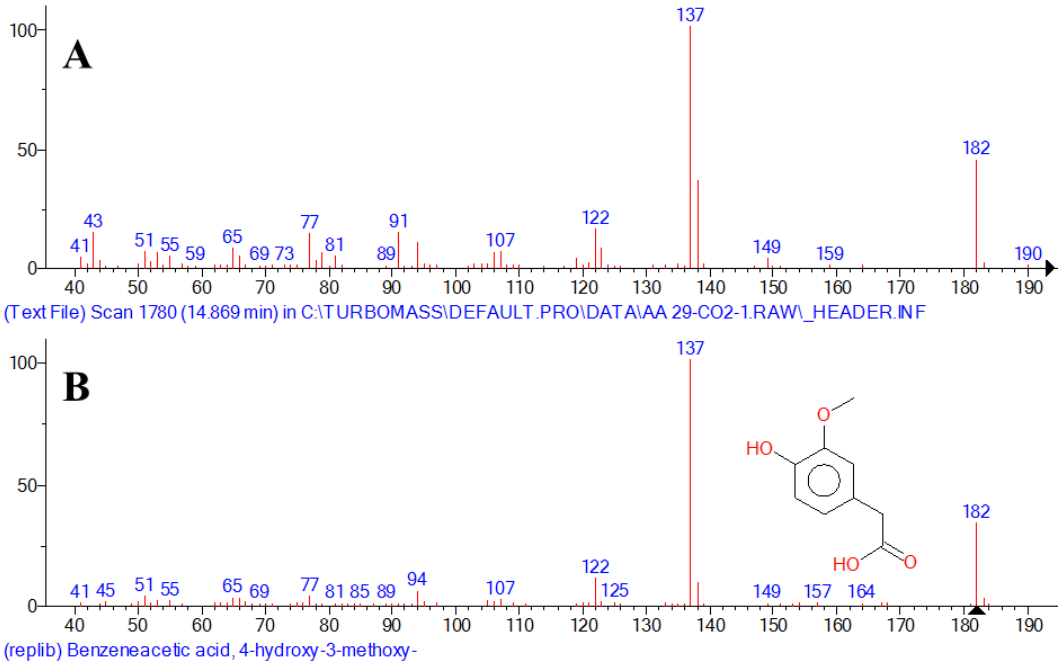

Figure A.189: Matching MS spectrum of peak number 24 MS in CO_2-1 extract GC-MS: A) MS of peak number 24 in CO_2-1 extract sample; B) MS of Benzeneacetic acid, 4-hydroxy-3-methoxy- according to NIST library.

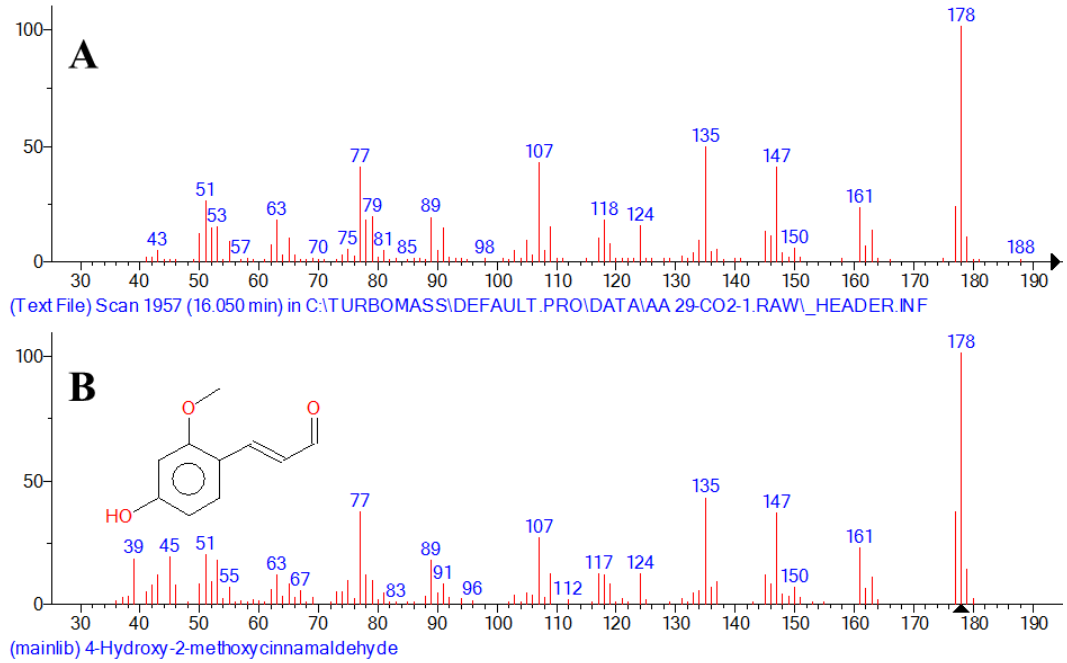

Figure A.190: Matching MS spectrum of peak number 26 MS in CO_2-1 extract GC-MS: A) MS of peak number 26 in CO_2-1 extract sample; B) MS of 4-Hydroxy-2-methoxycinnamaldehyde according to NIST library.

A.5.3 Mass spectra of identified phenolic peaks in CO_2-2 and their best library match

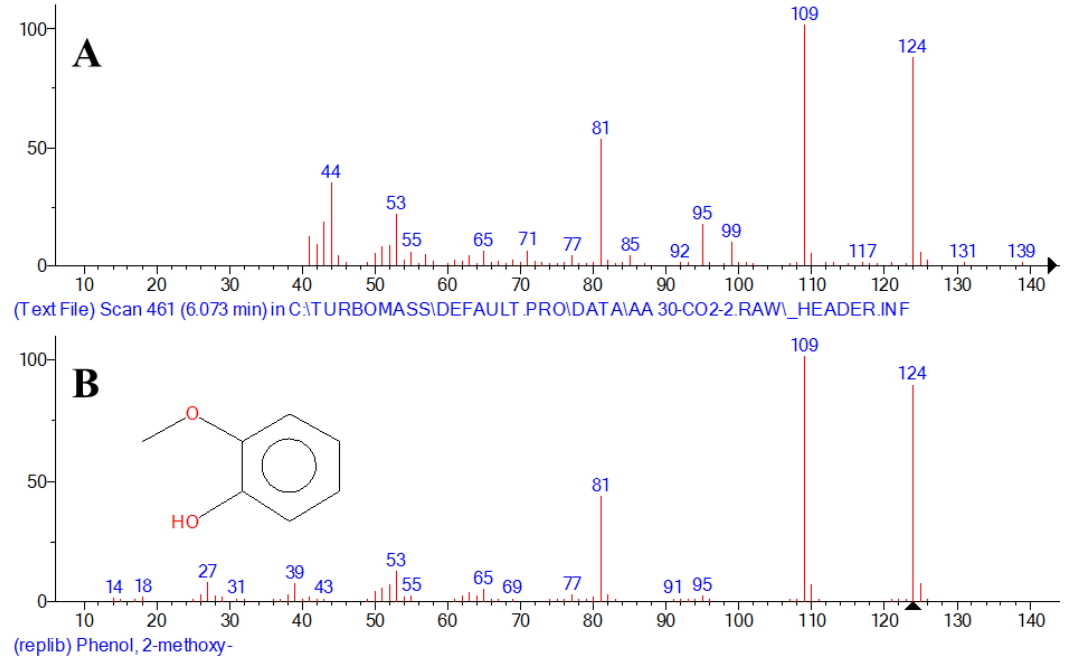

Figure A.191: Matching MS spectrum of peak number 4 MS in CO_2-2 extract GC-MS: A) MS of peak number 4 in CO_2-2 extract sample; B) MS of Phenol, 2-methoxy- according to NIST library.

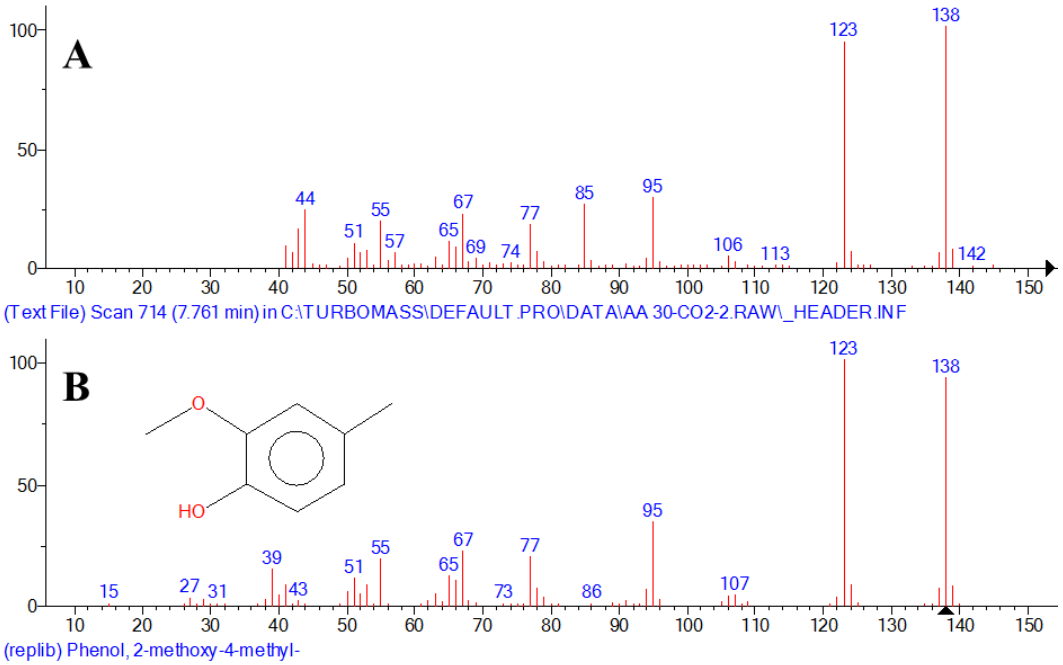

Figure A.192: Matching MS spectrum of peak number 7 MS in CO_2-2 extract GC-MS: A) MS of peak number 7 in CO_2-2 extract sample; B) MS of Phenol, 2-methoxy-4-methyl- according to NIST library.

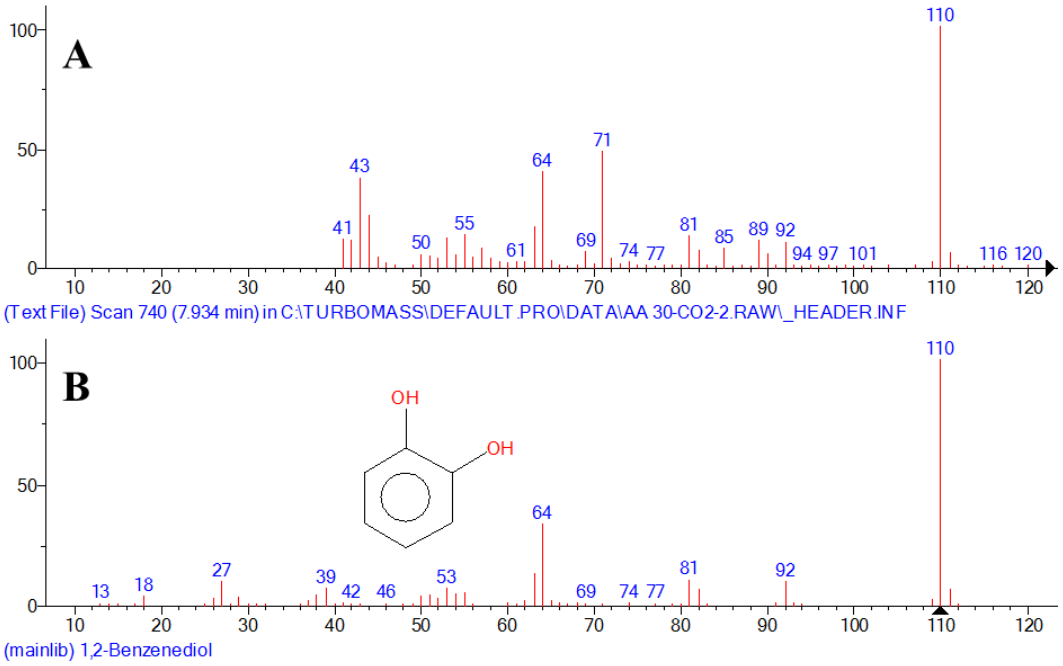

Figure A.193: Matching MS spectrum of peak number 8 MS in CO_2-2 extract GC-MS: A) MS of peak number 8 in CO_2-2 extract sample; B) MS of 1,2-Benzenediol according to NIST library.

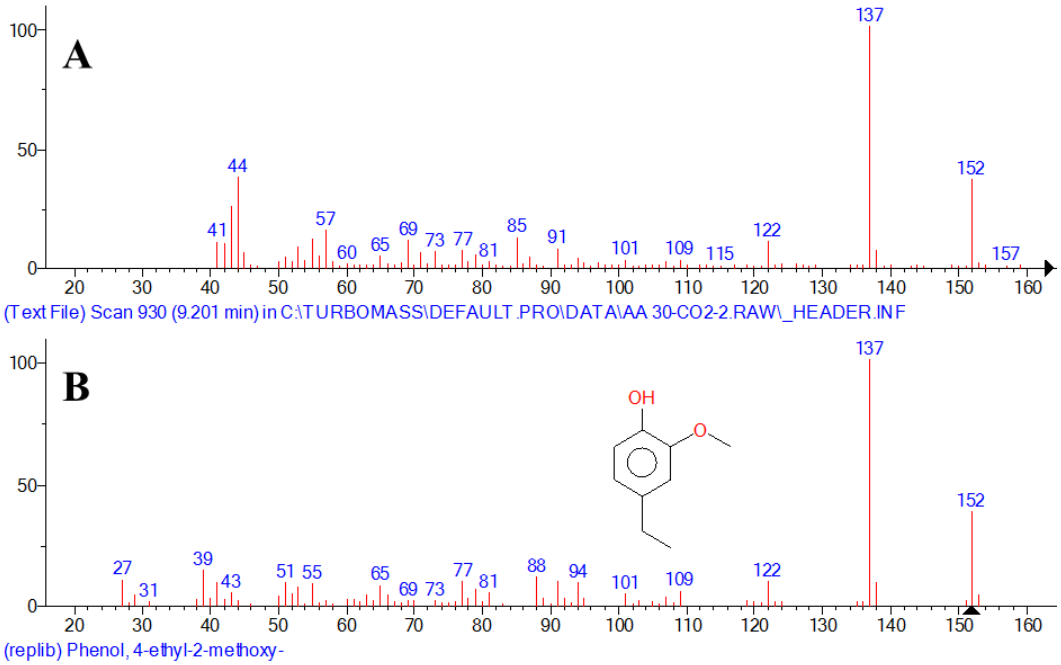

Figure A.194: Matching MS spectrum of peak number 10 MS in CO_2-2 extract GC-MS: A) MS of peak number 10 in CO_2-2 extract sample; B) MS of Phenol, 4-ethyl-2-methoxy- according to NIST library.

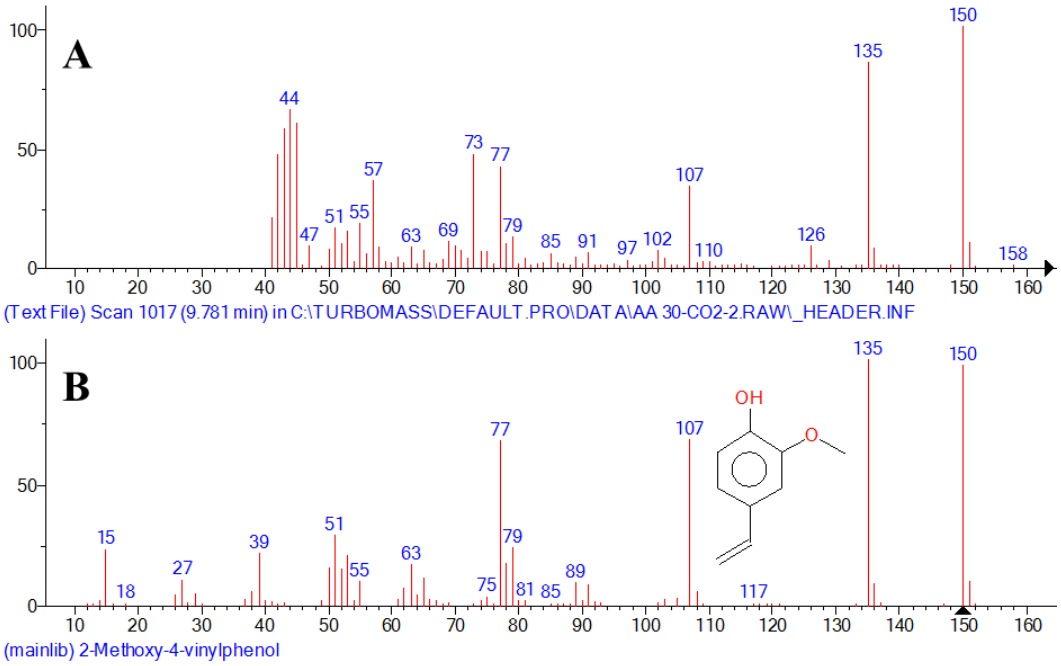

Figure A.195: Matching MS spectrum of peak number 12 MS in CO_2-2 extract GC-MS: A) MS of peak number 12 in CO_2-2 extract sample; B) MS of 2-Methoxy-4-vinylphenol according to NIST library.

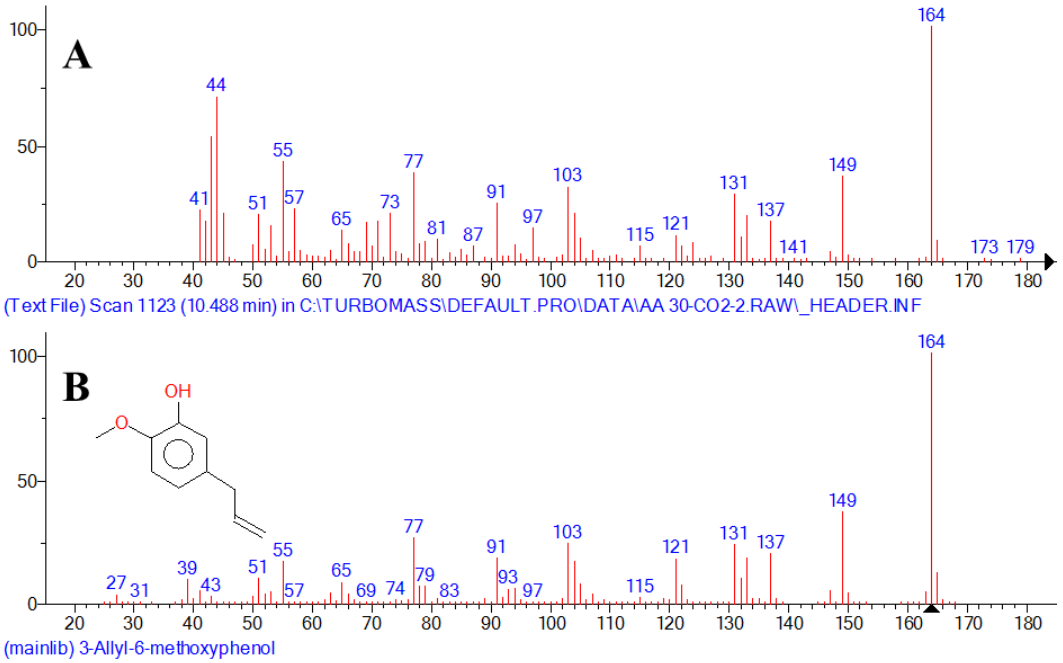

Figure A.196: Matching MS spectrum of peak number 14 MS in CO_2-2 extract GC-MS: A) MS of peak number 14 in CO_2-2 extract sample; B) MS of 3-Allyl-6-methoxyphenol according to NIST library.

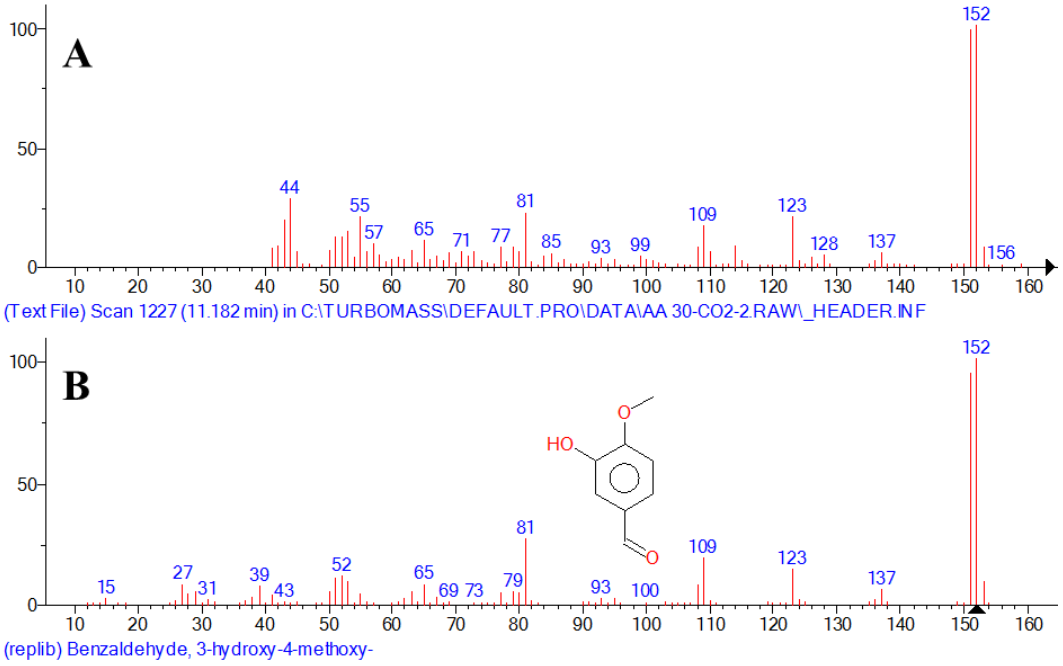

Figure A.197: Matching MS spectrum of peak number 16 MS in CO_2-2 extract GC-MS: A) MS of peak number 16 in CO_2-2 extract sample; B) MS of Benzaldehyde, 3-hydroxy-4-methoxy- according to NIST library.

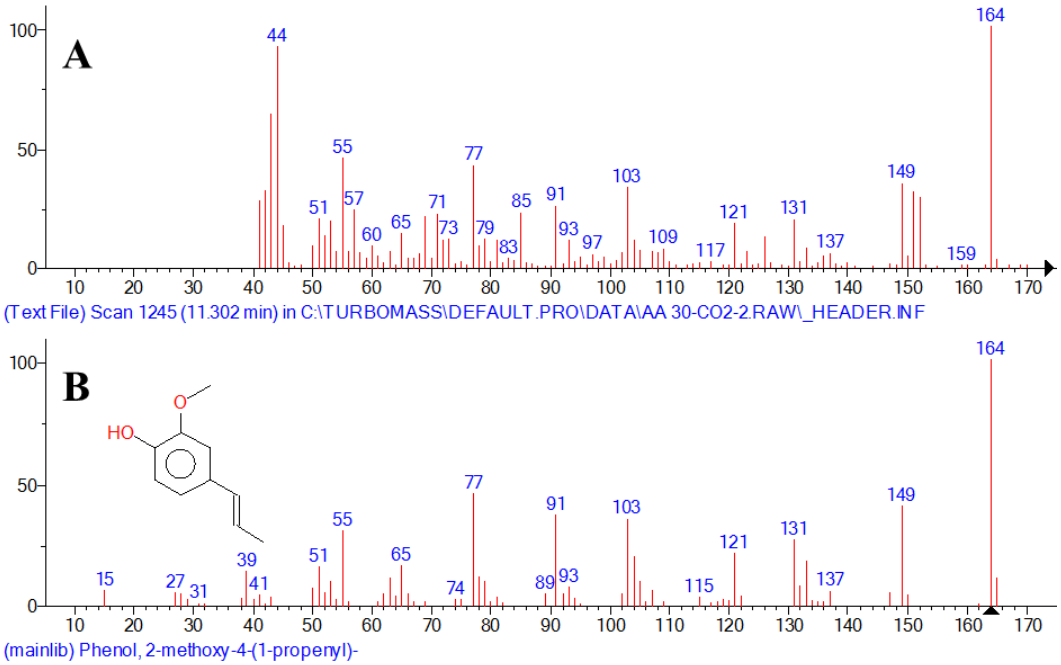

Figure A.198: Matching MS spectrum of peak number 17 MS in CO_2-2 extract GC-MS: A) MS of peak number 17 in CO_2-2 extract sample; B) MS of Phenol, 2-methoxy-4-(1-propenyl)- according to NIST library.

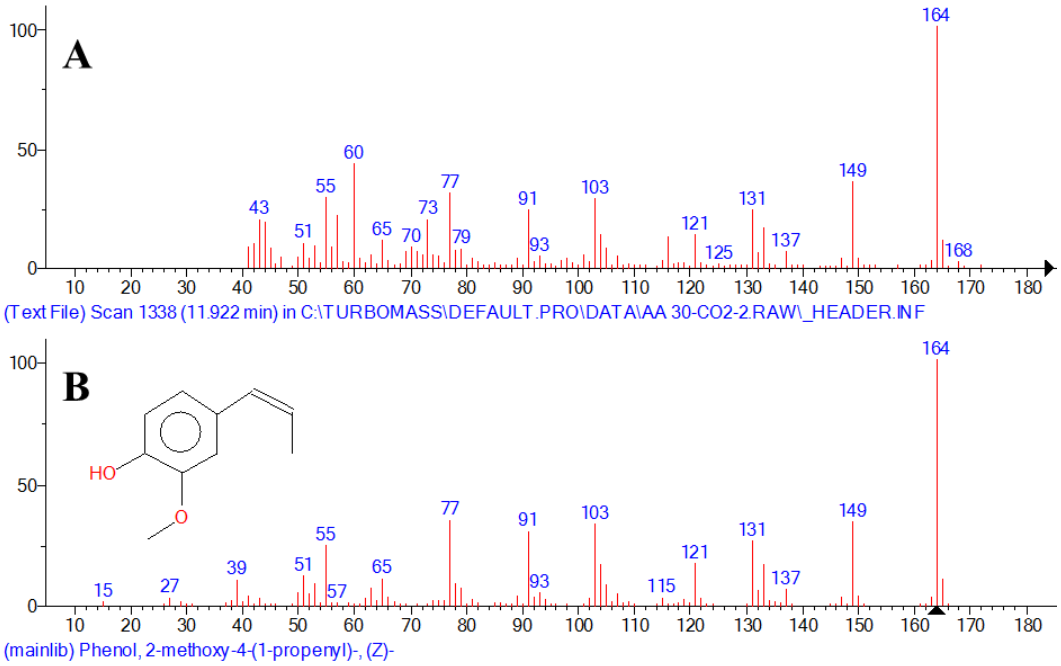

Figure A.199: Matching MS spectrum of peak number 18 MS in CO_2-2 extract GC-MS: A) MS of peak number 18 in CO_2-2 extract sample; B) MS of Phenol, 2-methoxy-4-(1-propenyl)-, (Z)- according to NIST library.

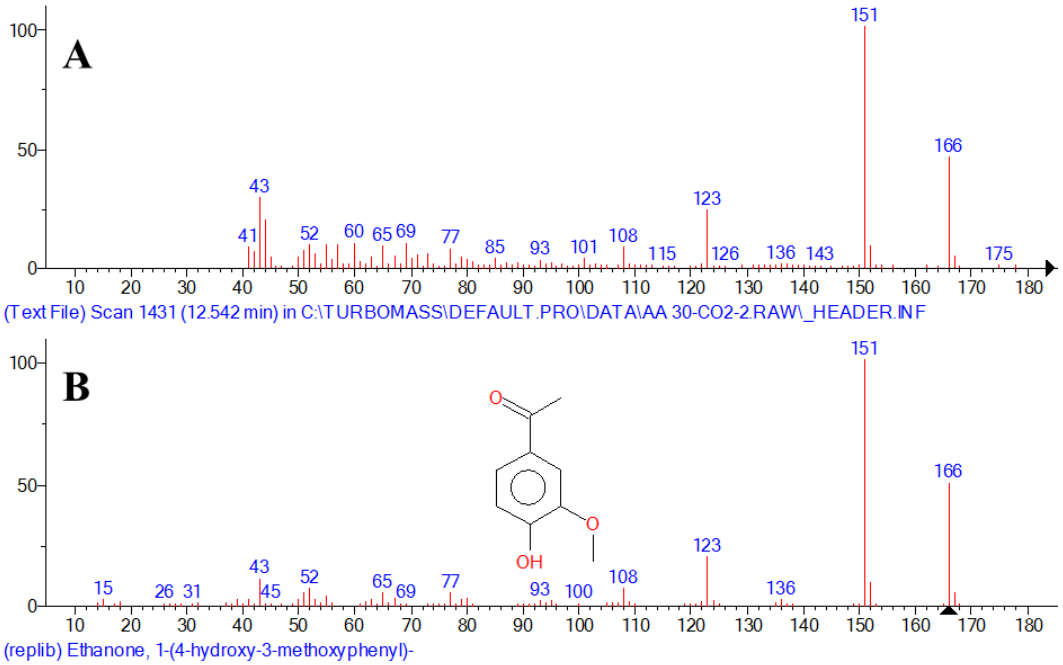

Figure A.200: Matching MS spectrum of peak number 20 MS in CO_2-2 extract GC-MS: A) MS of peak number 20 in CO_2-2 extract sample; B) MS of Ethanone, 1-(4-hydroxy-3-methoxyphenyl)- according to NIST library.

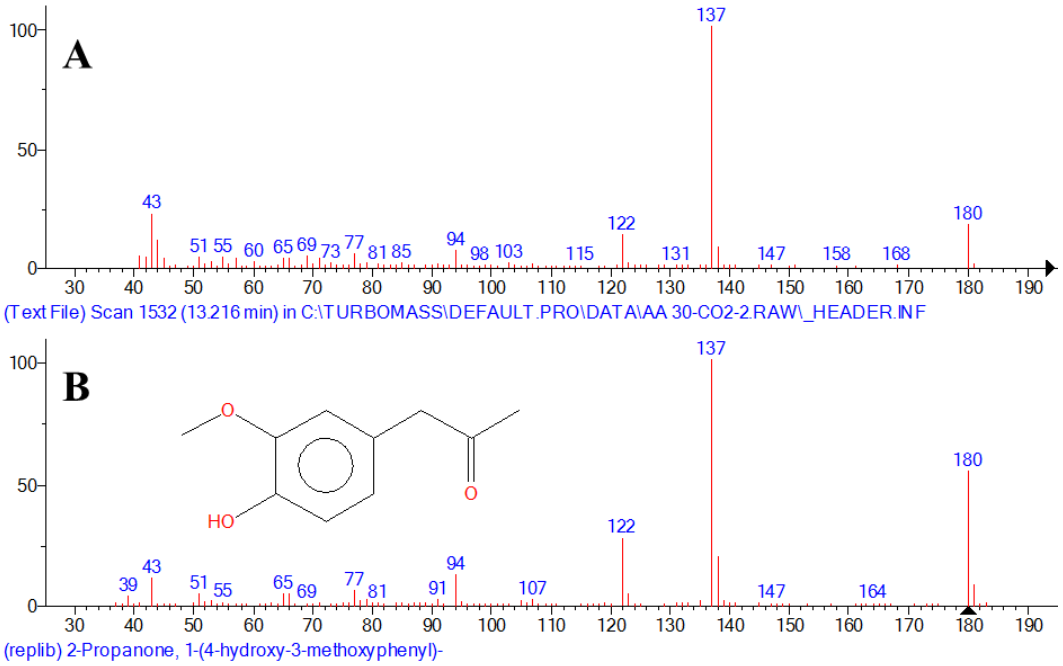

Figure A.201: Matching MS spectrum of peak number 21 MS in CO_2-2 extract GC-MS: A) MS of peak number 21 in CO_2-2 extract sample; B) MS of 2-Propanone, 1-(4-hydroxy-3-methoxyphenyl)- according to NIST library.

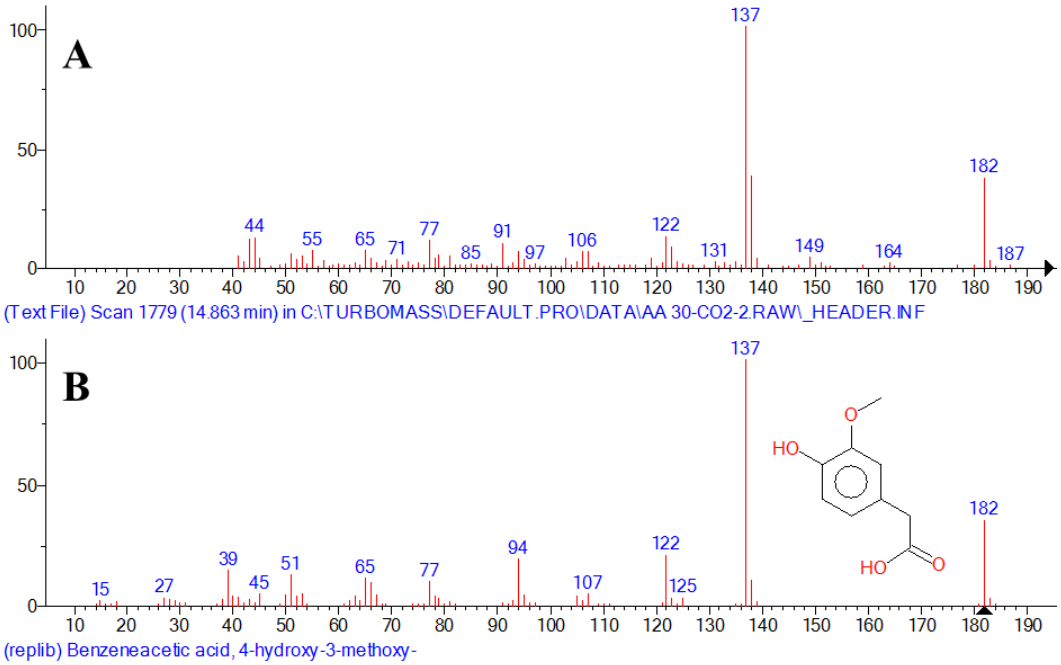

Figure A.202: Matching MS spectrum of peak number 24 MS in CO_2-2 extract GC-MS: A) MS of peak number 24 in CO_2-2 extract sample; B) MS of Benzeneacetic acid, 4-hydroxy-3-methoxy- according to NIST library.

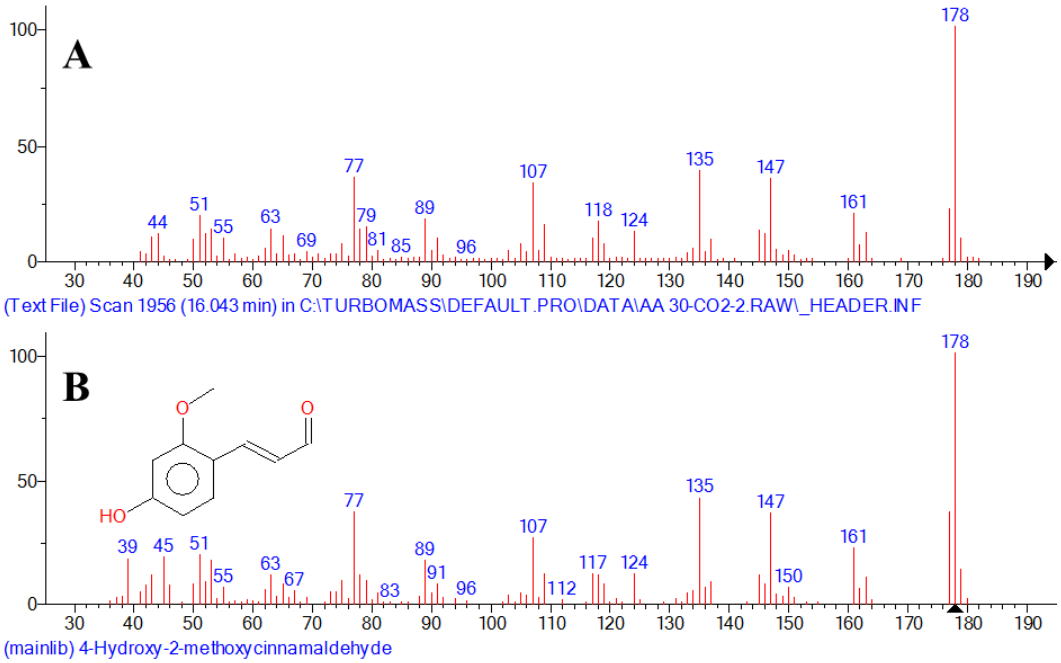

Figure A.203: Matching MS spectrum of peak number 26 MS in CO_2-2 extract GC-MS: A) MS of peak number 26 in CO_2-2 extract sample; B) MS of 4-Hydroxy-2-methoxycinnamaldehyde according to NIST library.

A.5.4 Mass spectra of identified phenolic peaks in CO_2-3 and their best library match

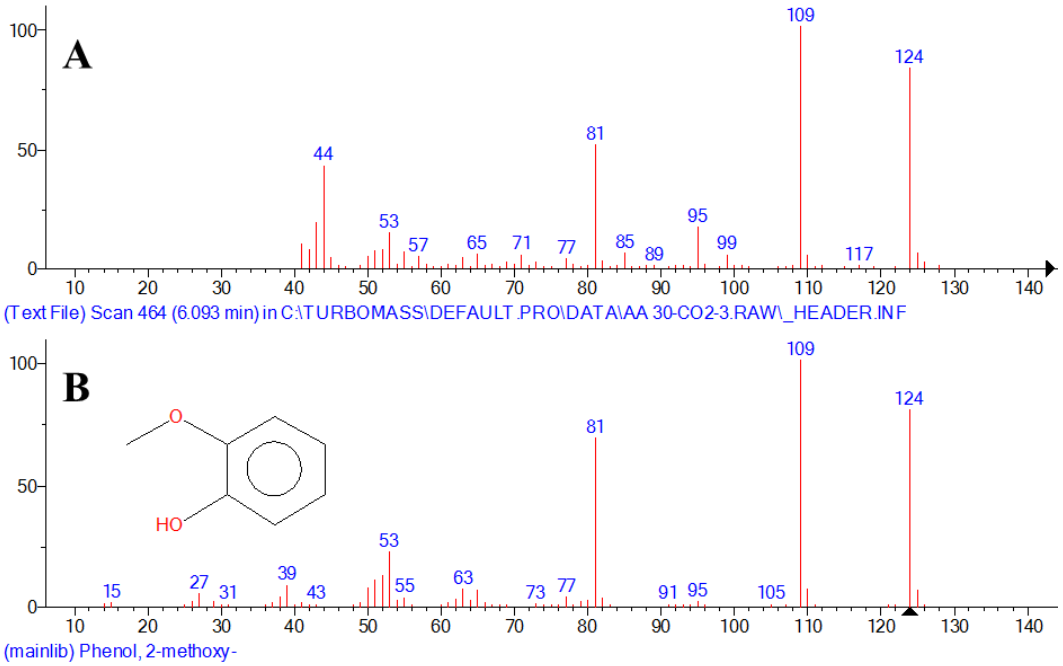

Figure A.204: Matching MS spectrum of peak number 4 MS in CO_2-3 extract GC-MS: A) MS of peak number 4 in CO_2-3 extract sample; B) MS of Phenol, 2-methoxy- according to NIST library.

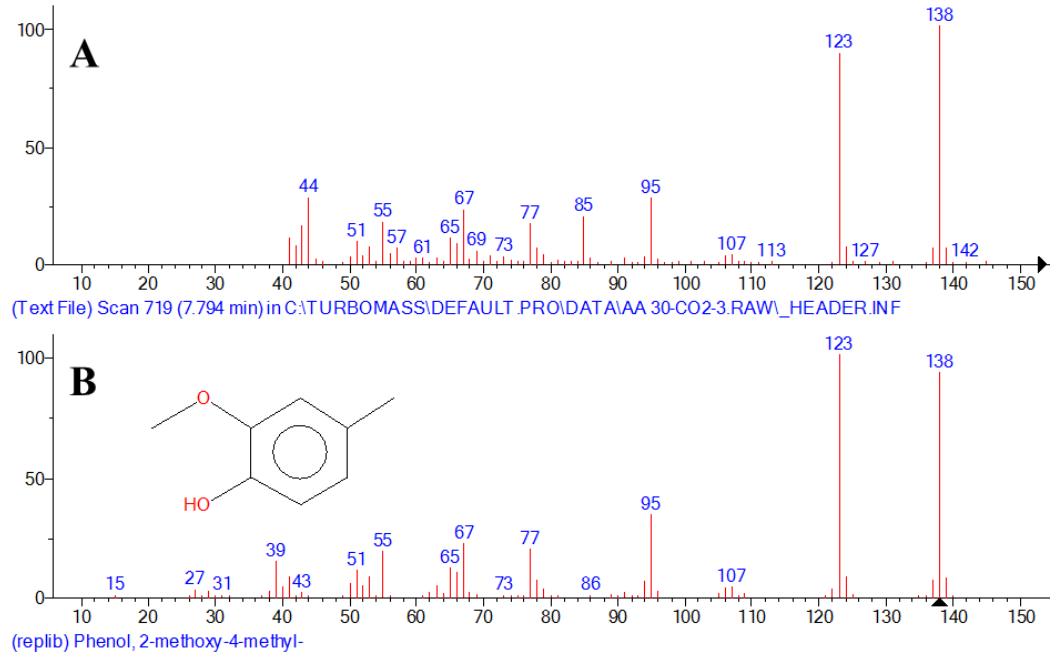

Figure A.205: Matching MS spectrum of peak number 7 MS in CO_2-3 extract GC-MS: A) MS of peak number 7 in CO_2-3 extract sample; B) MS of Phenol, 2-methoxy-4-methyl- according to NIST library.

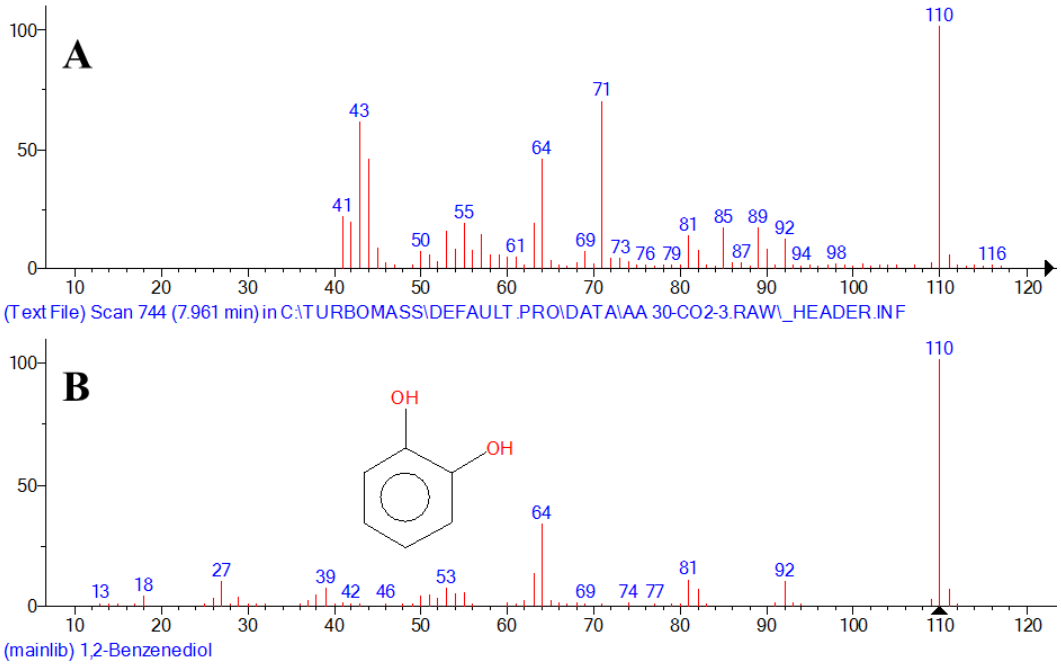

Figure A.206: Matching MS spectrum of peak number 8 MS in CO_2-3 extract GC-MS: A) MS of peak number 8 in CO_2-3 extract sample; B) MS of 1,2-Benzenediol according to NIST library.

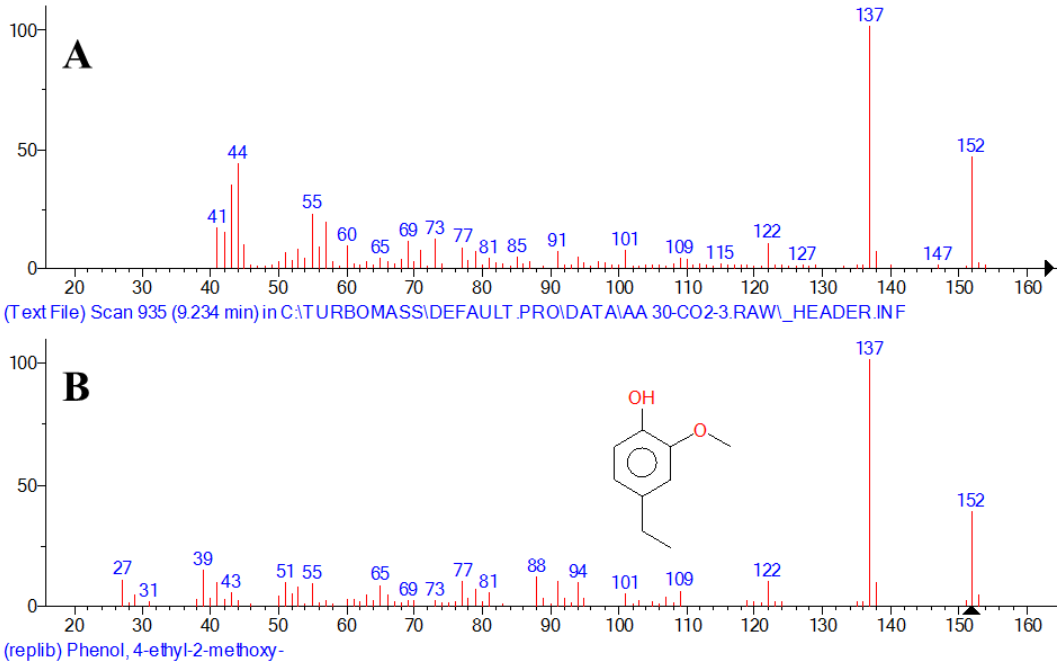

Figure A.207: Matching MS spectrum of peak number 10 MS in CO_2-3 extract GC-MS: A) MS of peak number 10 in CO_2-3 extract sample; B) MS of Phenol, 4-ethyl-2-methoxy- according to NIST library.

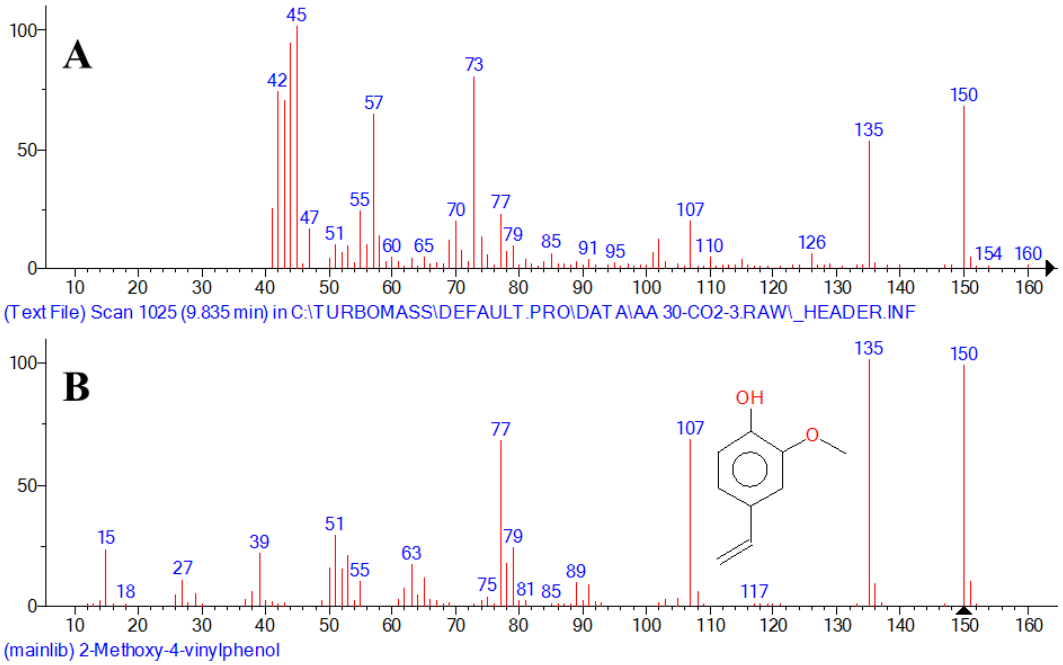

Figure A.208: Matching MS spectrum of peak number 12 MS in CO_2-3 extract GC-MS: A) MS of peak number 12 in CO_2-3 extract sample; B) MS of 2-Methoxy-4-vinylphenol according to NIST library.

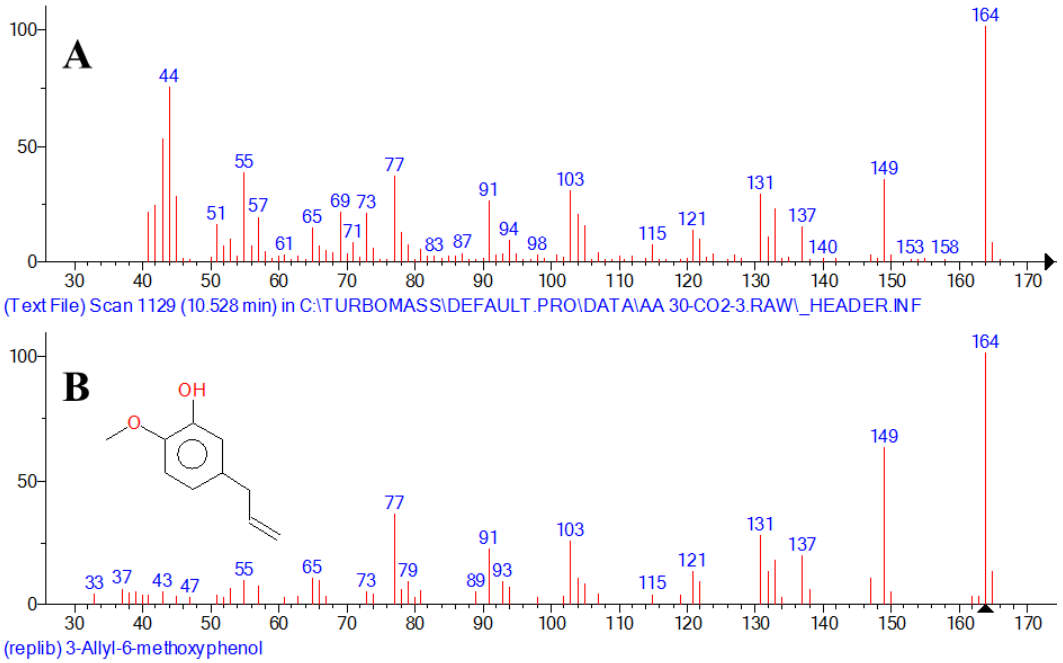

Figure A.209: Matching MS spectrum of peak number 14 MS in CO_2-3 extract GC-MS: A) MS of peak number 14 in CO_2-3 extract sample; B) MS of 3-Allyl-6-methoxyphenol according to NIST library.

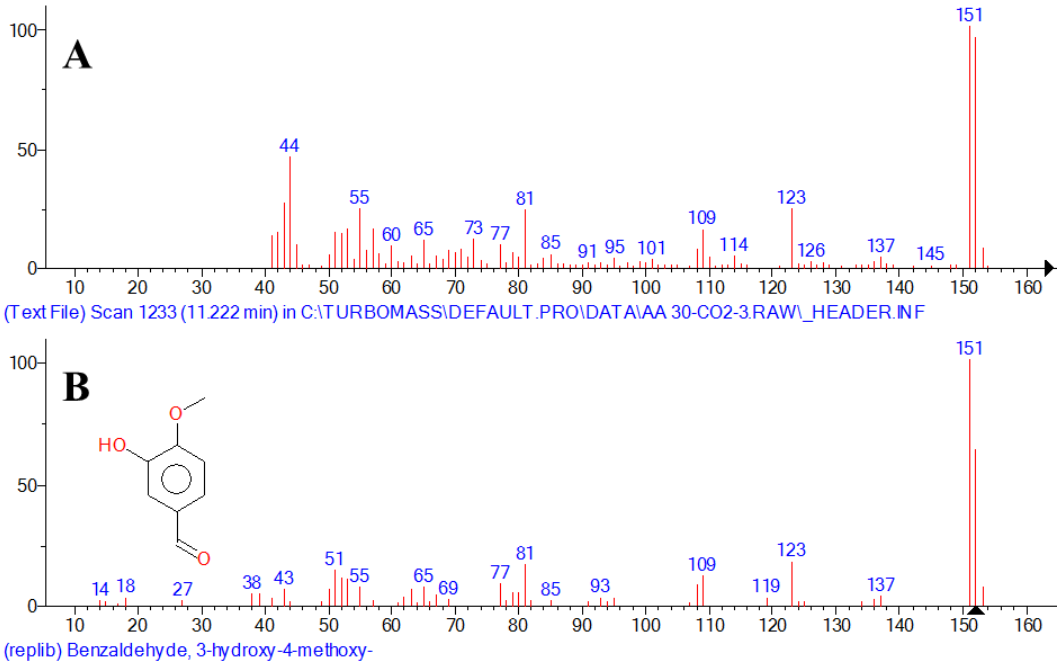

Figure A.210: Matching MS spectrum of peak number 16 MS in CO_2-3 extract GC-MS: A) MS of peak number 16 in CO_2-3 extract sample; B) MS of Benzaldehyde, 3-hydroxy-4-methoxy- according to NIST library.

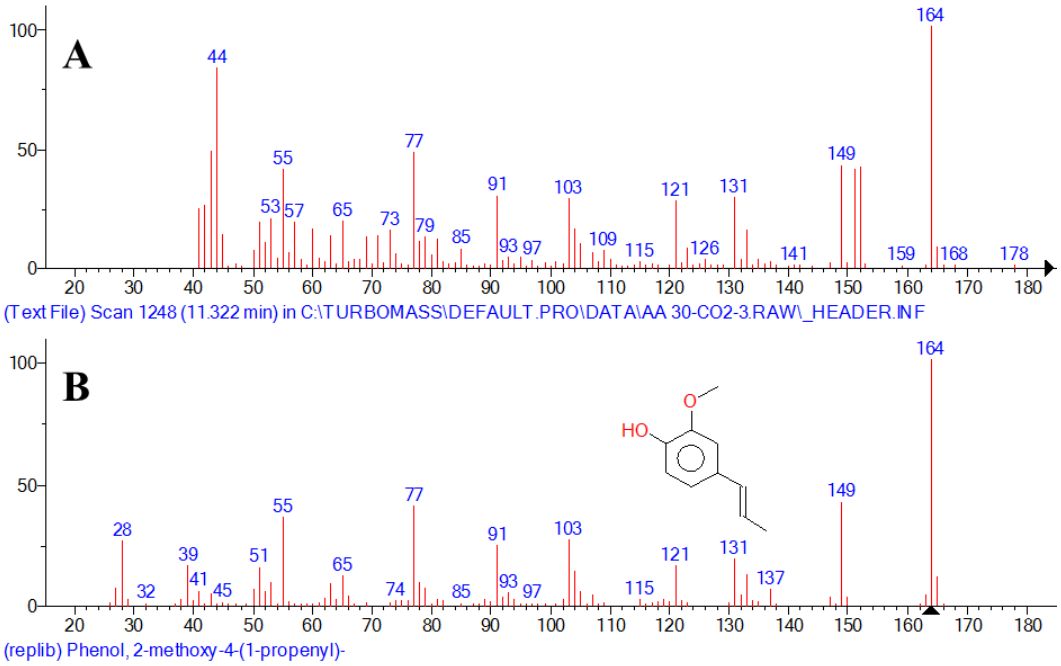

Figure A.211: Matching MS spectrum of peak number 17 MS in CO_2-3 extract GC-MS: A) MS of peak number 17 in CO_2-3 extract sample; B) MS of Phenol, 2-methoxy-4-(1-propenyl)- according to NIST library.

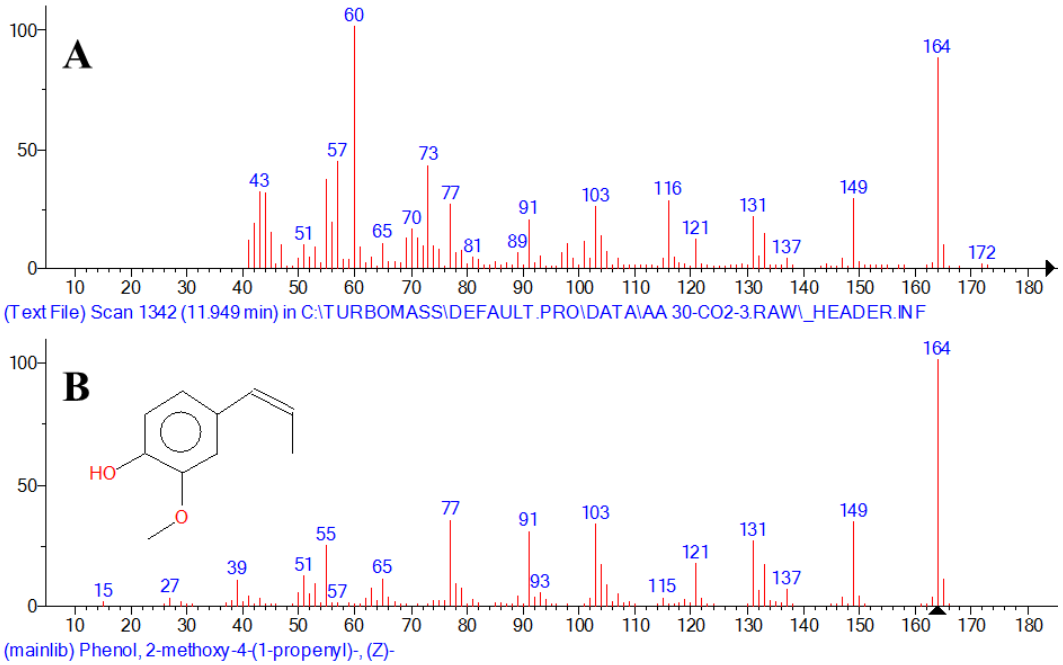

Figure A.212: Matching MS spectrum of peak number 18 MS in CO_2-3 extract GC-MS: A) MS of peak number 18 in CO_2-3 extract sample; B) MS of Phenol, 2-methoxy-4-(1-propenyl)-, (Z)- according to NIST library.

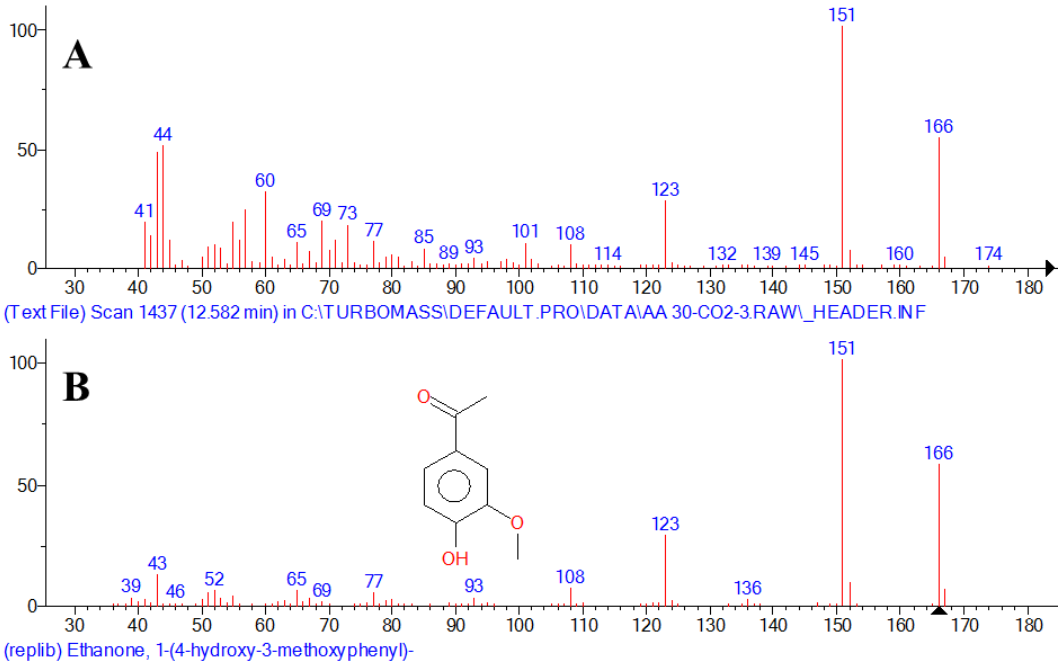

Figure A.213: Matching MS spectrum of peak number 20 MS in CO_2-3 extract GC-MS: A) MS of peak number 20 in CO_2-3 extract sample; B) MS of Ethanone, 1-(4-hydroxy-3-methoxyphenyl)- according to NIST library.

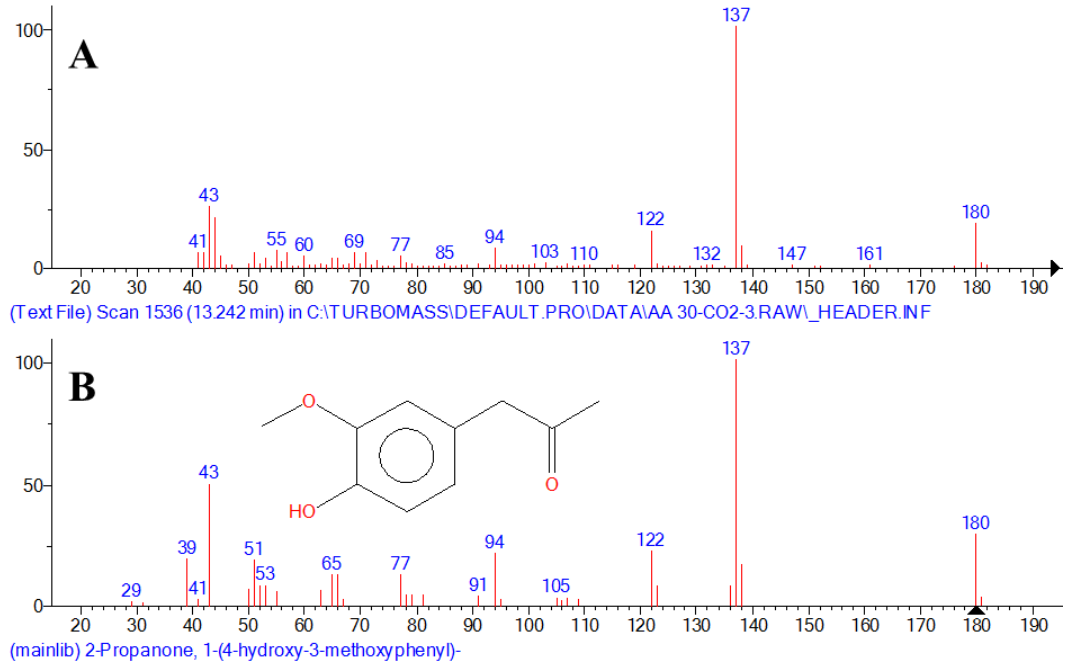

Figure A.214: Matching MS spectrum of peak number 21 MS in CO_2-3 extract GC-MS: A) MS of peak number 21 in CO_2-3 extract sample; B) MS of 2-Propanone, 1-(4-hydroxy-3-methoxyphenyl)- according to NIST library.

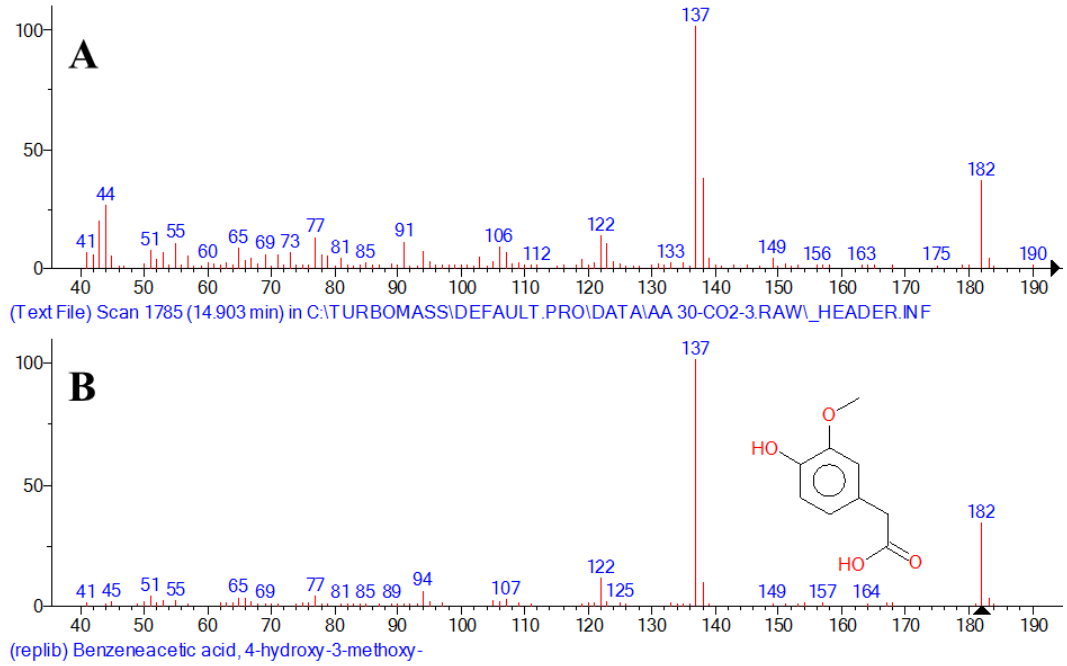

Figure A.215: Matching MS spectrum of peak number 24 MS in CO_2-3 extract GC-MS: A) MS of peak number 24 in CO_2-3 extract sample; B) MS of Benzeneacetic acid, 4-hydroxy-3-methoxy- according to NIST library.

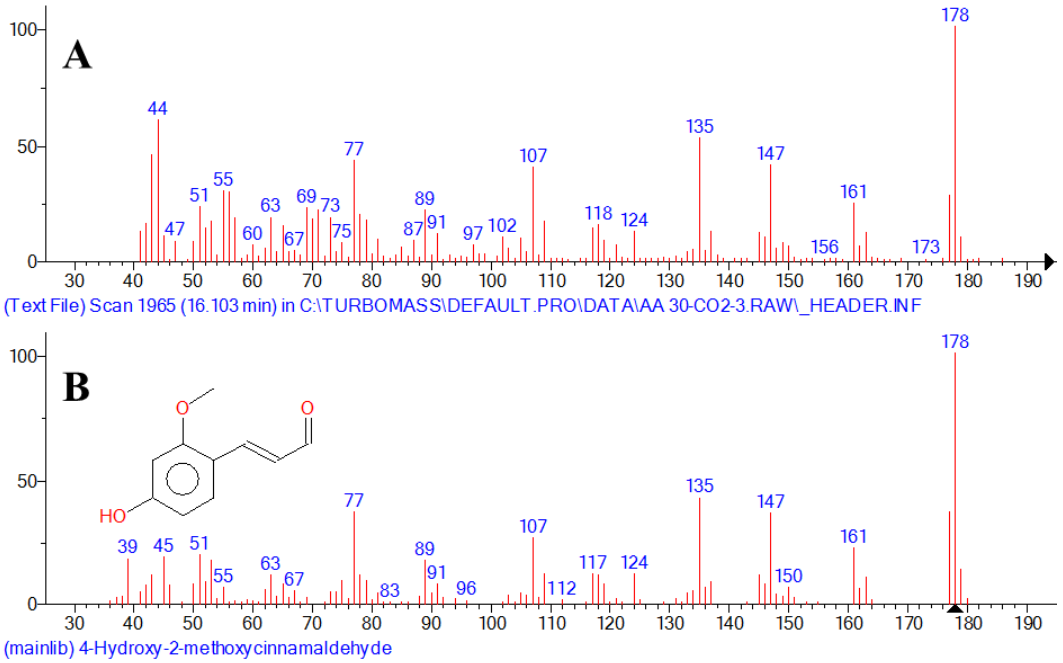

Figure A.216: Matching MS spectrum of peak number 26 MS in CO_2-3 extract GC-MS: A) MS of peak number 26 in CO_2-3 extract sample; B) MS of 4-Hydroxy-2-methoxycinnamaldehyde according to NIST library.

A.5.5 Mass spectra of identified phenolic peaks in CO_2-4 and their best library match

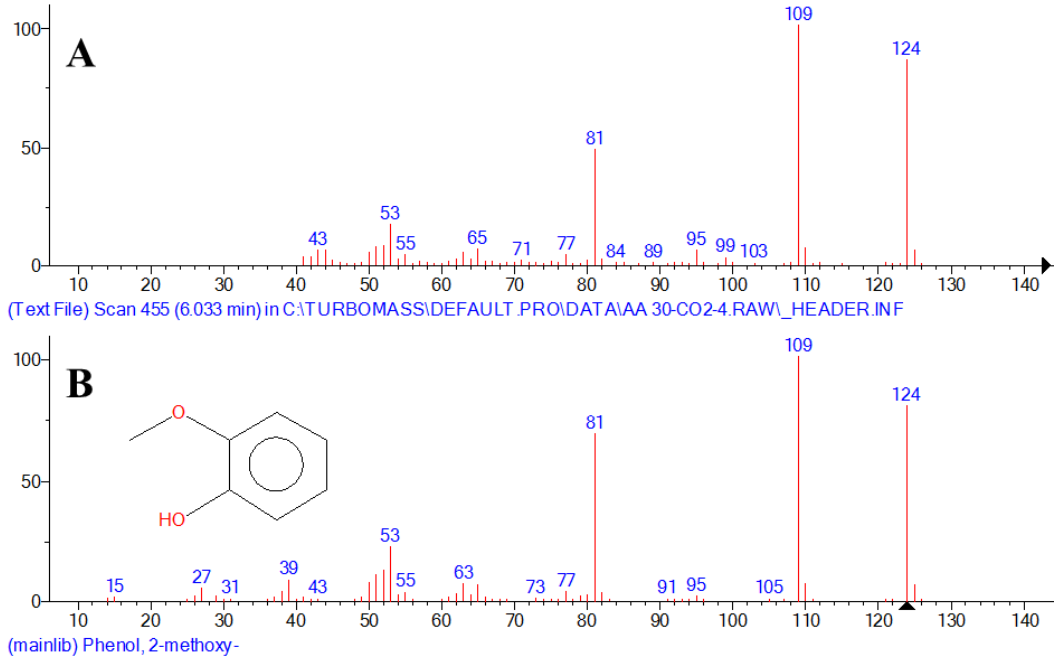

Figure A.217: Matching MS spectrum of peak number 4 MS in CO_2-4 extract GC-MS: A) MS of peak number 4 in CO_2-4 extract sample; B) MS of Phenol, 2-methoxy- according to NIST library.

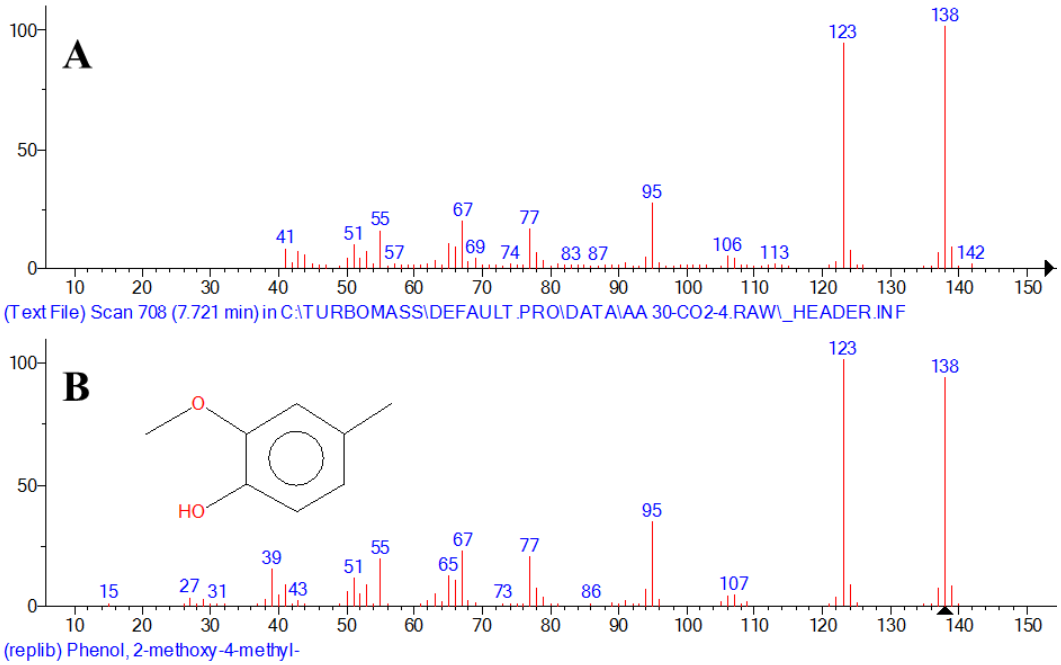

Figure A.218: Matching MS spectrum of peak number 7 MS in CO_2-4 extract GC-MS: A) MS of peak number 7 in CO_2-4 extract sample; B) MS of Phenol, 2-methoxy-4-methyl- according to NIST library.

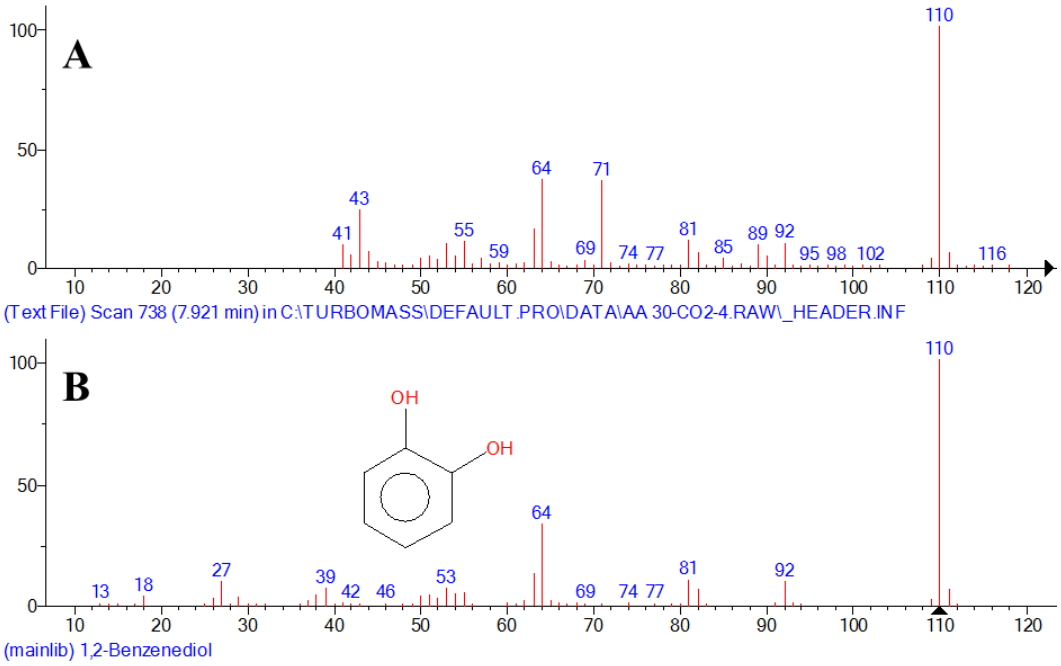

Figure A.219: Matching MS spectrum of peak number 8 MS in CO_2-4 extract GC-MS: A) MS of peak number 8 in CO_2-4 extract sample; B) MS of 1,2-Benzenediol according to NIST library.

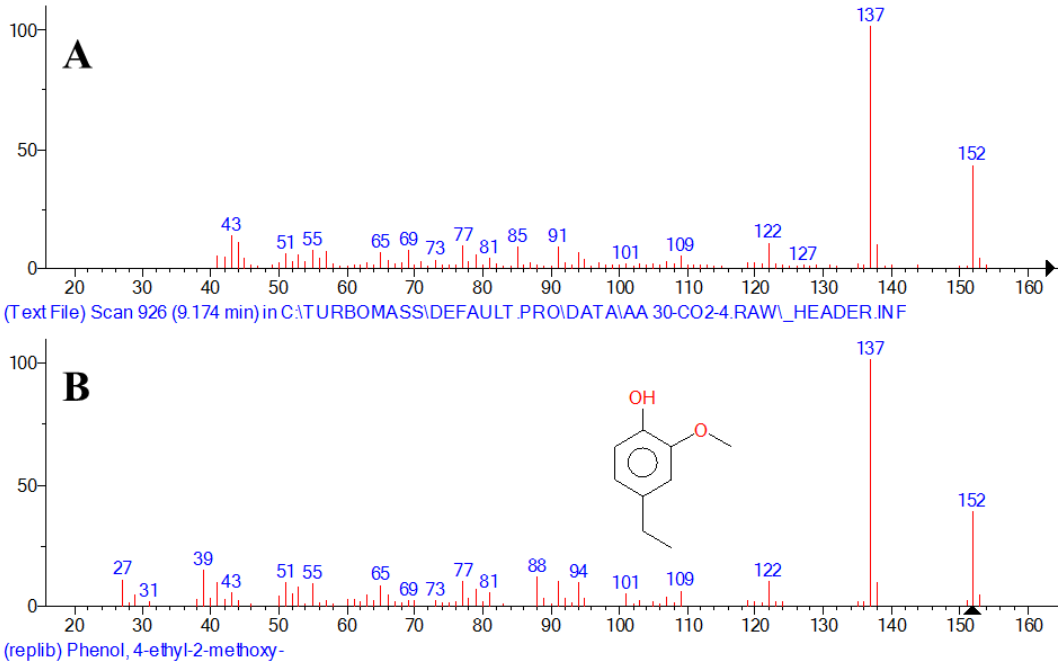

Figure A.220: Matching MS spectrum of peak number 10 MS in CO_2-4 extract GC-MS: A) MS of peak number 10 in CO_2-4 extract sample; B) MS of Phenol, 4-ethyl-2-methoxy- according to NIST library.

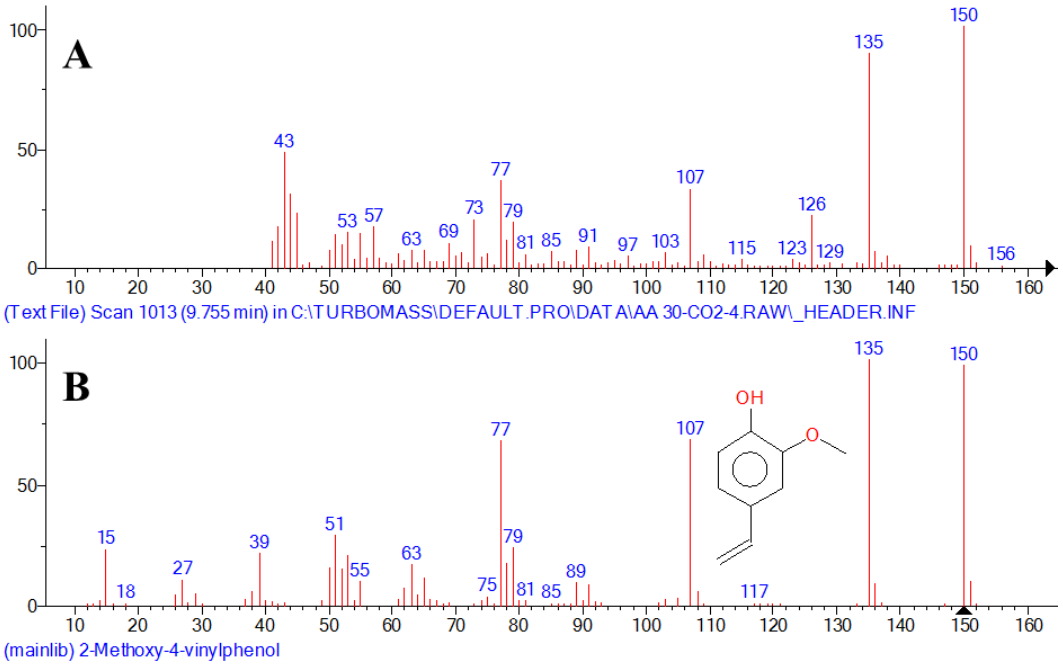

Figure A.221: Matching MS spectrum of peak number 12 MS in CO_2-4 extract GC-MS: A) MS of peak number 12 in CO_2-4 extract sample; B) MS of 2-Methoxy-4-vinylphenol according to NIST library.

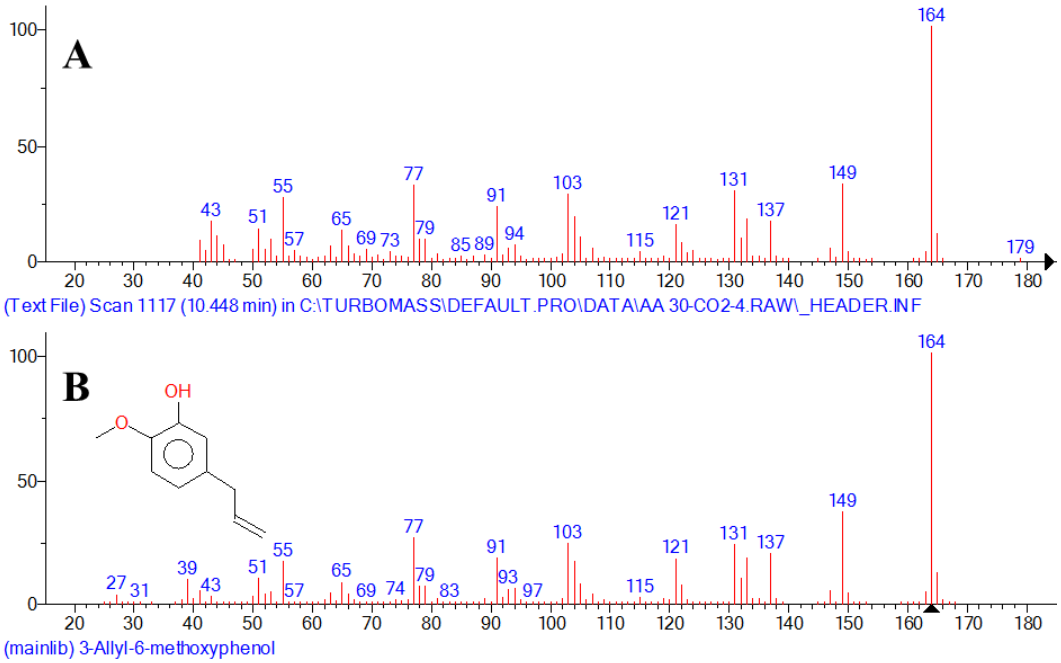

Figure A.222: Matching MS spectrum of peak number 14 MS in CO_2-4 extract GC-MS: A) MS of peak number 14 in CO_2-4 extract sample; B) MS of 3-Allyl-6-methoxyphenol according to NIST library.

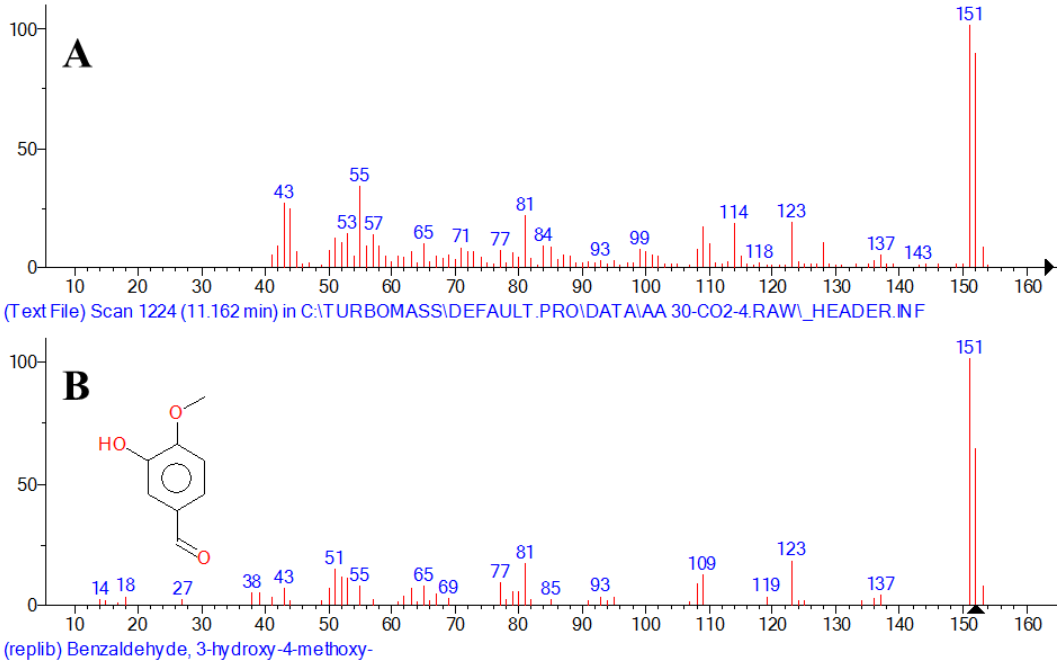

Figure A.223: Matching MS spectrum of peak number 16 MS in CO_2-4 extract GC-MS: A) MS of peak number 16 in CO_2-4 extract sample; B) MS of Benzaldehyde, 3-hydroxy-4-methoxy- according to NIST library.

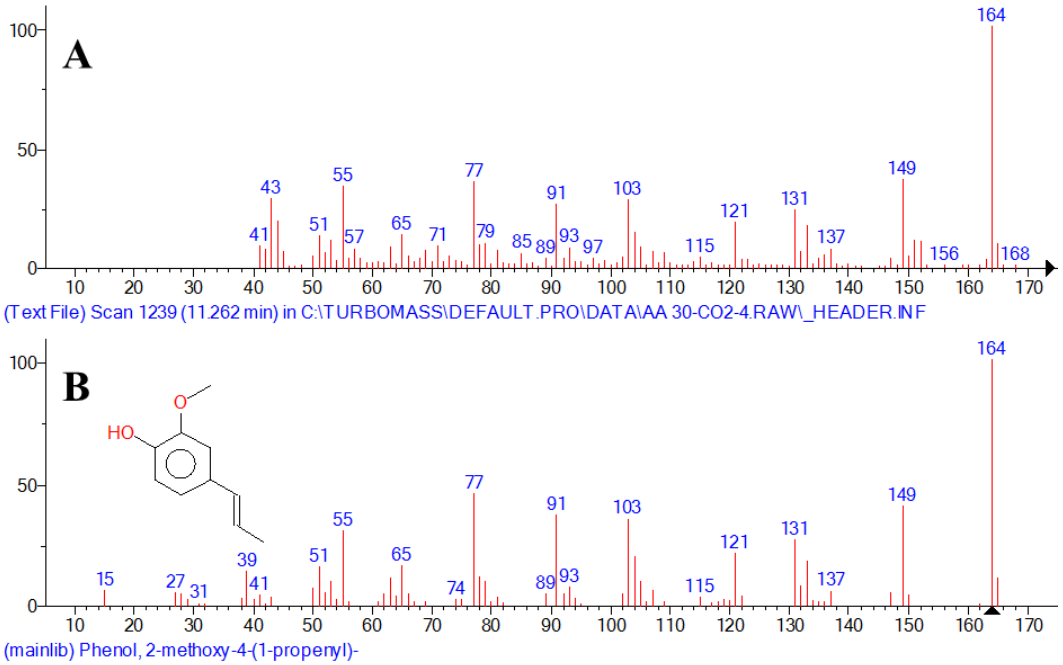

Figure A.224: Matching MS spectrum of peak number 17 MS in CO_2-4 extract GC-MS: A) MS of peak number 17 in CO_2-4 extract sample; B) MS of Phenol, 2-methoxy-4-(1-propenyl)- according to NIST library.

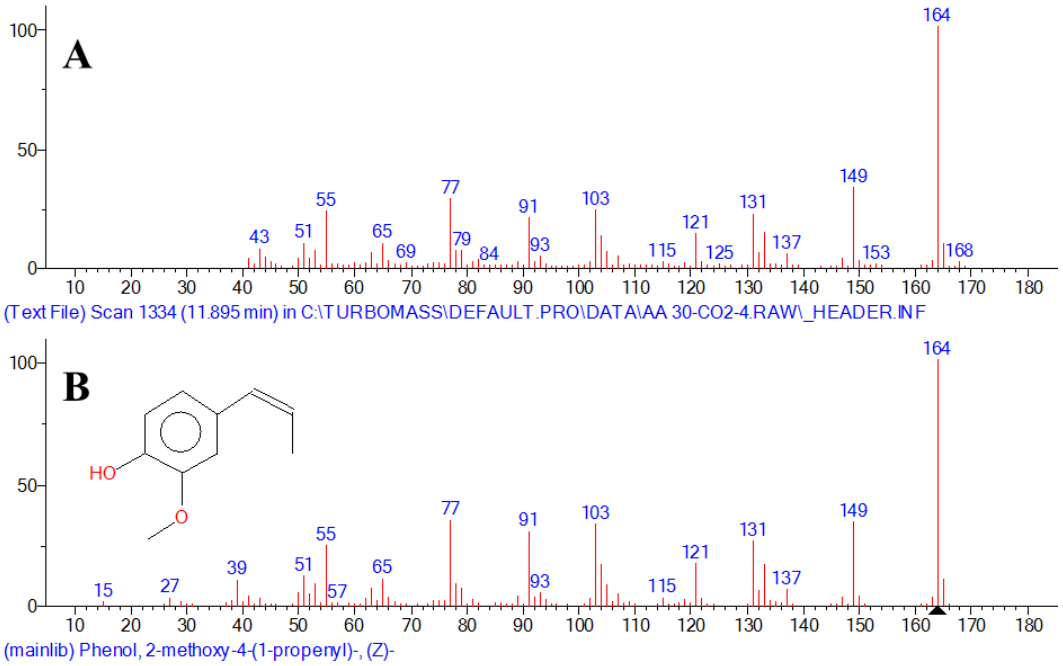

Figure A.225: Matching MS spectrum of peak number 18 MS in CO_2-4 extract GC-MS: A) MS of peak number 18 in CO_2-4 extract sample; B) MS of Phenol, 2-methoxy-4-(1-propenyl)-, (Z)- according to NIST library.

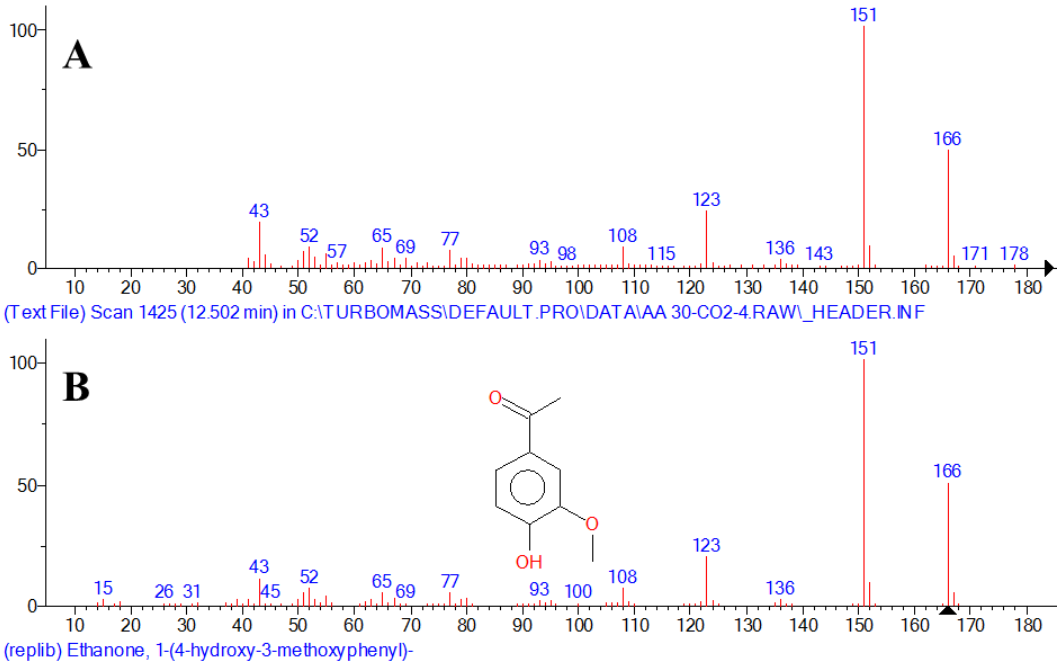

Figure A.226: Matching MS spectrum of peak number 20 MS in CO_2-4 extract GC-MS: A) MS of peak number 20 in CO_2-4 extract sample; B) MS of Ethanone, 1-(4-hydroxy-3-methoxyphenyl)- according to NIST library.

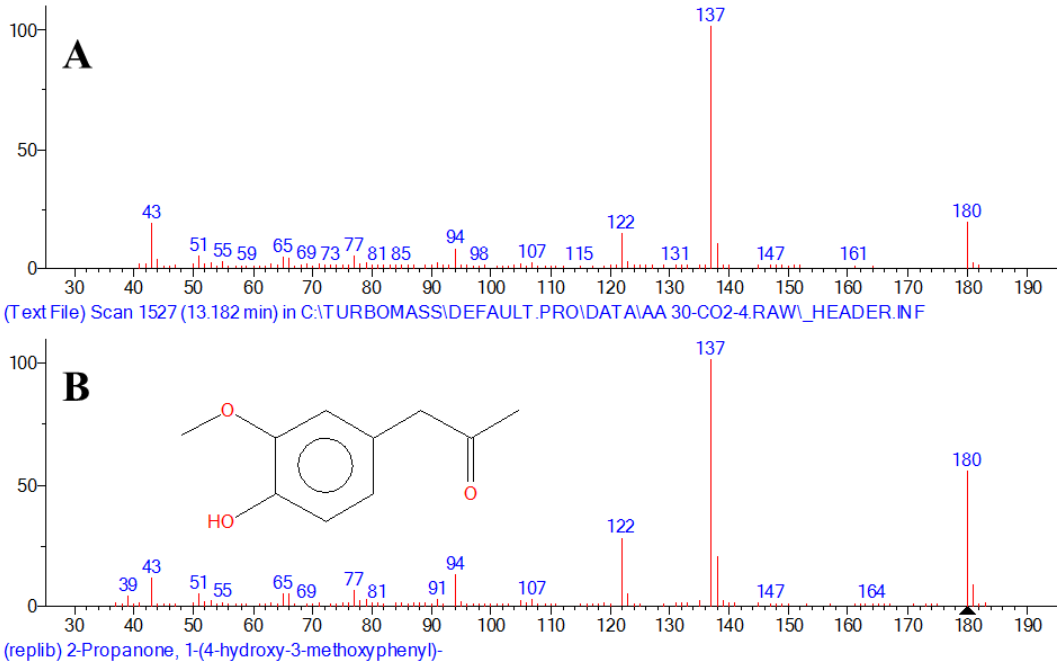

Figure A.227: Matching MS spectrum of peak number 21 MS in CO_2-4 extract GC-MS: A) MS of peak number 21 in CO_2-4 extract sample; B) MS of 2-Propanone, 1-(4-hydroxy-3-methoxyphenyl)- according to NIST library.

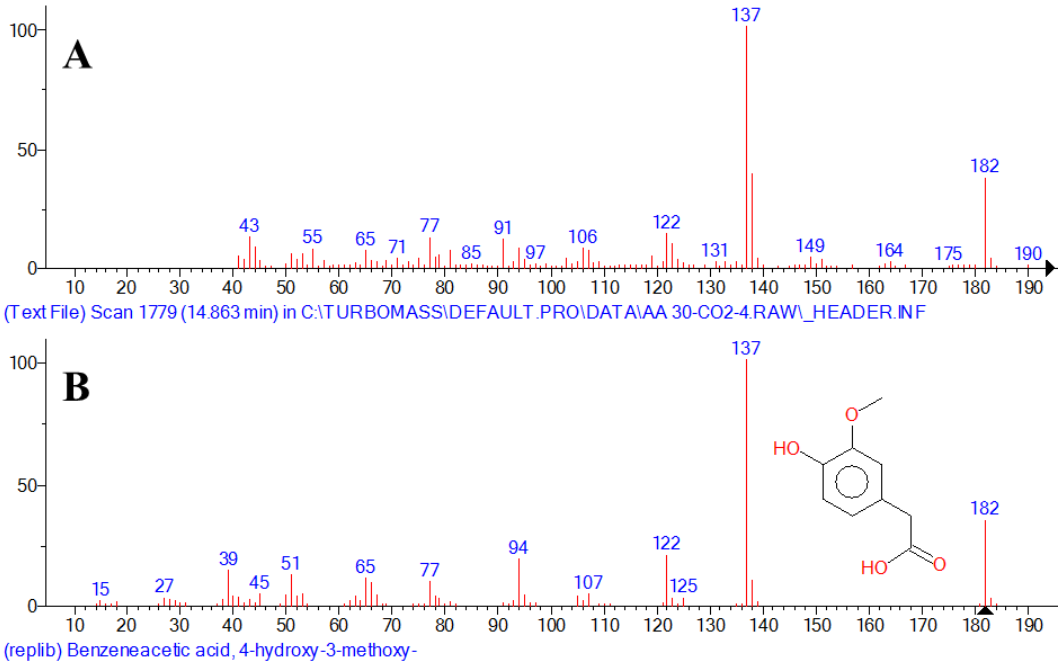

Figure A.228: Matching MS spectrum of peak number 24 MS in CO_2-4 extract GC-MS: A) MS of peak number 24 in CO_2-4 extract sample; B) MS of Benzeneacetic acid, 4-hydroxy-3-methoxy- according to NIST library.

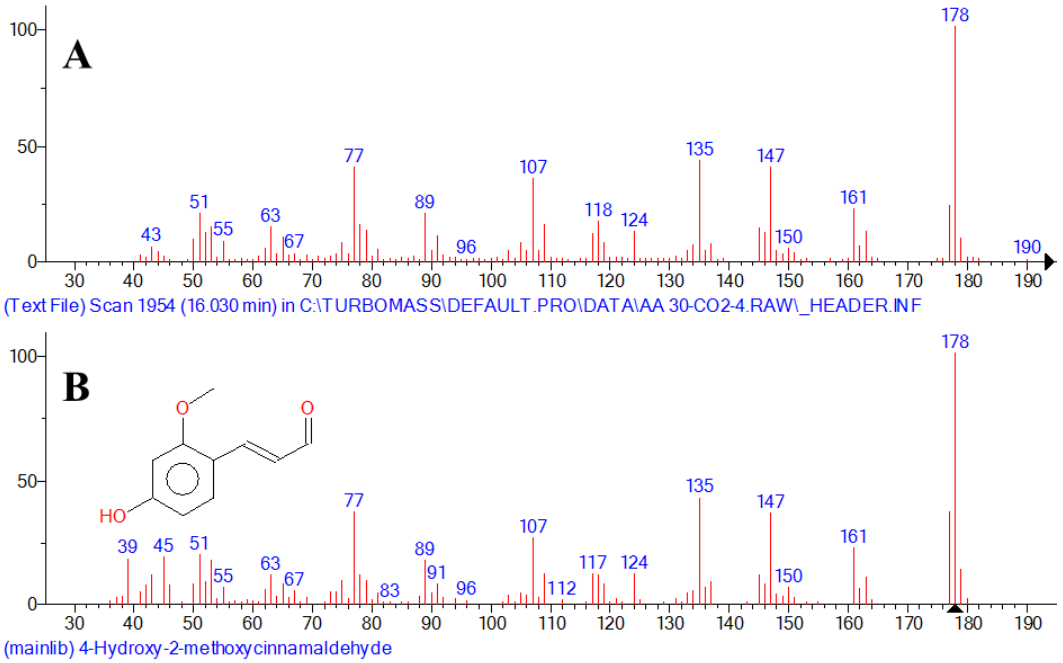

Figure A.229: Matching MS spectrum of peak number 26 MS in CO_2-4 extract GC-MS: A) MS of peak number 26 in CO_2-4 extract sample; B) MS of 4-Hydroxy-2-methoxycinnamaldehyde according to NIST library.

Appendix B: ECN Calculations

Table B.1: ECN reduction values by functional group used for analysis of phenols in all GC-FID experiments.

Functional Group	Structure	ECN Reduction	Source
Phenol	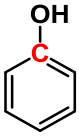	- 0.83	255, 368
Ether		- 1.00	253
Olefinic C	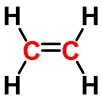	- 0.05	253
Carbonyl	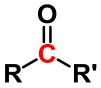	- 1.00	253
Carboxyl	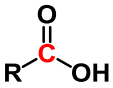	- 1.00	253, 254
Primary Alcohol	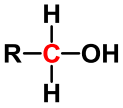	- 0.60	253
Secondary Alcohol	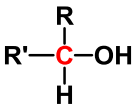	- 0.75	253
Ester	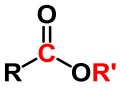	- 1.25	253, 255

Table B.2: ECN reduction by functional group for each identified phenolic compound including the standard compound.

Name	Structure	Group(s)	No. of C	Reduction	ECN
Phenol		phenol	6	0.83	5.17
Phenol, 2-methyl-		phenol	7	0.83	6.17
Phenol, 4-methyl-	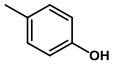	phenol	7	0.83	6.17
Phenol, 2-methoxy-	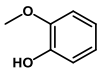	phenol + ether	7	0.83 + 1.00	5.17
Phenol, 2,5-dimethyl-		phenol	8	0.83	7.17
1,3-Benzenediol, 4-ethyl-	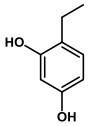	two phenol	8	2 x 0.83	6.34
Phenol, 2-methoxy-4-methyl-	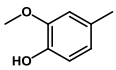	phenol + ether	8	0.83 + 1.00	6.17
1,2-Benzenediol		two phenol	6	2 x 0.83	4.34
1,2-Benzenediol, 3-methyl-	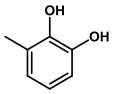	two phenol	7	2 x 0.83	5.34
Phenol, 4-ethyl-2-methoxy-	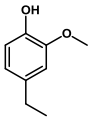	phenol + ether	9	0.83 + 1.00	7.17
1,2-Benzenediol, 4-methyl-	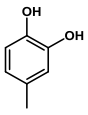	two phenol	7	2 x 0.83	5.34
2-Methoxy-4-vinylphenol	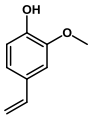	phenol + ether + two olefinic C	9	0.83 + 1.00 + (2 x 0.05)	7.07
Phenol, 4-(2-propenyl)-	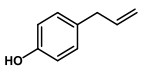	phenol + two olefinic C	9	0.83 + (2 x 0.05)	8.07

3-Allyl-6-methoxyphenol	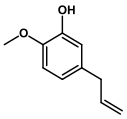	phenol + ether + two olefinic C	10	0.83 + 1.00 + (2 x 0.05)	8.07
Phenol, 2-methoxy-4-propyl-	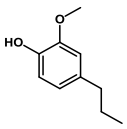	phenol + ether	10	0.83 + 1.00	8.17
Benzaldehyde, 3-hydroxy-4-methoxy-	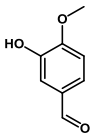	phenol + ether + carbonyl	8	0.83 + 1.00 + 1.00	5.17
Phenol, 2-methoxy-4-(1-propenyl)-	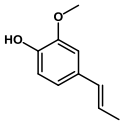	phenol + ether + two olefinic C	10	0.83 + 1.00 + (2 x 0.05)	8.07
Phenol, 2-methoxy-4-(1-propenyl)-, (Z)-	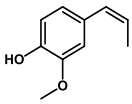	phenol + ether + two olefinic C	10	0.83 + 1.00 + (2 x 0.05)	8.07
3,7-Benzofurandiol, 2,3-dihydro-2,2-dimethyl-	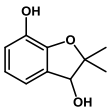	phenol + ether + secondary alcohol	10	0.83 + 1.00 + 0.75	7.42
Ethanone, 1-(4-hydroxy-3-methoxyphenyl)-	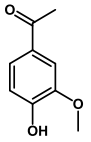	phenol + ether + carbonyl	9	0.83 + 1.00 + 1.00	6.17
Benzoic acid, 4-hydroxy-3-methoxy-, methyl ester	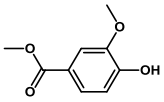	phenol + ether + ester	9	0.83 + 1.00 + 1.25	5.92
2-Propanone, 1-(4-hydroxy-3-methoxyphenyl)-	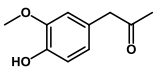	phenol + ether + carbonyl	10	0.83 + 1.00 + 1.00	7.17
Phenol, 4-(3-hydroxy-1-propenyl)-2-methoxy-	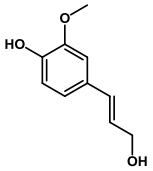	phenol + ether + two olefinic C + primary alcohol	10	0.83 + 1.00 + (2 x 0.05) + 0.60	7.47
Benzoic acid, 4-hydroxy-3-methoxy-	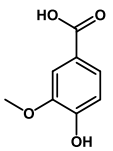	phenol + ether + carboxyl	8	0.83 + 1.00 + 1.00	5.17

Benzeneacetic acid, 4-hydroxy-3-methoxy-	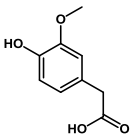	phenol + ether + carboxyl	9	0.83 + 1.00 + 1.00	6.17
4-((1E)-3-Hydroxy-1-propenyl)-2-methoxyphenol	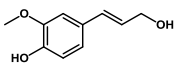	phenol + ether + two olefinic C + primary alcohol	10	0.83 + 1.00 + (2 x 0.05) + 0.60	7.47
4-Hydroxy-2-methoxycinnamaldehyde	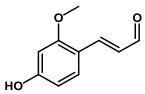	phenol + ether + two olefinic C + carbonyl	10	0.83 + 1.00 + (2 x 0.05) + 1.00	7.07
β-(4-Hydroxy-3-methoxyphenyl)propionic acid	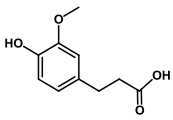	phenol + ether + carboxyl	10	0.83 + 1.00 + 1.00	7.17
Benzeneacetic acid, 4-hydroxy-3-methoxy-, methyl ester	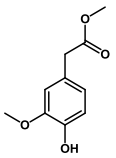	phenol + ether + ester	10	0.83 + 1.00 + 1.25	6.92
Phenylacetylformic acid, 4-hydroxy-3-methoxy-	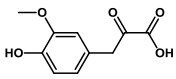	phenol + ether + carbonyl + carboxyl	10	0.83 + 1.00 + 1.00 + 1.00	6.17
Naphtho[2,3-c]furan-1,4-dione, 3,3a,9,9a-tetrahydro-6-hydroxy-7-methoxy-	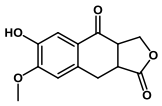	Phenol + ether + carbonyl + ester	13	0.83 + 1.00 + 1.00 + 1.25	8.92
2H-1-Benzopyran-7-ol, 3,4-dihydro-3-(4-hydroxy-2-methoxyphenyl)-	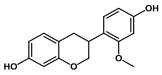	two phenol + two ether	16	(2 x 0.83) + (2 x 1.00)	12.34
Podocarpa-8,11,13-triene-7β,13-diol, 14-isopropyl-	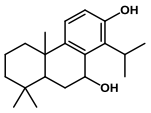	phenol + secondary alcohol	20	0.83 + 0.75	18.42
Phenol, 4-[2,3-dihydro-7-methoxy-3-methyl-5-(1-propenyl)-2-benzofuranyl]-2-methoxy-	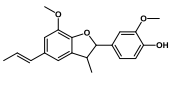	phenol + three ether + two olefinic C	20	0.83 + (3 x 1.00) + (2 x 0.05)	16.07
2(3H)-Furanone, dihydro-3,4-bis[(4-hydroxy-3-methoxyphenyl)methyl]-,	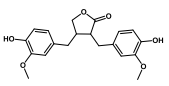	two phenol + two ether + ester	20	(2 x 0.83) + (2 x 1.00) + 1.25	15.09

(3R-trans)-					
Naphtho[2,3-c]furan-1(3H)-one, 3a,4,9,9a-tetrahydro-6-hydroxy-4-(4-hydroxy-3-methoxyphenyl)-7-methoxy-, [3aR-(3aα,4α,9aβ)]-	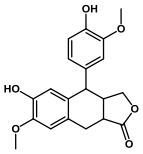	two phenol + two ether + ester	20	(2 x 0.83) + (2 x 1.00) + 1.25	15.09
Butylated Hydroxytoluene	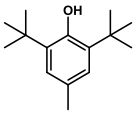	phenol	15	0.83	14.17

Appendix C: Phenolic Concentrations in Methyl Linoleate

Table C.1: The exact amounts of phenolic standard antioxidants blended with 2 ml methyl linoleate and their measured induction times at 120 °C and 1 bar of oxygen.

Antioxidant	Sample weight (mg)	Phenolic Concentration (mg/ml)	Phenolic Concentration (mol/dm^3) x10^{-3}	Phenolic Concentration (% w/w)	Induction time (min)
BHT	0	0	0	0	0
	2.7	1.35	6	0.15	54
	8.9	4.45	20	0.5	108
	17.8	8.9	40	1	148
	35.6	17.8	80	2	192
Eugenol	0	0	0	0	0
	8.9	4.45	27	0.5	23
	17.8	8.9	54	1	32
	35.6	17.8	108	2	34
	53.4	26.7	162	3	36
Catechol (1st test)	0	0	0	0	0
	2.7	1.35	12.3	0.15	38
	8.9	4.45	40.5	0.5	134
	17.8	8.9	81	1	80
	35.6	17.8	162	2	28
Catechol (2nd test)	0	0	0	0	0
	2.2	1.1	10	0.12	20
	4.4	2.2	20	0.25	63
	6.6	3.3	30	0.37	105
	8.8	4.4	40	0.49	109
	11	5.5	50	0.62	120
	13.2	6.6	60	0.74	105
Isoeugenol	0	0	0	0	0

Antioxidant	Sample weight (mg)	Phenolic Concentration (mg/ml)	Phenolic Concentration (mol/dm^3) x10^{-3}	Phenolic Concentration (% w/w)	Induction time (min)
	1.6	0.8	5	0.09	0
	3.3	1.65	10	0.19	6
	6.6	3.3	20	0.37	7
	9.9	4.95	30	0.56	16
	13.1	6.55	40	0.74	22
	19.7	9.85	60	1.11	31
Mixed phenolic	0	0	0	0	0
	1	0.5	3.7	0.06	0
	4	2	14.9	0.22	8
	8	4	29.8	0.45	22
	16	8	59.5	0.9	48
	32	16	119	1.8	76

Table C.2: The exact amounts of crude extracts blended with 2 ml methyl linoleate and their measured induction times at 120 $^{\circ}$C and 1 bar of oxygen.

Extract ID	Sample weight [a] (mg)	Phenolic Concentration [b] (mg/ml)	Phenolic Concentration [b] (mol/dm^3) x10^{-3}	Phenolic Concentration [b] (% w/w)	Induction time (min)
Crude bio-oil	0	0	0	0	0
	25	2.88	17.38	0.32	52
	50	5.75	34.75	0.65	98
	100	11.5	69.5	1.30	163
Water-soluble extract	0	0	0	0	0
	25	1.75	10.38	0.2	22
	50	3.5	20.75	0.4	48

Extract ID	Sample weight [a] (mg)	Phenolic Concentration [b] (mg/ml)	Phenolic Concentration [b] (mol/dm^3) x10^{-3}	Phenolic Concentration [b] (% w/w)	Induction time (min)
	100	7	41.5	0.79	87
Neutral extract	0	0	0	0	0
	25	1.38	8.63	0.16	8
	50	2.75	17.25	0.31	14
	100	5.5	34.5	0.62	18
Phenolic extract	0	0	0	0	0
	25	6.25	37.75	0.70	50
	50	12.5	75.5	1.41	108
	100	25	151	2.81	128
Organic acids extract	0	0	0	0	0
	25	4.75	29.13	0.53	45
	50	9.5	58.25	1.07	88
	100	19	116.5	2.14	100
Diethyl ether extract	0	0	0	0	0
	25	7	42.38	0.79	90
	50	14	84.75	1.57	175
	100	28	169.5	3.15	160
DCM extract	0	0	0	0	0
	25	1.63	9.75	0.18	4
	50	3.25	19.5	0.37	6
	100	6.5	39	0.73	10
Water-soluble residue	0	0	0	0	0
	25	0.13	1.13	0.01	0
	50	0.25	2.25	0.03	0

Extract ID	Sample weight [a] (mg)	Phenolic Concentration [b] (mg/ml)	Phenolic Concentration [b] (mol/dm^3) x10^{-3}	Phenolic Concentration [b] (% w/w)	Induction time (min)
	100	0.5	4.5	0.06	0

[a] Actual total extract weight blended with 2 ml methyl linoleate.

[b] As determined by Folin-Ciocalteu (FC) assay assume only mono-phenolic present.

Table C.3: The equivalent molar concentrations of each detected phenolic compound *via* GC-FID when blending 100 mg of crude bio-oil or its water-insoluble extracts with 2 ml methyl linoleate. [a]

Compound	Structure	Concentration (x10^{-3} mol/dm^3)				
		Crude bio-oil	Water-soluble extract	Neutral extract	Phenolic extract	Organic acids extract
Phenol		0	/	/	0.48	/
Phenol, 2-methyl-		/[b]	/	/	0.26	/
Phenol, 4-methyl-	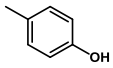	0	/	/	0.77	/
Phenol, 2-methoxy-	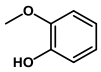	3.02	/	0.40	8.59	1.37
Phenol, 2,5-dimethyl-		/	/	/	0.06	/
1,3-Benzenediol, 4-ethyl-	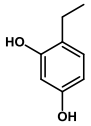	/	/	0.18	/	/
Phenol, 2-methoxy-4-methyl-	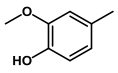	2.27	0.25	5.07	12.75	/
1,2-Benzenediol		4.25	3.28	/	/	2.11
1,2-Benzenediol, 3-methyl-	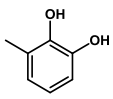	/	/	/	/	0.38

Compound	Structure	Concentration (x10^{-3} mol/dm^3)				
		Crude bio-oil	Water-soluble extract	Neutral extract	Phenolic extract	Organic acids extract
Phenol, 4-ethyl-2-methoxy-	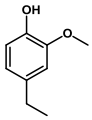	0.59	/	4.45	2.76	/
1,2-Benzenediol, 4-methyl-	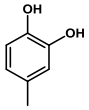	0.95	/	/	/	/
2-Methoxy-4-vinylphenol	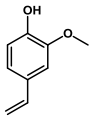	1.53	/	0.12	2.91	0.54
Phenol, 4-(2-propenyl)-	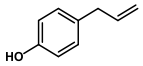	/	/	/	0.19	/
3-Allyl-6-methoxyphenol	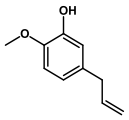	0.4	/	4.57	2.61	/
Phenol, 2-methoxy-4-propyl-	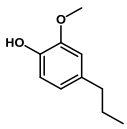	0.06	/	1.85	0.35	/
Benzaldehyde, 3-hydroxy-4-methoxy-	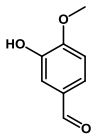	0.93	0.72	/	4.5	2.57
Phenol, 2-methoxy-4-(1-propenyl)-	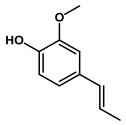	0.12	/	0.25	1.68	/
Phenol, 2-methoxy-4-(1-propenyl)-, (Z)-	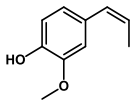	2.66	/	4.79	11.55	0.69
3,7-Benzofurandiol, 2,3-dihydro-2,2-dimethyl-	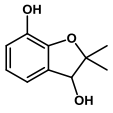	/	/	0.39	/	/
Ethanone, 1-(4-hydroxy-3-methoxyphenyl)-	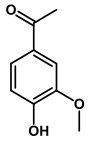	0.61	0.18	/	2.44	/

Compound	Structure	Concentration (x10^{-3} mol/dm^3)				
		Crude bio-oil	Water-soluble extract	Neutral extract	Phenolic extract	Organic acids extract
2-Propanone, 1-(4-hydroxy-3-methoxyphenyl)-	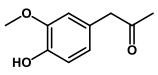	1.79	0.40	/	/	/
Phenol, 4-(3-hydroxy-1-propenyl)-2-methoxy-	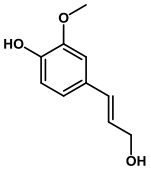	0.22	0.06	/	/	/
Benzoic acid, 4-hydroxy-3-methoxy-	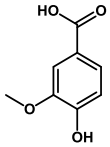	/	/	/	/	2.87
Benzeneacetic acid, 4-hydroxy-3-methoxy-	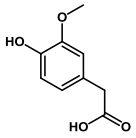	1.13	0.44	0	4.79	2.73
4-((1E)-3-Hydroxy-1-propenyl)-2-methoxyphenol	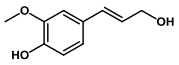	/	/	/	0.77	/
4-Hydroxy-2-methoxycinnamaldehyde	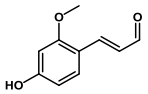	0.71	0.17	/	0.36	/
Benzeneacetic acid, 4-hydroxy-3-methoxy-, methyl ester	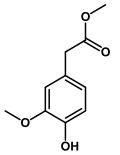	/	/	/	/	0.66
Phenylacetylformic acid, 4-hydroxy-3-methoxy-	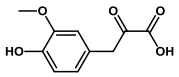	/	/	/	/	0.32
Naphtho[2,3-c]furan-1,4-dione, 3,3a,9,9a-tetrahydro-6-hydroxy-7-methoxy-	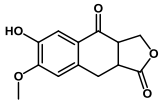	/	/	/	/	0.31
2H-1-Benzopyran-7-ol, 3,4-dihydro-3-(4-hydroxy-2-methoxyphenyl)-	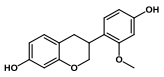	/	/	/	/	0

Compound	Structure	Concentration (x10^{-3} mol/dm^3)				
		Crude bio-oil	Water-soluble extract	Neutral extract	Phenolic extract	Organic acids extract
Podocarpa-8,11,13-triene-7β,13-diol, 14-isopropyl-	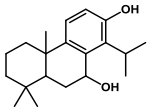	/	/	0.08	/	/
Phenol, 4-[2,3-dihydro-7-methoxy-3-methyl-5-(1-propenyl)-2-benzofuranyl]-2-methoxy-	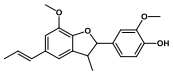	/	/	/	/	0
2(3H)-Furanone, dihydro-3,4-bis[(4-hydroxy-3-methoxyphenyl)methyl]-, (3R-trans)-	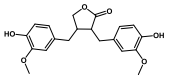	/	/	/	/	0.63
Naphtho[2,3-c]furan-1(3H)-one, 3a,4,9,9a-tetrahydro-6-hydroxy-4-(4-hydroxy-3-methoxyphenyl)-7-methoxy-, [3aR-(3aα,4α,9aβ)]-	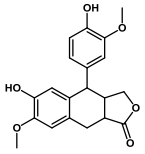	/	/	/	/	0.19
Total		~21.24	~5.52	~22.14	~57.81	~15.36

[a] Assuming that all GC-FID detected phenolics were fully dissolved in methyl linoleate.

[b] Not detected.

Table C.4: The equivalent molar concentrations of each detected phenolic compound *via* GC-FID when blending 100 mg of crude bio-oil or its water-soluble extracts with 2 ml methyl linoleate. [a]

Compound	Structure	Concentration (x 10^{-3} mol/dm^3)				
		Crude bio-oil extract	Water-soluble extract	Diethyl ether extract	DCM extract	Water-soluble residue
Phenol, 2-methoxy-		2.50	/	1.09	1.23	/
Phenol, 2-methoxy-4-methyl-	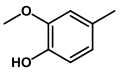	2.53	0.74	1.10	0.82	/
1,2-Benzenediol		1.50	1.18	11.10	/	/
Phenol, 4-ethyl-2-methoxy-	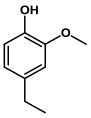	1.01	0.54	0.59	/	/
1,2-Benzenediol, 3-methyl-	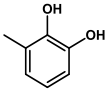	/[b]	/	2.26	/	/
2-Methoxy-4-vinylphenol	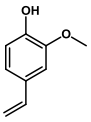	0.60	/	/	/	/
1,2-Benzenediol, 4-methyl-	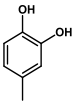	/	/	3.63	/	/
3-Allyl-6-methoxyphenol	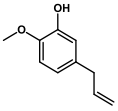	0.89	0.48	0.66	/	/
Phenol, 2-methoxy-4-propyl-	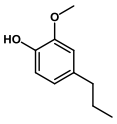	0.54	/	/	0.52	/
Benzaldehyde, 3-hydroxy-4-methoxy-	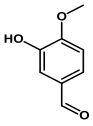	1.07	1.00	2.90	0.97	0.82
Phenol, 2-methoxy-4-(1-propenyl)-	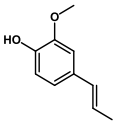	0.85	/	/	/	/

Compound	Structure	Concentration (x 10^{-3} mol/dm^3)				
		Crude bio-oil extract	Water-soluble extract	Diethyl ether extract	DCM extract	Water-soluble residue
Phenol, 2-methoxy-4-(1-propenyl)-, (Z)-	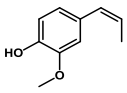	1.45	0.51	0.55	/	/
Ethanone, 1-(4-hydroxy-3-methoxyphenyl)-	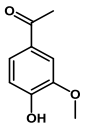	0.86	0.62	1.76	0.64	0.49
Benzoic acid, 4-hydroxy-3-methoxy-, methyl ester	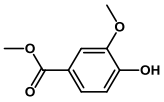	/	/	0.55	/	/
2-Propanone, 1-(4-hydroxy-3-methoxyphenyl)-	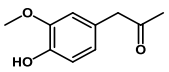	0.88	0.67	1.94	0.80	0.49
Benzeneacetic acid, 4-hydroxy-3-methoxy-	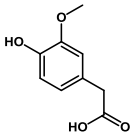	0.84	0.62	1.53	0.94	0.47
Phenylacetylformic acid, 4-hydroxy-3-methoxy-	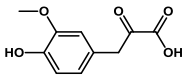	0.53	/	/	/	/
4-Hydroxy-2-methoxycinnamaldehyde	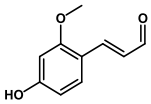	0.80	/	0.88	0.50	/
β-(4-Hydroxy-3-methoxyphenyl)propionic acid	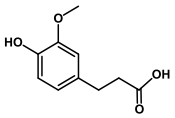	/	/	0.50	/	/
Total		~16.85	~6.36	~31.04	~6.42	~2.27

[a] Assuming that all GC-FID detected phenolics were fully dissolved in methyl linoleate.

[b] Not detected.

Appendix D: Microwave Pyrolysis

Table D.1 and Table D.2 show the recorded time, temperature and vacuum pressure at the beginning of phase formation (aqueous and bio-oil) per run during the 1st and 2nd microwave pyrolysis experiments. The microwave power was kept at 1200 W and the total procedure time per run was varying between 9 and 13 minutes, depending on the moment when crude bio-oil stops emerging from the microwave cavity.

Table D.1: Recorded observations during the 1st microwave pyrolysis experiment.

Run number	Time (second)	Temperature (°C)	Vacuum pressure (mbar)	Power (W)	Phase formation
1	60	52	22	1200	Aqueous
	165	124	95	1200	Bio-oil
2	90	54	31	1200	Aqueous
	200	108	62	1200	Bio-oil

Table D.2: Recorded observations during the 2nd microwave pyrolysis experiment.

Run number	Time (second)	Temperature (°C)	Vacuum pressure (mbar)	Power (W)	Phase formation
1	50	57	39	1200	Aqueous
	145	67	125	1200	Bio-oil
2	50	57	33	1200	Aqueous
	170	73	160	1200	Bio-oil
3	45	57	60	1200	Aqueous
	156	73	199	1200	Bio-oil
4	60	59	29	1200	Aqueous
	150	65	133	1200	Bio-oil
5	40	54	20	1200	Aqueous
	160	67	130	1200	Bio-oil

Run number	Time (second)	Temperature (°C)	Vacuum pressure (mbar)	Power (W)	Phase formation
6	45	50	20	1200	Aqueous
	165	70	130	1200	Bio-oil

The recorded temperature and vacuum pressure for the bio-oil formation in 1st microwave experiment (Table D.1) were slightly different in comparison with those stated in the 2nd microwave experiment (Table D.2). This is more likely due to the different microwave vessel used, where in the 1st microwave experiment the microwave vessel used was a homemade one.

As water is the only effective microwave absorber in wood, other important information to note is that the time gap between the 1st and the 2nd microwave pyrolysis experiments was 18 months. Therefore, moisture content of the woodchips is more likely to be affected by this time gap, which in turn affects the composition of the bio-oil produced. The moisture content of the woodchips used was not measured during the period of the 1st microwave pyrolysis experiment, however, it was measured after the 2nd microwave pyrolysis experiment and found to be *ca.* 7.5%, as demonstrated earlier in section 3.3 (Chapter 3).

Abbreviations

AD	Aerobic Digestion
ATR	Attenuated Total Reflectance
BDC	Biorenewables Development Centre
BDE	Bond Dissociation Energy
BHA	Butylated hydroxyanisole
BHT	Butylated hydroxytoluene
Bln	Billion
BOC	British Oxygen Company
CA	California
CFPP	Cold Filter Plugging Point
CHN	Carbon-Hydrogen-Nitrogen
CNSL	Cashew Nut Shell Liquid
CPA	Corrected Peak Area
DAD	Diode Array Detector
DCM	Dichloromethane
DMF	Dimethylformamide
DMSO	Dimethyl sulfoxide
DPPH	2,2-Diphenyl-1-picrylhydrazyl
DTBHQ	2,5-Di-*tert*-butyl-hydroquinone
DTBP	2,6-Di-*tert*-butylphenol
DTGS	Deuterated triglycine sulfate
ECN	Effective Carbon Number
EE	Eugenol Equivalent
ELSD	Evaporating Light Scattering Detector
EN	European Standard
EQ	Ethoxyquin
est	Estimated
f	Stoichiometric Inhibition Coefficient

FAME	Fatty Acid Methyl Ester
FC	Folin-Ciocalteu
FID	Flame Ionization Detector
FTIR	Fourier Transform Infrared
GC	Gas Chromatography
GPC	Gel Permeation Chromatography
HC	Hydrocarbon
HHV	Higher Heating Value
HMF	Hydroxymethylfurfural
$HO^{\bullet}$	Hydroxyl radical
HPLC	High Performance Liquid Chromatography
IB	Ionol BF200
ICP	Inductively Coupled Plasma
IEA	International Energy Agency
IP	Induction Period
IR	Infrared
IT	Induction Time
IUPAC	International Union of Pure and Applied Chemistry
k	Rate constant
KF	Karl Fisher
k_{inh}	Rate constant for inhibition
L	Litre – unit of volume
LC	Liquid Chromatography
MEK	Methyl ethyl ketone
Mln	Million
MPa	Megapascal – unit of pressure
MS	Mass Spectrometry
MSW	Municipal Solid Waste

MW	Molecular Weight
NIST	National Institute of Standards and Technology
NMP	*N*-Methyl-2-pyrrolidone
NMR	Nuclear Magnetic Resonance
O/BDPA	Octylated/butylated diphenylamine
PANA	*N*-Phenyl-1-naphthylamine
PDA	N, N′-di-sec-butyl-*p*-phenylenediamine
PG	Propyl gallate
PPA	Primary Peak Area
PUFA	Polyunsaturated Fatty Acid
PY	Pyrogallol
$R^{\bullet}$	Free radical or alkyl radical
RED	Renewable Energy Directive
RH	Lipid molecule
$RO^{\bullet}$	Alkoxyl radical
$ROO^{\bullet}$	Peroxyl radical
ROOH	Hydroperoxide
RRF	Relative Response Factor
SFC	Supercritical Fluid Chromatography
SFE	Supercritical Fluid Extraction
STA	Simultaneous Thermal Analyser
TBHQ	*Tert*-butyl-hydroquinone
TCI	Tokyo Chemical Industry
TG	Thermogravimetric
TGA	Thermogravimetric Analysis
THF	Tetrahydrofuran
TTBP	2,4,6-Tri-*tert*-butylphenol
UK	United Kingdome

US	United States
USA	United States of America
UV	Ultraviolet
Vis	Visible
ZDDP	Zinc dialkyl dithiophosphate

References

1. D. Meier, in *Advances in Biochemical Engineering/Biotechnology*, Springer, Berlin, Heidelberg, 2017, pp. 1-37.

2. M. R. Rover, P. A. Johnston, B. P. Lamsal and R. C. Brown, *Journal of Analytical and Applied Pyrolysis*, 2013, **104**, 194-201.

3. M. Serrano, A. Bouaid, M. Martínez and J. Aracil, *Fuel*, 2013, **113**, 50-58.

4. S. Jain and M. P. Sharma, *Fuel*, 2014, **116**, 14-18.

5. K. R. Spacino, D. Borsato, G. M. Buosi and L. T. Chendynski, *Fuel Processing Technology*, 2015, **137**, 366-370.

6. G. M. Buosi, E. T. da Silva, K. Spacino, L. R. C. Silva, B. A. D. Ferreira and D. Borsato, *Fuel*, 2016, **181**, 759-764.

7. P. T. Anastas and J. C. Warner, *Green Chemistry: Theory and Practice*, Oxford University Press, 2000.

8. P. T. Anastas and J. B. Zimmerman, *Environmental Science & Technology*, 2003, **37**, 94A-101A.

9. B. Gill, N. MacLeod, D. Clayton, R. Cowburn, J. Roberts and N. Hartley, *Biomass task force. Report to government*, London, UK: Defra, 2005.

10. J. Woods, F. Rosillo-Calle, R. Murphy, A. Strapasson, N. Burdett and M. Black, *The availability of sustainable biomass for use in UK power generation*, LCAworks, London, 2011.

11. P. Howes, J. Bates, M. Landy, S. O'Brien, R. Herbert, R. Matthews and G. Hogan, *UK and Global Bio-Energy Resource and Prices*, Report AEA/ED56029, AEA Technology plc, Didcot, 2011.

12. G. Berndes, M. Hoogwijk and R. van den Broek, *Biomass and Bioenergy*, 2003, **25**, 1-28.

13. F. Motasemi and M. T. Afzal, *Renewable and Sustainable Energy Reviews*, 2013, **28**, 317-330.

14. D. O. Hall, *Forest Ecology and Management*, 1997, **91**, 17-45.

15. N. L. Panwar, S. C. Kaushik and S. Kothari, *Renewable and Sustainable Energy Reviews*, 2011, **15**, 1513-1524.

16. D. Mohan, C. U. Pittman and P. H. Steele, *Energy & Fuels*, 2006, **20**, 848-889.

17. P. Roger, A. T. Mandla, S. H. James, M. R. Roger and S. R. Jeffrey, in *Handbook of Wood Chemistry and Wood Composites*, CRC Press, 2005, ch. 3, pp. 35-74.

18. R. C. Pettersen, in *The Chemistry of Solid Wood*, American Chemical Society, 1984, vol. 207, ch. 2, pp. 57-126.

19. A. Demirbaş, *Fuel*, 1997, **76**, 431-434.

20. H. Chung and N. R. Washburn, *Green Materials*, 2013, **1**, 137-160.

21. M. Staš, D. Kubička, J. Chudoba and M. Pospíšil, *Energy & Fuels*, 2014, **28**, 385-402.

22. J. L. McCarthy and A. Islam, in *Lignin: Historical, Biological, and Materials Perspectives*, American Chemical Society, 1999, vol. 742, ch. 1, pp. 2-99.

23. S. Laurichesse and L. Avérous, *Progress in Polymer Science*, 2014, **39**, 1266-1290.

24. E. Dorrestijn, L. J. J. Laarhoven, I. W. C. E. Arends and P. Mulder, *Journal of Analytical and Applied Pyrolysis*, 2000, **54**, 153-192.

25. W. Boerjan, J. Ralph and M. Baucher, *Annual Review of Plant Biology*, 2003, **54**, 519-546.

26. M. Baucher, B. Monties, M. V. Montagu and W. Boerjan, *Critical Reviews in Plant Sciences*, 1998, **17**, 125-197.

27. P. McKendry, *Bioresource Technology*, 2002, **83**, 47-54.

28. P. McKendry, *Bioresource Technology*, 2002, **83**, 37-46.

29. C. Wu and P. T. Williams, in *Waste as a Resource*, The Royal Society of Chemistry, 2013, pp. 1-43.

30. A. V. Herzog, T. E. Lipman and D. M. Kammen, in *OUR FRAGILE WORLD (OFW) Challenges and Opportunities for Sustainable Development*, ed. M. K. Tolba, EOLSS Publishers, Oxford, UK, 2001, vol. 1, pp. 505-536.

31. P.-w. He, S.-y. Luo, G. Cheng, B. Xiao, L. Cai and J.-b. Wang, *Renewable Energy*, 2012, **37**, 398-402.

32. S. Hurley, H. Li and C. Xu, *Bioresource Technology*, 2010, **101**, 9301-9307.

33. T.-Y. Mun, J.-O. Kim, J.-W. Kim and J.-S. Kim, *Bioresource Technology*, 2011, **102**, 7196-7203.

34. Y. Zhang, B. Li, H. Li and H. Liu, *Thermochimica Acta*, 2011, **519**, 65-71.

35. E. Cascarosa, L. Gasco, G. Gea, J. L. Sánchez and J. Arauzo, *Fuel*, 2011, **90**, 2798-2807.

36. S. Daggupati, R. N. Mandapati, S. M. Mahajani, A. Ganesh, R. K. Sapru, R. K. Sharma and P. Aghalayam, *Energy*, 2011, **36**, 1776-1784.

37. G. Gordillo, K. Annamalai and N. Carlin, *Renewable Energy*, 2009, **34**, 2789-2797.

38. L. Hongtao, C. Feng, P. Xia, Y. Kai and L. Shuqin, *Mining Science and Technology (China)*, 2011, **21**, 191-196.

39. H.-q. Li, H.-j. Han, M.-a. Du and W. Wang, *Bioresource Technology*, 2011, **102**, 4667-4673.

40. X. Shenqi, Z. Zhijie, X. Jie, Y. Guangsuo and W. Fuchen, *Fuel*, 2011, **90**, 1723-1730.

41. K. Stańczyk, N. Howaniec, A. Smoliński, J. Świądrowski, K. Kapusta, M. Wiatowski, J. Grabowski and J. Rogut, *Fuel*, 2011, **90**, 1953-1962.

42. W. Wang, H. Han, M. Yuan, H. Li, F. Fang and K. Wang, *Bioresource Technology*, 2011, **102**, 5454-5460.

43. N. Nipattummakul, I. I. Ahmed, S. Kerdsuwan and A. K. Gupta, *International Journal of Hydrogen Energy*, 2010, **35**, 11738-11745.

44. L.-p. Xie, T. Li, J.-d. Gao, X.-n. Fei, X. Wu and Y.-g. Jiang, *Journal of Fuel Chemistry and Technology*, 2010, **38**, 615-620.

45. T. Phuphuakrat, N. Nipattummakul, T. Namioka, S. Kerdsuwan and K. Yoshikawa, *Fuel*, 2010, **89**, 2278-2284.

46. M. He, Z. Hu, B. Xiao, J. Li, X. Guo, S. Luo, F. Yang, Y. Feng, G. Yang and S. Liu, *International Journal of Hydrogen Energy*, 2009, **34**, 195-203.

47. M. Thamavithya and A. Dutta, *Fuel Processing Technology*, 2008, **89**, 949-957.

48. G. Xiao, B.-s. Jin, Z.-p. Zhong, Y. Chi, M.-j. Ni, K.-f. Cen, R. Xiao, Y.-j. Huang and H. Huang, *Journal of Environmental Sciences*, 2007, **19**, 1398-1403.

49. W. Zhao, Q. Wang, Z. Zou, H. Liu, H. Zheng and L. Zhang, *Journal of Environmental Sciences*, 2009, **21**, S108-S111.

50. G. J. Stiegel and R. C. Maxwell, *Fuel Processing Technology*, 2001, **71**, 79-97.

51. A. Rentizelas, S. Karellas, E. Kakaras and I. Tatsiopoulos, *Energy Conversion and Management*, 2009, **50**, 674-681.

52. P. T. Williams, in *Waste Treatment and Disposal*, John Wiley & Sons, Ltd, 2005, pp. 325-366.

53. A. V. Bridgwater, *Chemical Engineering Journal*, 2003, **91**, 87-102.

54. A. V. Bridgwater and G. V. C. Peacocke, *Renewable and Sustainable Energy Reviews*, 2000, **4**, 1-73.

55. A. Demirbas, *Journal of Analytical and Applied Pyrolysis*, 2005, **73**, 39-43.

56. C.-H. Wu, C.-Y. Chang, C.-H. Tseng and J.-P. Lin, *Journal of Analytical and Applied Pyrolysis*, 2003, **67**, 41-53.

57. A. M. Cunliffe and P. T. Williams, *Journal of Analytical and Applied Pyrolysis*, 1998, **44**, 131-152.

58. E. A. Williams and P. T. Williams, *Journal of Analytical and Applied Pyrolysis*, 1997, **40**, 347-363.

59. W. Kaminsky and A. B. Kummer, *Journal of Analytical and Applied Pyrolysis*, 1989, **16**, 27-35.

60. F. Paradela, F. Pinto, A. M. Ramos, I. Gulyurtlu and I. Cabrita, *Journal of Analytical and Applied Pyrolysis*, 2009, **85**, 392-398.

61. R. Miranda, C. Sosa_Blanco, D. Bustos-Martínez and C. Vasile, *Journal of Analytical and Applied Pyrolysis*, 2007, **80**, 489-495.

62. A. A. Boateng, K. B. Hicks and K. P. Vogel, *Journal of Analytical and Applied Pyrolysis*, 2006, **75**, 55-64.

63. G. Maschio, C. Koufopanos and A. Lucchesi, *Bioresource Technology*, 1992, **42**, 219-231.

64. A. E. Pütün, *Energy Sources*, 2002, **24**, 275-285.

65. M. Balat, M. Balat, E. Kırtay and H. Balat, *Energy Conversion and Management*, 2009, **50**, 3147-3157.

66. D. Radlein and A. QUIGNARD, *Oil & Gas Science and Technology - Revue d'IFP Energies nouvelles*, 2013, **68**, 765-783.

67. M. F. Demirbas and M. Balat, *Journal of Scientific and Industrial Research*, 2007, **66**, 797.

68. E. d. Jong, H. Langeveld and R. v. Ree, *IEA Bioenergy Task 42 Biorefinery*, IEA Bioenergy, 2012.

69. J. H. Clark, V. Budarin, F. E. I. Deswarte, J. J. E. Hardy, F. M. Kerton, A. J. Hunt, R. Luque, D. J. Macquarrie, K. Milkowski, A. Rodriguez, O. Samuel, S. J. Tavener, R. J. White and A. J. Wilson, *Green Chemistry*, 2006, **8**, 853-860.

70. J. H. Clark, R. Luque and A. S. Matharu, *Annual review of chemical and biomolecular engineering*, 2012, **3**, 183-207.

71. M. FitzPatrick, P. Champagne, M. F. Cunningham and R. A. Whitney, *Bioresource Technology*, 2010, **101**, 8915-8922.

72. F. Cherubini, *Energy Conversion and Management*, 2010, **51**, 1412-1421.

73. V. L. Budarin, P. S. Shuttleworth, J. R. Dodson, A. J. Hunt, B. Lanigan, R. Marriott, K. J. Milkowski, A. J. Wilson, S. W. Breeden, J. Fan, E. H. K. Sin and J. H. Clark, *Energy & Environmental Science*, 2011, **4**, 471-479.

74. C. Wu, V. L. Budarin, M. J. Gronnow, M. De Bruyn, J. A. Onwudili, J. H. Clark and P. T. Williams, *Journal of Analytical and Applied Pyrolysis*, 2014, **107**, 276-283.

75. C. Wu, V. L. Budarin, M. Wang, V. Sharifi, M. J. Gronnow, Y. Wu, J. Swithenbank, J. H. Clark and P. T. Williams, *Applied Energy*, 2015, **157**, 533-539.

76. M. A. Surati, S. Jauhari and K. Desai, *Archives of Applied Science Research*, 2012, **4**, 645-661.

77. N. R. Nelly, G. G. Alexander and V. Z. Nikolai, *Russian Chemical Reviews*, 2005, **74**, 969.

78. C. Oliver Kappe, *Chemical Society Reviews*, 2008, **37**, 1127-1139.

79. J. M. Collins and N. E. Leadbeater, *Organic & Biomolecular Chemistry*, 2007, **5**, 1141-1150.

80. B. Bacsa, K. Horváti, S. Bõsze, F. Andreae and C. O. Kappe, *The Journal of Organic Chemistry*, 2008, **73**, 7532-7542.

81. R. Hoogenboom and U. S. Schubert, *Macromolecular Rapid Communications*, 2007, **28**, 368-386.

82. M. Bardts, N. Gonsior and H. Ritter, *Macromolecular Chemistry and Physics*, 2008, **209**, 25-31.

83. C. Holtze, M. Antonietti and K. Tauer, *Macromolecules*, 2006, **39**, 5720-5728.

84. M. Tsuji, M. Hashimoto, Y. Nishizawa, M. Kubokawa and T. Tsuji, *Chemistry – A European Journal*, 2005, **11**, 440-452.

85. V. Polshettiwar, M. N. Nadagouda and R. S. Varma, *Chemical Communications*, 2008, 6318-6320.

86. I. Bilecka and M. Niederberger, *Nanoscale*, 2010, **2**, 1358-1374.

87. S. Barlow and S. R. Marder, *Advanced Functional Materials*, 2003, **13**, 517-518.

88. O. Yoshikawa, T. Sonobe, T. Sagawa and S. Yoshikawa, *Applied Physics Letters*, 2009, **94**, 083301.

89. M. Gharibeh, G. A. Tompsett, K. S. Yngvesson and W. C. Conner, *The Journal of Physical Chemistry B*, 2009, **113**, 8930-8940.

90. J. R. Lill, E. S. Ingle, P. S. Liu, V. Pham and W. N. Sandoval, *Mass Spectrometry Reviews*, 2007, **26**, 657-671.

91. D. D. Young, J. Nichols, R. M. Kelly and A. Deiters, *Journal of the American Chemical Society*, 2008, **130**, 10048-10049.

92. K. M. Rahman and D. E. Thurston, *Chemical Communications*, 2009, 2875-2877.

93. P. Shuttleworth, V. Budarin and M. Gronnow, in *The Economic Utilisation of Food Co-Products*, The Royal Society of Chemistry, 2013, ch. 3, pp. 38-63.

94. S. A. Galema, *Chemical Society Reviews*, 1997, **26**, 233-238.

95. L. Zong, S. Zhou, N. Sgriccia, M. Hawley and L. Kempel, *The Journal of microwave power and electromagnetic energy: a publication of the International Microwave Power Institute*, 2003, **38**, 49-74.

96. T. Razzaq and C. O. Kappe, *ChemSusChem*, 2008, **1**, 123-132.

97. A. Corsaro, U. Chiacchio, V. Pistara and G. Romeo, *Current Organic Chemistry*, 2004, **8**, 511-538.

98. C. O. Kappe and D. Dallinger, *Nature Reviews Drug Discovery*, 2006, **5**, 51-63.

99. F. Mavandadi and Å. Pilotti, *Drug Discovery Today*, 2006, **11**, 165-174.

100. M. Larhed and A. Hallberg, *Drug Discovery Today*, 2001, **6**, 406-416.

101. D. M. P. Mingos and D. R. Baghurst, *Chemical Society Reviews*, 1991, **20**, 1-47.

102. C. Gabriel, S. Gabriel, E. H. Grant, E. H. Grant, B. S. J. Halstead and D. Michael P. Mingos, *Chemical Society Reviews*, 1998, **27**, 213-224.

103. A. Loupy and R. S. Varma, *Chimica Oggi - Chemistry Today*, 2006, **24**, 36.

104. S. S. Lam and H. A. Chase, *Energies*, 2012, **5**, 4209.

105. J. Anwar, U. Shafique, Z. Waheed uz, R. Rehman, M. Salman, A. Dar, J. M. Anzano, U. Ashraf and S. Ashraf, *Arabian Journal of Chemistry*, 2015, **8**, 100-104.

106. M. Nuchter, B. Ondruschka, W. Bonrath and A. Gum, *Green Chemistry*, 2004, **6**, 128-141.

107. D. M. P. Mingos, in *Microwave Assisted Organic Synthesis*, Blackwell Publishing Ltd., 2009, pp. 1-22.

108. B. L. Hayes, *Microwave synthesis: chemistry at the speed of light*, Cem Corporation, 2002, pp. 29-76.

109. A. D. L. Hoz, A. Diaz-Ortiz and A. Moreno, *Current Organic Chemistry*, 2004, **8**, 903-918.

110. D. J. Macquarrie, J. H. Clark and E. Fitzpatrick, *Biofuels, Bioproducts and Biorefining*, 2012, **6**, 549-560.

111. A. Domínguez, J. A. Menéndez, Y. Fernández, J. J. Pis, J. M. V. Nabais, P. J. M. Carrott and M. M. L. R. Carrott, *Journal of Analytical and Applied Pyrolysis*, 2007, **79**, 128-135.

112. V. L. Budarin, J. H. Clark, B. A. Lanigan, P. Shuttleworth, S. W. Breeden, A. J. Wilson, D. J. Macquarrie, K. Milkowski, J. Jones, T. Bridgeman and A. Ross, *Bioresource Technology*, 2009, **100**, 6064-6068.

113. Y. F. Huang, W. H. Kuan, S. L. Lo and C. F. Lin, *Bioresource Technology*, 2008, **99**, 8252-8258.

114. Y.-F. Huang, P.-T. Chiueh, W.-H. Kuan and S.-L. Lo, *Bioresource Technology*, 2013, **142**, 620-624.

115. V. L. Budarin, Y. Zhao, M. J. Gronnow, P. S. Shuttleworth, S. W. Breeden, D. J. Macquarrie and J. H. Clark, *Green Chemistry*, 2011, **13**, 2330-2333.

116. N. Ferrera-Lorenzo, E. Fuente, J. M. Bermúdez, I. Suárez-Ruiz and B. Ruiz, *Bioresource Technology*, 2014, **151**, 199-206.

117. F. Yu, S. Deng, P. Chen, Y. Liu, Y. Wan, A. Olson, D. Kittelson and R. Ruan, *Applied Biochemistry and Biotechnology*, 2007, **137**, 957-970.

118. F. Yu, R. Ruan and P. Steele, *Transactions of the American Society of Agricultural and Biological Engineers*, 2009, **52**, 1595-1601.

119. H. Lei, S. Ren and J. Julson, *Energy & Fuels*, 2009, **23**, 3254-3261.

120. M. Miura, H. Kaga, A. Sakurai, T. Kakuchi and K. Takahashi, *Journal of Analytical and Applied Pyrolysis*, 2004, **71**, 187-199.

121. J. P. Robinson, S. W. Kingman, R. Barranco, C. E. Snape and H. Al-Sayegh, *Industrial & Engineering Chemistry Research*, 2010, **49**, 459-463.

122. V. L. Budarin, P. S. Shuttleworth, M. De bruyn, T. J. Farmer, M. J. Gronnow, L. Pfaltzgraff, D. J. Macquarrie and J. H. Clark, *Catalysis Today*, 2015, **239**, 80-89.

123. H. Luo, L. Bao, L. Kong and Y. Sun, *Bioresource Technology*, 2017, **238**, 109-115.

124. A. V. Bridgwater, *Biomass and Bioenergy*, 2012, **38**, 68-94.

125. A. S. Pollard, M. R. Rover and R. C. Brown, *Journal of Analytical and Applied Pyrolysis*, 2012, **93**, 129-138.

126. J. Lehto, A. Oasmaa, Y. Solantausta, M. Kytö and D. Chiaramonti, *Applied Energy*, 2014, **116**, 178-190.

127. J. Piskorz, D. S. Scott and D. Radlein, in *Pyrolysis Oils from Biomass*, American Chemical Society, 1988, vol. 376, ch. 16, pp. 167-178.

128. J.-S. Kim, *Bioresource Technology*, 2015, **178**, 90-98.

129. N. S. Tessarolo, L. R. M. dos Santos, R. S. F. Silva and D. A. Azevedo, *Journal of Chromatography A*, 2013, **1279**, 68-75.

130. M. R. Rover and R. C. Brown, *Journal of Analytical and Applied Pyrolysis*, 2013, **104**, 366-371.

131. Y. Zhang, M. A. Dubé, D. D. McLean and M. Kates, *Bioresource Technology*, 2003, **90**, 229-240.

132. A. Sarin, *Biodiesel: Production and Properties*, The Royal Society of Chemistry, Dorchester, UK, 2012, pp. 1-4.

133. S. P. Singh and D. Singh, *Renewable and Sustainable Energy Reviews*, 2010, **14**, 200-216.

134. F. Staat and E. Vallet, *Chemistry and Industry*, 1994, **21**, 863-865.

135. D. Bajpai and V. K. Tyagi, *Journal of Oleo Science*, 2006, **55**, 487-502.

136. J. Yanowitz and R. Nelson, *Biodiesel Handling and Use Guide: Fourth Edition (Revised)*, Report NREL/TP-540-43672, National Renewable Energy Laboratory (NREL), 2009.

137. L. C. Meher, D. Vidya Sagar and S. N. Naik, *Renewable and Sustainable Energy Reviews*, 2006, **10**, 248-268.

138. S. K. Hoekman, A. Broch, C. Robbins, E. Ceniceros and M. Natarajan, *Renewable and Sustainable Energy Reviews*, 2012, **16**, 143-169.

139. E. Lotero, Y. Liu, D. E. Lopez, K. Suwannakarn, D. A. Bruce and J. G. Goodwin, *Industrial & Engineering Chemistry Research*, 2005, **44**, 5353-5363.

140. J. Thomson, *The Scot who Lit the World: The Story of William Murdoch, Inventor of Gas Lighting*, Janet Thomson, 2003.

141. M. Guo, W. Song and J. Buhain, *Renewable and Sustainable Energy Reviews*, 2015, **42**, 712-725.

142. G. Knothe, in *The Biodiesel Handbook*, eds. G. Knothe, J. V. Gerpen and J. Krahl, AOCS Publishing, Champaign, Illinois, USA, 2005, ch. 2, pp. 4-20.

143. G. Knothe, *INFORM - International News on Fats, Oils and Related Materials*, 2001, **12**, 1103-1107.

144. F. Ma and M. A. Hanna, *Bioresource Technology*, 1999, **70**, 1-15.

145. G. Chavanne, *Belgian Patent*, BE422,877, 1937.

146. H. Kazemian, B. Turowec, M. N. Siddiquee and S. Rohani, *Fuel*, 2013, **103**, 719-724.

147. M. M. Gui, K. T. Lee and S. Bhatia, *Energy*, 2008, **33**, 1646-1653.

148. Z. Yaakob, B. N. Narayanan, S. Padikkaparambil, S. Unni K and M. Akbar P, *Renewable and Sustainable Energy Reviews*, 2014, **35**, 136-153.

149. M. Canakci and H. Sanli, *Journal of Industrial Microbiology & Biotechnology*, 2008, **35**, 431-441.

150. A. Karmakar, S. Karmakar and S. Mukherjee, *Bioresource Technology*, 2010, **101**, 7201-7210.

151. OECD/FAO, *OECD-FAO Agricultural Outlook 2015-2024*, OECD Publishing, Paris, 2015.

152. *Directive 2009/28/EC of the European Parliament and of the Council of 23 April 2009 on the promotion of the use of energy from renewable sources and amending and subsequently repealing Directives 2001/77/EC and 2003/30/EC*, 2009.

153. J. Hu, Z. Du, C. Li and E. Min, *Fuel*, 2005, **84**, 1601-1606.

154. D. Y. C. Leung and Y. Guo, *Fuel Processing Technology*, 2006, **87**, 883-890.

155. M. S. Koçak, E. Ileri and Z. Utlu, *Energy & Fuels*, 2007, **21**, 3622-3626.

156. G. Karavalakis, S. Stournas and D. Karonis, *Fuel*, 2010, **89**, 2483-2489.

157. A. Schönborn, N. Ladommatos, J. Williams, R. Allan and J. Rogerson, *Combustion and Flame*, 2009, **156**, 1396-1412.

158. B.-F. Lin, J.-H. Huang and D.-Y. Huang, *Fuel*, 2009, **88**, 1779-1785.

159. C. J. Chuck, C. D. Bannister, J. G. Hawley, M. G. Davidson, I. La Bruna and A. Paine, *Energy & Fuels*, 2009, **23**, 2290-2294.

160. V. Nagaraju, N. Henein, A. Quader, M. Wu and W. Bryzik, *Effect of biodiesel (B-20) on performance and emissions in a single cylinder HSDI diesel engine*, Report 0148-7191, SAE Technical Paper, 2008.

161. O. Armas, K. Yehliu and A. L. Boehman, *Fuel*, 2010, **89**, 438-456.

162. K. Bunyakiat, S. Makmee, R. Sawangkeaw and S. Ngamprasertsith, *Energy & Fuels*, 2006, **20**, 812-817.

163. P. S. Mehta and K. Anand, *Energy & Fuels*, 2009, **23**, 3893-3898.

164. C. İlkiliç and R. Behçet, *Energy Sources, Part A: Recovery, Utilization, and Environmental Effects*, 2010, **32**, 839-850.

165. J. S. de Oliveira, P. M. Leite, L. B. de Souza, V. M. Mello, E. C. Silva, J. C. Rubim, S. M. P. Meneghetti and P. A. Z. Suarez, *Biomass and Bioenergy*, 2009, **33**, 449-453.

166. G. Karavalakis, F. Alvanou, S. Stournas and E. Bakeas, *Fuel*, 2009, **88**, 1078-1085.

167. H. Imahara, E. Minami, S. Hari and S. Saka, *Fuel*, 2008, **87**, 1-6.

168. O. Armas, J. J. Hernández and M. D. Cárdenas, *Fuel*, 2006, **85**, 2427-2438.

169. S. Taravus, H. Temur and A. Yartasi, *Energy & Fuels*, 2009, **23**, 4112-4115.

170. J. L. Harwood and F. D. Gunstone, in *The Lipid Handbook with CD-ROM, Third Edition*, CRC Press, 2007, pp. 37-141.

171. T. A. McKeon, B. K. Sharma, J. T. Lin, S. Z. Erhan, J. Alander and F. D. Gunstone, in *The Lipid Handbook with CD-ROM, Third Edition*, CRC Press, 2007, pp. 591-635.

172. R. K. Saluja, V. Kumar and R. Sham, *Renewable and Sustainable Energy Reviews*, 2016, **62**, 866-881.

173. B. R. Moser, *Journal of the American Oil Chemists' Society*, 2009, **86**, 699-706.

174. H. Tang, A. Wang, S. O. Salley and K. Y. S. Ng, *Journal of the American Oil Chemists' Society*, 2008, **85**, 373-382.

175. G. Aguilar, G. Mazzamaro and M. Rasberger, in *Chemistry and Technology of Lubricants*, eds. M. R. Mortier, F. M. Fox and T. S. Orszulik, Springer Netherlands, Dordrecht, 2010, pp. 107-152.

176. A. dos Reis Albuquerque, J. Maul, A. F. F. Vasconcelos, J. R. C. Filho, I. M. G. dos Santos and A. G. de Souza, *Journal of Thermal Analysis and Calorimetry*, 2014, **117**, 799-806.

177. J. Bolland, *Quarterly Reviews, Chemical Society*, 1949, **3**, 1-21.

178. C. E. Frank, *Chemical Reviews*, 1950, **46**, 155-169.

179. L. Bateman, *Quarterly Reviews, Chemical Society*, 1954, **8**, 147-167.

180. S. Zavgorodnii, *Russian Chemical Reviews*, 1961, **30**, 133-156.

181. D. Jun and A. M. Cyril, in *Lubricant Additives : Chemistry and Applications*, ed. L. R. Rudnick, CRC Press, Boca Raton, 2nd edn., 2009, pp. 3-50.

182. N. M. Emanuel, E. T. Denisov and Z. K. Maizus, *Liquid-Phase Oxidation of Hydrocarbons*, Plenum Press, New York, 1967, pp. 1-17.

183. A. V. Karyakin, *Russian Chemical Reviews*, 1961, **30**, 460.

184. M. Laguerre, J. Lecomte and P. Villeneuve, *Progress in Lipid Research*, 2007, **46**, 244-282.

185. S. W. Benson, *The Journal of Chemical Physics*, 1964, **40**, 1007-1013.

186. E. T. Denisov and I. B. Afanas'ev, *Oxidation and antioxidants in organic chemistry and biology*, CRC press, Boca Raton, 2005.

187. S. Al-Malaika, *Polymer Degradation and Stability*, 1991, **34**, 1-36.

188. A. F. Bickel and E. C. Kooyman, *Journal of the Chemical Society (Resumed)*, 1956, 2215-2221.

189. A. F. Bickel and E. C. Kooyman, *Journal of the Chemical Society (Resumed)*, 1953, 3211-3218.

190. C. J. Pedersen, *Industrial & Engineering Chemistry*, 1956, **48**, 1881-1884.

191. R. Shah, E. A. Haidasz, L. Valgimigli and D. A. Pratt, *Journal of the American Chemical Society*, 2015, **137**, 2440-2443.

192. E. A. Haidasz, R. Shah and D. A. Pratt, *Journal of the American Chemical Society*, 2014, **136**, 16643-16650.

193. M. B. Neiman, *Russian Chemical Reviews*, 1964, **33**, 13-27.

194. I. Tikhonov, V. Roginsky and E. Pliss, *International Journal of Chemical Kinetics*, 2009, **41**, 92-100.

195. C. E. Boozer, G. S. Hammond, C. E. Hamilton and J. N. Sen, *Journal of the American Chemical Society*, 1955, **77**, 3233-3237.

196. V. A. Roginsky, T. K. Barsukova, A. A. Remorova and W. Bors, *Journal of the American Oil Chemists' Society*, 1996, **73**, 777.

197. V. A. Roginskii, V. Z. Dubinskii, I. A. Shlyapnikova and V. B. Miller, *European Polymer Journal*, 1977, **13**, 1043-1051.

198. J. L. Bolland and P. T. Have, *Transactions of the Faraday Society*, 1947, **43**, 201-210.

199. J. L. Bolland and P. T. Have, *Discussions of the Faraday Society*, 1947, **2**, 252-260.

200. V. A. Roginskii, *Polymer Science U.S.S.R.*, 1982, **24**, 2063-2088.

201. E. T. Denisov, *Kinetics and Catalysis*, 2006, **47**, 662-671.

202. G. J. Moody, PhD Thesis, University of York, 2013.

203. G. Scott, in *Atmospheric oxidation and antioxidants*, ed. G. Scott, Elsevier, 1993, vol. 1, ch. 1, pp. 1-44.

204. A. P. Griva and E. T. Denisov, *International Journal of Chemical Kinetics*, 1973, **5**, 869-877.

205. H. Musso, *Angewandte Chemie International Edition in English*, 1963, **2**, 723-735.

206. K. Ley, E. Müller, R. Mayer and K. Scheffler, *Chemische Berichte*, 1958, **91**, 2670-2681.

207. J. Pospíšil, *Pure and Applied Chemistry*, 1973, **36**, 207-232.

208. H.-D. Becker, *The Journal of Organic Chemistry*, 1965, **30**, 982-989.

209. E. R. Altwicker, *Chemical Reviews*, 1967, **67**, 475-531.

210. E. T. Denisov and I. V. Khudyakov, *Chemical Reviews*, 1987, **87**, 1313-1357.

211. J. K. Becconsall, S. Clough and G. Scott, *Transactions of the Faraday Society*, 1960, **56**, 459-472.

212. G. Scott, *South African Journal of Chemistry*, 1979, **32**, 137-146.

213. S. L. Cosgrove and W. A. Waters, *Journal of the Chemical Society (Resumed)*, 1951, 388-391.

214. C. D. Cook, *The Journal of Organic Chemistry*, 1953, **18**, 261-266.

215. C. D. Cook, N. G. Nash and H. R. Flanagan, *Journal of the American Chemical Society*, 1955, **77**, 1783-1785.

216. R. F. Moore and W. A. Waters, *Journal of the Chemical Society (Resumed)*, 1954, 243-246.

217. J. K. Becconsall, S. Clough and G. Scott, *Proceedings of the Chemical Society*, 1959, **0**, 308-309.

218. R. Magnusson, *Acta Chemica Scandinavica*, 1966, **20**, 2211-2214.

219. E. L. Shanina and G. E. Zaikov, *International Journal of Polymeric Materials and Polymeric Biomaterials*, 1997, **38**, 99-128.

220. G. Scott, in *Atmospheric oxidation and antioxidants*, ed. G. Scott, Elsevier, 1993, vol. 3, ch. 8, pp. 205-222.

221. E. T. Denisov and V. V. Azatyan, *Inhibition of Chain Reactions*, Gordon and Breach, London, 2000.

222. S. G. Cohen, *Journal of the American Chemical Society*, 1947, **69**, 1057-1064.

223. G. Scott, *Polymer Engineering & Science*, 1984, **24**, 1007-1020.

224. G. Scott, *Bulletin of the Chemical Society of Japan*, 1988, **61**, 165-170.

225. A. K. Domingos, E. B. Saad, W. W. D. Vechiatto, H. M. Wilhelm and L. P. Ramos, *Journal of the Brazilian Chemical Society*, 2007, **18**, 416-423.

226. E. Sendzikiene, V. Makareviciene and P. Janulis, *Polish Journal of Environmental Studies*, 2005, **14**, 335-339.

227. C. Liang and K. Schwarzer, *Journal of the American Oil Chemists' Society*, 1998, **75**, 1441-1443.

228. Y. C. Liang, C. Y. May, C. S. Foon, M. A. Ngan, C. C. Hock and Y. Basiron, *Fuel*, 2006, **85**, 867-870.

229. F. Souza, F. Maia, S. Mazzetto, T. Nascimento and N. de Andrade, *Chemical and Biochemical Engineering Quarterly*, 2013, **27**, 327-334.

230. A. Ingendoh, *Lipid Technology*, 2010, **22**, 83-86.

231. W. E. Neff, E. Selke, T. L. Mounts, W. Rinsch, E. N. Frankel and M. A. M. Zeitoun, *Journal of the American Oil Chemists' Society*, 1992, **69**, 111-118.

232. R. L. McCormick, M. Ratcliff, L. Moens and R. Lawrence, *Fuel Processing Technology*, 2007, **88**, 651-657.

233. E. C. f. S. (CEN), *Fat and Oil Derivatives. Fatty Acid Methyl Esters (FAME). Determination of Oxidative Stability (Accelerated Oxidation Test), EN 14112: 2003*, Brussels, Belgium, 2003.

234. M. M. Rashed, M. A. Kalam, H. H. Masjuki, H. K. Rashedul, A. M. Ashraful, I. Shancita and A. M. Ruhul, *RSC Advances*, 2015, **5**, 36240-36261.

235. R. Sarin, M. Sharma, S. Sinharay and R. K. Malhotra, *Fuel*, 2007, **86**, 1365-1371.

236. Y.-H. Chen and Y.-M. Luo, *Fuel Processing Technology*, 2011, **92**, 1387-1393.

237. E. Subroto, R. Manurung, H. J. Heeres and A. A. Broekhuis, *European Journal of Lipid Science and Technology*, 2013, **115**, 909-920.

238. A. Y. Loo, K. Jain and I. Darah, *Food Chemistry*, 2008, **107**, 1151-1160.

239. L. S. de Sousa, C. V. R. de Moura, J. E. de Oliveira and E. M. de Moura, *Fuel*, 2014, **134**, 420-428.

240. G. El Diwani, S. El Rafie and S. Hawash, *International Journal of Environmental Science & Technology*, 2009, **6**, 369-378.

241. E. Christensen and R. L. McCormick, *Fuel Processing Technology*, 2014, **128**, 339-348.

242. Supriyono, H. Sulistyo, M. F. Almeida and J. M. Dias, *Fuel Processing Technology*, 2015, **132**, 133-138.

243. M. Mittelbach and S. Schober, *Journal of the American Oil Chemists' Society*, 2003, **80**, 817-823.

244. T. Vasileva, K. Stanulov and S. Nenkova, *Journal of the University of Chemical Technology and Metallurgy*, 2008, **43**, 65-68.

245. F. J. N. Maia, V. G. P. Ribeiro, D. Lomonaco, F. M. T. Luna and S. E. Mazzetto, *Industrial Crops and Products*, 2012, **36**, 271-275.

246. A. M. Salehi, G. Pages, I. Furó, G. Henriksson and M. Johansson, *Progress in Organic Coatings*, 2011, **72**, 325-333.

247. K. Doudin, S. Al-Malaika, H. H. Sheena, V. Tverezovskiy and P. Fowler, *Polymer Degradation and Stability*, 2016, **130**, 126-134.

248. R. M. Gallivan and P. K. Matschei, *US Patent*, US4209647, 1980.

249. A. Effendi, H. Gerhauser and A. V. Bridgwater, *Renewable and Sustainable Energy Reviews*, 2008, **12**, 2092-2116.

250. S. Wang, Y. Wang, Q. Cai, X. Wang, H. Jin and Z. Luo, *Separation and Purification Technology*, 2014, **122**, 248-255.

251. A. Olejniczak, A. Kucinska, A. W. Cyganiuk and J. P. Lukaszewicz, *Industrial & Engineering Chemistry Research*, 2012, **51**, 5117-5123.

252. C. J. Donahue and E. A. Rais, *Journal of Chemical Education*, 2009, **86**, 222.

253. J. C. Sternberg, W. S. Gallaway and D. T. L. Jones, in *Gas chromatography*, eds. N. Brenner, J. E. Collen and M. D. Weiss, Academic Press, New York, 1962, ch. XVIII, pp. 231-267.

254. J. T. Scanlon and D. E. Willis, *Journal of Chromatographic Science*, 1985, **23**, 333-340.

255. A. D. Jorgensen, K. C. Picel and V. C. Stamoudis, *Analytical Chemistry*, 1990, **62**, 683-689.

256. S.-H. Jung, S.-J. Kim and J.-S. Kim, *Bioresource Technology*, 2012, **114**, 670-676.

257. V. L. Singleton, R. Orthofer and R. M. Lamuela-Raventós, in *Methods in Enzymology*, Academic Press, 1999, vol. Volume 299, pp. 152-178.

258. A. L. Waterhouse, in *Current Protocols in Food Analytical Chemistry*, John Wiley & Sons, Inc., 2002.

259. A. Alfadhl, PhD Thesis, University of York, 2008.

260. M. S. Stark, J. J. Wilkinson, J. R. L. Smith, A. Alfadhl and B. A. Pochopien, *Industrial & Engineering Chemistry Research*, 2011, **50**, 817-823.

261. T. I. J. Dugmore and M. S. Stark, *Fuel*, 2014, **124**, 91-96.

262. T. I. J. Dugmore, PhD Thesis, University of York, 2011.

263. R. Luque, J. A. Menendez, A. Arenillas and J. Cot, *Energy & Environmental Science*, 2012, **5**, 5481-5488.

264. C. Yin, *Bioresource Technology*, 2012, **120**, 273-284.

265. A. W. Coats and J. P. Redfern, *Analyst*, 1963, **88**, 906-924.

266. A. Demirbas, *Progress in Energy and Combustion Science*, 2004, **30**, 219-230.

267. A. M. Azeez, D. Meier, J. Odermatt and T. Willner, *Energy & Fuels*, 2010, **24**, 2078-2085.

268. J. Werkelin, B.-J. Skrifvars and M. Hupa, *Biomass and Bioenergy*, 2005, **29**, 451-466.

269. C. Lievens, D. Mourant, M. He, R. Gunawan, X. Li and C.-Z. Li, *Fuel*, 2011, **90**, 3417-3423.

270. K. K. Pandey, *Journal of Applied Polymer Science*, 1999, **71**, 1969-1975.

271. C. Bonini and M. D'Auria, in *Biomass and Bioenergy: New Research*, ed. M. D. Brenes, Nova Science Publishers, Inc., New York, 2006, ch. 6, pp. 141-168.

272. J. P. Diebold, *A review of the chemical and physical mechanisms of the storage stability of fast pyrolysis bio-oils*, Report NREL/SR-570-27613, National Renewable Energy Laboratory, Colorado, 2000.

273. C. Lievens, J. Yperman, T. Cornelissen and R. Carleer, *Fuel*, 2008, **87**, 1906-1916.

274. C. Lievens, R. Carleer, T. Cornelissen and J. Yperman, *Fuel*, 2009, **88**, 1417-1425.

275. L. J. Bellamy, in *The Infra-red Spectra of Complex Molecules*, Springer Netherlands, Dordrecht, 1975, pp. 149-182.

276. M. R. Nimlos and R. J. Evans, *Fuel Chemistry Division Preprints*, 2002, **47**, 393-394.

277. J. L. Bishop, C. M. Pieters and J. O. Edwards, *Clays and Clay Minerals*, 1994, **42**, 702-716.

278. L. Ingram, D. Mohan, M. Bricka, P. Steele, D. Strobel, D. Crocker, B. Mitchell, J. Mohammad, K. Cantrell and C. U. Pittman, *Energy & Fuels*, 2008, **22**, 614-625.

279. S. Thangalazhy-Gopakumar, S. Adhikari, R. B. Gupta and S. D. Fernando, *Energy & Fuels*, 2011, **25**, 1191-1199.

280. C. A. Mullen, A. A. Boateng, K. B. Hicks, N. M. Goldberg and R. A. Moreau, *Energy & Fuels*, 2010, **24**, 699-706.

281. E. Alsbou and B. Helleur, *Energy & Fuels*, 2014, **28**, 578-590.

282. D. Meier and O. Faix, *Bioresource Technology*, 1999, **68**, 71-77.

283. M. Garcia-Perez, A. Chaala, H. Pakdel, D. Kretschmer and C. Roy, *Biomass and Bioenergy*, 2007, **31**, 222-242.

284. A. E. Pütün, B. B. Uzun, E. Apaydin and E. Pütün, *Fuel Processing Technology*, 2005, **87**, 25-32.

285. N. Ozbay, A. E. Pütün and E. Pütün, *International Journal of Energy Research*, 2006, **30**, 501-510.

286. C. A. Mullen, G. D. Strahan and A. A. Boateng, *Energy & Fuels*, 2009, **23**, 2707-2718.

287. N. R. Babij, E. O. McCusker, G. T. Whiteker, B. Canturk, N. Choy, L. C. Creemer, C. V. D. Amicis, N. M. Hewlett, P. L. Johnson, J. A. Knobelsdorf, F. Li, B. A. Lorsbach, B. M. Nugent, S. J. Ryan, M. R. Smith and Q. Yang, *Organic Process Research & Development*, 2016, **20**, 661-667.

288. H. Wikberg and S. Liisa Maunu, *Carbohydrate Polymers*, 2004, **58**, 461-466.

289. J. Banoub, G.-H. Delmas, N. Joly, G. Mackenzie, N. Cachet, B. Benjelloun-Mlayah and M. Delmas, *Journal of Mass Spectrometry*, 2015, **50**, 5-48.

290. C. Amen-Chen, H. Pakdel and C. Roy, *Bioresource Technology*, 2001, **79**, 277-299.

291. D. Takada, K. Ehara and S. Saka, *Journal of Wood Science*, 2004, **50**, 253-259.

292. D. C. Elliott and T. R. Hart, *Energy & Fuels*, 2009, **23**, 631-637.

293. L. Fele Žilnik and A. Jazbinšek, *Separation and Purification Technology*, 2012, **86**, 157-170.

294. Y. Fan, Y. Cai, X. Li, H. Yin, N. Yu, R. Zhang and W. Zhao, *Journal of Analytical and Applied Pyrolysis*, 2014, **106**, 63-70.

295. A. Demirbas, *Fuel Processing Technology*, 2007, **88**, 591-597.

296. M. Garcia-Perez, S. Wang, J. Shen, M. Rhodes, W. J. Lee and C.-Z. Li, *Energy & Fuels*, 2008, **22**, 2022-2032.

297. Q. Bu, H. Lei, S. Ren, L. Wang, J. Holladay, Q. Zhang, J. Tang and R. Ruan, *Bioresource Technology*, 2011, **102**, 7004-7007.

298. Q. Bu, H. Lei, S. Ren, L. Wang, Q. Zhang, J. Tang and R. Ruan, *Bioresource Technology*, 2012, **108**, 274-279.

299. M. Herrero, A. Cifuentes and E. Ibañez, *Food Chemistry*, 2006, **98**, 136-148.

300. Q. Lang and C. M. Wai, *Talanta*, 2001, **53**, 771-782.

301. E. Reverchon, *The Journal of Supercritical Fluids*, 1997, **10**, 1-37.

302. A. Dron, D. E. Guyeru, D. A. Gage and C. T. Lira, *Journal of Food Process Engineering*, 1997, **20**, 107-124.

303. F. Sahena, I. S. M. Zaidul, S. Jinap, A. A. Karim, K. A. Abbas, N. A. N. Norulaini and A. K. M. Omar, *Journal of Food Engineering*, 2009, **95**, 240-253.

304. M. Arshadi, A. J. Hunt and J. H. Clark, *RSC Advances*, 2012, **2**, 1806-1809.

305. R. S. Oakes, A. A. Clifford and C. M. Rayner, *Journal of the Chemical Society, Perkin Transactions 1*, 2001, 917-941.

306. W. K. Modey, D. A. Mulholland and M. W. Raynor, *Phytochemical Analysis*, 1996, **7**, 1-15.

307. E. Reverchon and I. De Marco, *The Journal of Supercritical Fluids*, 2006, **38**, 146-166.

308. F. Temelli, *The Journal of Supercritical Fluids*, 2009, **47**, 583-590.

309. H.-M. Yang, W. Zhao, K. Norinaga, J.-J. Fang, Y.-G. Wang, Z.-M. Zong and X.-Y. Wei, *Separation and Purification Technology*, 2015, **152**, 238-245.

310. C. Amen-Chen, H. Pakdel and C. Roy, *Biomass and Bioenergy*, 1997, **13**, 25-37.

311. J. Li, C. Wang and Z. Yang, *Journal of Analytical and Applied Pyrolysis*, 2010, **89**, 218-224.

312. Y. Wei, H. Lei, L. Wang, L. Zhu, X. Zhang, Y. Liu, S. Chen and B. Ahring, *Energy & Fuels*, 2014, **28**, 1207-1212.

313. Y. Kodera, K. Ukegawa and T. Nakayama, *American Chemical Society, Division of Petroleum Chemistry, Preprints;(United States)*, 1990, **35**.

314. B. P. Mudraboyina, D. Fu and P. G. Jessop, *Green Chemistry*, 2015, **17**, 169-172.

315. G. Knothe, *Fuel Processing Technology*, 2005, **86**, 1059-1070.

316. G. Knothe, *Fuel Processing Technology*, 2007, **88**, 669-677.

317. J. Hancsók, T. Kasza, S. Kovács, P. Solymosi and A. Holló, *Journal of Cleaner Production*, 2012, **34**, 76-81.

318. N. M. Ribeiro, A. C. Pinto, C. M. Quintella, G. O. da Rocha, L. S. G. Teixeira, L. L. N. Guarieiro, M. do Carmo Rangel, M. C. C. Veloso, M. J. C. Rezende, R. Serpa da Cruz, A. M. de Oliveira, E. A. Torres and J. B. de Andrade, *Energy & Fuels*, 2007, **21**, 2433-2445.

319. J. Pullen and K. Saeed, *Renewable and Sustainable Energy Reviews*, 2012, **16**, 5924-5950.

320. J. Van Gerpen, B. Shanks, R. Pruszko, D. Clements and G. Knothe, *Biodiesel Production Technology*, Report NREL/SR-510-36244, National Renewable Energy Laboratory (NREL), Golden, USA, 2004.

321. A. Bouaid, M. Martinez and J. Aracil, *Bioresource Technology*, 2009, **100**, 2234-2239.

322. G. Knothe and R. O. Dunn, *Journal of the American Oil Chemists' Society*, 2003, **80**, 1021-1026.

323. L. R. Mahoney, *Angewandte Chemie International Edition in English*, 1969, **8**, 547-555.

324. I. M. Rizwanul Fattah, H. H. Masjuki, M. A. Kalam, M. A. Hazrat, B. M. Masum, S. Imtenan and A. M. Ashraful, *Renewable and Sustainable Energy Reviews*, 2014, **30**, 356-370.

325. J. A. Waynick, *Characterization of Biodiesel Oxidation and Oxidation Products: Technical Literature Review. Task 1 Results*, Report NREL/TP-540-39096, National Renewable Energy Laboratory, Golden, USA, 2005.

326. Y. Yamamoto, E. Niki and Y. Kamiya, *Bulletin of the Chemical Society of Japan*, 1982, **55**, 1548-1550.

327. F. R. Mayo, *Accounts of Chemical Research*, 1968, **1**, 193-201.

328. M. S. Graboski and R. L. McCormick, *Progress in Energy and Combustion Science*, 1998, **24**, 125-164.

329. E. N. Frankel, W. E. Neff, W. K. Rohwedder, B. P. S. Khambay, R. F. Garwood and B. C. L. Weedon, *Lipids*, 1977, **12**, 908-913.

330. E. C. Zuleta, L. Baena, L. A. Rios and J. A. Calderón, *Journal of the Brazilian Chemical Society*, 2012, **23**, 2159-2175.

331. V. B. Oyeyemi, J. A. Keith and E. A. Carter, *The Journal of Physical Chemistry A*, 2014, **118**, 7392-7403.

332. J. A. Howard and K. U. Ingold, *Canadian Journal of Chemistry*, 1967, **45**, 793-802.

333. K. B. Clark, P. N. Culshaw, D. Griller, F. P. Lossing, J. A. M. Simoes and J. C. Walton, *The Journal of Organic Chemistry*, 1991, **56**, 5535-5539.

334. V. B. Oyeyemi, J. M. Dieterich, D. B. Krisiloff, T. Tan and E. A. Carter, *The Journal of Physical Chemistry A*, 2015, **119**, 3429-3439.

335. G. Knothe, *Energy & Fuels*, 2008, **22**, 1358-1364.

336. N. Singh, P. J. O'Malley and P. L. Popelier, *Physical Chemistry Chemical Physics*, 2005, **7**, 614-619.

337. E. T. Denisov and T. Denisova, *Handbook of antioxidants: bond dissociation energies, rate constants, activation energies, and enthalpies of reactions*, CRC press, Boca Raton, 2000.

338. Y. R. Luo, *Handbook of Bond Dissociation Energies in Organic Compounds*, CRC Press, Boca Raton, 2003.

339. M. Lucarini, P. Pedrielli, G. F. Pedulli, S. Cabiddu and C. Fattuoni, *The Journal of Organic Chemistry*, 1996, **61**, 9259-9263.

340. G. Brigati, M. Lucarini, V. Mugnaini and G. F. Pedulli, *The Journal of Organic Chemistry*, 2002, **67**, 4828-4832.

341. M. Lucarini and G. F. Pedulli, *Chemical Society Reviews*, 2010, **39**, 2106-2119.

342. R. Amorati, S. Menichetti, E. Mileo, G. F. Pedulli and C. Viglianisi, *Chemistry – A European Journal*, 2009, **15**, 4402-4410.

343. G. W. Burton, T. Doba, E. Gabe, L. Hughes, F. L. Lee, L. Prasad and K. U. Ingold, *Journal of the American Chemical Society*, 1985, **107**, 7053-7065.

344. M. Lucarini, G. F. Pedulli and M. Guerra, *Chemistry – A European Journal*, 2004, **10**, 933-939.

345. Y. Murakami, S. Ito, T. Atsumi and S. Fujisawa, *In vivo*, 2005, **19**, 1039-1043.

346. R. A. Larson, *Naturally Occurring Antioxidants*, CRC Press, Boca Raton, 1997, pp. 67-82.

347. M. S. Brewer, *Comprehensive Reviews in Food Science and Food Safety*, 2011, **10**, 221-247.

348. V. Bondet, W. Brand-Williams and C. Berset, *LWT - Food Science and Technology*, 1997, **30**, 609-615.

349. W. Brand-Williams, M. E. Cuvelier and C. Berset, *LWT - Food Science and Technology*, 1995, **28**, 25-30.

350. M.-E. Cuvelier, H. Richard and C. Berset, *Bioscience, Biotechnology, and Biochemistry*, 1992, **56**, 324-325.

351. A. Moure, J. M. Cruz, D. Franco, J. M. Domínguez, J. Sineiro, H. Domínguez, M. a. José Núñez and J. C. Parajó, *Food Chemistry*, 2001, **72**, 145-171.

352. M. Leopoldini, N. Russo and M. Toscano, *Food Chemistry*, 2011, **125**, 288-306.

353. S. V. Jovanovic, S. Steenken, M. Tosic, B. Marjanovic and M. G. Simic, *Journal of the American Chemical Society*, 1994, **116**, 4846-4851.

354. D. Procházková, I. Boušová and N. Wilhelmová, *Fitoterapia*, 2011, **82**, 513-523.

355. H. Li, A. Guo and H. Wang, *Food Chemistry*, 2008, **108**, 1-13.

356. K. Robards, P. D. Prenzler, G. Tucker, P. Swatsitang and W. Glover, *Food Chemistry*, 1999, **66**, 401-436.

357. M. D. Ryan, A. Yueh and W. Y. Chen, *Journal of The Electrochemical Society*, 1980, **127**, 1489-1495.

358. M. N. Peyrat-Maillard, M. E. Cuvelier and C. Berset, *Journal of the American Oil Chemists' Society*, 2003, **80**, 1007.

359. M. N. Peyrat-Maillard, S. Bonnely, L. Rondini and C. Berset, *LWT - Food Science and Technology*, 2001, **34**, 176-182.

360. T. Masuda, Y. Toi, H. Bando, T. Maekawa, Y. Takeda and H. Yamaguchi, *Journal of Agricultural and Food Chemistry*, 2002, **50**, 2524-2530.

361. E. Voisin and V. E. Williams, *Macromolecules*, 2008, **41**, 2994-2997.

362. J. W. Goodby, M. Hird, K. J. Toyne and T. Watson, *Journal of the Chemical Society, Chemical Communications*, 1994, 1701-1702.

363. N. Boden, R. J. Bushby and A. N. Cammidge, *Journal of the Chemical Society, Chemical Communications*, 1994, 465-466.

364. O. C. Musgrave and C. J. Webster, *Journal of the Chemical Society D: Chemical Communications*, 1969, 712-713.

365. O. C. Musgrave and C. J. Webster, *Journal of the Chemical Society C: Organic*, 1971, 1393-1397.

366. L. R. C. Barclay, C. E. Edwards and M. R. Vinqvist, *Journal of the American Chemical Society*, 1999, **121**, 6226-6231.

367. I. Tichonov, V. Roginsky and E. Pliss, *European Journal of Lipid Science and Technology*, 2010, **112**, 887-893.

368. C. L. Faiola, M. H. Erickson, V. L. Fricaud, B. T. Jobson and T. M. VanReken, *Atmospheric Measurement Techniques*, 2012, **5**, 1911-1923.